The hydrolysis of cirazoline and the mechanism of stabilization by SDDS

Jones, Christopher Buchan

Award date:
1988

Awarding institution:
University of Bath

THE HYDROLYSIS OF CIRAZOLINE AND THE MECHANISM OF STABILIZATION BY SDDS.

submitted by

CHRISTOPHER BUCHAN JONES, BPharm, MPS.

for the degree of Doctor of Philosophy

of the University of Bath

1988

This research has been carried out in the School of Pharmacy of the University of Bath under the supervision of D.J.G. Davies, MSc, PhD, FPS and B.J. Meakin, BPharm, FPS.

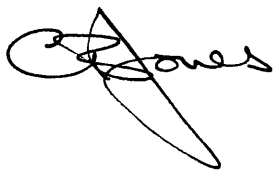

ProQuest LLC
789 East Eisenhower Parkway
P.O. Box 1346
Ann Arbor, MI 48106-1346

ACKNOWLEDGEMENTS

I wish to express my thanks to Mr. B.J. Meakin and Dr. D.J. Davies for the guidance, advice and discussion throughout this study. I would also like to acknowledge Dr. A. Casey and Dr. G.H. Dewar for their helpful discussions on imidazoline chemistry. I am indebted to the staff of the Pharmaceutics Department for their help and to many colleagues and friends for their interest and assistant.

I would also like to thank Miss Sarah Jenkins for patiently typing the manuscript.

Finally, I would like to thank my wife for her continual support, understanding and encouragement during all stages of this study.

This work was carried out with the aid of a grant award from the Science and Engineering Research Council.

To Sally

SUMMARY

This thesis principally examines the kinetics and mechanism of hydrolysis of cirazoline hydrochloride in aqueous solution and the stabilising effect of sodium dodecylsulphate (SDDS) which results from a variety of drug-surfactant interactions.

The introduction outlines the factors affecting hydrolysis kinetics and briefly reviews the stability and medicinal and physicochemical properties of imidazolines. The properties of surface active agents particularly micellization and solubilization are examined and separate sections are devoted to interactions between large organic ions of opposite charge and the effect of surfactants on reaction kinetics and equilibria. Experimental work is divided into seven sections dealing with materials and general methods; HPLC and UV analysis techniques; pK_a determination; NMR studies into imidazoline acidity; ion-pair and complex formation; micellization and solubilization; and kinetics of hydrolysis.

The poor stability of cirazoline relative to a series of other medicinal imidazolines was established. Examination of experimental data indicates that degradation of cirazoline is mediated through uncatalysed and specific base catalysed hydrolysis of the protonated species and that the relative instability of cirazoline is due to the presence of an ether linkage in the 2-substituent.

The interactions between cirazoline and dodecylsulphate ions in aqueous solution were studied in terms of ion-pair formation, complexation, micellization and solubilization. Aqueous, crystalline complex, liquid complex (coacervate) and micellar (pseudo)phases were identified. An automated conductimetric titration technique is described for the determination of ion-pair association constants, solid and liquid complex apparant solubility products (K_S'), CMC values, concentration of SDDS required to totally solubilize cirazoline (SOL_T) and cirazoline-SDDS micelle association constants (K_A). The effect of temperature, ionic strength and initial cirazoline hydrochloride concentration on K_S', CMC, SOL_T and K_A values were evaluated. NMR, DSC and solubility techniques were also employed in evaluating the interactions.

Experiments to investigate the effect of SDDS on the specific base catalysed hydrolysis were performed in the absence of buffer salts at pH 7.0 and at temperatures of 30°C and 50°C using 0.2 and 2 x 10^{-3} M initial concentrations of cirazoline hydrochloride. Complexation and micellar stabilization mechanisms were identified and a model is proposed for the prediction of rate modifying effects due to both these mechanisms.

The physicochemical nature and solubility of a series of imidazoline dodecylsulphate and cirazoline alkylsulphate complexes have also been studied and the results discussed in the light of their chemical structures.

ORIGIN AND SCOPE

Interactions occuring between large organic ions of opposite electrical charge are of importance in many areas of pharmacy, e.g. chemical, microbiological and physical stability of formulations, compatibility, analysis, drug design and drug absorption and distribution[119].

Tomlinson et al[180] have suggested that surfactants can protect oppositely charged drugs from hydrolysis by ion-pair or complex formation and micellar stabilization of labile drugs is a well documented phenomenon[41].

Cirazoline is a potent α-adrenergic agonist[14] but is rapidly hydrolysed in aqueous solution[15]. Davies et al[15,16] have shown that cirazoline may be stabilized by the addition of SDDS although poor tolerance of SDDS solutions have prevented its commercial use. This present work was initiated in an attempt to characterise much more definitively the hydrolysis of cirazoline and to study the interactions between cirazoline and dodecylsulphate ions in a fundamental manner in order to quantify more precisely the stability enhancing effect of SDDS.

CONTENTS

1. INTRODUCTION

1.1 DRUG STABILITY AND REACTION KINETICS

Drugs may be formulated into solid, semi-solid or liquid dosage forms. As such they are subject to chemical degradation due to the presence of, or exposure to water, oxygen, light and ionising radiation. The rates of such degradation processes are subject to modification by factors such as pH, temperature and the presence of excipients including electrolytes, buffers, cosolvents, surfactants, polymers and antioxidants. Additionally trace impurities such as metal ions and peroxides present in the drug sample, excipients or solvents may influence drug stability. Examples illustrating the effect of formulation on drug stability are widespread throughout the scientific literature and have been the subject of comprehensive reviews and texts[1-5].

1.1.1 General Hydrolysis Reaction Kinetics

The detailed theoretical treatment of kinetics associated with chemical hydrolysis reactions is the subject of many texts[6-10]. Consequently this section is confined to the expressions which have been used to interpret the experimental kinetic data described in section 8 and discussed in section 9.

The law of mass action states that the rate of a reaction, at constant temperature, is proportional to the product of the molar concentration of each reactant raised to a power equal to the number of molecules of the substance undergoing the reaction. Hydrolysis reactions are generally bimolecular processes involving an attacking

species and the substrate (S):

aS + b (attacking species) --> reaction products

The rate equation may therefore be described by equation 1.1.

$$\text{Rate} = -\frac{d\,[S]}{dt} = k.\,[S]^{a}.\,[\text{attacking species}]^{b} \quad (1.1)$$

Where [] indicates concentration and k is the reaction rate constant. The order of reaction, n, is an empirical observation and is defined as the sum of the exponents of the concentration terms that occur in the observed rate expression, i.e. n = (a+b). If the concentration of attacking species is kept constant throughout the hydrolysis process, then equation 1.1 may be reduced to:

$$\text{Rate} = -\frac{d\,[S]}{dt} = k_{obs}.\,[S]^{n} \quad (1.2)$$

Where k_{obs} is the observed rate constant and is equivalent to the product of the true bimolecular rate constant, k, and the concentration of attacking species raised to the power b. Hence in a controlled system whereby the attacking species concentration is maintained constant, many hydrolysis reactions are observed to follow first order kinetics (i.e. n = 1). For simple unit orders the observed reaction rate constant, k_{obs}, is readily obtained from the integrated form of the rate equation 1.2:

for, zero order reactions n=0 and $[S_t] - [S_o] = -k.t$ (1.3)

first order reactions n=1 and $\log_e[S_t]/[S_o] = -k.t$ (1.4)

second order reactions n=2 and $1/[S_t]-1/[S_o] = k.t$ (1.5)

Where $[S_o]$ is the initial substrate concentration and $[S_t]$ is the substrate concentration at time t. An alternative method of

determining first order rate constants is the Guggenheim method. This technique involves determining the change in substrate concentration, $\Delta[S]$, over a fixed time interval, Δt, for different initial concentration of substrate (equation 1.6):

$$\log_{10} \Delta[S] = \frac{-k.t}{2.303} + C \qquad (1.6)$$

Where C is a constant and t is time. Fractional order reactions often show a good fit to unit order equations (e.g. equations 1.3 to 1.5). These orders can be determined by studying the reaction at various initial substrate concentrations.

1.1.2 Factors Affecting Hydrolysis Reaction Kinetics

(a) Effect of pH and Substrate Species

The hydronium (H_3O^+) and hydroxide (OH^-) ions are often very effective catalysts for hydrolysis reactions and pH therefore has a marked effect on the rate of such reactions. This phenomenon is known as specific acid-base catalysis. For a substrate, S, undergoing simultaneous uncatalysed and specific acid and base catalysed hydrolysis reactions under pH controlled conditions, the observed first order rate of reaction may be given by:

$$-\frac{d[S]}{dt} = k_{obs}[S] = k_w[S][H_2O] + k_1[S][H_3O^+] + k_2[S][OH^-] \qquad (1.7)$$

$$\text{thus, } k_{obs} = k_0 + k_1[H_3O^+] + k_2[OH^-] \qquad (1.8)$$

Where k_{obs}, k_w, k_1 and k_2 are the observed, uncatalysed, specific acid and specific base catalysed reaction rate constants respectively; $[H_2O]$, $[H_3O^+]$ and $[OH^-]$ are the concentrations of water, hydronium and hydroxide ions respectively and [S] is the substrate concentration. In

dilute aqueous solution, $[H_2O]$ is large and constant and the water term may be written as k_0 (= k_w $[H_2O]$).

Many drug molecules are capable of existing in different ionic forms e.g. imidazolines may exist as the neutral(S) or protonated (SH^+) species. The fraction of each species present is dependent upon the pK_a of the substrate and the pH of the solution which may be calculated from equation 1.9:

$$pH = pK_a + \log_{10}\frac{[S]}{[SH^+]} - \log_{10} \gamma_{SH^+} \qquad (1.9)$$

Where γ_{SH^+} is the activity coefficient of the protonated species. Each species will be susceptible to hydrolysis at different rates. Under these circumstances equation 1.8 must be modified to account for the fraction of protonated (f_{SH^+}) and neutral (f_S) species:

$$k_{obs} = (k_0 + k_1 [H_3O^+] + k_2 [OH^-])f_{SH^+} + (k_3 + k_4 [H_3O^+] + k_5 [OH^-])f_S \qquad (1.10)$$

Where k_0, k_1 and k_2 are the rate constants for the uncatalysed, specific acid and specific base catalysed reactions respectively for species SH^+; and k_3, k_4 and k_5 are the equivalent rate constants for species S.

(b) General Acid-Base Catalysis

General acid-base catalysis is the rate modifying effect of Lowry-Brönsted acids and bases. Buffer salts in reactant solutions are known to act as Lowry-Brönsted acids and/or bases and can therefore contribute to the observed hydrolysis reaction rate. Thus the observed rate constant for a protonated base (such as the imidazolinium ion),

SH^+, in a buffer salt solution containing both a Lowry-Brönsted acid and base is given by:

$$k_{obs} = (k_0 + k_1[H_3O^+] + k_2[OH^-] + k_6[HA] + k_7[A^-] + k_8[B] + k_9[BH^+]).f_{SH^+} \qquad (1.11)$$

Where k_6, k_7, k_8 and k_9 are the rate constants due to attack of unionized acid, HA, its conjugate base, A^-, unionized base, B, and its conjugate acid, BH^+, respectively.

(c) Effect of Ionic Strength (I)

The ionic strength of a solution will have a direct influence on the rate of a reaction by its effect on the thermodynamic activities of reacting species and transition complex. This is known as the primary salt effect. Ionic strength, I, is defined by:

$$I = \frac{1}{2}\sum_1^i M_i z_i^2 \qquad (1.12)$$

Where the summation relates to the number of different ionic species in solution, i; M is the molar concentration and z is the charge of each ionic species. The relationship between the rate constant and I is given by the Bronsted-Bjerrum equation:

$$\log_{10}k' = \log_{10} k + 2(-\log_{10}\gamma_{\pm}) \qquad (1.13)$$

$$\text{and } -\log_{10}\gamma_{\pm} = Az_Az_BI^{1/2} \qquad (1.14)$$

Where k' is the rate constant at ionic strength I and k is the rate constant for any specific process i.e. $k = k_1$ or $k_2 \ldots, k_i$; z_A and z_B are the charges on the interacting ions and A is the Debye-Hückel constant which may be calculated from the relative permittivity and

temperature of the solution:

$$A = \sqrt{\frac{2\pi N}{1000.\ 2.303\ K_B^{3/2}} \cdot e^3 \frac{1}{(\epsilon T)^{3/2}}} = \frac{1.8246 \times 10^6}{(\epsilon T)^{3/2}} \text{ mol}^{-1/2}\ l^{1/2}\ K^{3/2} \qquad (1.15)$$

Where N = Avogadro's number

e = Charge on electron

K_B = Boltzmann's constant

T = Absolute Temperature (K)

ϵ = Relative permittivity

Equation 1.14 is usually valid at ionic strengths < 0.01M. For solutions of higher concentration (I < 0.1M) a modified form of the equation is used:

$$-\log_{10} \gamma_{\pm} = A\ z_A z_B \frac{I^{1/2}}{1 + Ba_i\ I^{1/2}} \qquad (1.16)$$

Where B is a second Debye-Hückel constant, also dependent upon the relative permittivity of the solvent and temperature (equation 1.17):

$$B = \left(\frac{8\pi Ne^2}{1000\ K_B}\right)^{1/2} \cdot \frac{1}{(\epsilon T)^{1/2}} = \frac{50.29 \times 10^8 \text{ cm}^{-1}\text{mol}^{-1/2} l^{1/2} K^{-1/2}}{(\epsilon T)^{1/2}} \qquad (1.17)$$

and a_i is the mean diameter of the reacting ions. For most aqueous electrolytes at 25°C the product $B.a_i$ is approximately unity and equation 1.16 reduces to:

$$-\log_{10} \gamma_{\pm} = A\ z_A z_B \frac{I^{1/2}}{1 + I^{1/2}} \qquad (1.18)$$

At moderately high ionic strengths, (0.1 - 1.0M), equation 1.16 must be further modified to account for the observed increase in $\gamma_{\pm}$ with

increasing ionic strength (equation 1.19):

$$-\log_{10} \gamma_{\pm} = \frac{A\, z_A z_B I^{1/2}}{1 + Ba_i . I^{1/2}} - CI \qquad (1.19)$$

Where C is an empirical constant.

Values of A and B for aqueous systems at different temperatures may be obtained from Robinson and Stokes[11].

If one or both of the interacting species are uncharged the product $z_A z_B = 0$ and equation 1.13 predicts an absence of ionic strength effects. An effect may be observed at higher ionic concentrations, (>0.1M), however, where activity effects for neutral species may become significant. Under these circumstances the effect is best described by:

$$\log k' = \log k + bI \qquad (1.20)$$

Where b is an empirical constant.

A secondary salt effect also exists which is due to the influence of ionic strength on the ionization constant, K_a (see equation 1.9). For a weak base:

$$K_a = \frac{[S][H^+]}{[SH^+]} \cdot \frac{\gamma_S . \gamma_{H^+}}{\gamma_{SH^+}} \qquad (1.21)$$

Where γ_S, γ_{H^+} and γ_{SH^+} are the activity coefficients of S, H^+ and SH^+ respectively. Since ionic strength influences activity coefficients according to Debye-Hückel Law (equations 1.14, 1.16, 1.18 and 1.19), it also affects the relative concentrations of the unprotonated, [S], and protonated, [SH^+], species and thus directly influences the rate of reaction (equation 1.10). Salt effects of this nature are produced by

both foreign salts and ionizable substrates. With strong acids and bases the secondary salt effect is small since the species are almost completely dissociated under all conditions.

(d) Effect of Relative Permittivity (ε)

The reaction rate of ionic species is influenced by a change in the relative permittivity of the medium due to modification of electrostatic interactions between the ions. For an interaction between two ions, the effect of relative permittivity, ε, on the reaction rate, k_ε is given by:

$$\log_{10} k_\varepsilon = \log_{10} k_{\varepsilon=0} - \frac{z_A z_B e^2}{K_B T r \varepsilon} \qquad (1.22)$$

Where $k_{\varepsilon=0}$ is the rate constant at infinite relative permittivity and r is the radius of the complex obtained from the reactants A and B and = $r_A + r_B$

Hence an increase in ε will result in a decrease in the reaction rate of oppositely charged reactants and an increase in the reaction rate of similarly charged reactants.

(e) Effect of Temperature

The rate of most hydrolytic reactions increases two-to-threefold with each 10°C rise in temperature. Two similar expressions based on classical collision theory (the Arrhenius equation, equation 1.23) and transition state theory (equation 1.24) have been derived to explain the relationship between temperature and rate constant, k:

$$k = A.e^{-E_a/RT} \qquad (1.23)$$

$$k = \frac{RT}{Nh} .e^{\Delta S^\ddagger/R} .e^{-\Delta H^\ddagger/RT} \qquad (1.24)$$

Where A = Frequency factor

E_a = Activation energy

$\Delta S^{\ddagger}$ = Standard entropy of transition complex formation

$\Delta H^{\ddagger}$ = Standard enthalpy of transition complex formation

h = Planck's constant

R = Gas constant

Equations 1.23 and 1.24 are useful in that the rate constant at any temperature may be extrapolated from a series of measurements at convenient temperatures.

1.2 2-IMIDAZOLINES

Imidazolines are five membered nitrogen heterocyclic compounds possessing a cyclic amidine arrangement of two nitrogen atoms. 2-substituted-2-imidazolines are partially reduced 4,5-dihydro-imidazoles which are substituted in the 2-position. The structure of cirazoline and other medicinal imidazolines is shown in figure 1.1.

1.2.1 Medicinal Uses

The pharmacological action of the 2-substituted-2-imidazolines is dependent upon the substituent structure and may be classified into three main groups[12,13]:

(i) α-Adrenergic Antagonist

Tolazoline and phentolamine are α-adrenergic antagonists with direct dilator action on the peripheral blood vessels, especially the arterioles and capillaries and therefore increase peripheral blood flow. They are mainly used in the treatment of peripheral vascular disorders due to arterial spasm or occlusion, e.g. Raynauld's disease.

2-R-2-imidazoline

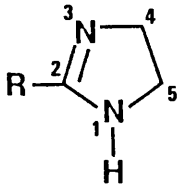

R=

2-methyl-2-imidazoline CH_3

Cirazoline

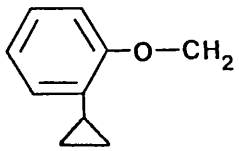

Fenoxazoline

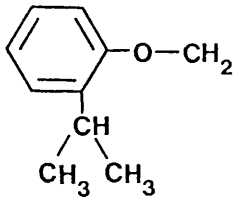

Tymazoline

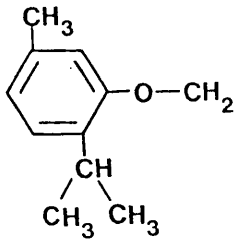

Antazoline

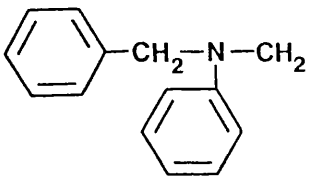

Phentolamine

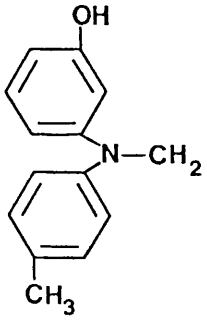

Figure 1.1 - Structure of 2-methyl-2-imidazoline and medicinal imidazolines (continued -->).

2-R-2-imidazoline

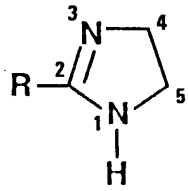

R=

Tolazoline

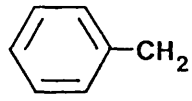

Naphazoline

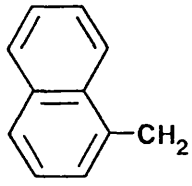

Tramazoline

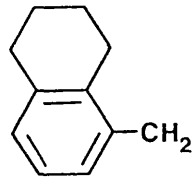

Xylometazoline

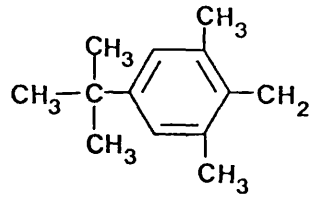

Oxymetazoline

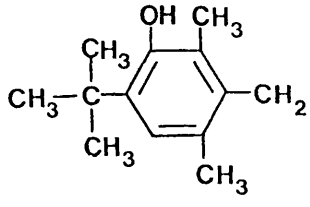

Cifenline

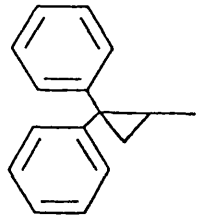

Figure 1.1 Continued - Structure of 2-methyl-2-imidazoline and medicinal imidazolines.

(ii) α-Adrenergic Agonists

Naphazoline, tramazoline, oxymetazoline, tymazoline, fenoxazoline and cirazoline are sympathomimetic agents with marked α-adrenergic activity. Naphazoline is a potent vasoconstrictor with rapid and prolonged action in reducing swelling and congestion when applied to mucous membranes. Cirazoline has been reported to have potent α-adrenergic agonist properties but its poor stability has prevented its widespread use[14-17]. This group of imidazolines is used in the form of nasal drops for the relief of nasal congestion and chronic and acute rhinitis.

(iii) H_1-antagonists

Antazoline is an H_1-antagonist and has the properties and uses of other non-imidazoline antihistamine agents such as promethazine. It is one of the least active and has a short duration of action. Local anaesthetic and anticholinergic properties have also been reported. Tymazoline has been reported to possess antihistamine properties but its α-adrenergic effects predominate.

In addition, Cifenline has recently been reported to have anti-arrhythmic properties[18].

1.2.2 Physiochemical Properties

Physiochemical properties of medicinal 2-substituted-2-imidazolines are summarised in table 1.1. These imidazolines are monoacidic bases and protonation occurs to give a resonance stabilized imidazolinium ion (figure 1.2)[23,24].

Imidazoline	Salt(s)	pK_a (25°C)	m.p. (°C)	UV Absorption Maxima (nm)	Exocyclic Methylene Acidity. Time for Total Exchange (hrs)
Cirazoline	HCl	9.44			>100
Fenoxazoline	HCl		174		-
Tymazoline	HCl	9.58	215-217		>100
Antazoline	HCl	10.23	240	242,292	84
Phentolamine	Mesylate	9.29	240	278	24
Tramazoline	HCl		172-174	267,275	-
Tolazoline	HCl	10.59	174	257,263	24
Naphazoline	HCl	10.48	168	271,281,288,291	84
Xylometazoline	HCl	10.85	>300	265	100
Oxymetazoline	HCl	10.54	300	280	100
2-methyl-2-imidazoline	-	11.09	105	218	No Exchange

Table 1.1 - Physicochemical characteristics of 2-methyl-2-imidazoline and medicinal imidazolines[13,19-22].

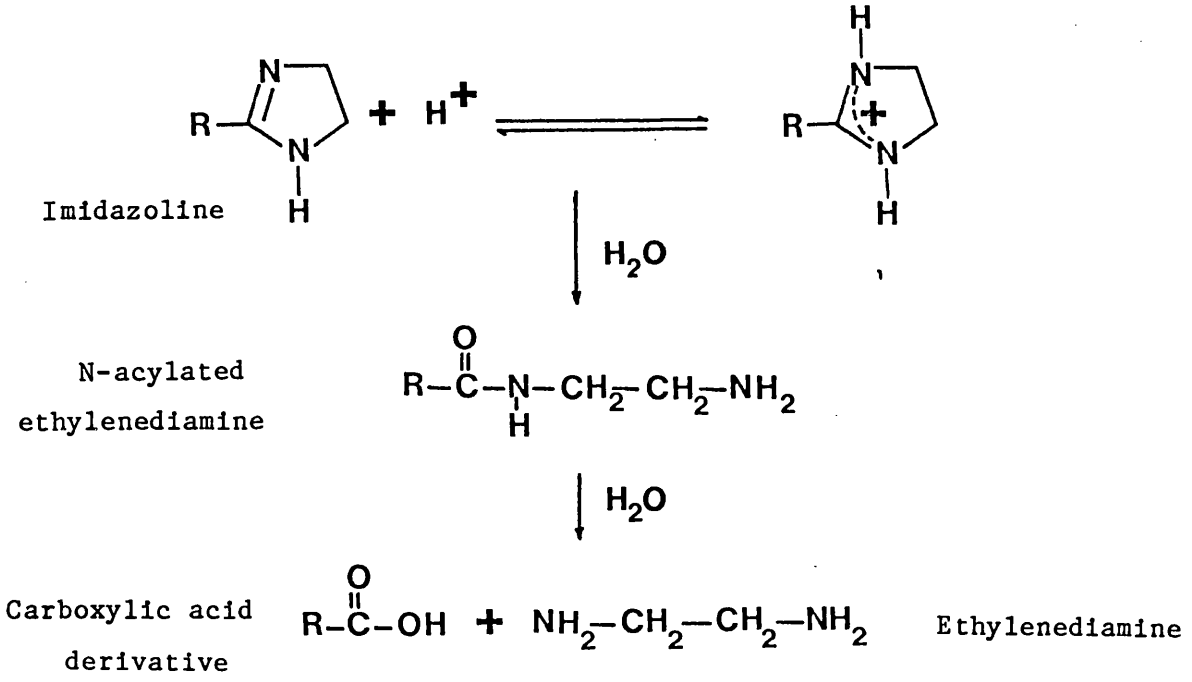

Figure 1.2 - General scheme for the protonation and hydrolysis of the 2-imidazoline ring showing hydrolysis of its primary degradation product.

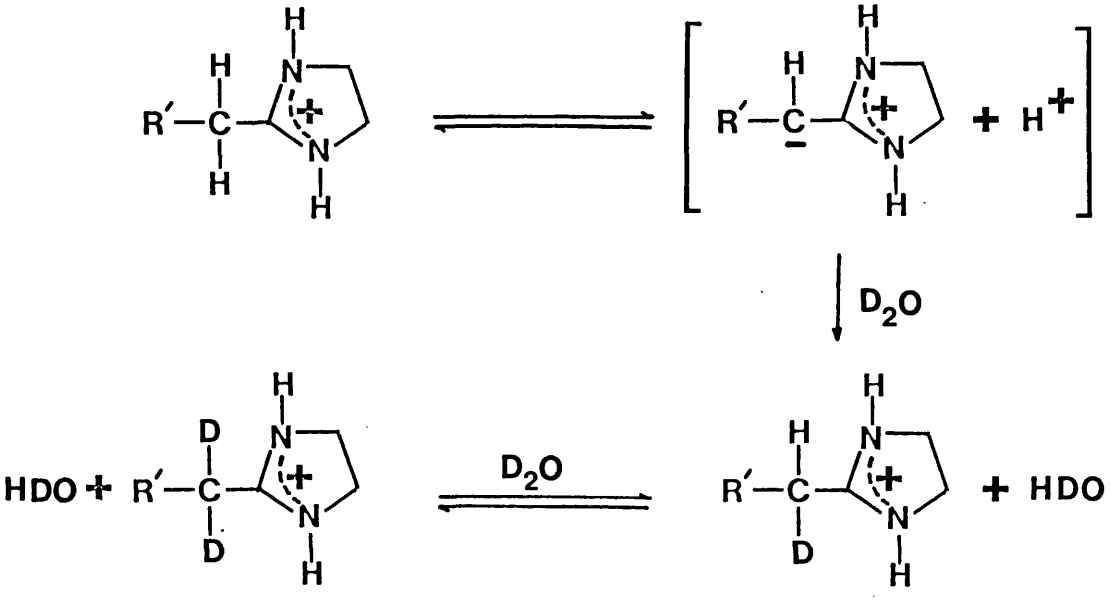

Figure 1.3 - Acidity of the imidazoline exocyclic methylene protons demonstrated by exchange with deuterium from deuterium oxide (D_2O).

The increase in acidity of the conjugate acid from 2-methyl-2-imidazoline (pK_a = 11.09)[19] to phentolamine (pK_a = 9.29)[21] follows the increase of electron withdrawing ability of the 2-substituent.

Kounterellis has obtained evidence for the acidity of the exocyclic methylene protons in nine 2-substituted-2-imidazolines[20]. Samples were analysed using proton magnetic resonance (PMR) and carbon magnetic resonance (CMR) spectroscopy using DMSO and D_2O as solvent. The relative acidity of the groups was assessed by determining the time required for complete exchange of the exocyclic methylene protons with the deuterium from D_2O, (figure 1.3). Acidity of the exocyclic methylene group was found to be dependent upon 2-substituent structure; table 1.1 shows the times given for complete exchange of the protonated species.

The differences in imidazoline acidity were explained by the relative electron withdrawing nature of the substituent and the presence of bulky ortho groups on the aromatic ring (figure 1.1) which restrict exchange due to steric hinderance. 2-methyl-2-imidazoline has an electron donating (methyl) group and consequently does not exchange. The acidity enhancement by electron withdrawing substituents results from stabilization of the intermediate carbanion through charge delocalization. The relatively low acidity of the exocyclic methylene groups in cirazoline and tymazoline was explained by the presence of bulky ortho groups. However, steric hinderance does not fully explain the weak acidity of cirazoline and tymazoline since xylometazoline has two methyl substituents which are closer to the exocyclic methylene group than the substituents in cirazoline and tymazoline and yet xylometazoline exchanges completely in 100 hours (table 1.1).

Comparison of exchange rates obtained by Kounterellis[20] is complicated by the use of different solvent systems; the ratio of imidazoline, DMSO and D_2O was varied to enable resolution of PMR peaks. Bimolecular reactions usually follow first or second order kinetics and reaction rates are therefore dependent upon the concentration of reactants (i.e. imidazoline, D_2O and OD^-). Changes in imidazoline and D_2O concentrations will therefore affect the exocyclic exchange rate. In addition, the pH (or pD) of the system was not controlled and the concentration of OH^- (OD^-) would therefore also have been different for each system, (imidazolines have pK_a values in the range 9.3-11.1 at 25°C, see table 1.1).

1.2.3 Stability of 2-Imidazolines

A highly characteristic property of the 2-substituted-2-imidazolines is their tendency to undergo hydrolysis with the formation of N-acylated ethylenediamines on treatment with acids and bases (figure 1.2)[23,24]. Further hydrolysis of these amide derivatives leads to formation of ethylene diamine and the carboxylic acid derivative. The rate of imidazoline hydrolysis is dependent upon substituent structure and species type (protonated or unprotonated). 2-aryl-2-imidazolines are generally more resistant to hydrolysis than 2-alkyl-2-imidazolines and early work indicated the protonated form to be more stable than the corresponding free base[23]. Hoffmann associated this with the highly symmetrical 2-imidazolinium ion structure relative to that of the uncharged molecule[23] (figure 1.2).

The effects of 2-alkyl substituents on the rate of hydrolysis of 1-hydroxyethyl-2-imidazoline in 95% ethanol, containing 3.75×10^{-2} M NaOH has been studied by Harnsberger and Riebsomer[25]. Half-life (minutes) for each substituent at 48.9°C, given in the rank order of

decreasing electron donating ability, was determined as: $-C(CH_3)_3$ = 612, $-CH(CH_3)_2$ = 187, $-C_{17}H_{35}$ = 115, $-C_5H_{11}$ = 118, $-C_2H_5$ = 80, $-CH_3$ = 150 and -H = 14. The ability of the 2-substituent to stabilize 2-imidazolines therefore follows the order of electron donating ability with the exception of the methyl substituent. The authors proposed that the reaction is due to specific base catalysis of the unprotonated species through hydrolytic attack on the $\delta+$ 2-carbon. 2-substituents with the ability to reduce the small positive charge through electron donation should therefore reduce the probability of attack by hydroxide ions. No explanation for the anomolous stability of the 2-methyl imidazoline was given however.

In a further study[26], the effect of pH on the hydrolysis of 1-hydroxyethyl-2-pentyl-2-imidazoline was reported. The rate of reaction in buffered one molar sodium perchlorate increased proportionally with pH up to pH 11.5 and then tailed off becoming independent of pH above pH 12.5. Harnsberger and Riebsomer explained the variation in rate of hydrolysis with pH by the formation of a complex between the imidazoline base and hydroxide ion. The initial reaction is fast and reversible while the reaction of the complex with water to form the observed hydrolysis products is rate controlling and irreversible. This mechanism has recently been supported in a study by Fernandez and Lamden[27] on the hydrolysis of 1-aryl-2-phenyl-2-imidazoline in boiling (80.7°C) 95% ethanolic solutions of potassium hydroxide.

This view that the imidazolinium ion is stable relative to the free base was contradicted by Martin and Parcell[28] who investigated the hydrolysis of 2-substituted 2-thiazolines and 2-methyl-2-imidazoline.

Hydrolysis was studied across the ionization region of 2-methyl-2-

imidazoline and a value of 2.6 ($\pm$0.1) min^{-1} M^{-1} was obtained for the specific base catalysed hydrolysis rate constant for the protonated species (k_2) at 25°C. These authors claimed that 'statements in the literature to the effect that the cationic form of imidazolines is more stable than the free base are kinetically incorrect'. A very low rate constant for the specific acid catalysed hydrolysis of the protonated species was predicted ($k_1 = 2.6 \times 10^{-7}$ min^{-1} M^{-1}).

The base catalysed hydrolysis of 2-nonyl-2-imidazoline has been studied by Savignac et al[29]. The effect of pH in the alkaline region on the degradation at 50°C was investigated using carbonate buffer (pH 9.7 - 10.4) and sodium hydroxide solution (pH 10.3 - 13.0). At pH 9.7 the observed rate constant was 2.5×10^{-5} s^{-1} which rose to 34.6×10^{-5} s^{-1} at pH 11.6, but became independent of pH above this value.

At high pH there is a very small proportion of the substrate present as the protonated species and the authors offer two possible explanations for the plateau in the stability-pH profile:

(i) due to attack of water on the neutral form of the substrate;
(ii) reaction of hydroxyl ion on the protonated species.

The second explanation was preferred and a correlation between the fraction of protonated substrate and k_{obs} was attempted. Difficulty in determining the pK_a of nonyl-2-imidazoline due to poor substrate solubility and stability and electrode response problems prevented production of definitive evidence for the theory. The conclusions reached in this work also contradict the mechanism suggested by Harnsberger and Riebsomer [25,26].

Savignac et al[29] point out that these reactions should be accompanied by a positive or zero entropy change which contradicts their

experimental value of -20 cal mol^{-1} K^{-1} for nonyl-2-imidazoline. Such a mechanism also supposes the accumulation of intermediate which was not indicated by their experimental data.

Reported data on the stability of medicinal 2-substituted imidazolines is limited. Stern et al[30] evaluated the hydrolysis of naphazoline and derived an equation relating the observed rate constant for the first order hydrolysis reaction (k_{obs}) to the specific base catalysed rate constants for the salt (k_2) and base (k_5) species and dissociation constant, K_a (equation 1.25):

$$\log k_{obs} = -pOH + \log\left(\frac{k_2\,[H_3O^+] + k_5.K_a}{K_a + [H_3O^+]}\right) \quad (1.25)$$

The effect of pH was investigated in the region pOH 0-8 at 25°C using various buffer systems to maintain pH. Experimental data in the range pOH = 4-7 showed a linear relationship between log k_{obs} and pOH with a slope of -1.00 indicating exclusive specific base catalysis of the protonated species in this pOH region (figure 1.4). A k_2 value of 182 $hours^{-1}$ M^{-1} at 25°C was obtained from the intercept. A plateau in the pOH-stability profile was observed in the pOH region 0.5-3 and the observed rate constant became independent of pOH. The nature of the profile indicated that hydolysis of free base does not contribute significantly to the overall rate constant under the experimental conditions, i.e. $k_2 >>> k_5$, although the authors calculated a value of k_5 = 0.187 $hours^{-1}$ M^{-1} at pH 13 using equation 1.24. Their treatment is suspect, however, since deviation between the experimental and theoretical stability-pOH profile (calculated using equation 1.25 and derived k_2 and k_5 values) occurs (figure 1.4). An activation energy of 16.4 kCal mol^{-1} and frequency factor of 1.91 x 10^{14} $hours^{-1}$ was determined from the variation of k_2 with temperature. Similar

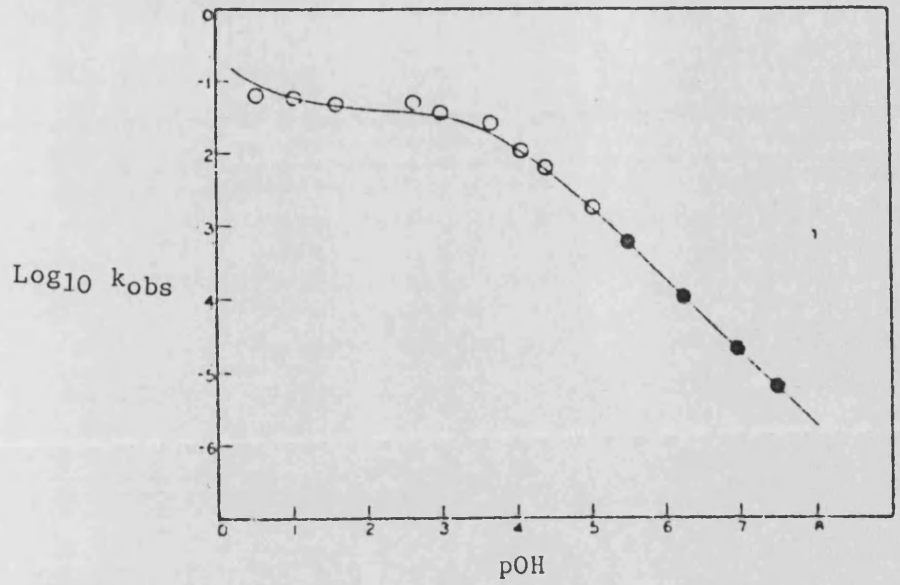

Figure 1.4 - Plot of $\log_{10} k_{obs}$ versus pOH for the hydrolysis of naphazoline at 25°C. Curves were calculated using equation 1.25 (from Stern et al[30]).

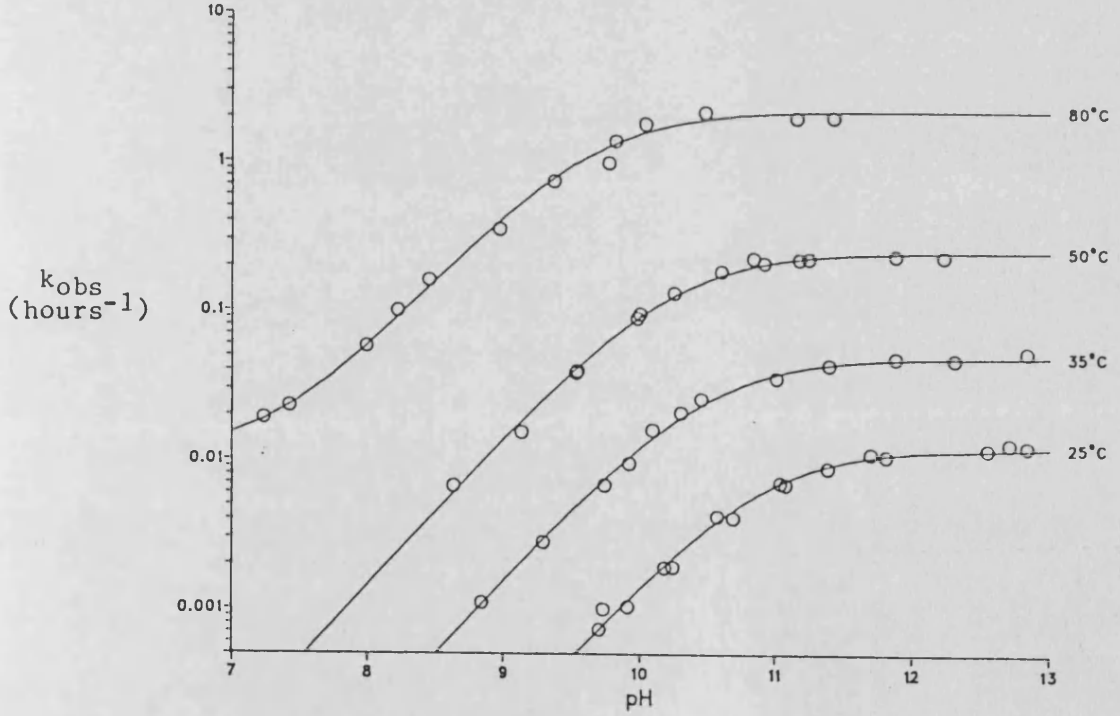

Figure 1.5 - Plots of k_{obs} ($\log_{10}$ scale) versus pH for the hydrolysis of cifenline at the temperatures indicated. Curves were calculated using equation 1.26 (from Ross et al[18]).

observations were obtained by Yamana et al[31] for the hydrolysis of oxymetazoline at 65° and 90°C, pOH 0.5-6.

The kinetics of hydrolysis of tymazoline[32], xylometazoline[33] and tolazoline[34] in the pH range 0.1-7.1 has been studied at various temperatures by Grabowska and co-workers. Results show the stability of these 2-imidazolines to be heavily dependent upon the nature of the 2-substituent. In phosphate buffer, pH 7.1 (25°C) and 70°C k_{obs} for xylometazoline, tolazoline and tymazoline were calculated as 4.48, 59.7 and 335 x 10^{-3} $hours^{-1}$ respectively. The reaction rate was pH dependent and the log k_{obs} - pH profile for xylometazoline and tolazoline showed evidence of specific acid catalysis which was absent in the tymazoline profile. A rapid rise in rate constants above pH about 3.5 occurred for all imidazolines indicating specific base catalysed hydrolysis.

Ross et al[18] have recently studied the hydrolysis of cifenline at pH 7.2 - 12.8, 25 - 80°C. First order rate constants at constant ionic strength (1.0 M KCl) were determined from data plotted according to the first order rate equation (equation 1.4) or by the Guggenheim method (equation 1.6). The $\log_{10} k_{obs}$-pH profile is shown in figure 1.5; lines were drawn using equation 1.26.

$$k_{obs} = \frac{k_0 + k_2 [OH^-]}{K_a [OH^-]/K_w + 1} \qquad (1.26)$$

Where K_w is the ionization constant for water.

The data are consistant with a mechanism involving reaction of the protonated species with water (at low pH and high temperature only) and hydroxide ion (equation 1.26). The authors were unable to fit these data to the mechanism proposed by Harnsberger and Riebsomer[25,26] and

concluded that the data support the simple ionization mechanism proposed by Martin and Parcell[28].

The hydrolysis of cirazoline hydrochloride has also been studied by Davies et al[15], Stroud et al[16] and Fedynec et al[17]. Davies et al determined the effect of pH on the observed first order rate constants in MacIlvaine's citrate-phosphate buffer (ionic strength 0.5 M) at 80°C[15]. The log k_{obs} -pH profile in the acid region (pH 2.9 - 7.0) showed potent specific base catalysis and the absence of specific acid catalysis. The slope of the profile in the region pH 5.0 - 7.0 was determined as 0.84 and the authors suggested a buffer catalysis effect. An activation energy and frequency factor of 99.3 $kJmol^{-1}$ and 4.86 x 10^9 s^{-1} were calculated at pH 4.6. At pH 7.0, 80°C the first order rate constant was 6.72 x 10^{-4} s^{-1}. Grabowska et al[33,34] found first order rate constants under approximately the same conditions (pH 7.1, 80°C) as: tolazoline = 4.45 x 10^{-5} s^{-1}, and xylometazoline = 3.89 x $10^{-6}s^{-1}$, thus highlighting the relatively poor stability of cirazoline. Davies et al postulated that the instability of cirazoline is due to the presence of the ether linkage which donates electrons to the benzene ring and makes the imidazoline ring more susceptable to hydrolytic attack[15].

1.3 SURFACE ACTIVE AGENTS

A surface active agent, is a compound which adsorbs strongly at an interface, for example between air-liquid, liquid-liquid and solid-liquid phases, and has the ability to lower the interfacial (surface) energy. Surface active materials include polymers such as proteins and smaller molecules such as soaps and detergents. The latter are known as association colloids due to their ability to aggregate in solution, forming particles of colloidal dimensions. The term "surfactant" is

often taken to mean this type of surface active agent which are characterised by the possession of both polar (hydrophilic) and non-polar (hydrophobic) regions on the same molecule.

The hydrophobic portion of the molecule is most commonly a flexible hydrocarbon chain although many compounds contain aromatic hydrophobic groups. Typically 8-20 carbon atoms are contained within this moiety. The hydrophilic portion may be ionized or consist of a non-ionic polar moiety and it is this feature which provides the most commonly used classification of surfactant structure; i.e. anionic, cationic, zwitterionic and non-ionic surfactants. This dual nature is responsible for the amphipathic nature of surfactants and it is the balance between the hydrophobic and hydrophilic parts of the molecule (ion) which gives the special properties associated with surface active agents.

In aqueous solution the hydrocarbon portion interacts only weakly with the water molecule and the strong self interaction between the water molecules arising from dispersion forces and hydrogen bonding act cooperately to "squeeze" the hydrocarbon out of the water. This phenomenon is termed the hydrophobic effect. However, the polar or ionic portion of the molecule, usually termed the head group, interacts strongly with the water via dipole-dipole or ion-dipole interactions and is solvated. An amphiphile will therefore, tend to accumulate at an interface in such an orientation that its hydrophilic head group is anchored in the aqueous phase with its hydrophobic portion in minimal contact with the water. These forces are also responsible for aggregation or micelle formation in surfactant systems; figure 1.6 illustrates some of the structures which may form in solutions of amphiphile molecules in water[35].

1.3.1 Micellization

Micelles may be defined as 'aggregates of colloidal dimensions existing in equilibrium with the molecules or ions from which they are formed'. Micelles may be small aggregates of nearly spherical shape but at higher concentration larger micelles which may be lamellar or rod-shaped may form. Such micellar aggregates together with the monomers from which they are formed constitute a single isotropic solution phase. Distinct liquid crystalline phases may exist and separation of surfactant-rich phases (coacervation) and solid crystals may occur (figure 1.6).

Micellization can be envisaged as the stepwise aggregation of monomers, S, using a multiple equilibrium model[36-39]:

$$S_1 + S_1 \overset{K_2}{\rightleftharpoons} S_2$$

$$S_1 + S_2 \overset{K_3}{\rightleftharpoons} S_3$$

$$S_1 + S_3 \overset{K_4}{\rightleftharpoons} S_4$$

$$S_1 + S_{N-1} \overset{K_M}{\rightleftharpoons} S_N$$

Where K_M is the micelle equilibrium constant and N is the aggregation number. In theory the multiple equilibrium model could result in a wide range of micellar sizes from dimers (S_2) to extremely large micelles (S_N). However, for typical surfactants the size distribution curve is bimodal, the peaks of which represent monomers (and possibly dimers and trimers) and monodisperse spherical micellar aggregates. This self association pattern may be rationalized in terms of the factors which promote and inhibit micellar growth. The impetus in micelle formation or cooperativity derives mainly from the entropic changes accompanying the transfer of hydrocarbon from an aqueous

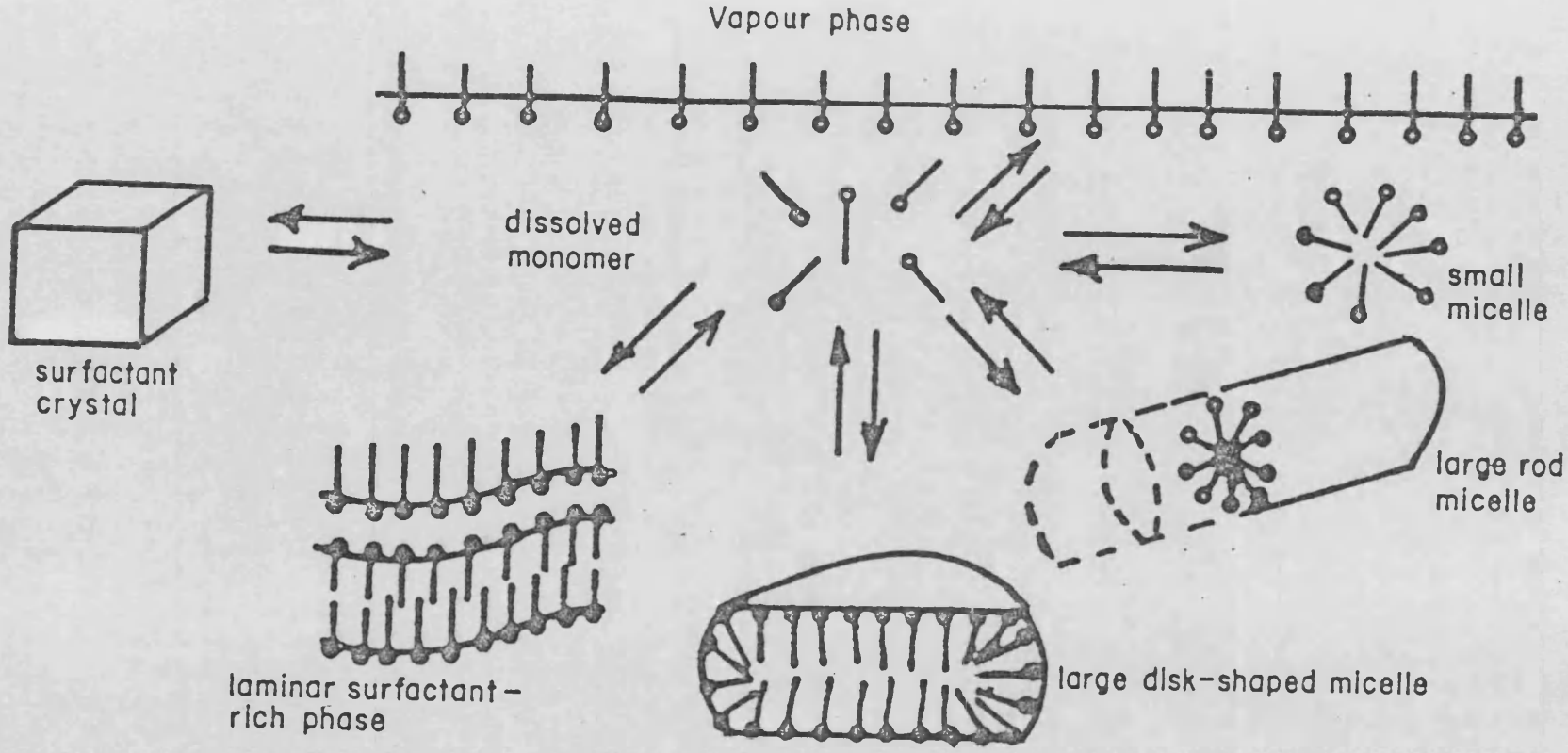

Figure 1.6 - Possible states of an amphiphile in water, (from Couper[35]).

environment to the micelle interior. The efficiency of shielding the hydrophobic group from the water increases with increase in aggregate size. Factors which limit micelle size (anti-cooperativity) for ionic surfactants arise from the progressive increase in charge repulsion between the headgroups at the micellar surface as the micellar size increases.

Two main approaches to the thermodynamic analysis of micellization have been widely used, viz the phase separation and mass action models. In the phase separation model the micelles (and counterions for ionic micelles) are considered to form a separate phase at the critical micelle concentration, CMC, whereas the basic mass action model assumes surfactant monomers, (counterions), and micelles are in association-dissociation equilibrium. When the aggregation number is large and concentrations close to the CMC are considered, both treatments result in equation 1.27 for the free energy change of micellization of one mole of surfactant (ΔG^{o}_{M}):

$$\Delta G^{o}_{M} = RT \log_e x_{CMC} + RT (1 - \alpha) \log_e x_Z \qquad (1.27)$$

Where x_{CMC} and x_Z are the mole fractions of monomer and counterion respectively, R is the gas constant, T is the absolute temperature and α is the degree of counterion dissociation.

In the absence of added electrolyte, equation 1.27 reduces to equation 1.28.

$$\Delta G^{o}_{M} = (2 - \alpha) RT \log_e x_{CMC} \qquad (1.28)$$

or expressed in molal concentration terms,

$$\Delta G^{o}_{M} = (2 - \alpha) RT \log_e CMC - (2 - \alpha) RT \log_e 55.5 \qquad (1.29)$$

The mass action approach is generally thought to be a more realistic treatment than the phase separation model. Assumptions and limitations to both methods have been discussed by Franks[40] and Attwood and Florence[41]. Thermodynamic models based on a modified mass action model[42], a multiple equilibrium model[43,44] and the Poisson-Boltzmann equation[45,46] have recently been proposed.

The large negative free energy of micellization results from a small, usually positive, enthalpy change, ΔH^{o}_{M}, and a large positive entropy change, ΔS^{o}_{M}. In general values of ΔH^{o}_{M} decrease with increasing temperature and may become negative at high temperatures. ΔH^{o}_{M} has been measured directly by calorimetry although more usually, it is estimated from the temperature dependence of the CMC, eg. in the absence of added electrolyte:

$$\Delta H^{o}_{M} = R\ (2 - \alpha)\left(\frac{d\ \log_e x_{CMC}}{d\ (1/T)}\right)_p \qquad (1.30)$$

The standard entropy of micellization is then obtained from equation 1.31.

$$\Delta G^{o}_{M} = \Delta H^{o}_{M} - T\,\Delta S^{o}_{M} \qquad (1.31)$$

Franks[40] has summarised changes in thermodynamic quantities for micellization of many surfactants under a variety of experimental conditions. Values for SDDS at 25°C have been reported as ΔH^{o}_{M} = -1.3 to + 2.2 kJ mol^{-1}; ΔS^{o}_{M} = 68.6 to 79.9 J mol K^{-1}, giving values of ΔG^{o}_{M} = -22 k J mol^{-1}.

Micellar aggregation is a highly dynamic and reversible process. Fast kinetic investigations of micellar solutions show two relaxation times with widely different time scales[47,48]. The slow process has been attributed to the micellization - dissolution equilibrium; use of

temperature jump, pressure jump and stopped flow techniques enabled an estimate of the micelle life-time in the region of 40 - 70 x 10^{-3} seconds to be obtained[48]. The fast process which has been detected using ultrasonic absorption, NMR and ESR techniques has a relaxation time of about 6 x 10^{-6} seconds[48] and has been identified with the exchange of monomers between the micellar species and the bulk solution. Experimental studies into the kinetics of micellization have been reviewed by Muller[49] and the topic has recently been discussed by Aniansson[50].

Evidence for the existence of micelles is based on the fact that physical properties of surfactant solutions exhibit an abrupt discontinuity which takes place over a narrow concentration range - the critical micelle concentration (CMC). The literature from 1926 up to 1966 has been critically surveyed by Mukerjee and Mysels who have published a collection of CMC values for over 700 compounds based on 333 references and shows some 70 methods have been used for CMC determinations[51]. Examples of physical properties used in the determination of CMC values include osmotic pressure, turbidity, solubilization, magnetic resonance, surface tension, conductivity and self diffusion; methods which have been employed more recently include positron anhilation techniques[52], electron paramagnetic resonance[53], and keto-enol tautomerism[54]. The sharpness of the inflexion point at the CMC depends upon the aggregation number, N, micellar equilibrium constant, K_M, and degree of dissociation α. Low N and K_M values result in a gradual change in physical property at the CMC.

Micellar aggregation has been the topic of much recent work and many reviews and proceedings of international symposia have appeared in the

literature (e.g. Surfactant Systems[41]; Micellization, Solubilization and Microemulsions[55], Solution Chemistry of Surfactants[56]; Solution Behaviour of Surfactants[57]; Surfactants in Solution[58]; Anionic Surfactants[210,211]; and Surfactants[59]). In this thesis anionic surfactants, and in particular SDDS, will be considered in detail but, where applicable, reference to other types of surfactant systems will be made.

1.3.1.1 STRUCTURE OF IONIC MICELLES

Pioneering work by McBain and Salmon[60] in 1920 suggested the formation of two types of micelle, spherical ionic micelles and lamellar neutral micelles. G.S. Hartley[61] later proposed that the association unit for ionic surfactants was spherical with a radius approximately equal to the length of a hydrocarbon chain. Many of the counterions were bound to the charged headgroups composing the micelle surface and the interior of the micelle had the properties of liquid hydrocarbon. The internal structure of micelles particularly the extent of water penetration and the conformation of alkylchains within the micelle core is the subject of considerable controversy. Currently five models are proposed:

(i) Hartley's 'Oil' Droplet Model[61]
(ii) Menger's 'Pincushion' Model[62]
(iii) Fromherz's 'Surfactant-block' Model[63]
(iv) Dill and Florey's 'Interphase (Lattice)' Model[64,65]
(v) Gruen's 'Standard Picture' Model[66,67]

The Hartley and Gruen models predict a smooth micelle surface, little water penetration into the core and minimal hydrocarbon-water contact at the micelle surface. Conversely a rough micellar surface with

extensive hydrocarbon-water contact is proposed by the Menger, Fromherz and Dill and Florey models. The Menger 'pincushion' model also predicts extensive penetration of water into the hydrocarbon core.

Much of the recent literature has re-supported the classical Hartley micelle concept as illustrated by the Gruen 'Standard Picture' model[66] (figure 1.7). The Gruen model predicts symmetrical aggregates in which, on average, each amphiphile has almost all of its hydrocarbon chain in the micelle core; the ionic headgroups, ions and water are almost totally excluded from the core; the chains are conformationally disordered (liquid like) and fill the core at approximately liquid n-alkane density throughout; the spatial freedom of movement is smallest for groups near the headgroup and increases along the chain; the chain may also, to a limited extent, exist outside the core and small voids may exist in the core as a consequence.

The layer surrounding the core is termed the Stern layer which contains, in addition to the hydrated polar head groups, a number of counterions given by $(1 - \alpha)N$. The Stern layer constitutes the inner part of the electrical double layer surrounding the micelle. The outer, more diffuse Gouy Chapman layer, contains the remaining αN counterions. The thin section of the diffuse layer up to the shear plane in addition to the core and the Stern layer are considered to form the kinetic micelle, which will migrate under an applied EMF.

In contrast to the micellar core, there is little doubt that the Stern layer of ionic micelles is heavily hydrated. Studies into pH-independent hydrolysis reactions and the extent of hydration of counterions suggest that the activity of water at the surface of

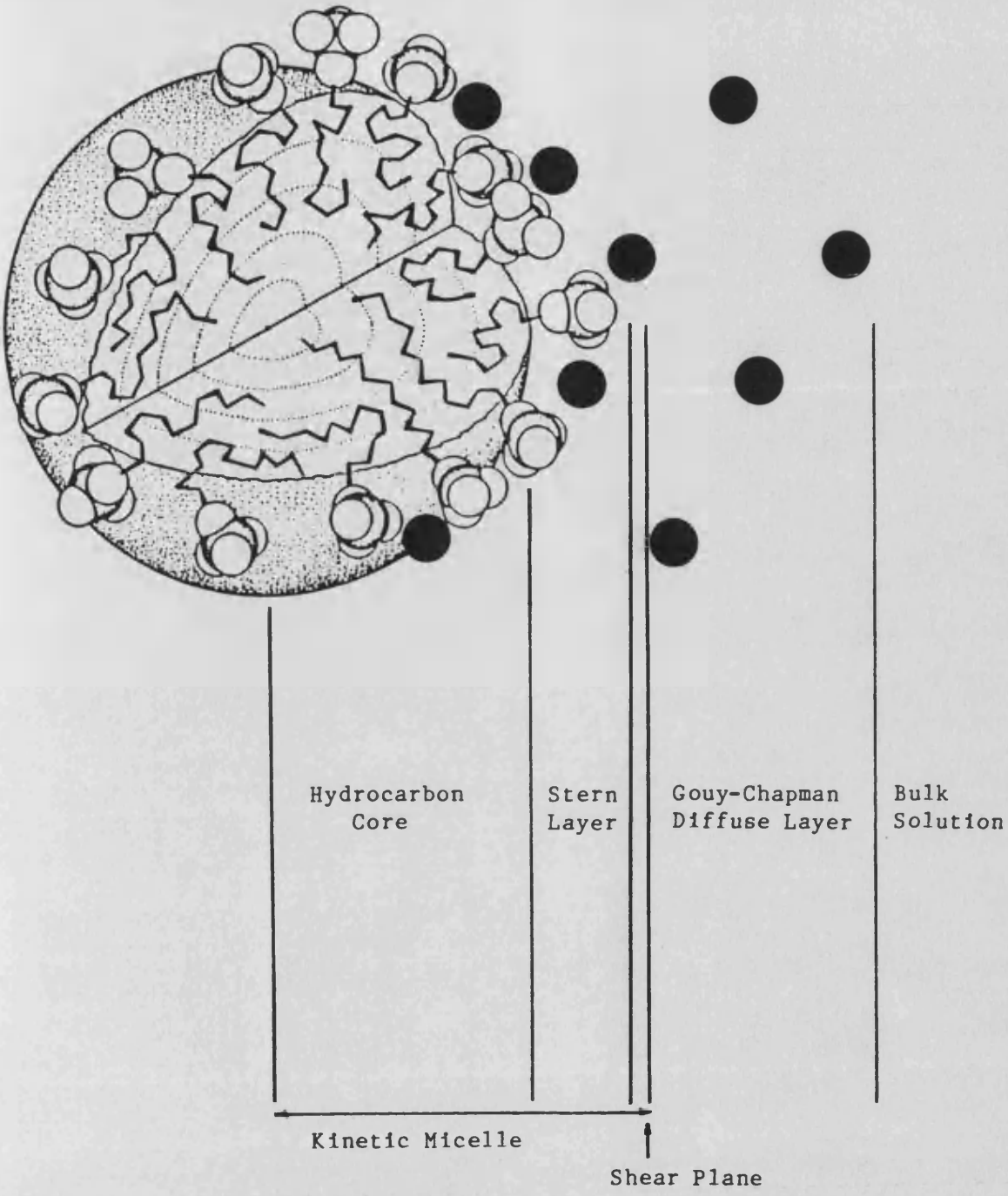

Figure 1.7 - Idealised structure of a SDDS micelle according to the Gruen 'Standard Picture Model'[66]. Hydrocarbon core, Stern layer, shear plane, and Gouy-Chapman diffuse layer are shown, (● = Na^+ counterions).

micelles is little different to bulk water[118]. There is general agreement that the relative permittivity, ϵ, of the Stern layer is intermediate between the value of 79 for water and two for hydrocarbons[41]. Mukerjee and Ray[117] found the effective ϵ was 36 near the headgroups of dodecylpyridimium iodide micelles and Beunen and Ruckenstein[70] predict a value of 65 - 70 at the outer compact layer and less than 7 at the inner layer of SDDS micelles. The low value of ϵ may be attributed to the large ionic concentration in the Stern layer and inner part of the diffuse layer. Cordes calculated that the concentration of charged groups at the micellar surface is about 3 - 5 M; 80% of these charges being neutralized directly through the incorporation of counterions[118].

The outer region of the ionic micelle is the Gouy-Chapman diffuse layer which contains the excess counterions necessary to neutralize the charge of the kinetic micelle. The distribution of ions in this layer follows the Boltzmann Law (equation 1.32).

$$n_{\pm} = n_o \exp^{\mp ze\psi/K_BT} \qquad (1.32)$$

Where $n_{\pm}$ are the concentration of anions and cation of valency $z_{\pm}$ at the part of the diffuse layer where the potential is ψ and n_o is the relevant concentration in the bulk, e is the electron charge, K_B is the Boltzmann constant and T in the absolute temperature.

The binding of counterions to a micelle may be viewed in chemical terms as a mass action type of ion-pairing or as a distribution in a Gouy-Chapman type of double layer. The mass action approach may be represented for an anionic micelle by equation 1.33.

$$NS^- + pZ^+ \overset{K_M}{\rightleftharpoons} [S_NZ_p]^{(N-p)-} \qquad (1.33)$$

Where S^-, Z^+ and $[S_NZ_p]$ correspond to the concentrations of the monomer, counterion and micelle respectively; N is the micelle aggregation number and K_M is the equilibrium constant for the association. The quantity (N-p) is the residual charge on the micelle and the degree of counterion dissociation, α, is given by equation 1.34, where β is the degree of counterion binding:

$$\alpha = 1 - \beta = \frac{(N - p)}{N} \qquad (1.34)$$

Instead of characterising counterion binding by a chemical equilibrium description involving specific complex formation (mass action model), Gouy-Chapman theory considers a continuous non-specific counterion distribution. The difficulty in unamibiguously dividing counterions into bound and free ions hence accounts for the different results obtained for β by different experimental techniques. Lindman and Wennerstrom[38] recognise the continuous counterion distribution principle but point out the usefulness of the degree of counterion association. The same authors list some general features of counterion binding for simple hydrophilic counterions as:

(i) β usually lies in the range 0.5 to 0.8,

(ii) different experimental approaches give the same general picture of counterion binding,

(iii) ion specificity is small among monovalent ions but may be important for size and shape and for phase equilibria,

(iv) ion competition effects may be marked (e.g. divalent ions replace monovalent ions),

(v) β is approximately independent of surfactant concentration, temperature and alkyl chain length,

(vi) β increases slightly with aggregate shape from spheres over rods to lamellae,

(vii) β is only slightly affected by added electrolyte.

However, the mass action model predicts a change in β with temperature, added electrolyte and dilution of the system and Lindman[48] cites these observations as failings of this approach. Gunnarsson et al[69], Jonsson and Wennerstrom[45], Beunen and Ruckenstein[70], and Frahm and Diekmann[71] have recently proposed models for counterion binding based on the Poisson-Boltzmann equation.

Franks[40] and Anacker[68] have summarised values of β for various surfactants determined using different experimental conditions and techniques; values for SDDS solutions at 25°C have been reported as between β = 0.62 and 0.86. Recent literature reports give β values for SDDS as 0.66 [72] and 0.74 [73] (EMF measurements) and 0.51 [74] (metal complex formation).

1.3.1.2 THE SIZE AND SHAPE OF MICELLES

A variety of evidence in support of an idealized spherical shape in the vicinity of the CMC has been reported for cationic, anionic and non-ionic sufactants[40]. However, several authors have shown from geometrical consideration that most of the common surfactants with a single hydrocarbon chain cannot form truely spherical micelles[41,75]. As the micellar radius is always limited by the maximum possible extension of the hydrocarbon chain, it is possible to establish the

greatest possible aggregation number, N_{max}, for spherical micelles of a given chain length. Schott calculated N_{max} as 39.2, 54.3, 72.0 and 92.2 for C_{10}, C_{12}, C_{14} and C_{16} surfactants, respectively[75]. These values are slightly lower than experimentally determined aggregation numbers of 41, 64, 80 and 100 respectively for sodium alkyl sulphates at 25°C[76], indicating some lack of micellar sphericity.

Tanford has proposed the formation of oblate and prolate ellipsoids to account for larger aggregation numbers, and from theoretical considerations, indicates that, except when head group repulsion is very strong, oblate ellipsoids are thermodynamically favoured over prolate ellipsoids[77,78]. Israelachivili et al rejected the oblate spheroid because of excessive curvature and proposed a disturbed oblate spheroid structure similar in shape to a red blood cell[79]. Further micellar growth was thought to lead to a cylindrical micelle with hemispherical ends.

Anacker[68] has reviewed the literature regarding micellar shape and discussed possible shapes in terms of core surface area per monomer. Figure 1.6 shows some suggested shapes of ionic micelles[35].

In contrast to many cationic micelles whose shape is often sensitive to concentration, SDDS micelles remain approximately spherical unless exposed to high electrolyte concentration[41]. The most obvious evidence of micellar growth and asymmetry is probably the dramatic increase in viscosity of the solution. Other methods used to determine micelle shape and molecular weight include light scattering, ultracentrifugation, membrane osmometry, magnetic resonance techniques, gel filtration, dye solubilization, potentiometric titration and hydrodynamics[40].

Typical values of aggregation number (N) range from about 20 for very small micelles to many hundred for large ones. For SDDS, N has been reported to be about 70 (25°C)[80] whilst fluorescent quenching techniques give the micelle radius (r) as 1.79 nm[81].

1.3.1.3 FACTORS AFFECTING CMC AND MICELLAR STRUCTURE

(a) Surfactant Structure

An increase in alkyl chain length results in an exponential decrease in CMC and a slight increase in aggregation number, N, and degree of counterion binding, β, due to the decreased charge density. Birdi has discussed the effect of alkyl chain length on the CMC, N and free energy of solubilization in alkylsulphate surfactant systems[82]. The structure, number and position of ionic head groups and the nature of the counterion also influence CMC and micellar size. For dodecylsulphates, inorganic counterion effects are more dependent upon valency than structure within a valency series; (CMC range 6.09 - 8.92 x 10^{-3} M, $Li^{+} > Na^{+} > K^{+} > Cs^{+}$; 1.66 - 2.2 x 10^{-3} M $Mn^{2+} > Cu^{2+} > Mg^{2+} > Co^{2+}$)[83].

The hydrophobicity of organic counterions also has a pronounced effect. For a series of alkyltrimethylammonium dodecylsulphates increasing alkylchain length from methyl to hexyl reduced the CMC at 25°C from 5.52 to 1.25 x 10^{-3} M [83]. A similar effect with increasing organic counterion hydrophobicity has been noted for cationic pyridinium surfactants[84]. Berr et al compared the micellar properties of SDDS and trimethyl ammonium dodecylsulphate (TMADDS) at 30°C; TMADDS micelles were found to be smaller and have a higher charge, smaller degree of aggregation and less but more deeply penetrating water than SDDS micelles[85]. These results were associated with the smaller size of the

sodium ion which allows a greater number of ions to fit in the available spaces around the sulphate head groups causing SDDS to have a smaller overall charge than TMADDS.

Counterions may induce striking viscoelastic behaviour in aqueous surfactant solutions. Gravesholt[86] compared the effect of substituted benzoate counterions with that of the conventional bromide counterion on the CMC and viscoelasticity of cetyltrimethylammonium (CTA) systems at 25° and 40°C. All organic salts studied had low CMC values compared to CTAB but rheological character was dependent upon molecular structure of the counterion; 2-hydroxybenzoate, 3-chlorobenzoate and 4-chlorobenzoate gave rise to viscoelasticity whereas 2-chlorobenzoate, 3-hydroxybenzoate and 4-hydroxybenzoate did not change the viscosity. The viscoelastic properties of CTA-salicylate were further investigated by Ulmius et al using PMR and linear dichroism techniques who attributed this behaviour to the presence of moderately large rod-shaped micelles which form long range periodic structures[87]. However, the secondary structure in viscoelastic amphiphile solutions must differ fundamentally from the ordinary spherical or rod-like micelles since such aggregates do not show any viscoelastic effect in pure CTAB solution even at high concentration.

Hoffmann et al have recently reported further studies into the viscoelastic nature of cetylpyridinium salicylate systems using small angle neutron scattering, SANS, static and dynamic light scattering, electric birefringence and rheological techniques[88]. At 25°C globular micelles form above the CMC of the system (1.5×10^{-4} M) but at a total concentration of 5×10^{-4} M transition to rod-like micelles

occurs. At a further characteristic concentration the rheological properties change and viscoelastic behaviour is observed.

High viscosities in CTA-tosylate surfactant systems have also been reported by Gamboa and Sepulveda[89]; a 7000 fold increase in relative viscosity at 25°C occurred as surfactant concentration was increased to 5×10^{-2} M. Sepulveda and Perez-Cotopoz[90] prepared a series of cetyltrimethylammonium alkylxanthate salts; methyl, ethyl, n-butyl and hexyl xanthate salts had very low solubility and precipitated from solution whereas propyl and amyl xanthate salts were extremely soluble and formed highly viscous solutions.

(b) Addition of Inorganic Electrolyte

Addition of electrolyte causes a reduction in the thickness of the ionic atmosphere surrounding the ionic head groups and a consequent decreased repulsion between them. This screening action is attributed to counterion binding which reduces the electrical work required for micelle formation. Electrolyte effects are primarily governed by the concentration and valency of the ions; an increase of either results in a decrease in CMC and increase in aggregation number.

The CMC of univalent ionic surfactants in the presence of added univalent salt, (CMC_I), was shown experimentally to be related to the total molar concentration of ions (equivalent to the concentration of added salt, C_Z, plus the concentration of surfactant at the CMC)[91], (equation 1.35). Subsequently Tartar derived a similar relationship based on Debye-Hückel theory[92].

$$\log_{10} CMC_I = a \log_{10} (C_Z + CMC) + b \qquad (1.35)$$

Where a and b are constants for a particular ionic group. Lange

calculated a as -0.503 for SDDS [93]. Backlund et al[73] found CMC values of SDDS varied from 8.1 - 1.5 x 10^{-3} M at 25°C as added NaCl increased from zero to 0.1 M giving values of a = -0.675 and b = -3.49.

The effect of electrolyte on the size and shape of SDDS micelles and in particular the sphere-to-rod transition has been the subject of many recent publications[41,68,73,94-104]. In 1980 Kratohvil[97] critically examined the literature values for aggregation number of SDDS in the presence of added sodium chloride. Mazer and co-workers used quasielastic light scattering to investigate the effects of temperature and sodium chloride concentration[94-96]. A dramatic increase in micellar weight and a change in shape from roughly spheroidal aggregates to a polydisperse distribution of spherocylindrical aggregates was observed at 0.45 M NaCl and 25°C (figure 1.8). Aggregation numbers of approximately 80 and 1000 were calculated for SDDS micelles at 25°C in the presence of 0.15 and 0.6 M NaCl respectively. At 18°C and in 0.6 M NaCl an aggregation number of about 1600 was found and the authors proposed a micellar shape corresponding to a prolate elipsoid with a semi-minor axis of 2.5 nm (equivalent to two elongated hydrocarbon chains) and semi major axis of 67.5 nm[95]. This work was subsequently critizised by Hayashi and Ikeda who found aggregation numbers of 97, 528 and 1630 in 0.1, 0.6 and 0.8 M NaCl respectively at 25°C[101]. Recent studies using quasielastic light scattering and flourescence quenching have been reported by Chang and Kaler[103] and Chen and co-workers[104] respectively.

The extent of counterion binding in micellar SDDS-NaCl systems has been studied by Backlund et al using Na^+ specific electrodes[73]. The degree of counterion association, β, was found to decrease slightly from 0.735 in the absence of NaCl to 0.707 in the presence of 0.036 M NaCl.

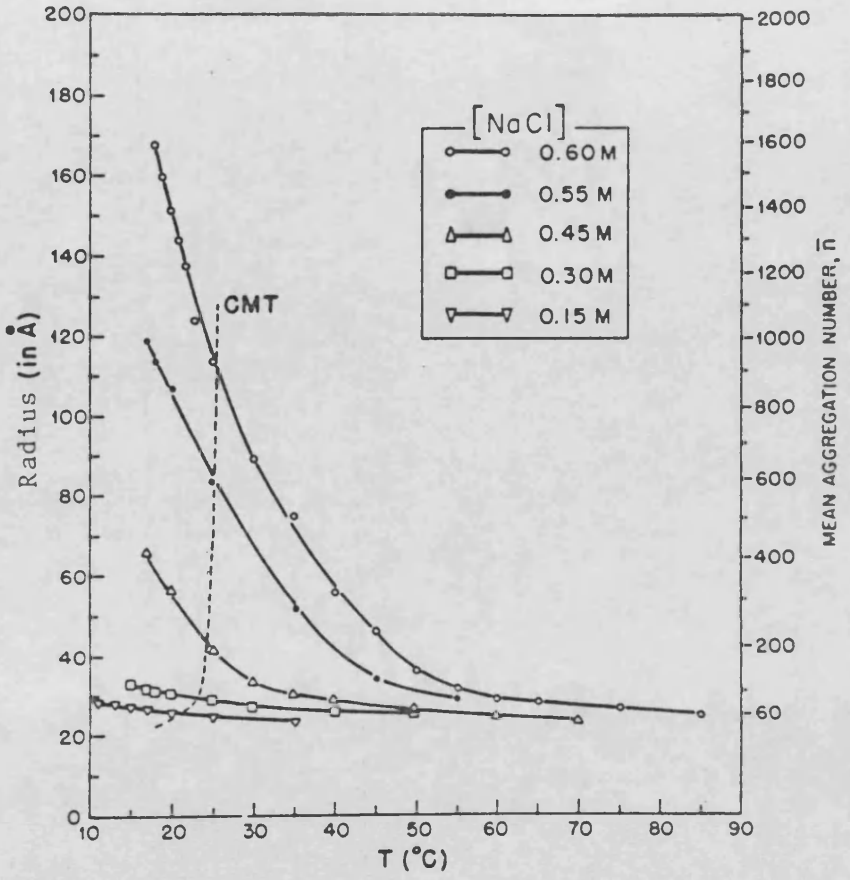

Figure 1.8 - Effect of sodium chloride concentration and temperature (T) on the mean aggregation number and radius of SDDS micelles (0.069M SDDS), (from Mazer et al[94]).

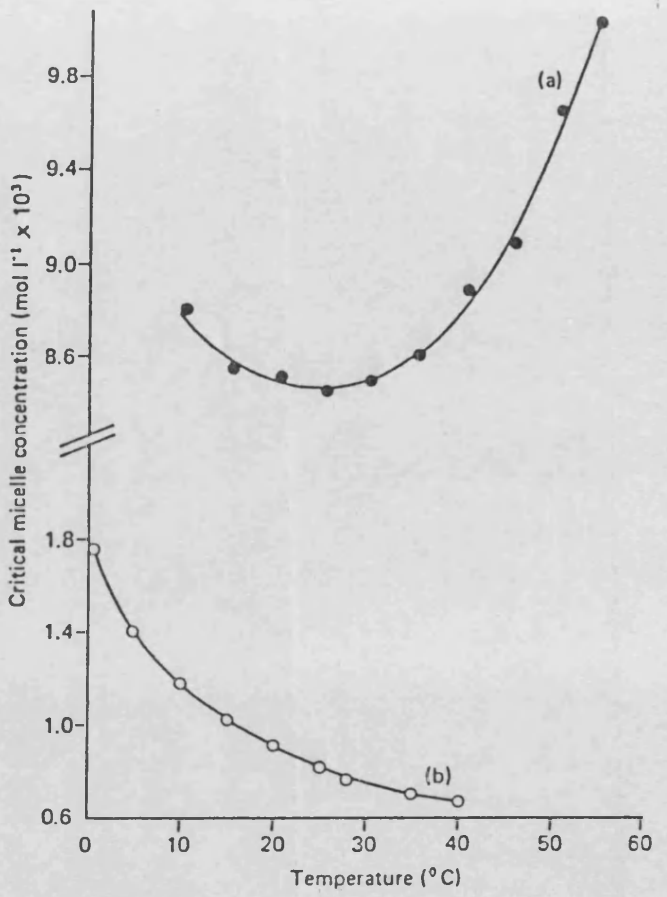

Figure 1.9 - Effect of temperature on the CMC of (a) SDDS , and (b) $CH_3(CH_2)_9(OCH_2CH_2)_5OH$, (from Goddard and Benson[109]).

Further increase in NaCl concentration to 0.3 M had no effect on β.

(c) Addition of Non-electrolyte

The addition of low molecular weight organic additives in aqueous solutions of surfactants is known to alter the CMC[51,105,106]. The most commonly studied additives have been urea and its derivitives, alcohols, sugars and hydrocarbons. Substances that affect the CMC of surfactants may be classified as penetrating (a solubilization phenomenon) and non-penetrating (a solvent phenomenon).

The interaction between unionised benzoic acid derivatives and dodecyl, tetradecyl and cetyltrimethylammonium bromide was investigated by Wan[107]. 2-hydroxybenzoic acid interacted with the surfactants leading to increased viscosity which reached a maximum at approximately the concentration where the surfactant solution became saturated with acid. Increasing concentrations of 2-hydroxybenzoic acid also changed the rheological behaviour from Newtonian to non-Newtonian. The interaction was found to be specific to 2-hydroxy substitution of benzoic acid as no viscosity effect was observed with benzoic acid, 3- and 4-hydroxybenzoic acid, acetylsalicylic acid, or 2, 3 and 4 substituted isomers of amino, chloro and nitro substituted benzoic acid. However, high viscosities have been reported in CTAB-benzoic acid systems in the presence of 0.1 M NaBr (relative viscosity = 585 in 0.1 M CTAB - 0.025 M benzoic acid[108]). These findings are somewhat different to those obtained with pure CTA salts by Gravesholt[86] (see section (a)). In this study CTA-3-chlorobenzoate and CTA-4-chlorobenzoate as well as CTA-salicylate was found to give viscous solutions.

(d) Temperature

The effect of temperature changes on the CMC of ionic surfactants is small in comparison with effects of added electrolyte and chemical structure of the amphiphile ion. A minimum in the CMC temperature curve, T_{min}, for ionic surfactants occurs typically between 20° and 30°C and has been reported as 26°C for SDDS[109,110]. Figure 1.9 shows the effect of temperature on the CMC of SDDS and the non-ionic surfactant, $CH_3(CH_2)_9(OCH_2CH_2)_5OH$ [111]. The effect of temperature increase on CMC is governed by two opposing factors; (a) dehydration of the monomers and (b) thermal agitation causing disruption of the structured water and reduction in the adhesion forces between monomers. Below T_{min} the effect of dehydration is dominant whereas above this temperature thermal agitation serves to increase the CMC.

The reduction in adhesive forces between monomers generally causes a reduction in micellar size of ionic surfactants with increase in temperature. Mazer et al[94,95] has studied the effect of temperature (10 - 90°C) on the size of SDDS micelles in sodium chloride solutions, (figure 1.8). A minimum micellar size corresponding to a sphere with a hydrated radius of about 2.5 nm is approached at high temperature in all NaCl concentrations.

1.3.2 Solubilization

The literature on solubilization by micelle forming surfactants is extensive and has been recently reviewed by Attwood and Florence[41] and Mukerjee[105,106]. Solubilization by colloidal surfactants is dependent upon the presence of a micellar phase and a characteristic feature is the existance of a critical, small range of concentrations below which there is no appreciable solubilization and above which the solubility

increases approximately linearly with the surfactant concentration. This CMC will generally be lower than the CMC of the system in the absence of solubilized species[105].

1.3.2.1 SOLUBILIZATION CAPACITY

The solubilization capacity may be defined as the saturation concentration of solubilizate for a given concentration of surfactant whilst maintaining a simple isotropic solution[41]. The saturated solubility of the solute may conveniently be expressed as the ratio of the number of moles of solubilizate to the number of moles of micellized surfactant, although other notations are used. For a particular surfactant this molar ratio is often found to remain constant above the CMC over a wide range of surfactant concentrations. However, this is not always so and care must be exercised in extrapolating data from one surfactant concentration to another[41].

1.3.2.2 MICELLE-WATER DISTRIBUTION CONSTANT

The distribution equilibrium of a solubilizate between micelles and the intermicellar solution may be determined under varying degrees of saturation.

The distribution of a solute, X, may be rationalized using the phase separation model for micellization and defined by the partition constant, K_p, (equation 1.36):

$$K_p = \frac{[X_{(M)}]}{[X_{(aq)}]} \qquad (1.36)$$

Where $[X_{(M)}]$ and $[X_{(aq)}]$ are the concentrations in the micellar and aqueous phases respectively. For a saturated system, K_p may be

obtained from the slope of a plot of saturated solubility of solubilizate in the surfactant system C_s, against micellized surfactant monomer concentration, $[S_{(M)}]$, (equation 1.37):

$$C_s = (K_p-1).\bar{v}.[X_{(aq)}].[S_{(M)}] + [X_{(aq)}] \qquad (1.37)$$

Where $\bar{v}$ is the partial molar volume of surfactant micelles.

Solubility data may also be treated by a mass action approach which leads to classical Langmuir (equation 1.38) and Scatchard (equation 1.39) binding equations:

$$r = \frac{nK_d\,[X_{(aq)}]}{1 + K_d\,[X_{(aq)}]} \qquad (1.38)$$

$$\frac{r}{[X_{(aq)}]} = nK_d - rK_d \qquad (1.39)$$

Where r is the mole ratio of bound solute to total solute, n is the maximum number of independent binding sites on the surfactant micelle and K_d is the intrinsic dissociation constant for the binding of solute molecules to one of the sites.

The micelle-water distribution equilibrium under unsaturated conditions has been determined by[41] dialysis, potentiometric titration, gel filtration, fluorescent quenching, NMR[112,113] and Raman spectroscopy[114].

1.3.2.3 LOCATION OF SOLUBILIZATE

Surfactant micelles are fluid-like in nature and solute molecules are distributed throughout the micelles with a rapid exchange between several states of different location, orientation and energy. Some locations and orientations may be greatly preferred, however, and it is

generally accepted that non-polar solubilizates such as aliphatic hydrocarbons are essentially dissolved in the hydrocarbon core of the micelles whereas semi-polar and polar solubilizates, e.g. fatty acids and alkanols, may be orientated radially in the micelle with the polar group either buried (deep penetration) or near the micellar surface (short penetration).

Mukerjee[105] has described a two state model for slightly polar solubilizates (e.g. benzene) involving a distribution between a 'dissolved state', associated with the core, and an 'adsorbed state' associated with the micelle/water interface. The mild surface activity of benzene in heptane/water systems and the extremely high surface-to-volume ratio in micelles allowed Mukerjee to predict a 7 to 1 ratio of 'adsorbed' to 'dissolved' benzene molecules in SDDS micelles. The distribution between the 'adsorbed state' and 'dissolved state' is expected to differ for solubilizates of different structures because of variations in surface activity and also with micellar size and shape.

Techniques described for determining the location of solubilizate in surfactant micelles include X-ray diffraction, adsorption spectrometry, NMR, fluoresence depolarization and electron resonance[41].

1.3.2.4 FACTORS AFFECTING SOLUBILIZATION

(a) Solubilizate and Surfactant Structure

The effect of surfactant structure on the solubilizing capacities is dependent upon the solubilization site within the micelle. In general, for solubilizates located in the micelle core, the solubilizing capacity shows a pronounced increase with increase in the alkyl chain length of the surfactant.

Ionic hydrophobic solutes may be solubilized within oppositely charged micelles by an ion-binding mechanism in addition to hydrophobic attraction forces (see section 1.4.3).

Solute polarity, polarizability, chain length, chain branching, molecular size, shape and structure have all been shown to affect solubility in surfactant micelles. No simple relationship exists between any single property of a solubilizate and its maximum additive concentration in a given surfactant solution. The solubility parameter of the solute and the surfactant determine the solubilization site of a particular solute and correct matching of these solubility parameters enables selection of the optimum surfactant to obtain maximum solubilization.

Solubilization of a series of n-alkanols in anionic and cationic micelles was investigated by Hoiland et al[115]. K_p values were calculated by a form of equation 1.36 and the standard free energy, ΔG^o_p, enthalpy, ΔH^o_p, and entropy ΔS^o_p, for the process:

$$\text{solubilizate}_{(aq)} \rightleftharpoons \text{solubilizate}_{(M)}$$

were calculated from equations 1.40 - 1.42:

$$\Delta G^o_p = -RT \log_e K_p \qquad (1.40)$$

$$\Delta H^o_p = \left(\frac{d\,\Delta G^o_p}{T}\right) \Big/ d(1/T) \qquad (1.41)$$

$$\Delta S^o_p = \frac{\Delta H^o_p - \Delta G^o_p}{T} \qquad (1.42)$$

The energetics of solubilization of n-hexanol in SDDS were determined as ΔG^o_p =-16.5 kJ mol^{-1}, ΔH^o_p = 4.1 kJ mol^{-1} and ΔS^o_p = 69 J mol^{-1} K^{-1},

thus indicating an endothermic reaction and an entropically driven solubilization process[115]. The mean molar standard free energy for the transfer of the alcohol from the aqueous to the micellar phase was approximately independent of surfactant type and was determined as -2.78 kJ mol^{-1} per methylene group at 298.2 K. This value is somewhat smaller than the reported standard free energy change for the transfer of alcohol from the aqueous to the pure state of $\Delta G^{o} = -3.31$ kJ mol^{-1} per methylene group[115].

The thermodynamics of solubilization of phenothiazine and its n-alkyl derivatives by sodium, manganese and zinc dodecyl sulphates has been studied by Moroi et al[116]. Thermodynamic parameters for the interaction between monomeric solubilizate molecules and vacant micelles were evaluated using the stepwise association model which also gives an association constant K_A for the solubilization process. Maximum additive concentrations of N-ethyl, N-methyl and phenothiazine became smaller as the hydrophobicity of the attached alkylchain increased. However, the rank order for K_A values is reversed reflecting the dependence of aqueous and micellar solubilities on alkyl chain length. Evaluation of thermodynamic parameters using equations 1.40 - 1.42 gave $\Delta G^{o} = -29.0$ kJ mol^{-1}, $\Delta H^{o} = -21.9$ kJ mol^{-1} and $\Delta S^{o} = 24$ J mol^{-1} K^{-1} and the authors therefore proposed that the sites of solubilization is the hydrophilic part of the micelles and not the micelle interior.

(b) Temperature

Temperature affects micellar solubilization by the following mechanisms:

(i) changes in solubilizate aqueous solubility,

(ii) changes in solubilizate micellar solubility,

(iii) changes in the properties of micelles.

Temperature effects are thus heavily dependent upon the nature of the solubilizate and surfactant and prediction of temperature effects is therefore difficult. In general, however, an increase in temperature results in an increase in the amount of solubilization.

(c) Additives

Electrolyte effects on solubilization by ionic surfactants close to the CMC are dominated by the increase in available micellar volume brought about by the reduction in CMC of the system. At higher surfactant concentrations well in excess of the CMC the situation is more complex. The effect of closer packing of surfactant within the micelle due to reduced repulsion of headgroups may lead to a reduction in the solubilizing capacity.

Non-electrolyte additives may have a synergistic or antigistic effect on solubilization. Additives which inhibit micellization naturally decrease the solubilizing capacity of surfactants.

1.4 INTERACTIONS BETWEEN IONIC SURFACE ACTIVE AGENTS AND OPPOSITELY CHARGED ORGANIC IONS

For ionic surfactants, aggregation of surfactant ions in dilute solutions below the critical micelle concentration, CMC, is minimal due

to electrostatic repulsion of the head groups. However, many examples of large organic ion-pairs and ion-triplets formed between surfactant ions and large organic ions of opposite charge have been described. These interactions are driven by electrostatic attraction reinforced by a strong hydrophobic effect; the relative contribution of each being dependent upon the structures of both ions and their immediate environment. The solubility of these ion-pairs/triplets is usually low in aqueous systems and phase separation due to complex formation occurs when the solubility has been exceeded. Solubilization occurs above the CMC of the system due to strong micellar binding of the oppositely charged organic ion.

Tomlinson et al have reviewed the literature (1965-80) on ion-pair and complex formation between large organic ions of opposite charge and have proposed a series of possible physicochemical equilibria between two large organic ions when one ion (B) is surface active and when the oppositely charged ion (A) can undergo aggregation or pseudomicellization[119]:

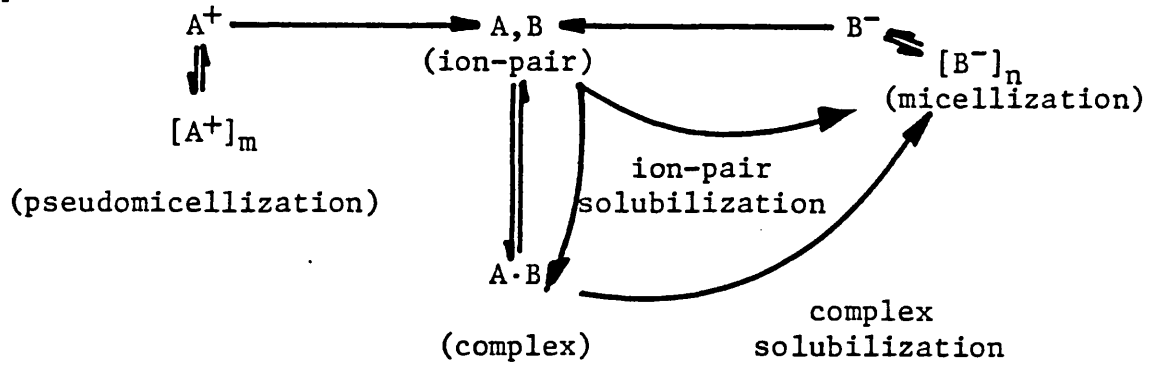

Such interactions are important in many areas of pharmacy and may affect chemical, microbiological and physical stability of formulations, and drug absorption and distribution[119,124,133,135,180,185-191,207-209].

Tomlinson et al have listed twenty methods reported in the literature for the study of large organic ion interactions[119]. For this work the

primary method used for investigating aggregation and ion-pair and complex formation was an automated conductimetric titration technique based on the method described by Mukhayer and Co-Workers[120-122].

1.4.1 Conductance

Ionic compounds such as salts of weak acids and bases dissociate in aqueous solution into ions which are free to carry (or conduct) current across the solution. Conductance is the reciprocal of resistance and is measured in units of Siemens (S). For a given electrolyte solution, conductance decreases proportionally with increasing distance between the electrodes, L, and increases proportionally with the cross-sectional area of the electrodes, A. Specific conductance, κ, is the conductance of an electrolyte measured using a standard cell comprising of electrodes of area 1 cm^2 spaced 1 cm apart. The ratio L/A is constant for any given conductivity cell and is referred to as the cell constant, K_{CELL}. The relationship between specific conductivity and conductivity, G, is shown in equation 1.43.

$$\kappa = \frac{L}{A} \cdot G = K_{CELL}\, G \qquad (Scm^{-1}) \qquad (1.43)$$

κ may be obtained by using the cell to measure the conductivity of an electrolyte solution of known specific conductivity at a given temperature.

Conductance will depend upon the concentration of ions present in the electrolyte solution. The comparative conductance behaviour of different electrolytes is therefore assessed by determining the ratio of specific conductance to ion concentration. Since electrolyte solutions of the same normality have the same charge concentration it is

more useful to utilise this form of expressing concentration rather than molarity. The equivalent conductivity, Λ, is defined by equation 1.44.

$$\Lambda = \frac{1000}{C} \qquad (1.44)$$

Where C is the concentration of ions in equivalents per litre. The equivalent conductivity of strong electrolytes at low concentration is found to be experimentally a linear function of the square root of concentration, decreasing as the concentration increases. Extrapolation to zero concentration yields the limiting equivalent conductivity Λ^o, and the equivalent conductivity at very low concentrations can therefore be represented by equation 1.45.

$$\Lambda = \Lambda^o - A\, C^{1/2} \qquad (1.45)$$

Where A is a constant for a given system and temperature. At infinite dilution, the motion of an ion is limited solely by its interaction with the surrounding solvent molecules, there being no other ions within a finite distance. Kohlrausch's law of the independent migration of ions states that the limiting equivalent conductance for an electrolyte is the sum of the limiting equivalent conductances for each of its constituent ions, $\lambda^o_{\pm}$ (equation 1.46).

$$\Lambda^o = \lambda^o_+ + \lambda^o_- \qquad (1.46)$$

Limiting ionic conductivities are very sensitive to change in temperature. Most aqueous electrolyte solutions have a temperature coefficient for conductivity close to 2% per degree at 25°C; temperature control of $\pm$ 0.05°C is therefore required for an experimental precision of 0.1%. At any given temperature, the

product of limiting ionic conductivity and viscosity of water, ($\lambda^o \eta^o$), for many ions is nearly constant suggesting that viscous forces account for most of the resistance to the motion of these ions in water.

For ideal solutions equivalent conductance should be independent of concentration. However, due to ion-ion interactions the effective ion concentration will not increase proportionally with chemical concentration and will therefore decrease with increasing concentration as activity corrections become more significant. Ion-ion interaction effects on conductance arise from electrophoretic and relaxation phenomenona.

(a) The electrophoretic effect arises when the solvated ion moves through a viscous medium and drags with it the solution in its immediate vicinity. Neighbouring ions therefore have to move, not in a stationary medium, but with or against the stream according to their charge relative to the first ion.

(b) The relaxation effect is due to the disturbance of the symmetrical distribution of the ion cloud around any given ion and will tend to decrease the velocity of ions. At equilibrum the ionic atmosphere is time average distributed with spherical symmetry and therefore exerts no net resultant force on a central ion. As the central ion moves to an off centre position it experiences a restoring force which rapidly dies away as the atmosphere is rearranged by the thermal motion of the constituent ions. The average restoring force experienced by the ion is called the relaxation effect.

These effects are concentration dependent, falling to zero at infinite dilution. The Onsager limiting law for conductivity relates the

limiting equivalent conductance at infinite dilution, Λ^o, to the equivalent conductance, Λ, at ionic strength, I, (equation 1.47).

$$\Lambda = \Lambda^o - \left[\frac{2.801 \times 10^6 |z_A z_B| q \Lambda^o}{(\varepsilon T)^{3/2} (1 + q^{1/2})} + \frac{41.25 (|z_A| + |z_B|)}{\eta (\varepsilon T)^{1/2}} \right] I^{1/2} \quad (1.47)$$

Where z_A and z_B are the charges on the respective ions, q is the mobility function, ε is the relative permittivity, T is the temperature (K) and η is the viscosity of the solution. A simplified form is given by equation 1.48:

$$\Lambda = \Lambda^o - (B_1 \Lambda^o + B_2) I^{1/2} \quad (1.48)$$

Where B_1 and B_2 are coefficients related to the relaxation and electrophoretic effects respectively and are available from standard tables[11]. For a solution 1:1 of electrolyte containing a single species of concentration, C, equation 1.48 becomes equation 1.49:

$$\Lambda = \Lambda^o - (B_1 \Lambda^o + B_2) C^{1/2} \quad (1.49)$$

For weak electrolytes, the degree of dissociation, α, decreases with increasing concentration (equation 1.50) which results in a marked reduction of Λ values as the overall concentration rises.

$$K^{eq} = \frac{\alpha^2 C}{1-\alpha} \quad (1.50)$$

Where K^{eq} is the ionization constant (equivalent to K_a for an uncharged weak acid and K_b for an uncharged weak base). The degree of dissociation can be obtained from the conductance ratio, equation 1.51.

$$\alpha = \frac{\Lambda}{\Lambda^o} \quad (1.51)$$

The Onsager limiting law (equation 1.48) is therefore, modified for 1:1 weak electrolytes to correct for α, equation 1.52.

$$\Lambda = [\Lambda^o - (B_1\Lambda^o + B_2)(\alpha C)^{1/2}]\alpha \qquad (1.52)$$

1.4.2 Ion Association and Complex Formation

The generalised form for the interaction between an anion, e.g. an anionic surfactant monomer, $S^{n-}(aq)$, and a cation, $X^{p+}(aq)$, in aqueous solution to form a sparingly soluble associated species, $S_pX_n\ (aq)$, and a complex, $S_pX_{n(c)}$, may be expressed by the following equilibria:

$$pS^{n-}(aq) + nX^{p+}(aq) \underset{K_{diss}}{\overset{K_{ass}}{\rightleftharpoons}} S_pX_n\ (aq) \rightleftharpoons S_pX_n(c)$$

Where K_{ass} and K_{diss} are the association and dissociation constants for $S_pX_{n(aq)}$.

1.4.2.1 ION-ASSOCIATION

K_{ass} is defined by equation 1.53:

$$K_{ass} = \frac{a\ S_pX_{n(aq)}}{(a_{S^{n-}(aq)})^p.(a_{X^{p+}(aq)})^n} \qquad (1.53)$$

For 1 : 1 electrolytes, such as cirazoline hydrochloride and sodium dodecylsulphate, the association may be defined by the ion-pair association constant, K_{ip}, (equations 1.54 - 1.56):

$$K_{ip} = \frac{a\ SX_{(aq)}}{a\ S^-_{(aq)} \cdot a\ X^+_{(aq)}} \qquad (1.54)$$

and at low ionic strengths ($<1\times10^{-4}$ M), where activity can be replaced

by molar concentration, [ ]:

$$K_{ip} = \frac{[SX_{(aq)}]}{[S^-_{(aq)}][X^+_{(aq)}]} \qquad (1.55)$$

$$\text{or,}\quad K_{ip} = \frac{[SX_{(aq)}]}{([NaS_{(aq)}]^T - [SX_{(aq)}])([XCl_{(aq)}]^T - [SX_{(aq)}])} \qquad (1.56)$$

Where $[NaS_{(aq)}]^T$ and $[XCl_{(aq)}]^T$ represent the total concentrations of the two interacting electrolytes (with sodium and chloride counterions).

Mukhayer and Davis[121] have described an automated conductimetric titration method whereby K_{ip} may be determined from observed deviation from theoretical conductivity values when the following assumptions are made:

(i) the degree of dimerisation (if any) of the surfactant and/or organic salt does not change appreciably during the titration,

(ii) the type of ion-pair association does not change appreciably during the titration,

(iii) activity effects with respect to the various ionic species can be ignored.

The technique involves titrating a moderately concentrated solution of surfactant into distilled water (titration I) and a dilute aqueous solution of the organic salt (titration II). The calculation of K_{ip} for a 1:1 ion-ion interaction (with sodium and chloride counterions) may then be described as follows:

the specific conductivity of the surfactant (κ_{NaS}) at any point during titration I is given by equation 1.57:

$$K_{NaS} \times 1000 = \Lambda^{o}_{NaS} [NaS_{(aq)}]^{T} \qquad (1.57)$$

If no ion-pair formation occurs during titration II the theoretical specific conductance of the mixture K_{mix} at any point in the titration would be given by equation 1.58:

$$K_{mix} \times 1000 = \Lambda^{o}_{NaS} [NaS_{(aq)}]^{T} + \Lambda^{o}_{XCl} [XCl_{(aq)}]^{T} \qquad (1.58)$$

However, since the formed ion-pairs are neutral and non-conducting, the experimentally observed specific conductivity (K'_{mix}) at any point during titration II is described by equation 1.59.

$$K'_{mix} \times 1000 = \Lambda^{o}_{NaS} ([NaS_{(aq)}]^{T} - [SX_{(aq)}]) + \Lambda^{o}_{XCl} ([XCl_{(aq)}]^{T} - [SX_{(aq)}]) + [SX_{(aq)}] (\lambda^{o}_{Na^{+}} + \lambda^{o}_{Cl^{-}}) \qquad (1.59)$$

Subtraction of equation 1.59 from 1.58 yields:

$$\Delta K_{mix} \times 1000 = (K_{mix} - K'_{mix}) \times 1000 = \Lambda^{o}_{NaS} [SX_{(aq)}] + \Lambda^{o}_{XCl} [SX_{(aq)}] - [SX_{(aq)}].(\lambda^{o}_{Na^{+}} + \lambda^{o}_{Cl^{-}}) \qquad (1.60)$$

$$\text{and} \quad [SX_{(aq)}] = \frac{\Delta K_{mix} \times 1000}{(\Lambda^{o}_{NaS} + \Lambda^{o}_{XCl}) - (\lambda^{o}_{Na^{+}} + \lambda^{o}_{Cl^{-}})} \qquad (1.61)$$

ΔK_{mix} at any given concentration of NaS may be calculated as follows:

the theoretical specific conductivity of the mixture, K_{mix}, when no ion-pairing takes place is given by equation 1.62:

$$K_{mix} = [K_{NaS} - K_{(aq)}] + [K_{XCl} - K_{(aq)}] \qquad (1.62)$$

Where $K_{(aq)}$ is the specific conductance of the conductivity water. K'_{mix} should also be corrected for the specific conductivity of the

solvent. Thus combining equations 1.60 and 1.62 gives ΔK_{mix} at any surfactant concentration:

$$\Delta K_{mix} = (K_{NaS} - K_{(aq)}) + (K_{XCl} - K_{(aq)}) - (K'_{mix} - K_{(aq)}) =$$
$$(K_{NaS} - K_{(aq)}) - (K'_{mix} - K_{XCl}) \qquad (1.63)$$

Experimental data from titrations I and II allow the solution of equation 1.63 for ΔK_{mix} and also provides Λ^{o}_{NaS} and Λ^{o}_{XCl}. $\lambda^{o}_{Na^+}$ and $\lambda^{o}_{Cl^-}$ are obtained from standard tables, hence equation 1.61 can be solved for $[SX_{(aq)}]$ at any point in titration II. Since $[NaS_{(aq)}]^T$ and $[XCl_{(aq)}]^T$ in titration II are also known, K_{ip} is thence calculated from equation 1.56.

Mukhayer[122] and Tomlinson et al[119] have collated the reported ion-pair association constants for various organic anions and cations at 25°C and have found a relationship between the total number of carbon atoms in the ion-pair and their association constants. K_{ip} values where the surfactant is SDDS were reported as 13 M^{-1} ($-Me_4N^+$), 19 M^{-1} ($-Et_4N^+$), 21 M^{-1} ($-Pr_4N^+$), 156 M^{-1} (benzyltriphenyl phosphonium) and 7280 M^{-1} ($-C_{10}H_{21}Me_3N^+$)[119].

1.4.2.2 COMPLEX FORMATION

Phase separation to form an insoluble hydrophobic complex occurs when the solubility of the associated species is exceeded. Hoyer and Doerr[123] have investigated the interaction of sodium and hydrogen dodecylsulphate with decyltrimethylammonium iodide and hydroxide. Decyltrimethylammonium-dodecylsulphate complex was prepared by two methods, (a) by mixing equimolar concentrations of aqueous decyltrimethylammonium hydroxide and hydrogendodecylsulphate solutions, and (b) by mixing equimolar concentrations of aqueous solutions of the corresponding salt forms and storage in an ice bath. Method (a)

produced a turbid microemulsion system which was stable for more than three years (diuturnal system) whereas method (b) resulted in precipitation and the formation of a crystalline solid. Dissolution of these crystals by heating resulted in a microemulsion system with similar properties to that obtained by method (a), except that of stability; within 3-4 hours gross phase separation occurred (caducous system).

Barry and Russell have investigated the interaction of commercial alkyltrimethylammonium bromides with amaranth (anionic dye) using surface tension, viscosity, light scattering, microscopy, microelectrophoresis, spectroscopy and phase studies[124]. Liquid droplets of complex were formed when dilute aqueous solutions of surfactant and dye were mixed, but floccules formed at high concentrations and at very high concentrations some viscoelastic systems were observed. The interaction product was termed a 'complex coacervate' and exhibited typical behaviour of coacervates in an electric field e.g. electrophoresis, disintergration and deformation. Coacervation describes the separation of a colloidal solution into two liquid layers, one of which is rich in colloidal component and the other poor. Barry and Gray studied complex coacervation of alkyltrimethylammonium bromides (C_{12} - C_{16}) with aqueous solutions of the anionic dyes tartrazine, amaranth, carmoisine and erythrosine and suggested the phenomenon was the result of rapid micellar growth[125]. For all these systems phase separation only occurred at certain mixing proportions and temperatures; an excess of dye or surfactant, presence of inorganic salt and increase in temperature all supressed coacervation. Their proposed theory of complex coacervation suggested the dye induces formation of surfactant micelles at concentrations that are well below the CMC of the pure surfactants in water; e.g. a forty

fold reduction in the CMC of tetradecylmethylammonium bromide at 40°C was predicted upon addition of 1.5×10^{-4} M amaranth.
Complex coacervation has also been reported in systems containing alkyltrimethylammonium bromide - di and trihydroxy bile salts[126], sodium dodecylsulphate - benzyltriphenylphosphonium chloride[127], alkylbenzyldimethylammonium chloride - sodium cromoglycate[128,129], alkylbenzyldimethylammonium chloride - indigo carmine[128] and sodium dodecylsulphate - tris (1,10-phenanthroline) iron (II)[130].

Lemordant and Gaboriaud[130] reported a turbid coacervate phase in the latter system which cleared with the formation of a crystalline precipitate upon standing. These crystals were isolated by filtration and were readily soluble in organic solvents. At high detergent to metal chelate ratios, red crystalline needles were formed instantaneously and simultaneously with the coacervate phase. Formation of crystalline complexes of methylviologen-didodecylsulphate, methylviologen-dialkyl sulphonates (C_{10} - C_{18})[131,132] and cetyltrimethylammonium-alkylxanthates[90] have also been reported.

Sepulveda and Perez-Cotopoz[90] prepared cetyltrimethylammonium-alkyl xanthates by mixing aqueous solutions of the surfactant bromide and xanthate potassium salts at 5°C. CTA-methyl-, ethyl-, butyl- and hexylxanthate salts formed solid complexes which were poorly soluble in water. CTA-propyl and amylxanthate complexes were also prepared but these salts had a high solubility in water giving viscous solutions. This unexpected behaviour was rationalized in terms of the odd/even alteration rule that is usually found in homologous alkyl series when a solid phase is involved (although the behaviour of the methylxanthate is obviously anomolous).

Solubility Product

Complexation between oppositely charged ions may be characterised by the stoichiometric solubility product, K_s. The dissociation constant for interaction in aqueous solution, K_{diss}, is defined by equation 1.64:

$$K_{diss} = \frac{(a_{S^{n-}(aq)})^p.(a_{X^{p+}(aq)})^n}{a_{S_pX_n(aq)}} \qquad (1.64)$$

At equilibrium, and in the presence of a separate complex phase $a_{S_pX_n(aq)}$ will be constant and equal to unity (saturated solution). The product of the ion activities is then constant and is known as the intrinsic solubility product which is defined by equation 1.65:

$$K_s = (a_{S^{n-}(aq)})^p.(a_{X^{p+}(aq)})^n \qquad (1.65)$$

Writing activities as the product of concentration, [], and activity coefficient, γ, (equation 1.66):

$$K_s = [S^{n-}(aq)]^p.[X^{p+}(aq)]^n.(\gamma_{S^{n-}(aq)})^p.(\gamma_{X^{p+}(aq)})^n \qquad (1.66)$$

The apparent solubility product, K_s', is defined by equation 1.67 and is related to the intrinsic solubility product, K_s, by equation 1.68.

$$K_s' = [S^{n-}(aq)]^p.[X^{p+}(aq)]^n \qquad (1.67)$$

$$K_s = K_s'.(\gamma_{S^{n-}(aq)})^p.(\gamma_{X^{p+}(aq)})^n \qquad (1.68)$$

For uni-univalent systems such as cirazoline hydrochloride and SDDS, K_s and K_s' may be expressed by equations 1.69 and 1.70 respectively.

$$K_s = (a_{S^-(aq)}).(a_{X^+(aq)}) = [S^-(aq)].[X^+(aq)].(\gamma_{\pm})^2 \qquad (1.69)$$

$$K_s' = [S^-(aq)][X^+(aq)] = K_s.(\gamma_{\pm})^{-2} \qquad (1.70)$$

Where $\gamma_{\pm}$ is the mean activity coefficient of the ions which at low ionic strengths (<1 x 10^{-4} M) approaches unity and $K_s' = K_s$. In the presence of complex, and when $SX_{(aq)} \rightarrow 0$, K_s' may be expressed by equation 1.71.

$$K_s' = ([S]^T - [SX_{(c)}])\,([X]^T - [SX_{(c)}]) \qquad (1.71)$$

Where $[S]^T$ and $[X]^T$ are the total concentrations of anion and cation mixed in the system and $[SX_{(c)}]$ is the concentration of precipitated complex. Hence, assuming K_s' is constant above the complexation point, $[SX_{(c)}]$, (and therefore $[S^-_{(aq)}]$ and $[X^+_{(aq)}]$), may be solved using the quadratic form of equation 1.71.

The solubility product for the interacting ions may be related to the aqueous solubilities of the formed salts, C_s, (equation 1.72):

$$C_s = \left(\frac{K_s}{n^n . p^p}\right)^{1/(n+p)} \qquad (1.72)$$

Which for a 1:1 salt becomes:

$$C_s = K_s'^{1/2} \qquad (1.73)$$

Equation 1.73 has been used by Sepulveda and Perez-Cotopoz in the determination of cetyltrimethylammonium-alkylxanthate solubility products[90]. A more accurate method for determination of K_s' which enables the exact stoichiometry of the interaction to be calculated is the automated conductimetric titration technique described by Mukhayer[122], Mukhayer et al[120], Mukhayer and Davis[121] and reviewed by Tomlinson et al[119]. For surfactant organic ion interactions, the technique involves titrating a concentrated solution of the surfactant against a dilute solution of the organic salt. In this way problems with micellization of the surfactant in the reaction vessel are usually

avoided. The end-point of the titration for the formation of insoluble complex is given by a marked change in gradient of the conductimetric titration trace (figure 1.10a) and the solution usually goes turbid at this point. The apparant stoichiometric solubility product may then be obtained from a knowledge of the concentrations of organic ion and surfactant at the end-point (equation 1.67) and the stoichiometry of the interaction.

An interesting phenomena was observed by Tomlinson and Davies[128] in the study of complexation between alkylbenzyldimethylammonium chlorides (ABDAC) and bischromones and ABDAC and indigo carmine. 'Typical' conductimetric titration traces (figure 1.10a) were obtained for the former systems but all ABDAC-indigo carmine systems produced the unusual and characteristic profiles shown in figure 1.10b where conductance rose to a maximum followed by a fall to a minimum and then a further rise. These 'atypical' conductimetric titration traces were explained by flocculation of indigo carmine in the presence of added surfactant. The end-point for the titrations in these systems was taken as the point where the initial fall off in conductivity occurs (point A in figure 1.10b) rather than where the sharp breakpoint occurs.

1.4.2.3 FACTORS AFFECTING IONIC INTERACTIONS

Tomlinson et al[119] have reviewed the literature on factors affecting ionic interaction and phase stability up to 1980; a brief summary of the literature is given here.

(a) Temperature

The onset and character of complex coacervation in ATAB-dye mixtures have been shown by Barry and Gray to be heavily dependent upon temperature, e.g. carmoisine-surfactant systems formed viscous gels

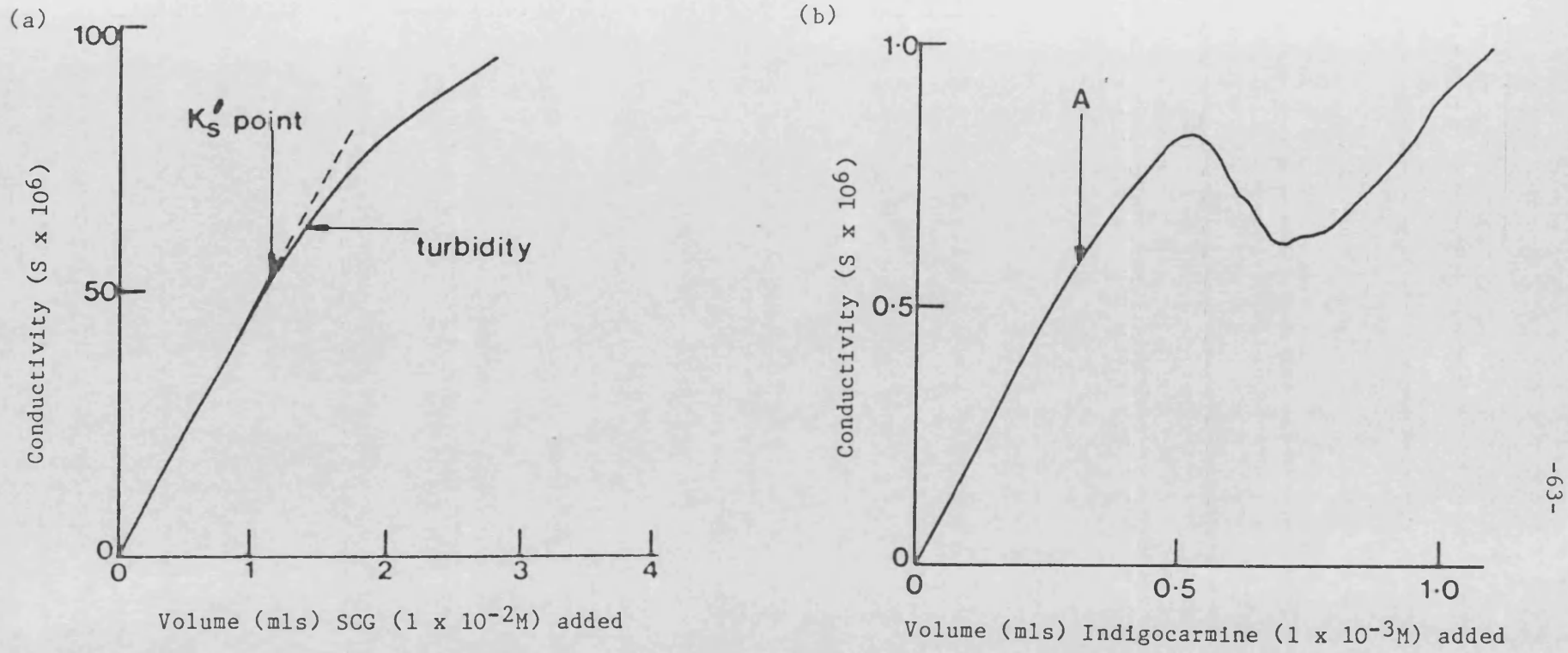

Figure 1.10 - Automated conductimetric titration trace for, (a) sodium cromoglycate (SCG) versus 2.6 x 10^{-4}M terdecylbenzyldimethylammonium chloride and (b) indigocarmine versus 1 x 10^{-5}M quindecylbenzyldimethylammonium chloride, at 25°C, (from Tomlinson and Davis[128])

below 40°C although at higher temperatures a dispersed phase consisting of isotropic oily droplets was produced[133]. For tartrazine-, erythrosine- and amaranth- surfactant systems, viscous mesomorphic phases were often produced which changed into isotropic oil droplets as the temperature rose.

Tomlinson et al observed that for six different interacting systems, changes in K_s' with temperature over the range 5° -60°C exhibit minima (T_{min}) between 14° and 20°C[119]. The relationship between K_s' and temperature was described by the polynomial expression, (equation 1.74) [119,129,134,135].

$$\log K_s' = A-BT+CT^2-DT^3 \qquad (1.74)$$

The standard free energy change, ΔG^o_f, standard enthalpy change, ΔH^o_f, and standard entropy change, ΔS^o_f, of complex formation was calculated using equations 1.75 to 1.77 since the activity of the saturated solution of the complex is taken as unity (see equation 1.64)[134]:

$$\Delta G^o_f = RT \log_e K_s \qquad (1.75)$$

$$\log_e K_s = \frac{\Delta H^o_f}{RT} - \frac{\Delta S^o_f}{R} \qquad (1.76)$$

$$\Delta G^o_f = \Delta H^o_f - T\Delta S^o_f \qquad (1.77)$$

Tomlinson et al have observed that for most reported systems, ΔH^o_f and ΔS^o_f are both positive and relatively high at low temperatures, but as the temperature is increased above the minimum, ΔG^o_f becomes more negative and the process becomes primarily enthalpically controlled with large negative ΔH^o_f values and smaller positive ΔS^o_f values[119]. Mukhayer and Davies explained these temperature effects on coacervate formation by coulombic and hydrophobic interactions[127]. At lower

temperatures the interaction process is controlled by entropic factors (hydrophobic interactions) and the stability of the coacervate increases (i.e. K_s decreases) with temperature. At higher temperatures the interaction process is controlled by enthalpic factors (coulombic interactions) and the stability of the coacervate decreases (i.e. K_s increases) with temperature. Although at higher temperatures ion-pair formation and complex coacervation between the hydrophobic ions may be reduced due to the melting of water structure, the temperature increase also lowers the relative permittivity which should result in an increase in ion-pair formation; and the resultant of these opposing effects is a large negative enthalpy and a small positive entropy of complex formation. However, positive ΔH^o_f and ΔS^o_f values have been obtained for alkylsulphate-alkylpyridinium and alkyltrimethylammonium ion systems[119], alkylbenzyldimethylammonium chloride - SGC systems[129], and phenothiazine -SDDS systems[135]. Table 1.2 shows selected thermodynamic parameters for complex formation in (a) BTPC -SDDS[134],
(b) dodecylbenzyldimethylammonium chloride - SCG[129], and
(c) chlorpromazine - SDDS systems[135].

However, the free energy of complex formation should be calculated with respect to mole fractions, or in molal terms using equation 1.78:

$$\Delta G^o_f = RT \log_e K_s - RT \log_e 55.5 \qquad (1.78)$$

Hence ΔG^o_f values calculated using equation 1.75, (and therefore, derived ΔS^o_f values calculated from equation 1.77), are not valid. ΔG^o_f and ΔS^of values for the systems in table 1.2 were recalculated using equations 1.78 and 1.77 respectively and are shown in parentheses in table 1.2.

System	Temp (°C)	$\log_{10} K_s$	ΔG^o_f (kJmol^{-1})	ΔH^o_f (kJmol^{-1})	ΔS^o_f (Jmol^{-1}K^{-1})
(a) BTPC-SDDS	5	-6.95	-37.0 (-46.3)	12.8	179 (212)
	10	-6.98	-37.8 (-47.3)	8.0	162 (195)
	30	-6.97	-40.4 (-50.5)	10.7	98 (131)
	50	-6.76	-41.8 (-52.6)	28.3	42 (75)
(b) DDBDAC-SCG	5	-	-51.9 (-61.2)	12.2	231 (264)
	35	-	-57.1 (-67.4)	-24.2	107 (140)
	50	-	-58.5 (-69.3)	-38.2	62 (96)
(c) CP-SDDS	10	-8.38	-45.4 (-54.9)	-24.5	74 (107)
	30	-8.03	-46.6 (-56.7)	-34.0	22.5 (75)
	50	-7.52	-46.6 (-57.4)	-46.6	1.5 (33)

Table 1.2 - Selected thermodynamic parameters for complex formation in (a) benzyltriphenylphophonium chloride - SDDS (BTPC-SDDS)[134], (b) dodecylbenzyldimethylammonium chloride - sodium cromoglycate (DDBDAC-SCG)[129], and chlorpromazine - SDDS (CP-SDDS)[135] systems at the temperature indicated.

(Figures in parentheses are ΔG^o_f and ΔS^o_f values calculated using equations 1.78 and 1.77).

(b) Structure

The effect of alkylchain length on K_s' has been studied in benzyltriphenylphosphonium chloride (BTPC) - sodium alkylsulphate systems[136,137], alkylbenzyldimethylammonium chloride (ABDAC) - sodium cromoglycate (SCG) systems[129,128], ABDAC - indigo carmine systems[128,129] and more recently in cetyltrimethylammonium bromide (CTAB) - alkyl xanthate[90] and alkyltrimethylammonium bromide (ATAB) - sodium saccharin (SS) systems[125]. An increase in hydrophobicity (alkylchain length) in all systems resulted in an enhanced interaction and a reduction in the solubility of the complex. The logarithm, of K_s', (or K_s), is linearly related to the number of methylene groups in the alkylchain, n, according to equation 1.79:

$$\log K_s' = a - bn \qquad (1.79)$$

where a and b are constants. Each additional methylene group in the alkylchain, n, has been found to provide a constant increment to the free energy of complexation of $d(\Delta G^o_f)_{/dn} = -3.5$ kJmol^{-1} (ATAB-SS)[125], -3.20 kJmol^{-1} (BTPC -sodium alkylsulphate)[136,137], and -3.17 kJmol^{-1} (ABDAC-SCG)[128,129]. A similar value (-3.5 kJmol^{-1}) was obtained by Sepulveda and Perez-Cotopoz[90] for the transfer of the methylene group attached to the xanthate moiety in CTAB-alkylxanthate systems at 25°C although Mukhayer and Davies reported a smaller value of -1.01 kJmol^{-1} for transfer in substituted phosphonium chloride - SDDS systems[138]. The latter workers compared the thermodynamics of transfer of the methylene group from aqueous phase to complex phase in BTPC - sodium alkylsulphate systems to that for the transfer to various other non-aqueous phases at 25°C[136]. Thermodynamic parameters for the complexation process show the

complex phase is consistant with a liquid-like or coacervate phase with some solid-like structure[136].

Values of the enthalpy, $d(\Delta H^{o}_{f})/dn$, and entropy, $d(\Delta S^{o}_{f})/dn$, of transfer of the methylene group from the aqueous environment to the BTP-alkylsulphate complex at 25°C have been estimated from plots of ΔH^{o}_{f} and ΔS^{o}_{f} versus alkylchain length, linear plots were obtained and $d(\Delta H^{o}_{f})/dn$ and $d(\Delta S^{o}_{f})/dn$ were calculated as approximately -2.0 $kJmol^{-1}$ and 5 $J\ mol^{-1}\ K^{-1}$ respectively[136]. Similar values of $d(\Delta H^{o}_{f})/dn$ = -1.50 $kJmol^{-1}$ and $d(\Delta S^{o}_{f})/dn$ = 11.2 $J\ mol^{-1}\ K^{-1}$ were obtained for ABDAC-SCG systems at 25°C [128,129].

The effect of substituents on the solubility of complexes has been examined by Mukhayer and Davies (substituted BTPC - SDDS systems)[138], Tomlinson and Davies (substituted ABDAC - SCG systems)[128], and Tomlinson et al (substituted phenothazines - SDDS systems)[135]. For the former system, the size of the cation (given by the molecular weight) was found to be a determining factor in the interaction[138]. A simple relationship did not, however, exist in the substituted ABDAC - SCG system; the presence of both methylene and chloro groups in the cation reduced K_s' but position of the chloro group and proximity to other chloro groups also influenced the interaction[128]. An excellent correlation between K_s' and the surface activity of the cations involved in the interaction, as measured by the CMC, was obtained, however. For five different systems, a linear relationship as expressed by equation 1.80 was found.

$$\log K_s' = A.\ \log CMC - B \qquad (1.80)$$

Where A and B are constants which have been determined as A = 3.16, B = 3.70 for ABDAC - SCG systems[128], A = 1.91, B = 3.06 for BTPC - SDDS systems[119], and A = 3.23, B = 6.26 for ABDAC - indigo carmine systems[119].

(c) Ionic Strength

Added electrolyte can greatly affect the stability of the complex coacervate phase[119,125,127,134]. In general, inorganic salts suppress coacervation and their effect increases with an increase in the valency of the inorganic ions[125]. Barry and Gray have shown that for tartrazine, amaranth and erythrosine - ATAB systems the extent of coacervation is decreased by the addition of salt[133]. However, coacervation in carmoisine-ATAB systems was increased upon addition of inorganic salts and a secondary coacervation area was observed in systems containing sodium citrate. Mukhayer and Davies[127] have investigated the effect of SDDS concentration on the solubility of BTPC-SDDS systems in the presence of added sodium chloride and found that the greater the concentration of SDDS in excess of the stoichiometric requirement, the less salt was required to supress coacervation. Complete supression of coacervation was obtained if sufficient salt was added; this was explained by charge screening of the interacting species causing a reduction in mutual attraction coupled with a lowering of the CMC of the system.

The effect of ionic strength on complex formation in the BTPC-SDDS system has been studied in terms of the solubility product of the system[134]. For uni-univalent ions such as in the BTPC-SDDS and cirazoline hydrochloride-SDDS systems, the intrinsic solubility product, K_s, may be expressed by equation 1.81 and 1.82.

$$K_s = (C_s \gamma_{\pm 0})^2 = (C_s' \gamma_{\pm i})^2 \qquad (1.81)$$

$$\log C_s' = \log C_s \gamma_{\pm 0} - \log \gamma_{\pm i} = \log C_s \gamma_{\pm 0} + AI^{1/2} \qquad (1.82)$$

Where C_s and C_s' are the concentrations of the large complexing ions at zero and at i concentrations of added electrolyte, and $\gamma_{\pm 0}$ and $\gamma_{\pm i}$ are

the mean ion activity coefficients at zero and i concentrations of added electrolyte. For the BTPC-SDDS system at 25°C and low ionic strength, (I<0.1 M), Mukhayer and Davis[134] found an approximately linear relationship between log C_s' and $I^{1/2}$ as predicted from equation 1.82. Above I = 0.1 M, however, solubility increased markedly more than predicted by equation 1.82 and this deviation was discussed in terms of:

(i) the large size of the ions and the high degree of hydration,

(ii) increased formation of BTP^+-DDS^-, BTP^+-Cl^- and DDS^--DDS^- ion-pairs at high ionic strength, and

(iii) micelle formation.

The authors summarised the effects of ionic strength on coacervate solubility by two separate processes; at low ionic strength, (I=<0.1 M), the activity coefficient decreases with increased electrolyte concentrations as predicted from the Debye-Hückel limiting law, (equation 1.14), and the complex is salted in; above I = 0.1 M aggregation of DDS^- monomers (micellization) occurs and the activity of the ions decreases markedly and the solubility of the complex shows a corresponding increase.

Strictly, the Debye-Hückel limiting law (equation 1.14) used in equation 1.82 is only valid at I < 0.01 M. However, this invalid approximation can not account for the observed increase in C_s' as at high ionic strengths (I = 0.1 - 1.0 M) $\gamma_\pm$ increases and may even become larger than unity (equation 1.19).

1.4.3 Micellar Binding of Oppositely Charged Organic Ions

1.4.3.1 ASSOCIATION CONSTANT

The association of an organic ion with an oppositely charged surfactant micelle may be defined by the equilibrium[90,139-142]:

$$X^+_{(aq)} + S^-_{(M)} \overset{K_A}{\rightleftharpoons} SX_{(M)}$$

and characterised by the association constant, K_A:

$$K_A = \frac{[SX_{(M)}]}{[X^+_{(aq)}][S^-_{(M)}]} \qquad (1.83)$$

Where $[SX_{(M)}]$ is the concentration of organic ion incorporated into micelles, $[X^+_{(aq)}]$ is the molar concentration of organic ion in water, and $[S^-_{(aq)}]$ is the concentration of micellized monomers of surfactant which are not bound to the organic ion, all expressed with respect to the total volume of the system.

The thermodynamics of the association process may be calculated using equations 1.84 - 1.86, where ΔG^o_A, ΔH^o_A and ΔS^o_A are the standard free energy, enthalpy and entropy change for the association process.

$$\Delta G^o_A = -RT \log_e K_A - RT \log_e 55.5 \qquad (1.84)$$

$$\log_e K_A = -\frac{\Delta H^o_A}{RT} + \frac{\Delta S^o_A}{R} - \log_e 55.5 \qquad (1.85)$$

$$\Delta G^o_A = \Delta H^o_A - T\Delta S^o_A \qquad (1.86)$$

The interaction between CTAB micelles and sodium p-toluenesulphate, sodium toluate, sodium benzenesulphonate and sodium phenylphosphate was investigated by Sepulveda using an UV absorption method which distinguished between free (or aqueous) and micellar bound anions[139].

Data were examined assuming that the micelles were composed of a certain number of sites each of which was accessible to one molecule of the corresponding anion. Results showed K_A values in the range 1.3 - 2.2 x 10^4 M^{-1} and the number of CTAB molecules per anion in the range 1.3 - 2.5.

In later studies transfer free energies for a variety of unionised, anionic and cationic benzene derivatives from water to CTAB[140,141] and SDDS[141] micelles were determined from K_A values. For a series of substituted phenols and phenoxide ions K_A values ranged from 0.026 - 0.43 x 10^4 M^{-1} for phenol to p-t-amylphenol and from 0.2 - 2.7 x 10^4 M^{-1} for their corresponding ions. The contribution of each methylene (or methyl) group to the free energy of transfer to CTAB micelles was calculated as -1.3 kJ mol^{-1} for both unionised and ionised species; the negative charge of the phenoxide ion was found to contribute -4.8 kJ mol^{-1} to the process. However, a recent comparison of binding constants for heterobi-, tri-and tetracyclic cations to SDDS micelles with those of the corresponding uncharged carbocyclic solubilzates showed that the difference between the neutral and charged compounds was small[142]. It was proposed that the opposing dual electrostatic effects of the positive charge which increases both water solubility and micellar interaction approximately cancelled, which resulted in no significant change in the value of the association constant[142].

The binding of alkylxanthates to CTAB micelles has been investigated in a comprehensive study by Sepulveda and Perez-Cotopoz[90]. The interaction was described by the solubility product, K_S, CMC and K_A. In the presence of precipitated CTAB-xanthate complex ($SX_{(C)}$) it was shown that the fraction (f) of total xanthate $[X]^T$ associated with micelles ($SX_{(M)}$)

is given by equation 1.87.

$$f = \frac{[SX_{(M)}]}{[X]^T} = \frac{K_A.K_S}{CMC.[X]^T}.[S]^T + \left(\frac{K_A.K_S}{CMC.[X]^T}\right)\left(\frac{K_S}{CMC} - CMC - [X]T\right) \quad (1.87)$$

Where $[S]^T$ is the total concentration of surfactant .K_A can therefore be calculated from the slope of a plot of f against $[S]^T$, providing $[SX_{(M)}]$, K_S and the CMC of the system are known.

Calculated K_S, CMC, and K_A values for CTAB - 1 x 10^{-4} M xanthate systems at 25°C are reproduced in table 1.3[90]. Free energies of transfer of xanthates from water to complex, (ΔG^o_f), and to CTAB micelles (ΔG^o_A), are also shown for each xanthate system. Increasing hydrophobicity of the alkyl xanthate ion results in a decrease in the CMC of the system and an increase in association constant (with the exception of methyl xanthate). The similarity in K_A (and ΔG^o_A) values for the lowest members of the series (methyl-propyl) was rationalized by considering the association of methyl and ethyl xanthates to be essentially electrostatic in nature and the hydrophobic contribution of the methyl and ethyl moieties is therefore minimal.

1.4.3.2 PHYSICOCHEMICAL NATURE OF IONIC SURFACTANT-ORGANIC ION AGGREGATES

Large organic ions of opposite charge often have a profound effect on the structure of ionic surfactant micelles. These interactions have been investigated by spectrophotometric, fluoresence, conductimetric, polarographic and stop-flow methods[143-148]. Abe et al[143] studied the binding of 4-phenylazo-1-naphthylamine with six sodium n-alkylsulphates and found the presence of 1.6 x 10^{-4} M dye reduced the CMC for each surfactant; e.g. the CMC of SDDS in the absence and presence of dye was reported as 8 x 10^{-3} and 2.1 x 10^{-3} respectively. Three distinct

XANTHATE	CMC $M \times 10^4$	K_s $M^2 \times 10^8$	ΔG^o_f $kJmol^{-1}$	K_A M^{-1}	ΔG^o_A $kJmol^{-1}$
-	8.0	-	-	-	-
Methyl	4.5	7.8	-30	768	-26
Ethyl	3.8	1.9	-32	675	-26
Propyl	2.0	-	-	904	-27
Butyl	1.1	0.16	-35	4108	-31
Amyl	0.4	-	-	19318	-34
Hexyl	-	0.0066	-39	-	-

Table 1.3 - Critical micelle concentration (CMC), solubility products (K_s), association constants (K_A), and transfer free energies of xanthates from water to solid CTAX (ΔG^o_f) and from water to CTAB micelles (ΔG^o_A) for each 1×10^{-4} M alkylxanthate - CTAB system at 25°C. (From Sepulveda and Perez-Cotopoz[90]).

processes were identified dependent upon SDDS concentration: (a) monomer complexation below the CMC of the dye-surfactant aggregate, (b) aggregation at surfactant concentrations between the dye-surfactant CMC and the CMC of the pure surfactant and, (c) aggregation at surfactant concentrations in excess of the pure surfactant CMC. Similar findings were reported by Sato et al[144] who investigated the interaction of 3,3'-diethylthiacarbocyanine iodide with SDDS; 1:1 aggregates and precipitate were formed at low SDDS concentrations or 'lower premicellar region'; an increase in SDDS concentration resulted in the formation of dye-rich induced micelles in the 'higher premicellar region'; further increases caused deaggregation of the dye due to dilution by SDDS and formation of ordinary micelles above the CMC. However, the CMC was not measured in the presence of the dye as this was assumed to have only a small effect on the CMC value. Similar conclusions were reached by Park and co-workers[145,146] in a study involving the interaction of methyl viologen and SDDS.

The rates of adsorption and absorption of positively charged dyes into anionic micelles of sodium alkylsulphates were investigated by Robinson et al[147,148] who proposed a two step mechanism; a very rapid diffusion controlled adsorption onto the micelle surface followed by slow intercalation or absorption into a more strongly bound site in the hydrocarbon interior of the micelle. A more recent study, however, concluded that the micellized site of dyes is close to the surface of SDDS micelles[206].

The effect of cationic surfactants on the size of SDDS micelles is varied. Almgren and Swarup [149,81] and Malliaris et al[150] found alkyltrimethylammonium bromide surfactants induced micelle growth the degree of which was dependent upon mole fraction of SDDS[150] whereas

symmetrical ions such as tetraalkylammonium and tetraphenylphosphonium ions have been reported to shrink micelles and act as spacers between the SDDS headgroups[81,149,151]. This latter effect is most marked with the most hydrophobic ion studied-tetraphenylphosphonium chloride - where 4.5×10^{-3} M and 16.6×10^{-3} M ion reduced the mean aggregation number of 5×10^{-3} M SDDS to 64.5 and 40.6 respectively at 20°C.

The effect of sodium tosylate (NaTOS) and sodium benzenesulphonate (NaBS) on the viscosity of CTAB micelles at 25°C was investigated by Gamboa and Sepulveda[152]. All systems exhibited non-Newtonian flow and relative viscosities were therefore calculated for zero flow rate. Relative viscosities increased with increasing CTAB concentration for both systems, e.g. for 5×10^{-2} M NaTOS, CTAB range 0.2 - 7×10^{-2} M, relative viscosities rose from 1.7 to 1×10^{5}. NaBS had a similar viscosity raising effect but to a lesser degree. The authors also demonstrated that if sufficient organic counterions were added to a micellar solution initially containing inorganic counterions, the micelle would finish up with only bound organic counterions and the system corresponded to a solution having the new micellar species, i.e. complete ion exchange. The viscosity raising effect of added sodium bromide was demonstrated by the addition of 5×10^{-2} M NaBr to 5×10^{-2} M CTA-TOS which increased the relative viscosity from 7×10^{3} to 1.6×10^{4} [152].

The high viscosities observed in these systems were interpreted in terms of micellar sphere-to-rod transition which occurs over a certain range of concentration of either surfactant or added salt. Axial ratios were calculated as 80, giving a rod length of 418 nm, for both CTAB-NaTOS and CTAB-NaBS systems. The transition was considered as coalesence of spherical micelles for which two negative and two

positive factors contributing to the free energy were identified. Negative contributions favouring coalesence arose from a decrease in the interfacial tension due to a decrease in micelle surface area and attractive van der Waals forces. Positive contributions inhibiting coalesence were due to the decrease in the number of kinetic particles which involved a decrease in the entropy of the system and repulsion of the head groups derived from their closer approximation in a cylindrical micelle. The second positive contribution could be diminished by increasing the ionic strength of the solution and/or by adding counterions that are strongly bound to micelles.

High viscosities and large micelle molecular weights in tetradecyltrimethylammonium bromide (TTAB) - sodium deoxycholates systems has been reported which is dependent upon mole percent of TTAB[126]. Such effects were not observed with TTAB - sodium cholate systems and it was concluded that the differences in micellar structure were due to the distribution of the hydroxyl groups on the steroid nucleus.

Davis et al[125] have recently reported the formation of viscoelastic gels in sodium saccharin - alkyltrimethylammonium bromide (SS-ATAB) mixtures. A rapid rise in viscosity occured at concentrations well above that necessary for the formation of a 1:1 complex which was explained by the formation of large rod-like micelles above the CMC of the system. The concentration of SS-ATAB at the critical viscosity point, CMC and onset of complex formation $(=(K_s)^{1/2})$ were all related to alkylchain length of surfactant, n, by equation 1.88.

$$\log C = a-bn \qquad (1.88)$$

Where C is concentration and a and b are constants for a given

concentration parameter. The contribution of the methylene group to micelle formation and complexation (obtained from b, equation 1.88) are identical indicating the similarity between the two processes.

1.5 SURFACTANT EFFECTS ON REACTION RATES AND EQUILIBRIA

The extensive literature regarding surfactant effects on reaction kinetics and chemical equilibria has been the subject of numerous reviews[118,153-160], recent examples are Attwood and Florence[41], Sudholter et al[161], Chaimovich et al[162] and Bunton[163]. Surfactant micelles are known to affect a diverse range of chemical reaction rates and may catalyse or inhibit reactions involving hydrolysis, oxidation, reduction, nucleophilic substitution, elimination, polymerisation, photochemical and electron transfer processes. The reaction pathway may also be influenced by the presence of surfactants and there are a number of examples of micellar control of reaction products and stereoselective synthesis[163,41,166]. In addition to producing kinetic effects, micelles may affect the equilibrium of chemical reactions and the term 'micellar catalysis' may therefore be regarded as somewhat incorrect as a 'true' catalyst must not shift the equilibrium to a considerable degree[165]. However, this term is much used in the literature and is useful because the surfactant is not utilized in the reaction and produces a marked effect on the reaction rate when added in low concentrations.

Reactivity in surfactant systems is of considerable pharmaceutical interest as optimization of surfactant type and concentration may enable stabilization of labile drugs and excipients and prevent unwanted interactions leading to destabilization of pharmaceutical products. The literature up to 1983 has been reviewed by Attwood and Florence and includes examples of micellar inhibited hydrolyses of

aspirin, indomethacin, chloramphenicol, procaine, p-aminobenzoate, p-aminophenylacetate, nicotinic acid esters, benzocaine and derivatives, homatropine, penicillin and cephalosporins[41]. Other recent examples include a five fold reduction in the rate of hydrolysis of indomethacin and related compounds by SDDS, (C_{16}TAB catalysed the reaction)[167]; inhibition of the acid catalysed hydrolysis of β-lactam antibiotics by polyoxyethylene-23 lauryl ether and CTAB, (SDDS catalysed the reaction[168]), pH dependent inhibition and catalysis of aspirin by CTAB and cetylpyridinium chloride[169], a mechanistic change in the acidic hydrolysis of diazepam by SDDS[166], and the inhibition of the base catalysed hydrolysis of cirazoline by sodium alkylsulphates[15,16], sodium dodecylethoxysulphates[16] and sodium polyoxyethylene sulphate[17].

Davies et al[15] investigated the rate modifying effect of SDDS on a 4×10^{-3} M solution of cirazoline hydrochloride at pH 7.0 and 40°C in the presence of McIlvaine's citrate-phosphate buffer (ionic strength = 0.5 M). Equimolar concentrations of cirazoline hydrochloride and SDDS resulted in the formation of an insoluble complex. Solubilization of this in excess SDDS above its CMC yielded marked stabilization; shelf lives, calculated for pH 4.6, increased from 18 weeks in the absence of surfactant to 8.7 and 14 years at concentrations of 3.0 and 6.0×10^{-2} M SDDS respectively.

In a later study, performed under similar experimental conditions, these workers investigated the effect of solubilization of cirazoline dodecylsulphate complexes in 10% PEG 400, 5% Tween 80, sodium alkylsulphates (C_{10} - C_{12}) and sodium dodecylethoxysulphates (E_2 - E_4) on the stability of cirazoline[16]. Solubilization by 10% PEG and within the non-ionic micelles of Tween 80 had no effect on the rate of

hydrolysis of cirazoline. The degree of stabilization afforded by solubilization in excess SDDS was found to be a function of both cirazoline and SDDS concentration. For 5×10^{-4} M cirazoline hydrochloride, no effect was observed at SDDS concentration at or below 1×10^{-3} M, indicating the absence of premicellar stabilization of the drug-surfactant complex (CMC = 4.5×10^{-4} M)[16]. At SDDS concentrations between $5.0 - 7.5 \times 10^{-3}$ M, marked stabilization occurred, the magnitude increasing with surfactant concentration (figure 1.11a). At higher concentrations of cirazoline hydrochloride (4×10^{-3} M) a similar stability-SDDS cocentration profile was produced except that the curve was shifted to higher SDDS concentrations due to an increase in the CMC of the system (figure 1.11a).

The effect of alkylsulphate chain length on cirazoline stabilization is shown in figure 1.11b[16]. For a given surfactant concentration the stabilizing effect was found to increase with increasing chain length which was explained in terms of changes in the CMC, micellar partitioning, aggregation number and complex association constants. A linear relationship was observed between the stabilizing factor and alkylchain length for a given concentration of surfactant[16].

The hydrophilic nature of sodium dodecylethoxysulphate surfactants (Empicols and Texapon ASV) was also investigated. A linear relationship with negative slope was obtained between the stabilization factor and number of ethylene oxide groups, reflecting the increase in CMC together with a decrease in micellar partition and complex association constants with increasing hydrophilic properties of the surfactants[16].

The stability of cirazoline hydrochloride (4×10^{-4} M) in the presence of 1.2×10^{-2} M sodium polyoxyethylene sulphate (E = 4) at pH 7 was

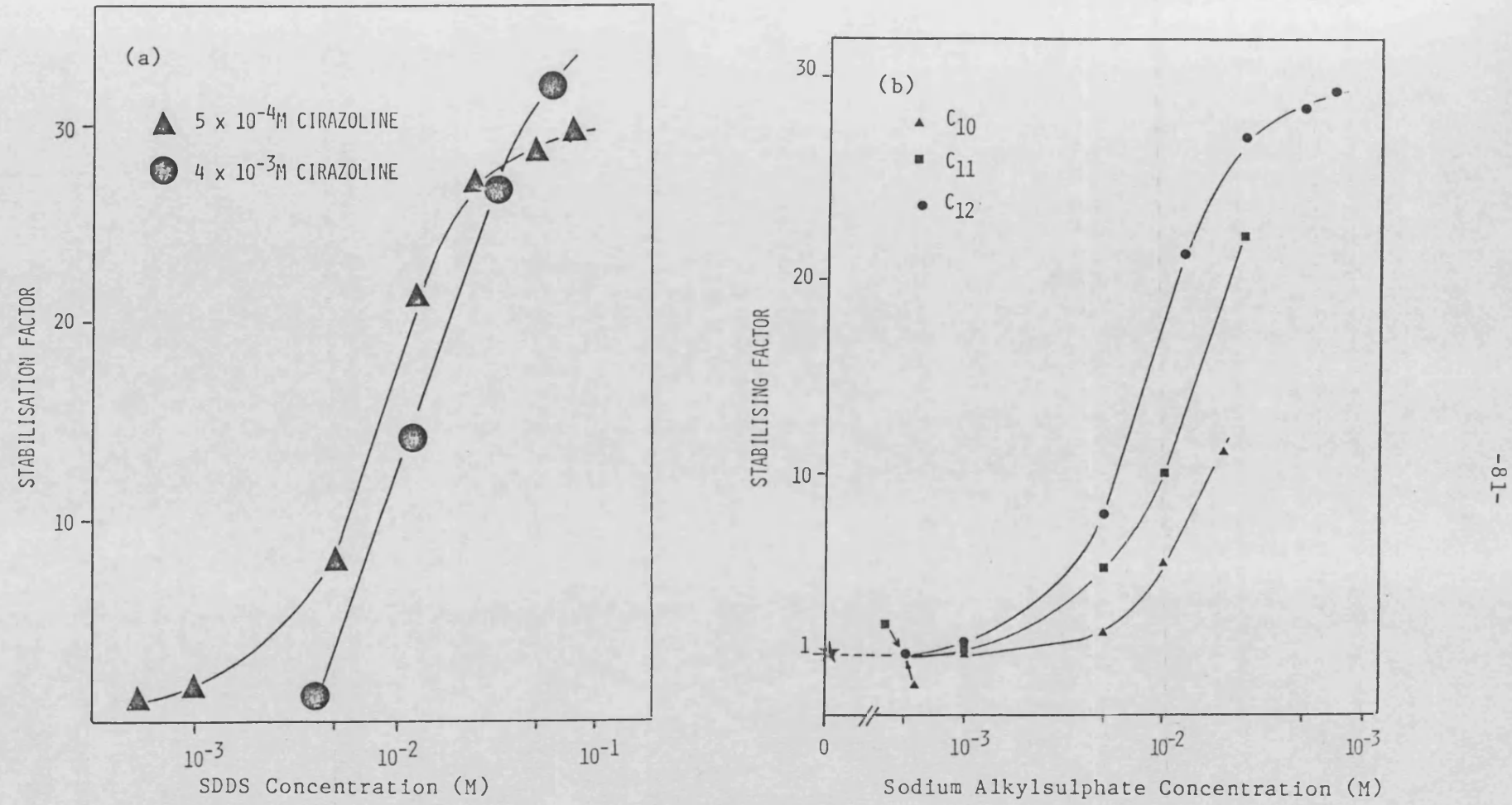

Figure 1.11 - Effect of sodium alkylsulphate concentration on the stabilization factor ($k_{(aq)}/k_{SDDS}$) for the hydrolysis of cirazoline hydrochloride at 40°C, pH 7.0, MacIlvaines buffer, ionic strength = 0.5M , (a) 5 x 10^{-4} and 4 x 10^{-3} M cirazoline hydrochloride in the presence of SDDS, and (b) 5 x 10^{-4} M cirazoline hydrochloride in the presence of sodium alkylsulphates (C_{10} - C_{12}), (from Stroud et al[16]).

also studied by Fedynec et al[17]; a mean stability factor of 4.0 was reported which was independent of temperature (22 - 50°C).

1.5.1 Mechanism of Micellar Effects on Reaction Rates

The interface formed at the ionic headgroups of micelles in the presence of a surrounding aqueous environment provides an unusual microenvironment in which chemical reactions may occur[118]. The mechanism of micellar effects on chemical reaction rates may be rationalised in terms of medium (or polarity) effects and proximity effects[165].

1.5.1.1 MEDIUM EFFECTS

Micelles have solvent properties different from those of water (section 1.3.1.1), e.g. they are less polar and therefore rate constants in the micellar environment could be different in accordance with dielectric constant changes[163], (section 1.1.2(d)). In addition the mutual orientation of the reactants in the micelle may influence the rate of reaction. These effects are difficult to quantify for bimolecular processes such as hydrolysis reactions, however, spontaneous unimolecular reactions provide a means of investigating reaction rates in micelles; e.g. anionic decarboxylations, arylsulphate anion decompositions and arylphosphate dianion decomposition reactions are slower in water than in less polar solvents and micellar catalysis at the surface of both cationic and nonionic micelles is observed[156,164]. (Anionic micelles have no effect on these reactions probably because the negatively charged substrates remain in the aqueous phase). In contrast $S_{N}1$ reactions are much faster in water than in less polar solvents and micellar inhibition is observed[156].

Comparison of aqueous $k^2_{(aq)}$, and micellar, $k^2_{(M)}$, bimolecular (2nd order) reaction rate constants is complicated by the need to assess a volume element for reactions within the micellar pseudophase; this is usually taken as the Stern layer because the micelle surface is the assumed reaction site for most micelle catalysed reactions.

Reported results indicate that micelles may have a catalytic effect, (i.e. $k^2_{(M)} > k^2_{(aq)}$, e.g. the reaction of azide ion with 2,4-dinitrochloronaphthalene, $k^2_{(M)}/k^2_{(aq)} = 400$); an inhibitory effect, (i.e. $k^2_{(M)} < k^2_{(aq)}$, e.g. acid catalysed benzidine rearrangment); or no significant effect, (i.e. $k^2_{(M)} \simeq k^2_{(aq)}$, e.g. the alkaline hydrolyisis of carboxylate or phosphate esters), on bimolecular reaction rates[164]. Published results for micellar effects on bimolecular reactions have recently been summarised by Romsted[164].

1.5.1.2 PROXIMITY EFFECTS

Proximity effects result from micelles bringing reactants together or by keeping them apart. The contribution of these effects is largely determined by the extent of the ionic (coulombic) and hydrophobic interactions between the reactants and the micelles.

In 1934 Hartley proposed a set of rules to predict the expected direction of micellar effects on the apparant pK_a (pK_a') shifts of acid-base indicators[170]. Anionic micelles should attract hydrogen ions from bulk solution and therefore increase the extent of protonation of solubilized weak bases and decrease the dissociation of solubilized weak acids. Conversely, cationic micelles should repel hydrogen ions and therefore have opposite effects to anionic micelles. The importance of these coulombic effects on the interaction between ionic micelles and reactive ions was recognised many years ago; for example

the rate of reaction of a variety of hydrophobic substrates with nucleophiles was increased by cationic surfactants because the micelles could incorporate both substrate and the reactive nucleophile[156]. These reactions were inhibited by anionic surfactants because the micelles incorporated the substrate but repelled the reactive nucleophile.

1.5.2 Factors Affecting Micellar Catalysis and Inhibition

For most systems the presence of surfactant micelles is necessary before substantial rate effects are observed. Hence factors which govern the amount and nature of the micellar pseudophase and the association of substrate(s) to the micelles also affect the extent of stabilization or catalysis (see sections 1.3.1.3, 1.3.2.4 and 1.4.3). However, surfactant and substrate structure, charge and the presence of additives, (particularly electrolytes), are also of fundamental importance.

1.5.2.1 SURFACTANT AND SUBSTRATE STRUCTURE

The nature and degree of the rate modifying effects due to the presence of surfactant micelles are difficult to predict. The coulombic and hydrophobic interactions which control micellar catalysis and inhibition are illustrated by the data in table 1.4, (from Bunton[157]). Coulombic interactions are evident but hydrophobic interactions are also important as shown by the effect on some reactions by non-ionic micelles. In general, for bimolecular reactions involving at least one charged species coulombic factors are of prime importance and the most potent effects are observed using ionic surfactants, (e.g. the base catalysed hydrolysis (saponification) of carboxylic esters, table 1.4.

Substrate	Reagent	Surfactant		
		Cationic	Anionic	Nonionic
Carboxylic ester[a]	OH^-	Catalysis	Inhibition	No effect
RCO.O--NO_2		Catalysis	Catalysis	
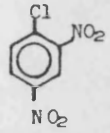	OH^-	Catalysis	Inhibition	No effect
$(PhO)_2PO.O$--NO_2	F^-	Catalysis	Inhibition	Inhibition
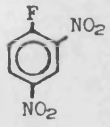	$PhNH_2$	Catalysis	Catalysis	Catalysis
XCH_2-CO.O--NO_2 [b]	OH^-	Catalysis		
$ArC(OMe)_3$	H^+, H_2O	Inhibition	Catalysis	

[a] Saponification by the $B_{Ac}2$ mechanism.

[b] Reaction by E1cB mechanism with formation of a ketene intermediate when X is strongly electron withdrawing.

Table 1.4 - Micellar catalysis and inhibition of some bimolecular reactions, (from Bunton[157]).

Reddy and Katiyar[171,184] investigated the effect of hydrophobic and coulombic interactions by studying the influence of a non-ionic surfactant, (Brij 35), and a series of cationic, (C_9TAB - C_{16}TAB), and anionic, (SOS-STDS), surfactants of increasing n-alkylchain length on the reaction of ethylviolet (EV^+, 9 x 10^{-6} M) with hydroxide ion. C_9TAB and C_{10}TAB exhibited negligible effects whereas C_{12}TAB - C_{16}TAB catalysed the reaction with 2 x 10^{-3} M OH^-, the extent of which increased with increasing alkylchain length. Anionic micelles strongly inhibited the reaction with 0.2 M OH^- and all alkylsulphate surfactants studied produced a similar maximal degree of rate retardation , associated with complete incorporation of EV^+ within the anionic micelles. The concentration of surfactant required to inhibit the reaction decreased with increasing alkyl chain length, however, (figure 1.12). Brij 35 micelles catalysed the reaction the degree of which increased with increasing concentration of hydroxide ion, (2 - 7 x 10^{-3} M).

The extent of catalysis by C_{16}TAB was correlated to the structure of the substrate; the more hydrophobic the substrate the greater the degree of catalysis. These results were discussed in terms of hydrophobic forces overcoming the unfavourable electrostatic force.

1.5.2.2 ELECTROLYTE

Added salts with non-reacting ions generally reduce the degree of micellar catalysis or inhibition of bimolecular reactions involving ionic reactants due to competition for micelle binding sites between the reactive ions and the added unreactive ions. Peturbation of micellar structure especially with hydrophobic counterions may also be important.

Added counterions significantly inhibited the $C_{16}TAB$ catalytic effect on reactions of EV^+ with OH^- at 3×10^{-3} M surfactant[171], the effectiveness being a function of the charge density:

$$NO_3^- > Br^- > Cl^- > SO_4^{2-} > CH_3CO_2^- > F^-$$

Similar effects were observed for the acid hydrolysis of trimethylorthobenzoate in anionic micelles where the degree of inhibition followed the order[153]:

$$R_4N^+ > CS^+ > Rb^+ > K^+ > Na^+ > Li^+ > \text{no salt}$$

Incorporated ions and buffers complicate the analysis of micelle catalysed reactions since they may act as general acid-base catalysts and also produce changes in the properties of micelles[172]. The effect of sodium hydroxide and borate, carbonate/bicarbonate and triethylamine/triethylammonium chloride buffers on the hydrolysis of N-methyl-N-(4'-nitrophenyl)-2-phenoxyacetamide at 65.5°C in the absence and presence of micelles of cetytrimethylammonium bromide (CTAB) was studied by Broxton[173]. The magnitude of catalysis was shown to be dependent on the buffer system used, the concentration of detergent, the concentration of buffer, the pH and the presence of added salts.

The effect of the nature and concentration of buffers on the base hydrolysis of p-nitrophenylcarboxylates catalysed by CTAB at 25°C was measured by Funasaki[172]. The rate constant-buffer concentration profile depended markedly upon the type of buffer and the following effects were noted:

(i) an increase in micellar concentration resulting from a decrease in CMC.

(ii) an incorporation of the base components of the buffers, (e.g. carbonate ion) into the micelles which act as catalysts.

(iii) an increase in bulk rate constant.

(iv) a decrease in surface hydroxide ion concentration with increasing ionic strength.

(v) a decrease in surface hydroxide ion concentration resulting from a decrease in the surface charge density which is brought about by penetration of the base components of buffers into micelles.

1.5.3 Quantitative Treatment Of Micellar Rate Effects - The Pseudophase Model

Micellization and micellar structure have been discussed in terms of various models (see section 1.3.1) but for kinetic studies it is most convenient to use the pseudophase model, i.e. a micelle is regarded as a submicroscopic aggregate which behaves as if it were a separate reaction medium with its own properties. Reactions may then be regarded as occurring in either the aqueous or the micellar pseudophase with reactants being rapidly equilibrated between the two. The quantitative estimation of micellar catalysis and inhibition is therefore dependent upon a knowledge of the distribution of reactants between aqueous and micellar pseudophases and calculation of the rate constants of reaction in each pseudophase.

1.5.3.1 MENGER AND PORTNOY ENZMYE MODEL[174]

Early work was pursued in the hope that micelles might function as simple models for enzymes[175]. The first real proposal of a general model for the quantitative analysis of micellar effects on reaction kinetics was the Menger and Portnoy Enzyme Model[174]. This model

assumes simple pseudophase partitioning of a single substrate, independent reactivity in the two pseudophases, a constant surfactant monomer concentration (equal to the CMC), absence of complexation between the substrate and surfactant monomer, and non-perturbation of micellization by the substrate.

The equilibrium distribution of a substrate, X, between the micellar and aqueous pseudophases can be described by:

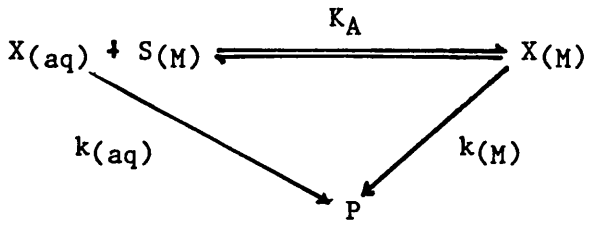

Where $X_{(aq)}$ and $X_{(M)}$ represent the substrate in the aqueous and micellar pseudophases respectively, $S_{(M)}$ is surfactant monomer in the micellar pseudophase, K_A is the substrate association constant, (defined by equation 1.83 or, alternatively written in terms of the concentration of micelles = $[S_{(M)}]/_N$, where N is the aggregation number), P is the reaction product and $k_{(aq)}$ and $k_{(M)}$ are the first order rate constants in the aqueous and micellar pseudophases respectively. The rate equation is given by equation 1.89:

$$\frac{d[P]}{dt} = k_{(aq)}[X_{(aq)}] + k_{(M)}[X_{(M)}] \qquad (1.89)$$

The overall observed first order rate constant, k_{obs}, is then given by equations 1.90 and 1.91 which have the same general form as the Michaelis-Menton and Lineweaver-Burke equations of enzyme kinetics respectively:

$$k_{obs} = \frac{k_{(aq)} + k_{(M)} K_A ([S]^T - CMC)}{1 + K_A ([S]^T - CMC)} \qquad (1.90)$$

$$\frac{1}{k_{(aq)} - k_{obs}} = \frac{1}{k_{(aq)} - k_{(M)}} + \frac{1}{(k_{(aq)} - k_{(M)})\, K_A\, ([S]^T - CMC)} \qquad (1.91)$$

Where $[S]^T$ is the total concentration of surfactant. K_A values determined kinetically for some micellar inhibited reactions agree reasonably well with those determined directly and for hydrophobic substrates are similar in magnitude to enzyme-substrate binding constants[157].

This model was originally applied to describe the micelle inhibited saponifation of 4-nitrophenylalkanoates in the presence of sodium laurate[174]. Menger and Portnoy concluded that $k_{(M)}$ for this reaction was within experimental error of zero. However, Quina and co-workers recently measured the extent of micellar inhibition of the alkaline hydrolysis of both long chain N-alkyl-4-cyanopyridinium ions and p-nitrophenylalkanoates[176] and concluded that the hydroxide ion reacts with the substrate within the micellar pseudophase and not just with unbound substrate in the aqueous phase.

This simple model has been applied successfully to micellar catalysed unimolecular reactions and to many micellar inhibited reactions when $k_{(aq)} >> k_{(M)}$. However, it fails to predict;

(a) the observed maximum in rate constants with increasing surfactant concentration for many micelle catalysed reactions;

(b) the effect of increasing unreactive hydrophilic electrolyte on reactions between charged substrates within ionic micelles[175].

For such reactions, the distribution of both reactants must be considered[157].

1.5.3.2 BEREZIN MODEL[165]

The limitations of the enzyme model led Berezin and co-workers to develop a much more general model which, in addition to the basic assumptions of the enzyme model[174], assumed that all substrates undergo independent pseudophase partitioning. Their model is valid for reactions involving only uncharged substrates in the presence of ionic surfactants and for most reactions carried out in the presence of non-ionic detergents[162]. However, for reactions involving ionic substrates in the presence of ionic detergents the assumption of simple pseudophase partitioning proves to be inadequate. Whilst the binding of organic substrates can be described by a simple partition (or association) constant, this approach cannot be used for the binding of hydrophilic ions to the surface of the micelle[162].

1.5.3.3 PSEUDOPHASE ION EXCHANGE MODEL[175,164]

Romsted extended the pseudophase model, retaining the fundamental assumptions of the Berezin model but treating the partitioning of hydrophilic ions in an entirely different fashion. The Stern layer of the micelle was considered to be saturated with respect to counterions, comprising a mixture of attacking ions, (Y), and inert ions (Z). These separate species were assumed to partition between the micellar Stern layer and the aqueous phase in accordance with an ion exchange equilibrium, (equation 1.92)[175,164,162]:

$$Y_{(aq)} + Z_{(M)} \rightleftharpoons Y_{(M)} + Z_{(aq)}$$

$$K_{Y/Z} = \frac{[Y_{(M)}][Z_{(aq)}]}{[Y_{(aq)}][Z_{(M)}]} \qquad (1.92)$$

Where the subscripts (aq) and (M) refer to the aqueous and micellar pseudophases respectively and $K_{Y/Z}$ is the ion exchange selectivity constant.

Using these assumptions, Romsted derived expressions that permit analysis and prediction of kinetic behaviour for several reaction types in micellar solution, including the effect of added inert salt on reaction rates[175]. The observed overall second order rate constant, k^2_{obs} was shown to be given by equation 1.93 [175]:

$$k^2_{obs} = \frac{k_{(M)}\ \beta\ K_p\ ([S]^T - CMC)\ D}{(K_p\ ([S]^T - CMC) + 1)([Y]^T - [Z]^T\ K_{Y/Z})} + \frac{k_{(aq)}}{K_p\ ([S]^T - CMC + 1)} \qquad (1.93)$$

Where β is the degree of counterion association (= constant) and D is the molar density of the micellar pseudophase in moles litre^{-1}.

The distribution of an uncharged organic substrate is described by a partition constant, K_p, (see section 1.3.2). If the substrate is a hydrophobic ion of opposite charge to the micelle then it should in theory be treated as an exchangeable ion. However, these ions bind strongly and their interactions with the micellar pseudophase may be described by a simple association constant[164], K_A, (see section 1.4.3.1), similar to that for neutral substrates. Association constants may be determined by a variety of techniques (e.g. solubility) or by selecting the value which gives the best fit to the kinetic data[164].

Modifications to the pseudophase ion exchange model have been put forward by Chaimovich and co-workers[162,177-179] and Berezin[165]. Quina et al have recently investigated the binding of OH^- to SDDS micelles and the effect of addert inert electrolyte (NaCl) on the rate of base

catalysed hydrolysis of N-aryl-4cyanopyridinium ion and p-nitrophenylalkanoate[176]. For totally bound substrate in a pH controlled system, a modified ion exchange formalism predicted the experimentally determined linear dependence of the observed first order rate constant, k_{obs}, on the concentration of added inert salt (NaCl), i.e. $k_{obs} \alpha C_Z$ [176].

1.5.3.4 LIMITATIONS OF THE PSEUDOPHASE MODELS

The pseudophase models assume that the substrate does not complex with surfactant monomer and that the substrate does not perturb micellization. These assumptions are not normally valid at low surfactant concentrations, particularly when the reactants and/or counterions are hydrophobic, and the simple pseudophase and ion exchange pseudophase models usually fail to predict observed behaviour in the CMC region[164]. Changes in the structure of micelles at higher surfactant concentrations may also result in the failure of pseudophase models[183]. Although the ion exchange model has been shown to correctly interpret the effect of substrate charge and chain length, buffers, pH and specific salt effects, it fails to describe the catalytic properties of cationic surfactants with reactive hydrophilic counterions such as OH^- or F^-[163,164]. The reason for this failure is not known although Romsted has postulated that one or more of the pseudophase assumptions is not valid, e.g. cooperative micelle formation and/or constant counterion binding[164].

1.5.4 Non-Micellar Surfactant Effects

With hydrophobic reactants, rate effects are often observed at surfactant concentrations below the CMC in water which could be caused by reactant-induced micellization or to reaction in sub-micellar

aggregates[163]. One example where monomeric surfactant may have been able to affect the rate of a chemical reaction is given by the reaction of triphenylmethane dyes with hydroxide ion (figure 1.12). Reddy and Katiyar[171] have reported a marked inhibition of the reaction in the presence of very low concentrations of alkylsulphate surfactants which they ascribed to the formation of sub-micellar aggregates (see section 1.3.1). However, an ion-pairing mechanism whereby alkylsulphate ions compete with hydroxide ions for the carbonium ion reactive site is a more probable explanation of the inhibition. Ion-pairing would also account for the effect of surfactant chain length on the reaction; the ion-pair association constant, K_{ip}, is a function of the hydrophobicity of the interacting ions (see section 1.4.2) and the higher alkylsulphate homologues would therefore be expected to interact more strongly with the cationic carbonium ion. At higher surfactant concentrations, solubilization by alkylsulphate micelles is probably the primary mechanism of inhibition.

Tomlinson et al[180] have suggested that for systems whereby the degrading species is ionised and the surfactant is of opposite electrical charge, then complexation between the two ions may be the prime stabilization mechanism. These workers presented theoretical and experimental treatments for the interaction between the cholinesters, acetylcholine chloride, and propionyl, butyl, myristyl and succincyl choline iodide with a series of alkylsulphates and demonstrated a relationship between ester hydrolysis half-life and the solubility product of the complex. The treatment presented predicted:

(i) the stability of the charged solute should increase linearly with an increase in alkylchain length of either ion;

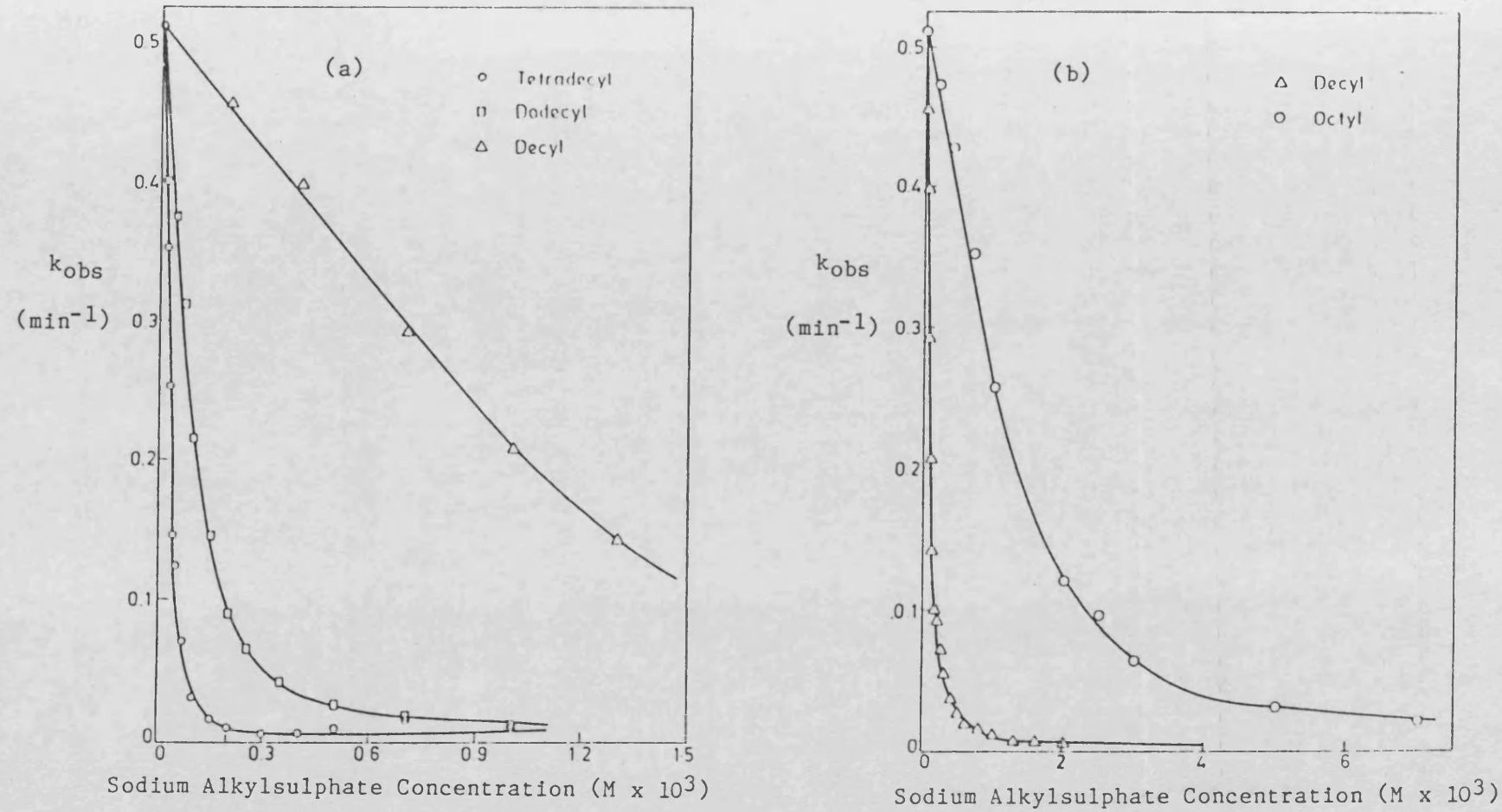

Figure 1.12 - Variation of the observed first order rate constant, k_{obs}, with concentration of sodium alkylsulphates for the reaction of ethylviolet (9×10^{-6} M) with OH^- (0.2 M), (a) sodium tetradecyl-, dodecyl-, and decylsulphates and (b) sodium decyl- and octylsulphates, (from Reddy and Katiyar[171]).

(ii) the stability should increase with increased concentration of surfactant;

(iii) an alteration in K_s should be reflected in a change in solute stability.

The stabilizing effect due to (i) and (ii) was demonstrated using data reported by Nogami for acylcholinester-SDDS and acetylcholine sulphate-SDDS systems[181]. In addition the decrease in stabilizing effect reported by Nogami[182] for methylene bromide-SDDS systems at 70°C upon increase in ionic strength was cited as an example of the effect of environmental changes on K_s ((ii), above). The authors argued that the increase in ionic strength should depress the CMC of the system thereby resulting in greater protection if micellar stabilization was the mechanism of protection against degradation. The K_s' of alkylsulphate-acetylcholine ester systems was shown to increase with increase in ionic strength and the complexation theory presented was used to explain the above results. However, the effect of electrolyte on the ability of ionic micelles to modify reactions between interacting ions (see section 1.5.2.2) was not taken into account in this treatment and it is this mechanism which is most likely to determine the observed reaction rate. Also, as these systems represent solubilized acylcholinesters in the absence of complex, it is more valid to consider micelle association constants rather than the solubility product which effectively describes the equilibrium between complex and aqueous phases.

2. MATERIALS AND METHODS

2.1 MATERIALS

2.1.1 Equipment

2.1.1.1 GLASSWARE

Grade A or B analytical glassware was used according to availability.

2.1.1.2 BALANCES

(i) Oertling R20 single pan

Maximum weight capacity : 200 g

Minimum division : 1 mg

(ii) Oertling TP31 single top pan

Maximum weight capacity : 220 g

Minimum division : 10 mg

2.1.1.3 ANALYTICAL EQUIPMENT

(i) Perkin Elmer 550S UV-VIS double beam spectrophotometer in conjunction with Perkin Elmer 561 recorder.

(Bodenseewerk Perkin Elmer & Co. GMBH, Uberhagen, W.G.)

Range : 195 - 750 nm

Wavelength accuracy: $\pm$ 0.5 nm

Wavelength reproducibility: $\pm$ 0.2 nm

Photomeric accuracy: $\pm$ 0.005A at 1A

Photomeric reproducibility: $\pm$ 0.002A at 1A

(ii) Jeol JNM GX 270 NMR spectrometer.

(iii) DuPont 910 differential scanning calorimeter with DuPont 9900 computer/thermal analyser.

(DuPont Company, Quilen Building, Wilmington, Delaware, U.S.A.)

Sample size : 0.5 - 100 mg

Temperature range: 170 to 600°C

Temperature reproducibility: $\pm$ 0.1°C

Calorimetric sensitivity : 6 μWcm^{-1} (RMS)

Calorimetric precision : 1%

Baseline stability : 20 μW

Thermocouples -	differential	chromel -constantan
	sample	chromel - alumel
	control	Plantinel II

(iv) HPLC

(a) Haskel pneumatic column packer

(Haskel Ltd., North Hylton Rd., Sunderland)

(b) SP1800 Liquid Chromatograph

(Spectraphysics Ltd., 17 Brick Knoll Park, St. Albans, Herts.)

Fitted with:

SP8110 Autosampler

SP9500 Communication interface device

SP8440 Variable wavelength detector (190 - 600 nm)

SP4100 Computing integrator

2.1.1.4 pH EQUIPMENT

(i) Phillips digital pH meters

	PW9410	PW9421
Display :	3½ LED	4½ LED
Range :	0 - 14.0 pH units	± 19.999 pH units
Resolution :	0.01 pH units	0.001 pH units
Instrument accuracy :	< 0.02 pH units	0.001 pH units
Temperature stability :	0.002 pH/K	0.001 pH/K
Isopotential point :	7.00 pH	7.00 pH

(ii) pH electrodes

(a) Phillips CAH 11 high temperature combined glass-silver/silver chloride electrode.

pH range : 0 - 14 pH units

Temperature range : 0 - 130°C.

(b) Phillips CE 1 combined glass-silver/silver chloride electrode.

pH range : 0 - 12 pH units

Temperature range : 0 - 70°C

(c) Radiometer 405-60 high temperature combined glass-silver/silver chloride electrode.

pH range : 0 - 12 pH units

Temperature range : 10 - 100°C

(iii) Radiometer pH stat assembly

(Electronic measuring instruments, Copenhagen, Denmark).

Accuracy of assembly : ± 0.05 pH

(a) TTT60 titrator

Accuracy : ± 0.02 pH (± 2 mv)

Stability : ± 0.1% (within ± 10°C temperature variations and ± 10% line voltage variation)

(b) ABU12 autoburette

Burette assembly type B220 (2.5 ml volume)

Accuracy : ± 2.5 µl ± 0.5%

Titrant flowrate : adjustable during titration from 1.25 to 160% of total burette volume min^{-1}.

(c) PHM61 pH meter

Range : 0 to ± 14 pH units (division 0.1 pH units)

0 to ± 1400 mv (division 10 mv)

Repeatability : ± 0.01 pH (1 mv)

Accuracy (25°C) : ± 0.03 pH

2.1.1.5 CONDUCTIMETRY

(i) Wayne Kerr B642 autobalance universal bridge

(Wayne Kerr Company Ltd., New Malden, Surrey).

Frequency : internal source/detection 1591.5 ± 0.5 Hz ($\omega = 10^4$)

Range : Conductivity 1×10^{-11} - 1×10^5 S

Resistance 1×10^{-5} - 1×10^{11} ohm

Capacitance 1×10^{-15} - 10 F

Inductance 1×10^{-9} - 1×10^7 H

Accuracy : ± 0.1% at 1591.5 Hz

Output : 0 - 100 mV from conductivity and capacitance meter circuits

Ambient temperature range : 0 - 40°C

(ii) Mullard E7591B dip-type conductivity cell

Nominal cell constant : 1.44

(iii) Servagor 120 Y-time recorder

(Gorez Metrawatt)

Recording width : 250 mm

Scale : 0 - 100 linear, 20 division

Chart speeds : 6 chart speeds - 3, 12, 60 cm min^{-1}or hr^{-1}

Range : 2, 5, 10, 20, 50, 200, 500 mV F.S.D.

(iv) Model 34/A syringe pump

(Sage Instruments, 540 Memorial Drive, Cambridge, U.S.A.)

Nominal flow rate range (5 ml syringe) : 1.2×10^{-3} -

2.7 mls min^{-1}

(v) Hamilton precision 5 ml gas tight syringe

(Bonaduz AG, P.O. Box 26 CH7402 Bonaduz, Switzerland).

2.1.1.6 PARTICLE SIZE ANALYSER

Coulter N4 MD sub-micron particle analyser with size distribution, processor analysis and multiple scattering angle detection. (Counter Electronics Ltd., Northwell Drive, Luton, Beds, LU3 3RH).

Sample particle size range :	3 to 300 nm
Sample molecular weight range :	10^4 - 10^{13} Daltons
Unimodal analysis reproducibility :	3% cv
Laser :	4 mW helium - neon (632.8nm)
Optics :	fibre optics located at 15.2, 21.1, 13.2, 41.9, 51.8 and 90°.
Temperature range :	0 to 90°C $\pm$ 0.2°C.

2.1.1.7 MISCELLANEOUS

(i) Water baths

(Grant Instruments, Barrington, Cambridge).

(a) Grant shaking water bath.

Shaking rate range : 20 - 200 min^{-1}

Temperature range : 0 - 80°C

(b) Grant heater stirrer type SU6 (in conjunction with Grant water bath).

Adjustable control thermostat range 0 to 80°C.

(ii) Magnetic stirrer/heater

(Rodwell Scientific Instruments, Brentwood)

(iii) Travelling vernier microscope

(Precision Tool and Instruments Co., Thornton Heath, Surrey).

(iv) Agla micrometer syringe outfit

(Wellcome Reagents Ltd., Beckenham, Kent).

Micrometer and Syringe (0.5 ml luer fitting) fitted with straight glass needle.

Accuracy : 5×10^{-5} at 0.01 ml increment.

(v) Buchi Rotavapor R110

(vi) Bath cooler (U-cool)

(Meslab Instruments Inc., Portsmouth N.H., U.S.A.)

(vii) Vacuum Oven

(viii) Filtration Units

Swinnex 25 mm filter holder in conjunction with Whatman cellulose nitrate membrane filters (25 mm), 0.45 μm pore size.

2.1.2 Chemicals

All chemicals other than imidazoline drugs used in this study were of AnalaR Grade (BDH Chemicals Ltd., Poole, England), or AR Grade (Fisons, Loughborough, England); with the exception of the following:

Apovincamine N-(cyclopropyl-2-phenoxy-acetyl) ethylene diamine (II) hydrochloride (CPAE hydrochloride	) Gifts from Synthelabo, 58 rue de la Glaciere, Paris, France.

Sodium dodecyl sulphate	Primar Grade	
Octan-1-ol	Puriss	) Koch Light Ltd., Haverhill, Suffolk.
Decan-1-ol	Hipure	
Tetradecan-1-ol	Genlab	
Acetonitrile Methanol Hexane Isopropanol		) HPLC Grade - Fisons, Loughborough, England.
Ethanol (absolute)		Burroughs
Sulphuric acid, 96%	Technical Grade	- Fisons, Loughborough, England
Sodium dichromate	Technical Grade	- Fisons, Loughborough, England
Soda Lime (4 - 10 mesh)	Lab. Reagent	- BDH Ltd., Poole, England
Silica gel (1-3 mm)	Lab Reagent	- Fisons, Loughborough, England

Glass wool	'Low in lead'	- BDH Ltd., Poole, England
1.0 M HCl solution	Convol	- BDH Ltd., Poole, England
1.0 M NaOH solution	Convol	- BDH Ltd., Poole, England

2.1.2.1 IMIDAZOLINES

Cirazoline hydrochloride and fenoxazoline hydrochloride were gifts from Synthelabo (58 rue de la Glaciere, Paris, France). Tolazoline hydrochloride, naphazoline nitrate, xylometazoline hydrochloride, and antazoline sulphate, were gifts from CIBA Laboratories, Horsham, West Sussex, England. 2-methyl-2-imidazoline was obtained as 'Genlab Grade' from Koch Light Ltd., Haverhill, Suffolk. All samples except cirazoline hydrochloride were used as received. 2-methyl-2-imidazoline was observed to contain high levels of moisture (estimated at 10%, see section 3.2); attempts to dry samples proved difficult and the material was therefore, used as received.

Purification of Cirazoline Hydrochloride

Samples of cirazoline hydrochloride were recrystallised twice from ethyl acetate : ethanol (3:1). Anhydrous cirazoline hydrochloride was used throughout the study and was prepared by drying purified samples to constant weight at 50°C, 900 mBar reduced pressure with silica gel desiccant. Samples were stored at ambient temperature over silica gel in a desiccator to prevent moisture uptake.

Characterisation

Samples of all imidazolines were characterised by HPLC and ultra-violet (UV) and nuclear magnetic resonance (NMR) spectroscopy. Purified, anhydrous cirazoline hydrochloride samples were also examined by differential scanning calorimetry (DSC) and infra-red spectoscopy (IR). UV spectroscopy gave the following absorption maxima (nm):

Cirazoline hydrochloride	275
2-methyl imidazoline	218
Tolazoline hydrochloride	256, 262
Naphazoline nitrate	270, 281, 288, 291
Xylometazoline hydrochloride	264
Antazoline hydrochloride	241, 292
Fenoxazoline hydrochloride	268, 274

These values are in good agreement with literature values (table 1.1). NMR spectra are shown in figures 5.1a to 5.7a and were consistent with structure. HPLC and NMR Chromatograms showed no evidence of impurities for all samples except fenoxazoline hydrochloride. HPLC chromatograms and NMR spectra of fenoxazoline hydrochloride showed an additional peak(s) corresponding to its primary hydrolysis degradation product (figure 3.9 and 5.2 respectively). The extent of degradation was estimated as 20% by NMR (see section 5.4). Fenoxazoline hydrochloride was therefore only used for degradation studies. The cirazoline hydrochloride IR spectum was consistent with structure and the DSC spectum (figure 2.1) showed a sharp melting point peak at 188.2°C. No peak associated with loss of water of hydration was

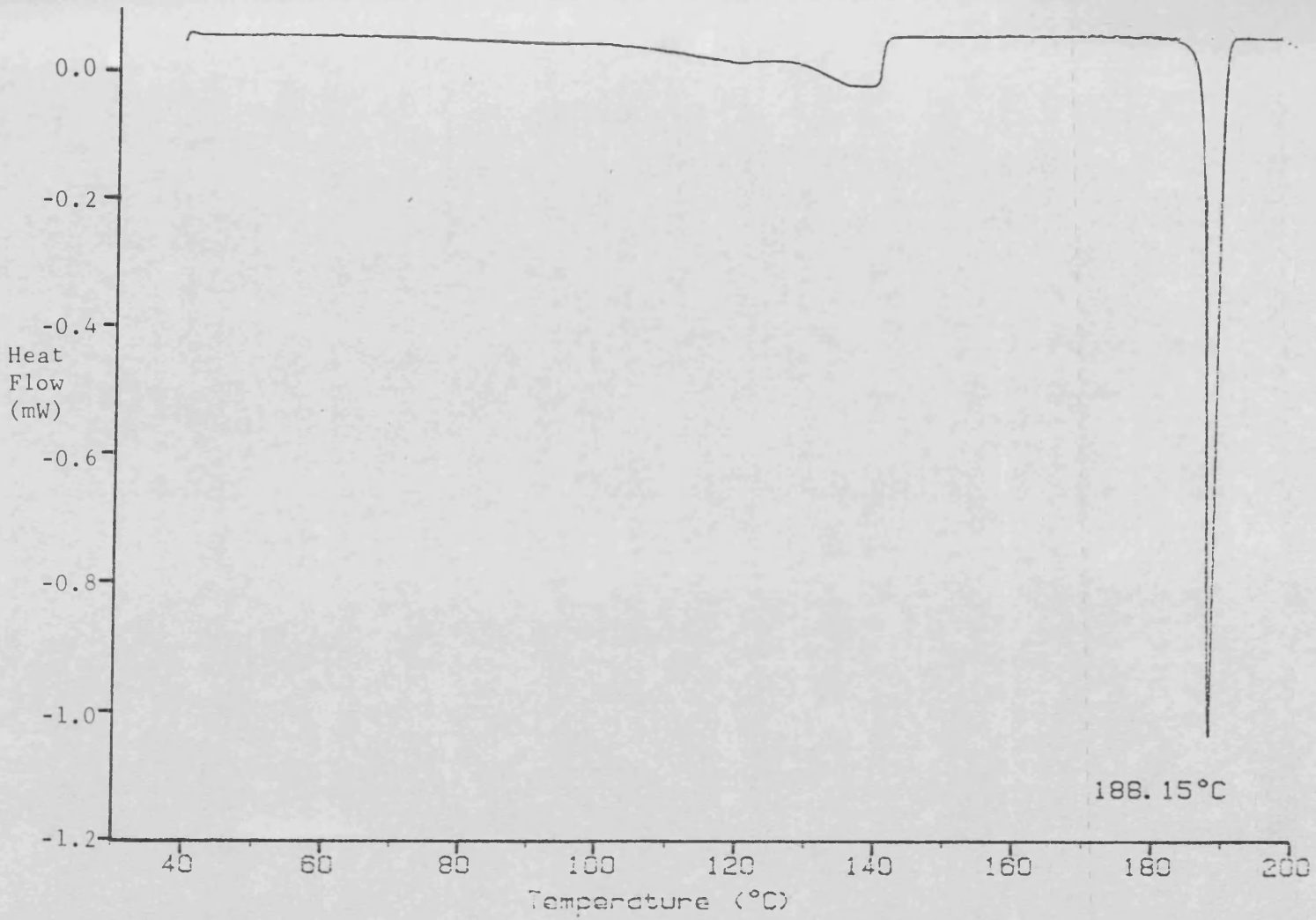

Figure 2.1 - Differential scanning calorimetry spectrum of anhydrous cirazoline hydrochloride.

observed, confirming the sample was anhydrous. The small peak at about 140°C is thought to be a crystalline transition.

2.1.2.2 SURFACTANTS

Purification of Sodium Dodecyl Sulphate (SDDS)

Commercial samples of surfactants often contain impurities including homologues and unreacted reagents. Although the SDDS sample used in this study was of Primar Grade, (>99% SDDS), hydrolysis to dodecan-1-ol may occur upon storage. SDDS was therefore subjected to the purification process described by Mukhayer and Davis[121].
The sample was Soxhlet extracted with petroleum ether, (40 - 60°), for 48 hours, dried and recrystallised twice from absolute ethanol. The resulting crystals were dried to constant weight at 40°C, 900 mBar reduced pressure. The purity of the sample was checked by surface tension and NMR Spectroscopy.

(a) Surface Tension

Impurities in a sample of surfactant may be detected by a characteristic minimum in surface tension - concentration curves. The technique used was the Wilhelmey Plate method; the equipment used in this laboratory has been described in detail by Shetewi[192].

The surface tension of a liquid, γ, is given by equation 2.1, where g is the acceleration of gravity and W is the weight in grams necessary to detach a thin glass microscope coverslip of thickness, t, and length, l, from the surface of the liquid.

$$\gamma = \frac{Wg}{2(l+t)} \qquad (2.1)$$

The dimensions of the coverslip were determined using a travelling microscope.

The accuracy of determination was checked by measuring the surface tension of toluene, acetonitrile (both HPLC grade) and double distilled water; the latter has a very high surface energy and is therefore easily contaminated. To minimise this risk, the surface tension data was obtained from freshly distilled water collected from a receiving vessel which had been left to overflow for at least 30 minutes.

Results obtained from single samples of each liquid are shown in table 2.1 together with known values obtained from the literature. Observed data are well in agreement with reported values and thus confirms the validity of the method.

Surface tension measurements were taken for 2-20 x 10^{-3}M concentration of purified SDDS; results are shown in table 2.2 and plotted graphically in figure 2.2. The absence of a minimum in the curve indicates that the material was pure.

The CMC of SDDS at 25°C was estimated as 8.40 x 10^{-3}M (literature value - mean 8.2 x 10^{-3}M, range 8.1 - 8.4 x 10^{-3} M)[51].

(b) NMR Spectroscopy

An NMR spectrum of a sample of purified SDDS was obtained using HDO as reference, (4.60 ppm). The spectrum and SDDS structure are shown in figure 2.3. The spectrum was consistant with structure and no anomalous peaks were detected. Assignments and integral values are shown together with the NMR data for sodium octyl sulphate, (SOS), sodium decyl sulphate, (SDS) and sodium tetradecyl sulphate, (STDS), in table 2.3. NMR analysis thus indicates the SDDS sample to be of high purity.

LIQUID	TEMP-ERATURE	OBSERVED SURFACE TENSION (mNM^{-1})	MEAN (S.D.)	REPORTED VALUE (193)
Double Distilled Water	25°C	71.98, 72.27, 72.03, 71.83	72.03 (0.18)	71.97
Toluene	30°C	28.03, 28.08, 28.08, 28.03	28.06 (0.03)	27.40
Aceto-nitrile	20°C	29.43, 29.43, 29.53	29.46 (0.06)	29.30

Table 2.1 - Surface tension values for water, toluene and acetonitrile.

SDDS CONCEN-TRATION M x 10^3	OBSERVED SURFACE TENSION (mNM^{-1})	MEAN (S.D.)
2.0	60.12, 60.12, 60,26, 59.92, 60.02	60.09 (0.13)
5.0	48.04, 47.75, 47.85, 47.94, 48.04, 48.04	47.94 (0.13)
8.0	40.89, 40.70, 40.75, 40.80	40.80 (0.08)
9.0	39.66, 39.76, 39.76	39.73 (0.06)
10.0	39.81, 39.76, 39.71	39.76 (0.05)
15.0	39.37, 39.37, 39.46, 39.42, 39.37	39.39 (0.04)
20.0	39.37, 39.42, 39.42	39.40 (0.03)

Table 2.2 - Surface tension data for aqueous solutions of purified SDDS at 25°C.

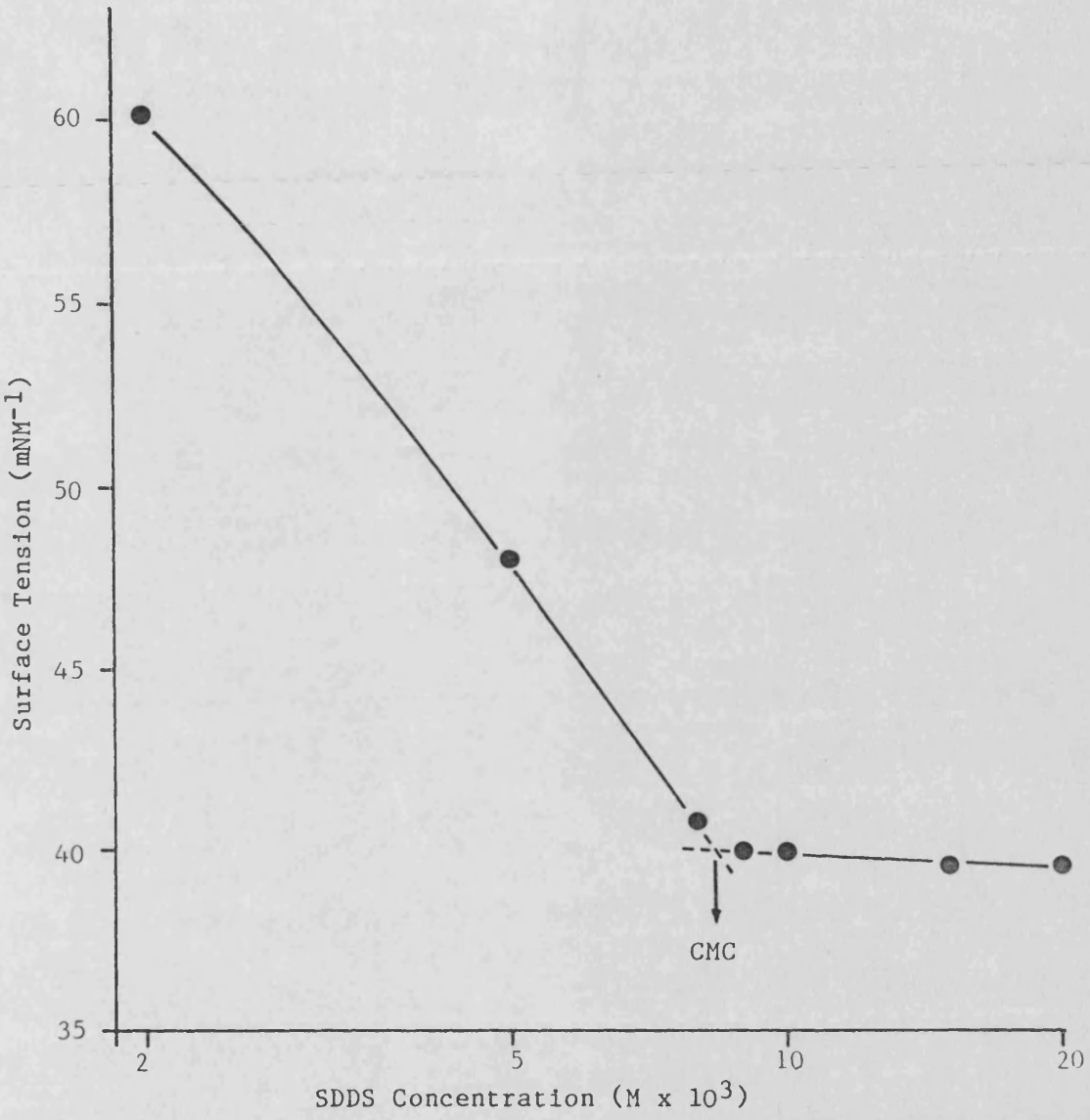

Figure 2.2 - Effect of concentration on surface tension of sodium dodecylsulphate solutions in double distilled water at 25°C.

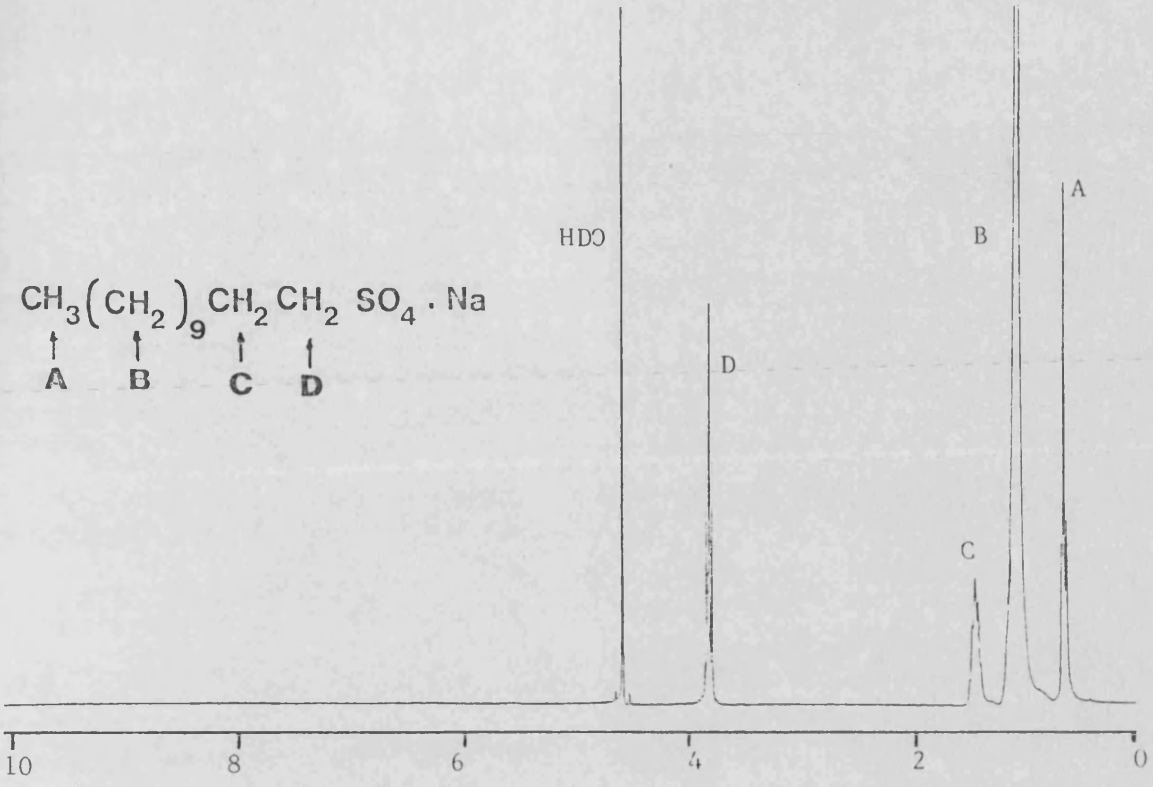

Figure 2.3 - Proton NMR spectra for sodium dodecylsulphate in D_2O, 20°C.

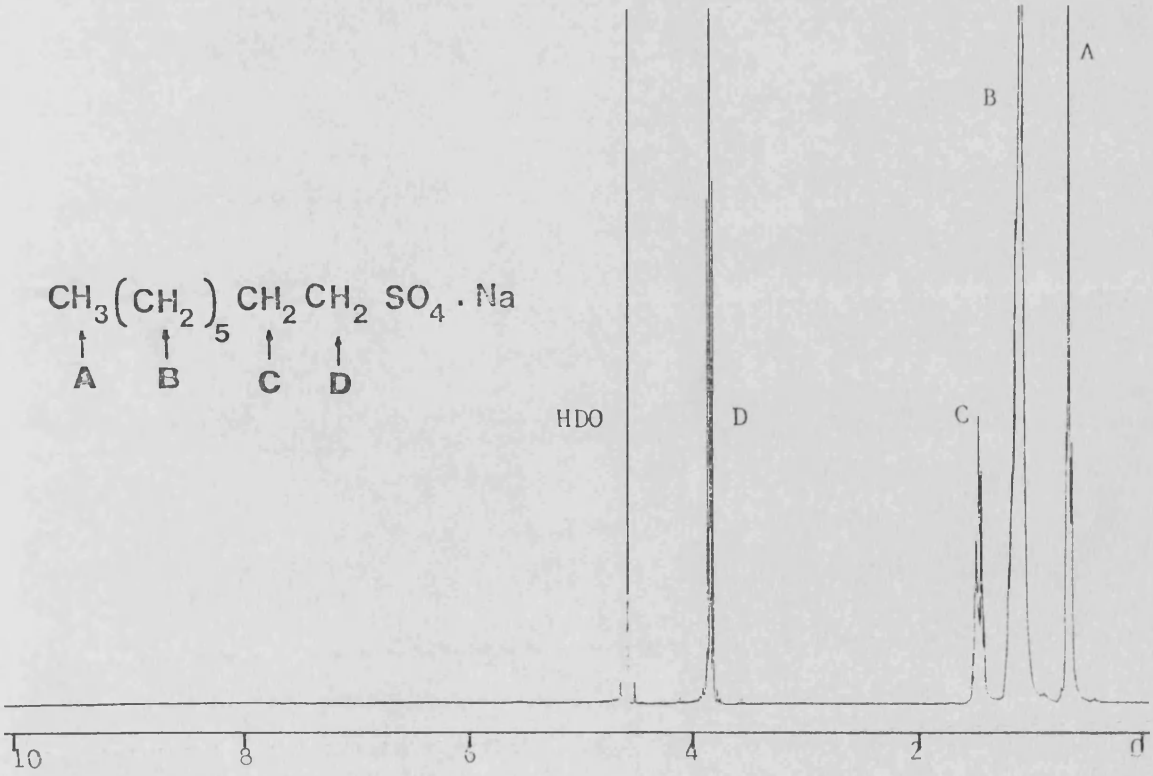

Figure 2.4 - Proton NMR spectra for sodium octylsulphate in D_2O, 20°C.

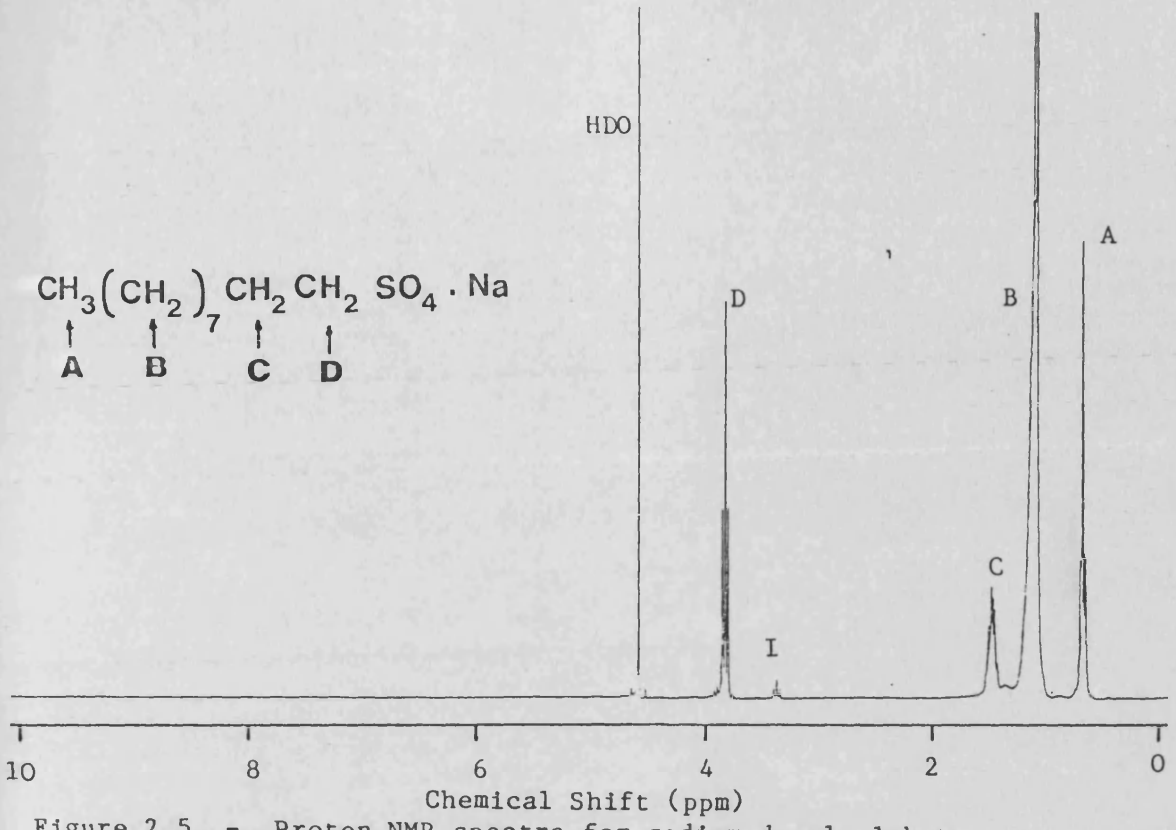

$CH_3(CH_2)_7 CH_2 CH_2 SO_4 . Na$

A B C D

Figure 2.5 - Proton NMR spectra for sodium decylsulphate in D_2O, 20°C. I = Impurity

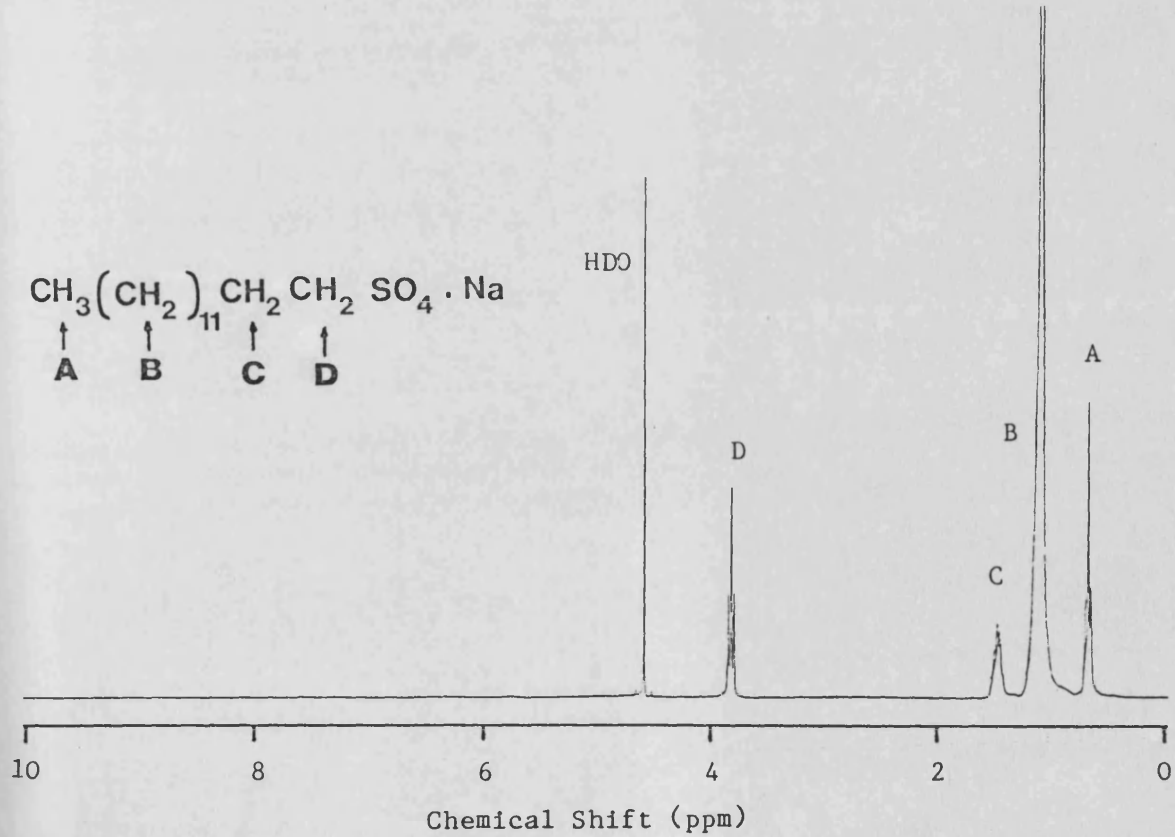

$CH_3(CH_2)_{11} CH_2 CH_2 SO_4 . Na$

A B C D

Figure 2.6 - Proton NMR spectra for sodium tetradecylsulphate in D_2O, 20°C.

Synthesis of Sodium Octyl, Decyl and Tetradecyl Sulphates

Sodium octyl sulphate, (SOS), sodium decyl sulphate (SDS) and sodium tetradecyl sulphate, (STDS) were synthesized from the corresponding alcohol and sulphuric acid. Purification was by extraction with butan-1-ol, Soxhlet extracton and recrystallistion from ethanol.

(a) Sodium Octyl Sulphate

96% H_2SO_4, (78.5g) was added dropwise over one hour to stirring octan-1-ol, (100.0g) in an ice bath. The resulting equimolar mix was then allowed to react at room temperature for 48 hours.

(b) Sodium Decyl Sulphate

96% H_2SO_4, (129.2g) was added dropwise over one hour to decan-1-ol (201.7g) in an ice bath. The resulting equimolar mix was then allowed to react at room temperature for 48 hours.

(c) Sodium Tetradecyl Sulphate

Tetradecan-1-ol is a solid at room temperature and excess sulphuric acid (4:1) was therefore used as solvent. 96% H_2SO_4 (191.2g) was added dropwise over one hour to tetradecan-1-ol (100.2g) at ambient temperature and left to react for five days.

(d) Purification

The following procedure was used for the purification of SOS, SDS and STDS:

The crude surfactant mix was diluted with distilled water and neutralised by the slow addition of solid sodium carbonate. The sodium alkyl sulphate was immediately extracted from the aqueous mix with butan-1-ol, (4 x 100 ml). The volume of the upper, butan-1-ol layer increased from 100 ml to approximately 250 ml upon shaking, indicating

the production of a ternary phase, (butan-1-ol : water : sodium alkyl sulphate). Evaporation to dryness at 70°C and 600 mm Hg reduced pressure, (Rotavapor R110) produced a solid residue of crude sodium alkyl sulphate and a distillate composed of two immisible liquids (butan-1-ol and water). The residue was Soxhlet extracted with petroleum ether (40 - 60°) for five days followed by diethyl ether for two days. The solid was dried overnight at ambient temperature and reduced pressure to remove traces of organic solvent.

Recrystallisation from ethanol was hampered by the presence of inorganic ions due to ternary phase production at the extraction stage. These ions were removed by filtering a hot solution of alkyl sulphate in ethanol before recrystallising at 4°C. This process was repeated and the resulting crystals dried to constant weight at ambient temperature and reduced pressure.

(e) Characterisation

SOS, SDS and STDS samples were examined by NMR. Samples were run in D_2O using HDO as reference, (4.60 ppm). Spectra are shown in figures 2.4 to 2.6 and are consistent with structure. No anomolous peaks were detected in the SOS and STDS spectra indicating a high degree of purity. A small triplet peak was observed at a chemical shift of 3.40 ppm in the SDS sample spectrum, however, indicating the presence of impurity (estimated at about 2%). NMR data are summarised in table 2.3.

2.1.2.3 DOUBLE DISTILLED WATER

Tap water was distilled through an all glass laboratory still and collected in vessels reserved solely for this purpose. This water was re-distilled using an all glass still fitted with a 25 cm long

Chemical Shift (ppm)	Peak Type	Assign-ment	Integration Observed (theoretical) number of protons per molecule SOS	SDS	SDDS	STDS
0.60-0.75	Triplet	A	2.89(3)	2.84(3)	2.95(3)	3.24(3)
1.00-1.25	Singlet	B	10.32(10)	13.64(14)	18.21(18)	21.80(22)
1.40-1.55	Pentlet	C	1.90(2)	2.59(2)	1.92(2)	1.93(2)
3.35-3.45	Triplet	Impurity	-	0.07	-	-
3.80-3.95	Triplet	D	1.90(2)	1.87(2)	1.92(2)	2.04(2)

Table 2.3 - NMR data for sodium alkyl sulphates in D_2O. (See figures 2.3-2.6 for explanation of assignment).

(SOS = sodium octyl sulphate, SDS = sodium decyl sulphate, SDDS = sodium dodecyl sulphate, STDS = sodium tetradecyl sulphate).

fractionating column containing cut glass, (pyrex), tubing. The resultant double distilled water was collected in glass containers reserved solely for this purpose. Such water was shown to have a surface tension of 72.03 mNM^{-1} and specific conductivity of less than 1×10^{-6} Scm^{-1} at 25°C.

2.2 GENERAL METHODS

2.2.1. Cleaning of Glassware

All glassware was immersed in chromic acid mixture for at least one hour, rinsed six times with tap water followed by three times with distilled water. Cleaned glassware was dried in a hot air oven before use or storage.

2.2.2 Ageing of Glassware

Glass and silica surfaces can acquire a negative charge when in contact with aqueous solution and positively charged species in solution can be attracted and adsorbed onto such surfaces. This effect is an important factor in studies involving cationic surfactants and may be relevant to solutions of protonated drugs such as cirazoline hydrochloride or other imidazoline salts. Alkyl sulphates and ion-pair/complexes may also be adsorbed on to surfaces by an hydrophobic attraction.

An ageing process was therefore applied to all glassware used for imidazoline and surfactant solutions. Glassware was presaturated for at least 24 hours with the same concentration of solution to be used in the study. The containers were washed with distilled water, dried and used for the relevant solution throughout the work without subjecting them to further chromic acid treatment.

2.2.3 Temperature Measurements

All temperature measurements at or below 50°C were made with reference to a calibrated mercury in glass thermometer range -5 to 50°C, graduated at intervals of 0.1°C (calibration factor = 1.000)[194]. A mercury in glass thermometer, range -10 to 110°C, graduated at intervals of 0.5°C was used for temperature measurements between 50 and 80°C.

2.2.4 Preparation of Buffers

The following standard buffer solutions were prepared according to Bates[195].

(a)	Equimolal (0.025 m) phosphate	pH 6.865 at 25°C
(b)	Potassium hydrogen phthalate (0.05 m)	pH 4.008 at 25°C
(c)	Borax (0.01 m)	pH 9.180 at 25°C

Buffers were stored in stoppered flasks at 4°C and discarded after four weeks.

2.2.5 pH-Measurement

2.2.5.1 TECHNIQUE FOR STANDARDISING pH METERS

Both types of pH meters (digital and pH-stat unit) were standardised prior to each experimental determination of pH using standard buffers. The pH electrode and standard buffers were equilibrated to the experiment temperature before use. Equimolal phosphate buffer was used in conjunction with either phthalate buffer (for experiment pH < 6.85) or borax buffer (for experiment pH >6.85). The pH of standard buffers at the required temperature was taken from Bates[195].

2.2.5.2 CHOICE OF pH ELECTRODE

The Phillips CE1 pH electrodes were used for pH measurement below 70°C and pH 12. For temperatures > 70°C and below pH 12 the Radiometer 405-60 pH electrode was used. The Phillips CAH-11 electrode was used for pH determinations of pH 12 and above.

2.2.5.3 pH-MEASUREMENT IN CIRAZOLINE - SDDS SYSTEMS

The response time and sensitivity of electrodes were found to decrease when used for long periods in mixtures of cirazoline and SDDS solutions; this is probably due to adsorption of cirazoline dodecyl sulphate onto the glass envelope. The electrode was therefore removed from such solution immediately after measurement and the electrode response checked using standard buffers. If any drift or sluggish response was noted, the electrode was washed in 95% ethanol, soaked for a few hours in 0.1 M HCl and recalibrated.

In practice, the change in electrode response was negligible if used for less than about 30 minutes.

2.2.5.4 EFFECT OF MAGNETIC STIRRER ON pH MEASUREMENT

The magnetic stirrers used with the automated pH-stat unit were found to significantly affect the pH readings of solutions, causing an apparent shift to lower pH values. This effect was investigated by monitoring the pH of NaOH, (0.1 M), HCl, (0.1 M) and phosphate buffer solution using the pH-stat assembly in conjunction with the Phillips CE1 electrode. A change of pH of - 0.10 pH units occurred when using

the magnetic stirrer. This change of pH was independent of the pH of the solution.

A correction factor of + 0.10 pH units was therefore applied to all pH readings measured using these magnetic stirrers.

3. ANALYTICAL

3.1 HPLC ANALYSIS

High performance liquid chromatography (HPLC) is probably now the technique of choice in pharmaceutical analysis and is the subject of several comprehensive reviews[196-198]. The different modes of chromatographic separation available with HPLC are given below:

1. Adsorption
2. Liquid - liquid partition
3. Reversed phase
4. Reversed phase ion-pair partition
5. Ion-exchange
6. Exclusion
7. Affinity

Detection techniques include UV absorption, refractive index, fluorescence, electrochemical, electron capture and mass spectrometry. Various parameters are used to characterise the efficiency of a chromatographic system.

The retention of a solute is indicated by the column capacity ratio, k' (equation 3.1):

$$k' = \frac{t_r - t_o}{t_o} \qquad (3.1)$$

Where t_r is the retention time of the given peak and t_o is the retention time of the solvent peak.

The efficiency of a chromatographic column is measured by the number of theoretical plates, N, to which the column is equivalent. N is calculated using equation 3.2:

$$N = 16 \frac{t_r^2}{W} = 5.54 \frac{t_r^2}{W_{1/2}} \qquad (3.2)$$

Where W is the base line width of the peak and $W_{1/2}$ is the peak width at half-height. Typical values of N lie in the range 1000 - 20,000 plates.

The resolution, R_s, of two chromatographic peaks is a measure of their separation, (equation 3.3):

$$R_s = 2 \frac{(t_2 - t_1)}{(W_1 + W_2)} \qquad (3.3)$$

Where t_1 and t_2 are the retention distances and W_1 and W_2 the peak base widths of peaks 1 and 2 respectively. For two Gaussian peaks, effective base line resolution is obtained for $R_s = 1.5$.

The selectivity , α, is defined as the ratio of the column capacity ratio of the two peaks of interest, (equation 3.4):

$$\alpha = \frac{k'_2}{k'_1} \qquad (3.4)$$

Quantification of sample concentration is achieved by reference to standard solutions. Two forms of reference are possible, namely internal standard and external standard techniques. The former method involves the inclusion of a standard substance of known concentration in the sample mixture. Ideally the internal standard should have a chemical structure similar to that of the sample but sufficiently different to enable resolution of the sample and standard peaks. The standard must be stable under the assay

conditions and other peaks in the chromatogram such as those due to degradation product(s), must not interfere with the standard peak. Sample concentration is expressed as peak height ratio, or preferably peak area ratio (sample peak area/internal standard peak area). Reference to peak area ratio/concentration calibration curves allows calculation of sample concentration, (see also section 3.1.6). The external standard technique involves the injection of a solution of known concentration alongside the unknown samples. Quantification of unknown samples is made by direct reference to the external standard peak height/area.

The advantages of the external standard method is that it is the simpler technique and only involves one chemical entity. The latter may be important when strict control of experimental conditions is not possible. The internal standard method, although more complicated in development, has the advantage that the injection volume is not critical for the determination.

3.1.1 Description

A reversed phase ion-pair stability indicating HPLC assay for cirazoline was developed from the method described by Davies et al[15]. The assay technique also allowed determination of the primary degradation product, CPAE. This ability to assay both reactant and product of the hydolysis allowed great versatility in determining the extent of cirazoline degradation and reaction rate constants.
A 100 mm x 5 mm Spherisorb ODS Column was used in conjunction with an aqueous sodium acetate buffer : acetonitrile (30 : 70) mobile phase system with apovincamine solution in acetronitrile as internal standard. The assay was modified by increasing the aqueous buffer concentration from 0.1 M to 0.2 M and reducing the flow rate

from 1.2 mls min^{-1} to 1.0 mls min^{-1}. This adjustment improved the assay by increasing sensitivity and reducing the total analysis time from seven to five minutes while retaining base line separation of peaks.

The HPLC conditions are summarised below:

Column	:	100 x 5 mm Spherisorb S5 ODS	
Mobile Phase	:	(i) Sodium acetate (aq) 0.4 M	150 mls
		(ii) Glacial acetic acid	40 mls
		(iii) Distilled water	110 mls
		(iv) Acetonitrile	700 mls
		pH adjusted to 5.2 with (i)/(ii)	
Flow Rate	:	1.0 ml min^{-1}	
Detection	:	UV at 275 nm	
Attenuation	:	0.02 - 0.08 AUFS	
Load	:	10 µl	
Chart Speed	:	0.5 cm min^{-1}	
Temperature	:	Ambient	
Internal Standard	:	Apovincamine (5 - 20 µg ml^{-1})*	
Injection	:	Minimum two per sample	

* Added as 12.5 - 100 µg ml^{-1} solution in acetonitrile because of poor aqueous solubility.

3.1.2 Preparation of Column and Evaluation of Performance

The 100 x 5 mm Spherisorb S5 ODS column used throughout was slurry packed in isopropanol and hexane at 7000 psi using a Haskel pneumatic column packer.

The reverse phase testing procedure of Bristow and Knox was used to evaluate column performance[199]. A test solute mix of phenol, anisole

and phenetole was chromatographed using methanol : water, (60 : 40) mobile phase. The number of plates was calculated for the last peak (phenetole) using equation 3.2 and was found to be 3033 plates (30330 plates metre $^{-1}$). This value is within the range normally observed in HPLC systems.

3.1.3 Specificity of Cirazoline and CPAE Assays

Separate solutions of 2 x 10^{-4} M cirazoline hydrochloride (aq), 2 x 10^{-4} M CPAE hydrochloride (aq), 10 μg ml^{-1} apovincamine (in 20% acetonitrile) and a mixture of the three solutions (in 20% acetonitrile) were chromatographed using the conditions described in section 3.1.1. Hydrochloric acid (final concentration of 4 x 10^{-3} M) was included in all solutions to inhibit degradation. A chromatogram of the mixture run at a chart speed of 4 cm min^{-1} (8 x normal) is given in figure 3.1. CPAE, cirazoline and apovincamine peaks had retention times of 2.0, 3.0 and 4.0 minutes respectively. Satisfactory base line separation resolution and selectivity were obtained for both CPAE/cirazoline (R_s = 2.1, α = 2.0) and cirazoline/apovincamine (R_s = 1.6, α = 1.5) peaks. Chromatographic parameters are shown together with HPLC data for other imidazolines in table 3.1.

The cirazoline assay was shown to be stability indicating by degrading 2 x 10^{-3} M cirazoline hydrochloride in equimolal phosphate buffer (0.025 m), pH 6.85 at 70°C down to about 60% residual concentration. Samples taken during the experiment were assayed and the results show a decrease in cirazoline peak size and the concomitant appearance of a peak with similar characteristics to the CPAE peak, thus confirming the hydrolysis of cirazoline to CPAE. An

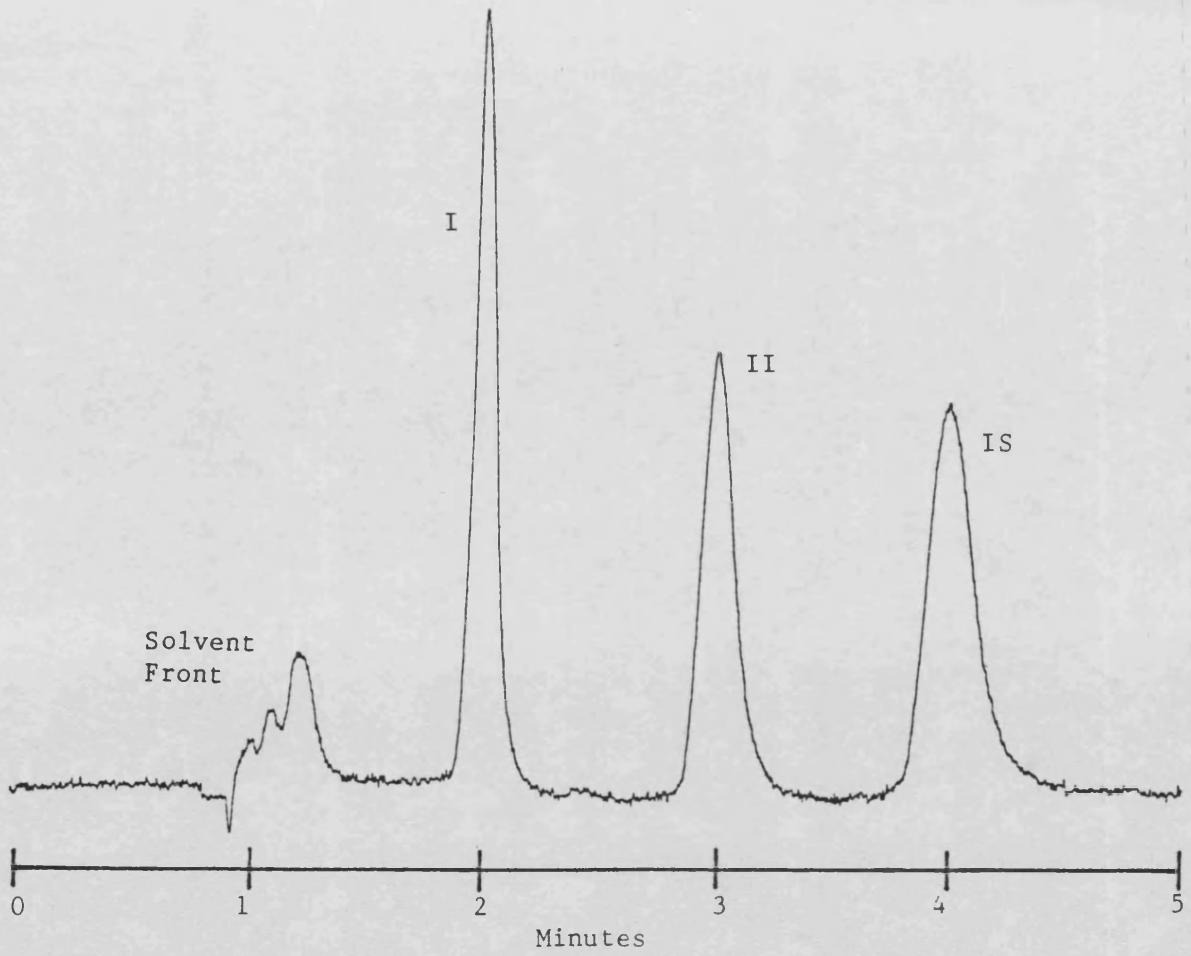

Figure 3.1 - HPL Chromatogram of a mixture of 2 x 10^{-4} M CPAE (I), 2 x 10^{-4} M cirazoline hydrochloride (II) and 10 μg ml^{-1} apovincamine (IS) in 20% acetonitrile, 4 x 10^{-3} M HCl. (Chart speed=40 mm min^{-1} (8 x normal), detection at 275 nm, 0.04 AUFS).

PARAMETER	CIR	ANT	FEN	NAP	TOL	XYL	CPAE
Detection Wavelength (nm)	275	275	275	275	240	240	275
I t_I	2.0	2.1	2.2	2.1	-	-	1.4
k'_I	1.1	1.2	1.3	1.1	-	-	2.0
II t_{II}	3.0	3.0	3.3	3.0	2.6	4.8	2.0
k'II	2.2	2.2	2.6	2.3	1.7	3.0	1.1
IS t_{IS}	4.0	4.0	4.0	4.0	-	-	4.0
k'_{IS}	3.3	3.3	3.3	3.3	-	-	3.3
I/II (α	2.0	1.9	2.1	2.1	-	-	(8.2)
I/II (R_s	2.1	1.5	2.5	2.4	-	-	1.4
II/IS(α	1.5	1.5	1.3	1.4	-	-	2.9
II/IS(R_s	1.6	1.5	1.0	1.5	-	-	3.4
N_{II} M^{-1}	19000	24000	18000	23000	7000	5000	26000
Total Analysis Time (mins)	5.0	5.0	5.0	5.0	3.0	6.0	3.0

Table 3.1 - Chromatographic parameters for the HPLC assay of imidazolines and CPAE. I = Degradation peak, II = Imidazoline or CPAE peak, IS = Internal Standard. (CIR = cirazoline, ANT = antazoline, FEN = fenoxazoline, NAP = naphazoline, TOL = tolazoline, XYL = xylometazoline.)

HPLC chromatogram of initial and partially degraded, (60% residual concentration), samples are given in figure 3.2.

A solution of CPAE hydrochloride was produced in situ by fully degrading a 0.01 M solution of cirazoline hydrochloride in sodium hydroxide at pH 8.0 and 80°C. After 24 hours the solution was neutralised with 0.1 M HCl and suitably diluted. The resultant chromatogram for the CPAE solution is shown in figure 3.3a. The CPAE assay was shown to be stability indicating by degrading a 1×10^{-3} M sample of CPAE hydrochloride in 0.1 M NaOH at 70°C. Samples taken over a 24 hour period were assayed and results showed a decrease in CPAE peak size and the concomitant appearance of a peak with a retention time of 1.4 minutes (figure 3.3b). This peak is thought to be associated with production of cyclopropyl-2-phenoxy-acetic acid.

The CPAE chromatogram, (figure 3.3a) shows the absence of significant peaks at retention times associated with cirazoline and the CPAE degradation product, indicating that all cirazoline had been converted exclusively to CPAE (figure 3.3a). This solution was used throughout the study as a standard solution of CPAE hydrochloride.

3.1.4 Linearity of Cirazoline and CPAE Assays

Calibration curves of peak area ratio against concentration were constructed for cirazoline and CPAE over the concentration range $0 - 36 \times 10^{-5}$ M. Solutions were prepared containing 20 $\mu g\ ml^{-1}$ apovincamine (internal standard) in 4×10^{-3} M HCl, 20% acetonitrile. Data and linear regression analysis results are given in table 3.2 and calibration curves are shown in figure 3.4. Results show peak area ratio to be proportional to concentration for both cirazoline and CPAE.

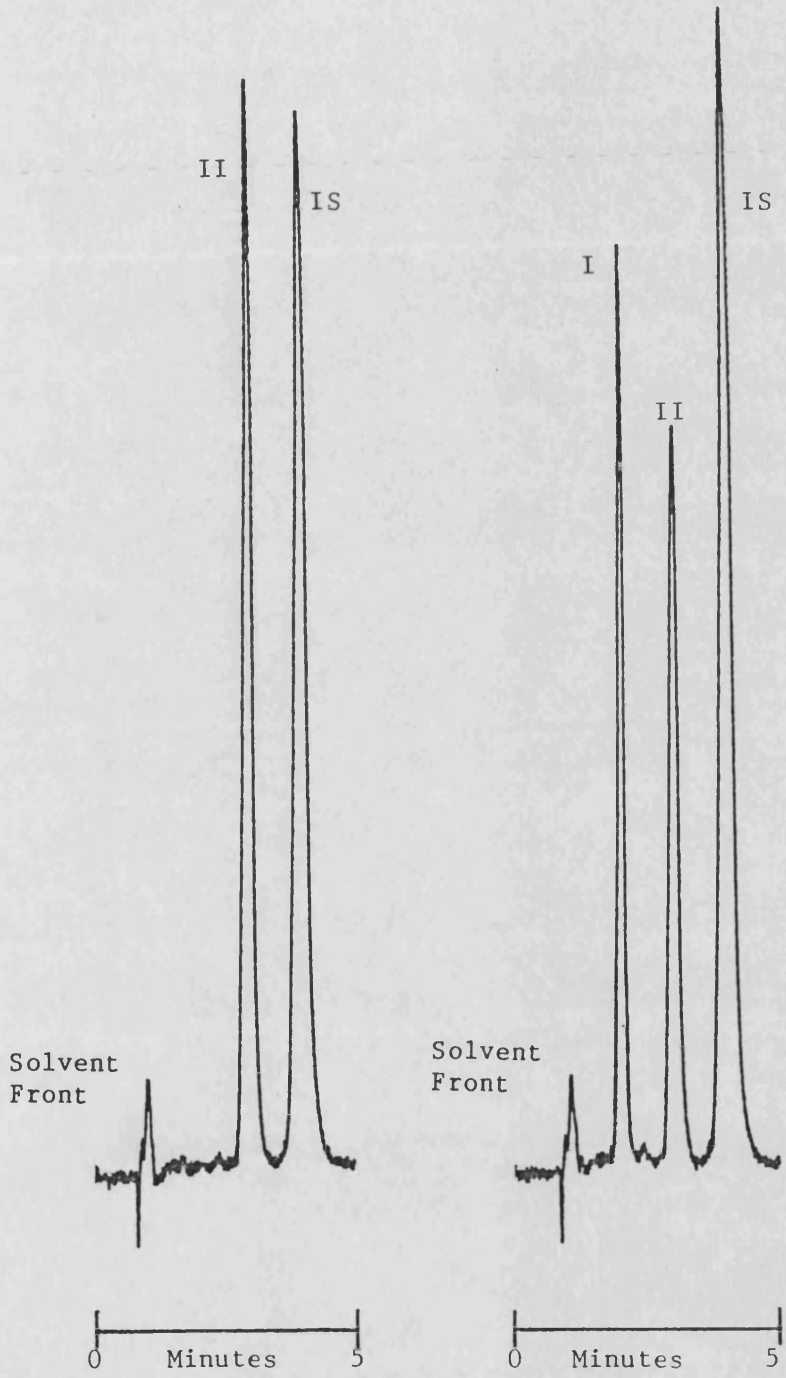

Figure 3.2 - HPL Chromatogram of 3.2×10^{-4} M cirazoline hydrochloride (II), (a) initial sample, (b) after storage in phosphate buffer pH 6.85, 70°C for 38 minutes. I = CPAE, IS = 20 µg ml^{-1} apovincamine. (Chart speed 5=mm min^{-1}, detection at 275 nm, 0.04 AUFS).

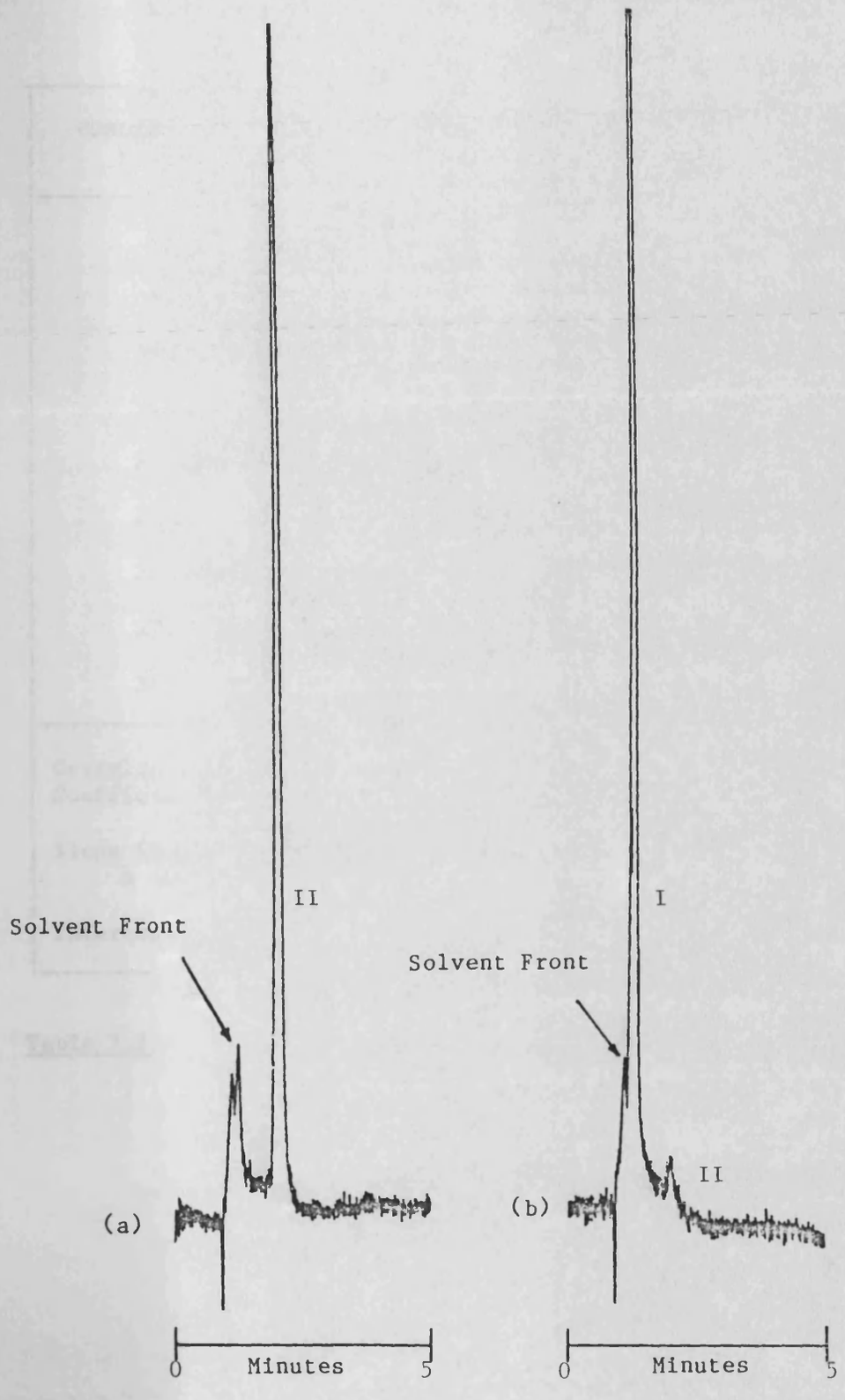

Figure 3.3 - HPL chromatogram of 1.6 x 10^{-4} M CPAE (II), (a) sample prepared by degrading 0.01 M cirazoline hydrochloride at pH 8.0, 80°C for 24 hours, (b) sample after 24 hours storage in 0.1 M NaoH, 70°C showing production of cyclopropyl-2-phenoxy-acetic acid (I). (Chart speed = 5 mm min^{-1}, detection at 275 nm, 0.02 AUFS).

CONCENTRATION M x 10^5	CIRAZOLINE MEAN PEAK AREA RATIO	CPAE MEAN PEAK AREA RATIO
4.0	0.0854	0.1090
8.0	0.1781	0.2281
12.0	0.2749	0.3379
16.0	0.4094	0.4682
20.0	0.5124	0.5763
24.0	0.6222	0.6956
28.0	0.7235	0.8211
32.0	0.8506	0.9522
36.0	0.9544	1.059
Correlation Coefficient	0.9996	0.9998
Slope (S.D.) x 10^{-3}	2.7515 (0.0321)	2.986 (0.0211)
Intercept(S.D.).	-0.0380 (0.0073)	-0.0142 (0.0047)

Table 3.2 - HPLC calibration data and linear regression analysis data for cirazoline and CPAE using apovincamine (20 μg ml^{-1}) as internal standard.

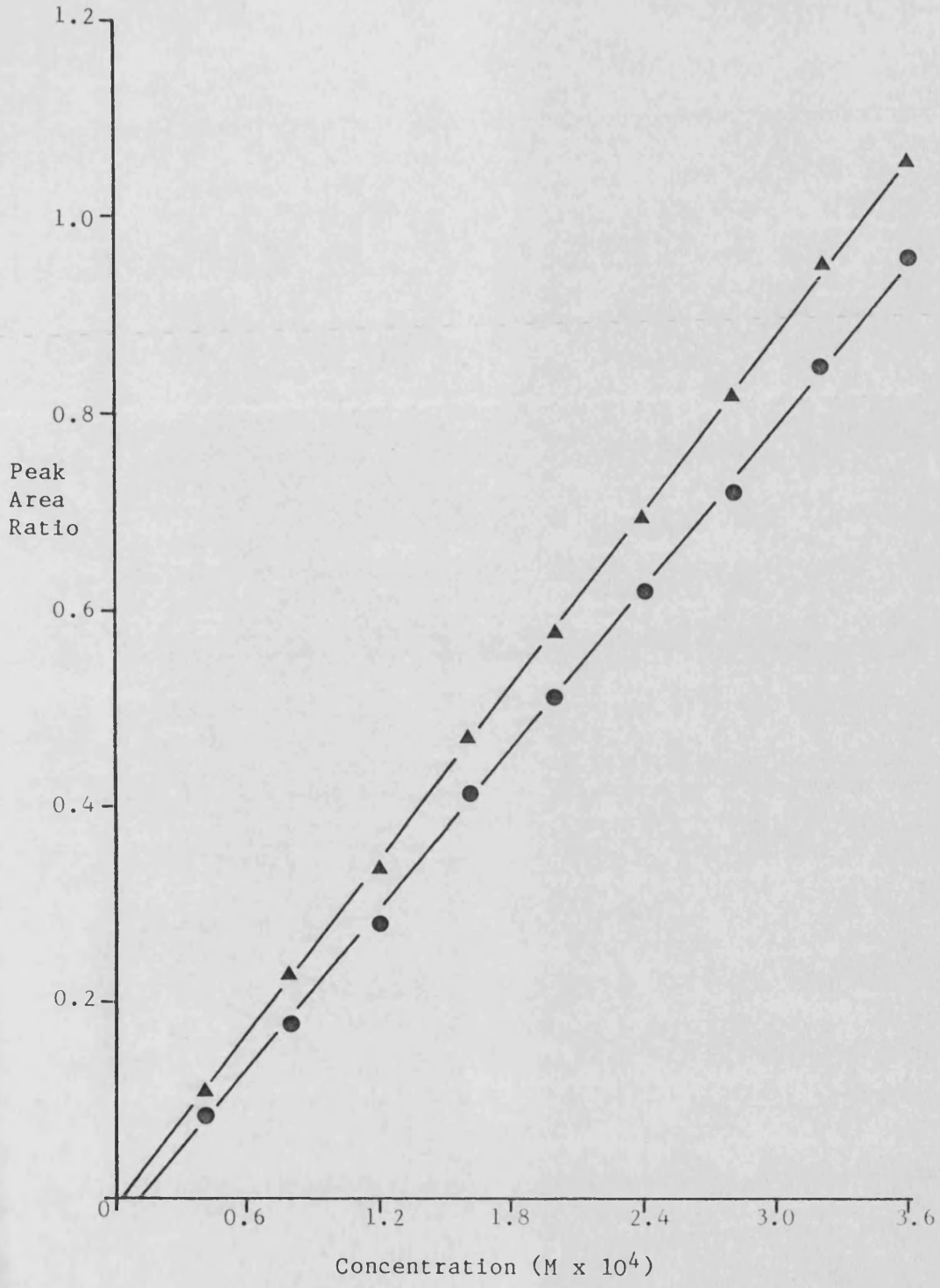

Figure 3.4 - HPLC calibration plot for cirazoline hydrochloride, (—●—), and CPAE, (—▲—), using 20 μg ml^{-1} apovincamine as internal standard.

Negative intercepts (> $\pm$ 2 S.D.s from the origin) were obtained for both cirazoline (intercept = -0.038) and CPAE (-0.014). The magnitude of the intercepts is small, however, and the error in first order rate constant determination resulting from the assumption that the calibration curves pass through the origin is considered to be minimal (<2%). The concentration of sample solutions was therefore calculated by reference to a single standard solution, which was injected at the start of each assay and repeated after every ten sample solutions. The molar concentration of sample was calculated from equation 3.5.

$$\text{Sample Concentration} = \text{Standard Concentration} \times \frac{\text{Mean Peak Area Ratio (Sample)}}{\text{Mean Peak Area Ratio (Standard)}} \quad (3.5)$$

The sensitivity of the assay at 0.04 AUFS was determined by assaying solutions of 3.0 - 30 x 10^{-6} M cirazoline hydrochloride and 3.2 - 32 x 10^{-6} M CPAE hydrochloride. The minimum detectable concentration at the normal sensitivity of 0.04 AUFS was found to be 10 x 10^{-6} M for cirazoline and 6.4 x 10^{-6} M for CPAE.

Samples taken from surfactant experiments contain SDDS which may affect the assays. This was tested by constructing calibration curves for cirazoline and CPAE in the absence and presence of 0.016 M SDDS. Calibration solutions were prepared containing cirazoline hydrochloride (0.8 - 4.8 x 10^{-4} M), CPAE hydrochloride (0.4 -2.4 x 10^{-4} M), internal standard (10 $\mu g\ ml^{-1}$) and 4 x 10^{-3} M HCl. The stability of cirazoline and CPAE solutions awaiting assay was evaluated by analysing the aqueous calibration solutions after storage for one and two months at ambient temperature. Linear regression analysis data on these calibration curves are shown in table 3.3.

	AQUEOUS		0.016 M SDDS SOLUTION	
	Cirazoline	CPAE	Cirazoline	CPAE
1 Month				
Number of Points	4	4	5	4
Correlation Coefficient	0.9994	0.9993	0.9992	0.9985
Slope x 10^{-3}	5.463	5.552	5.460	5.324
(S.D. x 10^{-3})	(0.132)	(0.150)	(0.129)	(0.207)
Intercept	-0.056	0.034	-0.081	0.007
(S.D.)	(0.031)	(0.026)	(0.034)	(0.026)
2 Months				
Number of Points	5	5		
Correlation Coefficient	0.9996	0.9998		
Slope x 10^{-3}	5.375	5.382		
(S.D. x 10^{-3})	(0.084)	(0.069)		
Intercept	-0.059	-0.050		
(S.D.)	(0.0222)	(0.011)		

Table 3.3 - Linear regression analysis data for calibration curves in the absence and presence of 0.016 M SDDS after one and two months storage under ambient condition. (Internal standard - apovincamine 10 μg/ml).

t-tests on the one month aqueous and SDDS solution data show the plots to be indistinguishable at the P = 0.05 level for both cirazoline (t_{calc} = 0.016, t_{tab} = 2.57) and CPAE (t_{calc} = 0.892, t_{tab} = 2.78). SDDS has therefore no effect on the cirazoline and CPAE assays. t-tests on the aqueous one month and two months storage data and one month SDDS solution and aqueous two months storage data show the plots to be indistinguishable at the P = 0.05 level for cirazoline (t_{calc} = 0.562, t_{tab} = 2.57 and t_{calc} = 0.552, t_{tab} = 2.45), and CPAE (t_{calc} = 1.030, t_{tab} = 2.57 and t_{calc} = 0.266, t_{tab} = 2.57). Storage over a two month period has therefore no effect on the cirazoline and CPAE assays. Solutions were normally assayed within one month of sampling.

3.1.5 Reproducibility of Cirazoline and CPAE Assays

The reproducibility of the cirazoline hydrochloride and CPAE assays was evaluated by assaying ten consecutive injections of a standard solution consisting of 3.2×10^{-4} M cirazoline hydrochloride, 2×10^{-4} M CPAE hydrochloride and 20 $\mu g\ ml^{-1}$ apovincamine in 4×10^{-3} M HCl, 20% acetonitrile. Statistical analysis on peak areas and peak area ratios is given in table 3.4. Cirazoline, CPAE and apovincamine peak areas were found to be reproducable (CV $\leq$ 3%) but greater precision was obtained from the use of peak area ratios (CV < 1.8%); thus justifying the use of internal standard.

	MEAN	S.D.	CV(%)
Peak Area (I)	12075	266	2.2
Peak Area (II)	16836	400	2.4
Peak Area (IS)	18189	554	3.0
Peak Area Ratio (I/IS)	0.6641	0.0121	1.8
Peak Area Ratio (II/IS)	0.9258	0.0152	1.6

Table 3.4 - Reproducibility of cirazoline and CPAE assays. Statistical analysis on ten consecutive injections of a mixture consisting of 3.2×10^{-4} M cirazoline hydrochloride (II), 2×10^{-4} M CPAE hydrochloride (I) and 20 $\mu g\ ml^{-1}$ apovincamine (IS).

3.1.6 Calculation of Percent Residual Cirazoline Concentration

The determination of percent residual concentration is used for calculation of reaction rate constants (Chapter 8) and is also a useful parameter in monitoring possible degradation during non-kinetic studies. The ability to assay both cirazoline and CPAE concentration allows three methods of calculation:

1. Cirazoline concentration alone.

The percent residual concentration (% RC) can be calculated from equation 3.6,

$$\% \text{ RC} = \frac{[\text{CIR}]_{\text{sample}}}{[\text{CIR}]_{\text{I}}} \times 100 \qquad (3.6)$$

Where $[\text{CIR}]_{\text{sample}}$ and $[\text{CIR}]_{\text{I}}$ are the molar cirazoline concentration of the sample and initial sample respectively. This method is the simplest of the three but suffers from the disadvantage of requiring an accurate knowledge of the initial sample concentration and may also be subject to error due to concentration changes in the reaction vessel caused by addition of titrant (from the pH stat) and from evaporation during the experiment.

2. CPAE concentration alone.

The percent residual concentration can be calculated using the molar CPAE concentration, (equation 3.7).

$$\% \text{ RC} = \frac{([\text{CIR}]_{\text{I}} - [\text{CPAE}]_{\text{sample}}) \times 100}{[\text{CIR}]_{\text{I}}} \qquad (3.7)$$

Where $[CPAE]_{sample}$ is the molar CPAE concentration in the sample. This method is necessary when representative sampling of cirazoline cannot be achieved. The calculation relies on representative sampling of CPAE, an accurate knowledge of the initial molar cirazoline concentration value and of the stability of CPAE under the experimental conditions.

3. Cirazoline and CPAE Concentration.

Percent residual concentration can be calculated using both cirazoline and CPAE concentrations from equation 3.8.

$$\% RC = \frac{[CIR]_{sample}}{[CIR]_{sample} + [CPAE]_{sample}} \times 100 \qquad (3.8)$$

This method relies on representative sampling for both cirazoline and CPAE and the latter must be stable under the experimental conditions. The method has the advantage of requiring only relative concentrations and not absolute values. Errors due to volume changes in the reaction flask (e.g. addition of titrant and evaporation) and pipetting are negated, thus improving the accuracy and precision of the assay. Direct sampling at temperatures other than 20°C is thus possible as the volume of the sample is not critical to the assay. The amount of degradation can be determined from one sample and does not rely on initial or other values. This is especially useful as a 'quality control' assay in the calculation of possible degradation. during non-kinetic experiments.

The three methods of calculation were tested by degrading cirazoline hydrochloride (2×10^{-3} M) in equimolal phosphate buffer, (pH 6.85, 70°C) using the method described in section 8.2.1a. CPAE is stable

under these conditions (as confirmed by absence of HPLC peak at 1.4 mins) and volume changes should be minimal as the experiment was rapid (about 40 minutes) and no titrant was used. All three methods should therefore be valid and give similar percent residual concentration values and rate constants. Results are shown in table 3.5 and figure 3.5. Total assay values (cirazoline plus CPAE concentration) were essentially constant during the degradation (Mean 1.903×10^{-3} M, S.D. 0.019, CV 1.02%) confirming the stability of CPAE under these conditions. Assay concentration values are less than the input concentration as sampling was performed at 70°C; the density of water at 70°C (0.9778) is approximately 0.98 times that at 20°C (0.9982). The slight degradation (1.5%) at time zero is due to the delay in taking the first sample in order to ensure complete mixing of the solutions (see section 8). All methods of calculation give similar results and derived rate constants, (t-tests for k_{obs} give t_{calc} : 1/2 = 1.388, 1/3 = 0.682, 2/3 = 1.279; t_{tab} = 2.120 at P = 0.05) showing that under ideal conditions all methods are valid. The data calculated using cirazoline and CPAE concentration values (equation 3.8), however, had the smaller relative standard deviation and wherever possible percent residual concentration was calculated by this method.

An example of kinetic data where degradation of CPAE was significant (as indicated by mass balance inconsistancies and detection of an HPLC peak corresponding to the CPAE degradation product), is given by the hydrolysis of cirazoline hydrochloride in 0.1 M HCl at 70°C. These data are shown in table 3.6 and figure 3.6. Percent residual concentration in these cases was calculated by reference to cirazoline concentration alone (method 1).

TIME (MINS)	CONCENTRATION (M x 10^3)			% RESIDUAL CONCENTRATION		
	CIR	CPAE	TOTAL	METHOD 1 (equation 3.6)	METHOD 2 (equation 3.7)	METHOD 3 (equation 3.8)
0	1.881	0.038	1.919	100.0	98.0	98.0
5	1.727	0.152	1.879	91.8	92.1	91.9
9	1.673	0.257	1.930	88.9	86.6	86.7
13	1.557	0.347	1.904	82.8	81.9	81.8
17	1.481	0.422	1.903	78.7	78.0	77.8
21	1.398	0.494	1.892	74.3	74.3	73.9
25	1.342	0.590	1.932	71.3	69.3	69.5
29	1.230	0.644	1.874	65.4	66.5	65.7
34	1.161	0.742	1.903	61.7	61.4	61.0
38	1.095	0.803	1.898	58.2	58.2	57.7
Mean (S.D.)			1.0934 (0.0194)			
Correlation Coefficient				0.9986	0.9996	0.9998
Slope x 10^2				-1.415	-1.374	-1.396
(S.D. x 10^2)				(0.026)	(0.014)	(0.010)
(RSD Slope)				(1.84%)	(1.02%)	(0.72%)
Intercept				4.604	4.588	4.589
(S.D.)				(0.006)	(0.003)	(0.002)
(Calculated % initial)				(99.88)	(98.30)	(98.40)
k_{obs} x 10^4 s^{-1}				2.36	2.29	2.33

Table 3.5 - Degradation of 2 x 10^{-3} M cirazoline [CIR] hydrochloride in phospate buffer pH 6.85 at 70°C. Residual concentrations and first order rate constants calculated according to equations 3.6 - 3.8.

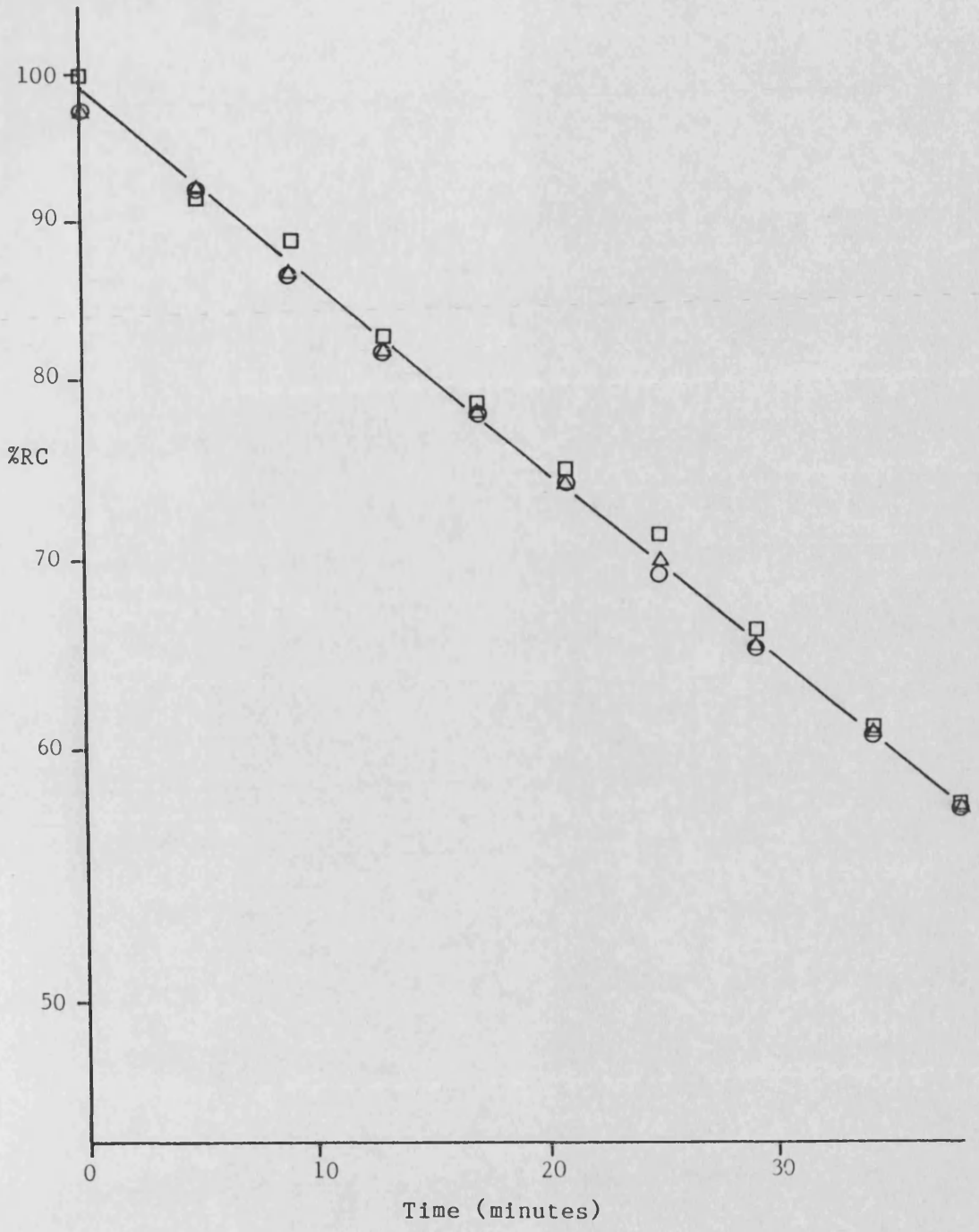

Figure 3.5 - First order plot for the degradation of 2 x 10^{-3} M cirazoline hydrochloride in phosphate buffer pH 6.85, 70°C. Percent residual concentration (%RC) values calculated using (a) equation 3.6, (—□—), (b) equation 3.7, (—○—), and (c) equation 3.8, (—△—).

TIME (MINS)	CONCENTRATION (M x 10^3)			% RESIDUAL CONCENTRATION		
	CIR	CPAE	TOTAL	METHOD 1 (equation 3.6)	METHOD 2 (equation 3.7)	METHOD 3 (equation 3.8)
0	1.500	0.023	1.523	100.0	98.5	98.5
26.5	1.317	0.143	1.460	87.8	90.6	90.2
47.5	1.170	0.214	1.384	78.0	86.0	84.6
71.5	1.057	0.265	1.322	70.5	82.6	80.0
96.9	0.997	0.301	1.298	66.4	80.2	76.8
120.3	0.885	0.319	1.204	59.0	79.0	73.5
143.3	0.798	0.319	1.117	53.2	79.0	71.4
168.5	0.723	0.296	1.019	48.2	80.5	70.9
196.1	0.667	0.317	0.984	44.5	79.2	67.8
215.3	0.638	0.318	0.956	42.5	79.1	66.7
Mean (S.D.)			1.227 (0.202)			
Correlation Coefficient				0.9963	0.8361	0.9711
Slope x 10^3				-3.986	-0.853	-1.704
(S.D. x 10^3)				(0.122)	(0.198)	(0.148)
(RSD Slope)				(3.1%)	(43.1%)	(8.7%)
Intercept				4.569	4.515	4.535
(S.D.)				(0.016)	(0.025)	(0.019)
(Calculated as % initial)				(96.45%)	(91.38%)	(93.22%)
k_{obs} x 10^7 s^{-1}				11.1	2.37	4.73

Table 3.6 - Degradation of 1.6 x 10^{-3} M cirazoline [CIR] hydrochloride in 0.1 M HCl at 70°C. Residual concentrations and first order rate constants calculated according to equations 3.6 - 3.8.

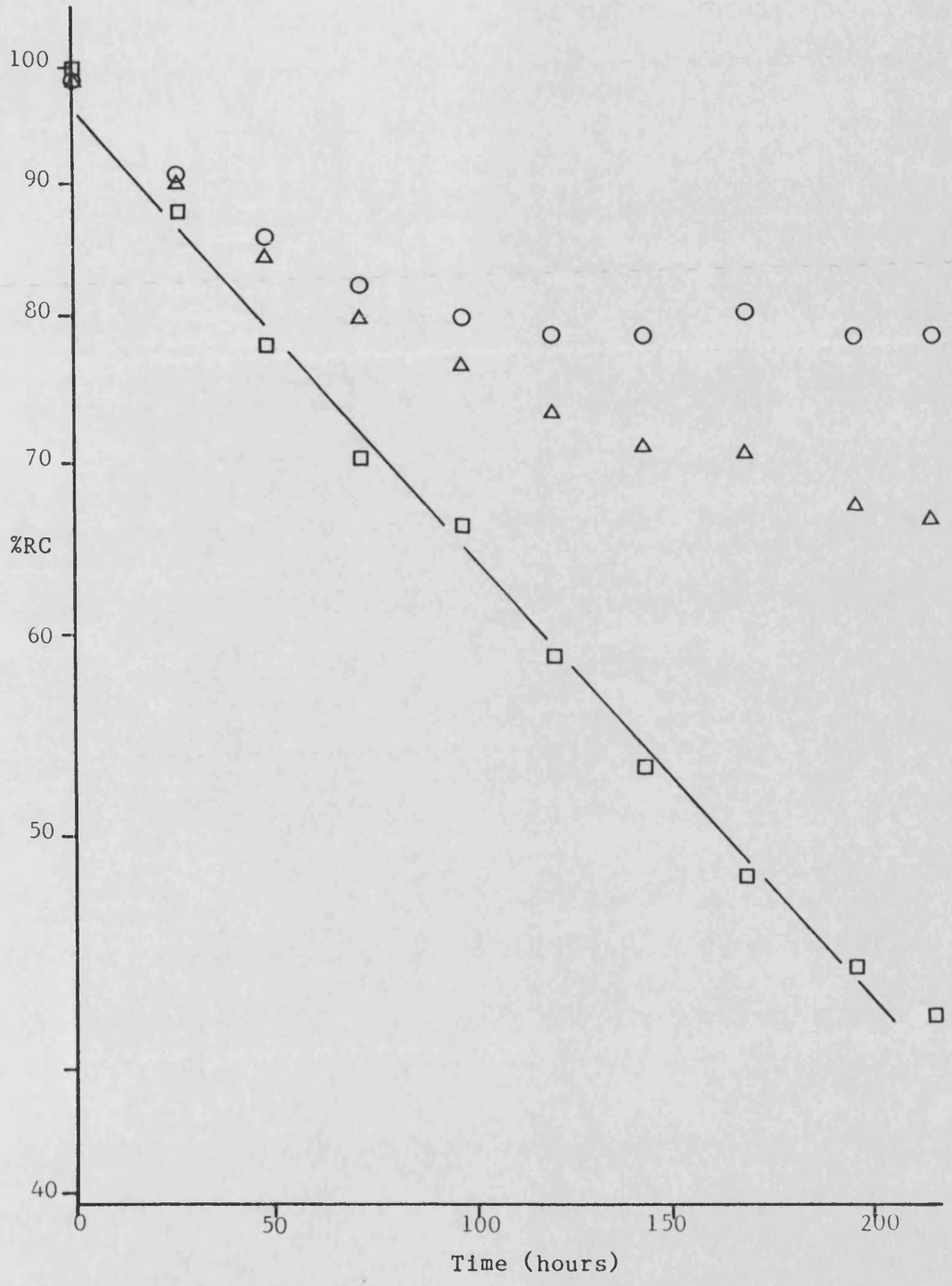

Figure 3.6 - First order plot for the degradation of 1.6×10^{-3} M cirazoline hydrochloride in 0.1 M HCl, 70°C. Percent residual concentration (%RC) values calculated using (a) equation 3.6, (—□—), (b) equation 3.7, (—○—), and (c) equation 3.8, (—△—).

In surfactant studies where cirazoline dodecylsulphate was precipitated from solution and representative sampling of cirazoline could not be achieved, calculation of percent residual concentration was made by reference to CPAE concentration alone (method 2, equation 3.7). An example of such data is given by the degradation of 2×10^{-3} M cirazoline hydrochloride in 1×10^{-3} M SDDS at pH 7.0 and 30°C, table 3.7 and figure 3.7.

3.1.7 Adaptation of HPLC Assay to Other Imidazolines

Antazoline, fenoxazoline and naphazoline samples were analysed using the HPLC conditions described for cirazoline with apovincamine as internal standard. HPL chromatograms of initial and partially degraded samples are shown in figures 3.8 to 3.10. Partial degradation in the initial fenoxazoline sample is evident (see section 2.1.2.1). Tolazoline and xylometazoline could not be detected at 275 nm as their UV absorbance at this wavelength is too low. Assays were therefore, carried out at a wavelength of 240 nm in the absence of internal standard and calculation was by reference to external standard peak areas. HPL chromatograms of initial and partially degraded solutions are shown in figures 3.11 and 3.12. Tolazoline and xylometazoline degradation product peaks were not detected on the HPL chromatograms. Chromatographic parameters are presented in table 3.1; satisfactory resolution (R_s) and selectivity (α) were obtained for all peaks except the fenoxazoline/internal standard peaks (R_s = 1.0, α = 1.3), figure 3.9. This fenoxazoline assay method was used, however, as satisfactory peak area ratio/concentration linearity was obtained.

Calibration curves were constructed for each imidazoline up to a concentration of 4.8×10^{-4} M and are shown in figures 3.13 to 3.15.

TIME (HOURS)	CONCENTRATION (M x 10^3) CIR	CPAE	TOTAL	% RESIDUAL CONCENTRATION METHOD 1 (equation 3.6)	METHOD 2 (equation 3.7)	METHOD 3 (equation 3.8)
0	2.000	0	2.000	100.0	100.0	100.0
3.42	1.242	0.028	1.270	62.1	98.6	97.8
8.42	1.036	0.066	1.102	51.8	96.7	94.0
20.2	0.969	0.185	1.154	48.4	90.8	84.0
29.8	1.767	0.237	2.004	88.3	88.2	88.2
44.2	1.596	0.326	1.922	79.8	83.7	83.1
51.3	1.571	0.342	1.913	78.6	82.9	82.1
56.8	1.451	0.371	1.822	72.5	81.5	79.7
68.4	1.308	0.464	1.772	65.4	76.8	73.8
74.8	1.296	0.508	1.804	64.8	74.6	71.8
Mean (S.D.)			1.676 (0.356)			
Correlation Coefficient				0.0374	0.9957	0.9648
Slope x 10^4				+3.115	-36.97	-39.50
(S.D. x 10^4)				(29.42)	(1.221)	(3.809)
(RSD Slope)				(944%)	(3.3%)	(9.6%)
Intercept				4.231	4.597	4.583
(S.D.)				(0.130)	(0.006)	(0.017)
(Calculated as % initial)				(68.79%)	(99.19%)	(97.81%)
k_{obs} x 10^6 s^{-1}				-	1.03	1.10

Table 3.7 - Degradation of 2 x 10^{-3} M cirazoline [CIR] hydrochloride in 1 x 10^{-3} M SDDS at pH 7.0, 30°C. Residual concentrations and first order rate constants calculated according to equations 3.6 - 3.8.

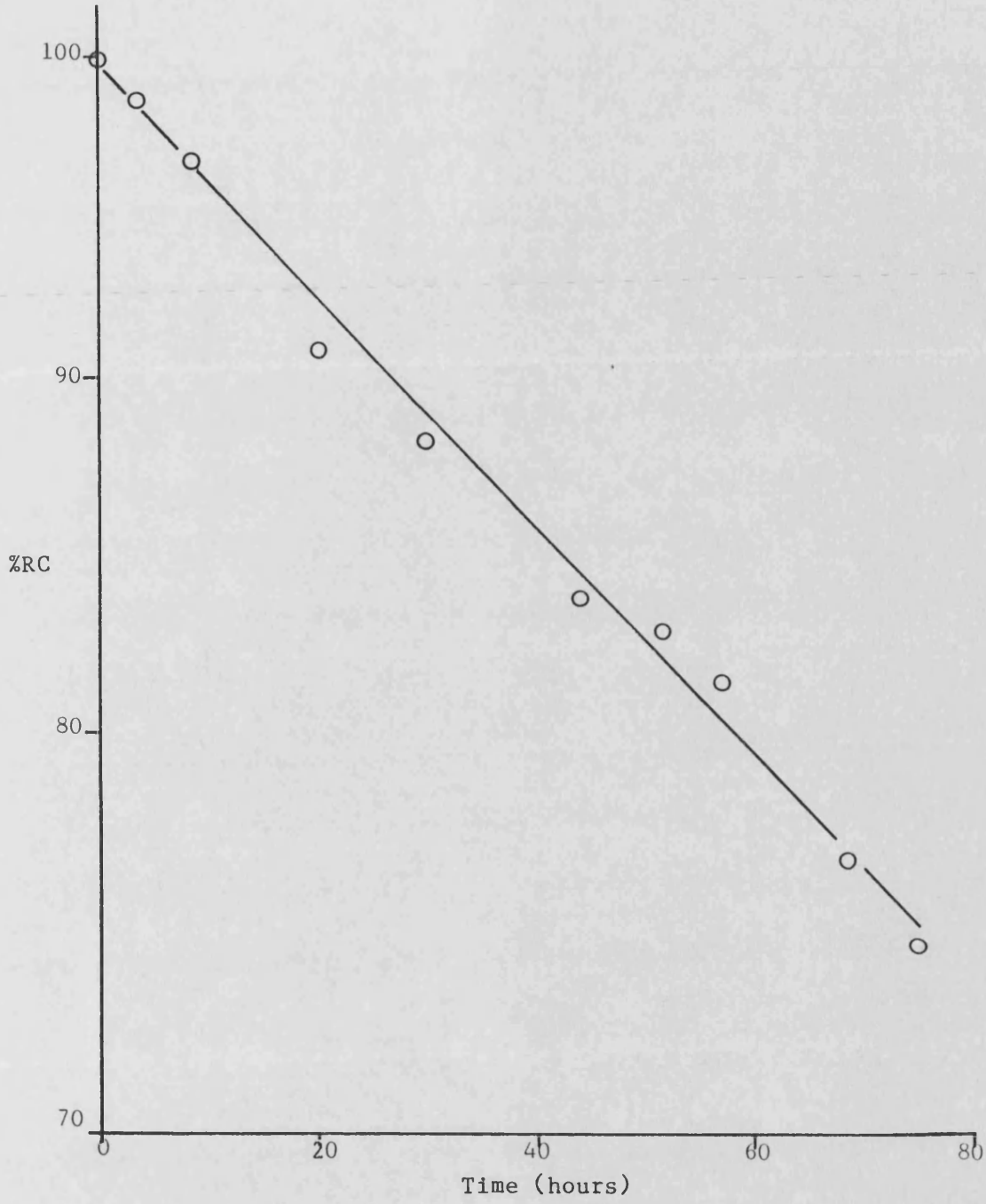

Figure 3.7 - First order plot for the degradation of 2 x 10^{-3} M cirazoline hydrochloride in 1 x 10^{-3} M SDDS, pH 7.0, 30°C. Percent residual concentration (%RC) values calculated using equation 3.6.

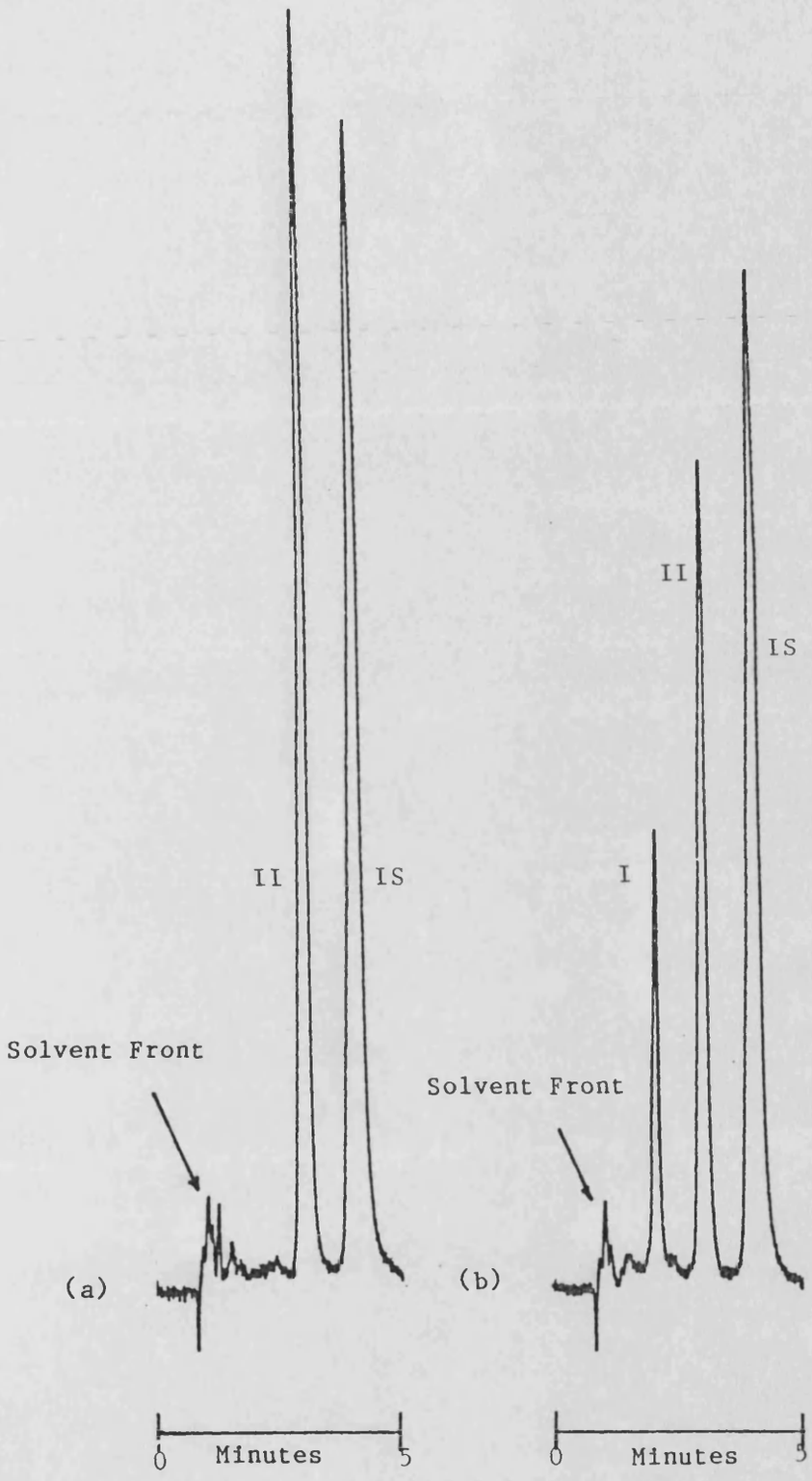

Figure 3.8 - HPL chromatogram of 3.2×10^{-4} M antazoline sulphate (II), (a) initial sample, (b) after storage in phosphate buffer pH 6.85, 70°C for 8.3 hours. I = degradation product, IS = 20 μg ml^{-1} apovincamine. (Chart speed = 5 mm min^{-1}, detection at 275 nm, 0.04 AUFS).

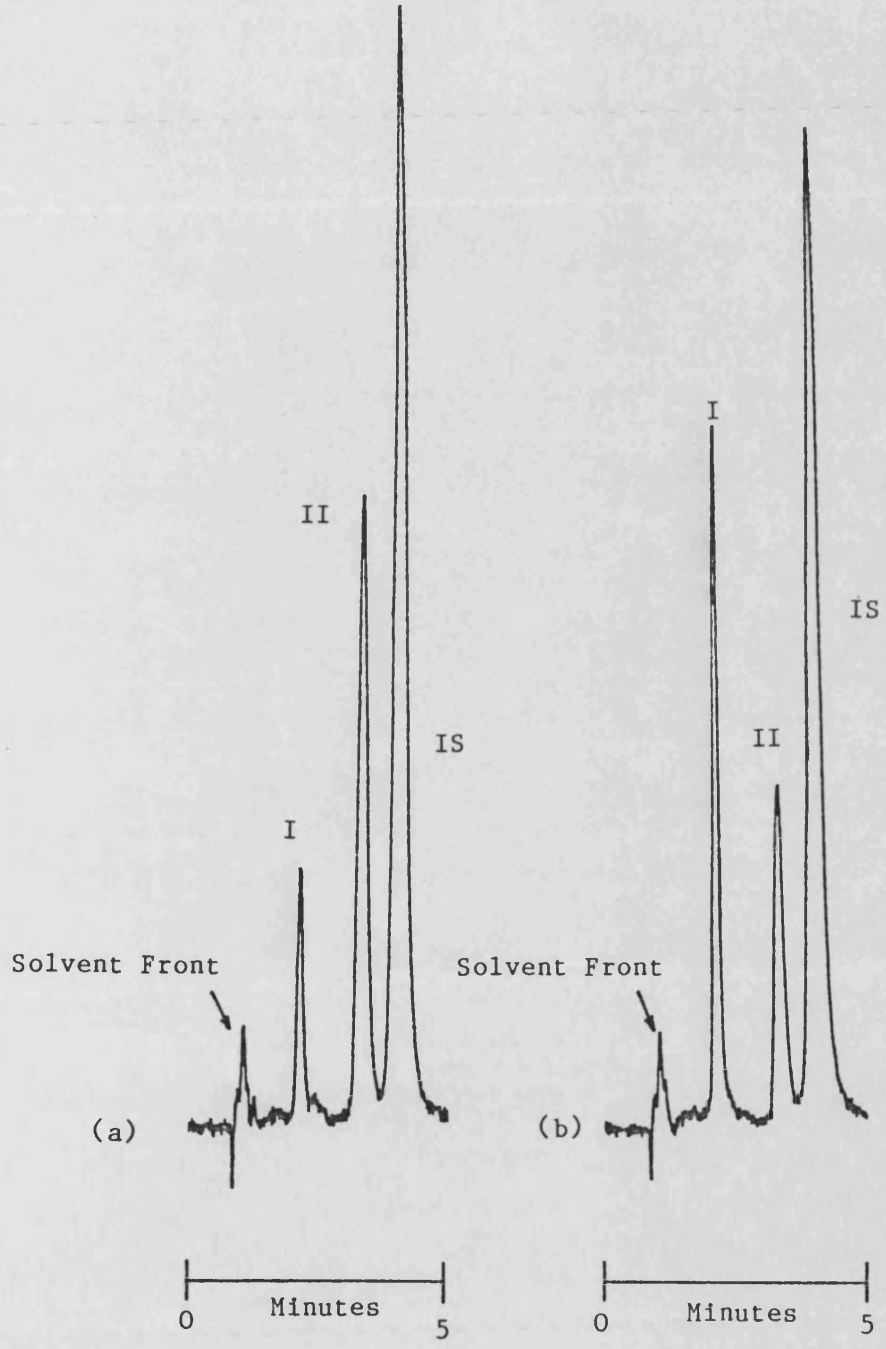

Figure 3.9 - HPL chromatogram of 3.2×10^{-4} M fenoxazoline hydrochloride (II), (a) Initial sample showing presence of degradation product (I), (b) after storage in phosphate buffer pH 6.85, 70°C for 38 minutes. IS = 20 µg ml^{-1} apovincamine. (Chart speed = 5 mm min^{-1}, detection at 275 nm, 0.04 AUFS).

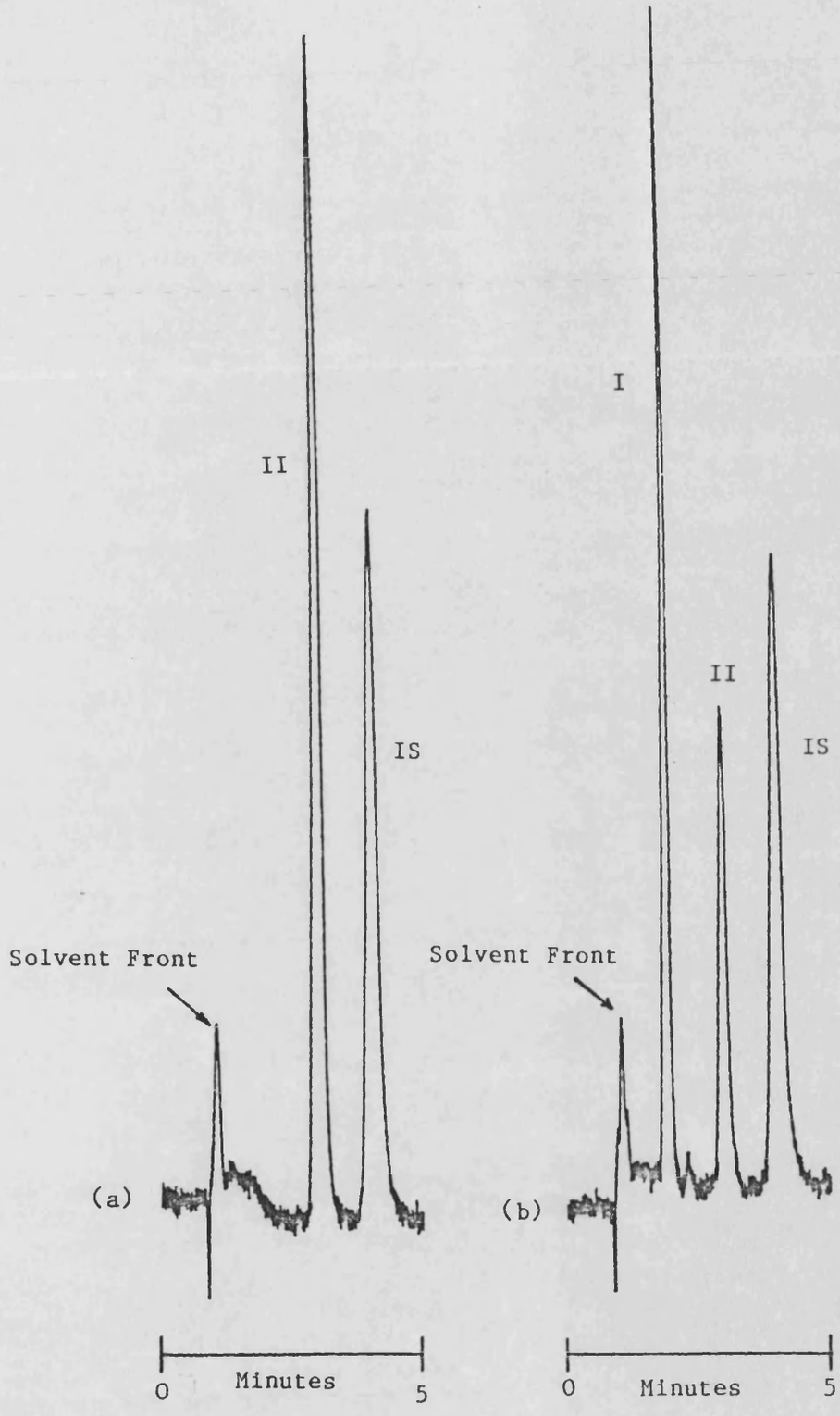

Figure 3.10 - HPL chromatogram of 6.4×10^{-5} M naphazoline nitrate (II), (a) initial sample, (b) after storage in phosphate buffer pH 6.85, 70°C for 77 hours. I = degradation product, IS = 10 μg ml^{-1} apovincamine. (Chart speed = 5 mm min^{-1}, detection at 275 nm, 0.04 AUFS).

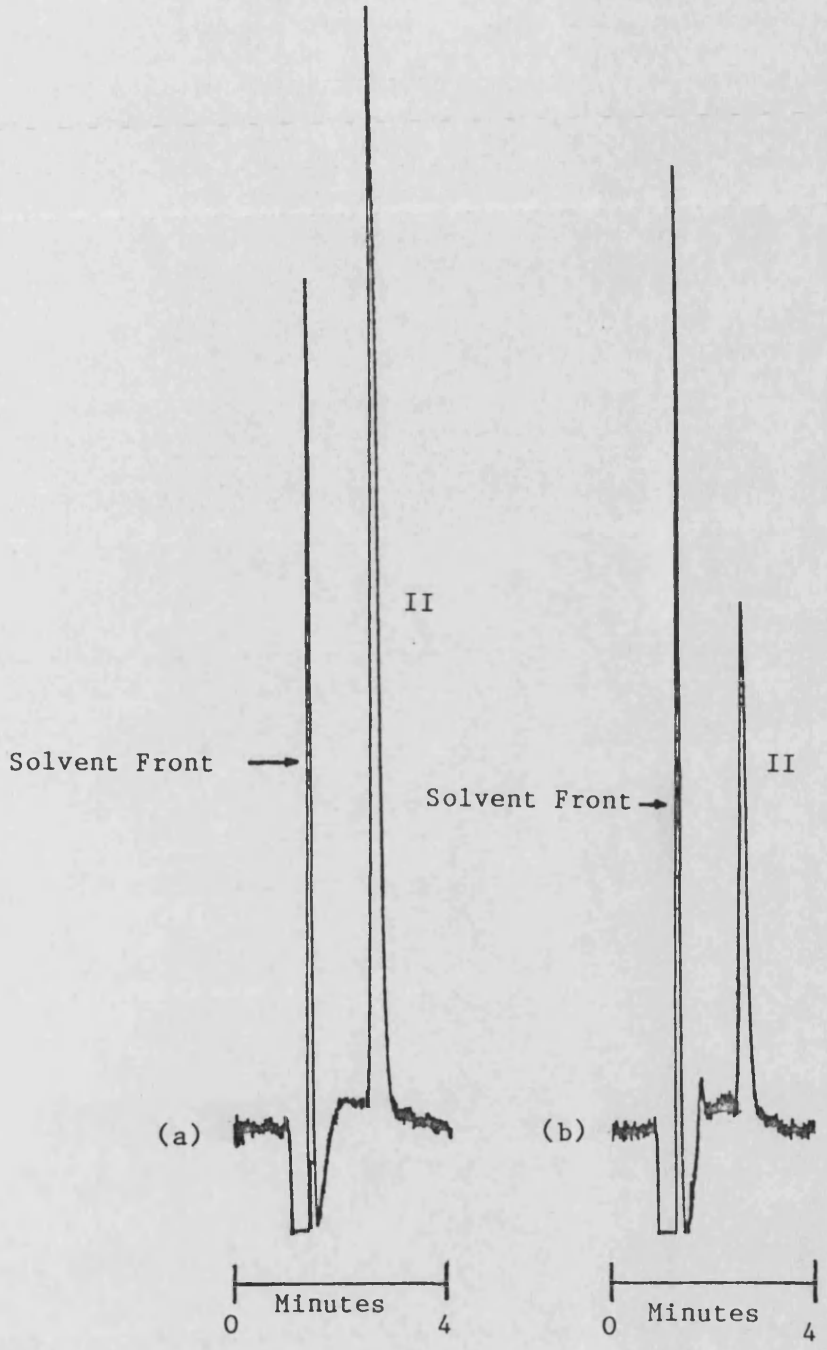

Figure 3.11 - HPL chromatogram of 3.2×10^{-4} M tolazoline hydrochloride (II), (a) initial sample, (b) after storage in phosphate buffer pH 6.85, 70°C for 51 hours. (Chart speed = 5 mm min^{-1}, detection at 240 nm, 0.04 AUFS).

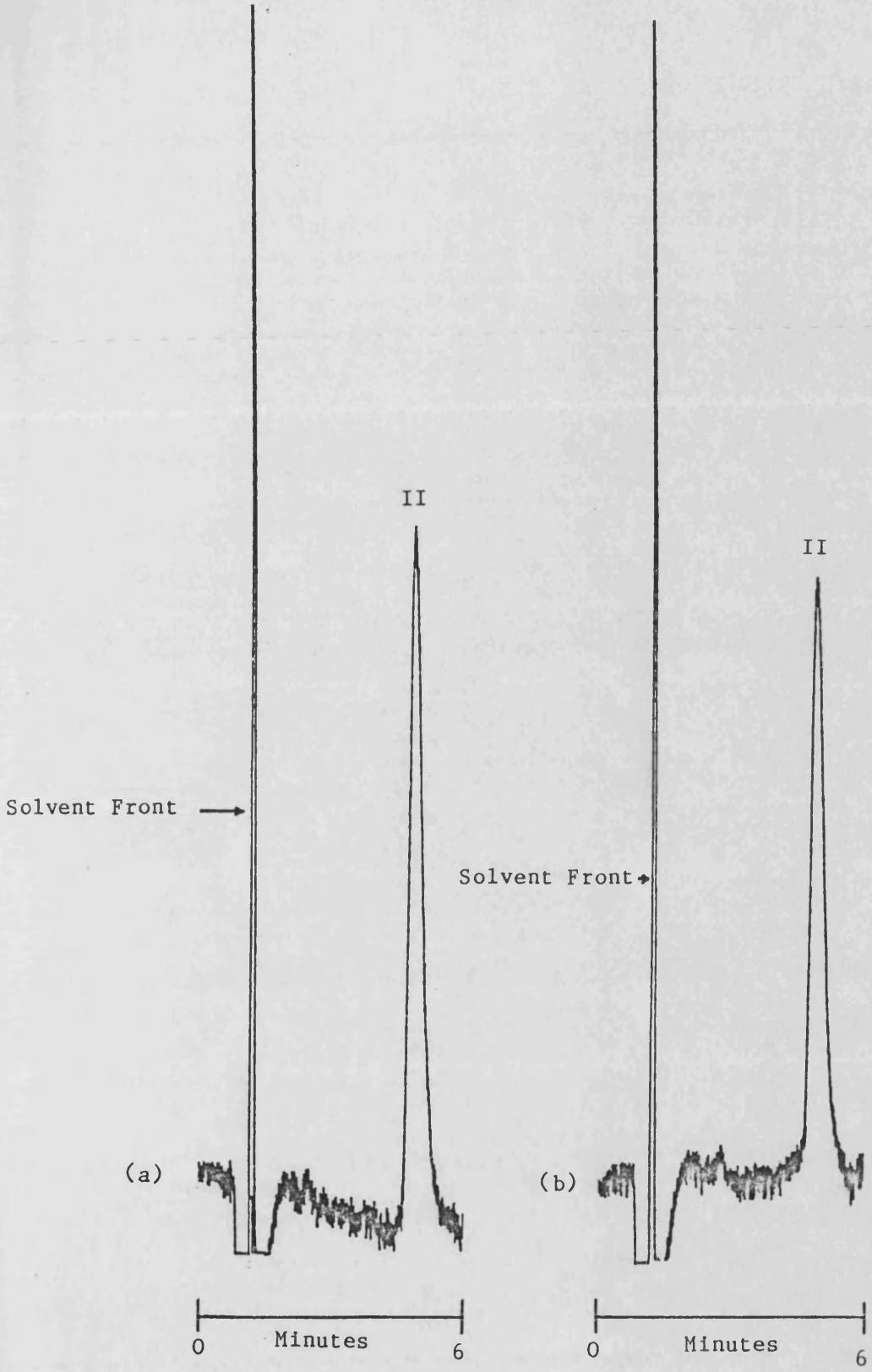

Figure 3.12 - HPL chromatogram of 1.6×10^{-4} M xylometazoline hydrochloride (II), (a) initial sample, (b) after storage in phosphate buffer pH 6.85, 70°C for 103 hours. (Chart speed = 5 mm min^{-1}, detection at 275 nm, 0.04 AUFS).

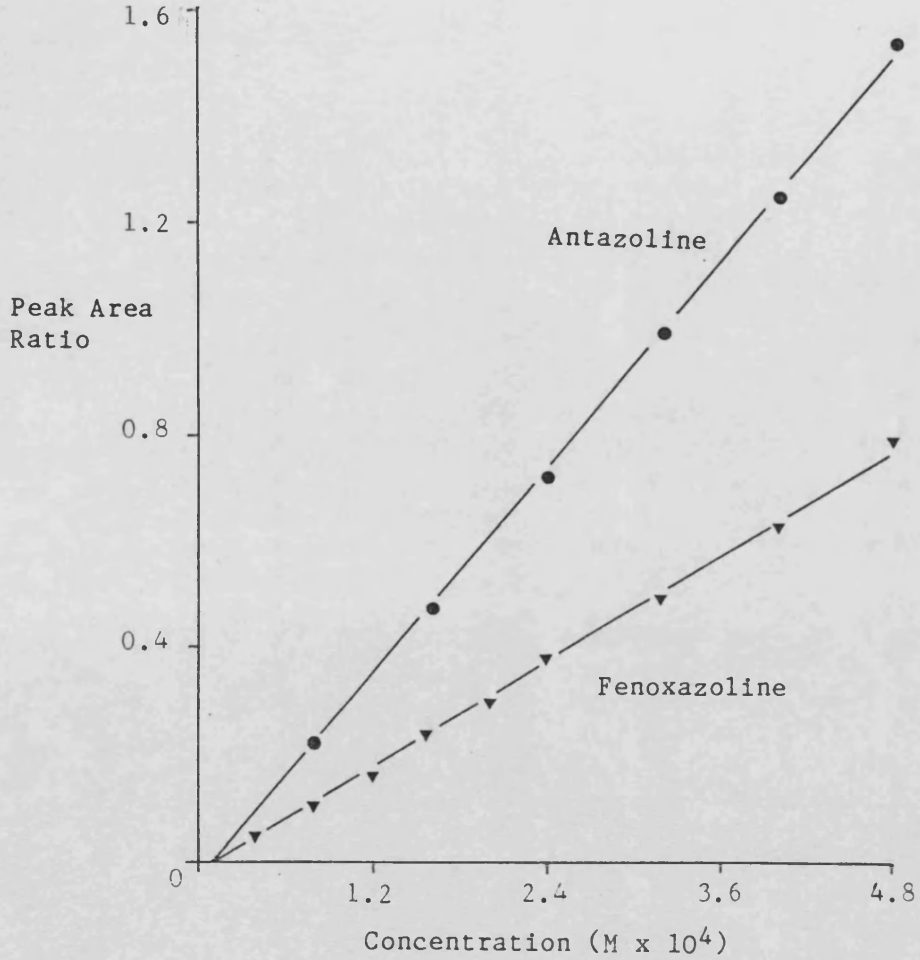

Figure 3.13 - HPLC calibration plots for antazoline sulphate (—●—) fenoxazoline hydrochloride (—▼—) using 20 μg ml^{-1} apovincamine as internal standard.

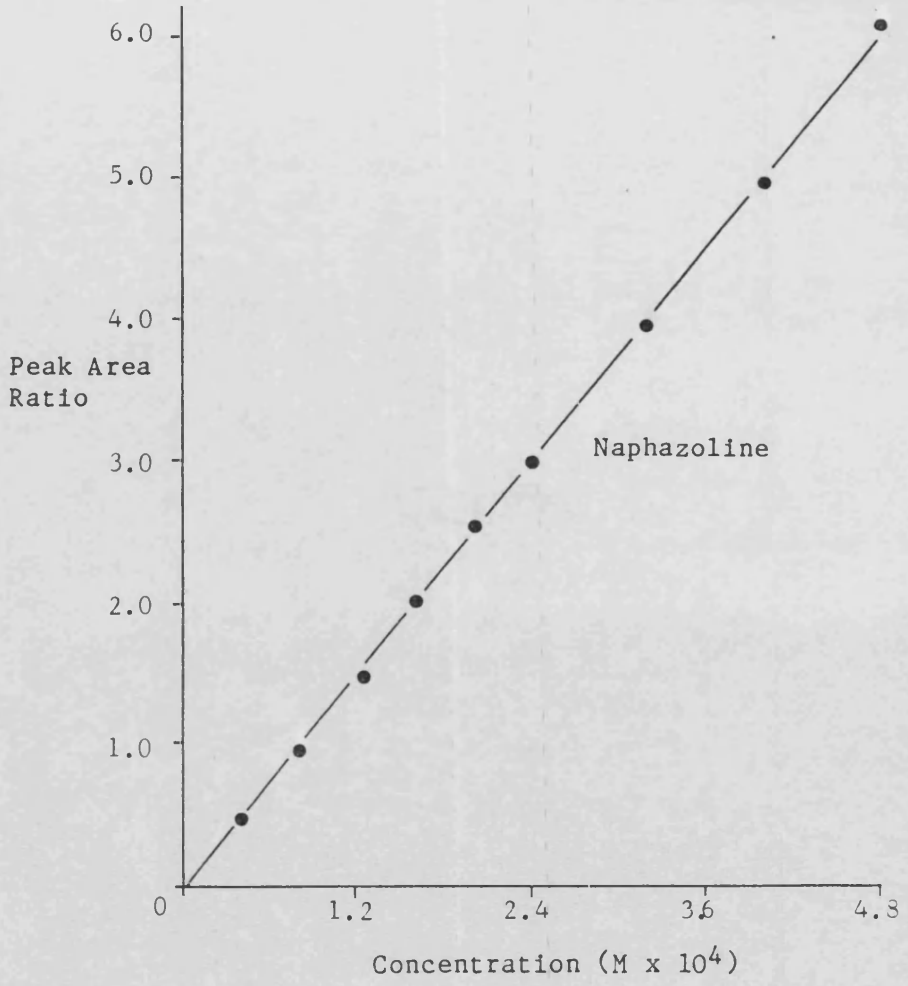

Figure 3.14 - HPLC calibration plot for naphazoline nitrate using 20 μg ml^{-1} apovincamine as internal standard. Detection at 275 nm.

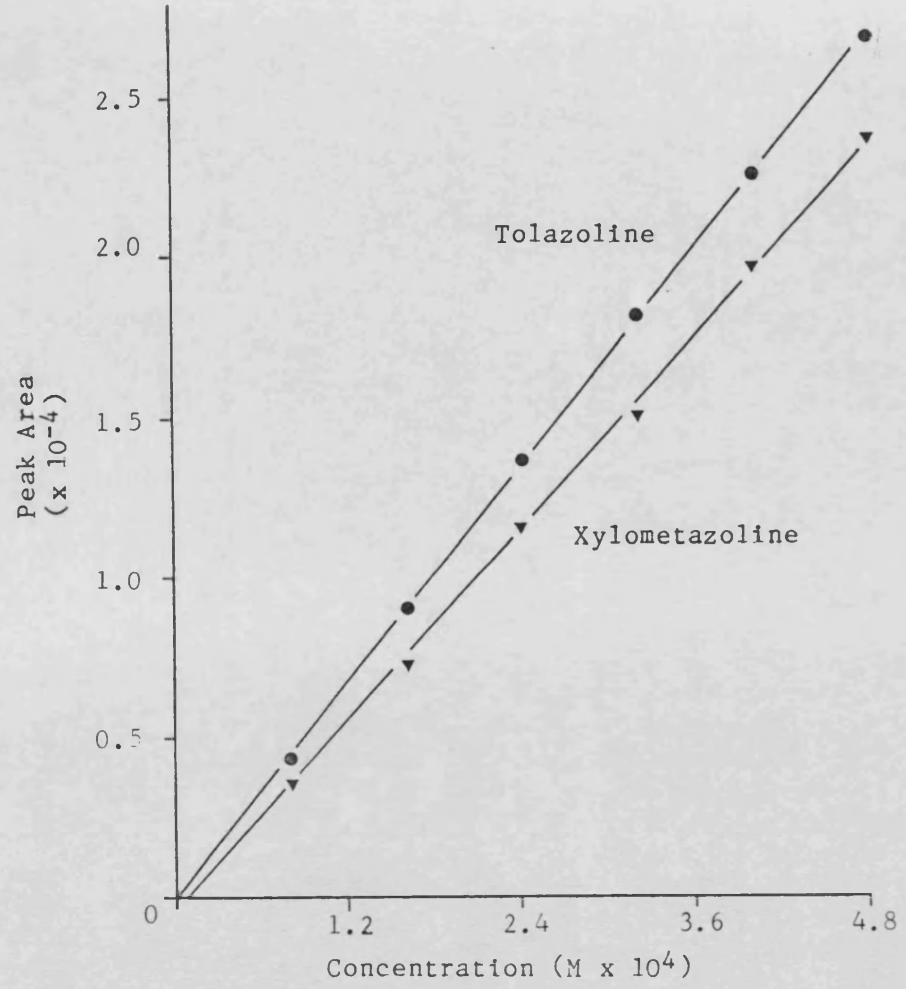

Figure 3.15 - HPLC calibration plots for tolazoline hydrochloride (—●—) and xylometazoline hydrochloride (—▼—). Detection at 240 nm.

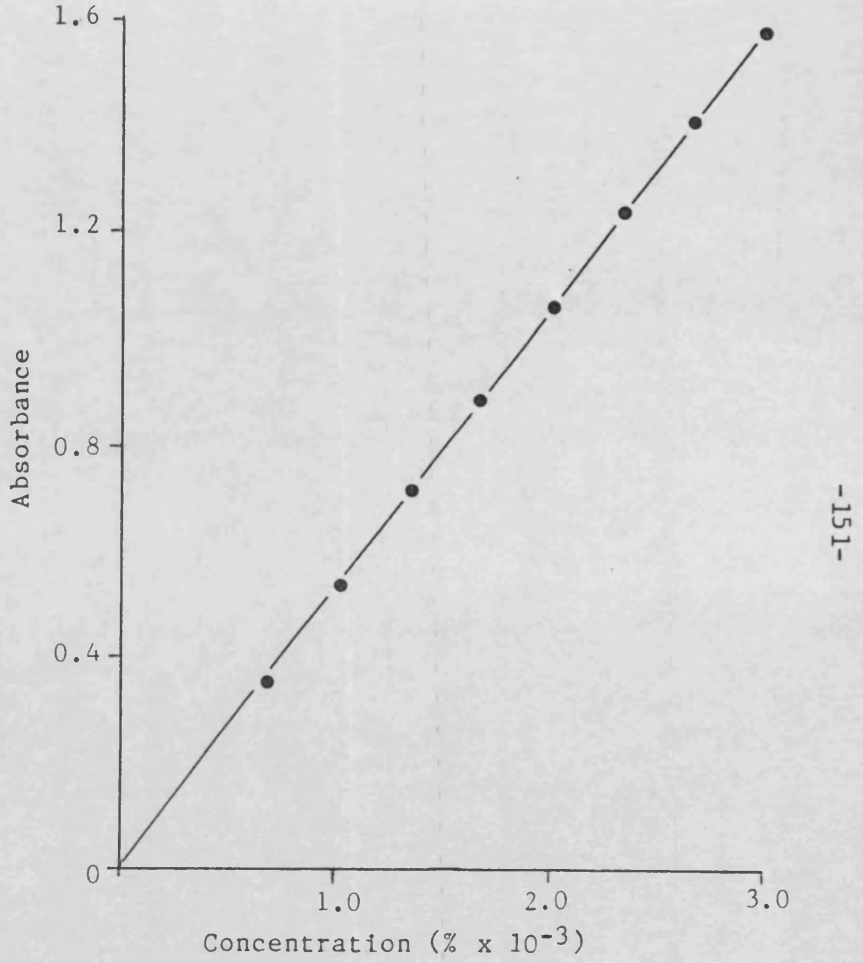

Figure 3.16 - Beer Lambert plot for 2-methyl-2-imidazoline in 4 x 10^{-3} M HCl at 218 nm.

Linear regression analysis data are summarised in table 3.8. Naphazoline and tolazoline calibration curves pass close to the origin (intercept < $\pm$ 2 S.D.s. from the origin), but antazoline, fenoxazoline and xylometazoline curves have negative intercepts, > 2 S.D.s. from the origin. The magnitude of the intercepts is small, however, and the error in first order rate constant determination resulting from the assumption that the calibration curves pass through the origin is considered to be minimal (<4%). All curves show the peak area (ratio) to be proportional to concentration. Sample concentration was therefore calculated by reference to a single standard solution which was assayed alongside the samples, (see equation 3.5).

2-methyl-2-imidazoline could not be analysed using the HPLC method as significant absorbance does not occur above the UV cut-off point of the mobile phase system; it was therefore assayed by UV spectrophotometry (section 3.2).

3.2 UV ASSAY OF 2-METHYL-2-IMIDAZOLINE

2-methyl-2-imidazoline was assayed by UV analysis at 218 nm using a Perkin Elmer 550S UV-VIS spectrophotometer with 1 cm pathlength quartz cuvettes. Absorbance was measured in duplicate against double distilled water and spectra were recorded on a Perkin Elmer 561 chart recorder.

A 0.05 M stock solution was prepared in 0.06 M HCl solution. This HCl concentration was chosen to ensure complete neutralisation of the free base and provide a sufficiently acidic environment to inhibit degradation during storage.

	ANT*	FEN*	NAP*	TOL	XYL
Number of Data Points	6	9	9	6	6
Correlation Coefficient	0.9996	0.9987	0.9998	0.9998	0.9993
Slope x 10^{-3}	3.287	1.679	12.70	56510	50570
(S.D. x 10^{-3})	(0.044)	(0.033)	(0.10)	514	965
(RSD Slope)	(1.3%)	(2.0%)	(0.8%)	(0.9%)	(1.9%)
Intercept	-0.050	-0.029	-0.055	7	-635
(S.D.)	(0.014)	(0.009)	(0.028)	160	301

Table 3.8 - Linear regression analysis data for imidazoline HPLC calibration plots (peak area (ratio) against molar concentration). (ANT = antazoline, FEN = fenoxazoline, NAP = naphazoline, TOL = tolazoline and XYL = xylometazoline).

* Peak area ratio (internal standard = 20 µg/ml apovincamine)

This stock solution was suitably diluted to provide eight concentrations in the range 0.672 - 3.024 x 10^{-3}% (0.8 - 3.6 x 10^{-4} M nominal) in 4 x 10^{-3} M HCl from which a Beer-Lambert plot was constructed, (figure 3.16). Linear regression analysis on the data expressed in % w/v concentration terms gave the following data:

Correlation coefficient:	0.99997
Slope x 10^{-2} (S.D. x 10^{-2}):	5.207 (0.016)
Intercept (S.D.):	0.017 (0.003)

Results show absorbance to be proportional to concentration with an $E^{1\%}_{1cm}$ value of 521 and an apparant molar extinction coefficient (ε) of 4.40 x 10^3 (literature value = 4.9 x 10^3 at 218 nm[28]). The difference between the calculated and literature ε values (10%) is probably due to the presence of water within the sample (see section 2.1.2.1). A positive intercept > $\pm$ 2 S.D.s. from the origin was obtained; the magnitude of the intercept was small, however, and the error resulting from the assumption that the calibration curve passes through the origin is considered to be minimal (<2%).

The assay was shown to be stability indicating by degrading a 0.0168% w/v solution in 0.1 M NaOH at 70°C. 4 ml samples were withdrawn at appropriate intervals, acidified with 5 mls of 0.1 M HCl and diluted to 25 mls, with distilled water. Absorbance was measured at 218 nm and the spectrum from 185 to 260 nm recorded. Samples showed a rapid fall in absorbance at 218 nm to a constant residual value 0.073. Spectra are shown in figure 3.17.

The percentage residual concentration (% RC) for the degradation of 2-methyl-2-imidazoline was calculated from equation 3.9:

$$\% \text{ RC} = \frac{A_t - 0.073}{A_I - 0.073} \times 100 \qquad (3.9)$$

Where A_I and A_t are the initial absorbance and absorbance after time t, respectively.

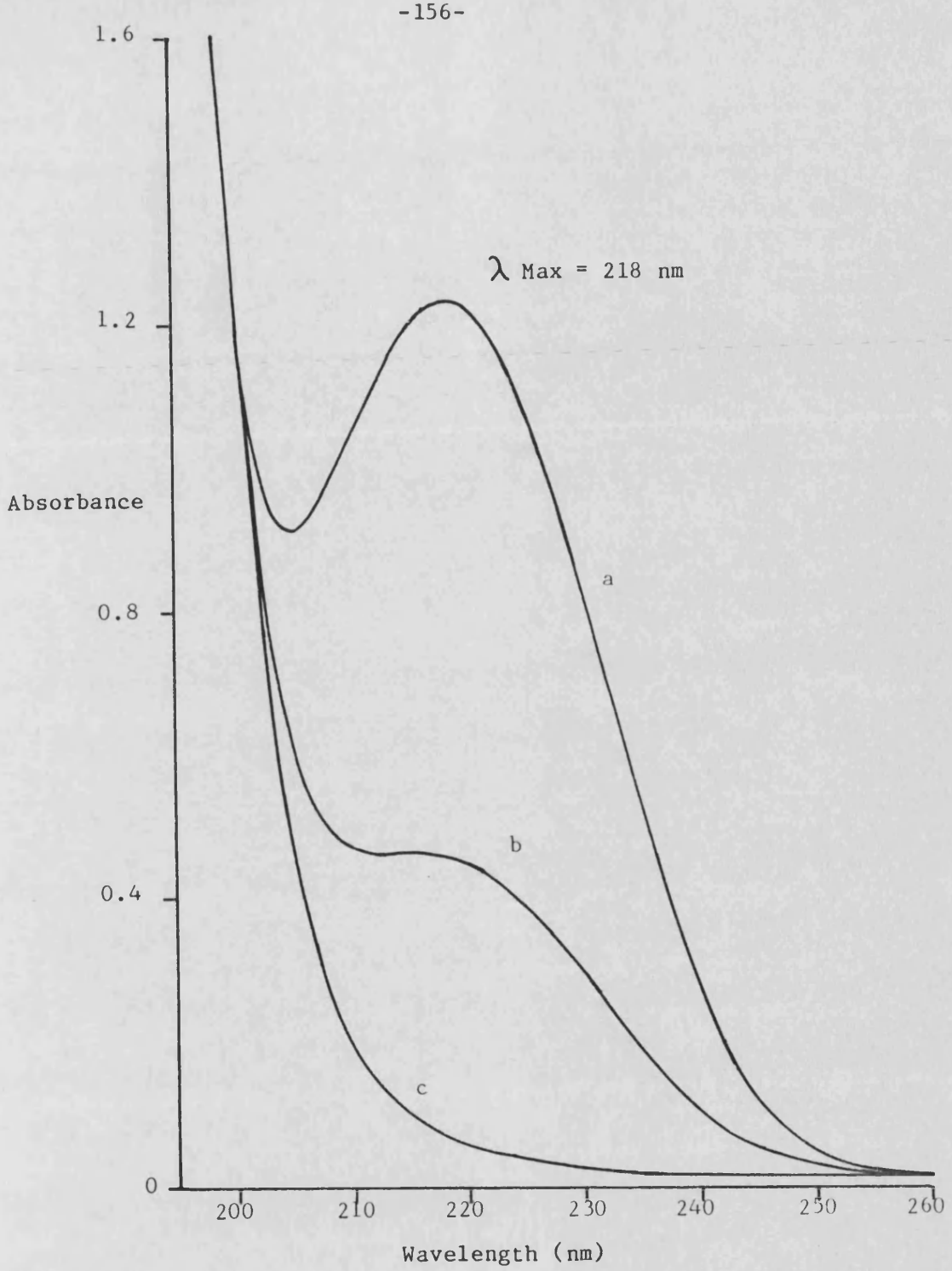

Figure 3.17 - UV spectra of 2-methyl-2-imidazoline (2.69 % w/v) after storage as a 1.68 x 10^{-2} % w/v solution in 0.1 M NaOH, (a) initial, (b) after 6 minutes and (c) after 104 minutes.

4. pK_a OF CIRAZOLINE AND CPAE

4.1 INTRODUCTION

pK_a values are of particular importance as a knowledge of the amount of ionised species is crucial when investigating ionic interactions. For the dissociation of cirazoline, the intrinsic or thermodynamic ionisation constant, K_a, is given by equation 4.1.

$$CIRH^+ \overset{K_a}{\rightleftharpoons} CIR + H^+$$

$$K_a = \frac{a_{H^+} . a_{CIR}}{a_{CIRH^+}} = - \text{antilog } pK_a \qquad (4.1)$$

Where a represents the activities of the various species. If the activities of the conjugate acid-base species are replaced by stoichiometric concentrations, $[CIRH^+]$ and $[CIR]$, an apparant ionisation constant, K_a', is obtained, (equation 4.2):

$$K_a' = \frac{a_{H^+} [CIR]}{[CIRH^+]} = - \text{antilog } pK_a' \qquad (4.2)$$

The thermodynamic and apparant pK_a values are related by equation 4.3:

$$pK_a' = pK_a - \log_{10} \cdot \gamma_{CIRH^+} \qquad (4.3)$$

Where γ_{CIRH^+} is the activity coefficient for the cirazoline cation, $CIRH^+$ and can be calculated from the Debye-Hückel equation (equation 1.16). Equations 4.1 and 4.2 may be written in the form of the Henderson-Hasselbalch equations, (equations 4.4 and 4.5 respectively):

$$pK_a = pH + \log_{10} \left(\frac{a_{CIRH^+}}{a_{CIR}} \right) \qquad (4.4)$$

$$pK_a' = pH + \log_{10} \frac{[CIRH^+]}{[CIR]} \qquad (4.5)$$

As ionic strengths approach zero, concentrations approximate closely to activities and $pK_a' \dashrightarrow pK_a$.

The pK_a values of weak bases such as cirazoline are particularly sensitive to temperature. Over temperature ranges where the standard enthalpy change (ΔH^o) and standard entropy change (ΔS^o) for ionisation are constant, the pK_a temperature dependency can be calculated from a form of the Van't Hoff equation (4.6):

$$pK_a = \frac{\Delta H^o}{2.303R} \cdot \frac{1}{T} - \frac{\Delta S^o}{2.303R} \qquad (4.6)$$

Where R is the gas constant and T is in degrees Kelvin. Plots of pK_a against T^{-1} should therefore be linear. Over extended temperature ranges where ΔH^o and ΔS^o may show variations, pK_a temperature profiles may show minima and temperature dependence can follow a virial equation:

$$pK_a = \frac{P}{T} + Q + RT \ldots\ldots \qquad (4.7)$$

Where P and Q are constants. For temperature ranges where equation 4.6 holds, Perrin has proposed an expression for the calculation of a temperature coefficient $\frac{-d(pK_a)}{dT}$ for the pK_a of monoacidic bases (equation 4.8)[200]:

$$-\frac{d(pK_a)}{dT} = \frac{pK_a - 0.9}{T} \qquad (4.8)$$

Techniques for determining the pK_a values of weak acids and bases include potentiometric titration, solubility, nuclear magnetic resonance spectoscopy, spectrophotometry and conductimetry. The method

employed for the determination of cirazoline pK_a was the potentiometric method described by Albert and Serjeant[201]. This method involves titrating a solution of the weak base or acid for which the pK_a is to be determined with a solution of strong acid or base. This method was chosen for its speed, an important factor as the stability of aqueous of cirazoline at high pH is poor. In view of this stability problem, special attention was given to minimising exposure of solutions to high pH; solutions were assayed after titration completion and the extent of degradation determined by reference to cirazoline and CPAE concentration. Titration of dilute solutions, (approximately 1×10^{-3} M), was used due to the poor solubility of the free base. Potassium hydroxide was used as titrant rather than sodium hydroxide as the potassium ion gives rise to less electrode error.

The presence of carbonate in the titrant solution produces inaccuracies in pK_a determination as exact concentrations of salt and free base must be known. Formation of potassium hydrogen carbonate will reduce the amount of titrant able to react with cirazoline. This will not be detected by standardization with a strong acid, as unlike weak acids such as cirazoline hydrochloride, strong acids will react with potassium hyrogen carbonate. Possible sources of carbonate contamination are:-

(a) Carbonate present on the surface of potassium hydroxide pellets.

(b) Carbonate present in water formed from equilibrium with carbon dioxide in the air.

To overcome these problems, carbonate free potassium hydroxide solution was prepared, freshly boiled and cooled double distilled water used throughout and all solutions were maintained below nitrogen.

4.2 EXPERIMENTAL

4.2.1 Preparation of Carbonate-Free Potassium Hydroxide

A small amount of glass wool was placed in the bottom of a quickfit dropping funnel and about 20 g of potassium hydroxide pellets added. Sufficient freshly boiled and cooled double distilled water was added to just cover the pellets. A soda-lime guard tube was fitted and the aqueous solution immediately drained to waste. After a repeat washing procedure, the dropping funnel was filled with more water, stoppered, and shaken until all the potassium hydroxide had dissolved. The soda-lime guard tube was replaced and the first 5 -10 mls of solution ran to waste. The remaining solution was collected in a quickfit conical flask and stored under nitrogen. The concentration of solution thus produced was determined by diluting a sample and titrating against 0.1 M HCl using methyl orange as indicator. The concentration of the stock solution of carbonate-free potassium hydroxide was found to be 0.3171 M.

4.2.2 Titration Procedure

The apparatus used for the determination of pK_a values is shown in figure 4.1.

Potentiometric titrations of cirazoline hydrochloride were carried out at 25°, 30°, 35° and 40°C in the presence of 0.1 M potassium chloride since the electrode response time was slow at very low ionic strengths. Titration of CPAE was carried out at 25°C.

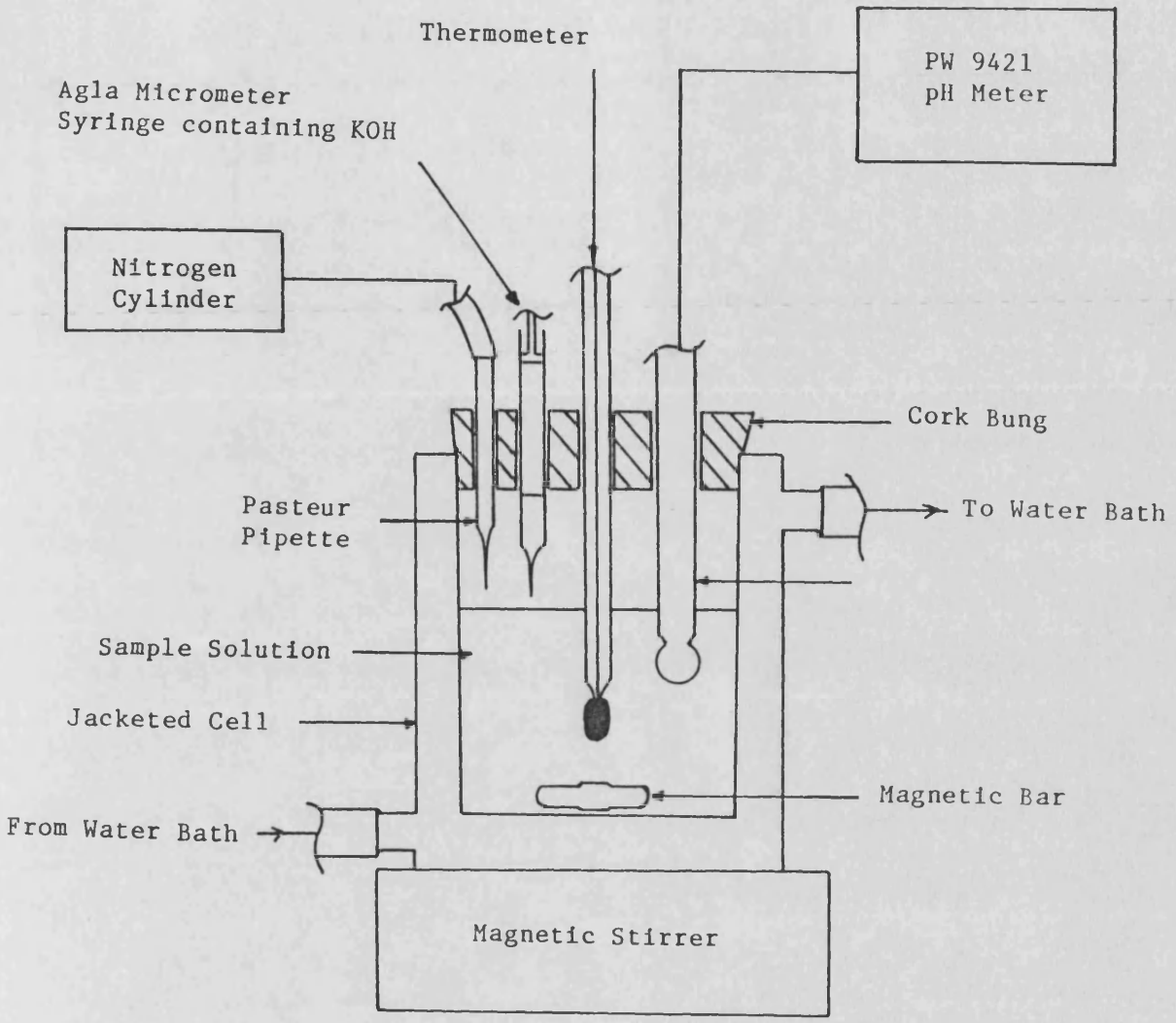

Figure 4.1 - Apparatus used for the determination of pK_a values by potentiometric titration.

Potassium chloride (1.49 g) and freshly boiled and cooled double distilled water (200 g) were weighed and transferred to the jacketed cell. About 50 mg of cirazoline hydrochloride or CPAE (approximately 1×10^3 M) were accurately weighed into the cell and the bung inserted. The tip of the nitrogen feed line was positioned about 1 cm above the solution and the flow rate adjusted to produce a slight impression on the surface. The thermometer and pH probe were immersed in the liquid and all other holes in the cork bung stoppered. The magnetic stirrer was switched on and the solution allowed to equilibrate to temperature.

The Agla micrometer syringe, fitted with a straight glass needle, was carefully filled with carbonate-free potassium hydroxide solution, minimising exposure to air. The syringe was inserted into the cell and positioned so as the tip of the needle was just above the surface of the liquid. The titration commenced by lowering the syringe into the stirring solution and adding the required volume of potassium hydroxide. After a few seconds the syringe was withdrawn from the solution and the pH of the still solution recorded. The titration continued until at least four pH readings were produced. The volume of titrant added was always <0.2% of the initial volume. Immediately the titration was complete, the solution was acidified with 0.1 M HCl and a sample taken for assay. The percent residual concentration was calculated by reference to cirazoline and CPAE concentration (method 3, equation 3.8, section 3.1.6).

4.2.3 Treatment of Experimental Data

Individual apparant pK_a values were calculated after each addition of titrant using the Henderson-Hasselbalch equation (equation 4.5). For very dilute concentrations of weak acid or base or at high pH,

allowance must be made for the hydroxyl ion concentration, $[OH^-]$, of the solution when calculating $[CIRH^+]$ and [CIR] which are derived from the ion balance equation (equation 4.9) and the mass balance equation (equation 4.10).

$$[CIRH^+] + [K^+] + [H^+] = [Cl^-] + [OH^-] \qquad (4.9)$$

$$[CIRHCl]^T = [CIRH^+] + [CIR] = [Cl^-] \qquad (4.10)$$

Where $[K^+]$ is the concentration of potassium ions and is equal to the concentration of titrant [KOH] added, $[Cl^-]$ is the concentration of chloride ions and is equal to the total concentration of cirazoline hydrochloride added, $[CIRHCl]^T$. The experimental data in tables 4.1 - 4.5 show that after the addition of the first increment of titrant, $[H^+]$ becomes negligible compared to values of [CIR]. Equation 4.9 may therefore be reduced to equation 4.11:

$$[CIRH^+] = [CIRHCl]^T + [OH^-] - [KOH] \qquad (4.11)$$

Combining equations 4.10 and 4.11 gives:

$$[CIR] = [KOH] - [OH^-] \qquad (4.12)$$

$[OH^-]$ for this work was calculated from the hydroxyl ion activity, a_{OH^-}, which was obtained from equation 4.13. pK_w' values were calculated from equation 4.14 using standard literature values for pK_w at each experimental temperature[201].

$$-\log_{10} a_{OH^-} = pK_w' - pH = -\log_{10}[OH^-] - \log_{10} \gamma_{OH^-} \qquad (4.13)$$

$$pK_w' = -\log_{10} K_w' = pK_w + 2 \log_{10} \gamma_{\pm} \qquad (4.14)$$

Where K_w' and K_w are the apparent and intrinsic ionisation constants for water and $\gamma_{\pm}$ is the mean ion activity coefficient. γ_{OH^-} and $\gamma_{\pm}$ were calculated as 0.75 using equation 1.18.

The cirazoline concentration terms used to calculate pK_a' values from equation 4.5 were therefore calculated from equations 4.11 and 4.12. Intrinsic pK_a values were then estimated from equations 4.3 and 1.19. Values of A and B were taken from Robinson and Stokes[11], the product Ba_i was estimated as unity and the ionic strength, I, was taken as 0.1 M.

4.3 RESULTS

Tables 4.1-4.5 show the titration data, derived species concentrations and apparant pK_a' values obtained in 0.1 m KCl over the temperature range 24.9-39.5°. Mean values and the range were assessed using the protocol of Albert and Serjeant[201]; the mean is derived by converting pK_a' to K_a', calculating the mean K_a' and hence the mean pK_a'. The range is the largest deviation of this value from those found experimentally. Results are set out in table 4.6; observed range values conform well within the proposed criterion of acceptance which is a scatter of $\pm$ 0.06.

Figure 4.2 shows a plot of pK_a' against T for cirazoline in 0.1 m KCl. Linear regression analysis gave the following results: correlation coefficient = 0.99997, slope (S.D.) = -2.677 (0.015) x 10^{-2}, intercept (S.D.) = 17.58 (0.04). The temperature coefficient ($-dpK_a'/_{dT}$) is given by the slope and was found to be 0.027 pH units K^{-1}. This is in good agreement with the calculated value of 0.029 pH units K^{-1} (equation 4.8). Figure 4.3 shows the pK_a -temperature data plotted according to the Van't Hoff equation (equation 4.6). Linear regression

analysis data and thermodynamic parameters for the protonation of cirazoline at 25°C are shown in table 4.7.

ΔH^{o} for cirazoline was calculated from the slope of the Van't Hoff plot (figure 4.2), ΔG^{o} was obtained from equation 4.15 and ΔS^{o} was calculated from equation 4.16.

$$\Delta G^{o} = 2.303\ RT\ pK_a \qquad (4.15)$$

$$\Delta G^{o} = \Delta H^{o} - T\,\Delta S^{o} \qquad (4.16)$$

The thermodynamic parameters in table 4.7 indicate that protonation of cirazoline to form $CIRH^{+}$ is driven by a large negative free energy change (-54 kJ mol^{-1}) which is derived from a large exothermic enthalpy change (-48.2 kJ mol^{-1}) and a small positive entropy change (+20 J mol^{-1} K^{-1}).

VOLUME KOH (mls)	pH	CONCENTRATION (M x 10^6) OH^-	$CIRH^+$	CIR	pK_a'
0	6.350	-	1028.7	-	-
0.15	9.002	23.9	815.0	213.7	9.583
0.20	9.169	35.2	747.1	281.6	9.593
0.25	9.306	48.2	680.9	347.8	9.598
0.30	9.433	64.7	618.2	410.5	9.611
0.35	9.549	84.5	558.8	469.9	9.624

Table 4.1 - Data from the potentiometric titration of 0.3171 M KOH against cirazoline hydrochloride in 0.1 m KCl at 24.9°C. Apparent pK_a (pK_a') values calculated using γ_{OH^-} = 0.75 and pK_w = 13.747.

VOLUME KOH (mls)	pH	CONCENTRATION (M x 10^6) OH^-	$CIRH^+$	CIR	pK_a'
0	6.496	-	1038.6	-	-
0.15	8.887	23.9	824.9	213.7	9.474
0.20	9.051	34.8	756.6	282.0	9.480
0.25	9.189	47.9	690.5	348.1	9.486
0.30	9.310	63.3	626.7	411.9	9.492
0.35	9.422	82.0	566.2	472.4	9.501

Table 4.2 - Data from the potentiometric titration of 0.3171 M KOH against cirazoline hydrochloride in 0.1 m KCl at 29.0°C. Apparent pK_a (pK_a') values calculated using γ_{OH^-} = 0.75 and pK_w = 13.633.

VOLUME KOH (mls)	pH	CONCENTRATION (M x 10^6) OH^-	$CIRH^+$	CIR	pK_a'
0	6.400	-	1038.6	-	-
0.15	8.726	26.3	827.3	211.3	9.319
0.20	8.887	38.1	759.9	278.7	9.323
0.25	9.022	52.1	694.7	343.9	9.327
0.29	9.119	65.1	644.3	394.3	9.332

Table 4.3 - Data from the potentiometric titration of 0.3171 m KOH against cirazoline hydrochloride in 0.1 m KCl at 34.9°C. Apparent pK_a (pK_a') values calculated using γ_{OH^-} = 0.75 and pK_w = 13.430.

VOLUME KOH (mls)	pH	CONCENTRATION (M x 10^6) OH^-	$CIRH^+$	CIR	pK_a'
0	6.257	-	898.2	-	-
0.15	8.674	32.7	693.3	204.9	9.203
0.20	8.839	47.7	629.1	269.1	9.208
0.25	8.965	63.8	566.0	332.2	9.196
0.30	9.106	88.2	511.2	387.0	9.227

Table 4.4 - Data from the potentiometric titration of 0.3171 m KOH against cirazoline hydrochloride in 0.1 m KCl at 39.5°C. Apparent pK_a (pK_a') values calculated using γ_{OH^-} = 0.75 and pK_w = 13.285.

VOLUME KOH (mls)	pH	CONCENTRATION (M x 10^6) OH^-	$CPAEH^+$	CPAE	pK_a'
0	7.131	-	826.2	-	-
0.15	8.660	10.9	599.5	226.7	9.082
0.20	8.848	16.8	526.2	300.0	9.092
0.25	9.013	24.5	454.7	371.5	9.101
0.30	9.176	35.7	386.7	439.5	9.120
0.35	9.340	39.1	310.9	515.3	9.121
0.40	9.515	58.5	251.1	571.1	9.156

Table 4.5 - Data from the potentiometric titration of 0.3171 m KOH against CPAE hydrochloride in 0.1 m KCl at 25.0°C. Apparent pK_a (pK_a') values calculated using γ_{OH^-} = 0.75 and pK_w = 13.747.

COMPOUND	TEMP-ERATURE (°C)	NO. OF TITRANT ADDITIONS	APPARANT pK_a'	THERMO-DYNAMIC pK_a	EXTENT OF CIRAZOLINE DEGRADATION (%)
Cirazoline	24.9	5	9.60±0.02	9.48±0.02	2.4
	29.0	5	9.49±0.01	9.37±0.01	3.0
	34.9	4	9.33±0.01	9.21±0.01	3.8
	39.5	4	9.21±0.02	9.09±0.02	7.2
CPAE	25.0	6	9.09±0.03	8.97±0.03	-

Table 4.6 - Apparant and thermodynamic pK_a values for cirazoline and CPAE at temperature indicated.

Correlation coefficient	0.99996
Slope (S.D.)	2.495×10^3 (0.016×10^3)
Intercept (S.D.)	1.112 (0.051)
ΔG°_{25}	-54.1 kJ mol^{-1}
ΔH°_{25}	-48.2 kJ mol^{-1}
ΔS°_{25}	+20 J mol^{-1} K^{-1}

Table 4.7 - Linear regression analysis results for the pK_a data plotted according to equation 4.6 and derived thermodynamic parameters for the protonation of cirazoline at 25°C.

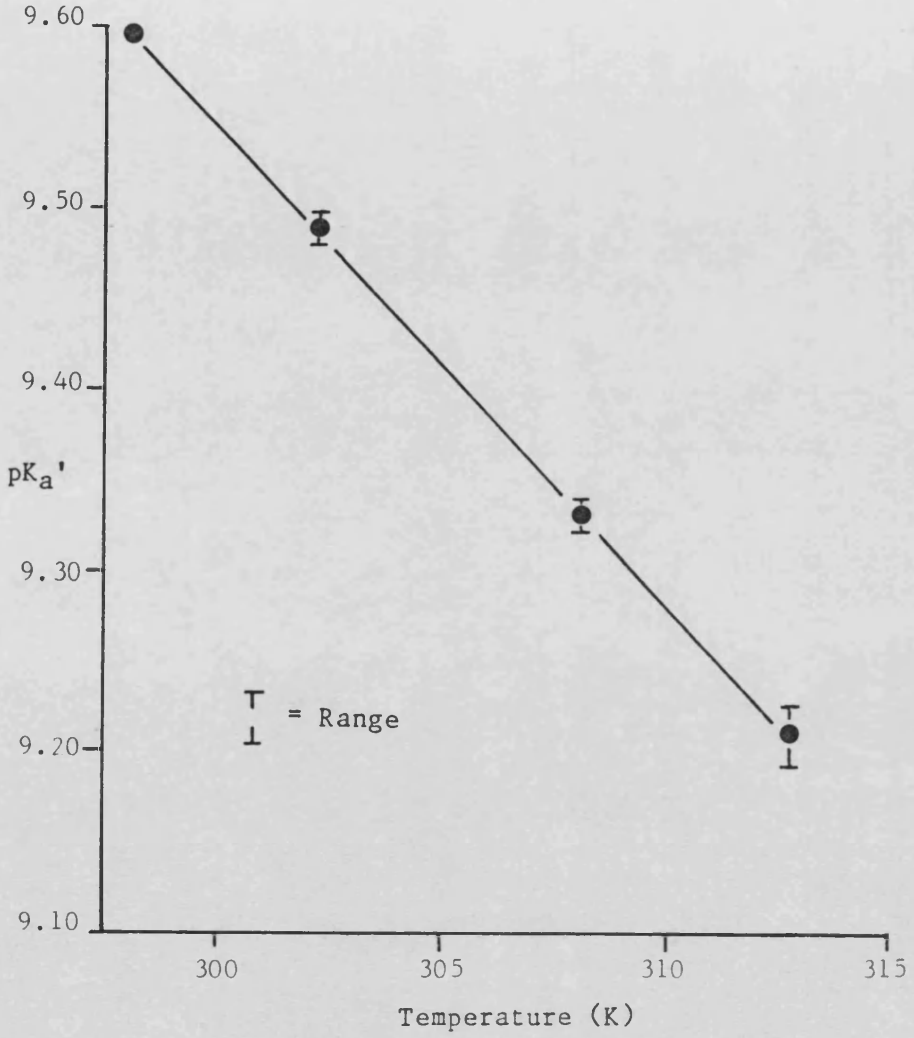

Figure 4.2 - Effect of temperature on the cirazoline hydrochloride apparant pK_a (pK_a') in 0.1 m KCl.

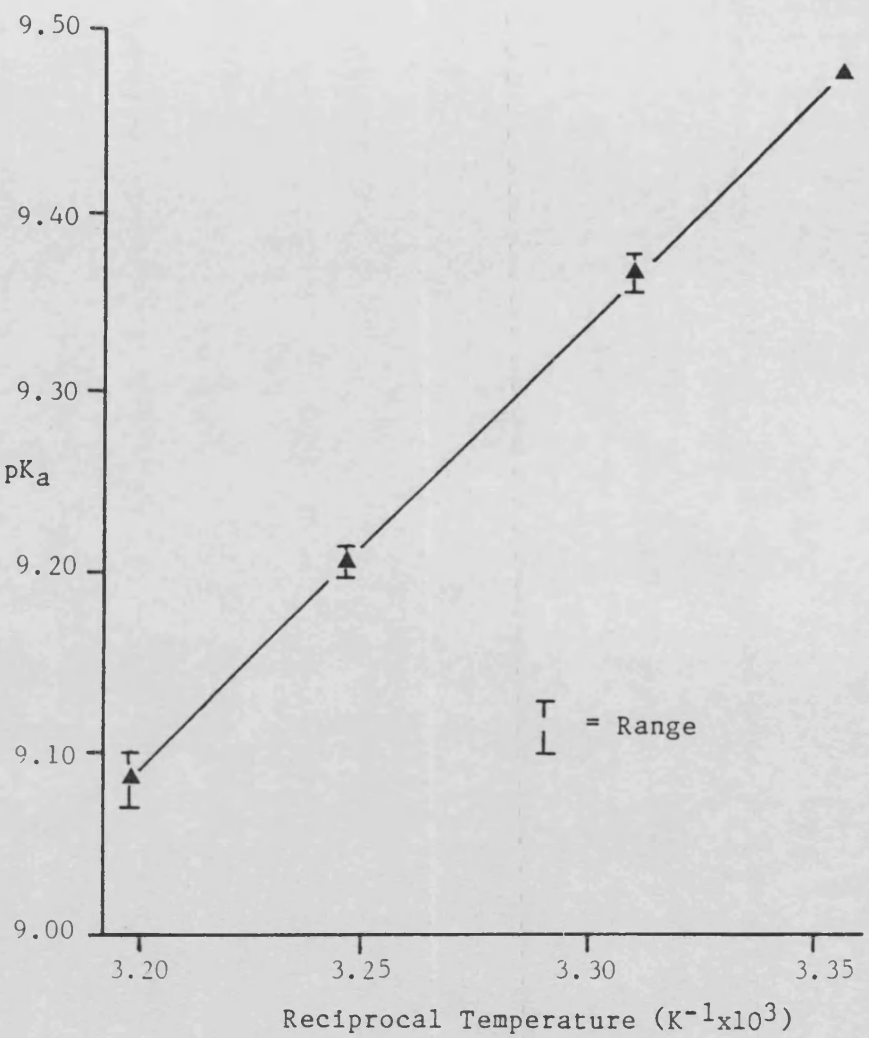

Figure 4.3 - Cirazoline hydrochloride intrinsic pK_a against reciprocal temperature, (Van't Hoff Plot).

5. 2-IMIDAZOLINE EXOCYCLIC METHYLENE ACIDITY

The acidity of the imidazoline exocyclic methylene group was investigated using nuclear magnetic resonance (NMR) spectroscopy under controlled 'pH' and temperature conditions in order to evaluate the mechanism of imidazoline hydrolysis.

5.1 NUCLEAR MAGNETIC RESONANCE SPECTROSCOPY

NMR spectroscopy is a standard technique used for determining the structure of organic molecules by providing information about the chemical environment of atoms, the number of atoms in each environment, and the structure of groups adjacent to each atom. Proton magnetic resonance (PMR) and ^{13}C NMR are the commonest forms of NMR which is based on observing resonance of these magnetic atoms induced by an applied electromagnetic field. NMR theory is the subject of many text books[202-204] and is outside the scope of this thesis. Interpretation of structure is based on the provision of NMR spectra from which chemical shifts (δ), peak area, spin-spin splitting and proton/deuterium (H/D) exchange can be determined.

The chemical shift, measured in parts per million (ppm) is a function of the electron density surrounding the nucleus and is determined relative to a standard peak e.g. tetramethylsilane, TMS, (0 ppm), HDO (4.6 ppm). In general the greater the chemical shift the lower the electron density surrounding the nucleus i.e. the nucleus is deshielded. The area under the resonance peak is proportional to the

number of nuclei responsible for the absorption. Integration of peak area therefore allows quantification of nuclei and aids elucidation of structure. Spin-spin coupling causes production of a fine structure in a spectrum and is due to the presence of neighbouring magnetic nuclei. The extent of peak splitting is a function of the number and type of nuclei causing the splitting. For splitting induced by vicinal protons, the number of peaks in the fine structure is given by the number of protons causing the splitting plus one. Proton/deuterium (H/D) exchange is the process whereby deuterium, which has no absorbance in the proton spectral region, exchanges with labile protons from the solute. This is performed by using D_2O as solvent or preferably by deuteration, i.e. adding D_2O to a sample dissolved in an inert solvent such as $CDCl_3$. Typical labile protons are those associated with acidic or basic functional groups; these protons exchange very rapidly and a total loss of peak occurs immediately upon addition of D_2O; such peaks are therefore not observed when the sample is prepared in D_2O. This effect is a useful tool in the identification of acidic or basic groups. More stable acidic or basic groups, such as methylene groups close to an electron withdrawing groups, exchange at a much slower rate. In these cases the relevant proton peak(s) may be observed to diminish in magnitude by repeatedly scanning the sample at appropriate time intervals. The rate of exchange (given from the rate of decrease in peak area) is therefore a measure of the acidity or basicity of the group.

5.2 METHOD

The exocyclic methylene acidity of cirazoline hydrochloride, antazoline sulphate, fenoxazoline hydrochloride, naphazoline nitrate, tolazoline

hydrochloride, xylometazoline hydrochloride and 2-methyl-2-imidazoline was investigated at 20°C in phosphate buffer 'pH' 6.9 using PMR. Spectra were generated using a Jeol JNM GX270 FT NMR spectrometer in the range δ = 0 to 10 ppm.

Solutions were prepared by dissolving 150 mg of sample in 5 mls of 0.025 m equimolal phosphate buffer 'pH' 6.9. The buffer was prepared according to Bates[195] except D_2O was used as solvent. The 'pH' of the final buffered samples was determined as 'pH' 6.9 $\pm$ 0.1 at 20°C. Unlike the other imidazoline samples, 2-methyl-2-imidazoline was only available as the free base; the hydrochloride salt was therefore prepared *in situ* by the addition of equimolar HCl and dilution to volume with phosphate buffer. The 'pH' of the final system was adjusted to 'pH' 6.9 using aqueous 1 M HCl.

A scan was performed immediately after sample preparation and repeated at appropriate intervals during the study. The HDO peak resulting from exchange of protons from the phosphate buffer salts with D_2O was used as the internal reference (δ = 4.60 ppm).

5.3 CALCULATION OF EXCHANGE RATE CONSTANTS

The number of protons associated with each absorption peak was calculated by peak area integration. For each sample, the number of protons (H) in each moiety of the molecule was calculated by reference to an inert 'standard' moiety within the molecule:

$$\text{Number of Protons in Moiety} = \text{Number of Protons in Standard Moiety} \times \frac{\text{Peak Area of Moiety}}{\text{Peak Area of Standard Moiety}} \qquad (5.1)$$

The moieties within the imidazoline structure were defined as:

A = Endocyclic methylene groups

B = Exocyclic methylene group

C = Substituent aromatic ring(s)

D-F = Substituent aliphatic group(s)

The aromatic ring (C) was used as the standard moiety for cirazoline, fenoxazoline, antazoline and tolazoline; the trimethyl groups (D) were used for xylometazoline and the endocyclic methylene group (A) was used for 2-methyl-2-imidazoline.

The rate of proton/deuterium exchange is given by:

$$-\frac{dH}{dt} = k_{EX}.H^n \qquad (5.2)$$

Where $-\frac{dH}{dt}$ represents the loss of protons with time, t; k_{EX} is the exchange rate constant; H is the number of protons in the moiety and n is the order of reaction. For a first order exchange (i.e. n = 1):

$$k_{EX} = \frac{1}{t} \log_e\left(\frac{H_o}{H_t}\right) \text{and,}$$

$$\log_e(\%\ RH) = \log_e\left(\frac{H_t}{H_o} \times 100\right) = \log_e 100 - k_{EX}.t \qquad (5.3)$$

Where H_o and H_t are the number of protons in the moiety at time zero and after time t, and %RH is the percent residual proton number. First order exchange rate constants were determined for each imidazoline by fitting data to the first order rate equation (equation 5.3) using least squares regression analysis.

5.4 RESULTS

Initial and final NMR spectra of each imidazoline are shown in figures 5.1 to 5.7. The number of protons in each of the moieties (A-F) was calculated as described in section 5.3 and results are presented in tables 5.1 to 5.7. First order H/D exchange plots for naphazoline, antazoline, xylometazoline and tolazoline are shown in figure 5.8.

The initial NMR spectrum of fenoxazoline hydrochloride (figure 5.2a) shows the sample to be impure and integration data (table 5.2) suggest an initial impurity level of about 20%. Chemical degradation (ring cleavage) was evident during the exchange for cirazoline and fenoxazoline, (the remaining compounds showed no such degradation). NMR spectra for cirazoline and fenoxazoline show a decrease in the number of protons associated with the exo-(B) and endocyclic (A) methylene groups with time (tables 5.1 and 5.2) and the appearance of three peaks of equivalent area at chemical shifts of δ = 3.0, 3.4 and 4.4 ppm. These peaks are consistant with the structure of the cirazoline and fenoxazoline hydrolysis degradation products (see figure 1.2). The first order rate constant (k_{obs}) for the cirazoline and fenoxazoline hydrolysis reaction in phosphate buffer 'pH' 6.9 in D_2O, 20°C was calculated from the endocyclic methylene proton (A) data using equation 5.4.

$$\log_e \left(\frac{H_t}{H_o} \times 100 \right) = \log_e 100 - k_{obs}.t \qquad (5.4)$$

k_{obs} (S.D.) values were calculated using least squares regression analysis as 2.08×10^{-7} (0.08×10^{-7}) s^{-1} and 1.79×10^{-7} (0.14×10^{-7}) s^{-1} for cirazoline and fenoxazoline respectively.

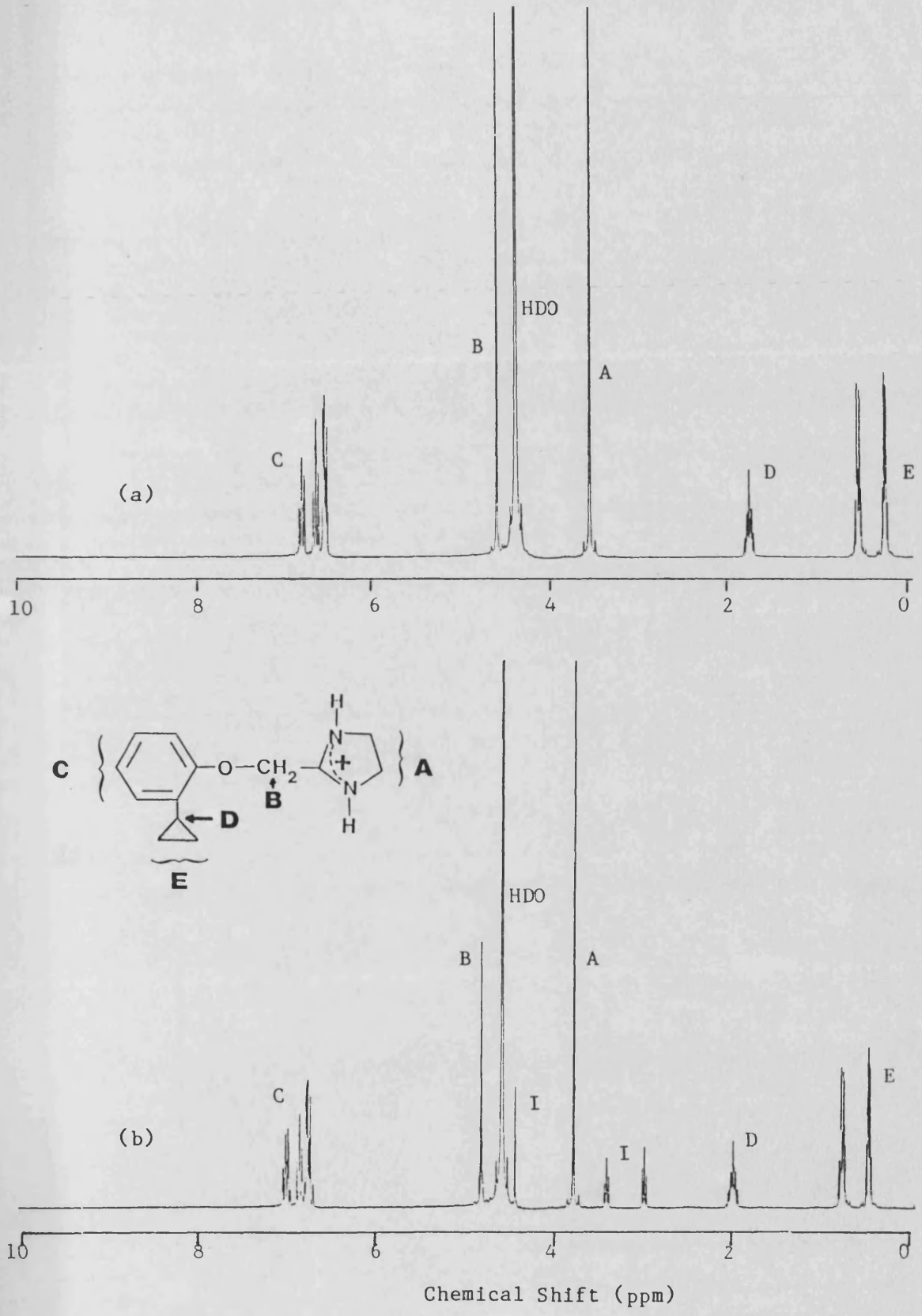

Figure 5.1 - Proton NMR spectra for cirazoline hydrochloride in phosphate buffer, 'pH' 6.9, in D_2O, 20°C; (a) initial, (b) after 336 hours. I = impurity/degradation product.

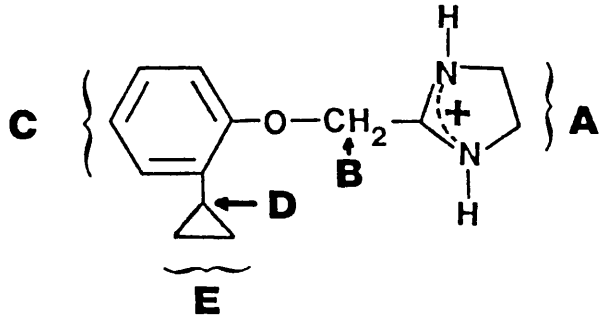

TIME	PROTON NUMBER					% RESIDUAL PROTON NUMBER		
(HRS)	H_A	H_B	H_C	H_D	H_E	% RH_A	%RH_B	%RH_B'
0	3.81	1.94	4.0	0.90	3.81	100	100	102
9	4.00	1.87	4.0	0.97	4.03	105	96.4	93.5
22	3.93	1.84	4.0	0.98	4.03	103	94.8	93.6
174	3.37	1.65	4.0	0.96	3.90	88.5	85.1	97.9
336	2.96	1.62	4.0	0.88	3.73	77.6	84.0	110
(ppm)	3.80	4.85	6.90	2.05	0.60			
Theoretical Proton Number	4	2	4	1	4			

Table 5.1 - Stability of cirazoline protons in phosphate buffer, 'pH' 6.9 in D_2O, 20°C. H_A = endocyclic methylene protons, H_B = exocyclic methylene protons, H_C = aromatic protons, H_D = substituent methine protons, H_E = substituent methylene protons, H_B' = corrected exocyclic methylene protons (see text for further explanation of this function).

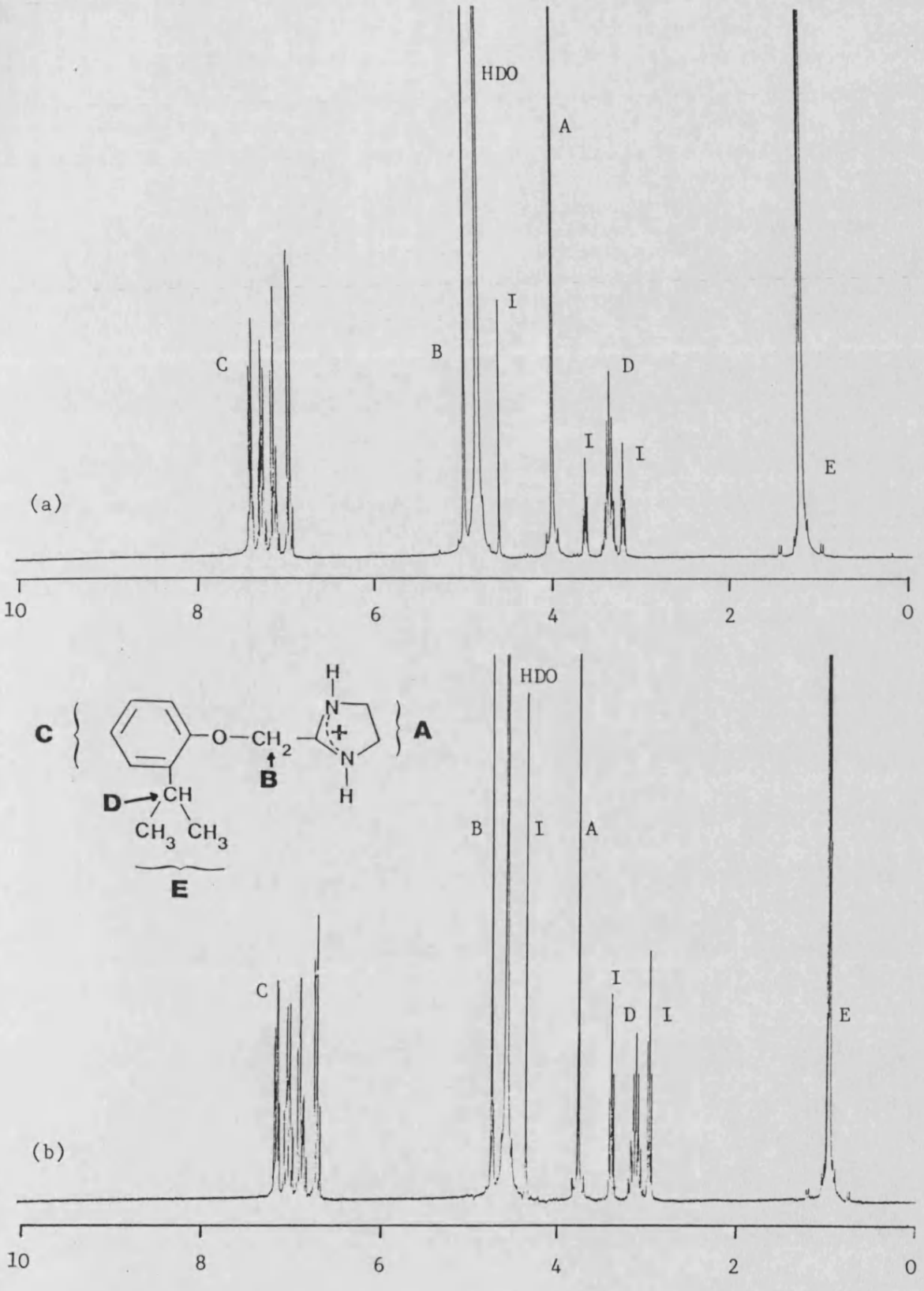

Figure 5.2 - Proton NMR spectra for fenoxazoline hydrochloride in phosphate buffer, 'pH' 6.9, in D_2O, 20°C; (a) initial, (b) after 336 hours. I = impurity/degradation product.

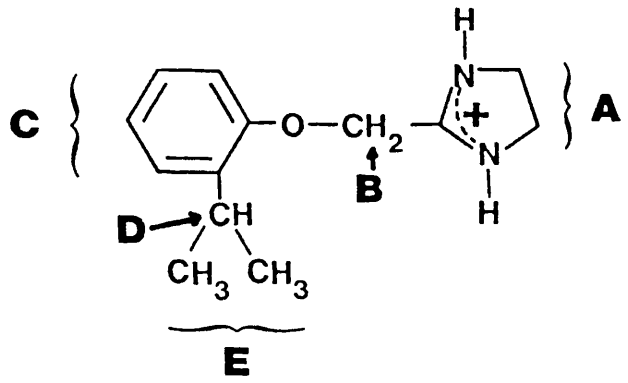

TIME (HRS)	PROTON NUMBER					% RESIDUAL PROTON NUMBER		
	H_A	H_B	H_C	H_D	H_E	% RH_A	$\%RH_B$	$\%RH_B'$
0	3.22	1.87	4.0	0.98	5.96	100	100	116
9	3.29	1.60	4.0	1.01	6.02	102	85.6	97.2
22	3.21	1.91	4.0	0.98	5.95	99.8	102	119
174	2.87	1.48	4.0	0.99	5.74	89.2	79.1	103
336	2.64	1.31	4.0	0.94	5.88	82.0	70.0	99.2
(ppm)	3.75	4.75	6.90	3.15	1.10			
Theoretical Proton Number	4	2	4	1	6			

Table 5.2 - Stability of fenoxazoline protons in phosphate buffer, 'pH' 6.9 in D_2O, 20°C. H_A = endocyclic methylene protons, H_B = exocyclic methylene protons, H_C = aromatic protons, H_D = substituent methine protons, H_E = substituent methylene protons, H_B' = corrected exocyclic methylene protons (see text for further explanation of this function).

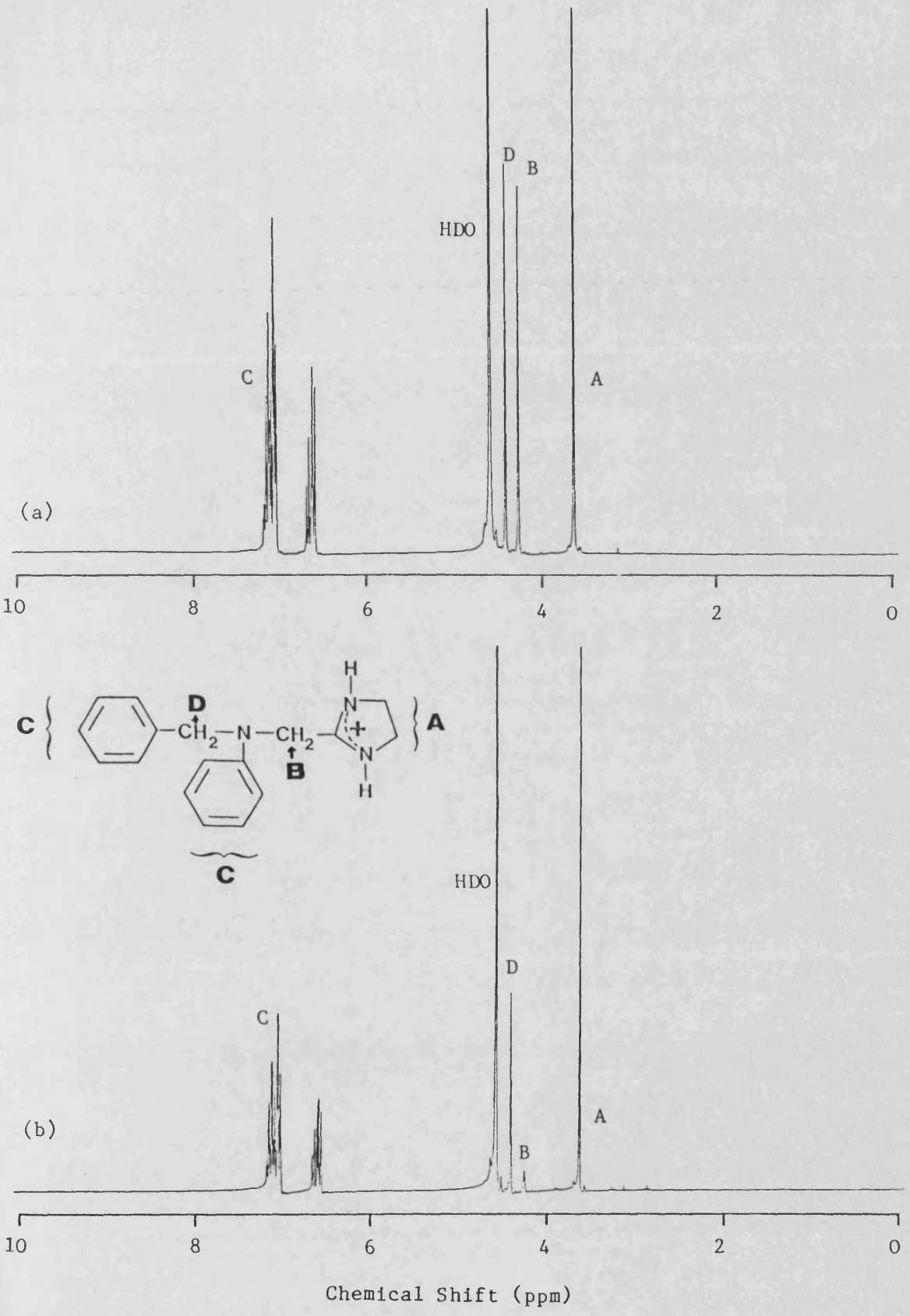

Figure 5.3 - Proton NMR spectra for antazoline sulphate in phosphate buffer, 'pH' 6.9, in D_2O 20°C, (a) initial, (b) after 678 hours.

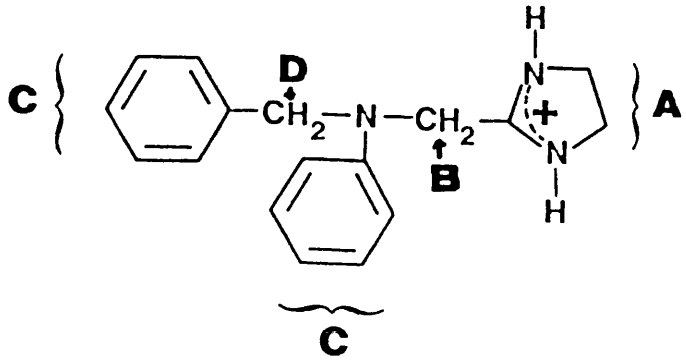

TIME (HRS)	PROTON NUMBER				% RESIDUAL PROTON NUMBER	
	H_A	H_B	H_C	H_D	% RH_A	% RH_B
0	3.91	1.85	10.0	1.85	100	100
9	3.93	1.97	10.0	2.05	101	107
22	3.90	1.70	10.0	1.83	99.7	91.9
174	3.94	1.52	10.0	2.08	101	82.2
336	3.80	1.11	10.0	1.88	97.1	60.0
530	3.75	0.76	10.0	1.79	95.9	41.1
678	3.87	0.66	10.0	2.12	99.0	35.7
(ppm)	3.60	4.30	6.90	4.45		
Theoretical Proton Number	4	2	10	2		

Table 5.3 - Stability of antazoline protons in phosphate buffer, 'pH' 6.9 in D_2O, 20°C. H_A = endocyclic methylene protons, H_B = exocyclic methylene protons, H_C = aromatic protons, H_D = substituent methylene protons.

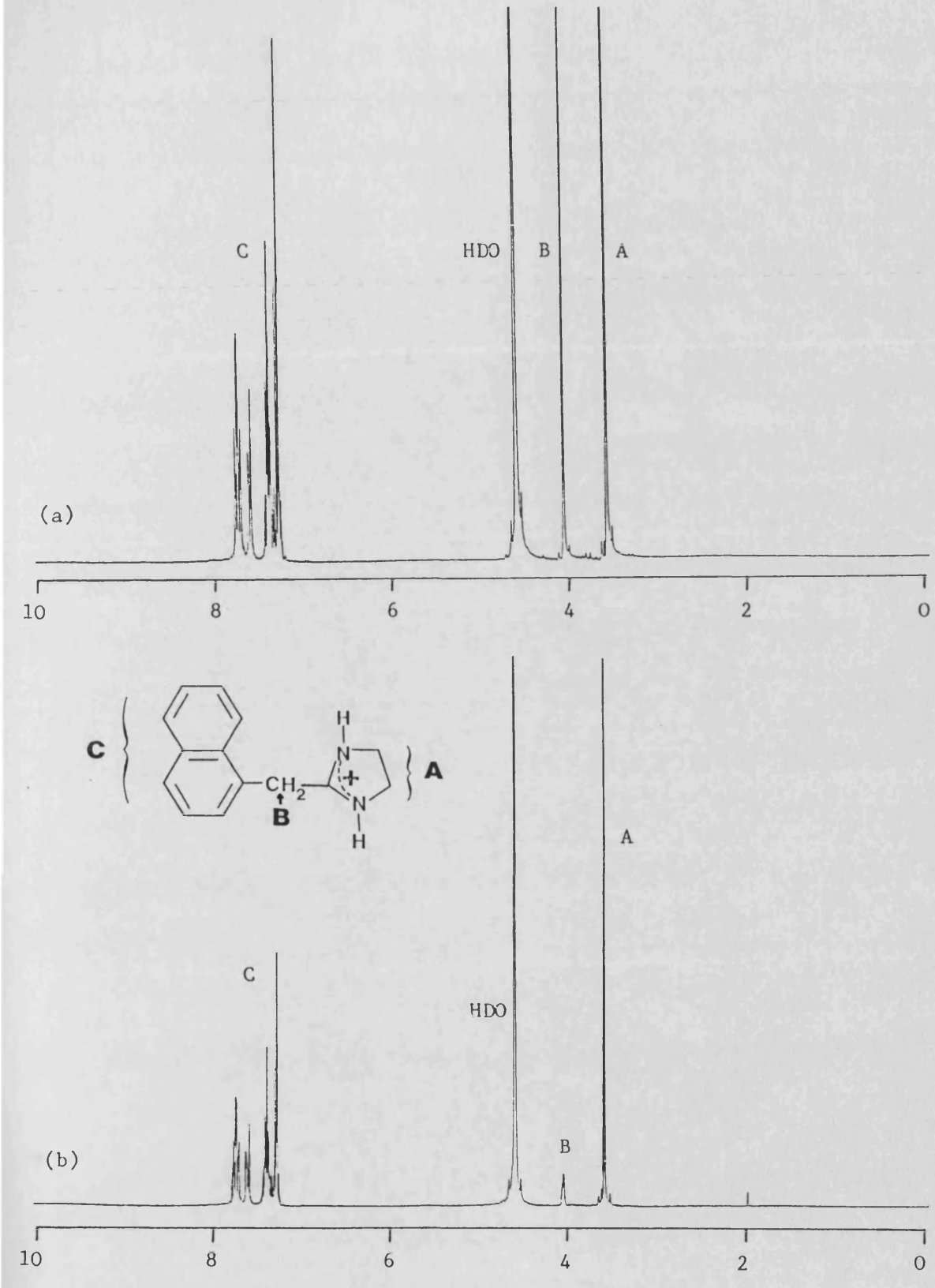

Figure 5.4 - Proton NMR spectra for naphazoline nitrate in phosphate buffer, 'pH' 6.9, in D_2O, 20°C; (a) initial, (b) after 264 hours.

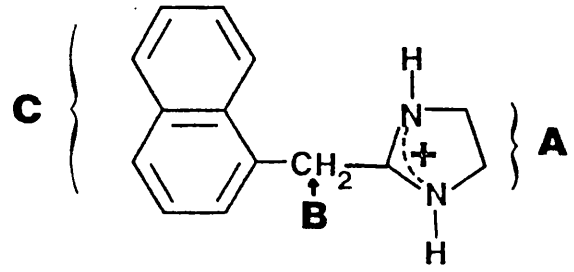

TIME	PROTON NUMBER			% RESIDUAL PROTON NUMBER	
(HRS)	H_A	H_B	H_C	% RH_A	%RH_B
0	4.17	1.97	7.0	100	100
10	3.99	1.81	7.0	95.7	91.9
22	3.96	1.66	7.0	94.9	81.5
174	3.97	0.67	7.0	95.2	34.0
264	4.02	0.34	7.0	96.4	17.8
(ppm)	3.55	4.00	7.50		
Theoretical Proton Number	4	2	7		

Table 5.4 - Stability of naphazoline protons in phosphate buffer, 'pH' 6.9 in D_2O, 20°C. H_A = endocyclic methylene protons, H_B = exocyclic methylene protons, H_C = aromatic protons.

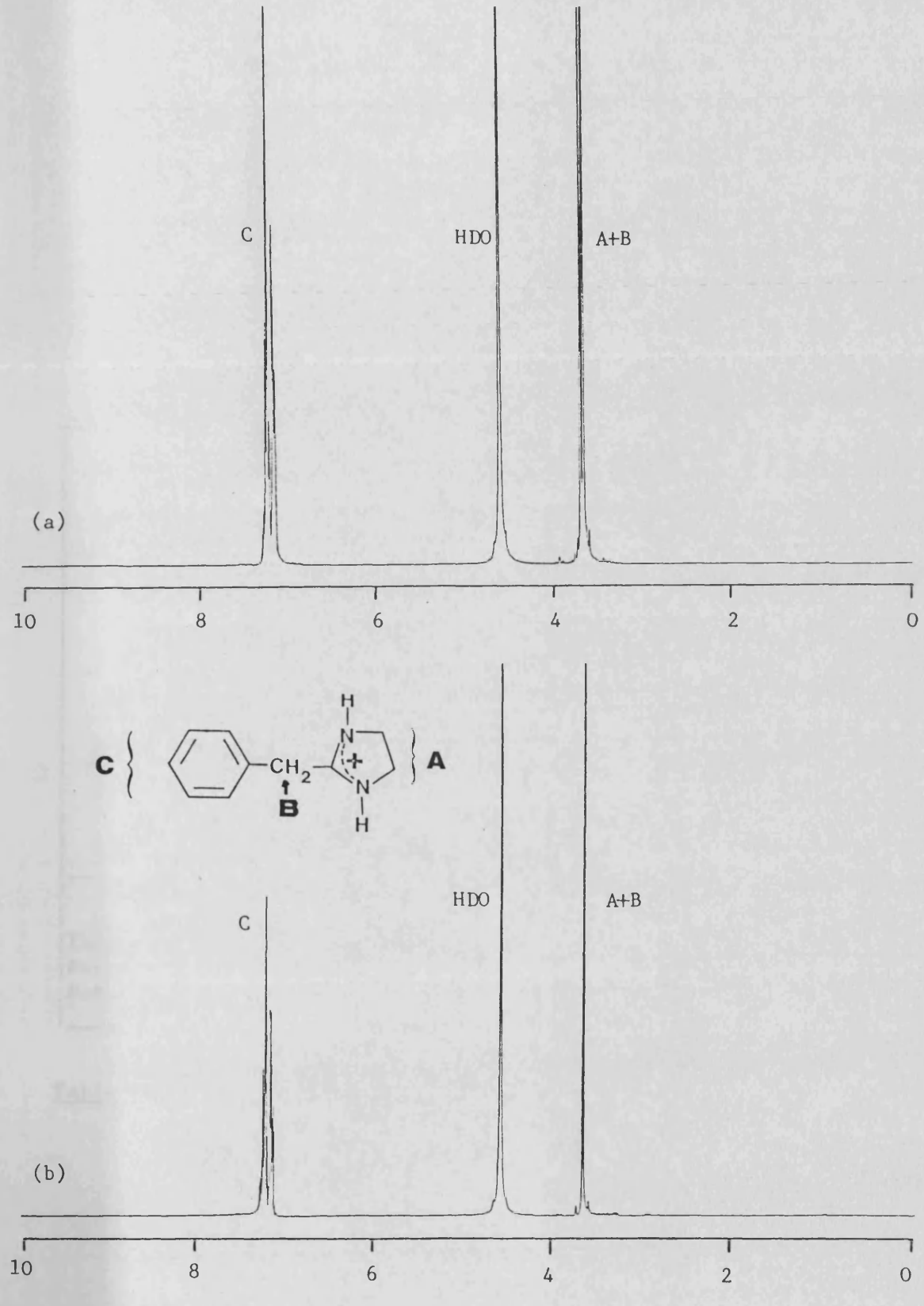

Figure 3.5 - Proton NMR spectra for tolazoline hydrochloride in phosphate buffer, 'pH' 6.9 in D_2O, 20°C, (a) initial, (b) after 678 hours.

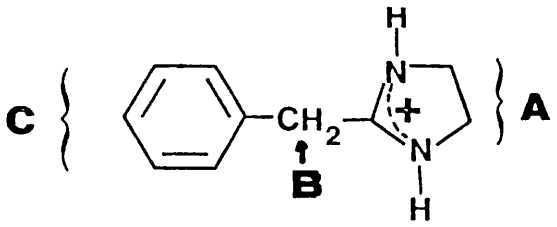

TIME (HRS)	PROTON NUMBER			% RESIDUAL PROTON NUMBER
	(H_A+H_B)	H_B	H_C	$\%RH_B$
0	6.16	2.05	5.0	100
9	6.13	2.02	5.0	98.4
22	6.03	1.92	5.0	93.6
174	5.21	1.10	5.0	53.7
530	4.38	0.46	5.0	13.3
678	4.28	0.27	5.0	8.5
(ppm)	3.70	3.70	7.20	
Theoretical Proton Number	6	2	5	

Table 5.5 - Stability of tolazoline protons in phosphate buffer, 'pH' 6.9 in D_2O, 20°C. H_A = endocyclic methylene protons, H_B = exocyclic methylene protons, H_C = aromatic protons.

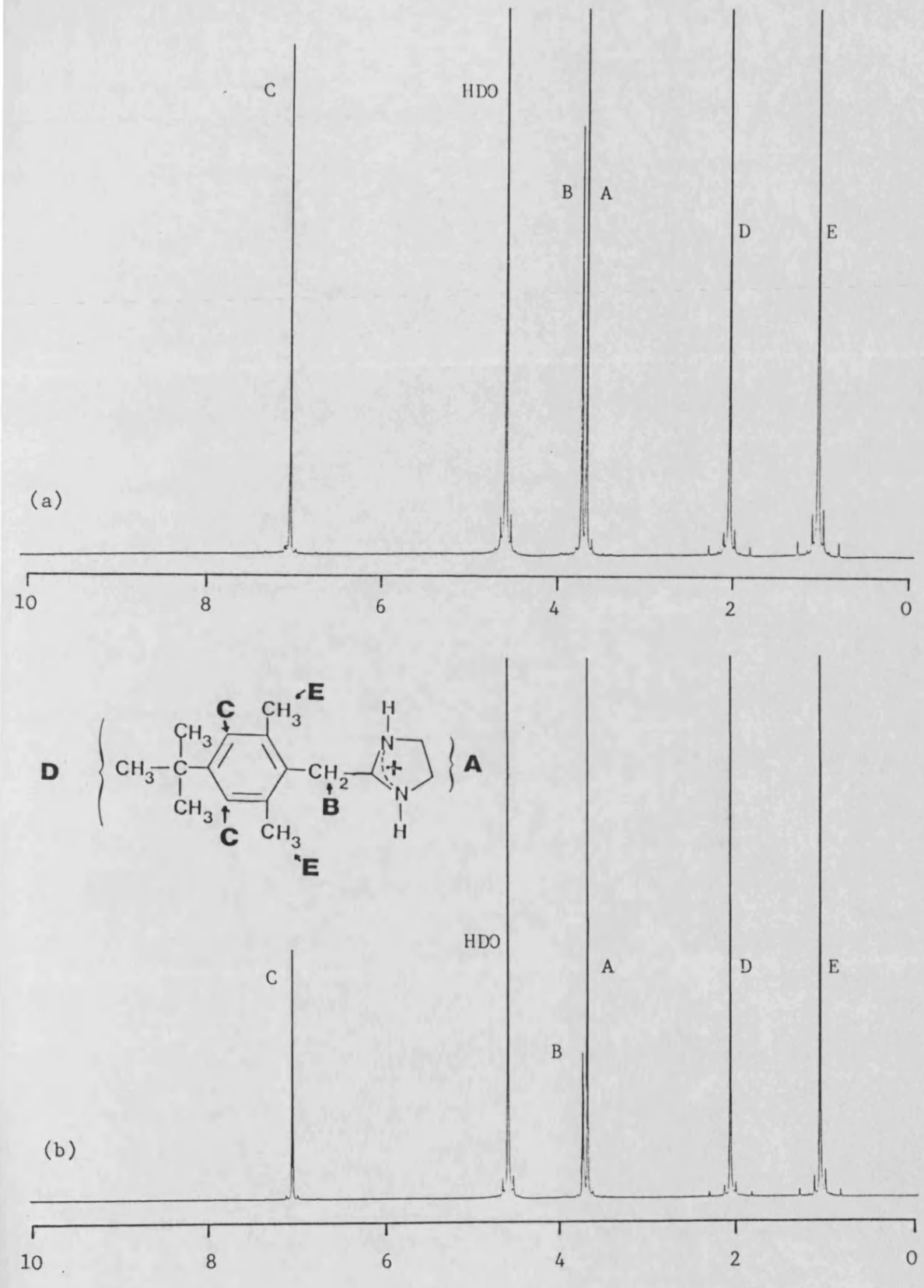

Figure 5.6 - Proton NMR spectra for xylometazoline hydrochloride in phosphate buffer, 'pH' 6.9, in D_2O, 20°C; (a) initial, (b) after 960 hours.

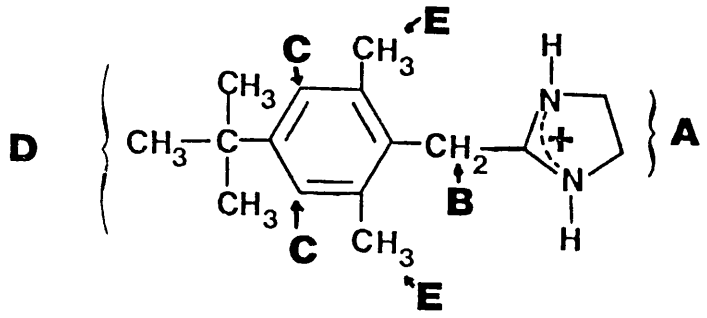

TIME (HRS)	PROTON NUMBER					% RESIDUAL PROTON NUMBER	
	H_A	H_B	H_C	H_D	H_E	% RH_A	%RH_B
0	3.86	2.09	1.95	5.99	9.0	100	100
10	3.67	2.15	1.94	6.02	9.0	95.1	103
22	3.82	1.98	2.05	5.93	9.0	99.0	94.7
174	4.01	2.02	1.99	6.00	9.0	104	96.7
336	3.85	1.81	1.92	5.92	9.0	99.8	86.6
530	3.90	1.85	1.94	5.98	9.0	101	88.5
960	3.86	1.64	1.99	6.05	9.0	100	78.5
(ppm)	3.65	3.75	7.05	2.10	1.10		
Theoretical Proton Number	4	2	2	6	9		

Table 5.6 - Stability of xylometazoline protons in phosphate buffer, 'pH' 6.9 in D_2O, 20°C. H_A = endocyclic methylene protons, H_B = exocyclic methylene protons, H_C = aromatic protons H_D = substituent methyl protons, H_E = substituent isobutyl protons.

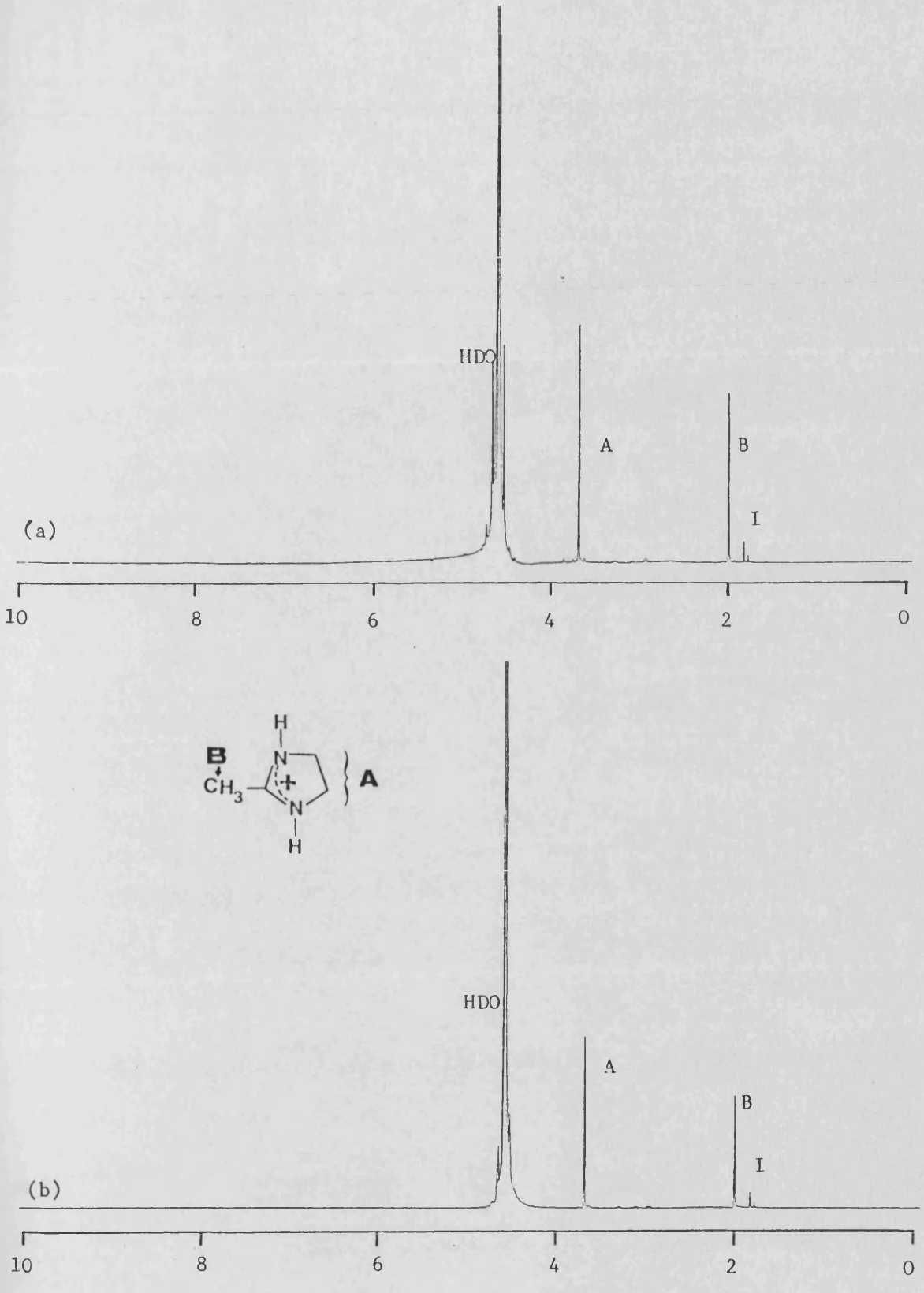

Figure 5.7 - Proton NMR spectra for 2-methyl-2-imidazoline hydrochloride in phosphate buffer, 'pH' 6.9, in D_2O, 20°C; (a) initial, (b) 360 hours. I = impurity/ degradation product.

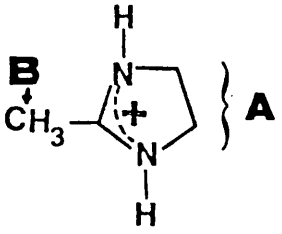

TIME (HRS)	PROTON NUMBER H_A	PROTON NUMBER H_B	% RESIDUAL PROTON NUMBER % RH_B
0	4.0	2.88	100
7	4.0	3.03	105
78	4.0	3.00	104
360	4.0	3.00	104
(ppm)	3.70	2.00	
Theoretical Proton Number	4	3	

Table 5.7 - Stability of 2-methyl-2-imidazoline protons in phosphate buffer 'pH' 6.9 in D_2O, 20°C. H_A = endocyclic methylene protons, H_B = exocyclic methyl protons.

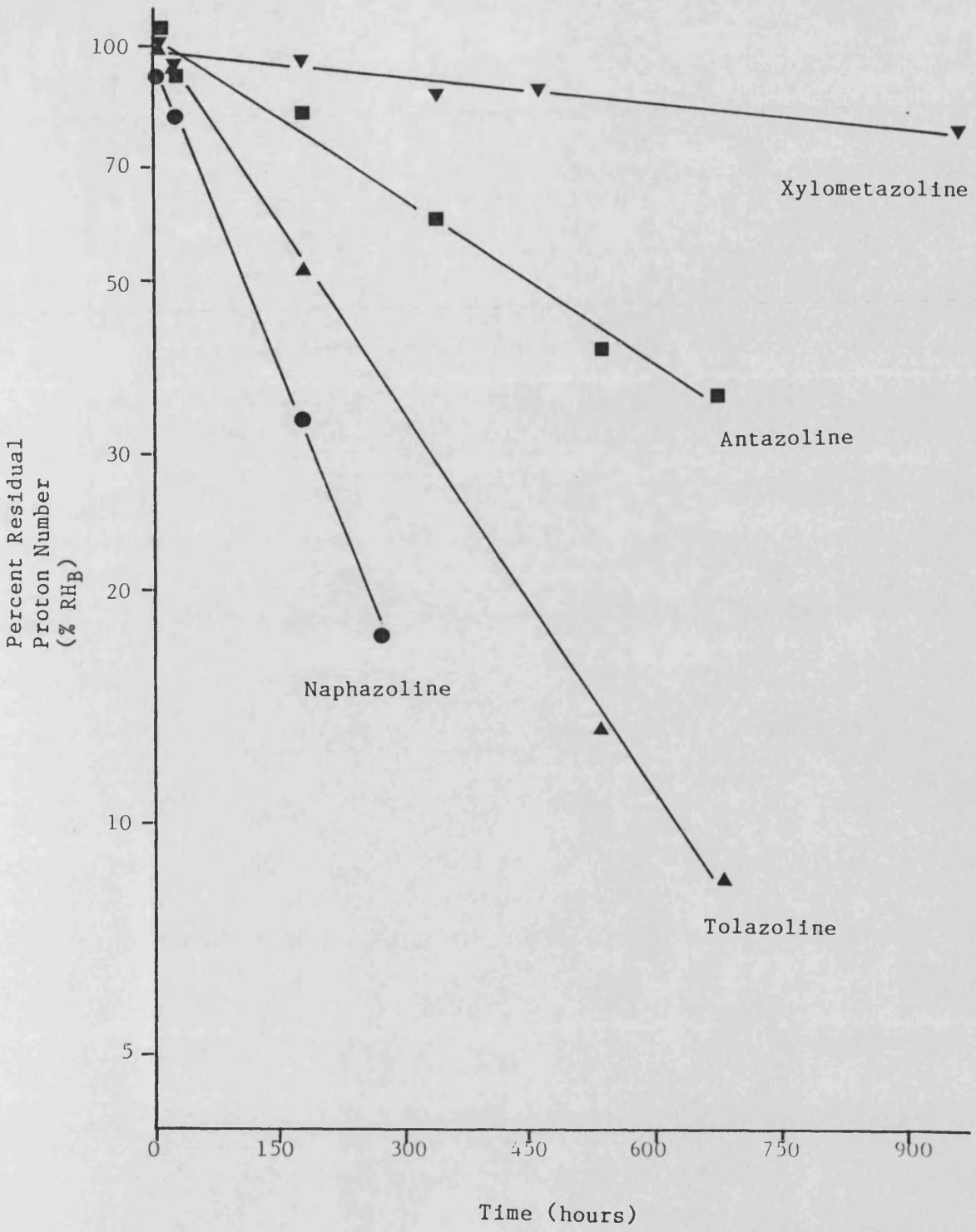

Figure 5.8 - First order plots for imidazoline exocyclic methylene proton (H_B)/deuterium exchange. Antazoline (—■—), naphazoline (—●—), tolazoline (—▲—), and xylometazoline (—▼—), in phosphate buffer 'pH' 6.9 in D_2O, 20°C.

In order to determine the extent of exocyclic methylene H/D exchange for undegraded cirazoline and fenoxazoline, the percent residual exocyclic methylene proton number was recalculated as a function of the endocyclic methylene proton number (H_A), using equation 5.5:

$$\% RH_B' = \frac{H_B}{H_A} \times \frac{4}{2} \times 100 \qquad (5.5)$$

Where % RH_B' is the corrected percent residual exocyclic methylene proton number and H_A and H_B are the number of endo and exocyclic methylene protons respectively. % RH_B' is therefore a measure of the extent of exchange for undegraded cirazoline and fenoxazoline. All other spectra showed the absence of peaks associated with imidazoline hydrolytic degradation products. The xylometazoline, naphazoline and antazoline endocyclic methylene proton number (H_A) remained constant and close to the theoretical value during the study; mean (S.D.) values were calculated as 3.85 (0.10), 4.02 (0.09) and 3.87 (0.07) respectively.

The tolazoline endo (A) and exocyclic (B) methylene protons had absorption peaks very close together and H_B could not be calculated directly. H_B was therefore calculated by subraction of H_A from the total methylene (H_A + H_B) protons (equation 5.6):

$$H_B = (H_A + H_B) - H_A \qquad (5.6)$$

H_A was assumed to be constant during the study and its value was determined from the spectrum at time zero (equation 5.7):

$$H_A = (H_A + H_B) \times \frac{4}{6}, \quad \text{at time zero} \qquad (5.7)$$

This calculation method is thought to be valid as the degradation (ring cleavage) rate of tolazoline is similar to naphazoline and antazoline

(section 8.3.5) and these samples did not degrade during the exchange study. The derived exocyclic methylene H/D exchange rate constant for each imidazoline are shown in table 5.8. Results indicate that 2-methyl-2-imidazoline, cirazoline and fenoxazoline have negligible exchange rates under the experimental conditions employed. Mean (S.D.) percent residual exocyclic methylene proton numbers were calculated as : 2-methyl-2-imidazoline % RH_B = 103 (2), cirazoline %RH_B' = 99.3 (6.7) and fenoxazoline % RH_B' = 107 (10).

Exocyclic methylene H/D exchange occurred in the antazoline, naphazoline, tolazoline and xylometazoline samples and the rate of exchange followed first order kinetics. The rates of exchange found in this study are much slower than observed by Kountourellis[20], where complete exchange occurred in 24-100 hours with these imidazolines when prepared in deuterated dimethylsulphoxide, DMSO. Under the conditions employed in this study (phosphate buffer in D_2O 'pH' 6.9, 20°C) half-lives determined from the first order rate equation (equation 5.3) are in the range 109-1080 hours (4.5-45 days). The rank order for the rate of exchange also differs; Kounterellis found reactivity in the order:

tolazoline>naphazoline = antazoline>xylometazoline

whereas these results indicate reactivity to be in the order:

naphazoline>tolazoline>antazoline>xylometazoline.

These discrepancies may be associated with the difference in experimental conditions employed.

The importance of the imidazoline ring in the mechanism of methylene H/D exchange is highlighted by the difference in stability of the antazoline exocyclic methylene protons (H_B) and substituent methylene protons (H_D). The exocyclic methylene group (B) is adjacent to the protonated imidazoline ring whereas the substituent methylene group

IMIDAZOLINE	$k_{EX(H_B)}$ (s^{-1}) (S.D.)	HALF LIFE (HRS)
2-Methyl-2-imidazoline	No Exchange	-
Xylometazoline	1.79×10^{-7} (0.12×10^{-7})	1080
Naphazoline	1.76×10^{-6} (0.05×10^{-6})	109
Tolazoline	1.16×10^{-6} (0.01×10^{-6})	165
Antazoline	4.44×10^{-7} (0.16×10^{-7}	433
Cirazoline	No Exchange *	-
Fenoxazoline	No Exchange *	-

Table 5.8 - Exocyclic methylene proton (H_B) exchange first order rate constants ($k_{EX(H_B)}$ for imidazolines in phosphate buffer 'pH 6.9' in D_2O, 20°C. (* = corrected first order rate constants ($k_{EX(H_B')}$).

(D) is adjacent to a phenyl ring. Both are bonded to the antazoline tertiary amine group. No H_D exchange was detected during the 678 hours (28 days) of the study (H_D mean = 1.94, S.D. = 0.14) whereas H_B exchanged with deuterium at a rate of 4.44×10^{-7} s^{-1}, giving a half-life of 433 hours (18 days).

6. ION-PAIR AND COMPLEX FORMATION IN IMIDAZOLINE-ALKYLSULPHATE SYSTEMS

6.1 INTRODUCTION

The interaction between cirazoline hydrochloride and SDDS in aqueous solution may be described in terms of ion-pair formation, complexation and micellization and solubilization. The relative amounts of cirazoline and SDDS in the aqueous (free ion), ion-pair, complex and micellar forms is dependent upon the concentrations of cirazoline hydrochloride and SDDS, temperature and presence of additives e.g. electrolyte. At SDDS concentrations well below the CMC of the system aggregation is absent and the system may be described in terms of the ion-pair association constant, K_{ip}, and the solubility product, K_s. These parameters were determined using an automated conductimetric titration procedure similar to the method described by Mukhayer and Davies[121]. In addition the physico-chemical nature of the formed cirazoline dodecylsulphate complex ($CIRH\text{-}DDS_{(c)}$) was investigated by visual observation, microscopy, NMR and DSC. Solubility products and complex formation were also investigated in cirazoline hydrochloride-sodium alkylsulphate (C_8 - C_{14}) systems and antazoline sulphate-, naphazoline nitrate-, xylometazoline hydrochloride- and tolazoline hydrochloride-SDDS systems.

6.2 EXPERIMENTAL

6.2.1 Automated Conductimetric Titrations

6.2.1.1 DESCRIPTION

The apparatus used for conductimetric titrations is shown diagramatically in figure 6.1. The sample solution (normally a solution of the imidazoline) was equilibrated to the desired temperature in a thermostatted beaker; temperature was maintained constant by water pumped from a water bath and cooler unit. The titration mixture was agitated continously by a magnetic stirrer. The conductance of the system was measured using a glass-platinum Mullard dip cell, (nominal cell constant 1.44) in conjunction with a Wayne Kerr conductivity bridge and recorded in the form of a continuous trace on a chart recorder. The surfactant solution was automatically pumped from a Hamilton precision syringe into the titration vessel at a known rate using a Braun motorized syringe pump. The delivery tubing was constructed from HPLC microbore tubing to prevent premature delivery of titrant.

6.2.1.2 DETERMINATION OF CELL CONSTANT

The cell constant was determined by measuring the conductivity of standard solutions of potassium chloride at 25°C. A range of potassium chloride solutions (1×10^{-3} - 2×10^{-2} M) was prepared using dried potassium chloride (analar) and double distilled water. The conductivity bridge was trimmed and calibrated as decribed in the instrument manual. Each solution in turn was equilibrated to 25°C in the jacketed beaker (figure 6.1) and the conductivity measured.

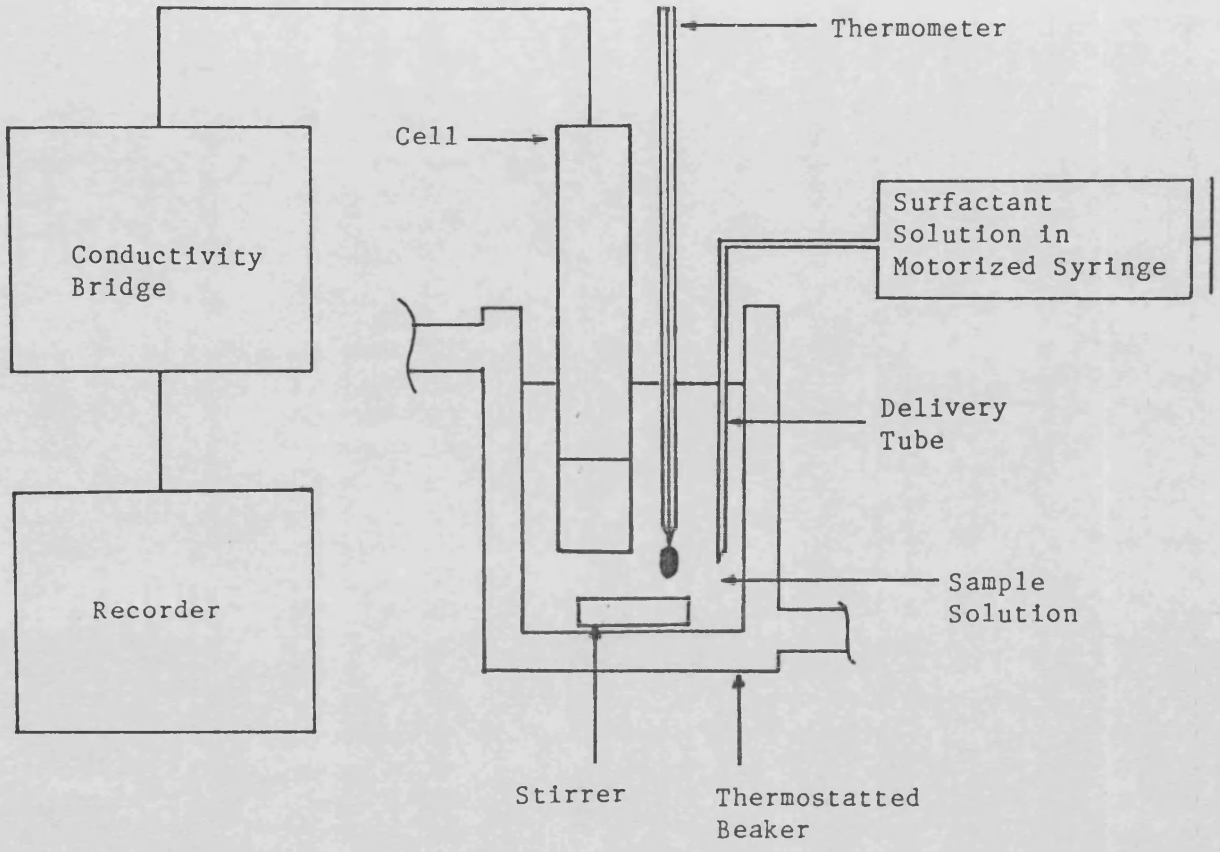

Figure 6.1 - Conductimetric titration apparatus.

The results, together with literature values and derived cell constants are shown in table 6.1. The mean cell constant was found to be 1.45; this value was used throughout.

6.2.1.3 SYRINGE CALIBRATION

The motorized syringe-pump unit was calibrated at each of the six flow rate settings used in the study. Different quantities of double distilled water at 20°C were titrated into a clean, dry, tared volumetric flask over a measured period of time (quartz stop watch). The weight delivered was determined and the volume flow rate calculated using the density of water at 20°C (0.9982). Results are shown in table 6.2.

6.2.1.4 CALIBRATION OF CONDUCTIVITY BRIDGE AND SERVOGOR 120 CHART RECORDER

The conductivity cell was disconnected and the desired bridge range selected. The chart recorder deflection was calibrated using the bridge conductivity meter output as follows: the chart recorder range switch was set to a full-scale deflection of '100'; 'calibrate /variable' switch 'to variable'; and 'zero/mV/V' switch to mV. The bridge meter sensitivity switch was switched to position '3' and the conductivity meter reading set to zero using the conductivity trim control. The chart recorder deflection was adjusted to zero using the 'zero' control. The bridge conductivity meter was then set to full-scale deflection and the chart deflection adjusted to full-scale using the variable control. The conductivity bridge was then trimmed and calibrated as described in the manual.

KCl M x 10^3	Conductivity S x 10^6	Corrected Conductivity S x 10^6	Literature Specific Conductivity κ(S x 10^6)	Cell Constant
Nil	0.7	-	-	-
1.0	102.9	102.2	147.0	1.438
2.0	202.0	201.3	294.7	1.464
5.0	492.5	491.8	717.8	1.460
10.0	965.3	964.6	1413.0	1.465
20.0	1916.0	1915.0	2767.0	1.445
			Mean	1.454
			S.D.	0.012
			CV	0.8%

Table 6.1 - Conductivity readings, literature specific conductivity values (calculated from equivalent conductivity values in Robinson and Stokes[11]), and calculated cell constants for a range of potassium chloride solutions at 25°C.

Flow Rate Setting	Flow Rate (μl min^{-1})	Mean Flow Rate (S.D.) (μl min^{-1})
6 (hr)	6.320, 6.267	6.294
8 (hr)	12.41, 12.36	12.39
9 (hr)	20.38, 20.25, 20.40, 20.42, 20.44	20.38 (0.08)
1 (min)	50.71, 50.41, 50.53, 50.45, 50.32	50.48 (0.15)
4 (min)	171.0, 174.4	172.7
5 (min)	247.5, 253.1, 253.3	251.3 (3.3)

Table 6.2 - Flow rate calibration data for automated syringe pump assembly at each flow rate setting shown, 20°C.

6.2.1.5 GENERAL PROCEDURE FOR CONDUCTIMETRIC TITRATIONS

The conductivity bridge and chart recorder were calibrated at the desired range settings as described in Section 6.2.1.4.
The Hamilton precision syringe was carefully filled with titrant and any bubbles of air removed. The syringe was loaded on to the motorized syringe pump and the microbore delivery tube unit fitted. An elastic band held the syringe plunger tight against the pump ram. The titrant was run to waste at a fast flow rate until all air bubbles from the delivery tube were removed from the system. The titration flow rate was selected and a few drops of titrant again run to waste to ensure correct gear location.

50 mls of sample solution were pipetted into the jacketed beaker, the thermometer inserted and the magnetic stirrer switched on. The beaker was covered with a layer of aluminium foil and the solution allowed to equilibrate with respect to temperature and dissolved gases. At temperatures above ambient it was necessary to remove gas bubbles from the beaker walls with the thermometer before proceeding. After equilibration, the magnetic stirrer was switched off and the aluminium cover removed. The conductivity cell was carefully inserted into the solution, ensuring complete removal of air from the measuring compartment. The cell was positioned just above the magnetic flea and close to the edge of the beaker to avoid the vortex. The tip of the syringe microbore delivery tube was positioned in a similar manner but on the opposite side of the beaker from the conductivity cell. A specially cut sheet of aluminium foil was placed on top of the beaker to minimise evaporation and contamination during the tiration. After a few minutes re-equilibration time the chart speed was selected and the titration started by simultaneously switching on the motorized syringe

pump unit and chart recorder. The conductivity meter reading was noted at the beginning and end of the titration to ensure the chart calibration was correct on each run.

6.2.1.6 CALCULATION OF CONCENTRATION

The concentration of added titrant at any point in the titration may be calculated using equations 6.1 and 6.2:

$$\text{Concentration (M)} = \text{Titrant concentration (M)} \times \frac{V}{(50+V)} \qquad (6.1)$$

$$V = F. \frac{1}{v} \qquad (6.2)$$

Where V is the volume of added titrant in mls, F is the flow rate in mls min^{-1}, 1 is the chart run length in mm, and v is the chart speed in mm min^{-1}; (preliminary checks showed the chart speed settings were correct).

The concentration of solute being titrated at any point in the titration is given by equation 6.3:

$$\text{Concentration (M)} = \text{Initial Concentration (M)} \times \frac{50}{(50+V)} \qquad (6.3)$$

6.2.1.7 VALIDATION OF TITRATION METHOD

The titration technique was validated by comparing the conductivity of potassium chloride solutions during titration (dynamic method) with the conductivity of stock solutions of known concentration (static method). Determinations were performed at 30°C and at the two principal flow rates used in the study (20.38 and 50.48 $\mu l\ min^{-1}$). The conductivity bridge and chart recorder were calibrated as previously described (section 6.2.1.4).

(a) Static Method

Solutions of 1 - 6 x 10^{-3} M potassium chloride were prepared from a 0.1 M stock solution. Each solution, in turn, was equilibrated to 30°C in the jacketed cell and the conductivity of the unstirred solution measured. Conductivity values were read off the bridge meter and also recorded on the chart recorder as a 'base line'. The 'static' specific conductivity values were calculated from both meter and chart readings.

(b) Dynamic Method

0.1 M potassium chloride was titrated into 50 mls of double distilled water at 30°C using the general method previously described (section 6.2.1.5). Flow rates of 20.38 and 50.48 µl min^{-1} were used at chart speeds of 12 cm hr^{-1} and 60 cm hr^{-1} respectively; chart range 0 - 1 x 10^{-3} S; conductivity bridge range '6'. Conductivity was recorded as a curve on the chart recorder from which a plot of specific conductivity against potassium chloride concentration was constructed. The 'dynamic' specific conductivity corresponding to 1.0, 2.0, 3.0, 4.0, 5.0 and 6.0 x 10^{-3} M potassium chloride solution was read from the graph using equations 6.1 and 6.2.

Results of 'static' and 'dynamic' experiments are shown in table 6.3. The results show a good agreement between 'static' and 'dynamic' specific conductivity values. The observed average difference between meter and static chart values (±0.9%) and meter and dynamic chart values (±2.0%) reflect the errors in calibrating and reading values off the chart recorder.

KCl Concentration M (x 10^3)	Conductivity (S x 10^6)			
	Static		Dynamic	
	Meter	Chart	20.38 µl min^{-1}	50.48 µl min^{-1}
1.0	112.6	114	115	114
2.0	220.2	223	224	226
3.0	330.8	333	336	336
4.0	435.6	440	446	444
5.0	543.7	548	552	551
6.0	650.1	654	661	660

Table 6.3 - 'Static' and 'dynamic' specific conductivity of potassium chloride solution at 30°C.

6.2.2 Differential Scanning Calorimetry

The physicochemical nature of the cirazoline alkylsulphate complex was investigated using differential scanning calorimetry (DSC). This is a thermal analysis technique in which the energy of a transition of a substance is measured as a function of temperature. The sample and reference material are subjected to a closely controlled increasing temperature programme and, in the event that a transition occurs in the sample, the thermal energy added to the sample or reference containers is varied in order to maintain both sample and reference at the same temperature. Because this energy input is precisely equivalent in magnitude to the energy absorbed or evolved in the particular transition, a recording of this balance energy between sample and reference yields a direct calorimetric measurement of the transition energy. Hence DSC not only yields the temperature of a particular transition but, also enables calculation of the enthalpy change of the transition.

In these studies the weight of the sample was not measured due to difficulty in sample preparation and the technique was therefore limited to the determination of transition temperatures and a qualitative indication of the nature of the transition (i.e. exothermic versus endothermic transition).

DSC curves were generated using a DuPont 910 differential scanning calorimeter with DuPont 9900 computer/thermal analyser. Aluminium, crimped pans (non-hermetic seal) were used. Sample and reference (air) pans were equilibrated automatically to the initial temperature.

6.3 RESULTS

6.3.1 Physicochemical Nature of Formed Complexes

The formation and physicochemical nature of cirazoline-alkylsulphate and imidazoline-dodecylsulphate complexes were investigated.

6.3.1.1 CIRAZOLINE-ALKYLSULPHATE SYSTEMS

Complexes of cirazoline octylsulphate (CIRH-OS, 0.05 M), cirazoline decylsulphate (CIRH-DS, 0.033 M), cirazoline dodecylsulphate CIRH-DDS, 0.01 M) and cirazoline tetradecylsulphate (CIRH-TDS, 0.005 M) were formed by mixing aqueous solutions of cirazoline hydrochloride and the appropriate sodium alkylsulphate in equimolar amounts at ambient temperature.

The CIRH-OS system immediately formed a white liquid-in-liquid dispersion which separated after about ten minutes to form a lower oily layer. Storage at 4°C for 24 hours resulted in the formation of a viscous supernatent and partial crystallization of the lower layer. After further storage at 4°C the viscosity reduced and the system consisted of a lower crystalline layer and a clear supernatent. CIRH-DS formed a liquid complex and the system appeared as a white milky dispersion. Slow crystallisation occurred upon storage at 4°C. CIRH-DDS and CIRH-TDS systems immediately formed a slightly viscous, grey dispersion which precipitated with time to form a white crystalline solid and clear supernatent. CIRH-DDS precipitated after 12-24 hours storage at ambient temperature whereas CIRH-TDS crystallised a few minutes after preparation.

The CIRH-DDS system was further investigated by preparing mixtures of different concentrations and mole ratio. Systems containing 2×10^{-3} M

cirazoline hydrochloride and 2 - 10 x 10^{-3} M SDDS were prepared at ambient temperature. The 10 x 10^{-3} M SDDS mixture was well above the CMC of that system (see table 7.4, section 7.1.2.2) and formed a stable isotropic solution with no apparant increase in viscosity. Systems containing other SDDS concentrations formed clear or slightly hazy viscous solutions which precipitated overnight at ambient temperature. Birefringence was not detected in these systems when viewed under polarized light indicating the absence of liquid crystalline phase. Figure 6.2 shows the equimolar (2 x 10^{-3} M) systems at 30°C, (a) immediately after preparation and (b) after 24 hours storage.

Samples of all crystalline cirazoline alkylsulphate complexes were isolated at 4°C using Whatman No. 1 filter paper and dried to constant weight at ambient temperature in a desiccator containing silica gel. Great care was needed in handling the hydrated CIRH-OS crystalline complex as rapid melting occurred with slight increase in temperature. The NMR spectra on the anhydrous complexes in $CDCl_3$ (Appendix 1), show all complexes to be of 1:1 stoichiometry, (CIRH-OS = 1:0.979, CIRH-DS = 1:0.946, CIRH-DDS = 1:0.996, and CIRH-TDS = 1:0.976). Figures 6.3 - 6.6 show photomicrographs of anhydrous and hydrated complexes at x 80 magnification.

Determination of Transition Temperature

The effect of temperature on the physical nature of the hydrated complexes was investigated by determining the temperature of transition from stable hydrated solid complex to stable hydrated liquid complex using DSC. The CIRH-DDS complex transition temperature was also determined by visual observation.

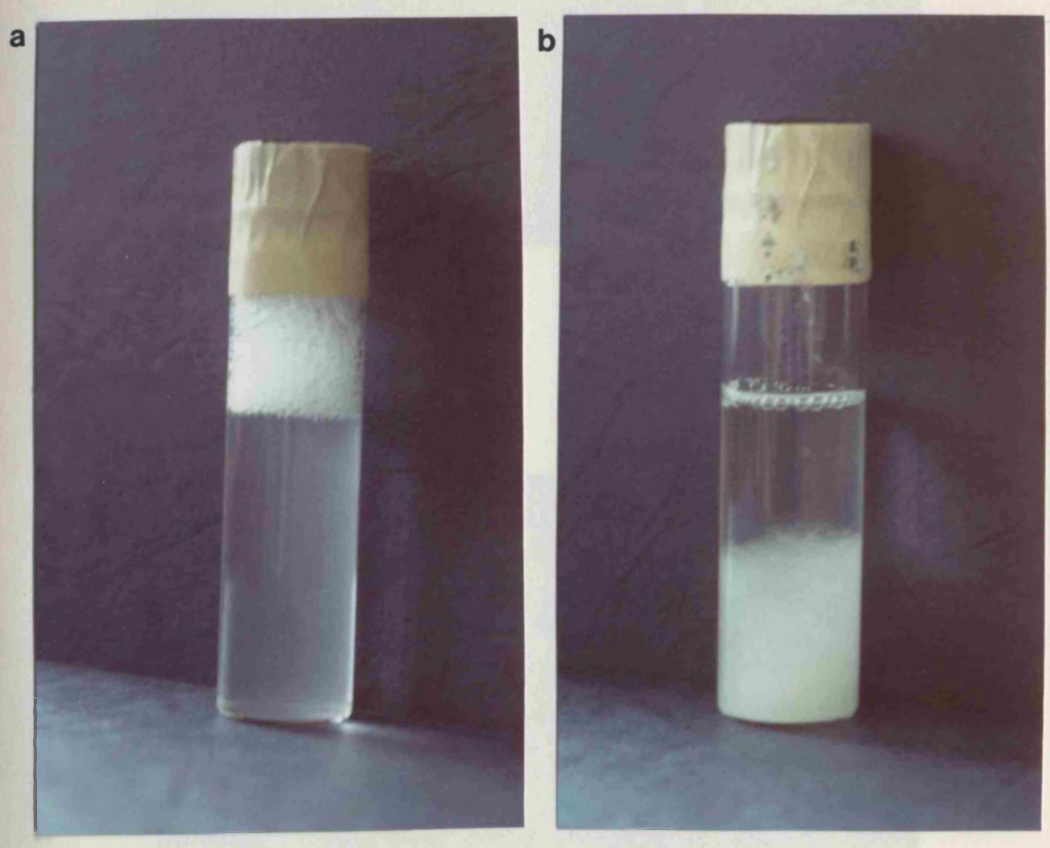

Figure 6.2 - Equimolar (2×10^{-3} M) cirazoline hydrochloride - SDDS system at 30°C, (a) immediately after preparation and (b) after 24 hours storage.

a

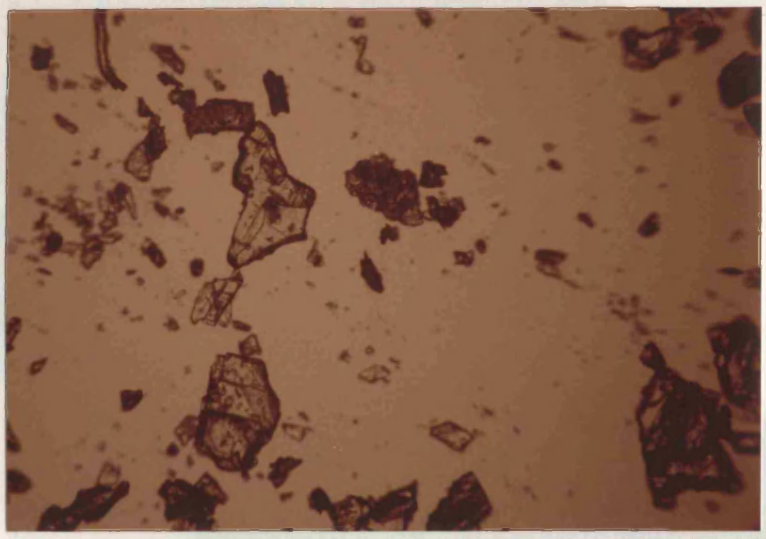

b

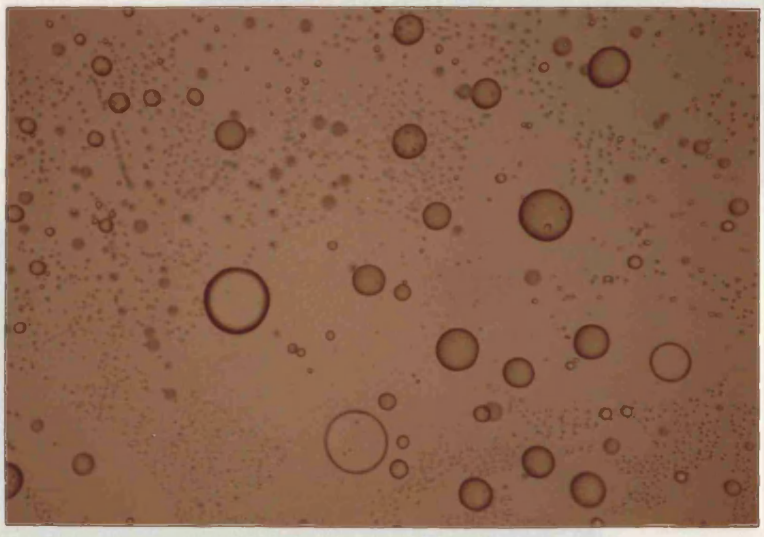

Figure 6.3 - Photomicrographs of cirazoline-octylsulphate complex at x 80 magnification, ambient temperature, (a) anhydrous, (b) hydrated in distilled water.

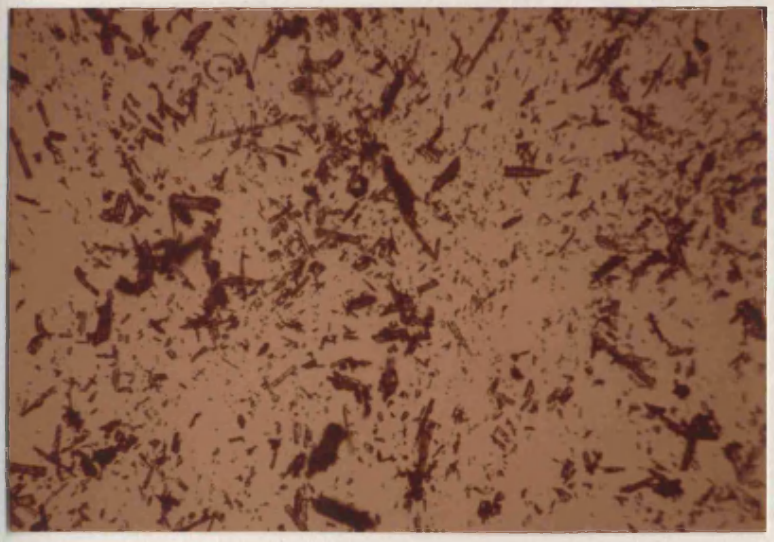

a

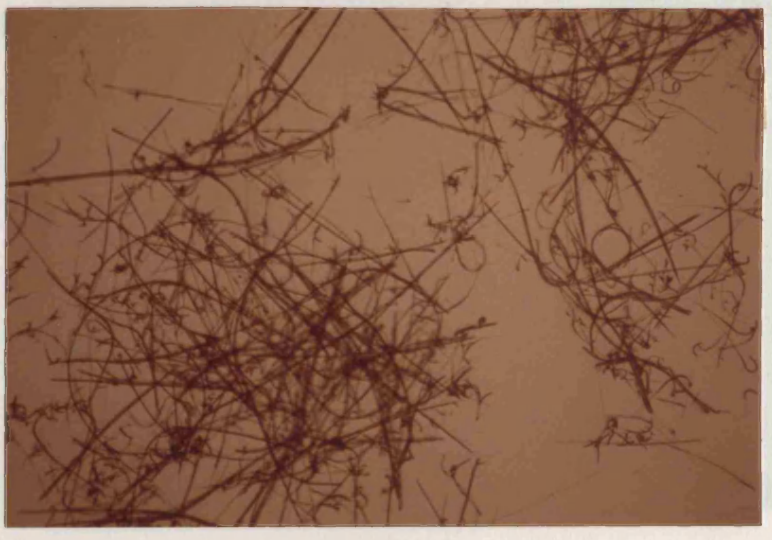

b

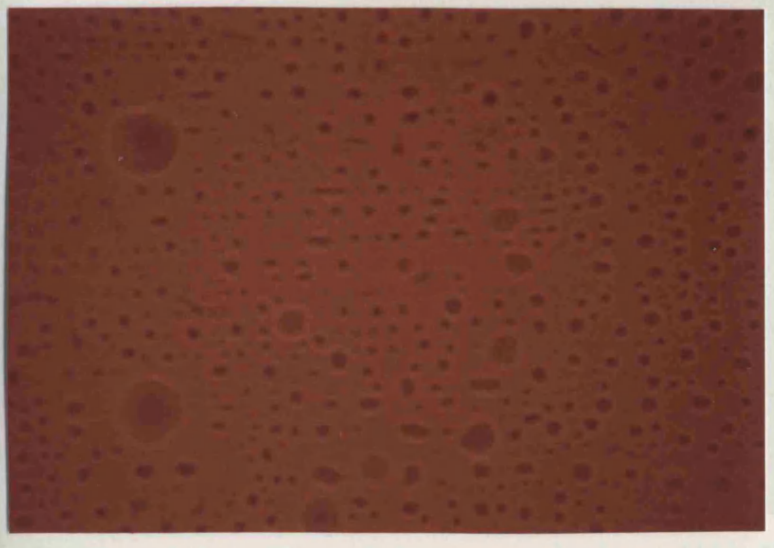

c

Figure 6.4 - Photomicrographs of cirazoline-decylsulphate complex at x 80 magnification, (a) anhydrous, ambient temperature, (b) hydrated in distilled water at ambient temperature and (c) hydrated in distilled water with warming.

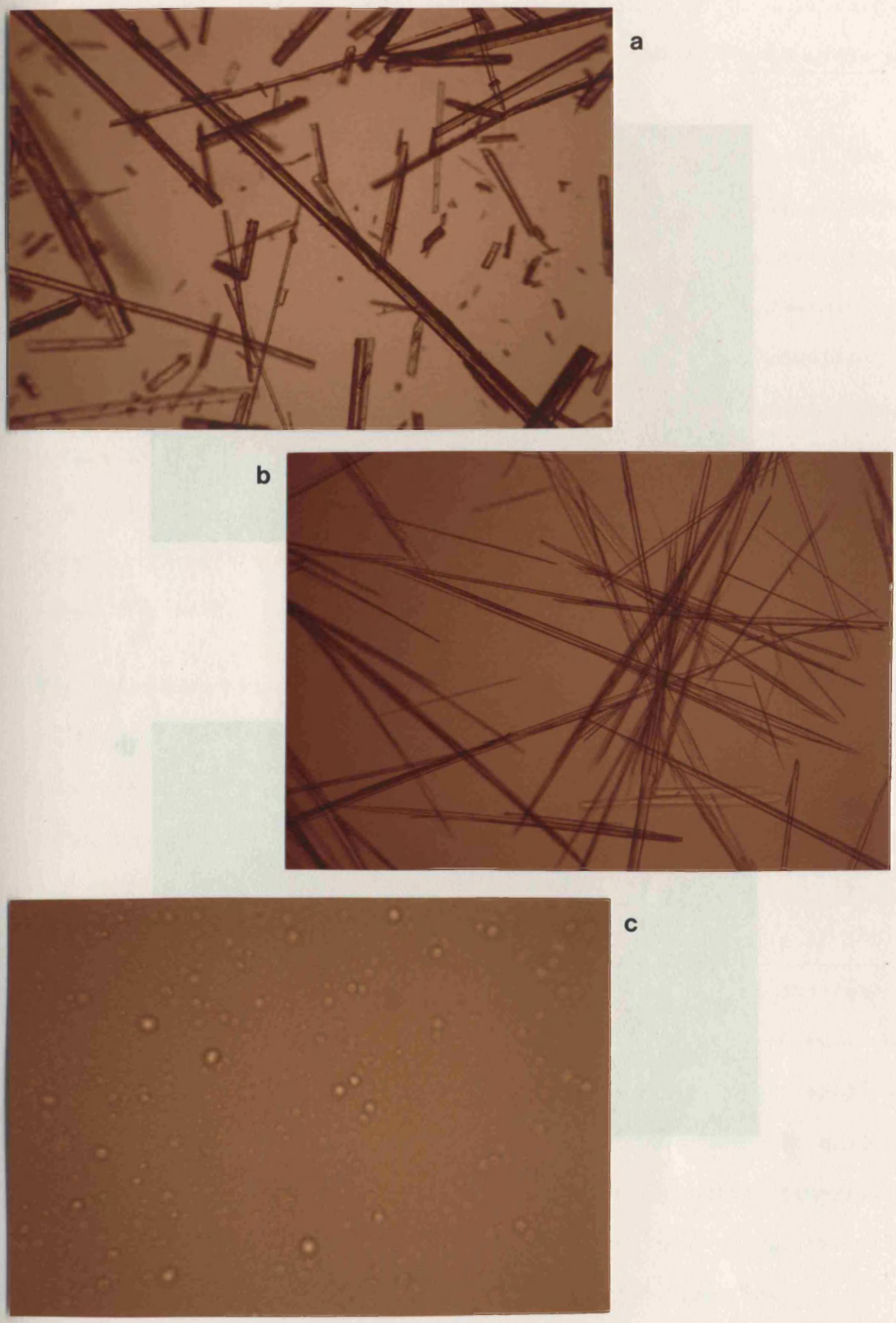

Figure 6.5 - Photomicrographs of cirazoline-dodecylsulphate complex at x 80 magnification, (a) anhydrous, ambient temperature, (b) hydrated in distilled water at ambient temperature and (c) hydrated in distilled water with warming.

a

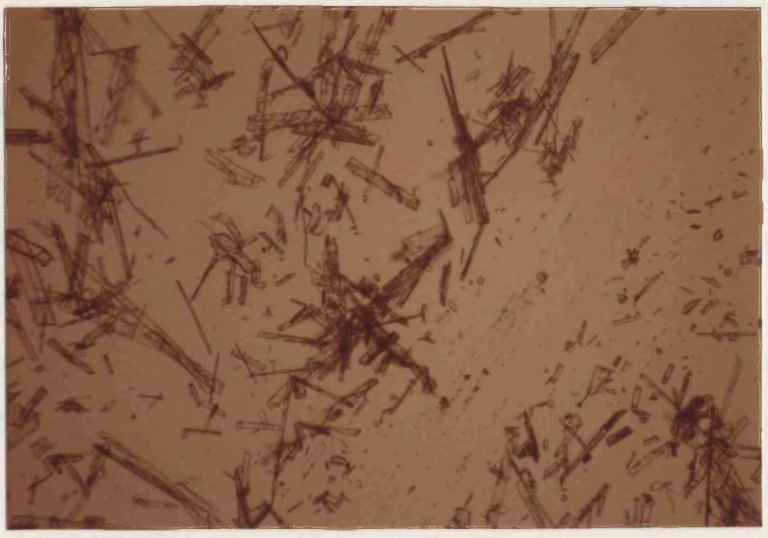

b

Figure 6.6 - Photomicrographs of cirazoline-tetradecylsulphate complex at x 80 magnification, ambient temperature, (a) anhydrous and (b) hydrated in distilled water.

Equimolar mixtures of cirazoline hydrochloride and SDDS were prepared at 1 x 10^{-3}, 2 x 10^{-3}, 3.3 x 10^{-3}, 1 x 10^{-2} and 5 x 10^{-2} M concentration levels and equilibrated at 25°C in a water bath. The temperature was increased in increments of about 1°C and the physical appearance of the system noted at each temperature. An equilibration time of at least one hour was allowed between temperature increase and assessment. The transition temperature was given by the formation of a grey liquid in liquid dispersion and the concomitant reduction in the amount of crystalline complex. Transition in each system occurred over a narrow temperature range (approximately 2°C) and all systems changed from a crystalline suspension to a grey dispersion in the temperature range 39 - 42°C.

The transition temperature of hydrated complexes was determined by DSC as follows: a small amount of anhydrous crystalline complex was placed in a sample pan and two drops of chilled distilled water were added using a pasteur pipette. The pan was crimped (non-hermetic seal) and the exterior dried carefully with a tissue. Samples were equilibrated to temperature in the DSC furnace and scanned at a ramp rate of 1°C min^{-1}. Large peaks with negative heat flow occurred which indicate endothermic solid -> liquid transitions. Figures 6.7 - 6.10 show the DSC spectrum for each system and indicate a transition temperature of 17.8°, 34.1°, 44.9° and 52.7°C for CIRH-OS, CIRH-DS, CIRH-DDS and CIRH-TDS systems respectively. The CIRH-DDS complex transition temperature was also determined at a ramp rate of 0.2°C min^{-1} and using crystalline complex formed <u>in situ</u> from aqueous solutions of cirazoline hydrochloride and SDDS; a transition temperature of 44.4°C was obtained for both these systems.

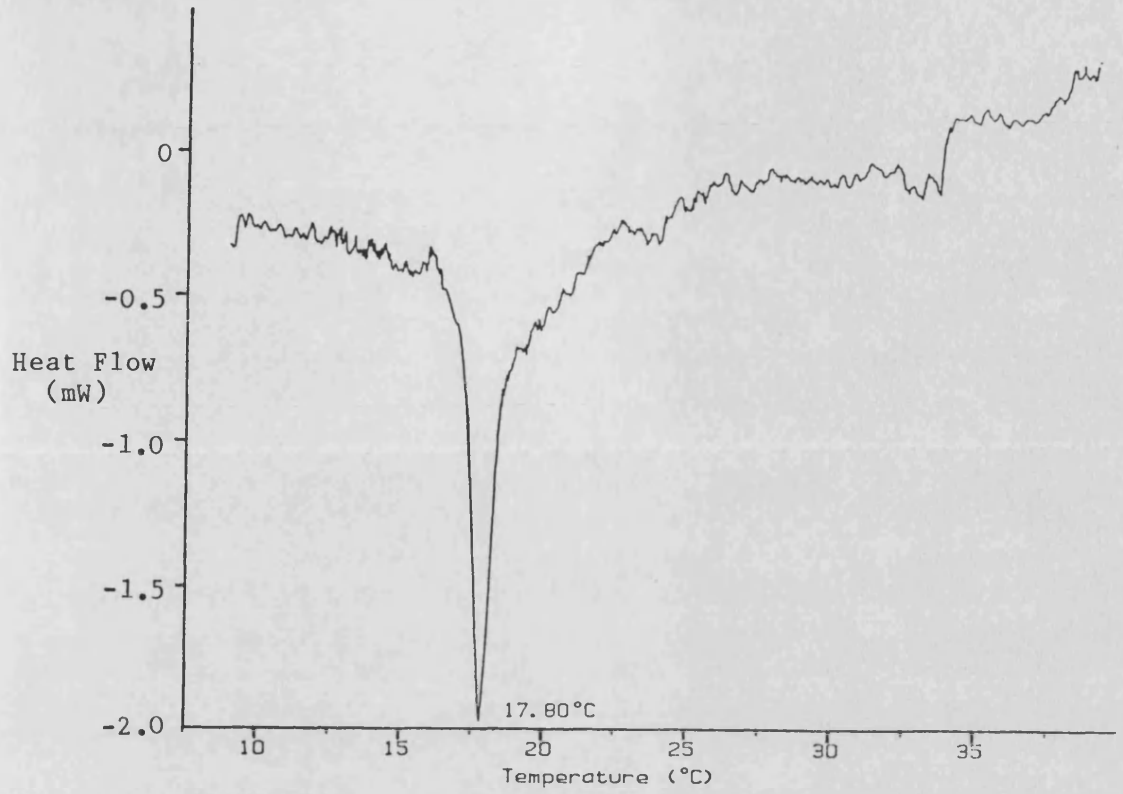

Figure 6.7 - DSC spectrum for cirazoline-octylsulphate complex in distilled water showing solid --> liquid complex transition endotherm, (ramp rate = $1^{o}C\ min^{-1}$).

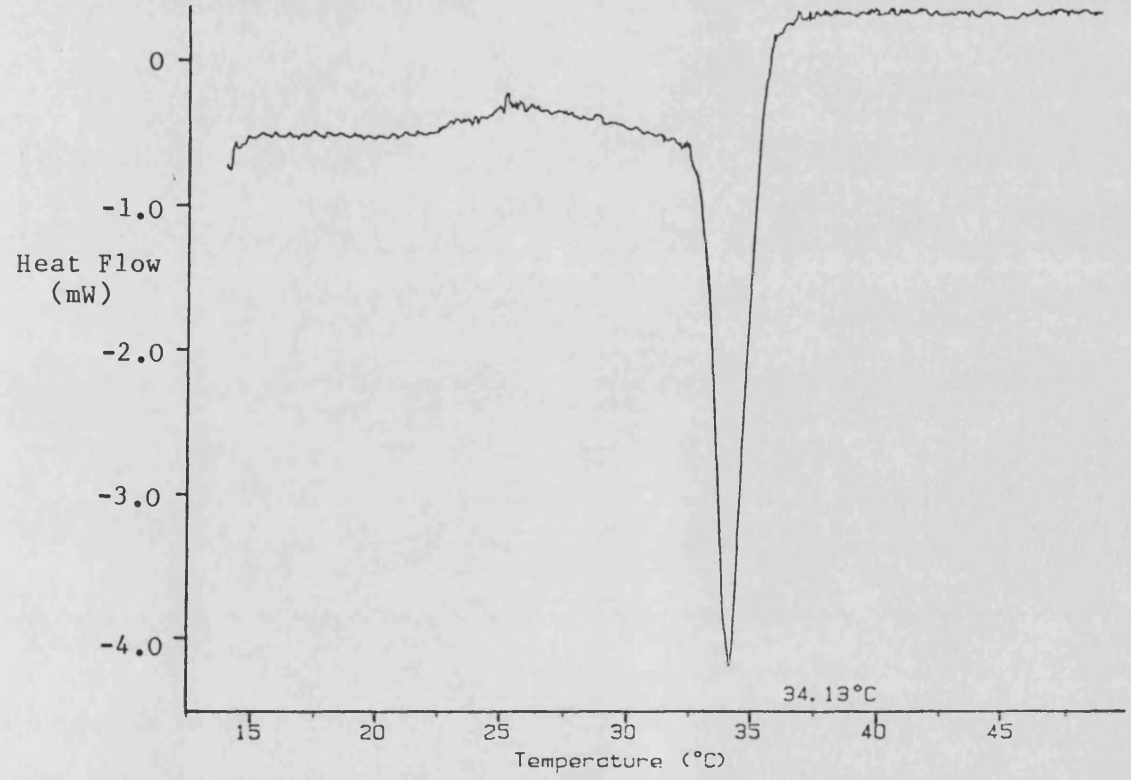

Figure 6.8 - DSC spectrum for cirazoline-decylsulphate complex in distilled water showing solid --> liquid complex transition endotherm, (ramp rate = $1^{o}C\ min^{-1}$).

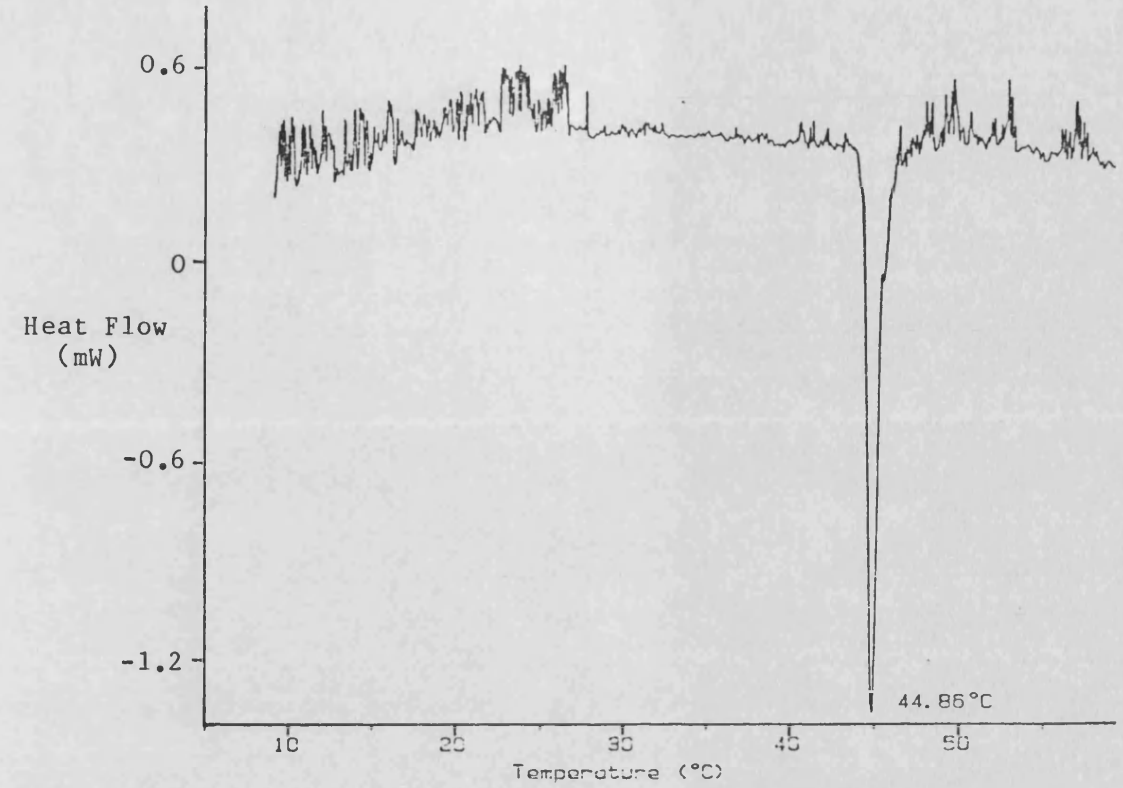

Figure 6.9 - DSC spectrum for cirazoline-dodecylsulphate complex in distilled water showing solid --> liquid complex transition endotherm, (ramp rate = $1^{o}C\ min^{-1}$).

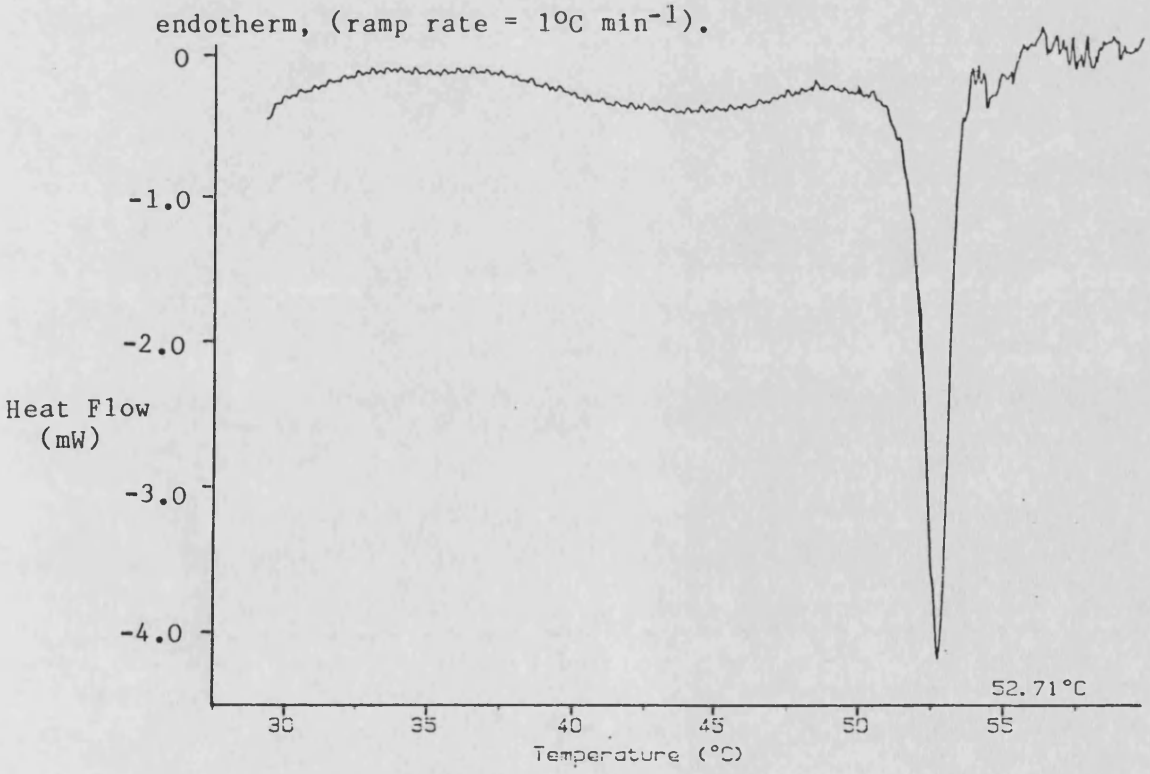

Figure 6.10 - DSC spectrum for cirazoline-tetradecylsulphate complex in distilled water showing solid --> liquid complex transition endotherm, (ramp rate = $1^{o}C\ min^{-1}$).

6.3.1.2 IMIDAZOLINE DODECYLSULPHATE SYSTEMS

1×10^{-3} M complexes of antazoline dodecylsulphate (ANTH-DDS), xylometazoline dodecylsulphate (XYLH-DDS), naphazoline dodecylsulphate (NAPH-DDS) and tolazoline dodecylsulphate (TOLH-DDS) were produced by mixing in equimolar quantities aqueous solutions of SDDS and the appropriate imidazoline salt at ambient temperature. The ANTH-DDS complex immediately produced large, white solid floccules which separated to the surface. The XYLH-DDS and NAPH-DDS systems formed grey, viscous liquid-in-liquid dispersions. The former precipitated slowly at 4°C to form long, needle-like crystals whereas the NAPH-DDS system remained unchanged as a liquid-in-liquid dispersion at 4°C during the period of the study (about four months). The TOLH-DDS system was a clear isotropic viscous liquid at ambient and 4°C which was stable over the period of the study.

6.3.2 Determination of Solubility Products

6.3.2.1 CIRAZOLINE DODECYLSULPHATE EQUILIBRIUM SOLUBILITY PRODUCT

The apparant equilibrium solubility product for the cirazoline hydrochloride-SDDS system was determined at 30°C by conductivity and turbidity measurements. Systems containing 2×10^{-4} M cirazoline hydrochloride and a range of SDDS concentrations were prepared and equilibrated to 30°C over a 24 hour period. The presence of insoluble phase was detected by measuring the apparant absorbance of each system in a 10 mm cuvette at 500 nm using a Perkin Elmer 550S UV-VIS spectrophotometer. Conductivity was measured using the jacketed beaker, Mullard conductivity dip-cell and Wayne-Kerr conductivity bridge in static mode (see section 6.2.1.7a).

The solubility product was calculated from a knowledge of the cirazoline hydrochloride concentration and the SDDS concentration associated with the appearance of insoluble phase (equation 1.67); a 1:1 stoichiometry was assumed for this calculation. This point is signified by an increase in the turbidity of the system and an inflexion in the conductivity-SDDS concentration profile. Turbidity and conductivity measurements are shown in table 6.4 and figure 6.11.

The turbidity data show a marked increase in apparant absorbance at an SDDS concentration of 6×10^{-4} M. Systems containing concentrations of SDDS at or above this value produced a highly flocculated, solid complex indicating the cirazoline-dodecylsulphate solubility product had been exceeded. The conductivity-SDDS concentration profile shows a deviation from linearity at the same SDDS concentration associated with complex formation. The system containing 5.75×10^{-4} M SDDS was a clear isotropic solution and the apparent solubility product at 30°C was therefore estimated at between 1.15×10^{-7} and 1.20×10^{-7} $moles^2 litre^{-2}$.

6.3.2.2 DETERMINATION OF SOLUBILITY PRODUCTS BY CONDUCTIMETRIC TITRATION

Solubility products were determined from the end-point of conductimetric titrations using equations 6.1 - 6.3 and 1.67.

(a) Description

Figure 6.12 shows the conductivity curve for the titration of 0.01 M SDDS into 1.5×10^{-3} M cirazoline hydrochloride at 50°C, flow rate 50.48 $\mu l\ min^{-1}$, chart speed 12 cm hr^{-1}, chart conductivity range 100 -200 $\times 10^{-6}$S; (the chart recorder trace is shown in Appendix 2).

[SDDS] M x 10^4	APPARANT ABSORBANCE AT 500 nm (AU) (a)	(b)	SPECIFIC CONDUCTIVITY (S x 10^6)(b)	OBSERVATION
NIL	0.002	0.004	23.90	CLEAR SOLUTION
4.5	0.002	0.002	57.28	"
5.0	0.002	0.004	60.64	"
5.5	0.001	0.003	64.67	"
5.75	0.001	0.002	66.67	CLEAR SOLUTION?
6.0	0.008	0.018	67.19	CRYSTALLINE SUSPENSION
6.5	0.028	0.027	70.34	"
7.0	0.040	0.045	74.08	"
7.5	0.100	0.083	77.95	"

Table 6.4 - Turbidity (apparant absorbance) and conductivity data for 2 x 10^{-4} M cirazoline hydrochloride-SDDS systems at 30°C.

(a) approximately 18 hours after preparation and

(b) approximately 24 hours after preparation.

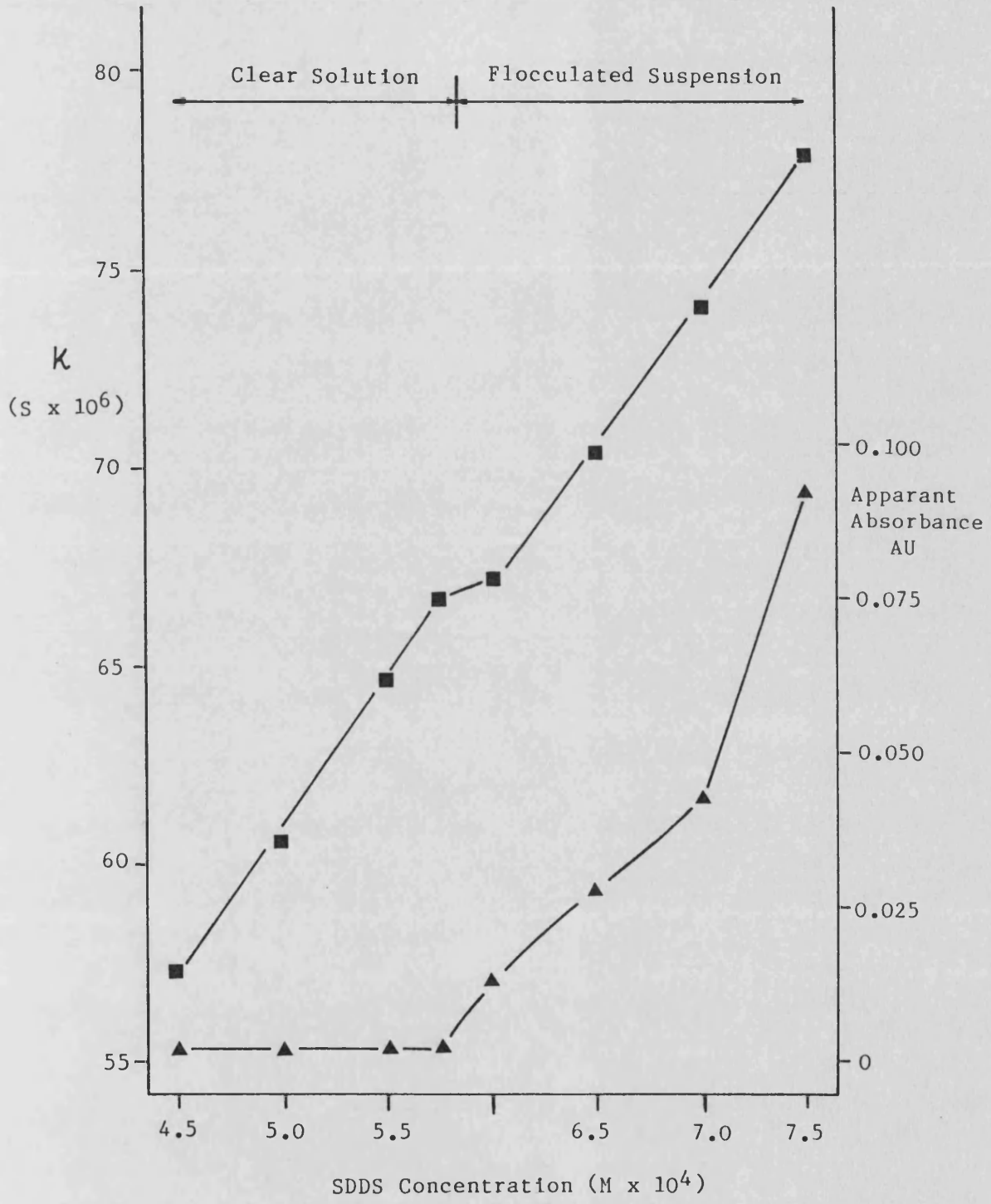

Figure 6.11 - Specific conductivity, K, apparant absorbance and physical appearance of 2 x 10^{-4} M cirazoline hydrochloride-SDDS systems, 30°C, after 24 hours equilibration.

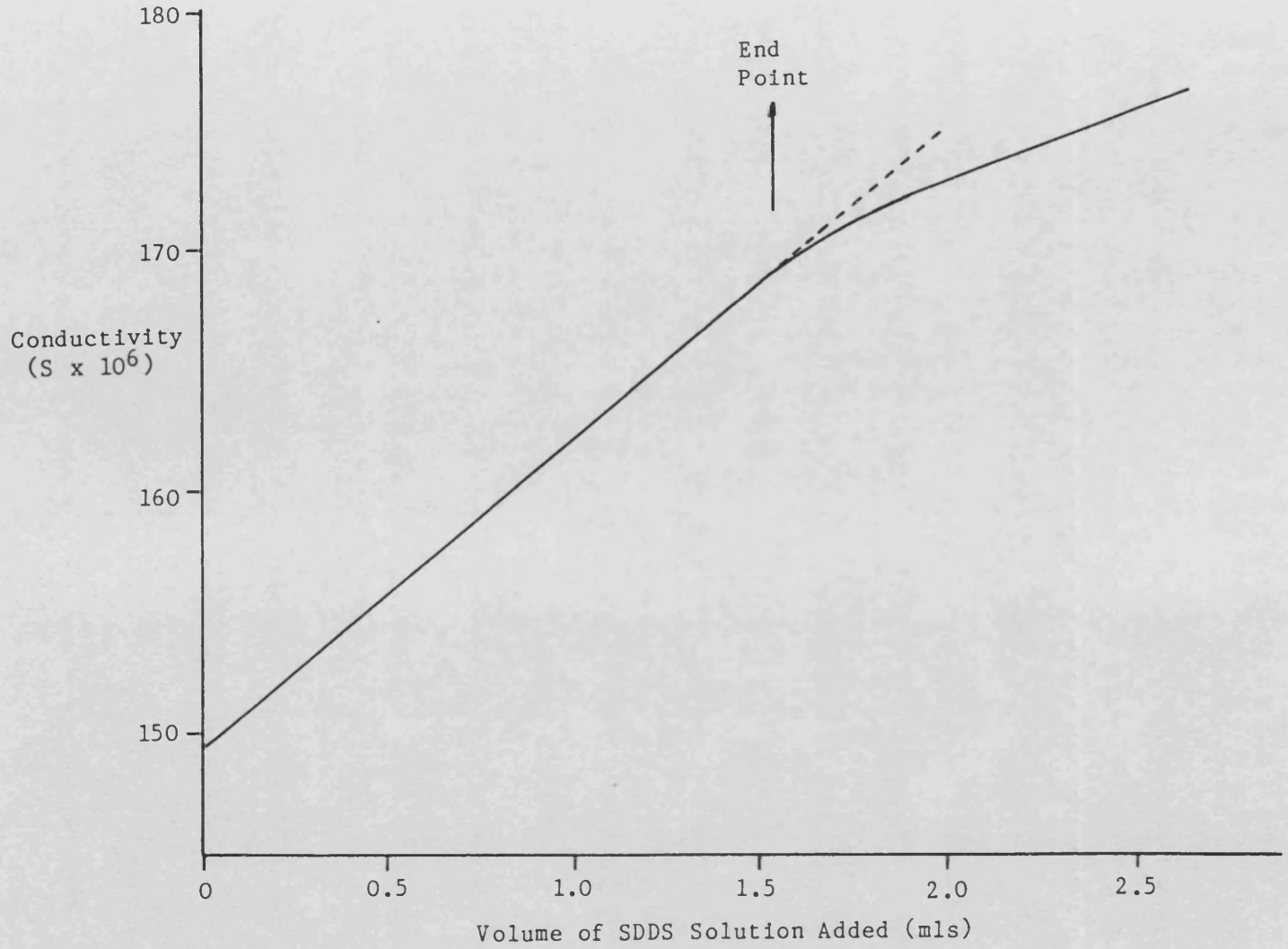

Figure 6.12 - Conductimetric titration trace for SDDS (0.01 M) against cirazoline hydrochloride (1.5×10^{-3} M) at 50°C. Flow rate = 50.48 µl min^{-1}, chart speed = 12 cm hr^{-1}, chart conductivity range = 100 - 200 x 10^{-6} S.

The CIRH-DDS complex is liquid at this temperature (see section 6.3.1) and the conductivity curve resembles literature examples (figure 1.10a). The end-point of the titration is given by the point of initial deviation from linearity in the conductivity curve concomitant with phase separation (figure 6.12). The incremental increase in conductivity with added titrant decreases after this point due to formation of insoluble non-conducting complex. At concentrations below and well above the end-point the conductivity curve is linear (accounting for dilution effects) but of different slope.

At 30°C the equilibrium CIRH-DDS complex is solid and conductivity curves show an abnormal decrease in conductivity associated with formation of a white flocculated dispersion. Figure 6.13 shows the conductivity curve for the titration of 0.01 M SDDS into 1 x 10^{-3} M cirazoline hydrochloride at 30°C; flow rate 20.4 µl min^{-1}, chart speed 12 cm hr^{-1}, chart conductivity range 70 - 90 x 10^{-6} S; (the chart recorder trace is shown in Appendix 2). The titration end-point for the solid complex solubility product is found to be given by extrapolation of the second linear curve to the first (figure 6.13). Verification for this is that the solubility product value of 1.16 x 10^{-7} $moles^2 litre^{-2}$ calculated by this method is in good agreement with the equilibrium K_s' value of 1.15 x 10^{-7} - 1.20 x 10^{-7} $moles^2 litre^{-2}$ (section 6.3.1). The peak in the conductivity curve is thought to represent supersaturation due to the formation of a metastable system (see section 6.3.1.1).

(b) Effect of Titration Flow Rate

The effect of flow rate was investigated by titrating 0.01 M SDDS solution into a 1 x 10^{-3} M solution of cirazoline hydrochloride at

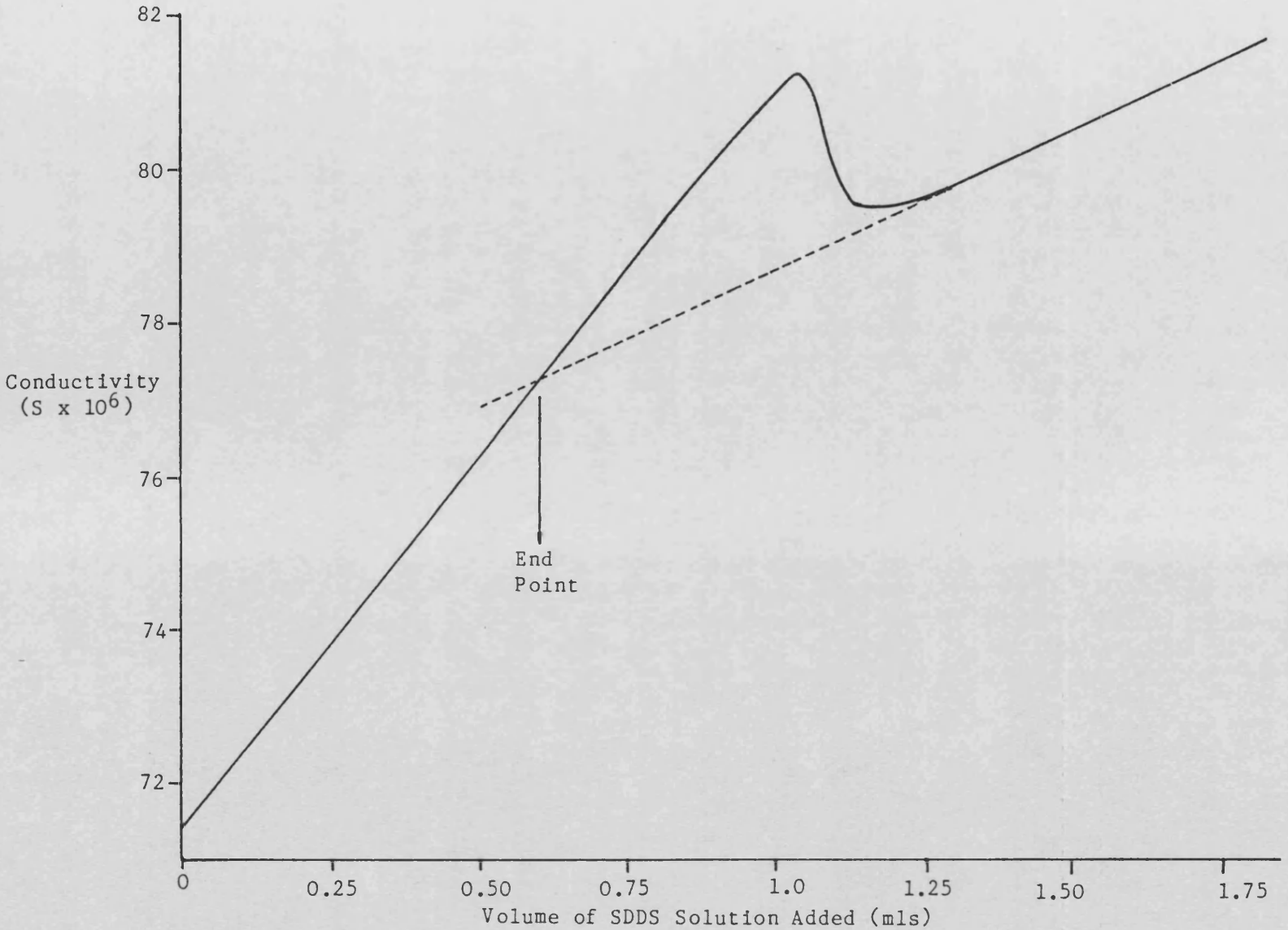

Figure 6.13 - Conductimetric titration trace for SDDS (0.01 M) against cirazoline hydrochloride (1×10^{-3} M) at 30°C. Flow rate = 20.38 µl min^{-1}, chart speed = 12 cm hr^{-1}, chart conductivity range = 70 - 90 x 10^{-6} S.

30°C. Flow rates of 6.29, 12.39, 20.38, 50.48 and 173 µl min^{-1} were used. The latter flow rate was selected as this is similar to the molar rate of addition used by Mukhayer et al[120]. The conductivity bridge and chart recorder were set to give a chart conductivity range of 70 -90 x 10^{-6} S. A chart speed of 3, 12 or 60 cm hr^{-1} was used as appropriate.

At flow rates of 6.29 - 50.48 µl min^{-1} characteristic conductivity curves associated with formation of solid complex were produced. The complex formed in this manner was similar in morphology to that observed in equilibrium studies (sections 6.3.1 and 6.3.2.1). At a flow rate of 173 µl min^{-1}, however, the characteristic decrease in conductivity associated with precipitation of solid complex was absent. The inflexion in the conductivity curve was a simple change in gradient, similar to that observed for the titration at 50°C (figure 6.12). The system changed in appearance at this point from a clear solution to a turbid, grey dispersion and the complex was liquid in nature. A change in specific conductivity-SDDS volume, plot constructed using data from titration curves at flow rates of 20.38 and 173 µl min^{-1} is shown in figure 6.14. Titration end-points are also shown for the calculation of the 'solid' and 'liquid' solubility products. Both profiles are linear with similar slope until phase separation occurs. The profiles differ thereafter with the formation of the liquid and solid complexes.

Calculated solubility product values at each flow rate is shown in table 6.5. Titration at flow rates of 6.29, 12.39, 20.38 and 50.48 µl min^{-1} was found to produce similar values and show good agreement with the equilibrium solubility product value (1.15 x 10^{-7} - 1.20 x 10^{-7} $moles^2 litre^{-2}$).

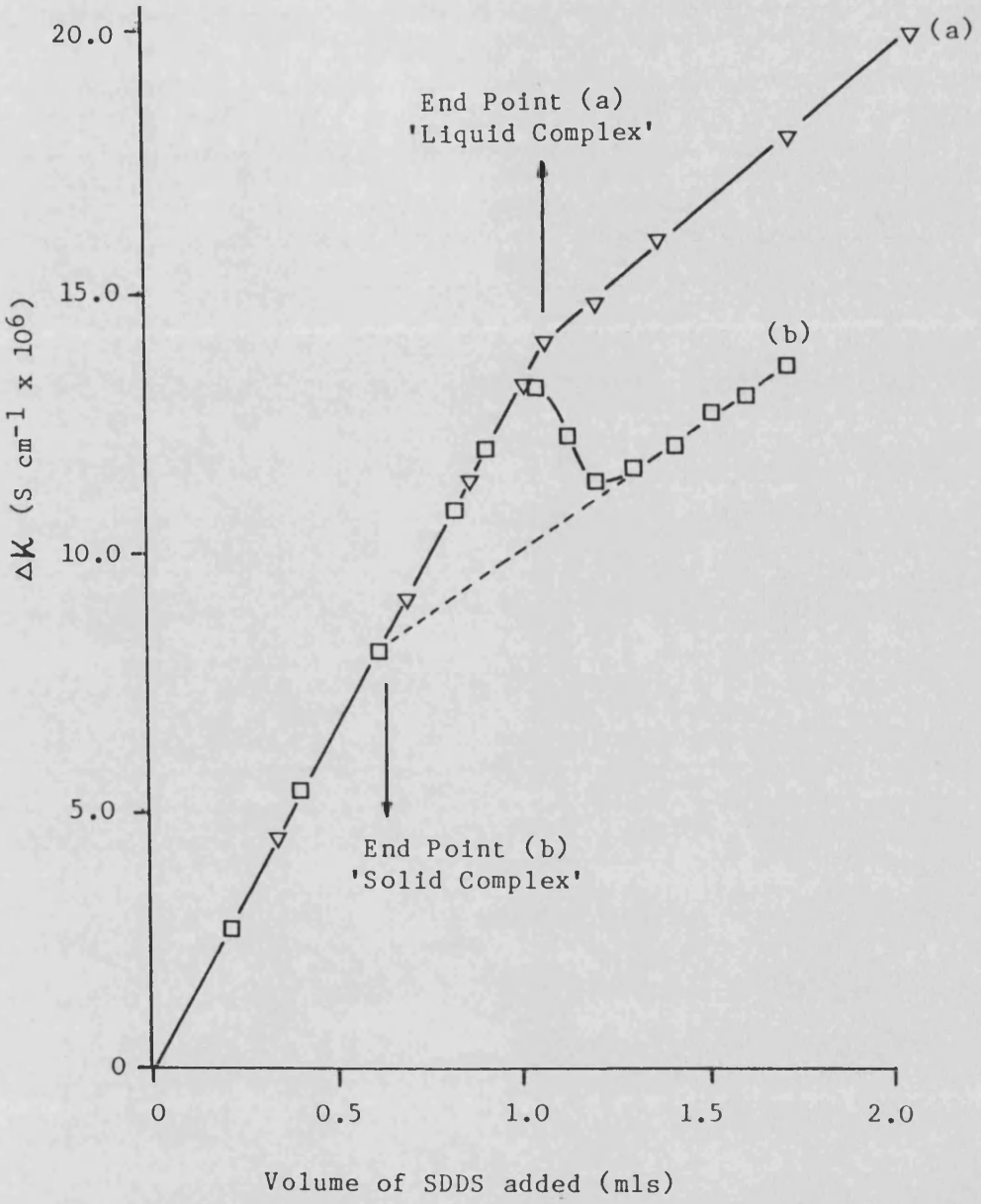

Figure 6.14 - Change in specific conductivity, ΔK, - SDDS volume plot for the titration of SDDS (0.01 M) against cirazoline hydrochloride (1 x 10^{-3} M) at 30°C and flow rates of (a) 173 µl min^{-1} (—▽—), and (b) 20.38 µl min^{-1} (—□—).

FLOW RATE ($\mu l\ min^{-1}$)	SOLUBILITY PRODUCT ($moles^2 litre^{-2}$)	COMPLEX
-	1.15 - 1.20 *	SOLID
6.29	1.17	"
12.40	1.19	"
20.38	1.16	"
50.48	1.23	"
172.7	2.04	LIQUID

Table 6.5 - The effect of titrant flow rate on calculated cirazoline-dodecylsulphate solubility product at 30°C. (* Equilibrium solubility product value).

The liquid complex system formed by titrating at a fast flow rate was found to precipitate with time, forming a white flocculated dispersion, similar in nature to the equilibrium complex. The liquid complex system is therefore thought to be metastable under these conditions.

(c) Reproducibility

The cirazoline dodecylsulphate solid complex solubility product at 30°C was determined seven times over a twelve month period by titrating 0.01M SDDS against 1 x 10^{-3} M cirazoline hydrochloride at a flow rate of 20.38 µl min^{-1}. The mean solubility product was found to be 1.17 x 10^{-7} (S.D. = 0.03 x 10^{-7}) $moles^2 litre^{-2}$. Four further titrations were performed at flow rates of 12.38 or 50.48 µl min^{-1} and the mean for all eleven solubility product values was calculated as 1.17 x 10^{-7} (S.D. = 0.03 x 10^{-7}) $moles^2 litre^{-2}$.

The CIRH-DDS liquid complex solubility product was determined twice at 50°C and twice at 37.5°C by titrating 0.01 M SDDS against 1 x 10^{-3} M cirazoline hydrochloride. At 50°C, flow rates of 20.38 and 50.48 µl min^{-1} were used and solubility product values were calculated as 4.27 x 10^{-7} and 4.10 x 10^{-7} $moles^2 litre^{-2}$ respectively. At 37.5°C, flow rates of 20.38 and 172.7 µl min^{-1} were used and gave solubility product values of 2.62 x 10^{-7} and 2.56 x 10^{-7} $moles^2 litre^{-2}$ respectively.

The reproducibility of the titration end-point measuring technique was evaluated by analysing a solid complex titration curve (0.01 M SDDS v 1 x 10^{-3} M cirazoline hydrochloride at 30°C), and a liquid complex titration curve (0.01 M SDDS v 1.5 x 10^{-3} M cirazoline hydrochloride at 50°C). Each conductivity curve was reproduced six times using a photocopier and the end-point and resulting solubility product value of

each curve determined. The mean solid and liquid complex solubility product was calculated as 1.16×10^{-7} (S.D. 0.01×10^{-7}) $mole^2 litre^{-2}$ and 2.78×10^{-7} (S.D. 0.04×10^{-7}) $moles^2 litre^{-2}$, respectively. These data therefore show the solid complex and liquid complex measuring techniques to be reproducible.

6.3.2.3 STOICHIOMETRY OF THE CIRAZOLINE HYDROCHLORIDE-SDDS INTERACTION

The interaction between cirazoline, ($CIRH^+$), and dodecylsulphate, (DDS^-), ions in aqueous solution may be represented by equation 6.4.

$$K_s' = [CIRH^+_{(aq)}]^n.[DDS^-_{(aq)}]^P \qquad (6.4)$$

Where K_s' is the apparant stoichiometric solubility product, [] are concentrations and n and p are the stoichiometric amounts of cirazoline and dodecylsulphate ions respectively. Rearrangement of equation 6.4 yields equation 6.5.

$$\log_{10} [DDS^-_{(aq)}] = \frac{1}{p} \log_{10} K_s' - \frac{n}{p} \log_{10} [CIRH^+_{(aq)}] \qquad (6.5)$$

The stoichiometry of the interaction (n:p) can thus be obtained from the slope of a plot of $\log_{10} [DDS^-_{(aq)}]$ against $\log_{10} [CIRH^+_{(aq)}]$ at the complexation end-point.

The stoichiometry of the solid and liquid complexes was determined by titrating 0.01 M SDDS into solutions of cirazoline hydrochloride at 30°C and 50°C respectively. All titrations were performed using a flow rate of 20.38 or 50.48 $\mu l\ min^{-1}$ and chart speed of 12 $cm\ hr^{-1}$. Table 6.6 shows the concentrations of cirazoline, $[CIRH^+_{(aq)}]_{ep}$, and dodecylsulphate, $[DDS^-_{(aq)}]_{ep}$, ions at the complexation end-point for each initial cirazoline hydrochloride concentration, $[CIRHCl]_I$, and temperature. Data plotted according to equation 6.5 are shown in

$[CIRHCl]_I$ ($Mx10^4$)	COMPLEXATION END-POINT ($Mx10^4$)		K_s' ($Moles^2\ litre^{-2}$ $x10^7$)
	$[CIRH^+(aq)]_{ep}$	$[DDS^-(aq)]_{ep}$	
Solid Complex (30°C)			
7.5	7.382	1.581	1.17
10.0	9.883	1.174	1.16
15.0	14.88	0.7759	1.16
20.0	19.88	0.5857	1.17
Liquid Complex (50°C)			
7.5	7.061	5.855	4.13
10.0	9.553	4.468	4.27
15.0	14.56	2.944	4.29
20.0	19.57	2.164	4.23

Table 6.6 - Conductimetric titration data for the interaction between cirazoline hydrochloride and SDDS at 30°C and 50°C. ($[CIRHCl]_I$ = initial cirazoline hydrochloride concentration, $[CIRH^+(aq)]_{ep}$ and $[DDS^-(aq)]_{ep}$ = cirazoline hydrochloride and SDDS concentrations at titration end-point respectively, K_s' = apparant solubility product calculated using a stoichiometry of 1 : 1).

figure 6.15. The slope of each curve was determined by linear regression analysis and the stoichiometry of the CIRH -DDS solid (30°C) and liquid (50°C) complexes was calculated as 1 : 1.004 (S.D. 1 : 0.007) and 1 : 0.978 (S.D. 1 : 0.020) respectively. The apparant solubility product, K_s', calculated using a stoichiometry of 1 : 1 is given for each titration in table 6.6.

Equation 6.4 indicates that a plot of $[DDS^-_{(aq)}]_{ep}$ against $[CIRH^+_{(aq)}]_{ep}^{-1}$ is linear with a slope of K_s' for interactions with a 1 : 1 stoichiometry. Such plots were constructed for solid (30°C) and liquid (50°C) data and are shown in figure 6.16. Linear dependence was observed for both sets of data and linear regression analysis data gave $K_s' = 1.17 \times 10^{-7}$ (S.D. 0.01×10^{-7}) moles^2 litre^{-2} for the solid complex at 30°C and $K_s' = 4.08 \times 10^{-7}$ (S.D. 0.10×10^{-7}) moles^2 litre^{-2} for the liquid complex at 50°C.

Intrinsic solubility product values, (K_s), were calculated using equation 1.70 and the Debye-Hückel equation, (equation 1.16). Values of the Debye-Hückel constant, (A), at 30°C and 50°C were obtained from standard literature tables[11], the product a_iB was taken as unity and ionic strength was calculated from the concentrations of cirazoline hydrochloride and SDDS at the titration end-point. The intrinsic solubility product for the solid complex at 30°C and liquid complex at 50°C were thus calculated as 1.09×10^{-7} and 3.88×10^{-7} moles^2 litre^{-2} respectively.

6.3.2.4 EFFECT OF TEMPERATURE

The effect of temperature on the cirazoline dodecylsulphate solubility product was studied by titrating 0.01 M SDDS into 1×10^{-3} M cirazoline hydrochloride at 10 - 50°C. Titration flow rates of 20.38 or

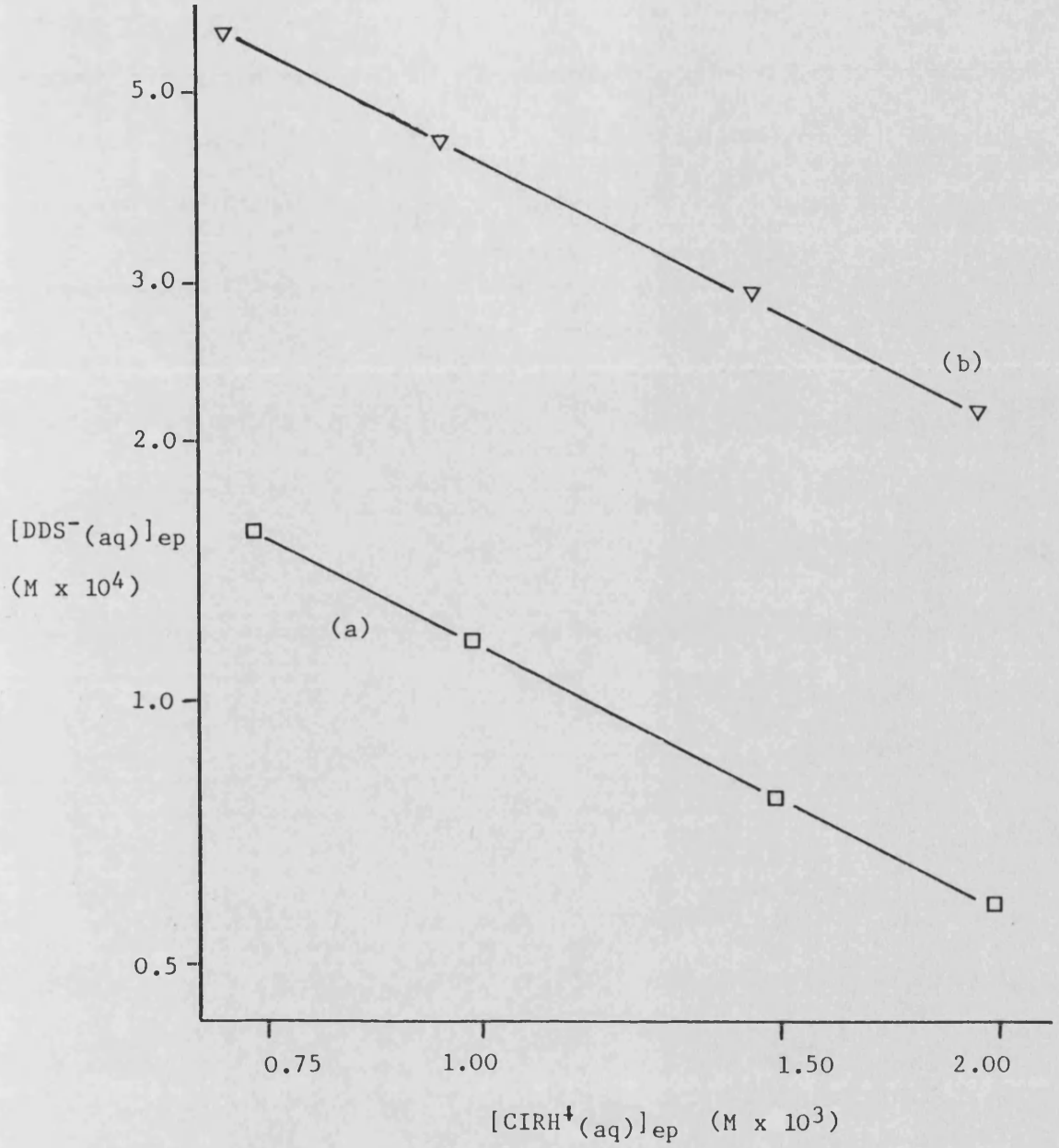

Figure 6.15 - Stoichiometry of the cirazoline-dodecylsulphate interaction (a) solid complex, 30°C, (—□—), (b) liquid complex, 50°C, (—▽—). Concentration of dodecylsulphate, $[DDS^-_{(aq)}]_{ep}$, and cirazoline, $[CIRH^+_{(aq)}]_{ep}$, ions at titration end point plotted according to equation 6.5.

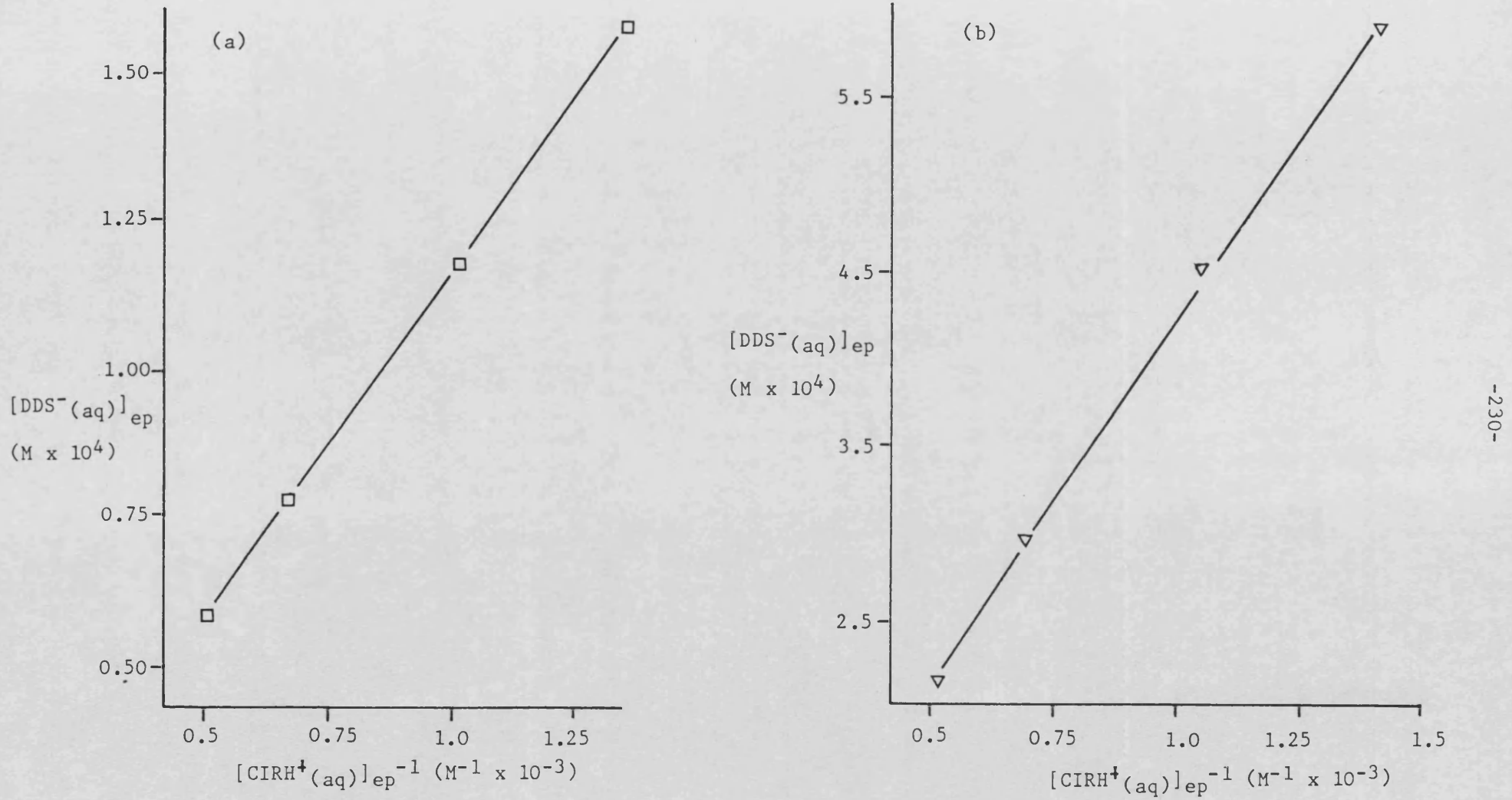

Figure 6.16 - Plot of dodecylsulphate concentration at titration end point, $[DDS^-(aq)]_{ep}$, against reciprocal cirazoline concentration at titration end point, $[CIRH^+(aq)]_{ep}^{-1}$, for (a) solid complex, 30°C and (b) liquid complex, 50°C.

173 $\mu l\ min^{-1}$ were used and conductivity traces were recorded at chart speeds of 12 cm hr^{-1} and 60 cm hr^{-1} respectively. Intrinsic solubility products were calculated from apparant solubility product values as described in section 6.3.2.3.

Apparent and intrinsic solubility products at each temperature are given in table 6.7. The nature of the formed complex at each temperature and titrant flow rate are also shown. At temperatures of 37.5°C and below, the nature of the formed complex and conductivity curve are dependent upon titration flow rate. Crystalline complex was formed at the slow flow rate (20.38 $\mu l\ min^{-1}$) and titration curves show the characteristic inflexions associated with sudden precipitation of solid complex. Titrations at the fast flow rate (173 $\mu l\ min^{-1}$) produced liquid complex and the inflexion in conductivity curves associated with phase separation was a simple change in gradient. These liquid complex systems were metastable and precipitated with time to form crystalline complex. Above 37.5°C, however, the solid complex did not form and only liquid complex was produced. The apparent solubility product, K_s', is plotted as a function of temperature in figure 6.17; both solid and liquid apparant solubility products increase with temperature in a curvilinear fashion.

Van't Hoff plots for the intrinsic solubility product - temperature data were linear (figure 6.18) for both solid and liquid complex systems; linear regression analysis data and thermodynamic parameters calculated using equations 1.76 to 1.78 are shown in table 6.8. These data indicate that solid complex formation is driven by a large negative enthalpy change, ΔH^o_f, but hindered by a negative entropy change, ΔS^o_f, reflecting the increased order in the solid phase. The

TEMPERATURE (°C)	SOLUBILITY PRODUCT (MOLES^2 LITRE^{-2} X10^8) K_s'	K_s	COMPLEX
(a) 20.38 x 10^{-3} mls min^{-1}			
9.90	2.02	1.88	Solid
15.00	3.13	2.91	"
20.10	5.23	4.87	"
25.05	7.51	6.99	"
30.15	11.5	10.7	"
35.20	18.1	16.9	"
37.60	21.7	20.2	"
37.60	25.6	23.8	Liquid
39.00	27.9	25.9	"
39.95	28.1	26.1	"
45.10	35.9	33.3	"
50.00	42.7	40.7	"
b) 173 x 10^{-3} mls min^{-1}			
20.00	14.1	13.1	Liquid
24.90	15.7	14.6	"
29.90	20.1	18.7	"
35.00	24.1	22.4	"
37.50	26.2	24.3	"

Table 6.7 - Effect of temperature on the cirazoline dodecylsulphate solubility product determined at a flow rate of (a) 20.38 µl min^{-1} and (b) 173 µl min^{-1}. (Initial cirazoline hydrochloride concentration = 1 x 10^{-3} M, titrant = 1 x 10^{-2} M SDDS).

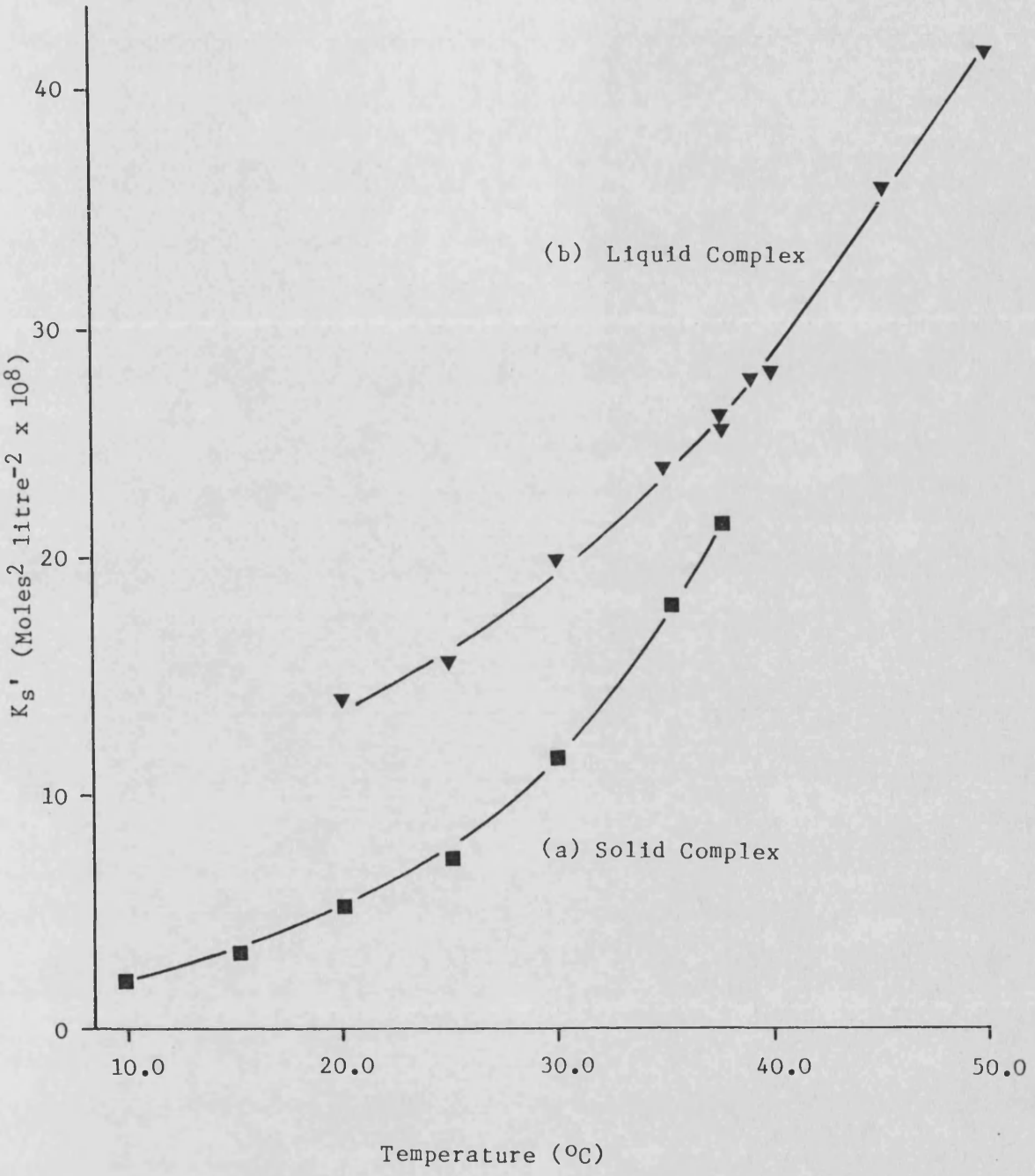

Figure 6.17 - Effect of temperature on the cirazoline-dodecylsulphate apparant solubility product, K_s', for (a) solid complex formation, (—■—), and (b) liquid complex formation, (—▼—).

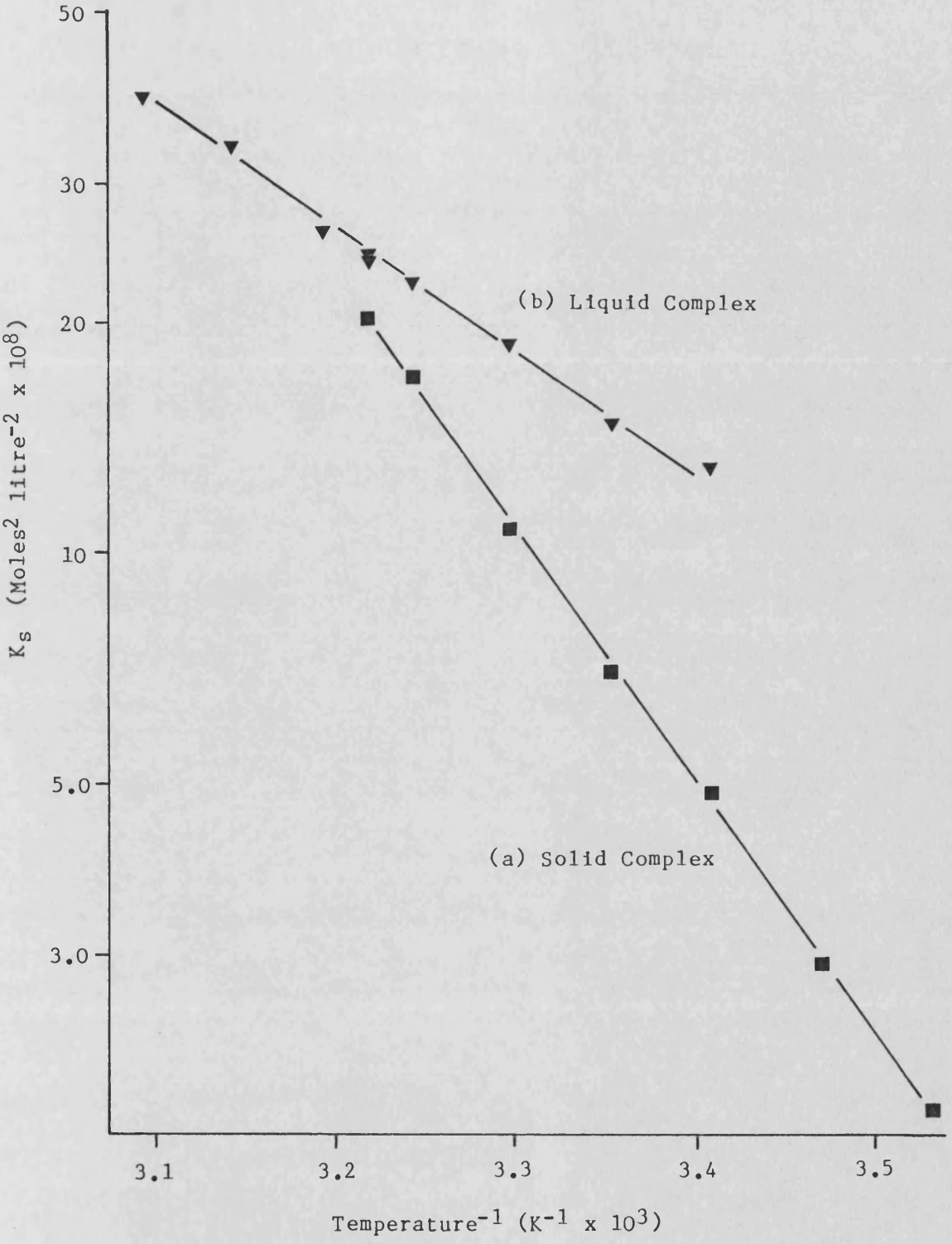

Figure 6.18 - Van't Hoff plots (intrinsic solubility product, K_s, on a $\log_{10}$ scale against reciprocal absolute temperature) for cirazoline-dodecylsulphate (a) solid complex formation (—■—) and (b) liquid complex formation (—▼—).

/

	SOLID COMPLEX	LIQUID COMPLEX
Correlation Coefficient	0.9996	0.9962
Slope (x 10^{-3})	-7.560	-3.515
S.D. of Slope (x 10^{-3})	0.100	0.109
R.S.D. of Slope	1.3%	3.1%
Intercept	8.908	-3.905
S.D. of Intercept	0.335	0.354
$\Delta G^{o}_{f,30^{o}C}(kJmol^{-1})$	-50.6	-49.1
$\Delta H^{o}_{f,30^{o}C}(kJmol^{-1})$	-62.9	-29.2
$\Delta S^{o}_{f,30^{o}C}(Jmol^{-1}k^{-1})$	-40.6	65.6

Table 6.8 - Linear regression analysis data for solid and liquid CIRH-DDS intrinsic solubility products plotted according to equation 1.76 and energetics of solid and metastable liquid complex formation at 30°C.

liquid phase separation process is driven by a combination of a negative enthalpy change and a positive entropy change.

Extrapolation of the solid complex curve to the liquid complex curve gives an intersection point at 42.5°C, K_s = 2.93 x 10^{-7} moles^{2}litre^{-2}.

6.3.2.5 EFFECT OF IONIC STRENGTH

The effect of ionic strength on the cirazoline-dodecylsulphate 'solid' solubility product was investigated at 30°C. 0.01 M SDDS was titrated at a flow rate of 20.38 µl min^{-1} into 1 x 10^{-3} M cirazoline hydrochloride solution in the presence of 1 x 10^{-4} - 1 x 10^{-3} M sodium chloride. Higher ionic strengths could not be studied successfully as the change in conductivity during the titration was too small relative to the high background conductivity. The 'solid' solubility product in the presence of 1 x 10^{-4} , 5 x 10^{-4} and 1 x 10^{-3} M sodium chloride was determined as 1.16 x 10^{-7} , 1.16 x 10^{-7} and 1.13 x 10^{-7} moles^{2}litre^{-2}. These results are similar to the solubility product in the absence of added sodium chloride (K_s' = 1.17 x 10^{-7} moles^{2}litre^{-2}) and show that low concentrations of electrolyte have minimal effect on the cirazoline dodecylsulphate solubility product.

6.3.2.6 EFFECT OF ALKYLSULPHATE CHAIN LENGTH

The effect of alkylsulphate chain length on the solubility product of cirazoline alkylsulphates was investigated at temperatures of 10°, 20°, 30° and 50°. Alkyl chain lengths of C_8 (cirazoline octylsulphate, CIRH-OS), C_{10} (cirazoline decylsulphate, CIRH-DS), C_{12} (cirazoline dodecylsulphate, CIRH-DDS) and C_{14} (cirazoline tetradecylsulphate, CIRH-TDS) were assessed.

(a) CIRH-OS

0.1 M sodium octylsulphate (SOS) was titrated at a flow rate of 20.38 or 50.48 $\mu l\ min^{-1}$ into 0.01 M cirazoline hydrochloride (10^{o} - $30^{o}C$) and 0.025 M cirazoline hydrochloride (30^{o} and $50^{o}C$). The higher cirazoline hydrochloride concentration was necessary because of the large solubility products observed at higher temperatures. Liquid complex was formed at all temperatures.

(b) CIRH-DS

0.05 M sodium decylsulphate was titrated at a flow rate of 12.39, 20.38 or 50.48 $\mu l\ min^{-1}$ into 2.5×10^{-3} M cirazoline hydrochloride. The (stable) complex form was liquid at $30^{o}C$ and $50^{o}C$ and solid at $10^{o}C$ and $20^{o}C$. Metastable liquid complexes could also be formed at the lower temperatures. The stoichiometry of the liquid complex at $30^{o}C$ was determined using 0.05 M SDS as titrant and initial cirazoline hydrochloride concentrations of 2.5×10^{-3}, 3.75×10^{-3} and 5×10^{-3} M. Data plotted according to equations 6.4 and 6.5 gave a stoichiometry of 1 : 1.02 (S.D. 1 : 0.18) and a mean K_s' value of 2.05×10^{-6} (S.D. 0.41×10^{-6}) $moles^2\ litre^{-2}$.

(c) CIRH-DDS

Data were taken from table 6.7.

(d) CIRH-TDS

Initial cirazoline hydrochloride concentrations of 5×10^{-5} - 5×10^{-4} M were used. STDS concentrations of 5×10^{-4} - 5×10^{-3} M were employed at flow rates of 12.39 or 20.38 $\mu l\ min^{-1}$. (Stable) liquid complex was formed at $50^{o}C$ and solid complex was produced at all lower temperatures. Metastable liquid complex could be

formed by fast titration (e.g. 50.48 $\mu l\ min^{-1}$) at the lower temperatures, however. A reliable estimate of the solid solubility product at 10°C could not be obtained; solid phase separation occurred but extrapolation of conductivity curves to determine the solubility product was difficult. This is probably due to the very low solubility product at this temperature and the slow rate of initial crystal nucleation. The stoichiometry of the solid CIRH-TDS complex was studied at 30°C using 5×10^{-3} M STDS and initial cirazoline hydrochloride concentrations 2.0, 3.0, 4.0 and 5.0×10^{-4} M. Data plotted according to equations 6.4 and 6.5 gave a stoichiometry of 1 : 0.93 (S.D. 1 : 0.03) and mean K_s' of 3.65×10^{-9} (S.D. 0.09×10^{-9}) $moles^2\ litre^{-2}$.

Intrinsic and apparant solubility products for CIRH-OS, CIRH-DS and CIRH-TDS systems at each temperature studied are shown in table 6.9. Titration conditions employed and nature of formed complex are also shown. Van't Hoff plots ($\log_{10} K_s$ versus K^{-1}) were constructed from these data and are shown in figure 6.19. In contrast to the behaviour of CIRH-DDS, the liquid K_s versus K^{-1} plots were non-linear. The temperature of transition from solid/metastable liquid systems to stable liquid complex systems is shifted to lower temperatures with a decrease in alkylchain length. Solid complex is observed at 30°C and below in the CIRH-TDS system, at 10°C and 20°C in the CIRH-DS system, and no CIRH-OS solid complex was observed in the temperature range studied. (Solid CIRH-DDS complex was formed at temperatures of 37.5°C and below, see section 6.3.2.4). The CIRH-DS solid complex is anomolous as it appears to be more stable than the liquid complex species; however, this is unlikely to be so and these results may be due to the close proximity of the solid and liquid end-points.

SYSTEM	TEMPERATURE (°C)	$[CIRHCl]_I$ (M)	[TITRANT] (M)	FLOW RATE ($\mu l\ min^{-1} \times 10^3$)	SOLUBILITY PRODUCT (Moles^2 litre^{-2}) K_s'	K_s	COMPLEX
CIRH-OS	10.00	0.01	0.1	50.48	3.87×10^{-5}	3.14×10^{-5}	Liquid
	20.10	0.01	0.1	50.48	4.42×10^{-5}	3.57×10^{-5}	Liquid
	30.00	0.01	0.1	20.38	5.00×10^{-5}	4.03×10^{-5}	Liquid
		0.025	0.1	20.38	6.28×10^{-5}	4.54×10^{-5}	Liquid
	50.00	0.025	0.1	20.38	10.2×10^{-5}	7.28×10^{-5}	Liquid
CIRH-DS	10.00	2.5×10^{-3}	0.05	20.38	1.62×10^{-6}	1.45×10^{-6}	Liquid
					1.70×10^{-6}	1.52×10^{-6}	Solid
	20.00	2.5×10^{-3}	0.05	12.39	1.89×10^{-6}	1.69×10^{-6}	Liquid
					2.12×10^{-6}	1.90×10^{-6}	Solid
	30.10*	$2.5\text{-}5\times10^{-3}$	0.05	20.38	2.05×10^{-6}	1.83×10^{-6}	Liquid
	50.00	2.5×10^{-3}	0.05	50.48	3.73×10^{-6}	3.32×10^{-6}	Liquid
CIRH-TDS	10.00	5×10^{-5}	5×10^{-4}	50.48	4.92×10^{-9}	4.84×10^{-9}	Liquid
	20.00	2×10^{-4}	1×10^{-3}	12.39	1.08×10^{-9}	1.05×10^{-9}	Solid
	30.00*	$2\text{-}5\times10^{-4}$	5×10^{-3}	20.38	3.65×10^{-9}	3.45×10^{-9}	Solid
		5×10^{-4}	5×10^{-3}	20.38	1.03×10^{-8}	9.78×10^{-9}	Liquid
	50.00	5×10^{-4}	5×10^{-3}	20.38	2.81×10^{-8}	2.66×10^{-8}	Liquid

Table 6.9 - The effect of temperature on cirazoline octylsulphate (CIRH-OS), cirazoline decylsulphate (CIRH-DS) and cirazoline tetradecylsulphate (CIRH-TDS) complex formation and apparant (K_s') and intrinsic (K_s) solubility products determined by conductimetric titration using initial cirazoline hydrochloride concentrations, $[CIRHCl]_I$, sodium alkylsulphate titrant concentrations, [titrant], and flow rates indicated. (* = data from stoichiometry determination).

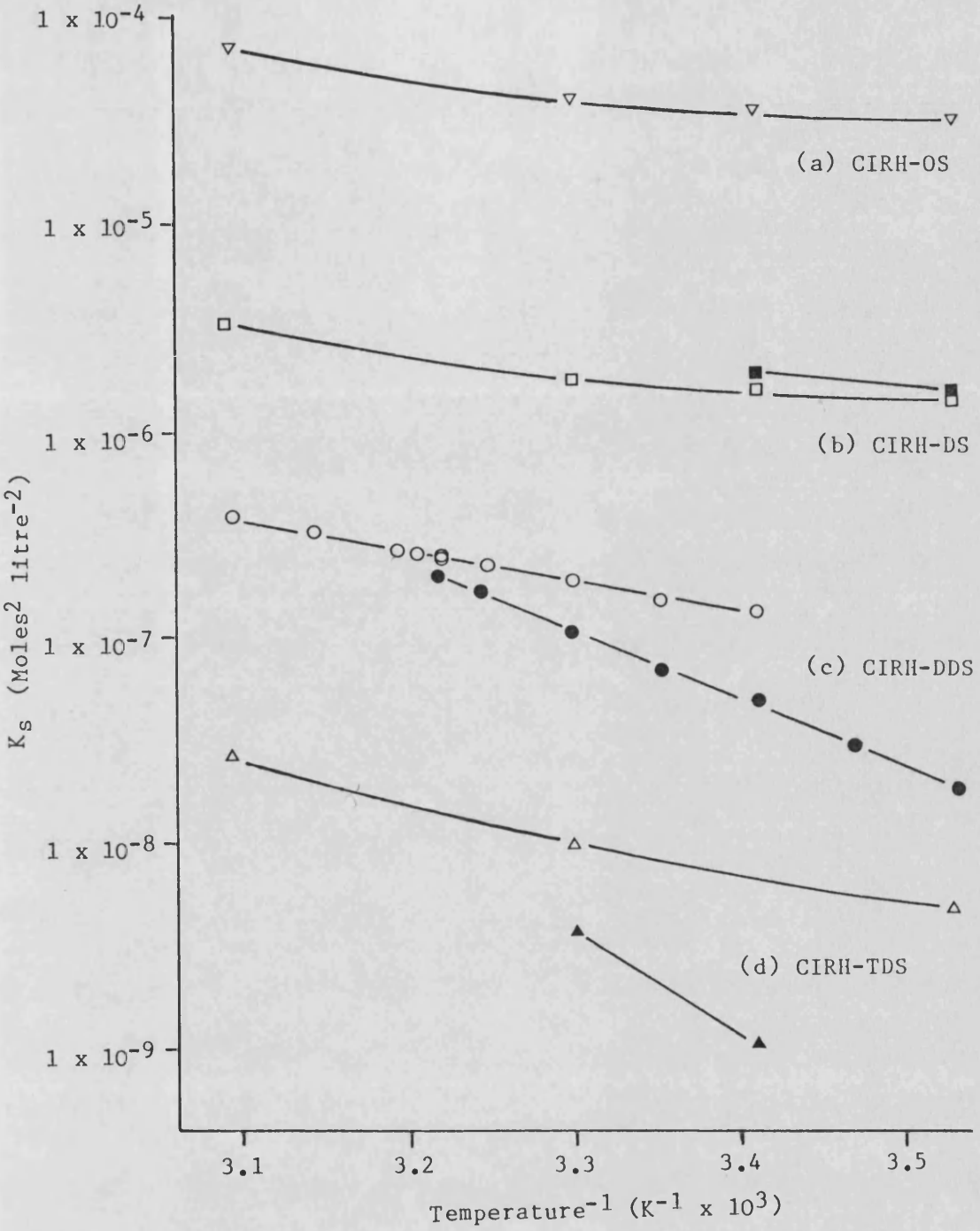

Figure 6.19 - Van't Hoff plots (intrinsic solubility product, K_s, on a $\log_{10}$ scale against reciprocal absolute temperature) for (a) cirazoline-octylsulphate, CIRH-OS, (—▽—), (b) cirazoline-decylsulphate, CIRH-DS, (—□—), (c) cirazoline-dodecylsulphate, CIRH-DDS, (—○—), (d) cirazoline-tetradecylsulphate, CIRH-TDS, (—△—). Solid symbols = solid complex, open symbols = liquid complex.

Alkyl chain length has a profound effect on aqueous solubility due to the hydrophobic nature of the methylene group. The standard free energy change upon complex formation, ΔG^{o}_{f}, is given by equation 1.78. Hence the contribution of each methylene group to the overall free energy change, $d(\Delta G^{o}_{f})/_{dn}$ may be obtained from a plot of $\log_{10} K_s$ against the number of methylene groups, n (equation 6.6).

$$\frac{d(\Delta G^{o}_{f})}{dn} = RT \frac{d \log_{10} K_s}{dn} \qquad (6.6)$$

Where R is the gas constant and T is absolute temperature. Figures 6.20 and 6.21 show the effect of number of methylene groups in the alkylchain on the cirazoline alkylsulphate solid and liquid intrinsic solubility product at each temperature studied. The liquid complex data and the limited solid complex data indicate a linear relationship between $\log_{10} K_s$ and n as predicted from equation 1.79. Linear regression analysis results for these data are shown in table 6.10. The free energy contribution per methylene group to the complexation process, $d(\Delta G^{o}_{f})/_{dn}$, was calculated from the slopes of these plots and equation 6.6 and is shown for each temperature and complex type in table 6.11. $d(\Delta G^{o}_{f})/_{dn}$ for the liquid complex formation was independent of temperature and calculated as -3.46 (S.D. 0.04) kJ mol^{-1}. $d(\Delta G^{o}_{f})/_{dn}$ for solid complex formation was greater than for liquid complex formation and was dependent upon temperature; at 10°, 20°, and 30°C $d(\Delta G^{o}_{f})/_{dn}$ was calculated as -5.17, -4.57 (S.D. = 0.06) and -4.44 kJ mol^{-1} respectively.

6.3.2.7 EFFECT OF IMIDAZOLINE STRUCTURE

The effect of imidazoline structure on complex formation and solubility product in imidazoline-DDS systems was investigated at 30°C. Antazoline dodecylsulphate (ANTH-DDS), xylometazoline

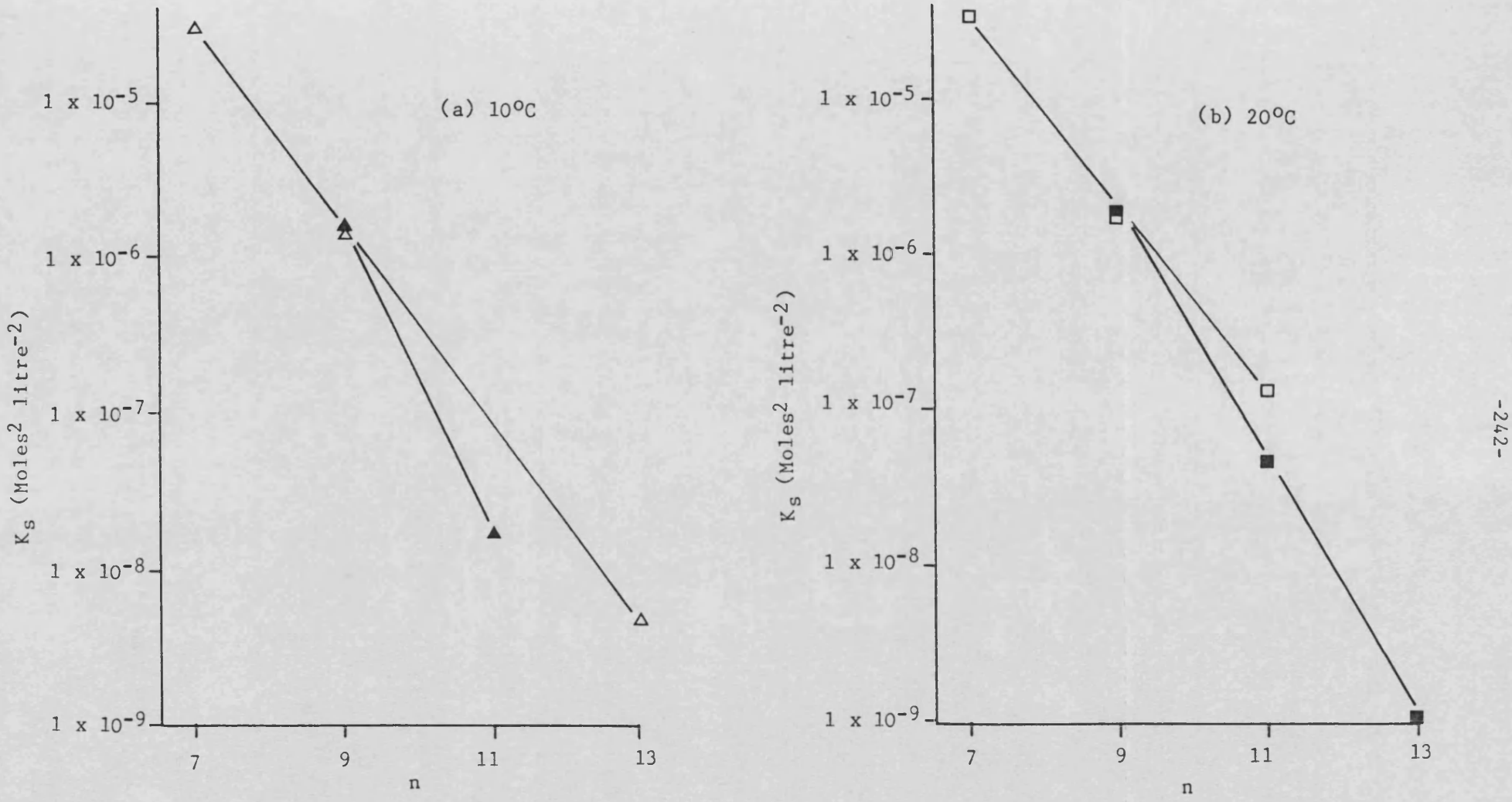

Figure 6.20 - Effect of number of methylene groups in the alkylchain, n, on the cirazoline-alkylsulphate intrinsic solubility product, K_s; (a) 10°C (—△—), (b) 20°C (—□—); open symbols = liquid complex, closed symbols = solid complex.

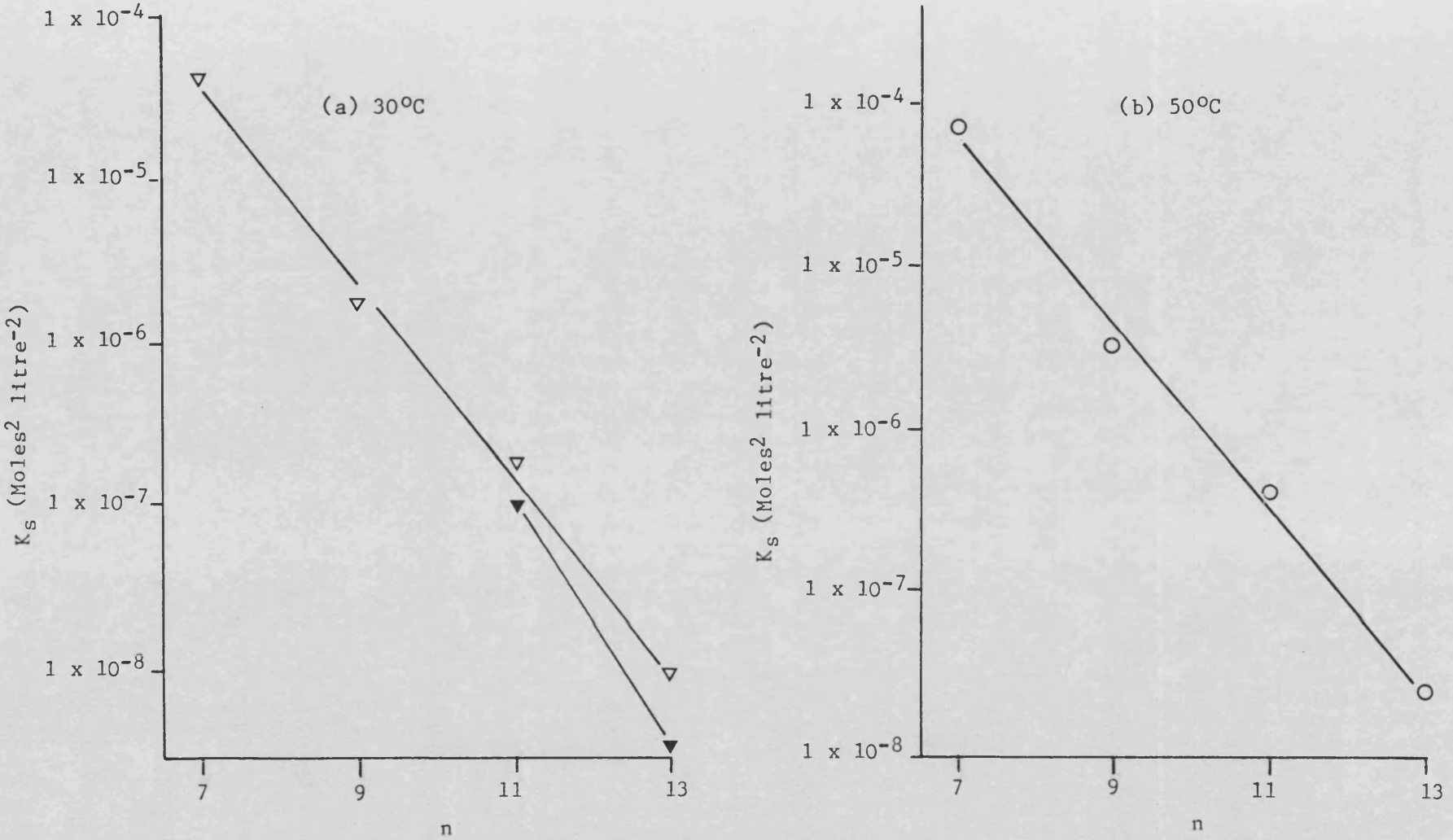

Figure 6.21 - Effect of number of methylene groups in the alkylchain, n, on the cirazoline-alkylsulphate intrinsic solubility product, K_s; (a) 30°C (—▽—), (b) 50°C (—○—); open symbols = liquid complex, closed symbols = solid complex.

COMPLEX	TEMPERATURE (°C) 10.0 LIQUID	20.0 SOLID	20.0 LIQUID	30.0 LIQUID	50.0 LIQUID
r	0.9998	0.9999	0.9987	0.9986	0.9978
Slope	-1.458	-1.875	-1.402	-1.383	-1.295
S.D. Slope	0.028	0.025	0.071	0.042	0.061
R.S.D. Slope	1.9%	1.3%	5.1%	3.0%	4.7%
Intercept	-0.2295	3.732	0.5091	0.4531	0.6418
S.D. Intercept	0.2767	0.277	0.6511	0.4040	0.6280

Table 6.10 - Linear regression analysis data for liquid and solid cirazoline alkylsulphate complex intrinsic solubility product data plotted according to equation 1.79, ($\log_e K_s$ versus n).

TEMPERATURE (°C)	$d(\Delta G^o_f)/dn$ (S.D.) $kJmol^{-1}$ SOLID	LIQUID
10.0	-5.17	-3.43 (0.07)
20.0	-4.57 (0.06)	-3.42 (0.17)
30.0	-4.44	-3.49 (0.11)
50.0	-	-3.48 (0.16)

Table 6.11 - Methylene group contribution to the free energy of cirazoline alkylsulphate complexation, $d(\Delta G^o_f)/dn$, for solid and liquid complexes at each temperature.

dodecylsulphate (XYLH-DDS), naphazoline dodecylsulphate (NAPH-DDS) and tolazoline dodecylsulphate (TOLH-DDS) were studied by titrating SDDS into imidazoline solutions at a flow rate of 12.39 or 20.38 $\mu l\ min^{-1}$. The stoichiometry and mean K_s' values of imidazoline DDS complexes were determined for all systems (except TOLH-DDS) using the method described for CIRH-DDS complex (section 6.3.2.3). Apparant and intrinsic solubility product, stoichiometry of interaction and nature of complex for each system are shown in table 6.12.

(a) ANTH-DDS

Solid complex was produced by all titrations and conductivity curves displayed the characteristic inflexions associated with sudden crystallization (see section 6.3.2.2). Accurate determination of ANTH-DDS solubility products could not be made, however as the degree of supersaturation was large (see section 6.3.2.2) and the formed complex was highly flocculated and adsorbed onto the titrant delivery tube, blocking the orifice.

(b) NAPH-DDS

Stable liquid complexes were formed and the inflexion in the conductivity curves was a simple change of gradient (see figure 6.12).

(c) XYLH-DDS

Both metastable liquid, and stable solid XYLH-DDS complexes were formed by titrating 0.01 M SDDS at a flow rate of 12.4 $\mu l\ min^{-1}$ into xylometazoline hydrochloride solutions. An initial liquid phase separation occurred followed by precipiation of crystalline complex. Solid and liquid solubility products were similar under these conditions and titration at a flow rate of 20.38 $\mu l\ min^{-1}$ was

$[IMIDAZOLINE]_I$ ($Mx10^4$)	[TITRANT] ($Mx10^3$)	FLOW RATE ($\mu l\ min^{-1}$)	NUMBER OF DETERMINATIONS	MEAN K_s' $Moles^2 litre^{-2}$ (S.D.$x10^8$)	(IMID:DDS) STOICHIOMETRY (S.D.)	COMPLEX
ANTH-DDS						
3.5-10.0	5.0-10.0	12.39,20.38	5	1.24(0.43)	1:0.94(0.22)	Solid
NAPH-DDS						
10.0-20.0	10.0	20.38	3	30.1(2.5)	1:0.97(0.10)	Liquid
XYLH-DDS						
5.0-20.0	10.0	12.39,20.38	5	9.19 (0.27)	1:1.03(0.03)	Liquid
7.5-20.0	10.0	12.39	4	8.86 (0.26)	1:0.99(0.03)	Solid
TOLH-DDS						
20.0	200	20.38	1	253	-	Liquid

Table 6.12 - Mean apparant solubility product (K_s'), stoichiometry and nature of formed complex for antazoline dodecylsulphate (ANTH-DDS), naphazoline dodecylsulphate (NAPH-DDS), xylometazoline dodecylsulphate (XYLH-DDS) and tolazoline dodecylsulphate (TOLH-DDS) systems determined by conductimetric titration using initial imidazoline concentration, $[Imidazoline]_I$, SDDS titrant concentration, [titrant], and flow rates indicated, 30°C.

sufficiently fast to prevent accurate measurement of the solid solubility product.

(d) TOLH-DDS

A single determination of the TOLH-DDS solubility product was made and resulted in the formation of stable liquid complex.

6.3.2.8 CPAE DODECYLSULPHATE SOLUBILITY PRODUCT

The apparant CPAE dodecylsulphate solubility product, K_s', at 30°C was determined in order to investigate the effect of CPAE formation on the structure of cirazoline hydrochloride-SDDS systems (see section 8.3.6). 0.01 M SDDS was titrated into 1 x 10^{-3} M CPAE solution at a flow rate of 20.38 µl min^{-1}. A stable liquid complex was formed and the solubility product was calculated as 2.43 x 10^{-7} $moles^2$ $litre^{-2}$. This is slightly greater than the liquid cirazoline dodecylsulphate solubility product, (K_s' = 2.01 x 10^{-7} $moles^2$ $litre^{-2}$ at 30°C), reflecting the more polar CPAE structure (figure 1.2).

6.3.3 Determination of Cirazoline dodecylsulphate and CPAE dodecylsulphate Ion-pair Association Constants

The cirazoline-dodecylsulphate and CPAE dodecylsulphate ion-pair association constants, K_{ip}, were determined at 30°C by the method described by Mukhayer and Davis[121] (see section 1.4.2.1). The latter was determined in order to investigate the effect of CPAE formation on the structure of cirazoline hydrochloride-SDDS systems (see section 8.3.6).

0.01 M SDDS was titrated at a flow rate of 20.38 µl min^{-1} into (a) double distilled water, (b) 1 x 10^{-3} M cirazoline hydrochloride and (c) 1 x 10^{-3} M CPAE hydrochloride. The chart conductivity range was

set at (a) 0 - 10 x 10^{-6} S, (b) 70 - 80 x 10^{-6} S and (c) 80 - 90 x 10^{-6} S. A chart speed of 60 cm hr^{-1} was used for all titrations.

The conductivity of eleven different concentrations of SDDS was measured from the blank titration curve (titration a). Specific K_{SDDS}, and equivalent Λ_{SDDS}, conductivities of these solutions were calculated using equation 1.43 and 1.44 respectively. Specific conductivities of the cirazoline hydrochloride-SDDS (titration b) and CPAE hydrochloride-SDDS (titration c) mixtures, K'_{mix}, at similar SDDS concentrations were then calculated using equation 1.43. The difference in specific conductivity due to interactions within the mixtures, ΔK_{mix}, the concentration of formed ion-pair, [CIRH-$DDS_{(aq)}$], and the ion-pair association constant, K_{ip}, were then calculated for each SDDS concentration using equations 1.63, 1.61 and 1.56. The equivalent conductivities of cirazoline hydrochloride, Λ_{CIR}, and CPAE hydrochloride, Λ_{CPAE}, at 30°C were calculated from the conductivity of the initial solutions. These values were assumed to be constant during the titrations since the increase in volume due to titrant addition was very small. The limiting ionic conductivities of sodium, $\lambda^{o}_{Na^+}$, and chloride, $\lambda^{o}_{Cl^-}$, ions were taken as 55.80 and 84.30 S eq^{-1} cm^2 respectively[11].

Table 6.13 shows the calculated cirazoline dodecylsulphate and CPAE dodecylsulphate ion-pair association constant at each SDDS concentration. K_{SDDS}, Λ_{SDDS}, K_{mix} and ΔK_{mix} values are also shown. Results indicate a mean ion-pair association constant of 232 (S.D. 20) for cirazoline dodecylsulphate and 248 (S.D. 9) for CPAE dodecylsulphate.

[SDDS] M($\times 10^5$)	Λ_{SDDS} S $eq^{-1}cm^2$	K_{SDDS} S cm^{-1}($\times 10^6$)	CIRH-DDS K_{mix}	ΔK_{mix}	K_{ip}	CPAE-DDS K_{mix}	ΔK_{mix}	K_{ip}
-	-	-	102.07	-	-	118.32	-	-
4.05	78.0	3.16	104.94	0.29	211	121.02	0.46	256
4.85	77.9	3.78	105.52	0.33	200	121.58	0.52	239
5.66	77.6	4.39	106.08	0.38	200	122.11	0.60	238
6.46	78.0	5.04	106.64	0.47	219	122.64	0.72	251
7.26	78.4	5.69	107.20	0.56	234	123.18	0.83	258
8.06	78.7	6.34	107.75	0.66	251	123.73	0.93	259
8.86	78.9	6.98	108.34	0.71	244	124.28	1.02	258
9.66	78.8	7.61	108.91	0.77	244	124.87	1.06	244
10.5	78.4	8.23	109.47	0.83	245	125.44	1.11	235
11.3	78.6	8.88	110.03	0.92	253	125.96	1.24	245
12.0	79.3	9.51	110.60	0.98	249	126.51	1.32	243

Table 6.13 - Cirazoline dodecylsulphate, CIRH-DDS, and CPAE dodecylsulphate, CPAEH-DDS, ion-pair association constants, K_{ip}, at 30°C. SDDS specific conducitivity, K_{SDDS}, SDDS equivalent conductivity, Λ_{SDDS}, specific conductivity of each mixture, K_{mix}, and difference in specific conductivity due to interaction of each mixture ΔK_{mix}, are also shown.

7. AGGREGATION IN CIRAZOLINE-DODECYLSULPHATE SYSTEMS

7.1 MICELLIZATION AND SOLUBILIZATION

7.1.1 Introduction

Formation of micelles above the CMC of cirazoline hydrochloride-SDDS systems allows interaction between cirazoline and micellar SDDS. The system may be characterised by the following parameters:

(i) its apparent CMC (CMC'); this is expressed in terms of the total SDDS concentration present in the system at its point of determination,

(ii) the true CMC (=$[DDS^-_{(aq)}]$); this is the concentration of free SDDS monomers present in the aqueous phase at the point of determination,

(iii) the solubilizing concentration of surfactant (SOL_T); this is the total SDDS concentration necessary to effect total solubilization of formed complex in a given system,

(iv) the association constant (K_A) for the interaction between cirazoline and SDDS micelles.

The interaction between cirazoline and SDDS micelles may be viewed in terms of:

(a) solubilization of the sparingly soluble neutral cirazoline dodecylsulphate ion-pair, (CIRH-DDS), due to partition into the micellar pseudophase which is characterised by the partition constant, K_p (equation 7.1):

$$\text{CIRH-DDS}_{(aq)} \overset{K_p}{\rightleftharpoons} \text{CIRH-DDS}_{(M)} \qquad (7.1)$$

$$K_p = \frac{[\text{CIRH-DDS}_{(M)}]}{[\text{CIRH-DDS}_{(aq)}]}$$

Where the subscripts $_{(aq)}$ and $_{(M)}$ refer to aqueous and micellar forms respectively.

(b) Mass action type binding of the cirazoline ion, $CIRH^{+}_{(aq)}$ to the negatively charged dodecylsulphate micelles, $DDS^{-}_{(M)}$, to form the electrically neutral cirazoline dodecylsulphate micellar species, $\text{CIRH-DDS}_{(M)}$; characterised by the association constant, K_A, (equation 7.2):

$$CIRH^{+}_{(aq)} + DDS^{-}_{(M)} \overset{K_A}{\rightleftharpoons} \text{CIRH-DDS}_{(M)}$$

$$K_A = \frac{[\text{CIRH-DDS}_{(M)}]}{[CIRH^{+}_{(aq)}][DDS^{-}_{(M)}]} \qquad (7.2)$$

The data treatment adopted in this thesis is based on the mass action binding model described by Sepulveda and Co-Workers[90, 139-141]. The association constant, K_A, may be obtained from a knowledge of $[\text{CIRH-DDS}_{(M)}]$, $[CIRH^{+}_{(aq)}]$ and $[DDS^{-}_{(M)}]$, (equation 7.2). For a saturated system, these parameters may be calculated from the CMC', SOL_T and the solubility product for the complex, K_s', (see section 6). The total concentration of cirazoline hydrochloride, $[CIRHCl]^T$, and SDDS,

$[SDDS]^T$, in the system are given by equations 7.3 and 7.4 respectively:

$$[CIRHCl]^T=[CIRH^+_{(aq)}]+[CIRH\text{-}DDS_{(M)}]+[CIRH\text{-}DDS_{(c)}] \quad (7.3)$$

$$[SDDS]^T=[DDS^-_{(aq)}]+[CIRH\text{-}DDS_{(M)}]+[DDS^-_{(M)}]+[CIRH\text{-}DDS_{(c)}] \quad (7.4)$$

Where $[DDS^-_{(M)}]$ is the concentration of dodecylsulphate in the micellar form which is not bound to cirazoline, and $[CIRH\text{-}DDS_{(c)}]$ is the concentration of precipitated complex.

At or below the CMC' of the system, $[CIRH\text{-}DDS_{(M)}] = [DDS^-_{(M)}] = 0$ and equations 7.3 and 7.4 reduce to equations 7.5 and 7.6 respectively:

$$[CIRHCl]^T = [CIRH^+_{(aq)}] + [CIRH\text{-}DDS_{(c)}] \quad (7.5)$$

$$[SDDS]^T = [DDS^-_{(aq)}] + [CIRH\text{-}DDS_{(c)}] \quad (7.6)$$

At the CMC' of the system, equation 7.6 may be written as:

$$CMC' = CMC + [CIRH\text{-}DDS_{(c)}] \quad (7.7)$$

The true CMC of the system and $[CIRH^+_{(aq)}]$ at the CMC' may then be calculated from a knowledge of K_s', (equations 7.8 and 7.9):

$$K_s' = [CIRH^+_{(aq)}].\ CMC \quad (7.8)$$

$$\text{or, } K_s' = ([CIRHCl]^T-[CIRH\text{-}DDS_{(c)}])(CMC'-[CIRH\text{-}DDS_{(c)}]) \quad (7.9)$$

At the total solubilization point, SOL_T, $[CIRH\text{-}DDS_{(c)}] = 0$ and equations 7.3 and 7.4 respectively reduce to equations 7.10 and 7.11 or 7.12:

$$[CIRH\text{-}DDS_{(M)}] = [CIRHCl]^T - [CIRH^+_{(aq)}] \quad (7.10)$$

$$[DDS^-_{(M)}] = [SDDS]^T - [DDS^-_{(aq)}] - [CIRH\text{-}DDS_{(M)}] \quad (7.11)$$

$$\text{or, } [DDS^-_{(M)}] = SOL_T - CMC - [CIRH\text{-}DDS_{(M)}] \quad (7.12)$$

Since the interaction being considered is between $CIRH^{+}_{(aq)}$ and $DDS^{-}_{(aq)}$ to form $CIRH\text{-}DDS_{(M)}$, $CIRH\text{-}DDS_{(c)}$ and $CIRH\text{-}DDS_{(aq)}$ do not interact directly with DDS^{-} micelles, but provide a reservoir for $CIRH^{+}_{(aq)}$ as it reacts with micelles then $CIRH^{+}_{(aq)}$, $CIRH\text{-}DDS_{(aq)}$ and CMC remain constant as $[SDDS]^{T}$ goes from CMC' to SOL_T and $CIRH\text{-}DDS_{(M)}$ results only from $CIRH\text{-}DDS_{(c)}$. Consequently if the volumes of the system at the CMC' and SOL_T are identical then:

$[CIRH\text{-}DDS_{(c)}]$ at the CMC' = $[CIRH\text{-}DDS_{(M)}]$ at the SOL_T, and equation 7.12 can be directly substituted in equation 7.7 to give equation 7.13:

$$[DDS^{-}_{(M)}] = SOL_T - CMC' \qquad (7.13)$$

Substitution of equations 7.8, 7.10 and 7.13 into equation 7.2 yields equation 7.14 from which K_A may be calculated.

$$K_A = \frac{([CIRHCl]^{T} - (K_s'/CMC))}{(SOL_T - CMC')} \cdot \frac{1}{(K_s'/CMC)} \qquad (7.14)$$

When the volume of the system is not constant, e.g. during a conductimetric titration, then equation 7.13 is not strictly valid and the volume change of the system between the CMC' and SOL_T must be considered.

7.1.2 Experimental

The SDDS concentration at the CMC', total solubilization concentration, SOL_T, and the cirazoline micelle-water association constant, K_A, were determined from solubility and conductometric titration studies.

7.1.2.1 SOLUBILITY STUDIES

The solubility of cirazoline hydrochloride at different ionic strengths in the presence of SDDS was determined by the following method.

Systems containing the required concentrations of cirazoline hydrochloride, SDDS and sodium chloride was prepared by mixing concentrated stock solutions and diluting to 25 mls. One ml of 0.01 M HCl (final concentration 4 x 10^{-4} M) was included in the formulation to inhibit cirazoline hydrolysis. A typical formulation for cirazoline hydrochloride (2 x 10^{-3} M)in the presence of SDDS (2.5 x 10^{-3} M) and sodium chloride (0.1 M) is given below.

Stock Solution (Concentration)	Volume (mls)	Final Concentration (M)
Cirazoline HCl (0.01 M)	5.0	2 x 10^{-3}
SDDS (0.01 M)	5.0	)
SDDS (6.25 x 10^{-3}M)	2.0	) 2.5 x 10^{-3}
Sodium Chloride (0.5 M)	5.0	0.1
HCl (0.01 M)	1.0	4 x 10^{-4}
Double distilled water to	25.0	

After making up to volume, the system was immediately shaken and transferred to a 3 dram glass vial. Polytetrafluoroethylene (PTFE) tape was wrapped around the screw thread of the vial and the top and screw thread covered with a layer of aluminium foil. The plastic top was screwed tightly on to the vial and sealed with a wrapping of autoclave tape. Vials were transferred to a constant temperature shaking water bath and shaken at a rate of 50 oscillations min^{-1}. The PTFE/aluminium foil acted as the primary barrier to moisture

ingression and the autoclave tape prevented the top from working loose as well as acting as a preliminary barrier to penetration. After equilibration the vials were sampled by filtering the system through Whatman 25 mm membrane filters (0.45 μm pore size) in Swinnex units. The first 5 mls of filtrate were run to waste and the second 5 mls collected in a 10 ml volumetric flask. 4 mls of this solution were immediately mixed with 1 ml of 0.1 M HCl and suitably diluted for assay. All filtration and sampling apparatus except the membrane filter were aged (as described for glassware, section 2) and warmed to approximately the experiment temperature prior to sampling.

(a) Effect of Filtering on Assay

Adsorption of cirazoline on to surfaces of the filtering apparatus may occur. To investigate the significance of any interaction, vials containing 5×10^{-3} M cirazoline hydrochloride, 1.2×10^{-2} M SDDS and 4×10^{-4} M HCl were equilibrated at 30°C for 24 hours. Under these conditions, cirazoline is totally solubilised and no solid phase is present. The vials were sampled directly and by the filtration technique. Assay results are shown in table 7.1 and indicate no significant difference between the filtered and unfiltered samples ($t_{calc} = 1.72$, $t_{tab} = 2.23$, $p = 0.05$).

(b) Determination of Equilibration Time

Six vials containing 5×10^{-3} M cirazoline hydrochloride, 9×10^{-3} M SDDS and 4×10^{-4} M HCl were held at 30°C in the shaking water bath. Under these conditions, cirazoline is partially solubilized and the system contains solid, aqueous and micellar phases. Samples were withdrawn at 24 hour intervals and assayed; results are shown in table 7.2 and indicate an equilibrium time of between 24 and 48 hours

VIAL	MEAN CIRAZOLINE CONCENTRATION (M X 10^3)	
	UNFILTERED	FILTERED
1	5.066	5.093
2	5.074	5.074
3	5.010	4.949
4	5.232	5.049
5	5.085	4.955
6	5.045	4.921
Mean	5.082	5.007
S.D.	0.077	0.074
Coefficient of variation	1.5%	1.5%

Table 7.1 - The effect of filtration on cirazoline assay. Vials contain 5 x 10^{-3} M cirazoline hydrochloride, 1.2 x 10^{-2} M SDDS and 5 x 10^{-4} M HCl.

VIAL	SAMPLE TIME (HRS)	MEAN CIRAZOLINE CONCENTRATION (M X 10^3)
1	0	2.281
2	24	2.022
3	48	1.974
4	72	1.923
5	96	2.094
6	120	1.959

Table 7.2 - Solubility equilbration time for 5 x 10^{-3} M cirazoline hydrochloride in the presence of 9 x 10^{-3} M SDDS and 4x 10^{-4} M HCl at 30°C and at a shaking rate of 50 oscillations per minute.

(vials 2 - 6, mean concentration = 1.99×10^{-3} M (CV = 3.3%)). In practice, samples were left to equilibrate for between 5 and 10 days. Degradation of cirazoline was not detected over this period.

(c) Calculation of CMC, SOL_T and K_A

The SDDS concentration at the CMC' and SOL_T can be obtained from inflexions in profiles of cirazoline solubility against SDDS concentration. Figures 7.13 and 7.14 (section 7.1.3.3) shows such profiles for 2×10^{-3} M and 5×10^{-3} M cirazoline hydrochloride - SDDS systems at 30°C. Equimolar concentration, CMC' and SOL_T points are indicated for each system. Below the CMC' of the system, the theoretical amount of cirazoline in solution may be predicted from K_S' values using the quadratic form of equations 7.5 and 7.9. Theoretical aqueous cirazoline solubility-SDDS concentration curves for each system were constructed using equation 1.70 and K_S values from table 6.7 and are shown as dashed lines in figures 7.13 and 7.14.

At SDDS concentrations below the equimolar concentration, i.e. when cirazoline is in excess, an increase in SDDS concentration causes a rapid decrease in the solubility of cirazoline due to hydrophobic complex formation, (figures 1.13 and 1.14). Above the equimolar concentration point the free SDDS concentration increases dramatically and micellization occurs at the CMC'. Cirazoline solubility increase in this region due to solubilization of the complex and the CMC' is given from the intersection of the linear solubilization curve with the theoretical solubility curve due to complex formation (figures 7.13 and 7.14).

At the SOL_T, all cirazoline is solubilized and further increase in SDDS concentration above this point has therefore no effect on the solubility of cirazoline and SOL_T is thus given by extrapolation of the linear solubilization curve to $[CIRHCl]^T$, (figures 7.13 and 7.14). K_A values were calculated using equation 7.14 and $[CIRH^+_{(aq)}]$ was calculated using equations 7.5 and 7.9. K_S' values were calculated from K_S values in table 6.7 and equation 1.70 (ionic strength = CMC' + added [NaCl]). CMC values were calculated from CMC' values using equations 7.7 and 7.9.

7.1.2.2 CONDUCTIMETRIC TITRATIONS

(a) Description

Aggregation and solubilization in cirazoline hydrochloride - SDDS systems was studied using the automated conductimetric titration technique described in section 6. SDDS solution (0.1 M or 0.2 M) was normally titrated into cirazoline hydrochloride solution at a flow rate of 20.38 or 50.48 $\mu l\ min^{-1}$, chart speed 12 cm hr^{-1}. Conductivity range was selected to give optimum deflection and was dependent upon cirazoline hydrochloride concentration, temperature and presence of electrolyte.

The initial phase of these titrations involves the formation of hydrophobic complex. The presence of a separate phase in the system was found to affect conductivity values through an obstruction effect. Robinson and Stokes[11] have described this effect and derived expressions for the specific conductivity and equivalent conductance of the electrolytes in relation to the volume fraction of the disperse phase. This treatment regards the disperse phase as insulating monodisperse spheres of low volume fraction in an aqueous

mixture of electrolytes. Mukhayer and Davis[121] have applied this treatment to account for differences in theoretical and experimental conductivity data in liquid complex systems. The correction gave reasonable agreement between theoretical and experimental conductivity data although differences were noted at higher concentrations. This approach, however, is not valid for crystalline complex systems as the assumption that the insoluble phase resembles monodisperse spheres clearly does not apply. In addition the highly flocculated nature of the solid cirazoline dodecylsulphate complex and its affinity for electrode and glass surfaces was found to cause an accumulation of complex in the measuring volume of the conductivity cell. This caused fluctuations in conductivity readings and increased the error in CMC' and SOL_T measurements.

The obstruction effect of the crystalline complex was overcome by continuously filtering the mixture using a specially designed jacketted cell, (figure 7.1). Crystals formed during the titration are held by the glass wool suspended in the jacketted cell. The glass wool is isolated from the conductivity dip-cell and magnetic flea by a specially designed glass insert. This consisted of an open vertical semi-circular shield attached to a lower cylindrical support which sat at the bottom of the jacketted cell. A coarse glass mesh covered the top of the support and divided the cell into upper and lower compartments. The magnetic flea was placed in the lower compartment, the dip-cell inserted into the sheild (which acted as an extension of the lower compartment) and the glass wool spread loosely throughout the upper compartment. The syringe was inserted through the glass wool and positioned so that the tip just protruded into the

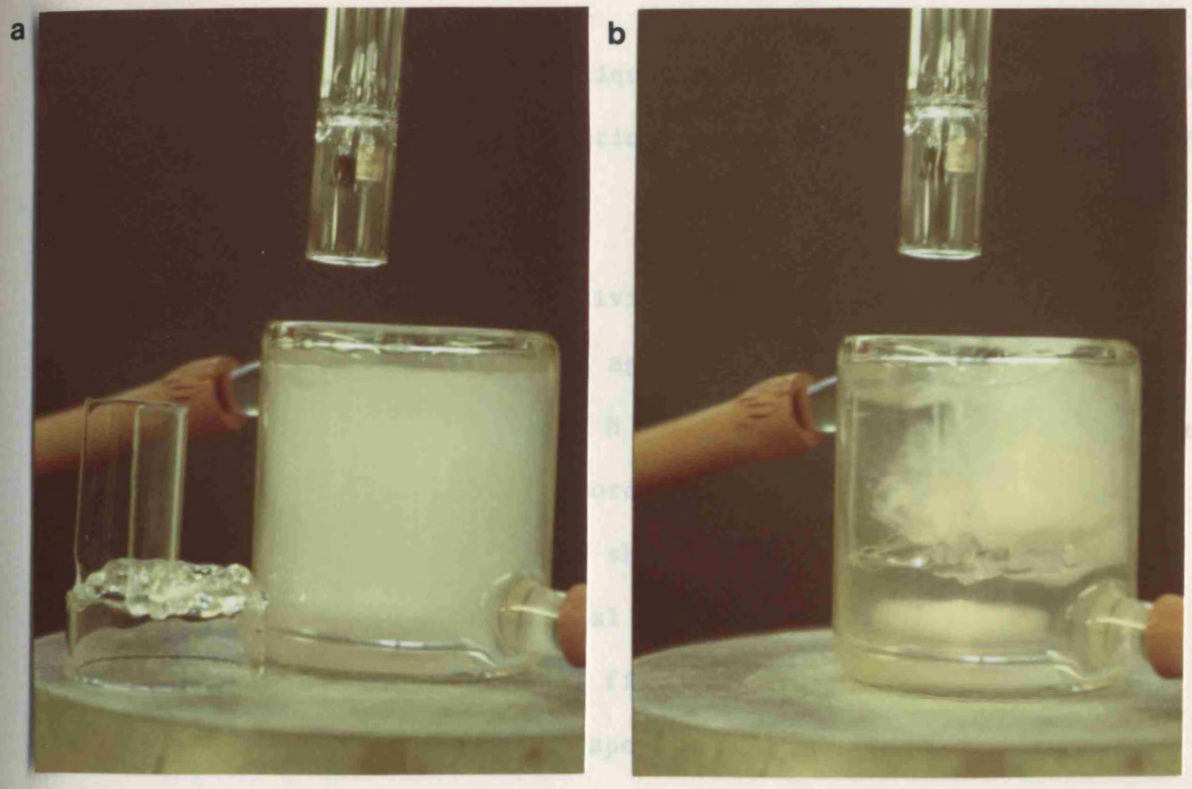

Figure 7.1 - Thermostated jacketted cell assembly for conductimetric titrations. 2×10^{-3} M cirazoline hydrochloride solution upon addition of 0.2 M SDDS, (a) showing stirring suspension of cirazoline dodecylsulphate in the absence of the glass insert and (b) showing glass insert and glass wool in position.

lower compartment. This arrangement allowed mixing of the filtrate and prevented glass wool and entrapped complex from interfering with conductivity measurements, (figure 7.1). One disadvantage of this assembly was that the glass wool increased the background conductivity in the system to approximately 15-50 x 10^{-6}S. This remained approximately constant during the titration.

The obstruction effect due to liquid complex formation was not such a serious problem and these titrations were performed in the absence of the insert.

The changes in specific conductivity - SDDS concentration profiles for the titration of 0.2 M SDDS against (a) double distilled water, (b) 2 x 10^{-3} M and (c) 5 x 10^{-3} M cirazoline hydrochloride at 30°C are shown in figure 7.2. Chart recorder traces for these titrations are shown in Appendix 3. Curve (a) shows a clear inflexion in conductivity at the CMC. A total of seven titrations were performed against double distilled water, five of which were in the absence and two in the presence of the specially designed glass insert; the mean (S.D.) CMC values were determined as 8.21 x 10^{-3} M (0.09 x 10^{-3} M) and 8.25 x 10^{-3} M respectively. These data are in agreement with reported CMC values for SDDS at 30°C (CMC = 8.2 - 8.5 x 10^{-3} M)[51] and indicate the specially designed glass insert does not affect the CMC.

Curve (b) is divided into six characteristic regions, distinguished by five inflexions, A - E. Each inflexion is associated with a change in the physico-chemical nature and appearance of the system. Prior to point A, the system was a clear solution which consisted primarily of cirazoline monomers and cirazoline dodecylsulphate ion-pairs. Point A marks the onset of phase separation and is equivalent

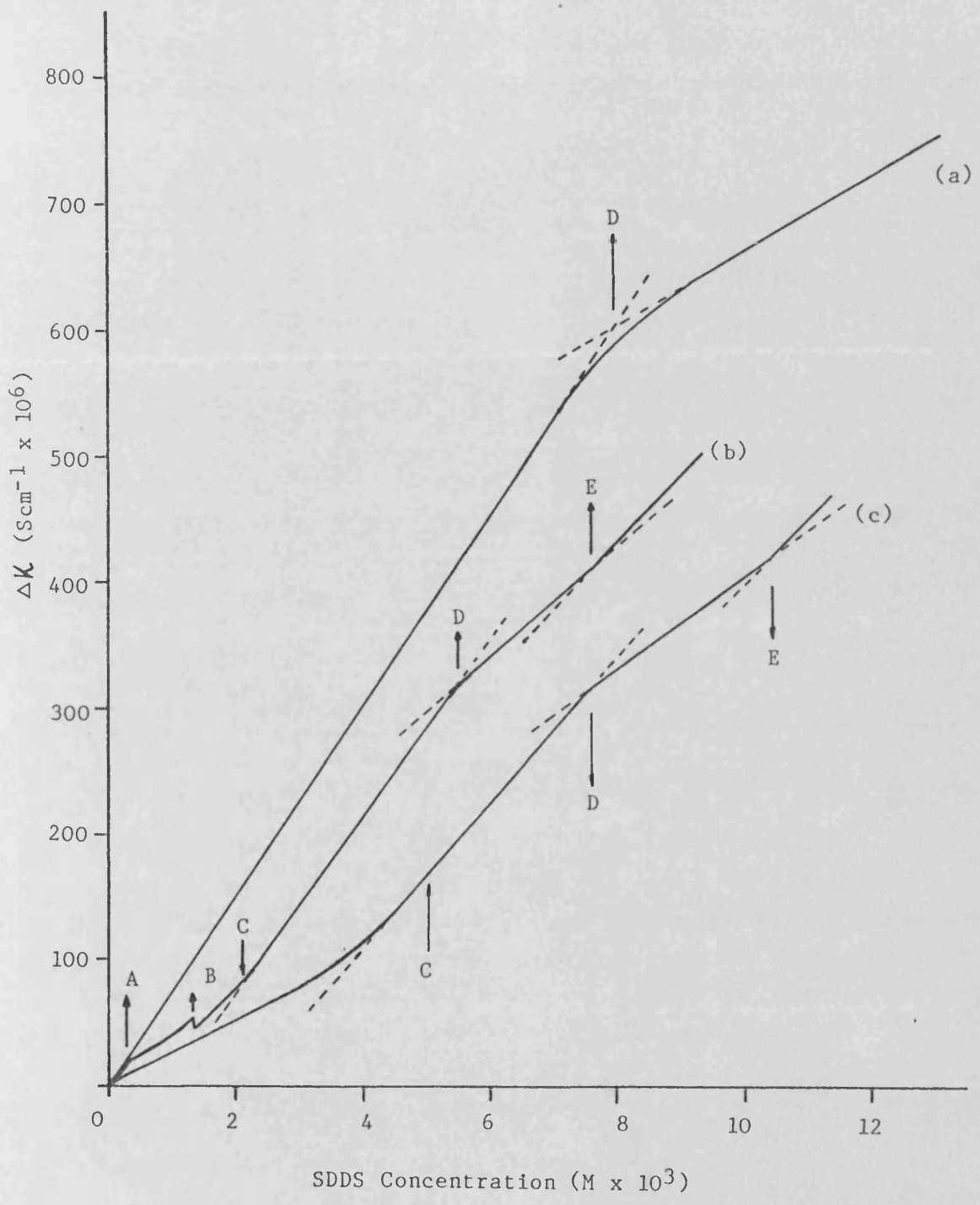

Figure 7.2 - Change in specific conductivity, ΔK, against SDDS concentration for the titration of 0.2 M SDDS into (a) double distilled water, (b) 2×10^{-3} M cirazoline hydrochloride and (c) 5×10^{-3} M cirazoline hydrochloride at 30°C. A = liquid complex phase separation, B = liquid --> solid complex transition, C = equimolar concentration, D = CMC' and E = SOL_T points.

to the inflexion used in the determination of the liquid complex solubility product (section 6). The system becomes turbid at this point and region A - B represents formation of metastable liquid complex. The region A - C is a non-linear curve, punctuated by a decrease in conductivity at point B. This inflexion is associated with a change in appearance from a grey liquid dispersion to a white flocculated suspension and precipitation of crystalline complex occurred at this point. Point C represents the cirazoline hydrochloride - SDDS equimolar point and further increase in SDDS concentration results in a linear curve, C - D. Inflexion D is followed by a second linear region, D - E, but of smaller slope. The concentration of crystalline complex reduces during this phase of the titration until, at point E, the system becomes a clear solution. Points D and E therefore represent the SDDS concentration at the CMC' and SOL_T of the system respectively. Further addition of SDDS results in an increase in conductivity and a non-linear curve.

The titration against 5 x 10^{-3} M cirazoline hydrochloride, curve (c), is similar to curve (b) except the inflexion points C - E are shifted to higher SDDS concentration. Points A (phase separation) and B (phase transition) are absent as crystalline complex was formed almost immediately upon addition of SDDS. The curve in the complex formation region (i.e. prior to point C) is initially linear but curves upwards as the SDDS concentration approaches the equimolar concentration point, C.

The form of the derived Onsager plots (equivalent conductivity of the mixture, Λ_{mix}, against square root of total concentration ($[CIRHCl]^T + [SDDS]^T)^{1/2}$, for the titrations against (a) 2 x 10^{-3} M and (b) 5 x 10^{-3} M cirazoline hydrochloride are shown in figure 7.3,

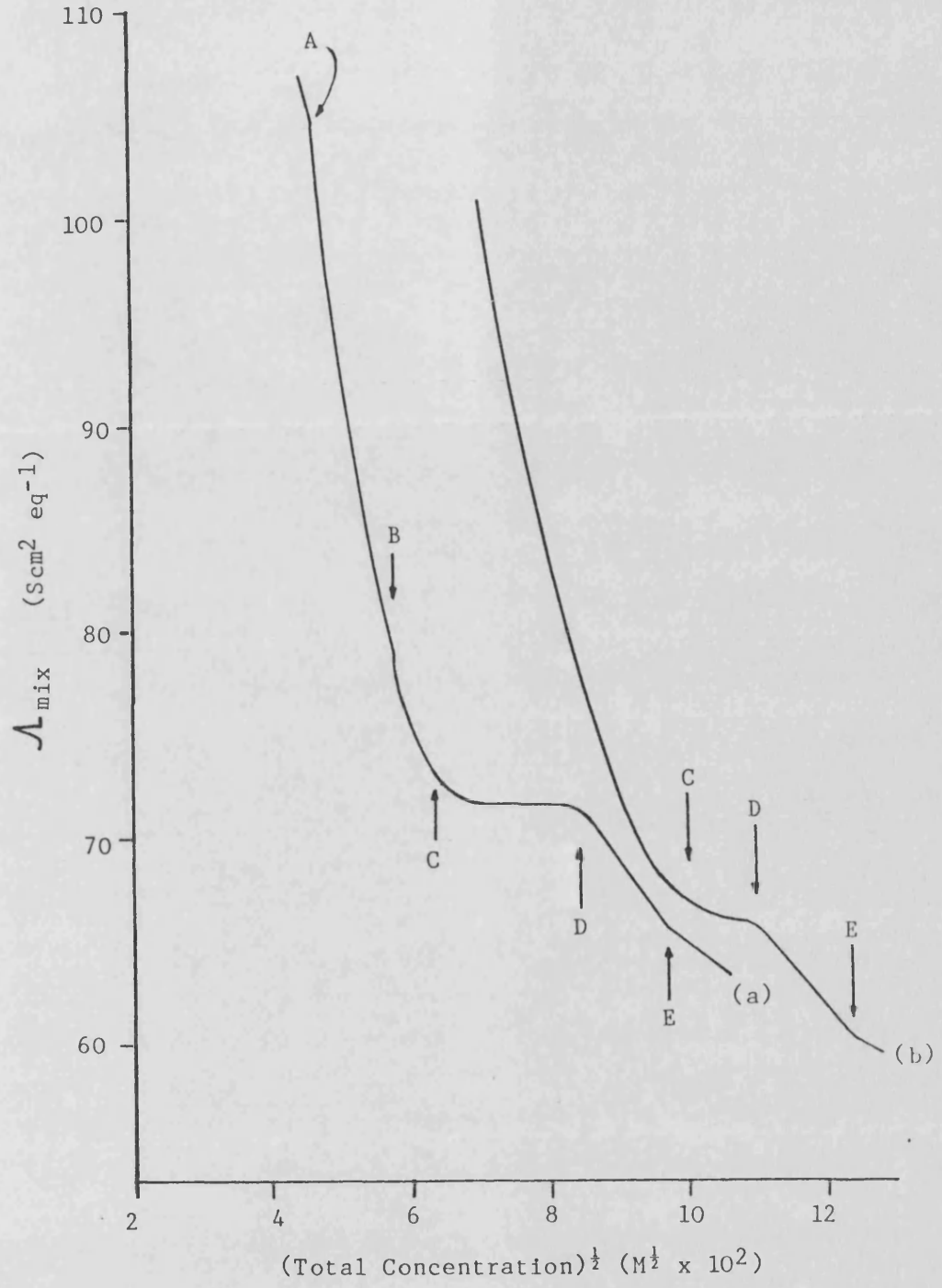

Figure 7.3 - Equivalent conductance of titration mixture, Λ_{mix}, against square root of total concentration of mixture (cirazoline hydrochloride + SDDS) for the titration of 0.2 M SDDS into (a) 2 x 10^{-3} M cirazoline hydrochloride and (b) 5 x 10^{-3} M cirazoline hydrochloride at 30°C. A = liquid complex phase separation, B = liquid --> solid complex transition, C = equimolar concentration, D = CMC' and E = SOL_T points.

these were obtained by taking at least 25 values from the recorder traces; (data points are not shown for the sake of clarity). For curve (a), addition of SDDS causes a rapid fall in Λ_{mix} indicating that cirazoline hydrochloride and SDDS are not behaving as independent strong electrolytes. Onset of complexation (point A) results in a rapid decrease in Λ_{mix} as ions are removed from solution. The phase transition point (B) is clearly shown as a discontinuity. Λ_{mix} continues to fall with increase in SDDS concentration until the equimolar concentration point (C) is exceeded. A region which is independent of concentration is then observed indicating the added SDDS is behaving as a strong electrolyte. The CMC' (point D) is associated with a decrease in Λ_{mix}. A decrease in the rate of fall of Λ_{mix} with concentration is observed at the SOL_T (point E). The nature of the inflexions at points C - E in curve (b) are similar to those observed in curve (a).

The conductivity curves in figure 7.2 relate to formation and solubilization of crystalline complex. Conductivity curves produced with liquid complex systems had different characteristics, however, Figure 7.4 shows the change in the specific conductivity - SDDS concentration profile for the titration of 0.1 M SDDS into 2 x 10^{-3} M cirazoline hydrochloride at 40°C, (the chart recorder trace is shown in Appendix 3). Point A in figure 7.4 marks the phase separation boundary and the system was turbid in the region A - E. No phase transition inflexion (B) occurred as the liquid complex is stable at this temperature (see section 6). The plot between onset of complexation and aggregation (region A - D) is a gentle upward curve with no inflexion at the equimolar concentration point (C). An upward discontinuity in the curve is observed at point D and the system gradually clears as further SDDS is added. At point E the

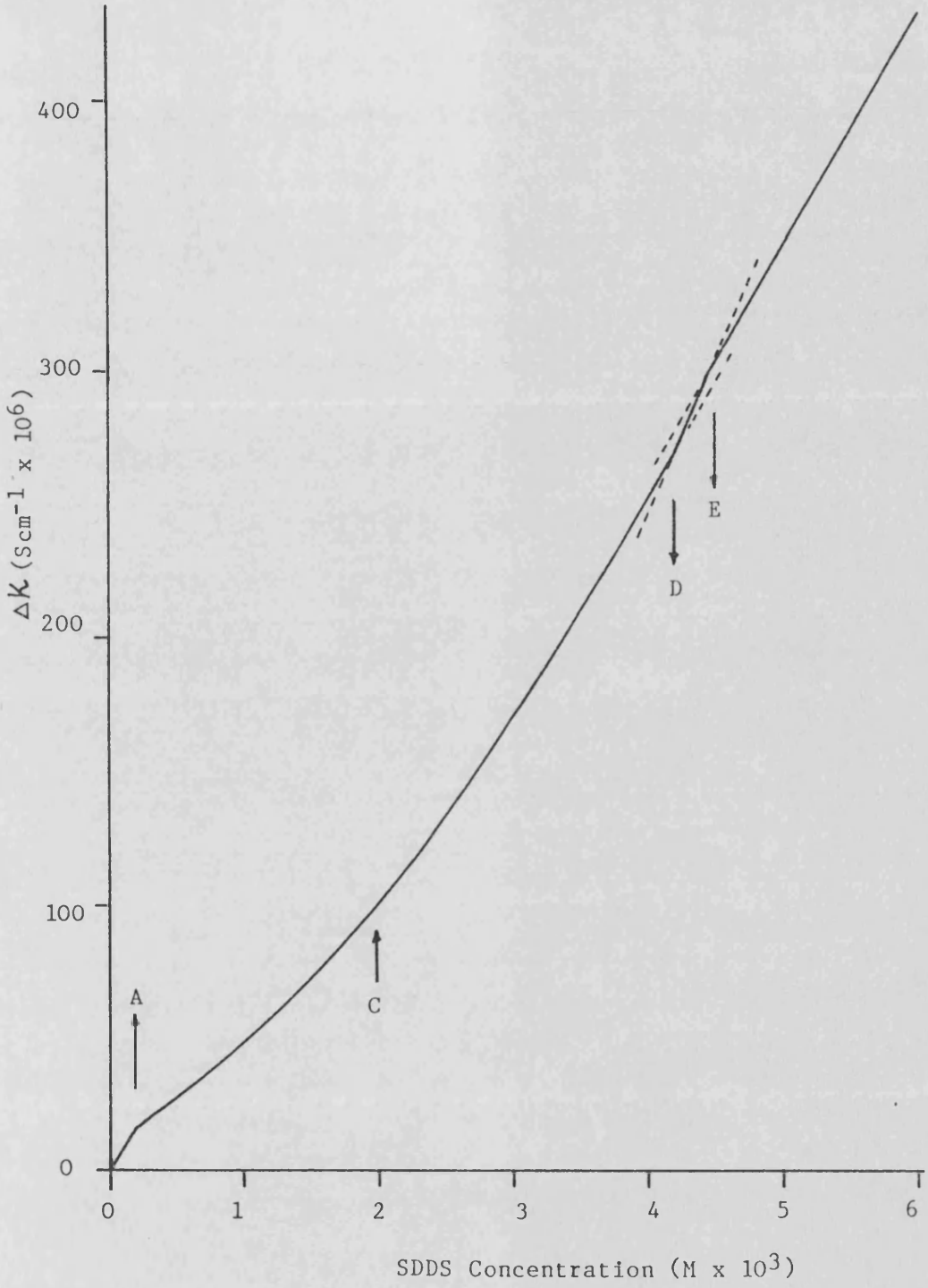

Figure 7.4 - Change in specific conductivity, ΔK, against SDDS concentration for the titration of 0.1 M SDDS into 2×10^{-3} M cirazoline hydrochloride at 40°C. A = liquid complex phase separation, C = equimolar concentration, D = CMC', and E = SOL_T points.

system is totally clear and a decrease in the rise in conductivity with SDDS concentration is observed. The curve beyond point E is linear over the SDDS concentration range studied. Visual observation indicates that region D - E is the solubilization region and, therefore, points, D and E are the CMC and SOL_T of the system respectively. However, these inflexions in the conductivity curve are the inverse of those observed with the solid complex system; i.e. an increase in the change in conductivity with concentration is observed at the CMC' and a decrease at the SOL_T. The Onsager plot (Λ_{mix} against $([CIRHCl]^T + [SDDS]^T)^{1/2}$, figure 7.5) is similar to the solid complex plots (figure 7.3) in that a dramatic fall in Λ_{mix} is observed due to ion-pairing and complexation. Λ_{mix} continues to fall beyond the equimolar concentration point (C) but unlike the solid complex plot, a shallow minimum in the curve is observed. An increase in Λ_{mix} with increase in concentration at the CMC' (point D) followed by a slight decrease in Λ_{mix} at the SOL_T (point E) then takes place.

(b) Calculation of CMC', SOL_T and K_A

CMC' and SOL_T points were determined by extrapolation of the appropriate regions of the conductivity curves (e.g. in figures 7.2 and 7.4). Inflexion points were normally taken directly from chart traces and the SDDS concentration calculated using equation 6.1. Conductivity curves for the solubilization of liquid complex were more difficult to analyse due to the non-linear nature of the profiles. Data points from these profiles are therefore, thought to be subject to appreciable error.

K_A values were determined using equation 7.14 as described in section 7.1.2.1(c). As the titration proceeds the system becomes

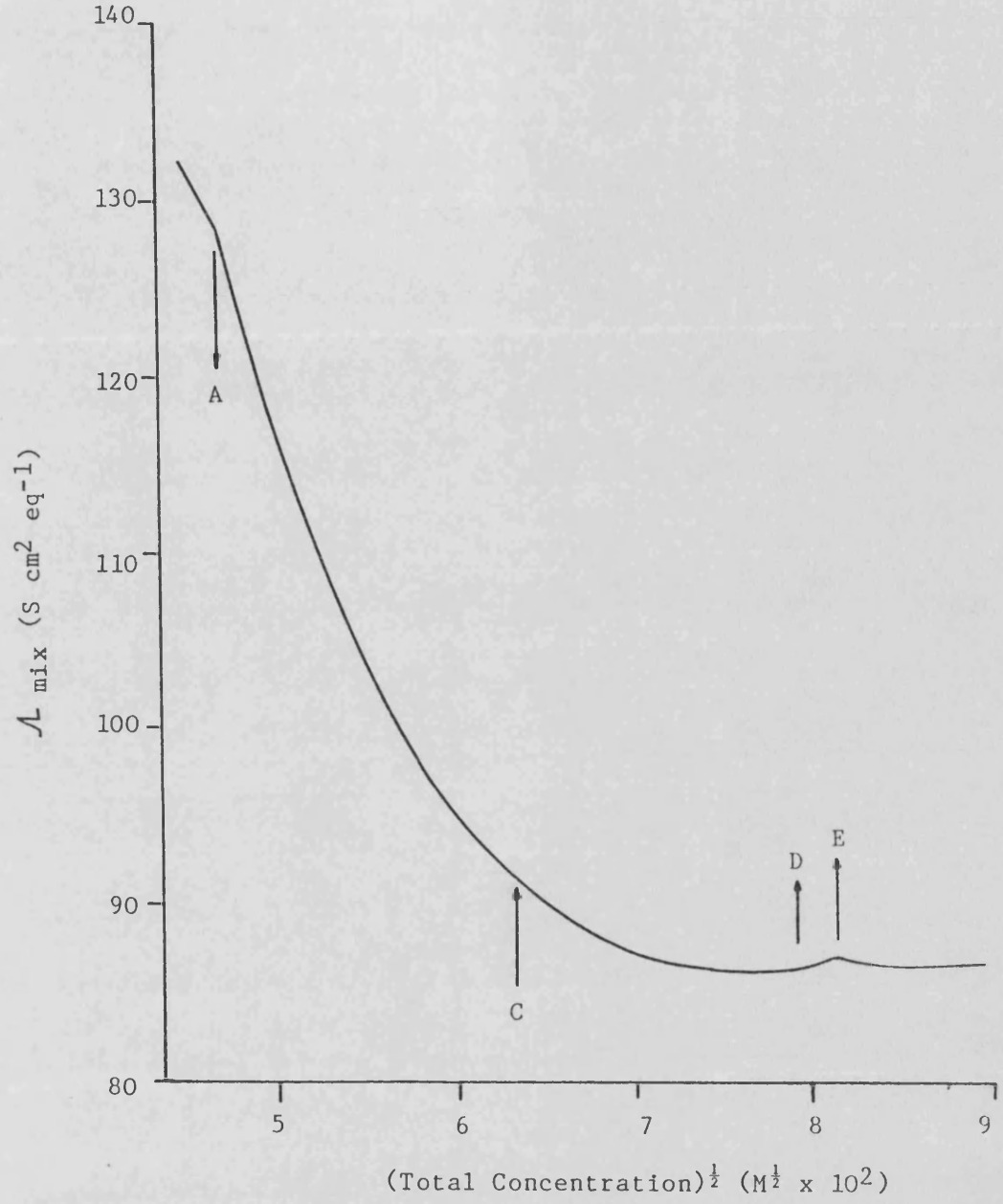

Figure 7.5 - Equivalent conductance of titration mixture, Λ_{mix}, against square root of total concentration of mixture (cirazoline hydrochloride + SDDS) for the titration of 0.1 M SDDS into 2 x 10^{-3} M cirazoline hydrochloride at 40°C. A = liquid complex separation, C = equimolar concentration, D = CMC and E = SOL_T points.

progressively more dilute with respect to cirazoline and equations 7.13 and 7.14 are not strictly valid. However, the volume change of the system between the CMC' and SOL_T was always small and the maximum error in using equation 7.14 for the calculation of K_A values in this thesis was calculated as 2.5%.

(c) Effect of Flow Rate

The effect of titrant flow rate on the calculated CMC', SOL_T and K_A values was determined. SDDS (0.2 M) was titrated into 2 x 10^{-3} M cirazoline hydrochloride at 30°C and at flow rates of 12.39, 20.38, 50.48 and 251.3 µl min^{-1}. Chart speeds of 3 - 60 cm hr^{-1} were used as appropriate and a chart conductivity range of 0 - 500 x 10^{-6} S was employed. Calculated CMC', SOL_T and K_A values are shown for each titration flow rate in table 7.3. At all but the fastest flow rate (251.3 µl min^{-1}) metastable liquid complex was formed initially but precipitated during the titration to form crystallation complex. Micellization and solubilization data at these flow rates therefore relate to the equilibrium solid complex species. At a flow rate of 251.3 µl min^{-1}, however, the crystalline complex did not form and the conductivity curve was similar in character to the titration curve at 40°C (figure 7.4). Accurate values could not be obtained for this system due to the fast titration speed.

The values in table 7.3 indicate that flow rate in not critical providing the titration is performed sufficiently slowly to enable the equilibrium system to form. Conductimetric titrations for the study of aggregation behaviour were therefore normally carried out at a flow rate of either 20.38 or 50.48 µl min^{-1}.

FLOW RATE ($\mu l\ min^{-1}$)	CMC' ($M \times 10^3$)	SOL_T ($M \times 10^3$)	K_A ($M^{-1} \times 10^{-4}$)	COMPLEX
12.39	5.20	7.04	2.7	Solid
20.38	5.22	6.79	3.3	Solid
50.48	5.27	6.79	3.4	Solid
251.3	-	-	-	Liquid

Table 7.3 - The effect of flow rate on the determination of CMC', SOL_T and K_A values by conductimetric titration. Data for the titration of 0.2 M SDDS against 2×10^3 M cirazoline hydrochloride at 30°C.

(d) Reproducibility

The reproducibility of the conductimetric titration technique for the determination of CMC', SOL_T and K_A values at 30°C was determined by titrating SDDS into 2 x 10^{-3} M cirazoline hydrochloride ten times over a seven month period. Table 7.4 shows SDDS concentration, flow rate and calculated CMC', SOL_T and K_A values for each titration. Statistical analysis shows the technique to give satisfactory reproducible values of CMC' (CV = 2%), SOL_T (CV = 3%) and K_A (CV = 7%).

7.1.3 Results

7.1.3.1 EFFECT OF CIRAZOLINE CONCENTRATION

The effect of initial cirazoline hydrochloride concentration on micellization and solubilization in cirazoline hydrochloride-SDDS systems was determined at 30°C by conductimetric titration. SDDS (0.1 or 0.2 M) was titrated at a flow rate of 20.38 or 50.48 $\mu l\ min^{-1}$ using a chart speed of 12 cm hr^{-1} and chart recorder range 0 - 500 x 10^{-6} S or 0 - 1000 x 10^{-6} S. Table 7.5 is a summary of the micellization and solubilization data for each initial cirazoline hydrochloride concentration. CMC values were calculated from the apparant CMC (CMC') using equations 7.9 and 7.7 and $[CIRH\text{-}DDS_{(M)}]$, $[DDS^-_{(M)}]$ and K_A values were calculated using equations 7.10, 7.13 and 7.14 respectively.

Figure 7.6 shows the effect of cirazoline concentration (corrected for titrant dilution) on (a) SOL_T, (b) total SDDS concentration in the system at the CMC (CMC'), and (c) true SDDS CMC. The presence of low concentrations of cirazoline in SDDS systems initially lowers

DATE	SDDS CONCENTRATION (M)	FLOW RATE ($\mu l\ min^{-1}$)	CMC' ($Mx10^3$)	SOL_T ($Mx10^3$)	K_A ($M^{-1}x10^{-4}$)
13.1.86	0.1	50.48	5.47	6.92	3.4
16.1.86	0.1	50.48	5.45	7.09	3.2
4.3.86	0.1	50.48	5.56	7.31	3.1
3.4.86	0.2	20.38	5.42	7.25	3.0
8.4.86	0.2	20.38	5.42	7.28	2.9
8.4.86	0.2	20.38	5.24	7.04	2.8
7.5.86	0.2	20.38	5.34	6.96	3.2
4.8.86	0.2	20.38	5.22	6.79	3.3
4.8.86	0.2	50.48	5.27	6.79	3.4
7.8.86	0.2	20.38	5.24	6.98	2.9
		Mean ($x\ 10^3$)	5.36	7.04	3.1
		S.D. ($x\ 10^3$)	0.12	0.19	0.2
		CV (%)	2.2	2.7	7.0

Table 7.4 - Reproducibility of the conductimetric titration technique for the determination of CMC', SOL_T and K_A values. Data for the titration of SDDS against 2×10^{-3} M cirazoline hydrochloride at 30°C.

CIRAZOLINE CONCENTRATION ($Mx10^3$)			SDDS CONCENTRATION ($Mx10^3$)				K_A
INITIAL	$[CIRH^+(aq)]$	$[CIRH\text{-}DDS(M)]$	CMC'	CMC	SOL_T	$[DDS^-(M)]$	(M^{-1} $x10^4$)
0.1	0.015	-	7.66	7.57	-	-	-
0.2	0.029	-	4.4[a]	4.2[a]	-	-	-
0.5	0.031	0.44	4.54	4.06	5.06	0.52	2.8
1.0[b]	0.032	0.91	4.76 (4.74-4.78)	3.81	5.76 (5.68-5.83)	1.00	2.8
1.5	0.034	1.37	5.09	3.67	6.43	1.34	3.0
2.0[c]	0.034	1.87	5.36 (5.22-5.56)	3.43	7.04 (6.79-7.31)	1.68	3.1
2.5	0.038	2.27	5.61	3.25	7.55	1.94	3.1
3.0	0.044	2.84	5.74	2.83	7.96	2.22	2.9
3.2	0.043	3.02	5.99	2.89	8.41	2.42	2.9
4.0[d]	0.048	3.76	6.46 (6.43-6.49)	2.59	9.47 (9.29-9.65)	3.01	2.6
5.0	0.048	4.68	7.48 (7.36-7.66)	2.66	10.73 (10.49-10.97)	3.25	3.1

a - approximate value

b - mean (range) of two determinations

c - mean (range) of ten determinations

d - mean (range) of three determinations

Table 7.5 - Effect of cirazoline hydrochloride concentration on micellization and solubilization in cirazoline hydrochloride-SDDS systems at 30°C.

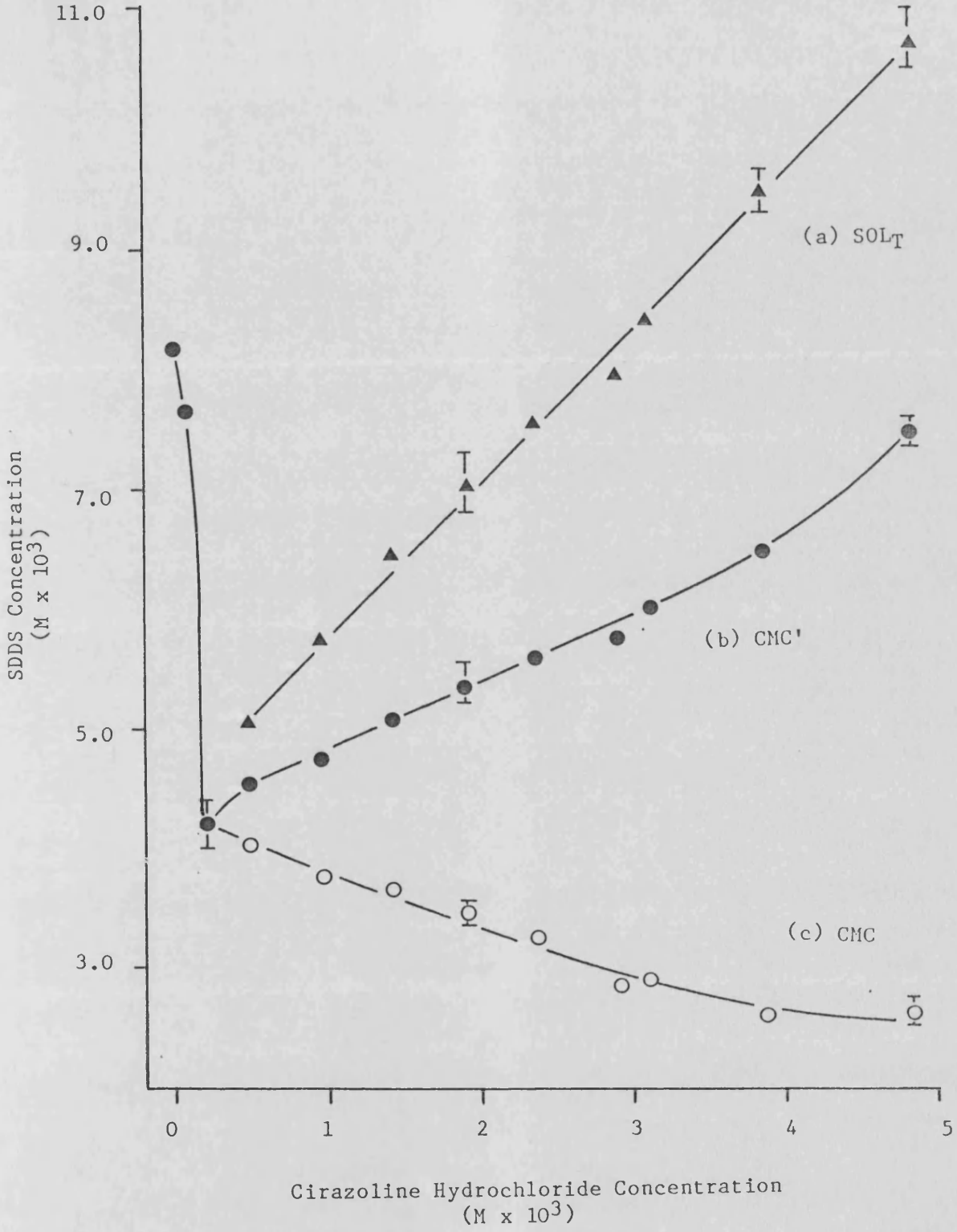

Figure 7.6 - Effect of cirazoline hydrochloride concentration (corrected for dilution) on (a) SOL_T, (b) CMC' and (c) CMC, for SDDS at 30°C.

the CMC', reaching a minimum at 2 x 10^{-4}M, further increase in cirazoline concentration then increases CMC'. This is due to the increased formation of CIRH-DDS complex and the consequent removal of dodecylsulphate ions from solution. The effect of cirazoline concentration on the micellization of SDDS is shown by the true SDDS CMC curve (c). This decreases with increase in cirazoline (and therefore complex) concentration. The SDDS concentration required to completely solubilize cirazoline (SOL_T) increases with increase in solubilizate (complex) concentration.

The molar ratio of cirazoline to dodecylsulphate moieties within the aggregates may be estimated from the slope of a plot of [CIRH-$DDS_{(M)}$] against ([$SDDS_{(M)}$] + [CIRH-$DDS_{(M)}$]), (figure 7.7). Linear regression analysis gave : regression coefficient = 0.9987, slope (S.D.) = 0.604 (0.012), and intercept (S.D.) = -2.34 x 10^{-4} (0.56 x 10^{-4}). The molar ratio of cirazoline to dodecylsulphate moieties within the aggregates is thus 0.6 : 1.

K_A values were independent of cirazoline concentration and gave a mean K_A value of 2.9 x 10^4 (S.D. = 0.2 x 10^4 M^{-1}).

7.1.3.2 EFFECT OF TEMPERATURE

The effect of temperature (10^o - 50^oC) on aggregation and solubilization within cirazoline hydrochloride - SDDS systems was investigated by conductimetric titration. Titrations were performed by titrating 0.1 or 0.2 M SDDS into 2 x 10^{-3} M cirazoline hydrochloride at a flow rate of 12.39, 20.38 or 50.48 µl min^{-1}. A chart speed of 3 or 12 cm/hr was used in conjunction with chart conductivity range 0 - 500 x 10^{-6} S.

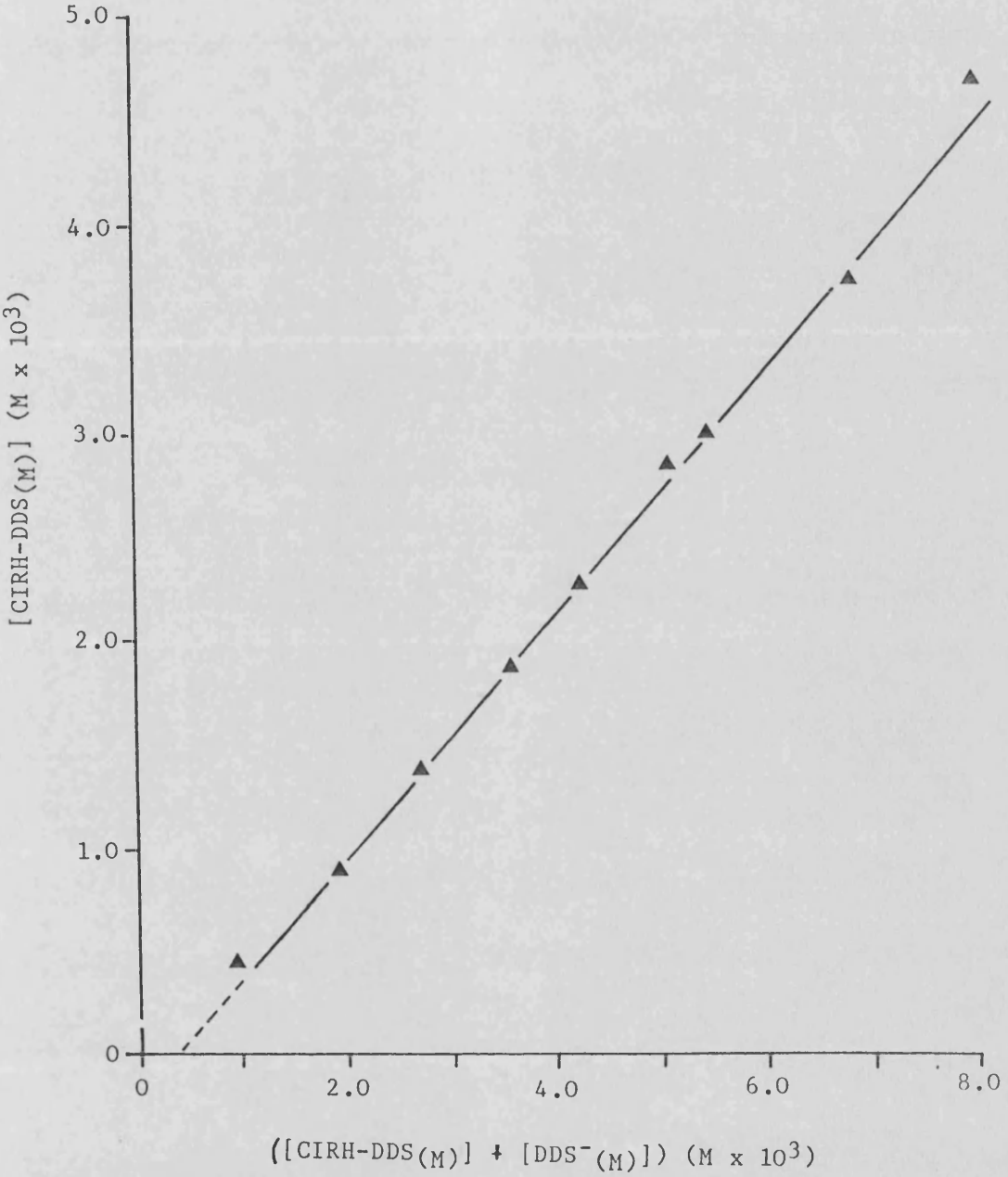

Figure 7.7 - Cirazoline : dodecylsulphate moiety ratio in aggregates. Plot of concentration of cirazoline in aggregates, ([CIRH-DDS$_{(M)}$], against total concentration of dodecylsulphate in aggregates, ([CIRH-DDS$_{(M)}$] + [DDS$^{-}_{(M)}$]). Concentrations expressed with respect to total volume of the system.

Solid CIRH-DDS complex was formed at temperatures of 35°C and below whereas liquid complex was produced at higher temperatures. Table 7.6 shows micellization and solubilization data at each temperature studied. The mole fraction of SDDS at the CMC, X_{CMC}, is also shown. K_A values were calculated using equation 7.14 and the solubility product values given in table 6.7. Figure 7.8 shows plots of CMC' and SOL_T against temperature are biphasic. Approximately linear decrease in both CMC' and SOL_T with temperature is observed for both crystalline and liquid CIRH-DDS systems with the break occurring at the transition temperature. For the solid complex system, the relative magnitudes of SOL_T and CMC' slopes indicate that solubilization is more sensitive to temperature change than the micellization process. The effect of temperature on the liquid complex values for CMC' and SOL_T is less pronounced and these solubilization and micellization processes appear to be equally affected by temperature.

The Van't Hoff plot for the derived true CMC (mole fraction) is biphasic with a non-linear plot for the crystalline complex systems with the inflexion corresponding to the transition point, (figure 7.9). The standard free energy change for the micellization process, ΔG^o_M, was calculated at each temperature using equation 1.29. The degree of dissociation, α, was taken as zero for these calculations (since cirazoline is strongly bound to the micelles). The standard enthalpy change for micellization, ΔH^o_M, at each temperature was determined from the slope of the curves and use of equation 1.30. The standard entropy change for micellization, ΔS^o_M, was calculated using equation 1.31. Table 7.7 is a summary of thermodynamic parameters for the micellization process at each temperature. ΔG^o_M is negative and ΔH^o_M and ΔS^o_M are positive at

TEMP. (°C)	$[CIRH^+_{(aq)}]$ ($Mx10^3$)	CMC' ($Mx10^3$)	CMC ($Mx10^3$)	X_{CMC} ($x10^5$)	SOL_T ($Mx10^3$)	AGGREGATE RATIO	K_A ($M^{-1}x10^{-4}$)
Solid Complex							
10	0.004	8.06 (7.96-8.15)	6.15	11.1	15	0.21	7.2
15	0.006	7.41 (7.38-7.44)	5.49	9.89	12.60	0.27	5.7
20	0.012	6.73 (6.72-6.74)	4.81	8.67	10.60	0.33	4.0
25	0.020	6.07 (6.01-6.12)	4.15	7.48	8.87	0.40	3.4
30[a]	0.034	5.36 (5.22-5.56)	3.43	6.18	7.04 (6.79-7.31)	0.52	3.1
35[b]	0.073	4.56 (4.35-4.74)	2.68	4.83	5.51 (5.38-5.72)	0.66	2.7
Liquid Complex							
37.5	0.107	4.40 (4.38-4.42)	2.59	4.67	4.75 (4.72-4.81)	0.83	4.8
40	0.119	4.33 (4.33-4.33)	2.54	4.58	4.66 (4.65-4.67)	0.84	4.5
45	0.157	4.21	2.45	4.44	4.58	0.82	3.0
50	0.196	4.00	2.28	4.11	4.40	0.81	2.2

a = Mean (range) of ten determinations, b = Mean (range) of four determinations

Table 7.6 - Effect of temperature on micellization and solubilization in 2 x 10^{-3} M cirazoline hydrochloride - SDDS systems. Unless otherwise indicated figures in parentheses represent range of two determinations. (X_{CMC} = mole fraction of SDDS at the CMC).

$$\text{Aggregate Ratio} = \frac{[\text{CIR-DDS}_{(M)}]}{[\text{CIRH-DDS}_{(M)}]+[\text{DDS}^-_{(M)}]}$$

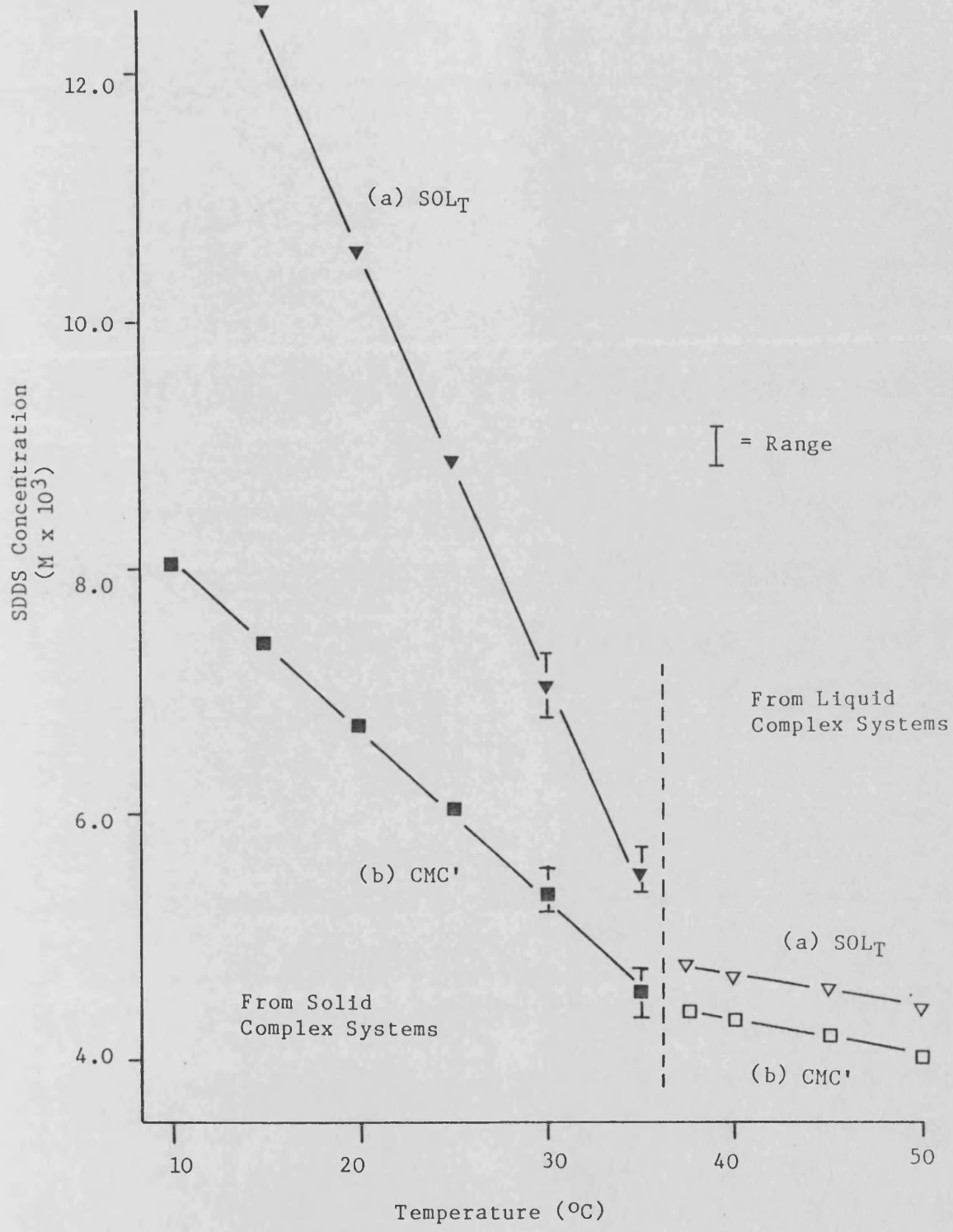

Figure 7.8 - Effect of temperature on the SDDS concentration at the (a) SOL_T, (b) CMC' for 2 x 10^{-3} M cirazoline hydrochloride-SDDS systems, 30°C.

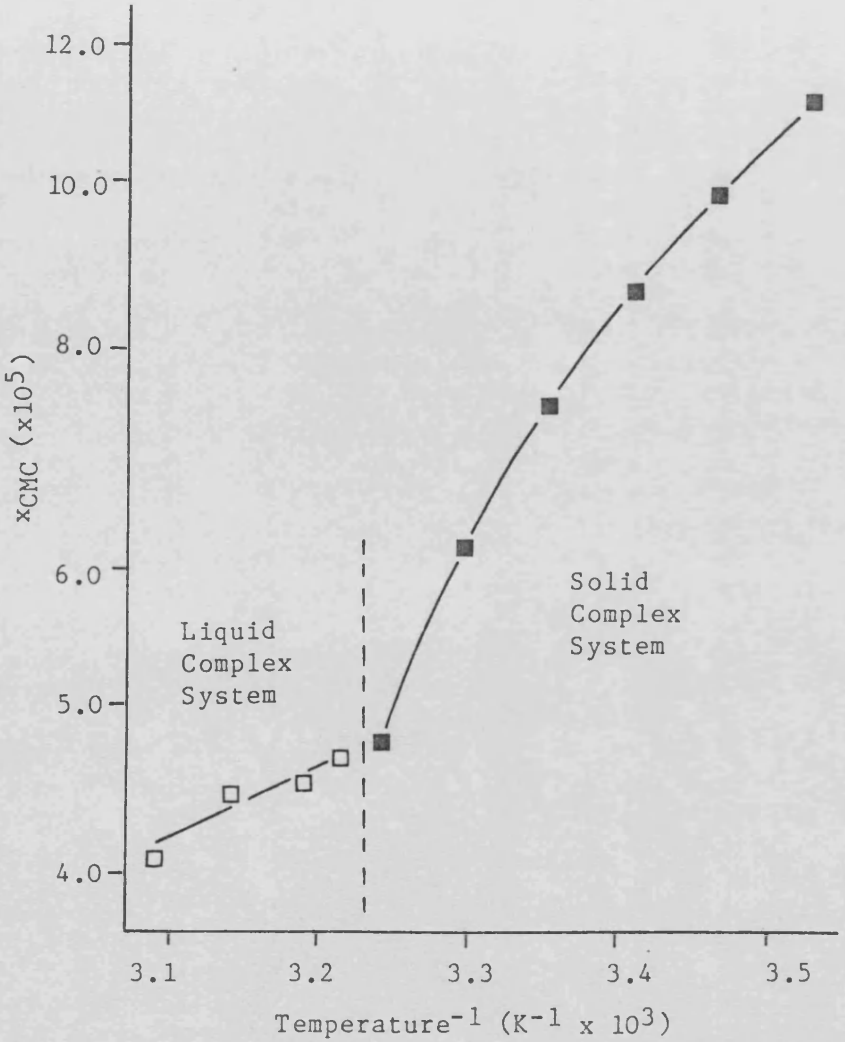

Figure 7.9 - Van't Hoff plot for micellization in 2 x 10^{-3} M cirazoline hydrochloride - SDDS system. Data plotted according to equation

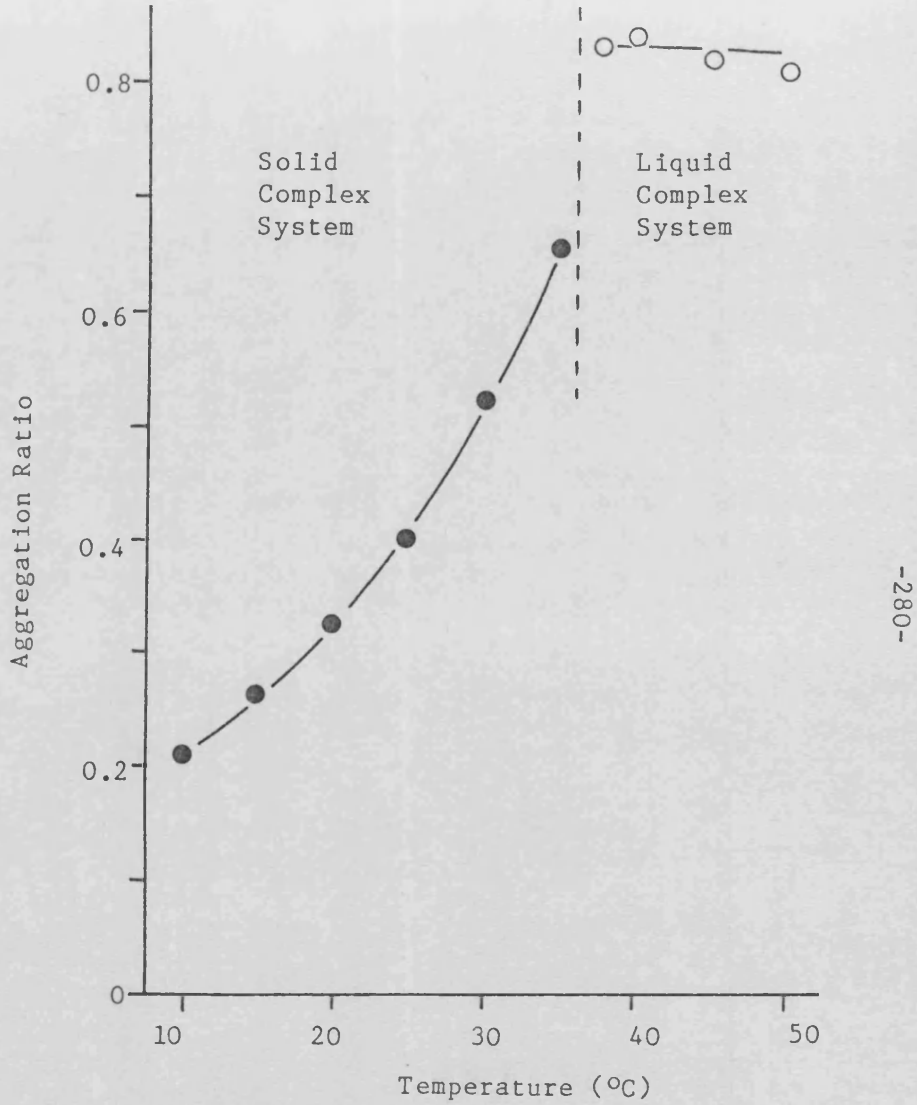

Figure 7.10 - The effect of temperature on the cirazoline:dodecylsulphate moiety ratio in aggregates.

TEMP (°C)	MICELLIZATION ΔG^{o}_{M} (kJmol^{-1})	ΔH^{o}_{M} (kJmol^{-1})	ΔS^{o}_{M} (Jmol^{-1}K^{-1})	SOLUBILIZATION ΔG^{o}_{A} (kJmol^{-1})	ΔH^{o}_{A} (kJmol^{-1})	ΔS^{o}_{A} (Jmol^{-1}K^{-1})
Solid Complex						
10	-43	11	90	-36	53	310
15	-44	17	210	-36	41	270
20	-46	21	230	-36	30	230
25	-47	27	250	-36	23	200
30	-49	33	270	-36	19	180
35	-51	42	300	-36	12	160
Liquid Complex						
37.5	-52	12	200	-38	5	300
40	-52	12	200	-38	5	300
45	-53	12	200	-38	5	300
50	-54	12	200	-38	5	300

Table 7.7 - Thermodynamics of micellization and solubilization processes in 2 x 10^{-3} M cirazoline hydrochloride-SDDS systems.

all temperatures studied. Micellization is therefore driven by a large positive entropy change and hindered by an endothermic enthalpy change. Micellization in liquid complex systems is driven by similar forces although ΔH^{o}_{M} and ΔS^{o}_{M} are somewhat less than for the solid complex system.

The effect of temperature on the ratio of cirazoline to dodecylsulphate moieties within the aggregates is shown in figure 7.10. The ratio increases with increase in temperature until the phase transition point is reached, e.g. at 10°C the ratio is 0.21 which rises to 0.65 at 35°C, thereafter remaining approximately constant at about 0.8.

For the solid complex system, K_A values decrease with increase in temperature and indicate the affinity of cirazoline ions for SDDS micelles diminishes as the temperature increases, (figure 7.11). A rapid increase in K_A occurs at the phase transition point; K_A for the association in the presence of liquid complex then falls rapidly with increasing temperature.

The Van't Hoff plot for the association of cirazoline ions to SDDS micelles is biphasic with a break corresponding to the transition temperature, (figure 7.12). The standard free energy change for the association process, ΔG^{o}_{A}, was calculated at each temperature using equation 1.84; the standard enthalpy change, ΔH^{o}_{A}, was determined from the slope of the curves and use of equation 1.85; and the standard entropy change, ΔS^{o}_{A}, was calculated using equation 1.86. These thermodynamic parameters are shown alongside micellization data in table 7.7. ΔG^{o}_{A} is negative and independent of temperature for each system. At low temperature the association process is driven by a large entropy change and hindered by a large enthalpy change.

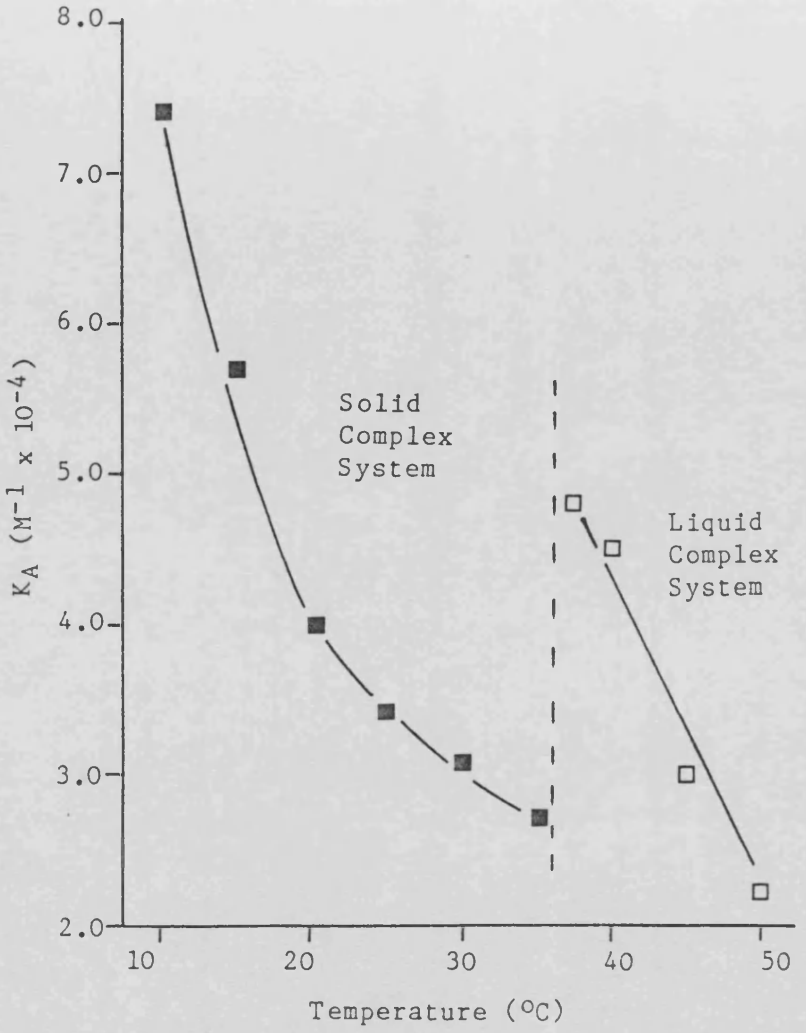

Figure 7.11 - The effect of temperature on the association constant (K_A) for the interaction between cirazoline and SDDS micelles.

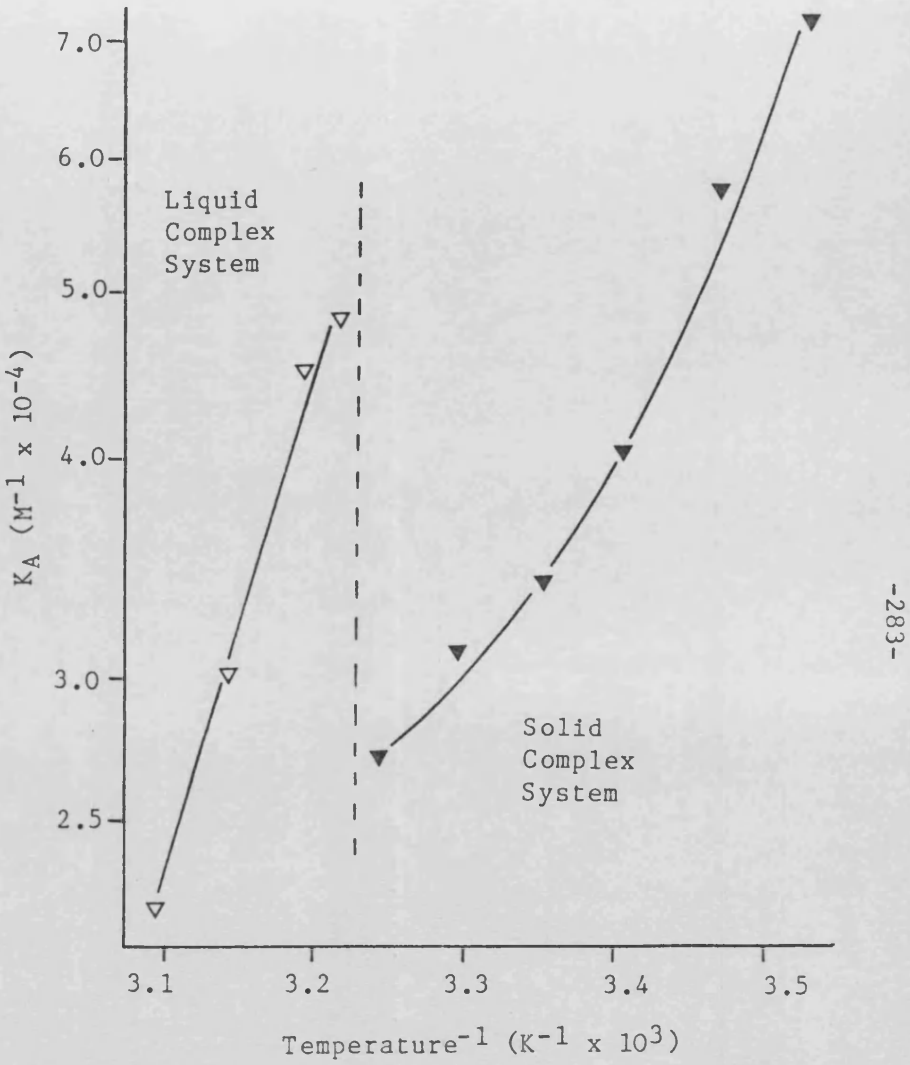

Figure 7.12 - Van't Hoff plot for the association of cirazoline to SDDS micelles. Data plo according to equation 1.85.

These values decrease with increase in temperature until the phase transition temperature is reached. The association in the presence of liquid complex is characterised by similar forces.

The validity and error in determining these values are discussed in section 9.

7.1.3.3 EFFECT OF IONIC STRENGTH

The effect of ionic strength (I) on aggregation and solubilization in 2×10^{-3} M and 5×10^{-3} M cirazoline hydrochloride - SDDS systems was studied at 30°C using both conductimetric titration ($I = 2 \times 10^{-3}$ - 1×10^{-2} M) and solubility ($I = 2 \times 10^{-3}$ - 1×10^{-1} M) methods. Ionic strength was adjusted by the inclusion of sodium chloride solution in the systems. Solid CIRH-DDS complex was formed in all systems. Conductimetric titrations were performed by titrating 0.1 M or 0.2 M SDDS into 2×10^{-3} M or 5×10^{-3} M cirazoline hydrochloride at a flow rate of 20.38 or 50.48 $\mu l\ min^{-1}$. Titrations were limited to sodium chloride concentrations of 0.01 M and below due to the high background conductivity of concentrated electrolyte solutions.

The effect of SDDS and sodium chloride concentration on the solubility of cirazoline is shown in tables 7.8 and 7.9. The physical nature of each system is also shown. Cirazoline solubility - SDDS concentration profiles in the absence and presence of sodium chloride and shown in figures 7.13 and 7.14. Theoretical aqueous solubility profiles (calculated using K_s values from table 6.7 and equations 1.70, 7.9 and 7.5), equimolar concentration, CMC' and SOL_T points are also shown. Below the CMC' of 2×10^{-3} M cirazoline hydrochloride-SDDS systems, cirazoline solubility falls with increase in SDDS concentration (table 7.8 and figure 7.13). Sodium chloride

[SDDS] ($Mx10^3$)	CIRAZOLINE CONCENTRATION ($M \times 10^3$)			
	ADDED SODIUM CHLORIDE CONCENTRATION (M)			
	NIL	0.01	0.05	0.1
0.8	1.163 (C)	1.204 (C)	1.205 (C)	1.180 (C)
1.2	0.815 (C)	0.830 (C)	0.833 (C)	0.840 (C)
1.6	0.489 (C)	0.459 (C)	0.493 (C)	0.523 (C)
2.0	0.268 (C)	0.304 (C)	0.334 (C)	0.432 (C)
2.25	-	-	-	0.510 (C)
2.50	-	-	-	0.674 (C,T?)
2.75	-	-	0.607 (C)	1.153 (C,T)
3.0	-	-	1.114 (C)	1.472 (C,T)
3.25	-	-	1.712 (C,T?)	1.882 (C,T)
3.50	-	-	2.004 (T)	2.095 (T)
3.75	-	-	2.003 (T)	2.079 (T)
4.0	-	-	2.025 (T)	1.982 (T)
4.5	0.269 (C)	-	-	-
5.0	0.301 (C)	-	-	-
5.5	0.419 (C)	-	-	-
6.0	1.291 (C)	-	-	-
6.5	1.872 (C)	-	-	-
7.0	2.035 (S)	-	-	-
7.25	2.017 (S)	-	-	-
8.0	2.01 (S)	-	-	-

Table 7.8 - The solubility of cirazoline in 2×10^{-3} M cirazoline hydrochloride-SDDS sytems in the absence and presence of 0.01, 0.05 and 0.1 M sodium chloride, 30°C. Symbols in parentheses represent physical nature of the system, S = clear solution, T = turbid with 'blue haze', C = crystalline suspension.

[SDDS] ($Mx10^3$)	CIRAZOLINE CONCENTRATION ($M \times 10^3$)			
	ADDED SODIUM CHLORIDE CONCENTRATION (M)			
	NIL	0.01	0.05	0.1
NIL	4.76 (S)	4.96 (S)	4.94 (S)	4.74 (S)
5.0	0.184 (C)	0.218 (C)	0.378 (C)	1.05 (C)
5.5	-	0.126 (C)	0.420 (C)	0.88 (C,T?)
6.0	0.086 (C)	0.130 (C)	0.887 (C)	1.61 (C,T)
6.5	-	0.268 (C)	1.80 (C,T)	2.18 (C,T)
7.0	0.168 (C)	0.811 (C)	2.51 (C,T)	2.98 (C,T)
7.5	-	1.37 (C)	3.28 (C,T)	4.36 (C,T)
8.0	0.641 (C)	1.90 (C)	4.14 (T)	4.33 (T)
8.5	1.09 (C)	2.74 (C)	4.00 (T)	4.50 (T)
9.0	1.66 (C)	3.32 (C)	4.09 (T)	4.61 (T)
9.5	2.21 (C)	-	-	-
10.0	2.87 (C)	4.88 (C)	3.98 (T)	4.40 (T)
10.5	3.34 (C)	-	-	-
11.0	3.89 (C)	-	-	-
12.0	4.66 (S)	4.93 (S)	4.78 (S)	4.80 (S)

Table 7.9 - The solubility of cirazoline in 5×10^{-3} M cirazoline hydrochloride-SDDS sytems in the absence and presence of 0.01, 0.05 and 0.1 M sodium chloride, 30°C. Symbols in parentheses represent physical nature of the system, S = clear solution, T = turbid with 'blue haze', C = crystalline suspension.

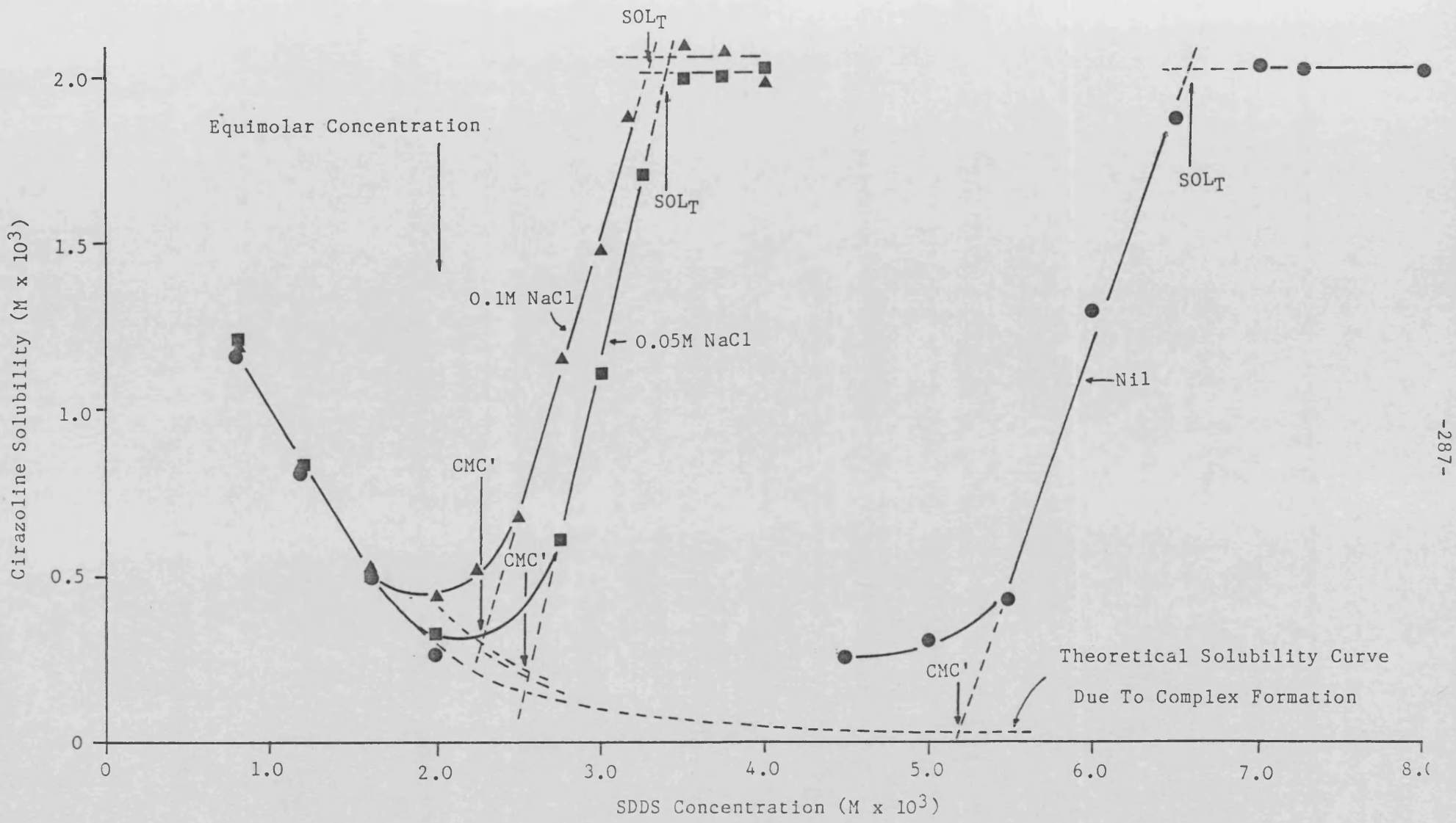

Figure 7.13 - The effect of added sodium chloride concentration on the solubility of cirazoline in 2 x 10^{-3} M cirazoline hydrochloride - SDDS systems at 30°C.

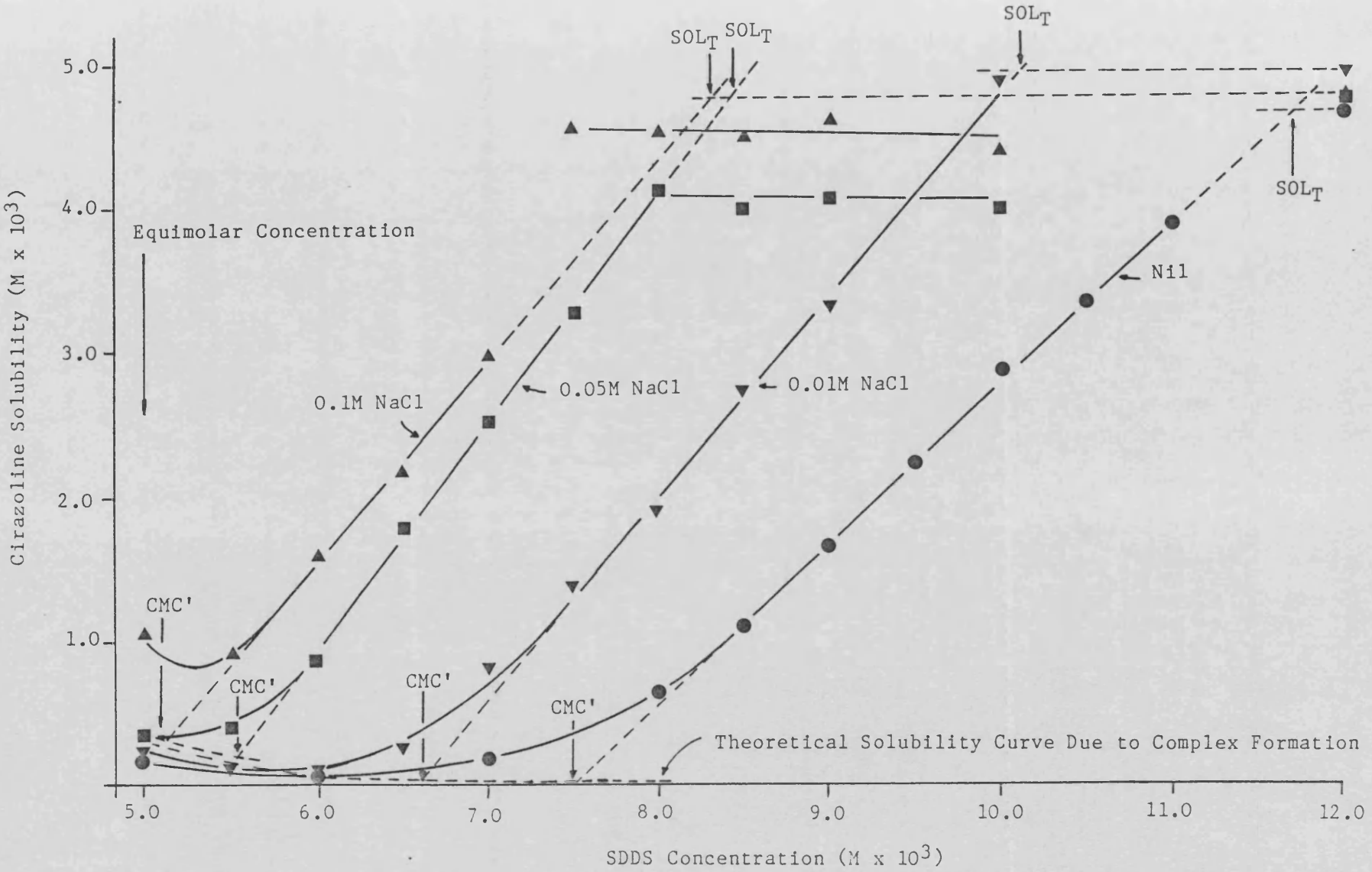

Figure 7.14 - The effect of added sodium chloride concentration on the solubility of cirazoline in 5 x 10^{-3} M cirazoline hydrochloride - SDDS systems at 30°C.

slightly increases the solubility of the cirazoline dodecylsulphate complex at a given SDDS concentration. The CMC' of the system is also lowered with increasing sodium chloride concentration and the solubility curves are shifted to lower SDDS concentration. The physical nature of the system is also affected by the presence of electrolyte. In the absence of sodium chloride partially solubilized systems appear as a suspension of crystalline complex, the quantity of which decreases as cirazoline is solubilized. After filtration the filtrate is a clear, non-viscous solution. In the presence of 0.05 and 0.1 M sodium chloride crystalline complex is again formed but the systems become viscous and turbid with a blue haze, (usually indicative of a colloidal suspension), as cirazoline is solubilized. The turbidity and high viscosity remain after filtration. Birefringence was not detected in these systems when viewed through polarised light indicating the absence of liquid crystalline phase.

Similar results were obtained with the 5×10^{-3} M cirazoline hydrochloride-SDDS systems (table 7.9, figure 7.14). In the absence of and presence of 0.01 M sodium chloride, partially solubilized systems are crystalline suspensions and the filtrate is a clear non-viscous solution. In the presence of 0.05 and 0.1 M sodium chloride, however, systems become increasingly viscous and turbid during the solubilization process. At SDDS concentrations $8 - 10 \times 10^{-3}$ M cirazoline is fully solubilized (i.e. crystalline complex is absent) but the analytical data shows cirazoline solubility is less than the input concentration. Results are erratic and indicate that the sampling technique is not valid in this SDDS concentration region. Clear solutions are formed at very high SDDS concentrations (12×10^{-3} M) well in excess of SOL_T. SOLT points were, therefore,

determined by extrapolation of the linear regions of the solubilization curves to $[CIRHCl]^T$ (figure 7.14).

Micellization and solubilization data for 2 x 10^{-3} M and 5 x 10^{-3} M cirazoline hydrochloride systems are summarised in tables 7.10 and 7.11 respectively.

CMC' values determined by conductimetric titration and solubility show reasonable agreement for both 2 x 10^{-3} M and 5 x 10^{-3} M cirazoline hydrochloride-SDDS systems.

The effect of ionic strength on the CMC and SOL_T is shown in figure 7.15. The 2 x 10^{-3} and 5 x 10^{-3} M cirazoline hydrochloride - SDDS CMC-ionic strength profiles are similar but SOL_T curves are shifted to higher SDDS concentration with increase in initial cirazoline concentration due to the greater amount of formed complex.

Increasing sodium chloride concentration decreases the CMC and SOL_T of both systems. The trend in the SOL_T curves closely follows that of the CMC curve, indicating that sodium chloride primarily affects micellization and not solubilization. Figure 7.16 shows the CMC data plotted according to equation 1.35 ($\log_{10}$ CMC v $\log_{10}$I). The plot is linear with a slope (S.D.) of -0.632 (0.017) which is similar to the reported values of -0.503[93] and -0.675[73] for pure SDDS systems and indicates that ionic strength affects the CMC of cirazoline hydrochloride -SDDS systems in a similar manner to that of the pure surfactant.

K_A values show a decrease in cirazoline association with SDDS micelles as ionic strength is increased, (tables 7.10 and 7.11), e.g. K_A in the absence and presence of 0.1 M sodium chloride was determined as about 3 x 10^4 and 0.4 x 10^4 respectively. However,

[NaCl] ($Mx10^3$)	I at CMC' ($Mx10^3$)	$[CIRH^+_{(aq)}]$ ($Mx10^3$)	SDDS CONCENTRATION ($Mx10^3$)			AGGREGATE RATIO	K_A ($M^{-1}x10^4$)
			CMC'	CMC	SOL_T		
NIL[c]	5.35	0.033	5.36 (5.22-5.56)	3.43	7.04 (6.79-7.31)	0.52	3.1
+NIL	5.25	0.033	5.25	3.29	6.55	0.60	4.0
0.1	5.55	0.033	5.45	3.53	7.05	0.54	3.4
0.5	5.77	0.036	5.27	3.35	6.94	0.53	3.1
1.0[b]	6.30	0.036	5.30 (5.17-5.45)	3.38	6.87 (6.79-6.96)	0.55	3.3
5.0	9.37	0.052	4.37	2.47	6.13	0.52	2.0
10.0[a]	13.9	0.066	3.93 (3.89-3.96)	2.03	5.56 (5.44-5.67)	0.53	1.8
+50.0	52.6	0.199	2.62	0.82	3.46	0.68	1.1
+100.0	102.2	0.348	2.19	0.54	3.32	0.59	0.42

Mean and range of a = two, b = three and c = ten determinations

Table 7.10 - The effect of ionic strength (I) on micellization and solubilization in 2 x 10^{-3} M cirazoline hydrochloride - SDDS systems at 30°C. Data determined by conductimetric titration and solubility (+) studies.

$$\text{Aggregate Ratio} = \frac{[CIRH\text{-}DDS_{(M)}]}{[CIRH\text{-}DDS_{(M)}] + [DDS^-_{(M)}]}$$

[NaCl] ($Mx10^3$)	I at CMC' ($Mx10^3$)	$[CIRH^+_{(aq)}]$ (M x 10^3)	SDDS CONCENTRATION ($Mx10^3$)			AGGREGATE RATIO	K_A ($M^{-1}x10^4$)
			CMC'	CMC	SOL_T		
NIL[a]	7.48	0.042	7.48 (7.36-7.66)	2.71	10.73 (10.49-10.97)	0.60	3.1
+NIL	7.50	0.049	7.50	2.55	11.65	0.54	2.4
+10	16.63	0.080	6.63	1.71	10.12	0.59	1.8
+50	55.6	0.212	5.57	0.78	8.55	0.62	0.76
+100	105.0	0.385	5.10	0.48	8.33	0.59	0.37

a = Mean and range of two determinations

Table 7.11 - The effect of ionic strength (I) on micellization and solubilization in 5 x 10^{-3} M cirazoline hydrochloride-SDDS systems at 30°C. Data determined from conductimetric titration and solubility (+) studies.

$$\text{Aggregate Ratio} = \frac{[CIRH\text{-}DDS_{(M)}]}{[DDS^-_{(M)}] + [CIRH\text{-}DDS_{(M)}]}$$

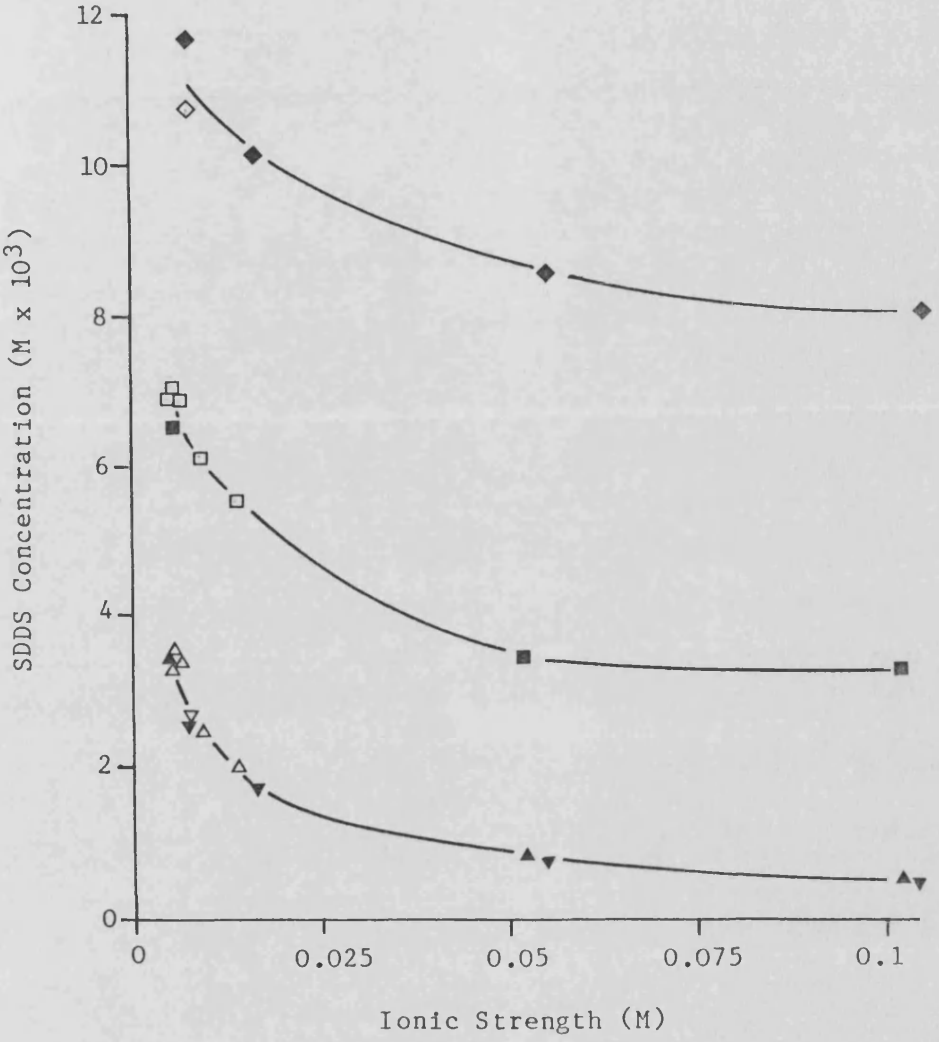

Figure 7.15 - The effect of ionic strength on the CMC and SOL_T of 2×10^{-3} M and 5×10^{-3} M cirazoline hydrochloride - SDDS systems at 30°C as determined by conductimetric titration (CT) and solubility (S) methods.

	2×10^{-3} M		5×10^{-3} M	
	CT	S	CT	S
SOL_T	-□-	—■—	—◇—	—◆—
CMC	-△-	—▲—	—▽—	—▼—

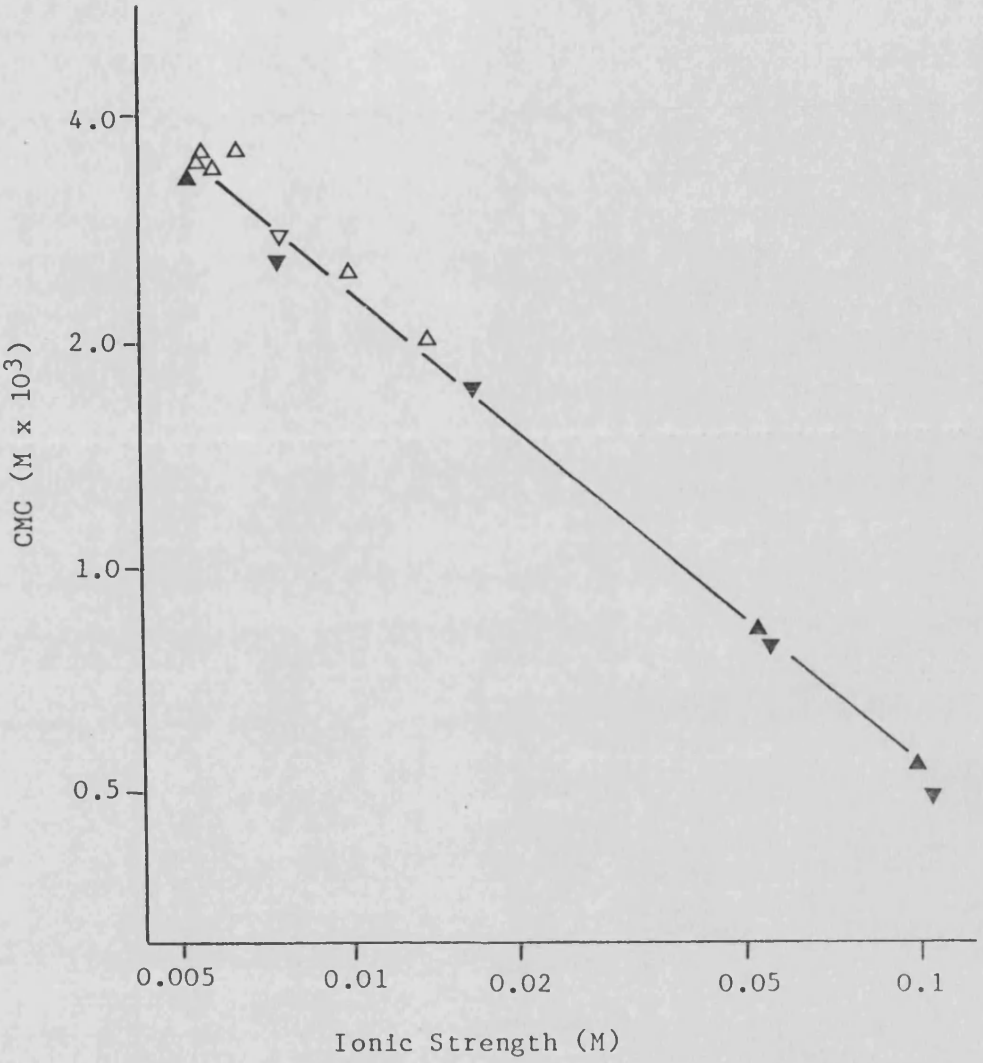

Figure 7.16 - The effect of ionic strength on the CMC of 2 x 10^{-3} M (—▲—), and 5 x 10^{-3} M (—▼—), cirazoline hydrochloride - SDDS systems at 30°C. Data plotted according to equation 1.35. Solid symbols = from solubility studies, open symbols=from conductimetric titration studies.

this trend is due to an increase in aqueous cirazoline solubility and the ratio of cirazoline to dodecylsulphate moieties within the aggregates remains approximately constant and independent of ionic strength at about 0.6 : 1.

7.2 PARTICLE SIZE ANALYSIS

7.2.1 Introduction

Particle size of 2 x 10^{-3} M cirazoline hydrochloride-SDDS systems was determined using the Coulter N4MD sub-micron particle size analyser. This is a is a photon correlation spectrometer (PCS) and estimates particle size from the diffusion coefficient, D, via the Stoke's-Einstein equation:

$$D = \frac{K_B T}{3\pi\eta r} \qquad (7.15)$$

Where K_B is the Boltzmann constant, T is the temperature, η is the viscosity of the diluent and r is the equivalent spherical hydrodynamic diameter. The PCS technique involves illuminating the particles with a laser and measuring the scattered light with photomultipliers. Brownian movement of the particles cause a constantly varying light intensity at the detector. Large, relatively slow moving particles change position slowly and cause slow intensity fluctuations; conversely, small quickly moving particles cause rapid intensity fluctuations. PCS sizes particles by characterising the time scale of these random intensity fluctuations. Detailed PCS theory is set out in standard texts[205].

The Coulter N4MD unimodal analysis provides an estimate of the mean equivalent spherical hydrodynamic diameter and standard deviation of

the distribution assuming a log-normal distribution. A knowledge of the sample temperature and the viscosity and refractive index of the diluent is required to achieve an estimate of particle size.

7.2.2 Experimental

Systems were designed to investigate the size of aggregates both saturated and unsaturated with respect to cirazoline.

Systems for particle size analysis were prepared by the method described for solubility studies (section 7.1.2.1). Samples were filtered (Whatman 25 mm membrane filter, 0.45 μm pore size) and re-equilibrated to temperature for 15 minutes within the Coulter N4MD sample compartment before commencement of particle size analysis. Six x three minute unimodal analyses were performed on each sample.

7.2.3 Results

The effect of SDDS and sodium chloride concentration on the particle size of cirazoline hydrochloride-SDDS systems was investigated at 30°C. Mixtures were prepared containing 2 x 10^{-3} M cirazoline hydrochloride in the absence and presence of 0.05 M and 0.1 M sodium chloride. SDDS concentrations at the CMC' and encompassing the SOL_T of the system were used.

Table 7.12 shows the mean number of counts, mean diffusion coefficient and mean particle diameter for each SDDS concentration in 0.05 M and 0.1 M sodium chloride. Standard deviation of mean diffusion coefficient and mean particle diameter are also shown. The particle size distribution of all samples was extremely broad. Figure 7.17 shows the mean particle diameter - SDDS concentration profile for systems containing 0.05 M and 0.1 M sodium chloride.

[SDDS] ($Mx10^3$)	MEAN NUMBER OF COUNTS ($s^{-1}x10^4$)	MEAN DIFFUSION COEFFICIENT (S.D.) ($cm^2s^{-1}x10^8$)	MEAN UNIMODAL PARTICLE DIAMETER (S.D.) (nm)
0.05 M NaCl			
2.50	17.9	4.57 (0.02)	122 (1)
2.75	46.9	4.20 (0.05)	133 (1)
3.00	86.3	4.16 (0.08)	134 (3)
3.25	147.0	3.27 (0.06)	170 (3)
3.50	175.0	2.77 (0.06)	200 (4)
3.75	182.0	3.10 (0.08)	180 (4)
4.00	211.0	3.56 (0.09)	156 (4)
0.1 M NaCl			
2.25	32.9	3.09 (0.08)	180 (5)
2.50	66.4	2.61 (0.16)	214 (12)
2.75	119.0	2.66 (0.05)	209 (4)
3.00	167.0	2.17 (0.25)	259 (28)
3.25	190.0	2.56 (0.11)	217 (9)
3.50	168.0	2.73 (0.05)	204 (4)
3.75	23.1	3.05 (0.02)	182 (1)
5.00	16.4	7.85 (0.07)	70.9 (1)
8.00	3.66	22.1 (5.0)	26.3 (5.7)

Table 7.12 - Unimodal particle size analysis data for 2 x 10^{-3} M cirazoline hydrochloride-SDDS systems at each SDDS concentration ([SDDS]) and sodium chloride concentration, 30°C. Data represent mean and standard deviation of six analyses per sample.

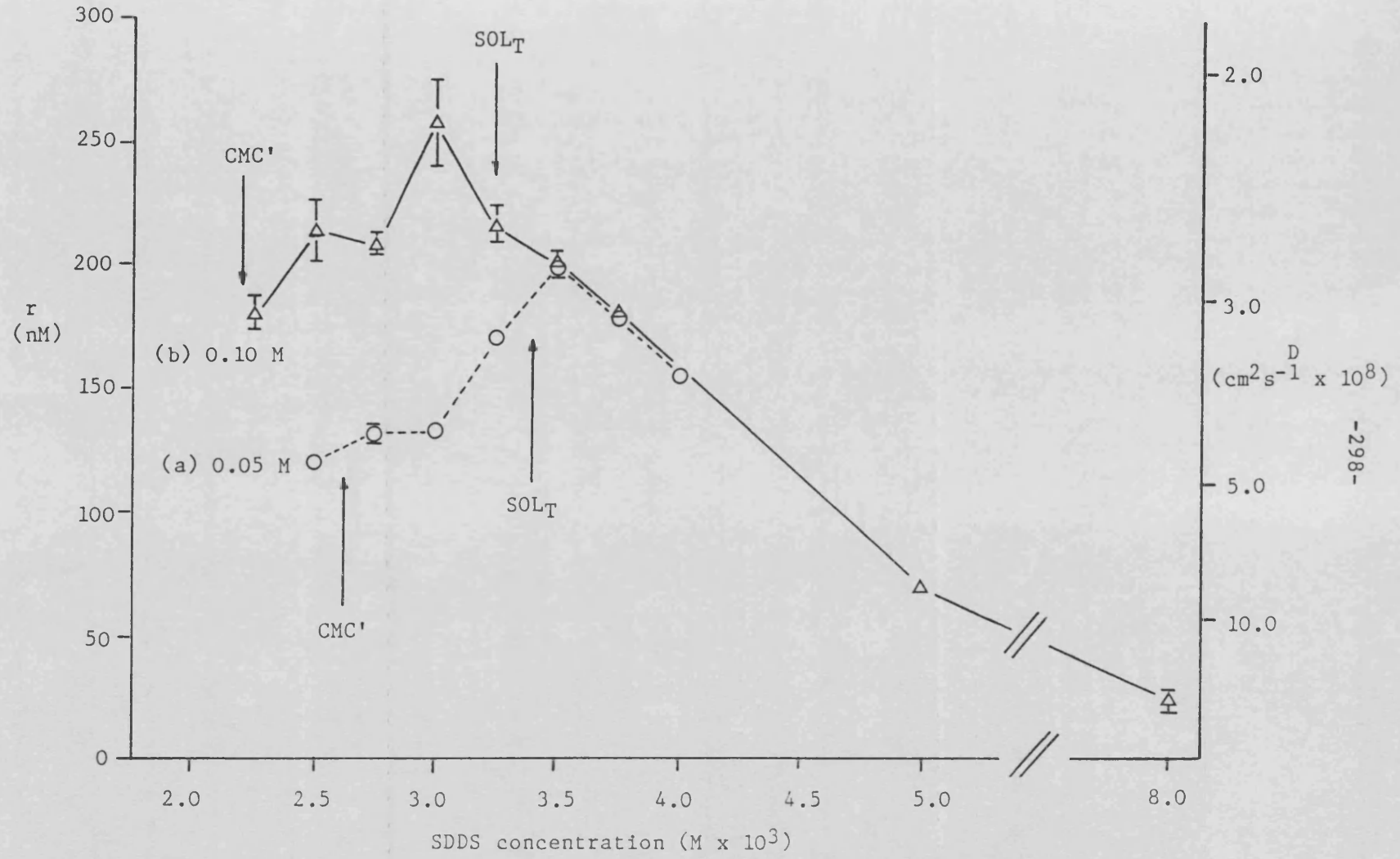

Figure 7.17 - Effect of SDDS concentration on the mean diffusion coefficient, D, and mean particle diameter, r, of aggregates in 2 x 10^{-3} M cirazoline hydrochloride-SDDS systems in the presence of (a) 0.05 M and (b) 0.10 M NaCl, 30°C.

CMC' and SOL_T of each system are shown (data obtained from table 7.10). Systems containing no added electrolyte were prepared using 4.5×10^{-3} - 5×10^{-2} M SDDS. Particle size analysis indicated a small particle size but the scattering intensity of these samples was insufficient for valid particle size analysis.

The particle size of SDDS aggregates in the presence of 2×10^{-3} M cirazoline hydrochloride and 0.05 M and 0.1 M sodium chloride is extremely large with a broad particle size distribution. In both systems the lowest SDDS concentration studies approximates to the CMC' of the system (2.19×10^{-3} M in 0.1 M NaCl, 2.62×10^{-3} M in 0.05 M NaCl, table 7.10). Increasing SDDS concentration above the CMC results in an initial increase in particle size up to a maximum associated with the total solubilization concentration, SOL_T, (3.32×10^{-3} M in 0.1 M NaCl, 3.46×10^{-3} M in 0.05 M NaCl, table 7.10). Further increases in SDDS concentration after total solubilization of cirazoline result in a decrease in particle size. For example, in 0.1 M NaCl the mean particle diameter rose from 180 nm close to the CMC to 259 nm at SDDS concentration near the SOL_T, then decreased to 26.3 nm at 8×10^{-3} M SDDS. Similar effects are observed with the 0.05 M NaCl system (figure 7.17). This suggests that particle size increases as the concentration of SDDS aggregates saturated with cirazoline increases, then decreases as the degree of unsaturation increases.

Electrolyte concentration has two effects on aggregation. Increasing electrolyte concentration decreases the CMC of the system and thereby increases the concentration of micellar surfactant at a given SDDS concentration. This effect is shown by the shift in peak particle size from 3.5×10^{-3} M SDDS in 0.05 M NaCl to 3.0×10^{-3} M SDDS in

0.1 M NaCl. Electrolyte concentration also affects the nature of the aggregates. In the absence of sodium chloride a small particle size was indicated (although scattering intensities were too low for valid analysis). In systems containing added electrolyte, for a given concentration of micellized SDDS, an increase in NaCl concentration caused an increase in the size of the aggregates. This effect is shown as a shift in the mean particle diameter - SDDS curve to higher particle diameter with increasing NaCl concentration (figure 7.17). The peak particle size diameter in the 0.1 M NaCl system is 259 nm and occurs at a micellar SDDS concentration of 0.75×10^{-3} M. In 0.05 M NaCl, however, peak particle diameter is smaller - 200 nm - and is associated with a slightly greater micellar SDDS concentration - 0.88×10^{-3} M.

8. KINETICS OF IMIDAZOLINE HYDROLYSIS

8.1 INTRODUCTION

First order rate constants for the hydrolysis of cirazoline and other imidazolines were determined at constant pH and temperature. Samples were withdrawn at known intervals during the hydrolysis, analysed and the percent residual concentration calculated by one of the methods described in section 3.1.6. Samples were normally taken at ten time intervals during each experiment. All data were fitted to the first order rate equation (equation 1.4) using linear regression analysis to obtain the observed first order rate constant.

Reactions in the absence of SDDS were usually followed down to a percent residual concentration below 60%. Due to the relatively slow rate in SDDS solutions, reactions in the presence of surfactant were normally only followed down to a percent residual concentration of about 80%. This limitation was also a result of the desire to avoid large amounts of degradation product which may disrupt the structure of the cirazoline-SDDS system.

pH control during degradation was effected either by pH-statting or the use of buffers.

(a) Buffered Solutions

The choice of a buffering system was dictated by the following:

(i) pH required,

(ii) chemical nature of buffer materials,

(iii) buffer capacity required,

(iv) dilution value,

(v) neutral salt effects,

(vi) temperature coefficient,

(vii) stability.

Kinetic studies in buffered systems were performed in equimolal (0.025 m) phosphate buffer, pH 6.87 at 25°. This system was chosen as this is an NBC primary standard, has good buffer capacity at pH 7 and a low temperature coefficient.

(b) pH Statting Technique

The pH-stat technique maintains pH by the addition of titrant to the reaction flask. The automated pH-stat assembly used in this study consisted of a two-necked, round bottomed reaction flask, magnetic stirrer, combined glass - silver/silver chloride pH electrode, PHM 61 pH meter, TTT60 titrator and ABU12 autoburette with micro-delivery tube. A diagramatic representation of the apparatus is shown in figure 8.1. The pH of the stirring reaction mixture is maintained by addition of titrant from the autoburette. Flow of titrant is controlled by the titrator, which is connected directly to the pH meter and autoburette. The required pH is set on the titrator through the end-point control. As the pH of the solution changes during the hydrolysis process, the titrator activates the autoburette and titrant is added to the reaction vessel. When the pH reaches the

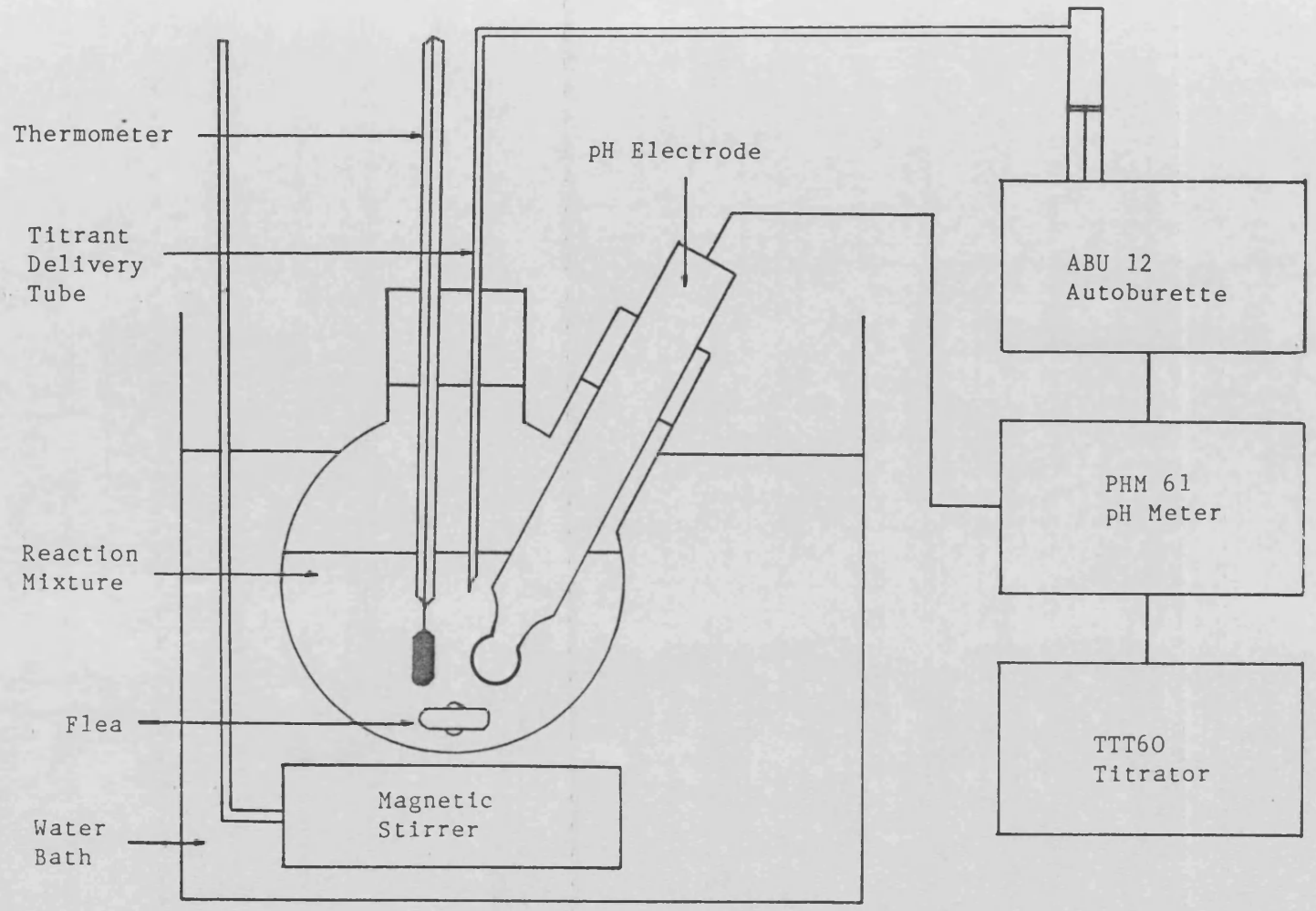

Figure 8.1 - Diagram of automated pH-stat apparatus.

required value, the titrator deactivates the autoburette and the flow of titrant is stopped. The rate of addition and concentration of titrant must be carefully selected to avoid pH drift, (insufficient titrant addition) or pH overshoot, (excess titrant addition) during the experiment.

In studies where the rate of hydrolysis- and hence rate of change of pH - is low (defined as kinetic reactions with half-life > 2 days), satisfactory pH control may be obtained by adding titrant manually. This technique was necessary for studies involving SDDS where the pH electrode cannot be left in the reaction mixture for long periods (section 2.2.5.3).

8.2 EXPERIMENTAL

8.2.1 General Procedures For Kinetic Studies

(a) Using Buffered Solution

95 ml of equimolal phosphate buffer solution were placed in a stoppered 200 ml volumetric flask and equilibrated in a constant temperature water bath. 5.0 ml of appropriate stock solution of drug was added and the flask shaken. A 4.0 ml sample was withdrawn after about 2 minutes equilibration time (= time zero), added to 1 ml of 0.1 M HCl to stop the reaction and suitably diluted for assay. Repeat 4 ml samples were withdrawn at appropriate intervals and similarly prepared for assay. The pH of the reaction mixture was measured at the start and end of the experiment and in all cases was found to be within $\pm$0.05 pH units of the stated pH of equimolal phosphate buffer at the reaction temperature.

(b) Using Automated pH-stat Apparatus

The pH required was set on the titrator of the pH-stat assembly and the burette filled with the appropriate concentrations of sodium hydroxide titrant (0.02 - 0.2 M). 95 mls of double distilled water were placed in the reaction flask and equilibrated in a constant temperature water bath. The magnetic stirrer was switched on and 5 ml of cirazoline hydrochloride stock solution were added to the reaction vessel. The pH-stat assembly was switched on and titrant delivered until the pH reached the required value. Further quantities of titrant were added automatically to counteract the fall in pH during hydrolysis. A 4 ml sample was withdrawn immediately after reaching the desired pH (=time zero), added to 1 ml of 0.1 M HCl to stop the reaction and suitably diluted for assay. 4 ml samples were withdrawn at appropriate intervals and similarly prepared for assay.

In studies involving high pH (> pH 9) or low pH (< pH 5), 95 ml of sodium hydroxide or hydrochloric acid solution of appropriate concentration were equilibrated to temperature and 5 ml of cirazoline hydrochloride stock solution added. This reduced the time and volume of titrant required to bring the cirazoline reaction solution to the desired pH.

In all automated pH-stat experiments the volume of titrant added was small (< 1 ml). The dilution effect is therefore minimal and was ignored in kinetic calculations.

(c) Using Manual pH-stat

The reaction mixture was prepared at room temperature by mixing the required amounts of stock solutions in a 100 ml volumetric flask and making up to volume (100 ml) with double distilled water. The mixture was immediately shaken, transferred to a stoppered 100 ml conical flask and equilibrated in a constant temperature water bath. The pH was then raised to pH 7.0 by the dropwise addition of sodium hydroxide solution (0.001-0.1 M). A 4 ml sample was withdrawn, (= time zero), and added to 1 ml of 0.1 M HCl to stop the reaction and suitably diluted for assay. 4 ml samples were withdrawn at appropriate intervals and similarly prepared for assay. pH was monitored throughout the experiment and adjusted as necessary by the dropwise addition of sodium hydroxide or hydrochloric acid solution (0.001 -0.01 M). Volume of titrant added and pH readings were recorded for each experiment. In all manual pH-stat experiments the volume of titrant added was small (< 2 ml). The dilution effect is therefore minimal and was ignored in kinetic calculations.

In studies involving SDDS, reaction mixtures were equilibrated for longer periods before commencing the kinetic study to allow for possible phase transitions. At 30°C, systems were left stirring for 24 hours, whereas at 50°C 1 hour was found to be sufficient. Assay results show the amount of degradation during equilibration to be negligible. Systems containing insoluble complex were continually stirred using a magnetic stirrer and flea to ensure intimate mixing of phases and to prevent deposition. During pH measurement the magnetic stirrer was switched off and readings were taken as rapidly as possible to minimise adsorption on to the electrode (see section 2.2.5.3).

pH measurements during kinetic experiments were normally within ± 0.05 pH units of the desired pH. Any trend in measured pH values was compensated for by adjusting the pH to a value slightly beyond the nominal pH (± 0.1 pH unit). As pH adjustment was usually carried out numerous times between samples, the mean pH is thought to be within ± 0.05 pH units of the desired pH.

8.2.2 Reproducibility of pH-statting Techniques

The degradation of cirazoline hydrochloride at 30°C was monitored twelve times using the manual pH-stat method (pH 7.0) on two different dates spaced five months apart, and three times using the automated pH-stat method (pH 7.1) on two different dates spaced nine months apart. Percent residual concentration was calculated by method 3 (section 3.1.6) and derived first order rate constants are shown in table 8.1.

The manual pH-stat data show satisfactory reproducibility (S.D. = 0.18, CV = 9%) and a t-test on the data obtained on 22.1.86 and 23.6.86 show the data to be indistinguishable at the P = 0.05 level (t_{calc} = 1.032, t_{tab} = 2.23). The automated pH-stat technique is also reproducible (S.D. = 0.16, CV = 6%). The mean k_{obs} value obtained by this technique is 32% greater than that obtained by the manual method. This is consistant with a pH difference of + 0.12 pH units (measured pH difference = + 0.10 pH units) assuming cirazoline is only subject to specific base catalysis under these conditions (see section 8.3.2).

METHOD	DATE	k_{obs} (S.D.) $s^{-1} \times 10^6$	Mean k_{obs} (S.D.) $s^{-1} \times 10^6$
Automated (pH 7.1)	29.4.85	2.73 (0.01)	
	22.1.85	2.72 (0.18)	
		2.47 (0.04)	
		TOTAL:	2.64 (0.16)
Manual (pH 7.0)	22.1.86	1.83 (0.11)	
		2.14 (0.14)	
		2.05 (0.40)	
		2.12 (0.11)	
		1.77 (0.23)	
		1.87 (0.09)	
		1.76 (0.11)	1.93 (0.16)
	23.6.86	2.02 (0.02)	
		2.30 (0.08)	
		1.98 (0.05)	
		1.94 (0.02)	
		2.25 (0.06)	2.10 (0.16)
		TOTAL:	2.00 (0.18)

Table 8.1 - Reproducibility of automated and manual pH-statting techniques. First order rate constants (k_{obs}) for the degradation of cirazoline hydrochloride at pH 7.1 (automated) and pH 7.0 (manual), 30°C determined on the date shown.

8.3 RESULTS

8.3.1 Order of Reaction

The order of reaction with respect to cirazoline hydrochloride concentration was determined using time and concentration based methods. All percent residual concentration values were calculated by reference to both cirazoline and CPAE concentrations (method 3, section 3.1.6).

8.3.1.1 TIME BASED METHODS

The order of reaction was calculated by three different methods: (i) fractional lifetime method, (ii) integration method and (iii) the Guggenheim method. The latter method is normally used for the determination of first order rate constants but a linear Guggenheim plot is indicative of first order kinetics.

Data were generated by degrading 2 x 10^{-3} M cirazoline hydrochloride at pH 7.1 and 60°C using the automated pH-statting technique. The hydrolysis was followed to a percent residual concentration of 12.5% - equivalent to three half-life periods. Results and calculated data are shown in table 8.2.

(i) Fractional Lifetime Method

The integrated form of equation 1.2 may be expressed by equation 8.1:

$$\log_{10} t_{1/y} = (1 - n) \log_{10} [S_o] \qquad (8.1)$$

Where $t_{1/y}$ is the time taken for the initial concentration of substrate, $[S_o]$, to fall by a fraction 1/y and n is the order of reaction. The order of reaction can therefore be determined from the slope of a plot of $\log_{10} t_{1/y}$ against $\log_{10} [S_o]$.

TIME (MINS)	PERCENT RESIDUAL CONCENTRATION	Δ[S] (Δt = 60 MINUTES)
0	100.0	50.9
20	77.5	39.1
40	61.1	-
60	49.1	24.8
80	38.4	19.1
95	32.6	-
120	24.3	11.7
140	19.3	-
160	15.1	-
180	12.6	-

Table 8.2 - Sample times, percent residual concentration values and Guggenheim calculated data, Δ[S], for the hydrolysis of cirazoline hydrochloride at pH 7.1, 60°C.

PERCENT RESIDUAL CONCENTRATION	$t_{3/4}$ (MINS)
100.00	24.0
75.00	24.0
56.25	25.5
42.19	25.5
31.64	24.0
23.73	23.3
17.80	23.3

Table 8.3 - Time taken for the percent residual concentration to decrease by successive fractions of 3/4 ($t_{3/4}$) for the hydrolysis of cirazoline hydrochloride at pH 7.1, 60°C.

The time taken for the percent residual concentration to decrease by successive fractions of 3/4 ($t_{3/4}$) was determined by plotting percent residual concentration against time (figure 8.2). Results are shown in table 8.3. A plot of $\log_{10} t_{3/4}$ against $\log_{10} [S_o]$ was constructed and the slope, determined by linear regression analysis, was found to be -1.796×10^{-2} M^{-1} (S.D. = 3.09×10^{-2} M^{-1}) and the order of reaction with respect to time was calculated as 1.018.

(ii) Integration Method

The order of reaction can be determined by plotting experimental data according to each of the integrated rate equations (equations 1.3 to 1.5). A linear plot is obtained when the integrated form of the correct rate law is used. For a first order reaction, a plot of percent residual concentration on a $\log_{10}$ scale versus time is linear with a slope equal to - k/2.303 (equation 1.4). Such a plot was constructed using data for the hydrolysis at pH 7.0, 60°C (figure 8.3). Linear regression analysis data gave a slope of -1.157×10^{-2} min^{-1} (S.D. = 0.009×10^{-2} min^{-1}) and correlation coefficient of 0.9998. The small error of slope (CV = 0.8%) and good correlation coefficient value indicate a linear plot which is consistant with a first order reaction.

(iii) Guggenheim Method

The Guggenheim method involves calculating the change in concentration, $\Delta[S]$, of a reactant over a fixed time interval, Δt. Equation 1.6 predicts a plot of $\Delta[S]$ on a $\log_{10}$ scale against time is linear for a first order reaction with a slope equal to $-\frac{k}{2.303}$.

A time interval of 60 minutes (approximately equivalent to the half-life of the reaction) was used. Data are give alongside the

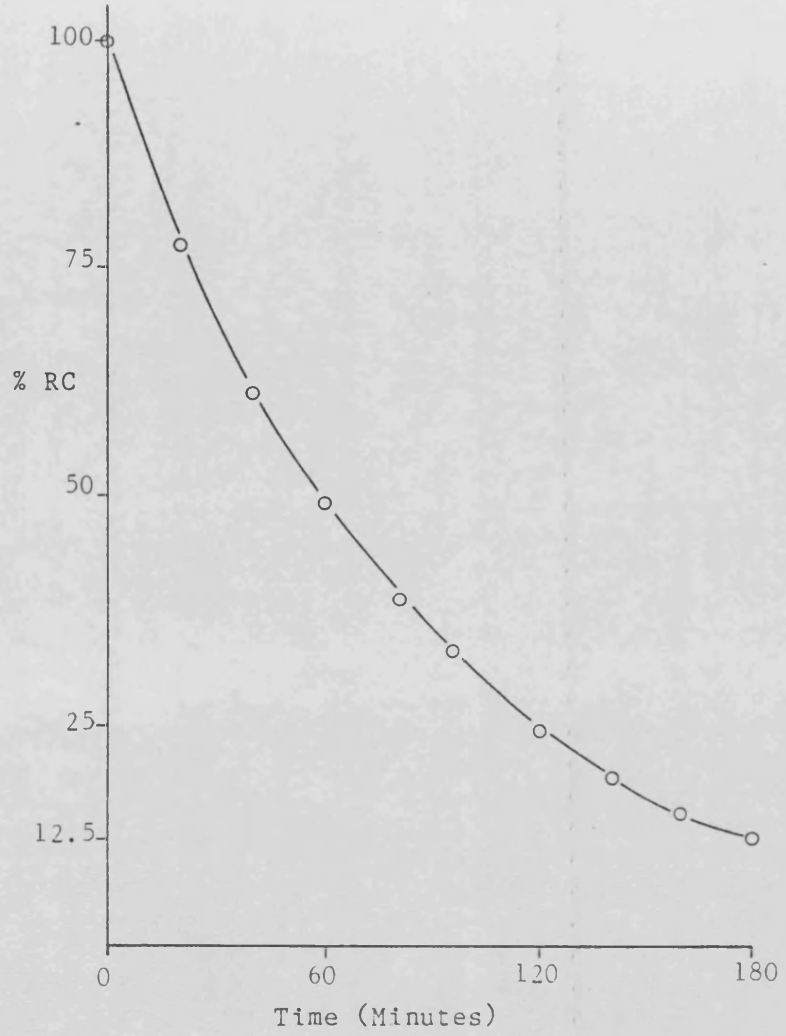

Figure 8.2 - Percent residual concentration (% RC) against time for the hydrolysis of cirazoline hydrochloride at pH 7.1, 60°C.

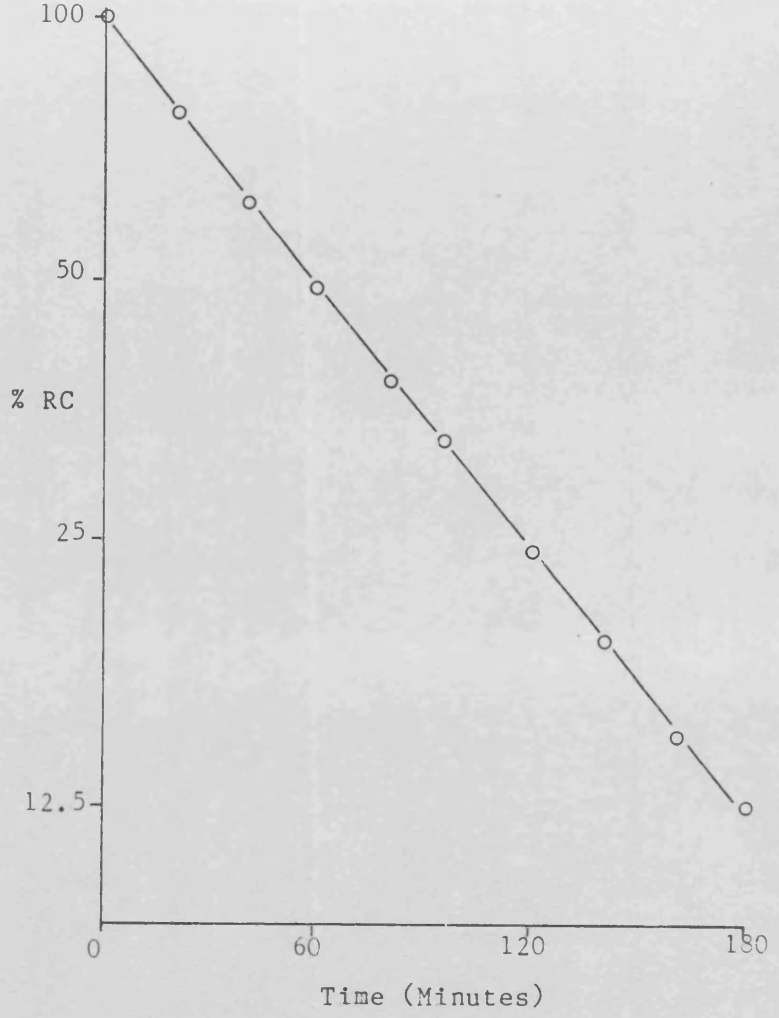

Figure 8.3 - Percent residual concentration (% RC) on a $\log_{10}$ scale against time for the hydrolysis of cirazoline hydrochloride at pH 7.1, 60°C. (First order plot).

hydrolysis data in table 8.2 and the Guggenheim plot is shown in figure 8.4. Linear regression analysis on the Guggenheim data gave a slope of -1.217×10^{-2} min^{-1} (S.D. = 0.014×10^{-2} min^{-1}) and a correlation coefficient of 0.9998. The small error of slope (CV = 1.2%) and good correlation coefficient indicate a linear plot and a first order reaction.

8.3.1.2 CONCENTRATION BASED METHODS

The order with respect to concentration may be determined by the Van't Hoff method of initial rates. Equation 1.2 may be written in the form:

$$\log_{10}\left(\frac{-d[S]}{dt}\right)_o = \log_{10} k_{obs} + n \log_{10} [S_o] \qquad (8.2)$$

Where the subscript $_o$ denotes initial values. A plot of $\log_{10}$ initial rate against $\log_{10}$ initial substrate concentration thus yields the order of reaction with respect to concentration from the slope.

Hydrolysis reactions were conducted at pH 7.0 and 30°C using the manual pH-statting technique. Initial cirazoline hydrochloride concentrations of 2×10^{-4} - 5×10^{-3} M were used and reactions were followed down to a percent residual concentration of about 50%. Results are shown in table 8.4.

The initial rate of each reaction was determined by plotting percent residual concentration against time and drawing a tangent to the curve at time zero, as shown for 5×10^{-3} M initial concentration in figure 8.5. The initial rate was calculated from the product of initial concentration, $[S_o]$, and the slope of the tangent. Results are shown in table 8.5. A plot of $\log_{10} (-d[S]/_{dt})_o$ against $\log_{10}$

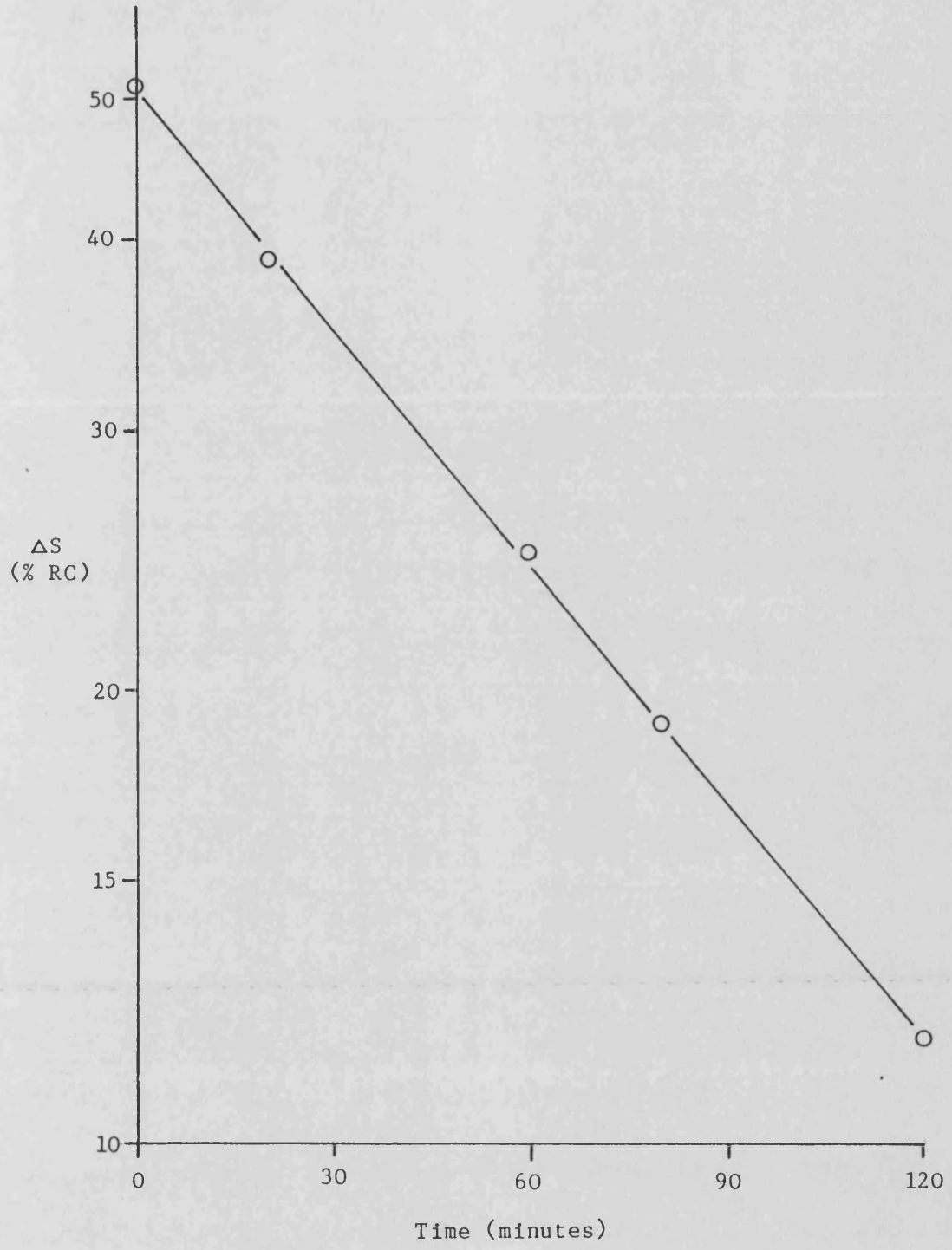

Figure 8.4 - Guggenheim plot for the hydrolysis of cirazoline hydrochloride at pH 7.1, 60°C. Data plotted according to equation 1.6, ΔS = change in percent residual concentration (% RC), Δt = time interval = 60 minutes.

TIME (HOURS)	PERCENT RESIDUAL CONCENTRATION				
	2×10^{-4}M	5×10^{-4}M	1×10^{-3}M	2×10^{-3}M	5×10^{-3}M
0	100.0	100.0	-	100.0	99.2
4.2	-	97.5	96.5	96.9	96.2
18.1	88.4	89.3	87.3	89.4	88.4
27.8	82.6	83.7	82.1	83.3	82.6
42.1	73.2	73.8	75.1	74.7	73.8
51.7	68.7	68.2	69.5	69.3	69.0
66.2	58.8	60.9	62.4	62.9	62.1
75.7	55.4	56.4	58.7	58.0	58.7
90.8	47.9	49.4	51.8	52.3	53.0
99.4	42.4	46.6	47.3	48.5	50.0

Table 8.4 - Sample times and percent residual concentration values for the hydrolysis of cirazoline hydrochloride at pH 7.0, 30°C at each initial concentration shown.

CIRAZOLINE CONCENTRATION (M)	INITIAL RATE ($M\ s^{-1} \times 10^8$)
2×10^{-4}	0.0352
5×10^{-4}	0.0855
1×10^{-3}	0.182
2×10^{-3}	0.338
5×10^{-3}	0.841

Table 8.5 - Initial rate of hydrolysis of cirazoline hydrochloride at pH 7.0, 30°C at each initial concentration.

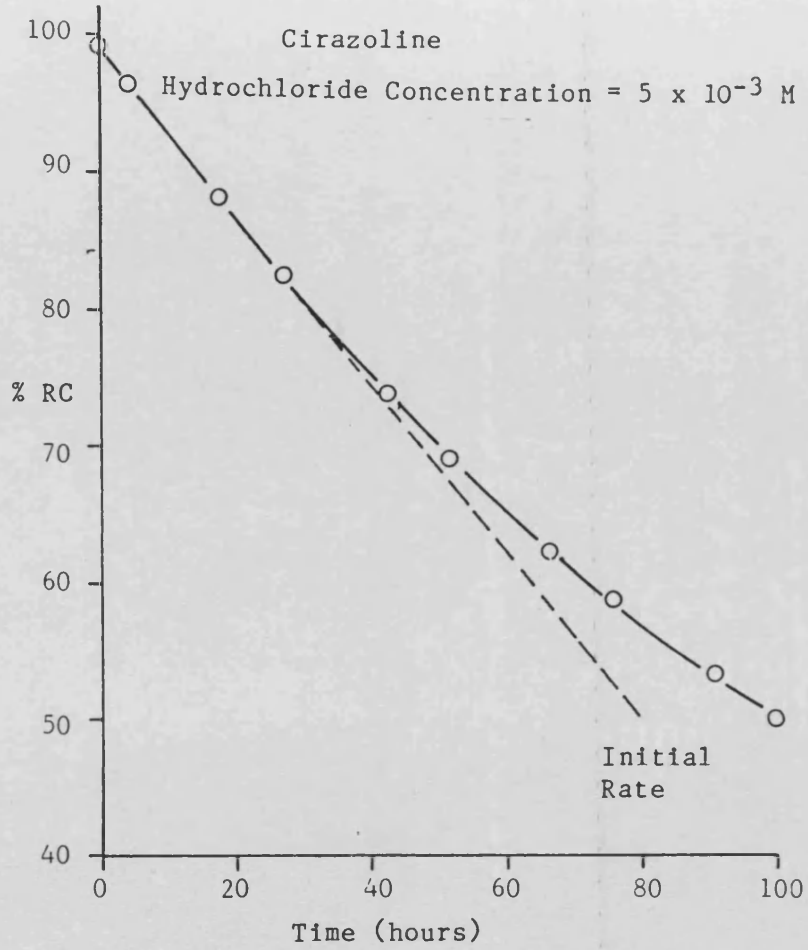

Figure 8.5 - Percent residual concentration (% RC) against time for the hydrolysis of cirazoline hydrochloride at pH 7.0, 30°C.

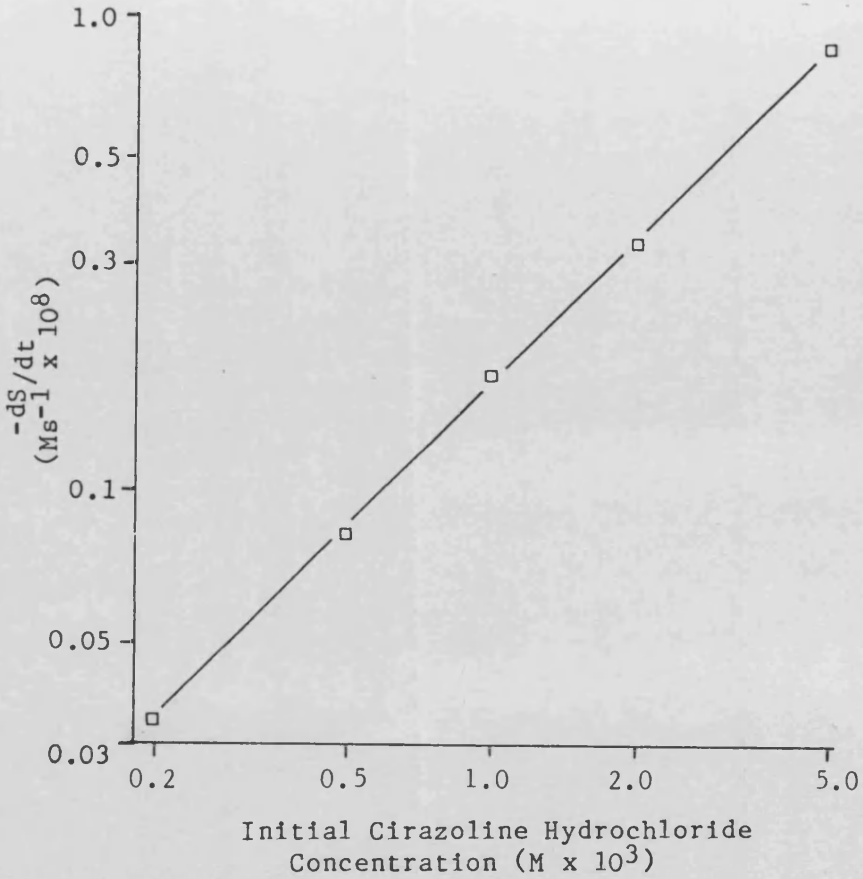

Figure 8.6 - Double $\log_{10}$ plot of initial rate of cirazoline hydrochloride hydrolysis ($-dS/dt$) against initial cirazoline hydrochloride concentration for the reaction at pH 7.0, 30°C.

$[S_o]$ was constructed and the slope determined by linear regression analysis (figure 8.6). The order of reaction with respect to concentration was found to be 0.988 (S.D. = 0.014).

8.3.2 Effect of pH

The effect of pH on the hydrolysis of 2×10^{-3} M cirazoline hydrochloride was studied using the automated pH-statting technique. The large range in rate constants necessitated two experiment temperatures - reactions at pH $\leq$7.1 were performed at 70°C and those at pH $>$ 7.1 at 25°C. Percent residual concentration was calculated by reference to both cirazoline and CPAE concentration (method 3, equation 3.8, section 3.1.6) except for the reaction at pH 1.1, 70°C where hydrolysis of CPAE was significant; percent residual concentration was therefore calculated by method 1 (equation 3.6, section 3.1.6). The reaction at pH 13.1 was undertaken at an initial cirazoline concentration of 4×10^{-4} M due to the poor solubility of the cirazoline free base.

The observed rate constant, k_{obs}, at each pH for reactions at 70°C and 25°C are shown in tables 8.6 and 8.7 respectively. Theoretical rate constants calculated as shown in section 8.3.2.1 are also given. Observed and theoretical pH profiles at 70°C and 25°C are shown in figures 8.7 and 8.8 respectively. The observed pH profile at 70°C shows the hydrolysis of cirazoline to be almost independent of pH in moderately strong acidic solutions (pH <3). Above about pH 4 the rate constant increases dramatically with pH indicating cirazoline hydrochloride is susceptable to specific base catalysis. The observed first order rate constant is extremely sensitive to pH change in the region pH 7.1 - 9.1 but becomes independent of pH above about pH 11.

pH	a_{OH^-} (M)	k_{obs} (S.D.) (s^{-1} x 10^6)	f_{SH^+}	$\frac{k_{obs}-k_o}{f_{SH^+}}$ (s^{-1}x10^6)	k_2 ($M^{-1}s^{-1}$)	k_T (s^{-1}x10^6)
1.1*	1.905×10^{-12}	1.03(0.03)	>0.999	-	-	1.18
2.1	1.905×10^{-11}	1.20(0.02)	>0.999	-	-	1.18
3.1	1.905×10^{-10}	1.32(0.01)	>0.999	-	-	1.23
4.1	1.905×10^{-9}	1.68(0.01)	>0.999	0.4	262	1.68
4.6	6.023×10^{-9}	2.73(0.05)	>0.999	1.4	257	2.75
5.1	1.905×10^{-8}	5.50(0.06)	>0.999	4.2	227	6.15
6.1	1.905×10^{-7}	60.2(1.0)	0.995	59.2	311	50.6
7.1	1.905×10^{-6}	451(7)	0.952	472	248	474

Table 8.6 - The effect of pH on the hydrolysis of 2 x 10^{-3} M cirazoline hydrochloride at 70°C. k_{obs} = observed first order rate constant, f_{SH^+} = fraction of protonated cirazoline species calculated using pK_a' = 8.40, k_2 = specific base catalysed rate constant calculated using equation 8.4, k_T = theoretical rate constant calculated using equation 8.6, k_o = uncatalysaed reaction rate constant, a_{OH^-} = hydroxyl ion activity calculated using pK_w = 12.82. (* = 1.6 x 10^{-3} M cirazoline hydrochloride).

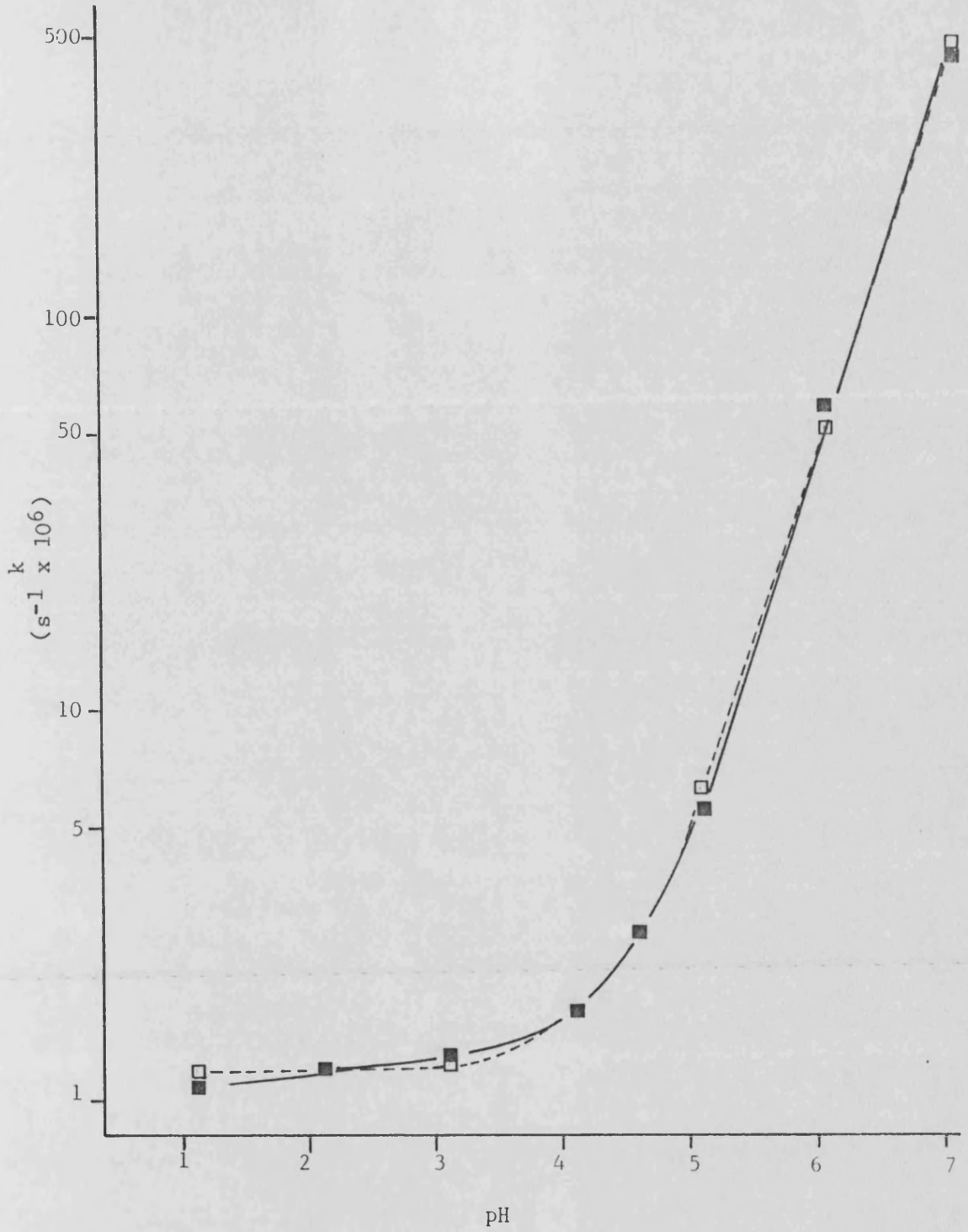

Figure 8.7 - Observed, (—■—), and theoretical, (--□--), stability-pH profiles, (first order rate constant on $\log_{10}$ scale against pH), for the hydrolysis of cirazoline hydrochloride at 70°C. Theoretical rate constants calculated using equation 8.6.

pH	a_{OH^-} (M)	k_{obs} (S.D.) (s^{-1} x 10^6)	f_{SH^+}	k_{obs}/f_{SH^+} (s^{-1})	k_2 ($M^{-1}s^{-1}$)	k_T ($s^{-1}x10^6$)
7.1	$1.259x10^{-7}$	1.24(0.02)	0.9960	$1.25x10^{-6}$	9.93	0.92
7.6	$3.981x10^{-7}$	3.96(0.04)	0.9876	$4.01x10^{-6}$	10.07	2.90
8.1	$1.259x10^{-6}$	8.36(0.10)	0.9617	$8.69x10^{-6}$	6.90	8.92
8.6	$3.981x10^{-6}$	25.6(0.3)	0.8882	$2.88x10^{-5}$	7.23	26.1
9.1	$1.259x10^{-5}$	64.2(0.3)	0.7153	$8.98x10^{-5}$	7.13	66.4
9.6	$3.981x10^{-5}$	116 (1)	0.4427	$2.62x10^{-4}$	6.58	130
10.1	$1.259x10^{-4}$	171 (1)	0.2008	$8.52x10^{-4}$	6.77	186
10.6	$3.981x10^{-4}$	193 (1)	$7.359x10^{-2}$	$2.62x10^{-3}$	6.59	216
11.1	$1.259x10^{-3}$	202 (1)	$2.450x10^{-2}$	$8.25x10^{-3}$	6.55	227
12.1	$1.259x10^{-2}$	213 (1)	$2.506x10^{-3}$	$8.50x10^{-2}$	6.75	233
13.1*	$1.259x10^{-1}$	206 (3)	$2.511x10^{-4}$	$8.20x10^{-1}$	6.52	233

Table 8.7 - The effect of pH on the hydrolysis of 2 x 10^{-3} M cirazoline hydrochloride at 25°C. k_{obs} = observed first order rate constant, f_{SH^+} = fraction of protonated cirazoline species calculated using pK_a' = 9.50, k_2 = specific base catalysed rate constant calculated using equation 8.8, k_T = theoretical rate constant calculated using equation 8.10, a_{OH^-} = hydroxyl ion activity calculated using pK_w = 14.00 (* = 4 x 10^{-4} M cirazoline hydrochloride).

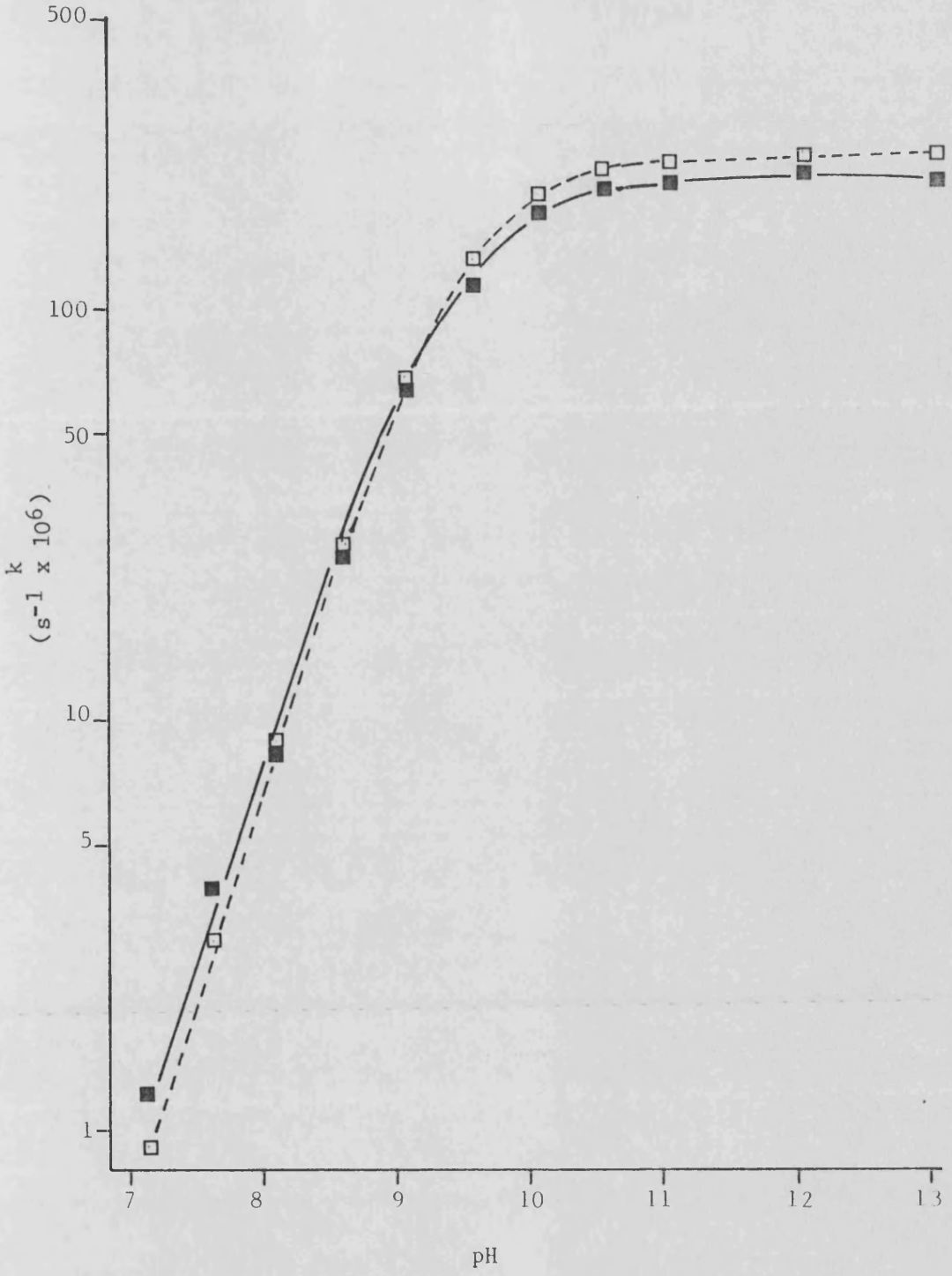

Figure 8.8 - Observed, (—■—), and theoretical, (--□--), stability-pH profiles, (first order rate constant on $\log_{10}$ scale against pH), for the hydrolysis of cirazoline hydrochloride at 25°C. Theoretical rate constants calculated using equation 8.10.

8.3.2.1 TREATMENT OF DATA AND CALCULATION OF THEORETICAL RATE CONSTANTS

(a) Calculation of k_o and k_2 values at 70°C

At pH 1-3 the hydrolysis is almost independent of pH which is characteristic of an uncatalysed reaction involving attack of neutral water. It may therefore be assumed that in this pH range the base (and acid) catalysed reaction(s) are negligible and providing also that the hydrolysis of the free base species is negligible (pK_a = 8.4 at 70°C, section 4.2.4), equation 1.10 reduces to equation 8.3:

$$k_{obs} = k_o \qquad (8.3)$$

as $k_2\ [OH^-] = k_1\ [H_3O^+] = 0$ and $f_{SH^+} \cong 1$ at pH 1-3.

The mean k_o values (pH 1.1-3.1) was thus calculated as 1.18×10^{-6} (S.D. 0.15×10^{-6}) s^{-1}. Ionic strength effects at low pH (<3) are discussed in section 8.3.2.1 c).

At pH >3.1 the base catalysed reaction becomes significant and providing the contribution from the free base hydrolysis to the overall reaction is minimal, the reaction may be described by equations 8.4 and 8.5.

$$k_{obs} = (k_o + k_2\ [OH^-]).f_{SH^+} \qquad (8.4)$$

and at low ionic strengths when $a_{OH^-} \cong [OH^-]$,

$$\log_{10}\left(\frac{k_{obs}}{f_{SH^+}}\right) - k_o = \log_{10} k_2 - pK_w + pH \qquad (8.5)$$

Figure 8.9 shows the pH 4.1 - 7.1 data plotted according to equation 8.5. Linear regression analysis gave: correlation coefficient = 0.9991, slope = 1.007 (SD 0.024) and intercept = -10.44 (SD 0.13).

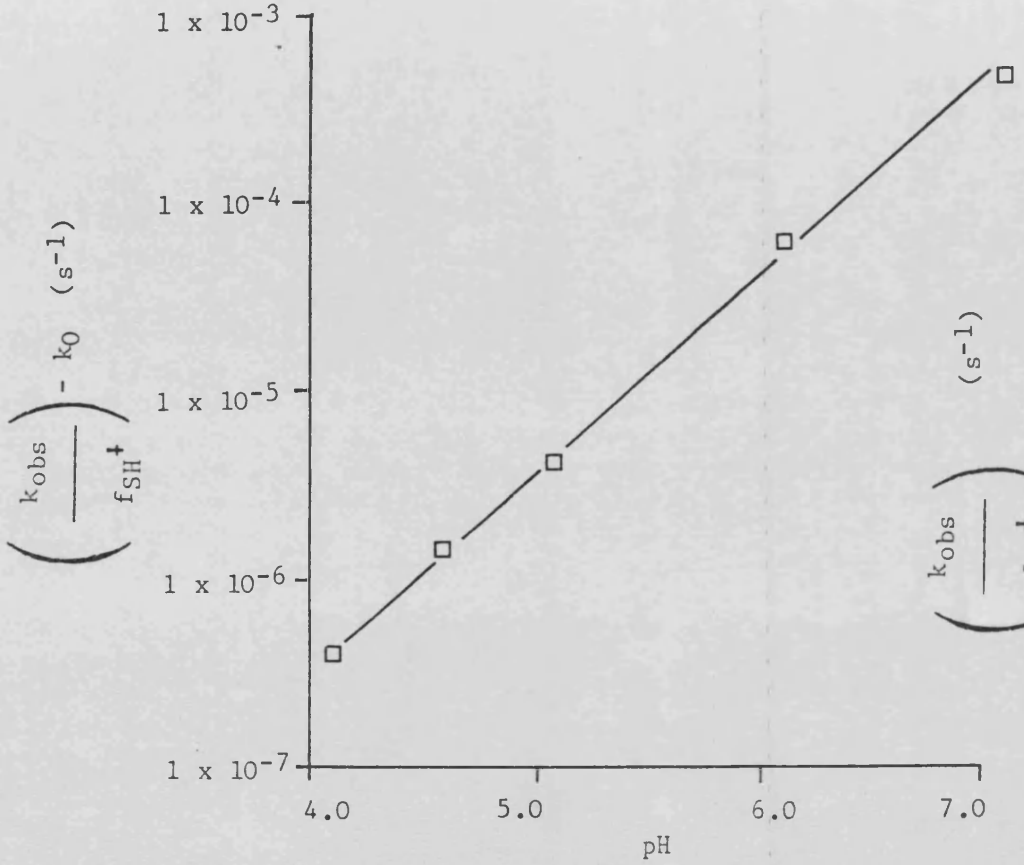

Figure 8.9 - The effect of pH on the hydrolysis of cirazoline hydrochloride at 70°C. Data plotted according to equation 8.5

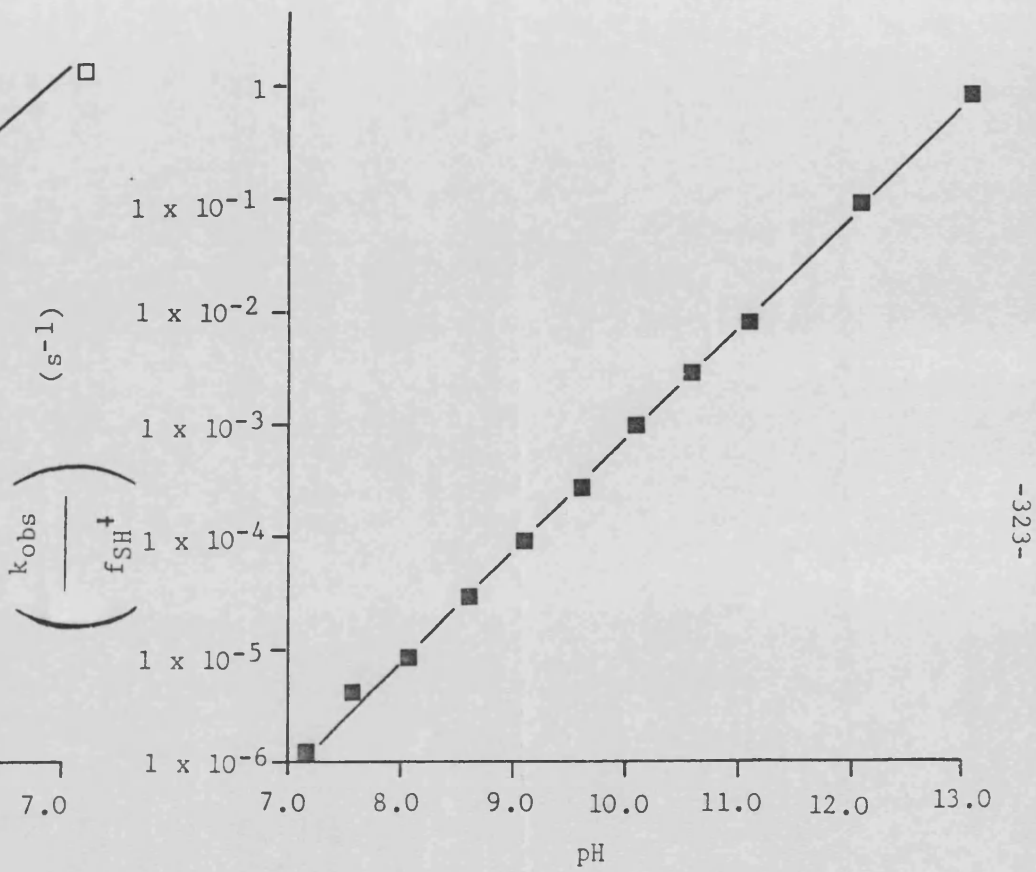

Figure 8.10 - The effect of pH on the hydrolysis of cirazoline hydrochloride at 25°C. Data plotted according to equation 8.9

The linear plot with slope close to unity confirms that equations 8.4 and 8.5 adequately describe the overall reaction in the pH 4.1 - 7.1 region. k_2 was determined at each pH (4.1 - 7.1) using equation 8.4 (table 8.6) and gave mean k_2 = 261 (S.D. 31) M^{-1} s^{-1} at 70°C.

A theoretical rate constant k_T was calculated at each experimental pH between 1.1 and 7.1, 70°C using equation 8.6:

$$k_T = (k_O + k_2 [OH^-]).f_{SH^+} = (1.18 \times 10^{-6} + 261 [OH^-]).f_{SH^+} \ s^{-1} \quad (8.6)$$

k_T values at each pH are shown in table 8.6 and the theoretical pH profile is shown in figure 8.7. The theoretical pH profile shows good agreement with the observed pH profile in the region pH 1.1 - 7.1 and demonstrates the validity of equations 8.4 and 8.6.

(b) Calculation of k_2 at 25°C.

At 25°C and pH >7 the uncatalysed and (any) specific acid catalysed reaction rates will be negligible and equation 1.10 reduces to equation 8.7:

$$k_{obs} = (k_2 [OH^-]).f_{SH^+} + (k_5[OH^-]).f_S \quad (8.7)$$

In the absence of free base hydrolysis equation 8.7 further reduces to equation 8.8:

$$k_{obs} = (k_2[OH^-]).f_{SH^+} \quad (8.8)$$

$[OH^-]$ will increase tenfold for every unit increase in pH but the fraction of protonated species, f_{SH^+}, will decrease with increase in pH due to formation of free base species(S). The pK_a of cirazoline at 25°C was determined as 9.48 (section 4.3) giving a pK_a' of 9.50 in 2×10^{-3} M solution (equation 4.3). Use of the simple Henderson-Hasselbalch equation (equation 4.5) indicates that cirazoline is

present as >99% SH^+ at a pH below 7.5 and >99% S at a pH above 11.5. Above pH 11.5, f_{SH^+} decreases approximately tenfold for every unit increase in pH and the reaction rate for the protonated species should therefore be constant above pH 11.5, which is the case observed experimentally (figure 8.8).

At low ionic strengths $a_{OH^-} \cong [OH^-]$ and equation 8.8 may be written in the form of equation 8.9:

$$\log_{10}\left(\frac{k_{obs}}{f_{SH^+}}\right) = \log_{10} k_2 - pK_w + pH \qquad (8.9)$$

Observed rate constant data plotted according to equation 8.9 are shown in figure 8.10. At high pH (>11), $a_{OH^-} \neq [OH^-]$ and equation 8.9 is not strictly valid. These ionic strength effects are discussed in section 8.3.2.1 (c). Linear regression analysis gave : correlation coefficient = 0.9997, slope = 0.9731 (S.D. 0.0085), and intercept = -12.88 (S.D. 0.08). The linear plot with slope close to unity confirms that equation 8.8 and 8.9 adequately describe the overall reaction in the pH region 7.1 - 13.1, 25°C. k_2 was determined at each pH (7.1 - 13.1) using equation 8.8 (table 8.7) and gave mean k_2 = 7.37 (S.D. 1.32) $M^{-1}\ s^{-1}$ at 25°C.

A theoretical rate constant, k_T, at 25°C was calculated at each experimental pH using equation 8.10:

$$k_T = k_2.[OH^-].f_{SH^+} = 7.37.[OH^-].f_{SH^+} \quad s^{-1} \qquad (8.10)$$

The theoretical pH profile is shown in figure 8.8 and shows good agreement with the observed profile indicating equation 8.10 is satisfactory in describing the cirazoline hydrolysis in the pH region 7.1 - 13.1, 25°C.

(c) Correction for Ionic Strength Effects

The ionic strength, I, of the reaction mixtures varies with the pH of the solution. At intermediate pH's (pH 4 - 10) I is essentially constant at 2 x 10^{-3} M due to the concentration of cirazoline hydrochloride. At low pH (<3) and high pH (>11) ionic strength will increase significantly above this level due to the high concentrations of hydrochloric acid and sodium hdroxide, respectively.

At low pH (1-3), the increase in ionic strength with decreasing pH has three possible effects on the rate of reaction (section 1.12(c));

(i) a decrease in the base catalysed reaction (section 8.3.4),

(ii) an increase in any acid catalysed reaction,

(iii) a slight modification in the neutral water (uncatalysed) reaction.

The observed slight downward trend in k_{obs} values with decreasing pH - and hence increasing ionic strength - is typical of electrolyte effects an ion-dipole reactions and further suggests that the dominant reaction in this pH region is between the cirazoline ion and neutral water.

At high pH, the specific base catalysis of the protonated cirazoline species may be described by equation 8.11:

$$k_T' = k_2'.[OH^-].f_{SH^+} \qquad (8.11)$$

Where k_T' is the calculated apparant reaction rate constant and k_2' is the apparant specific base catalysed reaction rate constant. For a given pH and temperature, an increase in ionic strength will tend to:

(i) decrease the rate of reaction due to increased shielding of the reacting ions, i.e. decrease k_2', (equation 1.13 and section 8.3.4), and

(ii) increase the rate of reaction due to an increase in pK_a' (equation 4.3) and fraction of protonated species, f_{SH^+}, (equation 4.5).

These two factors will have opposing effects which tend to cancel out; e.g. at pH 12.1, $[OH^-]$ = 0.014 M ($\gamma_\pm$ = 0.88), I = 0.016 M, pK_a' = 9.54, f_{SH^+} = 2.747 x 10^{-3} M and k_2' = 6.41 which gives k_T' = 247 x 10^{-6} s^{-1} (equation 8.11). This value is similar to the k_T value at pH 12.1 of 233 x 10^{-6} s^{-1} (table 8.7) which is calculated ignoring activity effects. Similarly at pH 13.1, $[OH^-]$ = 0.170 M ($\gamma_\pm$ = 0.74), I = 0.174 M, pK_a' = 9.63, f_{SH^+} = 3.387 x 10^{-4} and k_2' = 4.18 giving k_T' = 241 x 10^{-6} s^{-1} (equation 8.11) which is similar to the k_T value of 233 x 10^{-6} s^{-1} at pH 13.1 (table 8.7).

8.3.3 Effect of Temperature

The effect of temperature on the specific base catalysed hydrolysis (pH 7.1) and the uncatalysed (neutral water) hydrolysis (pH 1.1) of cirazoline hydrochloride was examined. Experiments at pH 7.1 were performed at 25 - 70°C using the automated pH-statting technique. An initial cirazoline hydrochloride concentration of 2 x 10^{-3} M was used and percent residual concentration was calculated by reference to both cirazoline and CPAE concentration (equation 3.8, section 3.1.6).

Experiments at pH 1.1 were carried out at temperatures of 50 - 80°C in 0.1 M HCl; no pH-statting was required as the buffer capacity of the HCl was sufficient to maintain pH. An initial cirazoline hydrochloride concentration of 1.6×10^{-3} M was used and percent residual concentration was calculated by reference to cirazoline concentration alone (equation 3.6, section 3.1.6) as CPAE degradation was significant under these conditions.

The observed rate constant at each temperature and pH is shown in table 8.8. k_2 and k_o values were calculated for each temperature using equations 8.8 and 8.3 respectively and are also shown in table 8.8. k_2 and k_o data were plotted according to the Arrhenius relationship ($\log_{10}$ k versus T^{-1}, equation 1.23, figure 8.11), and Transition State relationship ($\log_{10}$ k/T versus T^{-1}, equation 1.24). Linear regression analysis data and derived frequency factor, A, and activation energy, E_a, and standard enthalpy change, $\Delta H^{\ddagger}$, and standard entropy change, $\Delta S^{\ddagger}$, values for transition state formation are shown in table 8.8.

8.3.4 Effect of Ionic Strength

The effect of ionic strength on the hydrolysis of 2×10^{-3} M cirazoline hydrochloride was determined at pH 7.0 and 30°C. Control of pH was by the manual pH-stat technique and percent residual concentration was calculated by method 3 (section 3.1.6). Ionic strength was varied by the inclusion of different concentrations of sodium chloride (1×10^{-3} - 1×10^{-1} M) in the formulation. The concentration of cirazoline hydrochloride (2×10^{-3} M) was included in the calculation of total ionic strength of each system.

TEMPERATURE (°C)	k_{obs} (S.D.) (s^{-1} x 10^6) pH 7.1	pH 1.1	k_2 $M^{-1}s^{-1}$	k_o $M^{-1}s^{-1}x10^6$
25.0	1.24(0.02)	-	9.93	-
30.0	2.64(0.16)*	-	14.4	-
40.0	10.6 (0.2)	-	29.1	-
50.0	34.4 (0.4)	0.131(0.015)	50.8	0.131
60.0	193 (1)	-	164.0	-
70.0	451 (7)	1.11 (0.03)	248.0	1.11
75.0	-	1.81 (0.07)	-	1.81
80.0	-	2.59 (0.14)	-	2.59

	Equation 1.24		Equation 1.23	
	k_2	k_o	k_2	k_o
Correlation coefficient	0.9921	0.9992	0.9927	0.9992
Slope (S.D.) x 10^{-3}	-3.126 (0.198)	-4.860 (0.139)	-3.265 (0.198)	-5.007 (0.138)
Intercept (S.D.)	8.977 (0.624)	5.654 (0.408)	11.91 (0.63)	8.618 (0.405)
A (s^{-1})	-	-	8.13 x 10^{11}	4.15 x 10^8
E_a (KJ mol^{-1})	-	-	62.5	95.9
ΔH^* (kJ mol^{-1})	-59.9	-93.0	—	—
ΔS^* (J mol^{-1} k^{-1})	-25.7	-89.3	—	—

Table 8.8 - The effect of temperature on the hydrolysis of 2 x 10^{-3} M cirazoline hydrochloride at pH 7.1, and 1.6 x 10^{-3} M cirazoline hydrochloride in 0.1 M HCl (pH 1.1) Linear regression analysis results for the k_2 and k_o data plotted according to equation 1.23 ($\log_{10}k$ versus T^{-1}) and equation 8.24 ($\log_{10} k/T$ versus T^{-1}). Derived frequency factor, A, activation energy, E_a, standard enthalpy change, ΔH^*, and standard entropy change, ΔS^*, of transition state formation for each reaction are also shown.

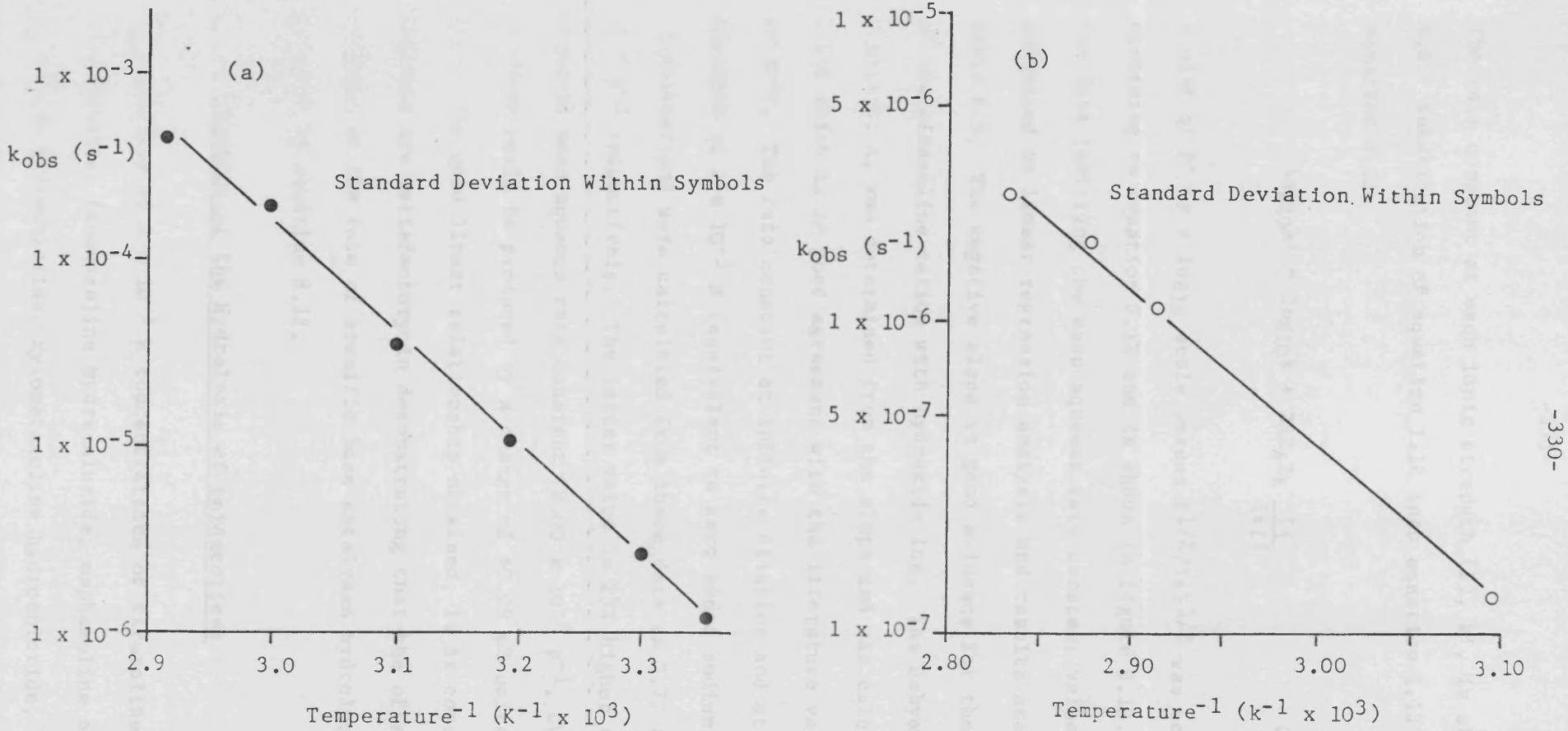

Figure 8.11 - Arrhenius plots for the hydrolysis of cirazoline hydrochloride (a) at pH 7.1 and (b) in 0.1 M HCl (pH 1.1).

The rate constant at each ionic strength (I), k', is shown in table 8.9. Substitution of equation 1.18 into equation 1.13 yields equation 8.12:

$$\log_{10}k' = \log_{10}k + 2AZ_AZ_B \frac{I^{\frac{1}{2}}}{1+I^{\frac{1}{2}}} \qquad (8.12)$$

A plot of k' on a $\log_{10}$ scale versus $I^{1/2}/1+I^{1/2}$ was constructed according to equation 8.12 and is shown in figure 8.12.
The data (omitting the mean aqueous rate constant value) were subjected to linear regression analysis and results are shown in table 8.9. The negative slope is good evidence for the interaction of the cirazoline cation with hydroxide ion. The Debye-Hückel constant, A, was determined from the slope and was calculated as 0.503 which is in good agreement with the literature value of 0.516 at 30°C. The rate constant at infinite dilution and at an ionic strength of 2×10^{-3} M (equivalent to zero added sodium chloride concentration) were calculated from these data as 2.72 and 2.47×10^{-6} s^{-1} respectively. The latter value is 23% higher than the observed mean aqueous rate constant (2.00×10^{-6} s^{-1}, CV = 9%); such an error could be produced by a change of +0.09 pH units or +1.3°C. Due to the good linear relationship obtained, it is considered that the data are satisfactory in demonstrating that the effect of ionic strength on the rate of specific base catalysed hydrolysis is governed by equation 8.12.

8.3.5 Kinetics of the Hydrolysis of Imidazolines

The stability of 2×10^{-3} M concentrations of cirazoline hydrochloride, fenoxazoline hydrochloride, naphazoline nitrate, tolazoline hydrochloride, xylometazoline hydrochloride, antazoline sulphate and 2-methyl-2-imidazoline was determined at 70°C using

NaCl CONCENTRATION (M)	I (M)	$\frac{I^{1/2}}{1+I^{1/2}}$ (x10^2)	OBSERVED RATE CONSTANT (S.D.) k'(s^{-1} x 10^6)
NIL	2 x 10^{-3}	4.281	2.00 (0.18)*
1 x 10^{-3}	3 x 10^{-3}	5.193	2.40 (0.06)
5 x 10^{-3}	7 x 10^{-3}	7.721	2.32 (0.09)
1 x 10^{-2}	1.2 x 10^{-2}	9.869	2.14 (0.06)
5 x 10^{-2}	5.2 x 10^{-2}	18.57	1.81 (0.04)
1 x 10^{-1}	1.02 x 10^{-1}	24.21	1.54 (0.03)

Correlation Coefficient : 0.9962

Slope (S.D.) : -1.005 (0.052)

Intercept (S.D.) : -5.564 (0.007)

Table 8.9 - The effect of ionic strength on the hydrolysis of cirazoline hydrochloride at pH 7.0,30°C. Linear regression analysis results for the 1 x 10^{-3} M - 1 x 10^{-1} M data plotted accorded to equation 8.12 (figure 8.12). * = mean and standard deviation of twelve experiments.

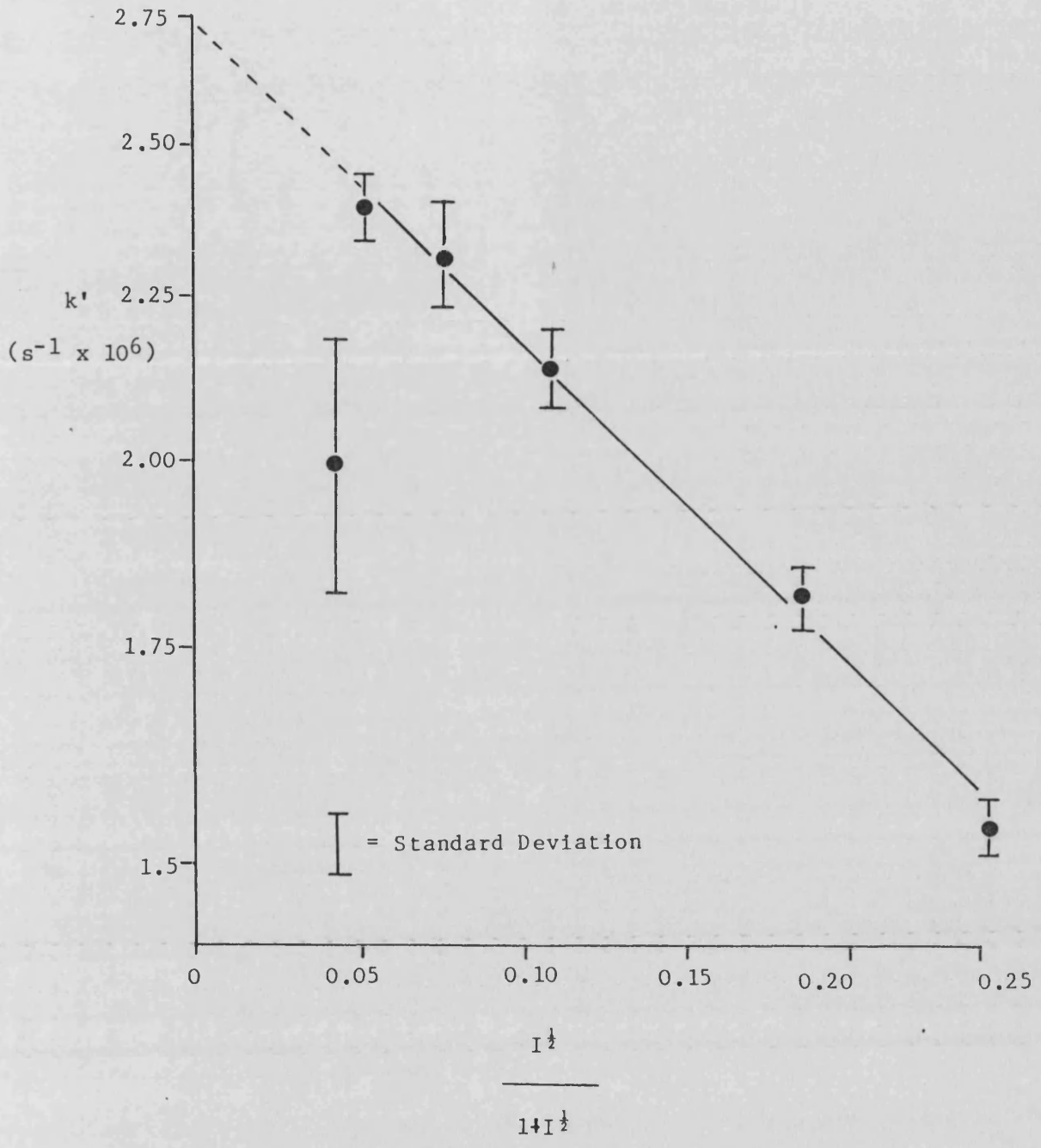

Figure 8.12 - The effect of ionic strength on the hydrolysis of cirazoline hydrochloride at 30°C. Data plotted according to equation 8.12.

phosphate buffer pH 6.85. Under these conditions all imidazolines are present as >95% protonated species (sections 1.2 and 4). Imidazolines were assayed using the methods described in sections 3.1.1 and 3.1.7. Percent residual cirazoline concentration was calculated using method 3 (equation 3.8, section 3.1.6). Table 8.10 shows the observed first order rate constant and half-life (calculated using equation 1.4) for each imidazoline. The results show that stability decreases in the order: xylometazoline > 2-methyl-2-imidazoline > naphazoline > tolazoline > antazoline > cirazoline > fenoxazoline.

Cirazoline and fenoxazoline are structurally closely related (figure 1.1) and contain an ether linkage between the imidazoline ring and the aromatic moiety. These compounds are by far the least stable being about 35 times more prone to hydrolysis than tolazoline.

8.3.6 Effect of SDDS on Kinetics of Cirazoline Hydrolysis

The effect of ion-pair formation, complex formation and micellar solubilization on the specific base catalysed hydrolysis of cirazoline was investigated using SDDS. The effect of added electrolyte on the hydrolysis of solubilized cirazoline was also studied.

8.3.6.1 EFFECT OF SDDS CONCENTRATION

The amount of ion-paired, complexed and solubilized cirazoline depends upon the total concentration of cirazoline and SDDS present in the system. In this work the effect of these interactions was investigated by constructing cirazoline stability - SDDS concentration profiles at fixed cirazoline hydrochloride

IMIDAZOLINE	OBSERVED RATE CONSTANT (S.D.) (s^{-1} x 10^{-6})	HALF-LIFE (HOURS)
Xylometazoline	0.564 (0.08)	341
2-methyl-2-imidazoline	2.79 (0.01)	69.0
Naphazoline	3.21 (0.15)	60.0
Tolazoline	6.79 (0.14)	28.4
Antazoline	10.5 (0.5)	18.3
Cirazoline	233 (2)	0.826
Fenoxazoline	243 (9)	0.792

Table 8.10 - The effect of imidazoline structure on the hydrolysis reaction rate constant and half-life in phosphate buffer pH 6.85, 70°C.

concentrations. Stabilization was measured by a stability factor - defined as the ratio of the aqueous first order rate constant in the absence of SDDS, $k_{(aq)}$, to that obtained in the presence of SDDS, k_{SDDS} - hence the greater the stability factor the greater the stabilizing effect of SDDS.

Kinetic studies were undertaken at pH 7.0 using the manual pH-stat technique. Percent residual concentration was calculated using method 3 (equation 3.8, section 3.1.6) except in the presence of CIRH-DDS complex when method 2 (equations 3.7) was used. Temperatures of 30° and 50°C were employed to investigate the solid and liquid complex systems respectively. Experiments at 30°C were limited to 28 days duration due to microbial contamination.

Table 8.11 shows the first order rate constant for the hydrolysis of 2×10^{-4} M cirazoline hydrochloride at 30°C in the presence of 1×10^{-4} - 2×10^{-2} M SDDS. Standard deviation of rate constant, stability factor and the physical appearance of each system are also shown. The stability factor was plotted as a function of SDDS concentration on a $\log_{10}$ scale and is shown in figure 8.13. The solubility product of the CIRH-DDS complex under these conditions was determined as 1.17×10^{-7} moles^2 litre^{-2} (section 6.3.2.2(c)), and the SDDS concentration at the CMC' of the system was estimated at 4.4×10^{-3} M (table 7.5) by conductimetric titration. Hence concentrations of SDDS in the range 5.9×10^{-4} M - 4.4×10^{-3} M will result in phase separation due to complex formation. The SDDS concentrations associated with phase separation and micellar solubilization and the physical nature of the systems are shown on the profile. At concentrations below the solubility product the systems are clear and the stability factor is close to unity,

[SDDS] ($Mx10^3$)	RATE CONSTANT (S.D.) ($s^{-1} \times 10^7$)	STABILITY FACTOR (k_{aq}/k_{SDDS})	APPEARANCE
NIL	20.0 (1.7)*	-	CLEAR SOLUTION
0.1	14.9 (0.4)	1.34	"
0.2	19.1 (0.8)	1.05	"
0.4	17.5 (1.2)	1.14	"
1.0	10.8 (1.2)	1.85	FLOCCULATED SUSPENSION
3.0	2.75 (0.11)	7.27	"
5.0	1.35 (0.05)	14.8	CLEAR SOLUTION
7.0	0.556 (0.025)	36.0	"
8.0	0.304 (0.024)	65.8	"
10.0)) 20.0)	No significant degradation after 27 days		"

Table 8.11 - The effect of SDDS concentration, [SDDS], on the hydrolysis of 2×10^{-4} M cirazoline hydrochloride at pH 7.0, 30°C. * Mean and standard deviation of 12 determinations.

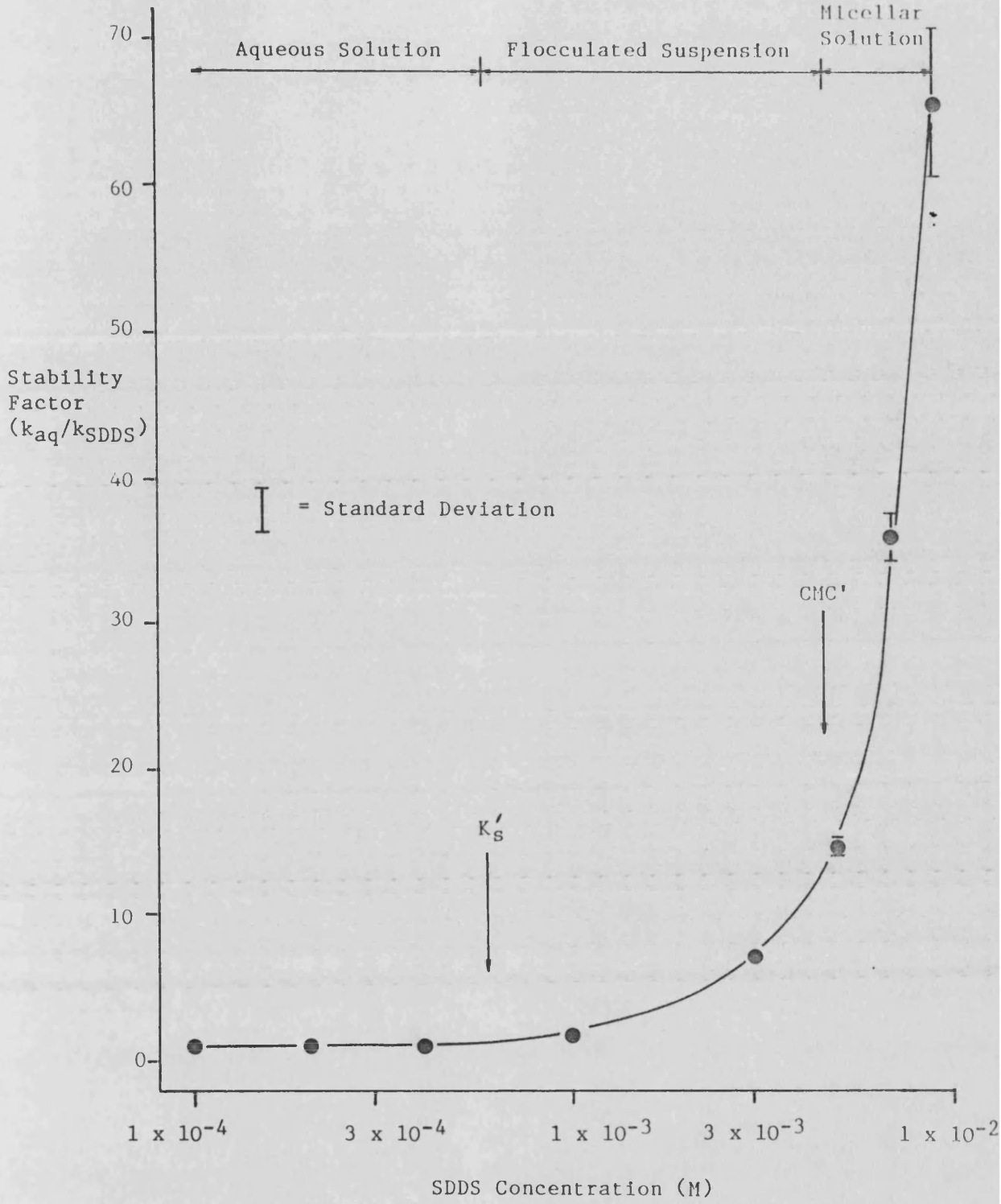

Figure 8.13 - 2 x 10^{-4} M cirazoline hydrochloride stability-SDDS concentration profile, 30°C. Plot of stability factor (k_{aq}/k_{SDDS}) against SDDS concentration ($\log_{10}$ scale) for the hydrolysis at pH 7.0, 30°C.

indicating that the formation of ion-pairs did not affect the rate of cirazoline hydrolysis. At concentrations of SDDS above the solubility product, but below the CMC' of the system a floculated suspension is formed confirming that phase separation occurred. The stability factor increases dramatically with increasing SDDS concentration around the CMC' of the system indicating that solubilization by SDDS is a potent method of stabilization. A 66 fold increase in stability was observed with 8×10^{-3} M SDDS and negligible degradation occurred over a 27 day period at SDDS concentrations of 1×10^{-2} and 2×10^{-2} M.

The extent of complexation in the 2×10^{-4} M cirazoline hydrochloride-SDDS systems was too small to allow assessment of any stabilizing effect. A profile was therefore constructed using a tenfold greater concentration of cirazoline hydrochloride. Table 8.12 gives the first order rate constant for the hydrolysis of 2×10^{-3} M cirazoline hydrochloride at 30°C in the presence of 3×10^{-4} - 3×10^{-2} M SDDS. Standard deviation of rate constant, stability factor and the appearance of each system are also shown. Under these conditions, the concentration of SDDS required to produce an insoluble complex is 5.85×10^{-5} M and all systems in this profile are therefore above the solubility product. The SDDS concentration at the CMC' of the system was determined as 5.36×10^{-3} M (S.D. = 0.12×10^{-3} M) by conductimetric titration and as 5.25×10^{-3} M from solubility studies (tables 7.4 and 7.10). The total solubilization concentration, SOL_T, was calculated as 7.04×10^{-3} M SDDS (S.D. = 0.19×10^{-3} M) by conductimetric titration and 6.51×10^{-3} M SDDS from solubility studies. The resultant stability profile is given in figure 8.14, which also shows CMC' and SOL_T points and the physical nature of the system. The stability factor increases from

[SDDS] ($Mx10^3$)	RATE CONSTANT (S.D.) ($s^{-1} \times 10^7$)	STABILITY FACTOR ($k_{(aq)}/k_{SDDS}$)	APPEARANCE
NIL	20.0 (1.7)*	-	CLEAR SOLUTION
0.3	16.1 (1.2)	1.24	FLOCCULATED SUSPENSION
0.5	12.4 (0.6)	1.61	"
1.0	10.3 (0.3)	1.94	"
2.0	2.37 (0.18)	8.44	"
3.0	0.736 (0.041)	27.2	"
5.0	0.307 (0.021)	65.1	"
5.5	0.525 (0.028)	38.1	"
6.5	0.360 (0.026)	55.6	"
7.0	0.350 (0.011)	57.1	CLEAR SOLUTION
10.0	0.198 (0.009)	101	"
20.0	0.110 (0.010)	190+	"
30.0	0.091 (0.010)	220+	

Table 8.12 - The effect of SDDS concentration, [SDDS], on the hydrolysis of 2×10^{-3} M cirazoline hydrochloride at pH 7.0, 30°C. * Mean and relative standard deviation of 12 determinations. + = Approximate value.

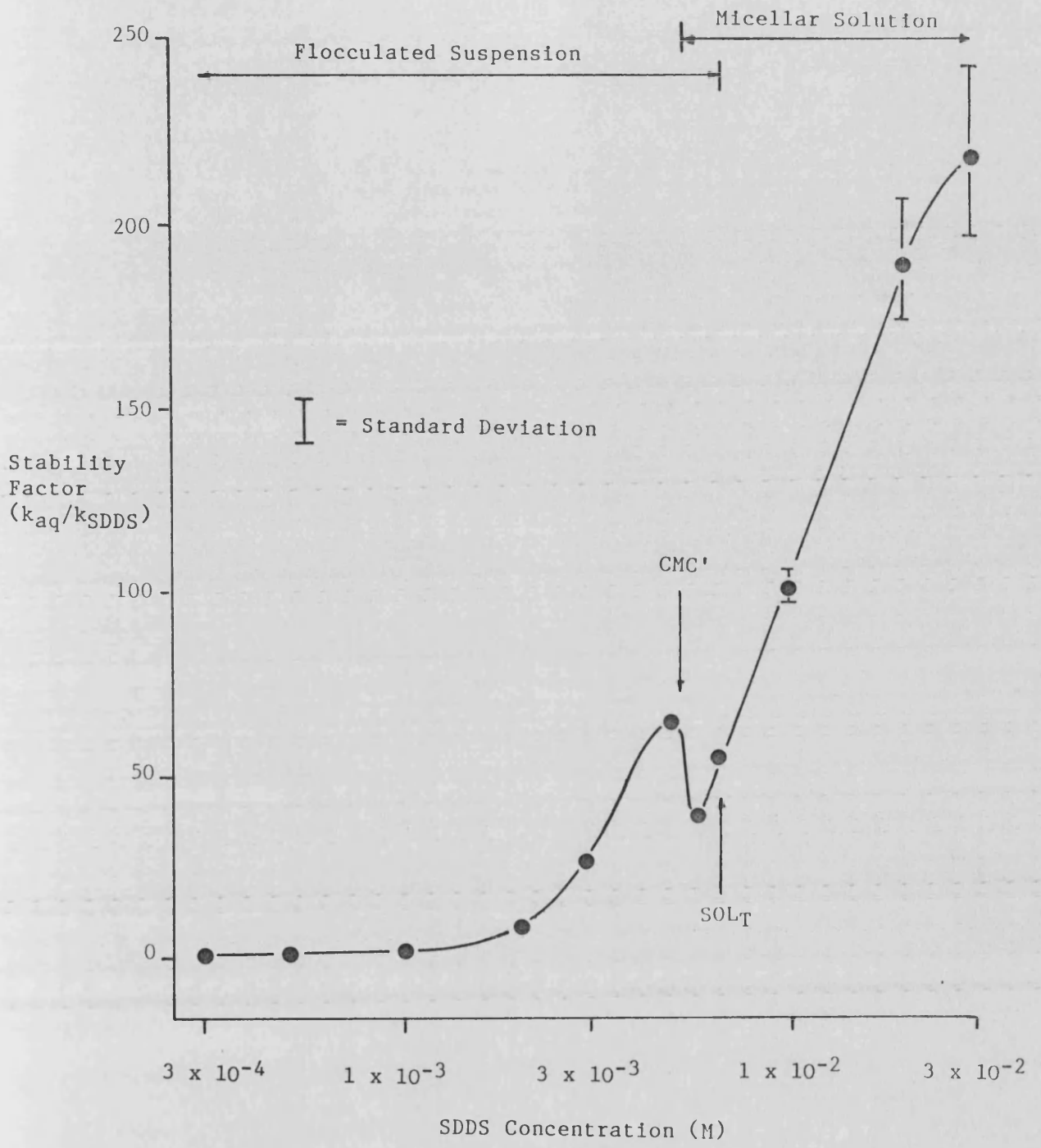

Figure 8.14 - 2×10^{-3} M cirazoline hydrochloride stability-SDDS concentration profile, 30°C. Plot of stability factor (k_{aq}/k_{SDDS}) against SDDS concentration ($\log_{10}$ scale) for the hydrolysis at pH 7.0, 30°C.

1.24 at 3 x 10^{-4} M SDDS to 65.1 at 5 x 10^{-3} M SDDS as cirazoline is removed from solution to form the solid CIRH-DDS complex. In the CMC' region, however, the stability factor decreases to 38.1 as the complex is solubilized. Further increases in SDDS concentration beyond the total solubilization point result in formation of a clear solution and a marked increase in stability. Only slight cirazoline degradation was observed at 2 x 10^{-2} M and 3 x 10^{-2} M SDDS and the stability factors were approximately 190 and 220, respectively.

The profiles at 30°C involve the formation of the solid CIRH-DDS complex. The effect of liquid complex formation on cirazoline stability was investigated at 50°C; the rate of aqueous cirazoline hydrolysis is approximately 16 times greater at this temperature than at 30°C and this therefore allowed the effect of high SDDS concentrations to be evaluated. Table 8.13 shows the first order rate constant for the hydrolysis of 2 x 10^{-3} M cirazoline hydrochloride at 50°C in the presence of 2 x 10^{-3} - 1 x 10^{-1} M SDDS. Standard deviation of rate constant, stability factor and the appearance of each system are also presented. The solubility product for the liquid complex at 50°C was determined as 4.19 x 10^{-7} moles^2 litre^{-2} (section 6.3.2.2(c)) and all systems are therefore above the solubility product. The SDDS concentration at the CMC' and SOL_T under these conditions was determined by conductimetric titration as 4.00 x 10^{-3} M and 4.40 x 10^{-3} M, respectively (table 7.6). These CMC' and SOL_T points and the nature of the system are shown on the stability profile (figure 8.15). The stability factor increases as the complex separates to form a liquid dispersion. Solubilization into micelles further increases the degree of stabilization but no inflexion around the initial micellization and solubilization region is evident under these conditions (see figure 8.14). The stability

[SDDS] ($Mx10^3$)	RATE CONSTANT (S.D.) ($s^{-1} \times 10^7$)	STABILITY FACTOR ($k_{(aq)}/k_{SDDS}$)	APPEARANCE
NIL	310 (4)	-	CLEAR SOLUTION
2.0	139 (2)	2.23	LIQUID DISPERSION
3.0	81.0 (1.1)	3.83	"
4.0	46.7 (1.3)	6.64	"
4.5	38.6 (0.2)	8.03	"
5.0	31.3 (0.8)	9.90	CLEAR SOLUTION
10.0	7.33 (0.15)	42.3	"
20.0	3.31 (0.04)	93.7	"
40.0	2.57 (0.03)	121	"
60.0	2.45 (0.02)	126	"
100.0	2.68 (0.04)	116	"

Table 8.13 - The effect of SDDS concentration, [SDDS], on the hydrolysis of 2×10^{-3} M cirazoline hydrochloride at pH 7.0, 50°C.

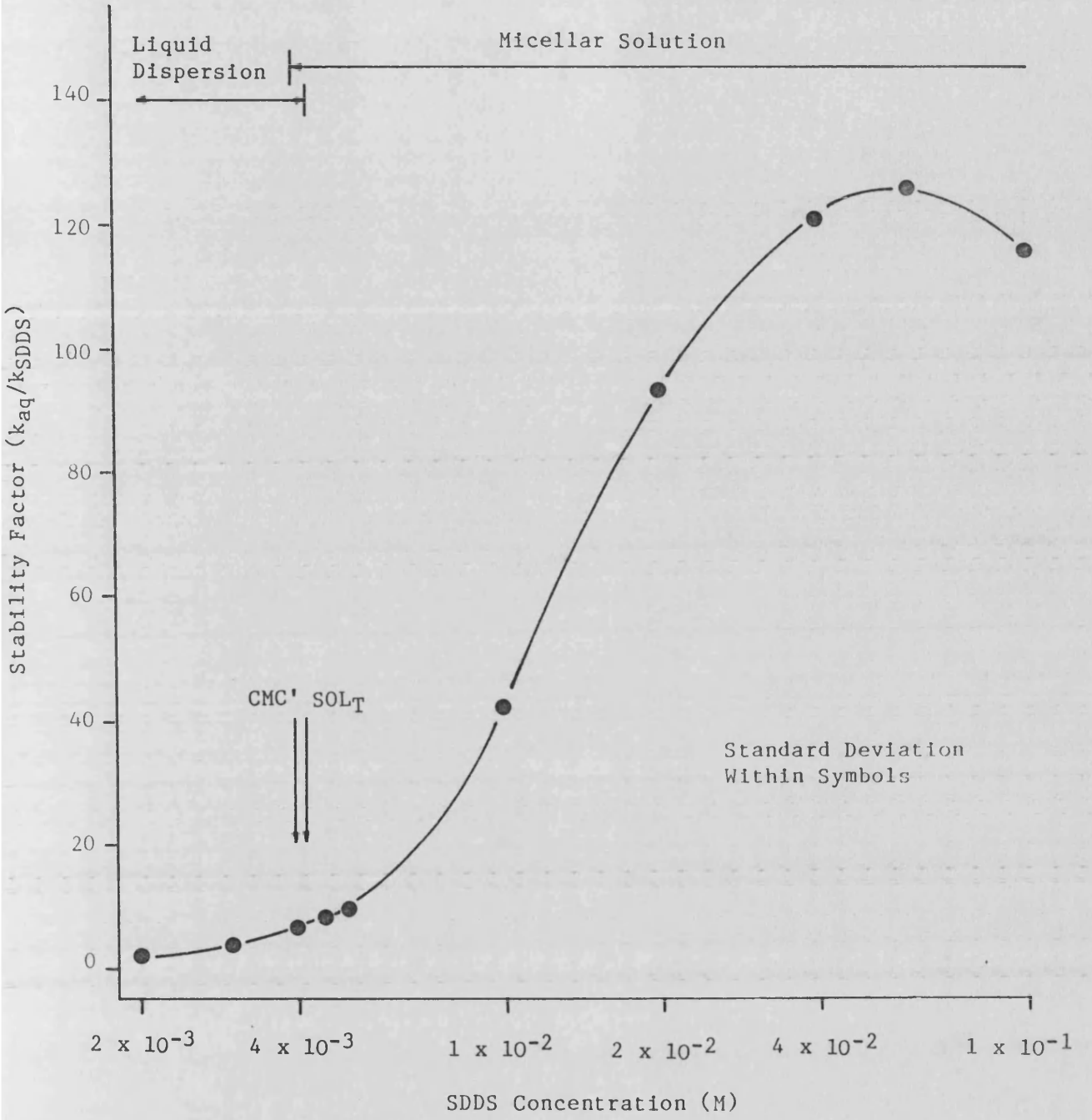

Figure 8.15 - 2 x 10^{-3} M cirazoline hydrochloride stability-SDDS concentration profile, 50°C. Plot of stability factor (k_{aq}/k_{SDDS}) against SDDS concentration ($\log_{10}$ scale) for the hydrolysis at pH 7.0, 50°C.

profile peaks at a stability factor of 126 at 0.06 M SDDS; further increase in SDDS concentration to 0.1 M results in a slight decrease in stability.

8.3.6.2 EFFECT OF IONIC STRENGTH

The effect of added electrolyte on the hydrolysis of solubilized cirazoline hydrochloride was investigated at pH 7.0, 30°C using the manual pH-stat technique. Systems were prepared containing 2×10^{-3} M cirazoline hydrochloride, 7×10^{-3} M SDDS and 1×10^{-3} - 1×10^{-1} M concentrations of sodium chloride.

Addition of electrolyte will have opposing effects on the aqueous and micellar reaction rate constants. The aqueous rate constant decreases as the electrolyte concentration increases according to equation 8.12, (table 8.9), whilst the micellar rate constant will increase due to reduced repulsion of hydroxide ions from the micellar surface. An increase in electrolyte concentration will also reduce the CMC of the system, increasing the volume of micelles.

Table 8.14 shows the first order rate constants and their standard deviations for the hydrolysis of 2×10^{-3} M cirazoline hydrochloride at pH 7.0, 30°C in the presence of 7×10^{-3} M SDDS and 1×10^{-3} M - 1×10^{-1} M concentration of sodium chloride, k'_{SDDS}. Stability factors are given with respect to:

(1) the aqueous rate constant, $k_{(aq)}$;

(2) the rate constant in the appropriate aqueous concentration of sodium chloride, $k'_{(aq)}$; and

(3) the change in concentration of micellar SDDS, $([S]^T\text{-CMC}')_{(aq)}/([S]^T\text{-CMC}')_{NaCl}$,

where $[S]^T$ is the total concentration of surfactant and

[NaCl] (M)	Ionic Strength (M)	k'_{SDDS} ($s^{-1}x10^8$) (S.D.)	STABILITY FACTOR 1	2	3
NIL	$2.0x10^{-3}$	3.50 (0.11)	57.1	57.1	57.1
$1.0x10^{-3}$	$3.0x10^{-3}$	4.22 (0.13)	47.4	56.9	52.4
$5.0x10^{-3}$	$7.0x10^{-3}$	4.39 (0.12)	45.6	52.9	33.0
$1.0x10^{-2}$	$1.2x10^{-2}$	4.26 (0.19)	46.9	50.3	26.9
$5.0x10^{-2}$	$5.0x10^{-2}$	4.79 (0.15)	41.8	37.8	14.2
$1.0x10^{-1}$	$1.02x10^{-1}$	7.04 (0.18)	28.4	21.9	7.5

Table 8.14 - The effect of added sodium chloride concentration, [NaCl], on the hydrolysis of solubilized cirazoline hydrochloride, pH 7.0, 30°C. Systems contain 2 x 10^{-3} M cirazoline hydrochloride and 7 x 10^{-3} M SDDS.

Stability Factors:-

$$(1) = \frac{k_{(aq)}}{k'_{SDDS}}$$

$$(2) = \frac{k'_{(aq)}}{k'_{SDDS}}$$

$$(3) = \frac{k'_{(aq)}}{k'_{SDDS}} \cdot \frac{([S]^T\text{-}CMC')_{(aq)}}{([S]^T\text{-}CMC')_{NaCl}}$$

subscripts (aq) and NaCl refer to systems in the absence and presence of sodium chloride .

Therefore (1) is an expression of the overall stabilizing effect due to the presence of SDDS and sodium chloride, (2) compensates for the increased aqueous stability in the presence of sodium chloride (3) compensates for the increased aqueous stability and change in concentration of micellar SDDS due to sodium chloride. $k'_{(aq)}$ and CMC' values were taken from tables 8.9 and 7.10 respectively.

All three methods of expressing stability show a decrease in protection afforded by SDDS with an increase in electrolyte concentration. Compensation for change in aqueous stablity and micelle concentration reveals a dramatic decrease in potency of micellar stabilization with increase in sodium chloride concentration.

9. DISCUSSION

9.1 THE AQUEOUS HYDROLYSIS OF CIRAZOLINE

Cirazoline is a monoacidic base and can, therefore, exist in two forms, i.e. protonated and unprotonated. The relative amount (mole ratio) of each species under given conditions is governed by the pK_a' of cirazoline and the pH of the system, (equation 4.5). Hence a knowledge of the cirazoline pK_a' is essential for investigating the mechanism and kinetics of aqueous hydrolysis, (equation 1.10).

Cirazoline pK_a' determination was hampered by problems with aqueous solubility and stability under the experimental conditions employed. These problems were minimised by restricting potentiometric titrations to the half-neutralisation point (4-5 determination per titration). The extent of degradation was dependent upon temperature, being greatest at 40°C where a maximum of 7.2% CPAE formed during the titration (table 4.6). Results showed good reproducibility within a given titration ($\pm$0.03 pH units maximum).

The pK_a of cirazoline was determined as 9.48 $\pm$ 0.02 at 25°C which is in good agreement with the reported value of 9.44[21] (see table 1.1). The cirazoline pK_a-temperature dependence is typical of monoacidic bases and falls with increasing temperature. Using the data in table 4.7 and equation 4.6, the pK_a at 30°, 50° and 70° was calculated as 9.34, 8.83 and 8.38 respectively.

Although hydrolysis reactions are bimolecular they often follow first order kinetics at constant pH. Kinetic studies performed under pH-statted conditions in the absence of buffer salts showed the hydrolysis of cirazoline hydrochloride to follow first order kinetics (section 8.3.1). The degradation of 2 x 10^{-3} M cirazoline at pH 7.1, 60°C was followed over three half-lives and the data analysed by three different time-based methods (section 3.1.6). The fractional life-time method (equation 8.1) gave an order of reaction of 1.018 (SD 0.039) and linear plots were obtained when the data were plotted according to the integrated first order equation (equation 1.4) and the Guggenheim equation (equation 1.6), thus indicating a first order reaction. The order of reaction was also found to be first order by a concentration based method. Degradation studies were carried out over the concentration range 0.2-5 x 10^{-3} M at pH 7.0, 30°C. Results analysed by the Van't Hoff method of initial rates gave an order of reaction of 0.988 (S.D. 0.014).

Two mechanisms of hydrolysis of cirazoline hydrochloride were identified (section 8.3.2), namely a neutral water reaction (attack of molecular water on protonated cirazoline) and a base catalysed reaction (attack of hydroxide ion on protonated cirazoline). No acid catalysed reaction or free base hydrolysis were observed. The overall reaction rate may be described by equation 8.4 which reduces to equation 8.8 at high pH when the uncatalysed (neutral water) reaction is negligible and may be ignored. Equation 8.4 is a form of equation 1.26 and indicates that the observed rate constant is a function of the uncatalysed (k_0) and specific base catalysed (k_2) reaction rate constants, hydroxide ion concentration ($[OH^-]$) and fraction of protonated cirazoline species (f_{SH^+}). Hence the stability of cirazoline may be predicted from a

knowledge of pH, pK_w, k_0, k_2 and pK_a. Figure 9.1 shows theoretical stability-pH profiles for the hydrolysis of 2 x 10^{-3} M cirazoline hydrochloride in the absence of added electrolyte and buffer salts at 30, 50 and 70°C. Data were calculated using equations 8.6, 1.23, 4.2, 4.3, 1.16 and 4.6, data from tables 4.7 and 8.8 and literature values for K_w[201]. The rate constant at pH 4.6, 70°C (k_T = 2.6 x 10^{-6} s^{-1}) predicted from these data is similar to that reported by Davies et al for the hydrolysis of cirazoline under similar conditions but using McIlvaines citrate-phosphate buffer at ionic strength 0.5 M to maintain pH, (k_{obs} = 3.72 x 10^{-6} s^{-1})[15]. The difference in rate constants may be due to the high ionic strength and in particular presence of general acid/base catalysis in the buffered system[15].

pH has a profound effect on the rate of hydrolysis of cirazoline through its effect on both the concentration of hydroxide and cirazoline ions. Below pH 3, [OH^-] is extremely low and the reaction rate is governed by the uncatalysed reaction and is, therefore, independent of pH. Above pH 3 the rate of reaction increases dramatically due to an increase in the rate of the base catalysed reaction. In the pH range 5 to 8 the stability-pH profile is linear but above pH 8 the relative increase in hydrolysis rate with pH decreases due to formation of the stable free base species. Above pH 10-11 the reaction rate is independent of pH. This effect is due to two opposing factors being in balance i.e. the increase in the concentration of OH^- and the decrease in the concentration of protonated species with increasing pH.

Like most reactions, the rate of hydrolysis of cirazoline increases with an increase in temperature (section 8.3.3). The data in table 8.8 show that the specific base catalysed reaction has a much lower energy

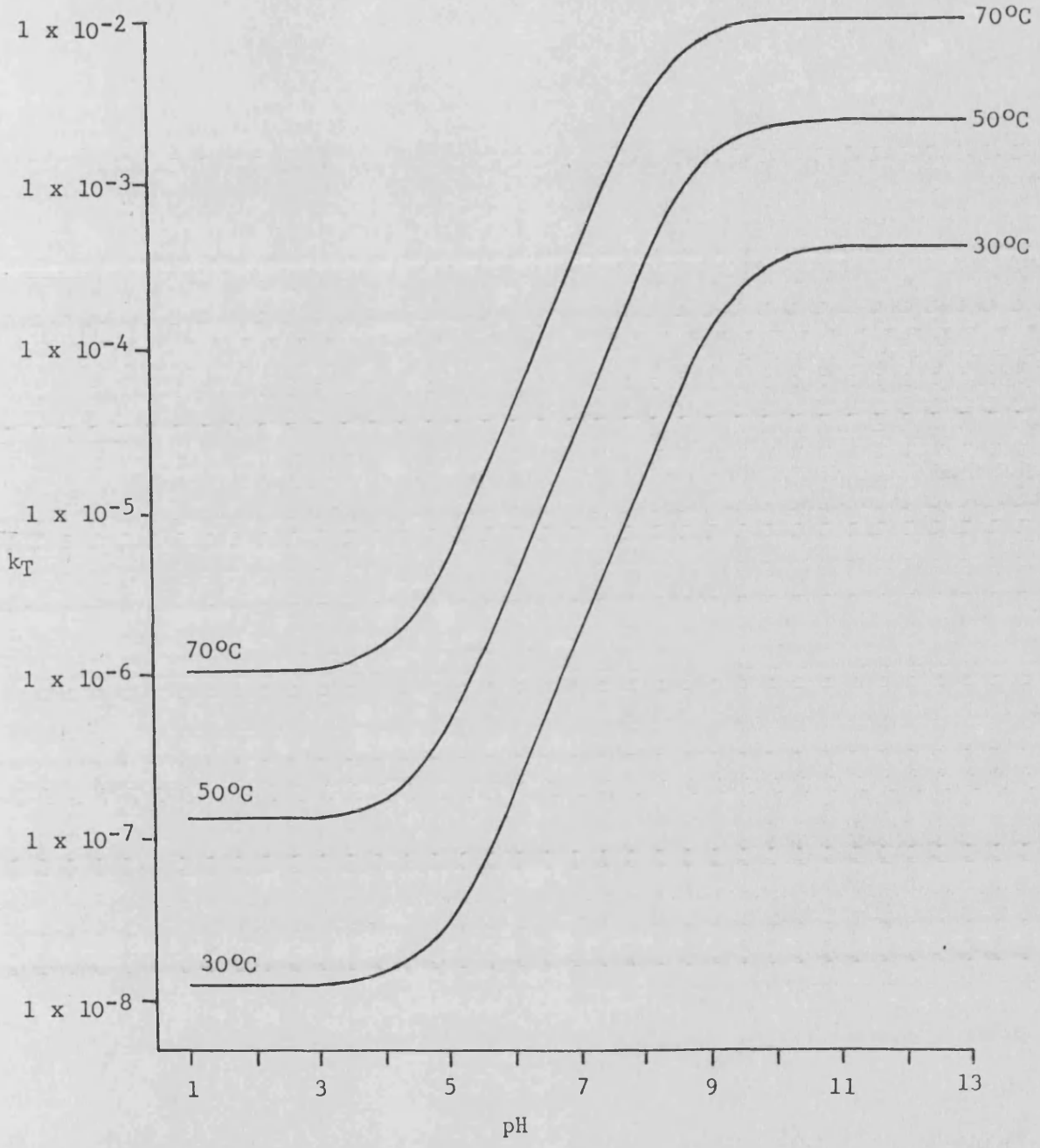

Figure 9.1 - Theoretical stability - pH profiles for the hydrolysis of 2 x 10^{-3}M cirazoline hydrochloride in the absence of added electrolyte and buffer salts at each temperature shown. Theoretical rate constants, k_T , calculated using equation 8.6 and data from tables 4.7 and 8.8 and literature values for K_w[201].

of activation (62.5 kJ mol^{-1}) and enthalpy of transition state formation (59.9 kJ mol^{-1}) than the uncatalysed reaction (95.9 and 93.0 kJ mol^{-1} respectively) which is a typical feature of catalytic behaviour. The frequency factor is approximately 2000 times greater for the catalysed reaction which may be explained by charge attraction effects. The entropy of transition state formation is negative for both reactions although numerically the entropy associated with the neutral water reaction is far greater, (-89.3 J mol K^{-1}), than for the catalysed reaction, (-25.7 J mol K^{-1}).

This difference in entropy change may be explained by the difference in the degree of solvation and hence water structure around the charged and uncharged species. In the neutral water reaction, both the cirazoline reactant and transition state species are charged and solvated whereas the base catalysed reaction involves the loss of two highly solvated ions to form an uncharged transition state species. Also, the neutral water reaction transition state species will be more bulky and sterically unfavoured relative to the transition state species in the base catalysed reaction.

For temperatures in the range 30°-70°C the reaction at pH 7 represents the optimum condition for studying the reaction of hydroxide ion with cirazoline ion. At this pH, the slopes of the observed stability profiles (figures 8.7 and 8.8) are approximately unity (indicating the expected absence of general acid-base catalysis), that the rate of the uncatalysed reaction is negligible and that the fraction of protonated cirazoline species is close to unity; use of equation 4.5 indicates that the fraction of protonated species at pH 7.0 is 0.996 and 0.962 at 30° and 70°C respectively. Specific base catalysed hydrolysis at pH 7 is also supported by the effect of ionic strength on k_{obs} at 30°C

(table 8.9). k_{obs} decreased with increasing ionic strength, I, according to equation 1.18, the calculated slope of 0.503 from figure 8.12 being close to the literature value of 0.516 at 30°C[11]. These results are consistant with a reaction between two oppositely charged ions such as hydroxide and cirazoline ions. However, k_{obs} in the absence of added electrolyte ($I = 2 \times 10^{-3}$ M) was calculated from the slope of figure 8.12 to be 23% higher than the mean k_{obs} value (CV = 9%). this observation is thought to be due to an error in the experimental conditions empolyed, i.e. a slightly higher pH and/or temperature. Such a reaction rate could be produced by a pH of 7.09 or a temperature of 31.3°C.

The stability of cirazoline relative to a series of other imidazolines with different 2-substituents was determined at pH 6.85, 70°C (section 8.3.5). Degradation studies were performed on 2×10^{-3} M concentrations of cirazoline hydrochloride, fenoxazoline hydrochloride, anatazoline sulphate, tolazoline hydrochloride, naphazoline nitrate, xylometazoline hydrochloride and 2-methyl-2-imidazoline using 0.025 equimolal phosphate buffer to maintain pH. This was considered acceptable despite possible general acid-base catalysis as only comparative stability of the imidazolines was required. The observed rate constants for xylometazoline and tolazoline (table 8.10) agree reasonably well with the data reported by Grabowska for the reactions in phosphate buffer at pH 7.1, 70°C[33,34]. Assuming specific base catalysed hydrolysis and $f_{SH^+} = 1$ in this pH region, rate constants for the reaction at pH 7.1, 70°C may be calculated from the data in table 8.10 using equation 8.8. Rate constants for xylometazoline and tolazoline under these conditions were calculated as, (literature value[33,34] in parentheses); 1.0×10^{-6} (1.2×10^{-6}) s^{-1} and 1.2×10^{-5} (1.7×10^{-5}) s^{-1} respectively.

Imidazoline	pK_a	Stability k_{tol}/k_{imid}	H_B δ(ppm)	Exchange k_{tol}/k_{imid}
Cirazoline	9.44	0.028	4.85	No Exchange
Fenoxazoline	-	0.029	4.75	No Exchange
Antazoline	10.23	0.65	4.30	0.38
Naphazoline	10.48	2.12	4.00	1.51
Tolazoline	10.59	1.00	3.70	1.00
Xylometazoline	10.85	12.2	3.75	0.152
2-methyl-2-imidazoline	11.09	2.44	2.00	No Exchange

Table 9.1 - pK_a, stability and NMR exocyclic methylene (H_B) data for imidazolines. k_{tol}/k_{imid} = substituent stability factor for hydrolysis (from table 8.10) and H_B exchange (from table 5.8). H_B chemical shifts (δ) from tables 5.1 to 5.7.

Using the data from table 8.10, a substituent stability factor was calculated for each imidazoline which are shown alongside pK_a data (from table 1.1) and NMR data in table 9.1. This factor is defined as the ratio of the tolazoline rate constant to the rate constant of the other imidazoline (k_{tol}/k_{imid}). Tolazoline was selected as the reference imidazoline as its stability is in the centre of the stability range.

A feature of some 2-substituted imidazolines in solution is exocyclic methylene exchange[20]. As part of the study into the mechanism of hydrolysis of cirazoline, the acidity of the imidazoline exocyclic methylene protons was investigated using NMR (section 5). This technique allowed the number of protons in each moiety to be monitored over a period of time. Reactions were performed under as similar conditions as possible to the degradation studies ('pH' = 6.85 in 0.025 equimolal phosphate buffer), with the exception of temperature. The temperature of the exchange studies was selected as 20°C as rapid exchange was predicted from literature data[20].

Common protons to all the medicinal imidazolines studied are the endocyclic protons (H_A) and the exocyclic protons (H_B), (section 5.3). H_A for all compounds studied had chemical shifts in the range δ = 3.55 - 3.80 indicating similar endocyclic electrical characteristics for all imidazolines. Any hydrolysis of imidazolines was detected by a decrease in the intensity of the H_A peak and a concomitant appearance and increase in intensity of peaks corresponding to degradation products (figure 1.2). All imidazolines except cirazoline and fenoxazoline were stable under the conditions of the experiment; these imidazolines slowly degraded, the observed reaction rate for cirazoline

(2.08 (S.D. 0.08) x 10^{-7} s^{-1}) being similar to that calculated for pH 6.85, 20°C using equations 8.6 and 1.23, (3.5 x 10^{-7} s^{-1}).

H_B chemical shifts were dependent upon the nature of the 2-substituent and are summarized in table 9.1.

First order H_B exchange occurred with antazoline, naphazoline, tolazoline and xylometazoline but no exchange was detected for cirazoline, fenoxazoline and 2-methyl-2-imidazoline. A substituent exchange factor defined as the ratio of the tolazoline exchange rate constant to the exchange rate constant of the imidazoline (k_{tol}/k_{imid}) was calculated and is also shown in table 9.1.

The data in table 9.1 show a reasonable trend between the stability of the imidazoline and its basicity (defined by pK_a). This trend follows the electron withdrawing ability of the 2-substituent as demonstrated by the chemical shifts of the exocyclic methylene protons (H_B). For example, cirazoline (pK_a = 9.44, H_B δ = 4.85) degrades 87 times faster than 2-methyl-2-imidazoline (pK_a = 11.09, H_B δ = 2.00) at pH 6.85, 70°C. As the electron withdrawing strength of the substituent increases, the ability of the imidazoline group to donate electrons decreases causing a reduction in basicity and pK_a. This inductive effect also increases the positive charge on the quaternary carbon and increases the reaction rate with hydroxide ion.

The major exception to the correlation between basicity and stability is given by the data for xylometazoline. The electron withdrawing ability of the xylometazoline substituent is predicted to be approximately similar to that for tolazoline and naphazoline. This is reflected in the H_B chemical shift and pK_a data. However, xylometazoline is found to be considerably more stable than the other

imidazolines studied. Xylometazoline has two methyl groups in the 2 and 6 position of the aromatic ring (see figure 1.1) which would present considerable obstruction to attack by hydroxyl ions at the 2-position of the imidazoline ring. Thus the main stabilizing property in xylometazoline is not an inductive effect but steric hinderance. Also naphazoline is slightly more stable, and cirazoline and fenoxazoline are appreciably more unstable than predicted from inductive effects (see pK_a and H_B chemical shifts, table 9.1). These findings may be explained using the exocyclic methylene exchange data in table 9.1. For cirazoline, fenoxazoline, antazoline, naphazoline and tolazoline, a clear relationship exists between H_B acidity and stability; i.e.

naphazoline > tolazoline > antazoline > cirazoline = fenoxazoline

No exchange was detected in the samples of cirazoline or fenoxazoline over a 14 day period indicating a low level of acidity. These imidazolines are extremely unstable relative to the other medicinal imidazolines studied. A possible explanation for these observations is outlined in figure 9.2, which shows the proposed mechanism of base catalysed hydrolysis and exocyclic methylene exchange. Charge effected attack of hydroxide ion at the 2-position of the imidazoline ring leads to formation of the unstable quaternary intermediate. The reaction may then follow one of two pathways leading to either hydrolysis (A) or exchange of H_B (B). For a given imidazoline, both processes may occur, the favoured pathway being dependent upon the nature of the 2-substituent (represented by R' in figure 9.2). This imbalance between the velocity of the two reactions confers either stability (exchange pathway favoured) or instability (hydrolysis pathway favoured). The substituent determines the relative velocity of the pathways by its

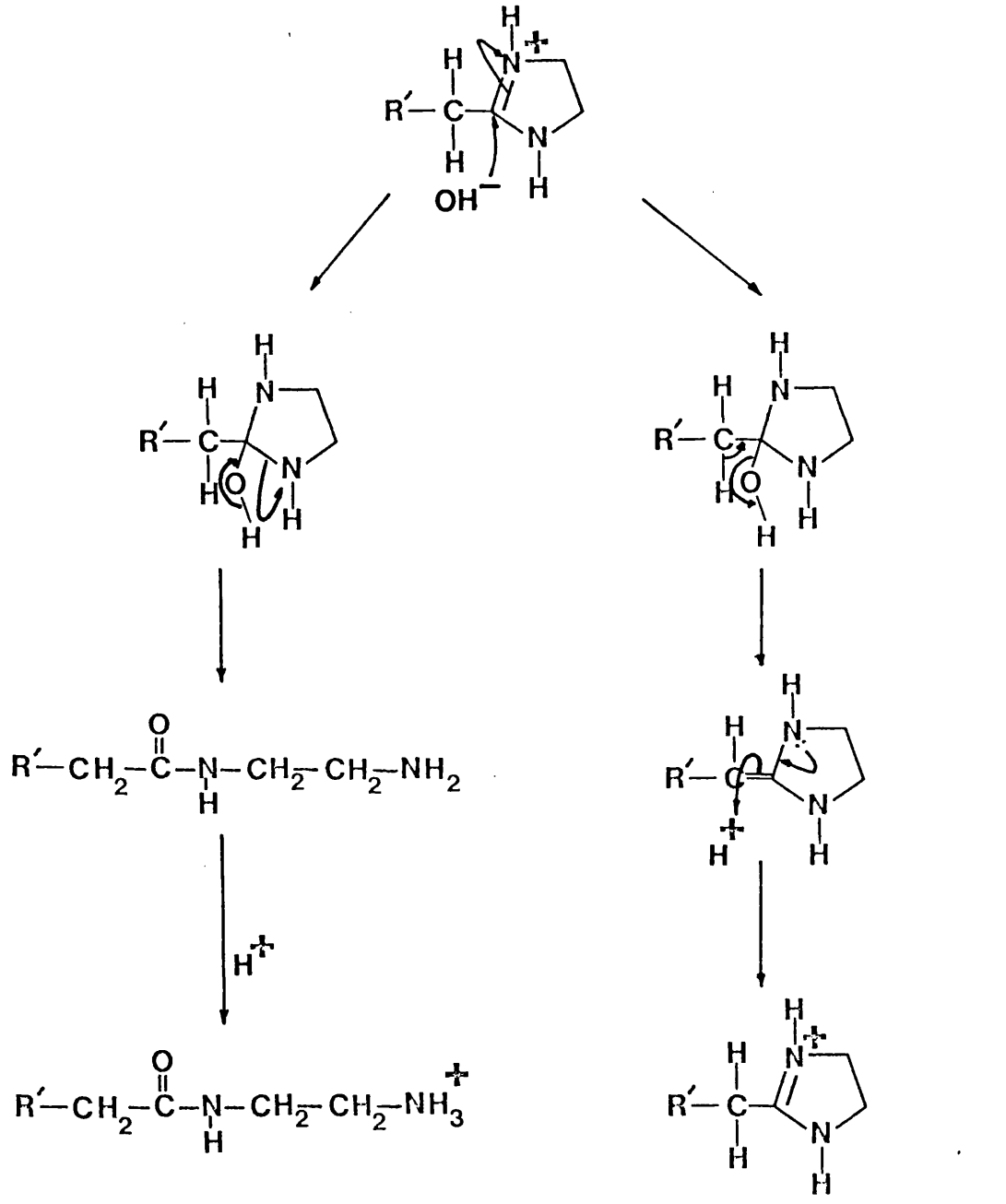

Figure 9.2 - Proposed mechanism for the base catalysed hydrolysis (ring cleavage) and exocyclic methylene proton exchange reactions for the 2-(R'-CH_2)-2-imidazolinium ion.

ability to stabilize the intermediate, e.g. by charge delocalization or resonance. Figure 9.3 shows the extensive resonance structures possible for the intermediate in the tolazoline reaction.

This resonance is inhibited by atoms which prevent conjugation with the aromatic ring; for example substituents with an oxygen atom spaced between the aromatic ring and the exocyclic methylene group (e.g. in cirazoline and fenoxazoline, figure 1.1) will strongly inhibit conjugation, whereas the presence of a nitrogen atom (e.g. in antazoline) will allow limited conjugation. Substituents with a larger aromatic moiety than tolazoline (e.g. in naphazoline) will allow greater conjugation and increased acidity and stability.

2-methyl-2-imidazoline does not possess an aromatic substituent and consequently does not have acidic protons. Stability is, therefore, only due to the presence of the electron donating methyl group. Xylometazoline has a very low rate of exchange which is probably due to the low rate of initial hydroxyl ion attack caused by steric hinderance.

Additional evidence for the proposed mechanism arises from the numerical similarity between the observed rates of cirazoline hydrolysis (pathway A) and naphazoline, tolazoline and antazoline exchange (pathway B). The first order rate constant for the hydrolysis of cirazoline under the conditions of the NMR experiments was calculated as 2×10^{-7} s^{-1} which is similar to the first order rate constants for antazoline, tolazoline and naphazoline exchange ($4 - 20 \times 10^{-7}$ s^{-1}).

Direct comparison of the imidazoline hydrolysis and exchange data is difficult due to the differences in solvent (H_2O/D_2O), pH (or pD),

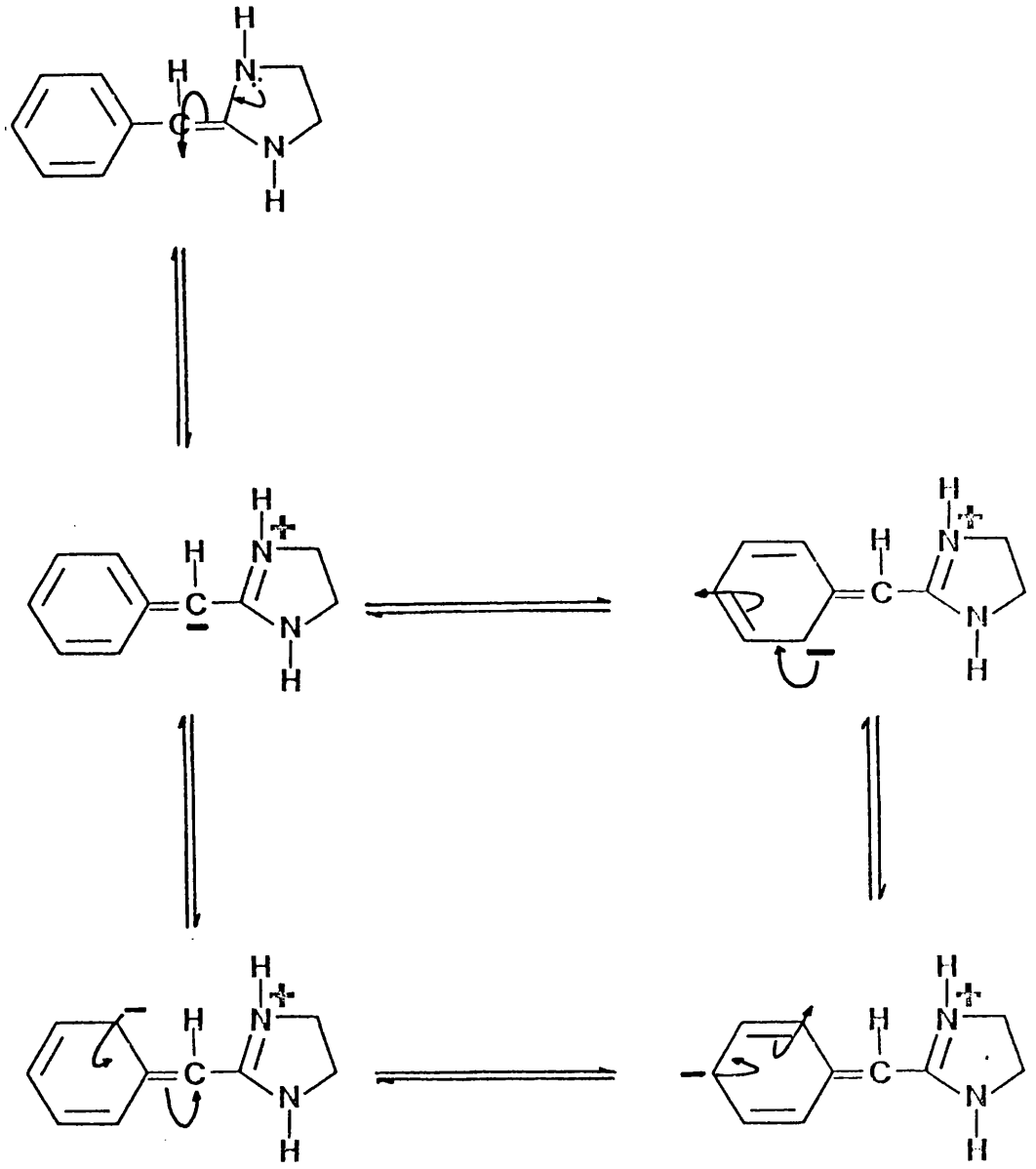

Figure 9.3 - Possible resonance structures for the intermediate formed during the exchange of tolazoline exocyclic methylene protons.

solute concentration and in particular temperature. More direct evidence comes from the behaviour of the antazoline substituent methylene protons (H_D in figure 5.3 table 5.3). No exchange occurred with H_D protons whereas H_B exchanged with deuterium at a rate of 4.4×10^{-7} s^{-1}, giving a half life of 18 days. These data suggest that the protonated imidazoline ring is fundamental to the exchange process.

The proposed mechanism also predicts an increase in exocyclic methylene exchange with an increase in pH, similar to the stability-pH profile (e.g. figure 9.1). This would, therefore, account for the observation by Kounterellis that the free base species of the imidazolines exchanges more rapidly than the protonated species[20] (c.f. early stability reports, section 1.2.3).

The mechanism of imidazoline hydrolysis whereby ring cleavage is due to specific base catalysis of the unprotonated species as proposed by Harnsberger and Riebsomer[25,26] and Fernandez and Lamden[27] is inconsistant with the data in this thesis which support the findings of Martin and Parcell[28], Savignac et al[29] and Ross et al[18]. They indicate that the imidazolinium ion is the labile species and hydrolysis is mediated through attack of neutral water (at low pH) and hydroxide ion (at medium and high pH).

9.2 PHYSICOCHEMICAL NATURE OF CIRAZOLINE HYDROCHLORIDE-SDDS SYSTEMS

The interaction between cirazoline hydrochloride and SDDS in aqueous solution was studied in terms of ion-pair formation, complexation, micellization and solubilization. Aqueous, solid and liquid complex and micellar (pseudo)phases were identified, the relative amounts of each being dependent upon the concentrations of cirazoline hydrochloride and SDDS, temperature and electrolyte. The equilibria

formed between these species were described by the ion-pair association constant, K_{ip}, apparant, (K_s'), and intrinsic, (K_s), solubility products, apparant, (CMC'), and true, (CMC), critical micelle concentrations, the SDDS concentration required to completely solubilize cirazoline, (SOL_T), and the cirazoline micellar association constant, (K_A). These parameters and the physicochemical nature of the formed (pseudo)phases were investigated by automated conductimetric titration, solubility, microscopy, NMR, DSC and PCS techniques.

9.2.1 Ion Pair Formation

Formation of cirazoline dodecylsulphate ion-pairs was demonstrated using an automated conductimetric titration technique (section 6.2) based on the method described by Mukhayer and Davis[121]. At 30°C, K_{ip} was determined as 232 (S.D. = 20) which is in good agreement with reported values for similar sized ions[119]. CPAE dodecylsulphate was found to have a similar K_{ip} value of 248 (S.D. = 9) at 30°C, again consistant with the similarity in the size of the cirazoline and CPAE ions.

9.2.2 Complex Formation

At concentrations of cirazoline hydrochloride and SDDS above the solubility product but below the SOL_T of the system, phase separation occurred to form cirazoline dodecylsulphate complex. Both solid and liquid complex forms were produced dependent upon temperature. Solid complex systems formed at ambient temperature and below resulting in a highly flocculated suspension. Microscopic examination of the suspension and isolated complex revealed long needle-like crystals, (figure 6.5a and b). Liquid complex formed at higher temperatures and produced a grey dispersion or 'coacervate' consisting of discrete

'oily' globules in water, (figure 6.5c). However, formation of solid complex was time dependent and metastable liquid complex and/or metastable viscous solutions were readily produced by mixing aqueous solutions of cirazoline hydrochloride and SDDS at ambient temperature. These systems crystallised with time to form solid complex. Surfactants are known to inhibit crystallization and formation of these metastable systems is indicative of supersaturation[41].

The solubility of the solid and liquid complexes was determined by measuring the solubility product using the automated conductimetric titration technique (section 6.3.2). (This method also enabled the stoichiometry of the interaction to be rapidly and accurately determined). Conductivity curves for titrations involving the formation of liquid complex resembled literature examples in that the phase separation point is given by a deviation from linearity, (figures 1.10a and 6.12). Titrations involving the formation of solid complex, however, were characterised by a sudden fall in conductivity and rapid phase separation leading to the production of a crystalline suspension. Continued addition of titrant resulted in a further increase in conductivity and a linear titration curve of smaller slope than the initial precomplex region (figure 6.13). This behaviour was similar to that reported by Tomlinson and Davis[128] for the titration of indigo carmine against quindecylbenzyldimethylammonium chloride at 25°C, (see section 1.4.2.2 and figure 1.10b). The inflexions in the curves were attributed by these authors to coacervate flocculation phenomena due to the presence of ionic salts and titration end-points were taken as the initial deviation from linearity. However, for the cirazoline hydrochloride-SDDS system in this study it was found that the titration end-point for the solid complex solubility product was given by extrapolation of the second linear region to the first, (figure 6.13).

A solubility product value of 1.17×10^{-7} moles^2 litre^2 was calculated by this method which is in good agreement with the equilibrium K_s' value of $1.15 - 1.20 \times 10^{-7}$ moles^2 litre^{-2} determined by turbidimetry and static conductimetry (section 6.3.2.1). The peak in the conductivity curve shown in figure 6.13 is thought to represent supersaturation due to formation of a metastable system; the extrapolated curve in figure 6.13 therefore represents a theoretical conductivity curve in the absence of supersaturation.

The automated conductimetric method for the determination of solid complex solubility products was found to be reproducible, (CV = 2.6% for eleven determinations). K_s' values for the liquid complex system were determined in duplicate at 37.5°C and 50°C and gave values within $\pm$ 2% of the means.

For a given complex species, titrant flow rate was not critical for K_s' determination (e.g. at 30°C solid complex $K_s' = 1.16 - 1.23 \times 10^{-7}$ moles^2 litre^{-2} at flow rates of 6.29 - 50.48 µl min^{-1}, (table 6.5); liquid complex $K_s' = 2.56$ (37.6°C) and 2.62 (37.5°C) $\times 10^{-7}$ moles^2 litre^{-2} at flow rates of 20.38 and 173 µl min^{-1}, (table 6.7). However, metastable liquid complex could be formed by fast titration, e.g. 173 µl min^{-1}, table 6.5. This effect is similar to that observed during the bulk mixing of cirazoline hydrochloride and SDDS aqueous solutions, (section 6.3.1), and is caused by the liquid complex K_s' being exceeded before onset of crystallization. Metastable liquid complex K_s' values were obtained from inflexions in conductivity curves in a similar manner to that described for the stable liquid complex species. For some temperature conditions, optimization of flow rates enabled calculation of both metastable liquid and solid K_s' values from a single titration.

The stoichiometry of the CIRH-DDS complexes was found to be 1 : 1, (solid 1 : 1.004, liquid 1 : 0.978), by the initial phase separation method, (equations 1.67 and 6.5). NMR analysis of isolated crystalline complex dissolved in $CDCl_3$ confirmed the 1 : 1 stoichiometry of the solid complex (1 : 0.996) (section 6.3.1.1, Appendix I).

Attempts to measure the effect of ionic strength on the solubility of solid complex by conductimetric titration (section 6.3.2.5) were limited by the high background conductance of electrolyte solutions. Results on systems containing low levels of added sodium chloride ($0.1 - 1 \times 10^{-3}$ M; I = $2.1 - 3 \times 10^{-3}$ M) showed no effect on K_s'. Solubility studies on both 2×10^{-3} M and 5×10^{-3} M cirazoline hydrochloride-SDDS mixtures at 30°C showed an increase in complex solubility as ionic strength increased over the ranges I = 0.002 -0.102 M and 0.005 -0.105 M (tables 7.8 and 7.9). However, these data were not sufficiently accurate to determine the quantitative relationship between solubility and ionic strength. Mukhayer and Davis have shown that the solubility of complexes increases with ionic strength according to equations 1.70 and 1.82[134]. Intrinsic solubility products and apparant solubility products at a given ionic strength were therefore calculated from the data in table 6.7 using equations 1.70 and 1.16.

The effect of temperature on the CIRH-DDS K_s' was determined over the range 10 - 50°C. At temperatures at or below 37.5°C, both stable solid complex and metastable liquid complex could be formed, dependent upon titrant flow rate. Above this temperature solid complex could not be formed even at slow flow rates. The solubility of both complex forms increased with increasing temperature, (figure 6.17). Van't Hoff plots, (figure 6.18), show a linear relationship between $\log_{10} K_s$ and

T^{-1} for both solid and liquid complexes but of different slope; the solubility of the solid complex having a greater temperature dependence. The linear plots in figure 6.18 are unusual in that previous reports for a variety of interacting systems over a similar temperature range indicate the presence of a temperature of maximum solubility (minimum K_s')[134]. Like most of the reported systems at higher temperatures (table 1.2), the CIRH-DDS liquid complex (coacervate) phase separation process is driven by a large negative free energy change (-49.1 kJ mol^{-1} at 30°C) which is due to a combination of a negative enthalpy change, (ΔH^o_f = -29.2 kJ mol^{-1}) and a positive entropy change, (ΔS^o_f = +65.6 J mol^{-1} K^{-1} at 30°C), indicating favourable contributions from both coulombic and hydrophobic interactions. This gain in entropy upon complexation or coacervate formation is probably due to loss of water structure.

The data in table 6.8 indicate that solid complex formation, although driven by a free energy change (ΔG^o_f = -50.6 kJ mol^{-1} at 30°C) similar to that for the liquid complex, is controlled by different factors. Crystallization of complex results in a larger negative enthalphy change, (ΔH^o_f = -62.9 kJ mol^{-1}), but a marked decrease in entropy, (ΔS^o_f = -40.6 J mol K^{-1} at 30°C). Thus solid complex formation is driven by coulombic forces but is inhibited by entropic factors. The latter is probably due to the high internal order within the crystals masking water structuring or hydrophobic effects.

The solid and liquid complex Van't Hoff plots intersect at a point equivalent to a transition temperature of 42.5°C and K_s of 2.93 x 10^{-7} $moles^2$ $litre^{-2}$, (figure 6.18). Below this temperature the negative free energy of solid complex formation is numerically greater than for liquid complex formation, (e.g. at 30°C, $\Delta G^o_{f,solid}$ = -50.6 kJ mol^{-1},

$\Delta G^{o}_{f,liquid}$ = -49.1 kJ mol^{-1}) and the solid complex is the stable form. At 42.5°C, $\Delta G^{o}_{f,solid} = \Delta G^{o}_{f,liquid}$ = -50.0 kJ mol^{-1} and both complexes are stable and in equilibrium. Above this temperature, $\Delta G^{o}_{f,solid}$ is numerically less than $\Delta G^{o}_{f,liquid}$ and the liquid complex system is the stable species.

The temperature of transition from solid to stable liquid complex was also determined by DSC and visual observation, (section 6.3.1.1). Macroscopic visual determination was performed by observing the change from an aqueous flocculated suspension of solid complex to a grey dispersion of liquid complex as the temperature was increased in small increments (1°C). DSC on a sample of solid CIRH-DDS complex suspended in water showed a large endothermic peak due to melting of the hydrated complex from which the temperature of transition was obtained. The endothermic nature of the transition from solid to liquid complex is consistant with that predicted from the ΔH^{o}_{f} values in table 6.8, ($\Delta H^{o}_{f,solid}$ = -62.9 kJ mol^{-1}, $\Delta H^{o}_{f,liquid}$ = -29.2 kJ mol^{-1}, i.e. $\Delta H^{o}_{solid \rightarrow liquid}$ = +33.7 kJ mol^{-1}). Unfortunately due to sample preparation problems the enthalpy change of transition could not be determined by DSC.

Transition temperatures for hydrated CIRH-DDS complex determined by each method show reasonable agreement and are summarised below:

Visual macroscopic appearance (section 6.3.1.1)	39° - 42°C
DSC (section 6.3.1.1)	44.6°C (43.0-46.2°C)
Temperature dependence of K_s' (section 6.3.2.4)	42.5°C

Subsequent work has indicated a transition temperature of 42.9°C by DSC.

The hydrophobic effect in complex formation was demonstrated by the formation of cirazoline octylsulphate, decylsulphate, and tetradecylsulphate complexes (sections 6.3.1.1 and 6.3.2.6). Complexation was similar to the CIRH-DDS systems in that both crystalline and liquid (coacervate) species were formed depending upon temperature (section 6.3.1.1). Metastable liquid complex and/or metastable viscous solutions could also be obtained by preparing systems above the solid complex solubility product. Isolation of the solid complexes was more difficult for the lower alkylchain homologues due to their high solubility, the low temperature required for crystallization and the slow rate of crystal formation. The stoichiometry of the complexes was found to be 1 : 1 by NMR (see section 6.3.2.6 and Appendix 1).

Determination of K_s' values was hampered by both high (CIRH-OS) and low (CIRH-TDS) solubilities of the complexes. The latter was particularly troublesome for the solid CIRH-TDS system at low temperature due to the high degree of supersaturation and the consequent greater degree of extrapolation required to obtain titration end-points. Unlike CIRH-DDS systems, Van't Hoff plots showed a non-linear relationship between $\log_{10} K_s'$ and T^{-1}, (figure 6.19), indicating temperature dependence of ΔH^o_f.

The temperature of transition from solid complex to liquid complex increased with increasing chain length; DSC gave hydrated complex melting points of 17.8, 34.1, 44.6 and 52.7°C for CIRH-OS, -DS, -DDS and -TDS complexes respectively. This shift in transition temperature was also observed in the limited K_s' temperature dependence data determined by conductimetric titration, (figures 6.20 and 6.21).

The solubilities of the cirazoline alkylsulphate complexes was consistant with interactive reports for other complex systems in that K_s is related to the number of methylene groups in the alkylchain according to equation 1.79[125,128,129,136,137]. The free energy change due to the transfer of a methylene group from the aqueous phase to the liquid complex phase was independent of temperature (10 - 50°C) and was calculated as $d(\Delta G^o_f)/_{dn}$ = -3.46 (S.D. = 0.04) kJ mol^{-1} (table 6.11). This is similar to previously reported values in the range -3.2 to -3.5 kJ mol^{-1} for various liquid coacervate systems[125,128,129,136,137] and suggests partial structuring within the liquid complex phase[136]. $d(\Delta G^o_f)/_{dn}$ data for solid complexes were limited but suggest a greater methylene group contribution to the free energy change upon crystalline complex formation compared to liquid (coacervate) formation (e.g. at 20°C $d(\Delta G^o_f)/_{dn}$ = -4.57 (S.D. = 0.06) and -3.42 (S.D. = 0.17) kJ mol^{-1} respectively). The data in table 6.11 also indicate temperature dependence for the free energy associated with transfer of a methylene group to solid complex, $d(\Delta G)/_{dn}$ increasing with decreasing temperature.

These physicochemical phenomena were not specific to cirazoline alkylsulphate systems. Formation of crystalline complexes and/or stable and metastable viscous solutions and liquid complexes was also observed in a total of four other imidazoline-SDDS systems studied (sections 6.3.1.2 and 6.3.2.7). The nature and solubility of formed complex was dependent upon the imidazoline 2-substituent (table 6.12). Tolazoline and naphazoline have unsubstituted aromatic moieties (figure 1.1) and formed viscous liquid complex systems with SDDS. No solid complex species was formed in these systems even at low temperature (4°C). NAPH-DDS was more soluble than the (metastable) CIRH-DDS liquid complex at 30°C ($K_{s'}$ = 3.01 and 2.01 x 10-7 moles2

litre^{-2} respectively) but was much less soluble than TOLH-DDS complex (K_s' = 2.53 x 10^{-6} moles^2 litre^{-2} at 30°C) which reflects the more hydrophobic nature of the naphazoline 2-substituent (figure 1.1). Xylometazoline, like cirazoline, readily formed both solid and liquid complexes with SDDS. K_s' values for the liquid and solid XYLH-DDS species are also similar and indicate a transition temperature close to 30°C. Slow crystallization from liquid complex occurred at 4°C. Antazoline is a much larger molecule than the other imidazolines studied (figure 1.1) and at 30°C only formed a poorly soluble solid complex (K_s' = 1.24 x 10^{-8} moles^2 litre^{-2}). Solid complex precipitated immediately when antazoline sulphate and SDDS solutions were mixed at room temperature and no metastable viscous solution or liquid complex species were produced. However, extensive supersaturation did occur during conductimetric titrations making accurate determination of K_s' difficult.

CPAE and SDDS also interacted to form a liquid complex or coacervate system at 30°C, (K_s' = 2.43 x 10^{-7} moles^2 litre^{-2}).

9.2.3 Aggregation and Solubilization

A mathematical approach to aggregation in cirazoline hydrochloride-SDDS systems has been discussed in section 7.1.1 involving the partition constant (K_p) for the solubilization of the neutral ion-pair by SDDS micelles (equation 7.1) and the equilibrium constant (K_A) for the binding of the protonated cirazoline ion to the negative SDDS micelles. Sepulveda and Perez-Cotopoz[90] derived equation 1.87 for the calculation of K_A but this requires an assay capable of distinguishing between 'free' and 'bound' (micellar) solute. Consequently the simple treatment described in section 7.1.1 leading to equation 7.14 for the calculation of K_A has been adopted in this thesis. This approach, like

that of Sepuveda and Perez-Cotopoz relies on the following assumptions (terminology is fully defined in section 7.1.1);

(i) the concentration of ion-pair in aqueous solution is small and constant,

(ii) equation 7.8 is valid at the CMC of the system,

(iii) the aqueous concentration of cirazoline and dodecylsulphate remain constant in the presence of micelles.

A knowledge of the total cirazoline concentration, the aqueous cirazoline concentration and the concentration of SDDS at the CMC' and SOL_T is required for the determination of K_A, (equation 7.14). These parameters were determined using the solubility and automated conductimetric titration techniques described in sections 6.2 and 7.1.2.

The solubility method was used to detemine CMC' and SOL_T values at 30°C from the effect of SDDS concentration on the solubility of cirazoline. Crystalline complex was formed above the solubility product and below the SOL_T; the amount of cirazoline was determined by filtration and subsequent HPLC assay (chapter 3). However, this solubility technique was slow and laborious as it involved preparation, equilibration and assay of numerous systems. In addition, CMC' and SOL_T values were often difficult to determine from theoretical and observed solubility curves.

A far quicker and precise method for the study of aggregation was the automated conductimetric titration technique described in sections 6.2.1 and 7.1.2.2 which enabled the determination of CMC', SOL_T, aggregate ratio and K_A values within a matter of hours. For the

2 x 10^{-3} M cirazoline hydrochloride solid complex system at 30°C, the method was shown to be reproducible, (CV for CMC' = 2%, SOL_T = 3%, K_A = 7%, table 7.4), and independent of titrant flow rate at 12.4 - 50.5 µl min, (CMC' = 5.20 - 5.27 x 10^{-3} M, SOL_T = 6.79 - 7.04 x 10^{-3} M, K_A = 2.7 - 3.4 x 10^4 M^{-1}, table 7.3). However, fast titration (251.3 µl min^{-1}) resulted in the CMC' being exceeded before crystallization of solid complex and measured parameters, therefore, relate to aggregation in metastable liquid complex system.

A reasonable correlation between parameters determined from conductimetric titrations and solubility studies was obtained; CMC' = 5.36 and 5.25 x 10^{-3} M, SOL_T = 7.04 and 6.55 x 10^{-3} M and K_A = 3.1 and 4.0 x 10^4 M^{-1} for the 2 x 10^{-3} M cirazoline hydrochloride system (table 7.10) and CMC' = 7.48 and 7.50 x 10^{-3} M, SOL_T = 10.73 and 11.65 x 10^{-3} M and K_A = 3.1 and 2.4 x 10^4 M^{-1} for the 5 x 10^{-3} M cirazoline hydrochloride system (table 7.11). The observed differences in values determined by the two techniques may be due to the limited solubility data available.

A problem associated with the measurement of conductivity in disperse systems is the obstruction effect caused by the presence of non-conducting particles. This was a potentially serious problem with crystalline complex systems but was overcome by continuously filtering the mixture using a specially designed glass cell (figure 7.1). This assembly was shown to have no effect on aggregation (SDDS CMC at 30°C = 8.25 x 10^{-3} M in the absence and 8.21 (S.D. = 0.09) x 10^{-3} M in the presence of the assembly). However, the presence of the glass wool in the assembly increased the background conductivity to approximately 15 - 50 x 10^{-6} S and an alternative to glass wool would, therefore, be preferable.

The conductimetric titration method involved titrating SDDS into a solution of cirazoline hydrochloride and calculating CMC' and SOL_T points from inflexions in the conductivity chart traces. The nature of these inflexions was dependent upon the type of complex formed; for the solid complex systems (e.g. 2 x 10^{-3} M cirazoline hydrochloride, 30°C, figure 7.2) inflexions were noted at the liquid complex phase separation, complex transition, equimolar concentration, CMC' and SOL_T points.

At the phase separation and phase transition points, conductivity curves resembled those for complexation, (section 6.3.2.2). Further addition of SDDS to the system beyond the phase transition point produced a linear response until the equimolar concentration point was approached, (e.g. curve c, figure 7.2). In this region the concentration of $CIRH^+_{(aq)}$ decreases rapidly and after the equimolar concentration point little complex is formed and the majority of dodecylsulphate remains as the free ion species, ($DDS^-_{(aq)}$). This results in a linear conductivity curve, (figure 7.2) and the Onsager plots, (figure 7.3, region C-D) indicate that the added SDDS is behaving as a strong electrolyte with little or no interaction between added SDDS and formed complex. The equimolar concentration point is further evidence of a 1 : 1 stoichiometry in the solid complex.

The sharp inflexion in conductivity curves at the CMC' (curves b and c in figures 7.2 and 7.3) is indicative of formation of aggregates with a large aggregation number, micelle equilibration constant and counterion binding (see section 1.3.1). The SOL_T point is characterised by an increase in conductance and a decrease in equivalent conductance. These conductance changes are consistant with the formation of a more highly conducting species, e.g. the formation of smaller and/or more

highly charged aggregates due to dilution of saturated aggregates with free dodecylsulphate ions, ($DDS^-_{(M)}$).

For the liquid complex system (e.g. 2 x 10^{-3} M cirazoline hydrochloride-SDDS system, 40°C, figure 7.4) inflexions at the phase separation point, CMC' and SOL_T were evident. Unlike the solid complex system (c.f. figures 7.2 and 7.4) the conductivity curve between the phase separation and aggregation points, (region A-D), is non-linear with no obvious inflexions at the equimolar concentration point (point C). The increase in conductivity at the CMC' indicates the formation of more highly conducting species due to aggregation. This is abnormal and may be explained by the liquid nature of the complex being solubilized. Partitioning into or more likely, adsorption of dodecylsulphate monomers on to the complex phase is likely to occur due to the surface active properties of SDDS. The composition of the formed complex phase will not, therefore, be of 1 : 1 stoichiometry in the presence of excess SDDS but will be rich in dodecylsulphate. When the concentration of aqueous dodecylsulphate ($DDS^-_{(aq)}$) reaches the CMC aggregation and solubilization of complex occurs. This 'liberates' the dodecylsulphate associated with the liquid complex phase resulting in increased micellar dodecylsulphate ($DDS^-_{(M)}$) and an increase in conductivity. At the SOL_T all complex phase has been solubilized and the relative increase in conductivity with SDDS concentration, therefore, decreases. Adsorption and/or partioning of $DDS^-_{(aq)}$ into the complex phase is also consistant with inflexions in the Onsager plot (figure 7.5). This explanation predicts that equation 7.8 for the determination of [$CIRH^+_{(aq)}$] (CMC) at the apparent CMC (CMC'), and equations 7.10-7.14 for the determination of K_A values are not valid for liquid complex systems.

The effect of cirazoline hydrochloride concentration (0.2 - 5 x 10^{-3} M) on the interaction with SDDS was studied at 30°C by conductimetric titration (section 7.1.3.1). Results indicate a potent CMC' decreasing effect at low cirazoline concentrations followed by an increase in CMC' and SOL_T at higher concentrations due to increased formation of crystalline complex, (table 7.5, figure 7.6). The true CMC, however, continues to decrease with increase in cirazoline hydrochloride concentration which is probably due to the increase in inorganic electrolyte concentration (Na^+ and Cl^-) with increasing complex formation. Addition of electrolyte was shown to have a similar effect on reducing the CMC in CIRH-DDS aggregation systems as on the pure SDDS system (figure 7.16). The true CMC-ionic strength plots for 2 x 10^{-3} and 5 x 10^{-3} M cirazoline hydrochloride-SDDS systems are similar and indicate that the amount of formed complex per se does not affect the CMC of the system, (figure 7.15).

An indication of the structure of formed cirazoline dodecylsulphate aggregates was obtained by determining the molar ratio of cirazoline to dodecylsulphate moieties within the aggregates. For the system at 30°C, a plot of micellar cirazoline concentration against micellar dodecylsulphate concentration was linear from which the cirazline : dodecylsulphate moiety ratio was calculated as 0.60 : 1. This is an extremely high ratio of solubilizate to surfactant and indicates a strong interaction between cirazoline and SDDS micelles which is reflected in the high K_A value of 2.9 x 10^4 (S.D. = 0.2 x 10^4). These parameters are similar in value to those reported for CTAB - sodium p-toluenesulphate, toluate, benzenesulphonate and phenylphosphate systems by Sepulveda et al[139,90], (CTAB; organic ion molar ratio = 1 : 0.4 - 1 : 0.77 and K_A = 1.3 - 2.2 x 10^4 M^{-1}).

The effect of added electrolyte (1×10^{-4} - 1×10^{-1} M NaCl) on aggregation and solubilization was studied by conductimetric titration and solubility studies at 30°C, (section 7.1.3.3). The CMC' and SOL_T for 2×10^{-3} and 5×10^{-3} M cirazoline hydrochloride-SDDS systems decreased with increasing electrolyte concentration (tables 7.10 and 7.11, and figure 7.15). However, electrolyte primarily affects the degree of aggregation and has minimal effect on the association of cirazoline to SDDS micelles; the cirazoline : dodecylsulphate moiety ratio within the aggregates for both 2×10^{-3} and 5×10^{-3} M cirazoline systems was approximately constant at 0.57 (S.D. = 0.05) : 1. This is consistant with literature reports of ion exchange between large organic ions (such as $CIRH^+$) and small inorganic ions (such as Na^+) at the surface of micelles, (see section 1.3.1 and 1.5.3.3). Although the composition of the aggregates remains approximately independent of ionic strength, the solubility of cirazoline in the aqueous phase increases with increasing electrolyte concentration resulting in a reduction in K_A values, (tables 7.10 and 7.11).

Particle size analysis using photon correlation spectroscopy (section 7.2) showed that electrolyte had a profound effect on the size of cirazoline dodecylsulphate aggregates (table 7.12 and figure 7.17). No valid analysis was obtained in the absence of added sodium chloride indicating a small aggregate size. Extremely large aggregates were detected in the presence of added 0.05 and 0.1 M NaCl, however, (e.g. mean diameter = 259 nm for 2×10^{-3} M cirazoline hydrochloride - 3×10^{-3} M SDDS - 0.1 M NaCl system at 30°C). Maximum aggregate size was greater in 0.1 M NaCl than in 0.05 M NaCl systems but in both cases corresponded to the SOL_T of the system indicating that size is a function of:

(i) the amount of cirazoline solubilized,

(ii) the degree of cirazoline saturation within the aggregates,

(iii) the concentration of electrolyte.

The increase in particle size of saturated aggregates with increase in the amount of solubilized cirazoline suggests that systems containing higher initial concentrations of cirazoline hydrochloride will result in larger aggregates upon solubilization. This is supported by the solubility data for 5 x 10^{-3} M cirazoline hydrochloride-SDDS systems in the presence of 0.05 and 0.1 M NaCl (table 7.9 and figure 7.14). These samples were filtered through a 0.45 μm filter to remove excess complex before assay. As the SDDS concentration approached the SOL_T for the system, the cirazoline assay values became erratic and were lower than predicted. These data are consistant with the formation of extremely large aggregates (>450 nm) which were filtered from solution during sample preparation.

Larger aggregate size in cirazoline-SDDS-NaCl system is also indicated by the highly viscous nature of solubilized systems. Visual observation indicated that in the presence of 0.05 and 0.1 M NaCl, systems became increasingly viscous and turbid during the solubilization process. This turbidity and viscosity was reduced in systems well above the SOL_T of the system, (e.g. 5 x 10^{-3} M cirazoline systems, table 7.9).

Temperature was found to have a profound effect upon aggregation. Micellization and solubilization was studied over the range 10 - 50°C by conductimetric titration at an initial cirazoline hydrochloride concentration of 2 x 10^{-3} M. for the solid complex system (< 35°C) both the true and apparent CMC (CMC') decreased with increase in temperature. The sensitivity of the CMC to temperature change is

reflected in the unusually high enthalpy values for micellization, ΔH^{o}_{M}, (11-42 kJ mol^{-1}, table 7.7). For pure SDDS, ΔH^{o}_{M} has been reported as -1.3 to +2.2 kJ mol^{-1} at 25°C[40] and the change in CMC with temperature is slight in the range 20 - 30°C but increases at higher and lower temperatures[111], (figure 1.9). The continuous fall in CMC values with rise in temperature for the systems studied here is probably due to the increase in cirazoline dodecylsulphate aqueous solubility with temperature (figure 6.17). The presence of small quantities of cirazoline in the aqueous phase has a potent CMC decreasing effect, (figure 7.6), and increase in temperature will, therefore, reduce the CMC of the system. The effect of temperature on ΔS^{o}_{M} is also unusual; pure surfactant systems usually exhibit a decrease in ΔS^{o}_{M} with increase in temperature due to the reduction in water structuring.

The effect of temperature on the ability of aggregates to solubilize pre-formed cirazoline dodecylsulphate crystalline complex is shown by the rapid fall in SOL_T as temperature is increased from 10° to 35°C (figure 7.8). This increase in solubility is brought about by an increase in both aqueous cirazoline solubility (tables 6.7 and 7.6) and the interaction between $CIRH^{+}_{(aq)}$ and $DDS^{-}_{(M)}$ (table 7.6); the molar ratio of cirazoline to dodecylsulphate moieties within the aggregates increases from 0.21 : 1 at 10°C to 0.66 : 1 at 35°C. The result of these two factors is a decrease in the affinity of $CIRH^{+}_{(aq)}$ to $DDS^{-}_{(M)}$ as shown by the fall in K_A values from 7.2 x 10^4 M^{-1} at 10°C to 2.7 x 10^4 M^{-1} at 35°C, (table 7.6 and figure 7.11). At low temperatures the association process is characterised by large positive entropy and enthalpy changes. Unlike the micellization process the magnitude of these parameters decreases with temperature increase, (table 7.7).

A sharp inflexion in CMC' and SOL_T-temperature curves is observed corresponding to the phase transition temperature of the systems, (figure 7.8). The temperature of transition is slightly lower in these systems compared to the transition temperature of pure complex systems (36°C versus 39 - 44.6°C); it is not clear whether this is due to a real effect of excess SDDS in the system or to the formation of metastable systems. The effect of temperature on the CMC' and SOL_T in liquid complex systems is less pronounced than with the solid complex system and micellization and solubilization appear to be equally affected by temperature. This inflexion in the CMC'-temperature curve is probably due to the change in complex solubility characteristics, (figure 6.17).

Clear inflexions in the plots of CMC (Van't Hoff plot, figure 7.9), K_A (figure 7,11 and Van't Hoff plot, figure 7.12), and aggregate ratio, (figure 7.10), against temperature are also apparant. However, the values of these parameters for aggregation and solubilization rely on the validity of equations 7.8 - 7.14. These equations are not thought to be valid for the liquid complex systems due to partitioning and/or adsorbtion of dodecylsulphate into the complex phase. Such effects would lead to erroneously high CMC, aggregate ratio and K_A values when using the treatment described in section 7.1.1.

9.2.4 Structure of Cirazoline Dodecylsulphate Systems

The interactions and formed structures possible within cirazoline hydrochloride-SDDS systems are outlined in figure 9.4. At very low concentrations of cirazoline and dodecylsulphate ion-association occurs to form electrically neutral ion pairs, $CIRH\text{-}DDS_{(aq)}$ but complex and micellar (pseudo)phases are absent. The equilibrium between the free ions and the ion-pair is quantified by the ion-pair association

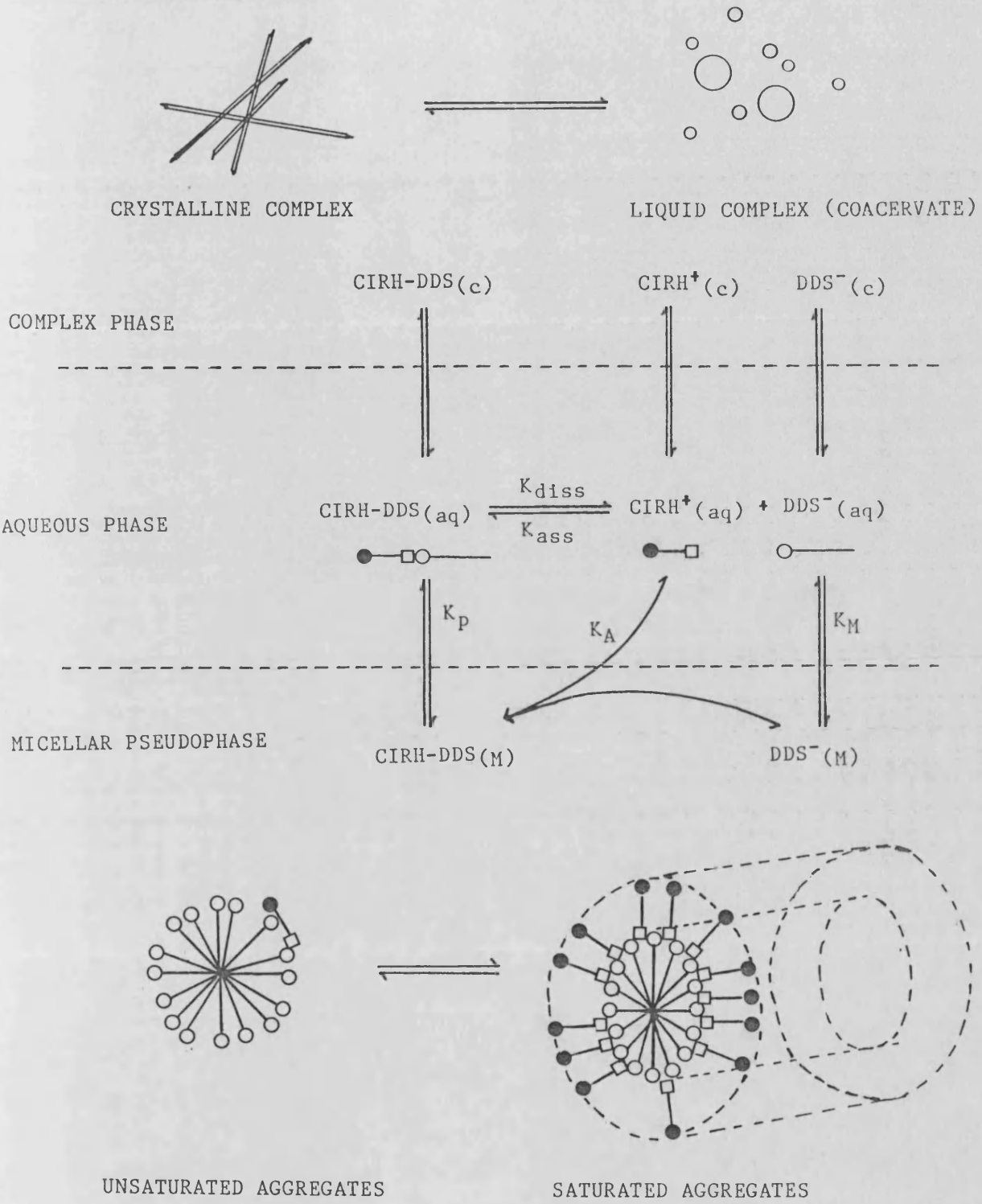

Figure 9.4 - Possible interactions and structures in cirazoline dodecylsulphate systems.

constants, (K_{ass} or K_{ip} equations 1.53 and 1.54), and the corresponding dissociation constant (K_{diss}, equation 1.64). At concentrations of SDDS below the CMC' of the system an increase in either cirazoline or SDDS concentration leads to increased ion-pair formation, (equation 1.54), until the apparant solubility product (K_s' equation 1.70) is reached. At this point phase separation occurs and cirazoline dodecylsulphate complex is formed. Complex may be crystalline or liquid (coacervate) in nature dependent upon temperature. However, if the CMC' of the system is less than the SDDS concentration necessary to exceed the solubility product then phase separation will not occur.

Interaction between complex and free cirazoline and/or dodecylsulphate ions is possible due to adsorption and/or partitioning into the complex phase. This is thought to be more important for the liquid complex systems in the presence of excess SDDS and adsorption onto complex crystals is thought to be minimal. Addition of excess SDDS to the system (i.e. [SDDS] > [CIRHCl]) leads to an increase in free dodecylsulphate ion ($DDS^-_{(aq)}$) concentration and aggregation occurs at the CMC of the system (K_M, equation 1.33). Formation of the SDDS micellar pseudophase allows its interaction with $CIRH\text{-}DDS_{(aq)}$, (K_p, equation 1.36) and $CIRH^+_{(aq)}$, (K_A, equation 1.83). Interaction of cirazoline with the dodecylsulphate aggregates by either mechanism leads to dissolution of complex in order to maintain the $CIRH\text{-}DDS_{(aq)}$ and $CIRH^+_{(aq)}$ concentration. At the SOL_T point sufficient micellar pseudophase is present to completely dissolve the complex and the system clears to form a micellar solution.

Between the CMC' and SOL_T points both aqueous and micellar (pseudo) phases are saturated with respect to cirazoline. Large aggregates are thought to be formed in this region probably due to cooperative

interaction between cirazoline aromatic moieties within the aggregates, (figure 9.4). Further addition of SDDS above the SOL_T leads to formation of unsaturated aggregates and a reduction in the concentration of $CIRH\text{-}DDS_{(aq)}$ and $CIRH^+_{(aq)}$. Aggregate size decreases due to reduced interaction between the cirazoline aromatic moieties until, in dilute cirazoline micellar solutions, approximately spherical micelles are formed as evidenced by observed viscosity changes.

The interactions and system of events just described refer to equilibrated systems. However, above the solubility product metastable systems may occur due to slow nucleation and/or slow rate of complex crystal formation. Metastable systems may take the form of liquid complex (coacervate) or large aggregates leading to viscous micellar solutions (sections 1.4.3.2 and 6.3.1). These phenomena are particularly important when solutions of cirazoline hydrochloride and SDDS are bulked (section 6.3.1) and during conductimetric titrations (sections 6.3.2 and 7.1.2.2).

Figure 9.5 shows predicted phase diagrams for the cirazoline hydrochloride-SDDS system at 10 - 50°C together with that in the presence of 0.1 M NaCl at 30°C. The aqueous solution - suspension/coacervate boundary was calculated using equation 1.70 and the K_s' values in table 6.7, (K_s' at 30°C for the systems in 0.1 M NaCl was calculated as 1.86×10^{-7} moles^2 litre^2 using equations 1.70 and 1.16). The aqueous micellar solution boundary represents the CMC' of the systems and the suspension/coacervate - micellar solution boundary represents the SOL_T of the system. These values for the system at 30°C with no added electrolyte were taken from table 7.5. Values for other systems were estimated from data in tables 7.5, 7.6, 7.10 and 7.11 and are, therefore, approximate.

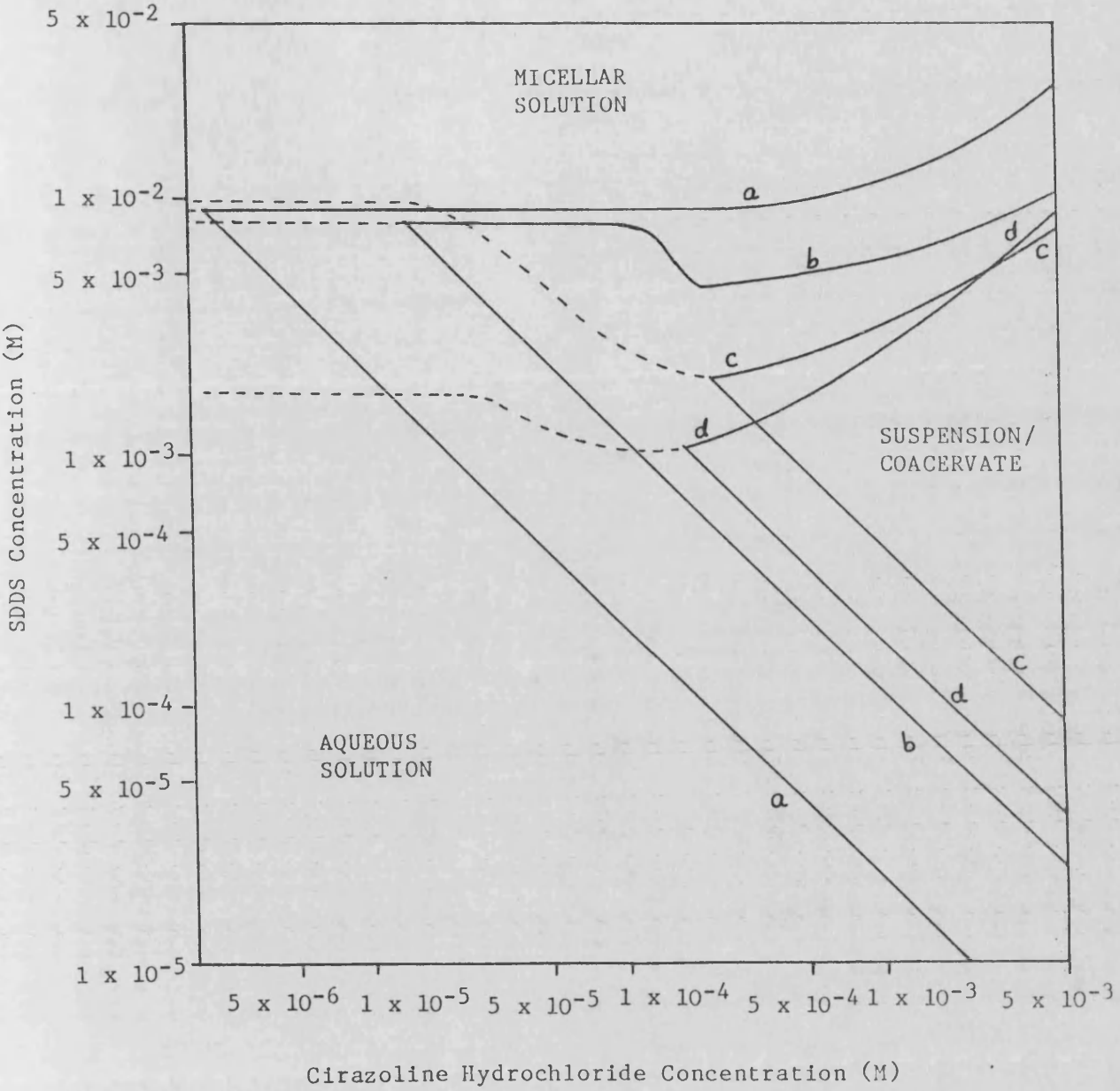

Figure 9.5 - Predicted phase diagram for cirazoline hydrochloride-SDDS systems at (a) 10°C, (b) 30°C, (c) 50°C and (d) 30°C in the presence of 0.1 M NaCl. Solid lines represent the suspension/coacervate - aqueous/micellar solution boundary; dashed lines represent the aqueous solution - micellar solution boundary.

An increase in temperature increases the solubility of cirazoline in SDDS systems due to an increase in aqueous solubility (K_s'), a decrease in the CMC' of the system and an increase in the capacity of aggregates to interact with or 'solubilize' cirazoline. Addition of electrolyte also increases the solubility of cirazoline in SDDS systems although addition of sodium chloride does not affect the capacity of aggregates to solubilize cirazoline.

At moderately high electrolyte concentrations (0.05 and 0.1 M) extremely large saturated aggregates formed which resulted in a viscous system (section 7.1.3.3). These structures may result from flocculation of cylindrical aggregates due to a reduction in charge repulsion. Similar effects have been noted for a variety of large organic ion-ionic surfactant systems, (section 1.4.3.2). A highly interactive meshwork of aggregates may then result due to interaction of aromatic moieties from different aggregates or regions of aggregates resulting in an increased viscosity of the system. Birefringence was not detected in these systems indicating the absence of liquid crystalline phase (section 7.1.3.3).

The ability of the organic ion to associate with aggregates and produce viscous solutions may be due to the structure of the ion and its ability to interact at the surface of the aggregates. Hence simple aromatic moieties (e.g. in tolazoline, tosylate and benzenesulphonate ions) may interact strongly to form rod-like micelles and viscous solutions even in the absence of added electrolyte. Bulky organic ions may have limited self-interaction or cooperativity resulting in decreased association.

9.3 THE EFFECT OF SDDS ON THE HYDROLYSIS OF CIRAZOLINE

The effect of SDDS concentration on the hydrolysis of cirazoline at pH 7.0 was studied at two initial cirazoline hydrochloride concentrations (0.2 and 2 x 10^{-3} M) and at two temperatures involving formation of crystalline complex (30°C) and liquid complex (50°C). The effect of added electrolyte (1 x 10^{-3} M - 0.1 M Nacl) on the hydrolysis of cirazoline in the 2 x 10^{-3} M cirazoline hydrochloride - 7 x 10^{-3} M SDDS system was also investigated. Kinetic studies were performed using the manual pH stat technique in the absence of added buffer salts. Aqueous hydrolysis of cirazoline under these conditions was shown to be due to specific base catalysed hydrolysis of the protonated species (section 8.3.2 and 9.1). The cirazoline degradation product, CPAE, was shown to have similar properties to cirazoline with respect to its interaction with SDDS (see K_{ip}, K_s' values, section 6) and will, therefore, cause minimal disruption to the structure of the system. However, kinetic studies were generally not followed beyond 80% residual cirazoline concentration to avoid large amounts of CPAE formation.

In the absence of added electrolyte, moderately low concentrations of SDDS had a potent stabilizing effect; e.g. for the 2 x 10^{-4} M cirazoline hydrochloride system at 30°C, 0.008 M SDDS resulted in a 66 fold increase in stability (table 8.11); addition of 0.03 M SDDS to 2 x 10^{-3} M cirazoline hydrochloride increased its stability at 30°C by 220 times (table 8.12), and addition of 0.06 M SDDS to 2 x 10^{-3} M cirazoline hydrochloride resulted in a 126 fold increase in stability at 50°C (table 8.13).

A knowledge of K_{ip}, K_s', CMC' and SOL_T and careful selection of concentrations enabled the contribution of each cirazoline containing

species to be evaluated, i.e. free aqueous ion, $CIRH^{+}_{(aq)}$; ion pair, $CIRH\text{-}DDS_{(aq)}$; complex, $CIRH\text{-}DDS_{(c)}$; and solubilized cirazoline $CIRH\text{-}DDS_{(M)}$ species, (figure 9.4). Degradation may proceed at different rates for each species leading to equation 9.1 which defines the overall first order rate constant for protonated cirazoline in the presence of SDDS, k_{SDDS}:

$$k_{SDDS} = k_{(aq)}.f_{(aq)} + k_{(ip)}.f_{(ip)} + k_{(c)}.f_{(c)} + k_{(M)}.f_{(M)} \qquad (9.1)$$

Where $k_{(aq)}$, $k_{(ip)}$, $k_{(c)}$ and $k_{(M)}$ are the relevent first order rate constants and $f_{(aq)}$, $f_{(ip)}$, $f_{(c)}$ and $f_{(M)}$ are the fractions of $CIRH^{+}_{(aq)}$, $CIRH\text{-}DDS_{(aq)}$, $CIRH\text{-}DDS_{(c)}$ and $CIRH\text{-}DDS_{(M)}$ in the overall system respectively.

The effect of ion-pair formation was studied using the 2×10^{-4} M cirazoline hydrochloride SDDS system. SDDS concentrations up to 5.9×10^{-4} M resulted in formation of an homogeneous aqueous solution as concentrations of cirazoline and dodecylsulphate are below the solubility product and CMC' of the system (figure 9.5). The observed stability factor is close to unity for these systems indicating that formation of ion-pairs does not significantly influence the rate of cirazoline hydrolysis, (table 8.11 and figure 8.13), and that $k_{(ip)}.f_{(ip)} = k_{(aq)}.f_{(aq)}$. (Use of equations 1.55 and 1.70 predicts that $[CIRH\text{-}DDS_{(aq)}] = 2.7 \times 10^{-5}$ M ($f_{(ip)} = 0.14$) at the phase separation point and the vast majority of cirazoline is, therefore, present as $CIRH^{+}_{(aq)}$.

Equation 9.1 may be simplified using the assumptions that formed complex is inert (i.e. $k_{(aq)} >> k_{(c)} \rightarrow 0$) and $k_{(ip)}.f_{(ip)} = k_{(aq)}.f_{(aq)}$, equation 9.2:

$$k_{SDDS} = k_{(aq)}.f_{(aq)} + k_{(M)}.f_{(M)} \qquad (9.2)$$

Equation 9.2 may be written in terms of a stability factor (see section 8.3.6):

$$\text{Stability Factor} = \frac{k_{(aq)}}{k_{SDDS}} = \frac{k_{(aq)}}{k_{(aq)} \cdot f_{(aq)} + k_{(M)} \cdot f_{(M)}} \qquad (9.3)$$

and below the CMC' of the system when $f_{(M)} = 0$, equation 9.3 further reduces to equation 9.4:

$$\text{Stability Factor} = \frac{k_{(aq)}}{k_{SDDS}} = \frac{1}{f_{(aq)}} \qquad (9.4)$$

The stabilizing effect due to complex formation was investigated by studying systems between the complex separation point and the CMC' of the system. In this region $f_{(M)} = 0$ and the amount of formed complex - and hence concentration of remaining free aqueous cirazoline ion - was calculated using equation 1.71. Theoretical stability factors for each system were calculated using equation 9.4 and are shown alongside observed stability factors (from tables 8.11 - 8.13) and calculated $f_{(c)}$ and $f_{(aq)}$ values in tables 9.2 —— 9.4.

Calculation of the contribution of the solubilized cirazoline species to the overall reaction requires a knowledge of $k_{(M)}$ and $f_{(M)}$. These parameters were calculated using the Menger and Portnoy kinetic model (section 1.5.3.1) and the Lineweaver-Burke equation (equation 1.91). Table 9.5 shows the transformed experimental data obtained in this study and derived K_A and $k_{(M)}$ values for each of the experimental systems. Only data above the SOL_T were used and data for the higher SDDS concentrations at 50°C were excluded because of high ionic strength effects. Figure 9.6 shows the Lineweaver-Burke plots for each system. $f_{(M)}$ values for each system were determined using the K_A values in table 9.5 and equation 7.2 and are shown in tables 9.2 - 9.4

[SDDS] (M x 10^3)	$f_{(c)}$	$f_{(M)}$	$f_{(aq)}$	STABILITY FACTOR	
				THEORETICAL	OBSERVED
0.1	0	0	1.000	1.0	1.3
0.2	0	0	1.000	1.0	1.1
0.4	0	0	1.000	1.0	1.1
1.0	0.3685	0	0.6315	1.6	1.9
2.0	0.6860	0	0.3140	3.2	-
3.0	0.8225	0	0.1775	5.6	7.3
4.0	0.8720	0	0.1280	7.7	-
5.0	0	0.9406	5.938×10^{-2}	15	15
7.0	0	0.9856	1.436×10^{-2}	43	36
8.0	0	0.9896	1.041×10^{-2}	52	66
10.0	0	0.9933	6.719×10^{-3}	64	-

Table 9.2 - The distribution of cirazoline and observed and theoretical stability factors for the 2×10^{-4} M cirazoline hydrochloride-SDDS system at 30°C. $f_{(c)}$, $f_{(M)}$ and $f_{(aq)}$ = fractions of cirazoline distributed in the complex, micellar and aqueous (pseudo)phases respectively. Theoretical stability factors were calculated using equation 9.3 and $k_{(aq)} = 2.00 \times 10^{-6}$ s^{-1}, $k_{(M)} = 1.82 \times 10^{-8}$ s^{-1}, $K_A = 2.64 \times 10^4$ M^{-1} and CMC' = 4.40×10^{-3} M.

[SDDS] ($M \times 10^3$)	$f_{(c)}$	$f_{(M)}$	$f_{(aq)}$	STABILITY FACTOR	
				THEORETICAL	OBSERVED
0.3	0.1170	0	0.8830	1.1	1.2
0.5	0.2130	0	0.7870	1.3	1.6
1.0	0.4470	0	0.5530	1.8	1.9
2.0	0.8290	0	0.1710	5.9	8.4
3.0	0.9470	0	5.300×10^{-2}	19	27
4.0	0.9715	0	2.845×10^{-2}	35	-
5.0	0.9805	0	1.925×10^{-2}	52	65
5.4	0.9835	0	1.725×10^{-2}	58	-
5.5	0.9010	0.0818	1.725×10^{-2}	57	38
6.5	0.3160	0.6668	1.725×10^{-2}	51	56
7.0	0	0.9835	1.725×10^{-2}	49	57
10.0	0	0.9935	6.530×10^{-3}	100	101
20.0	0	0.9979	2.075×10^{-3}	182	190
30.0	0	0.9988	1.235×10^{-3}	215	220
50.0	0	0.9993	6.85×10^{-4}	240	-
100.0	0	0.9997	3.20×10^{-4}	270	-

Table 9.3 - The distribution of cirazoline and observed and theoretical stability factors for the 2×10^{-3} M cirazoline hydrochloride-SDDS system at 30°C. $f_{(c)}$, $f_{(M)}$ and $f_{(aq)}$ = fractions of cirazoline distributed in the complex, micellar and aqueous (pseudo)phases respectively. Theoretical stability factors were calculated using equation 9.3 and $k_{(aq)} = 2.00 \times 10^{-6}$ s^{-1}, $k_{(M)} = 6.82 \times 10^{-9}$ s^{-1}, $K_A = 3.28 \times 10^4$ M^{-1}, CMC' = 5.36×10^{-3} M and $SOL_T = 7.0 \times 10^{-3}$ M.

[SDDS] ($M \times 10^3$)	$f_{(c)}$	$f_{(M)}$	$f_{(aq)}$	STABILITY FACTOR	
				THEORETICAL	OBSERVED
2.0	0.6735	0	0.3265	3.1	2.2
3.0	0.8385	0	0.1615	6.2	3.8
4.0	0.9027	0	0.0973	10.3	6.6
4.4	0	0.9027	0.0973	9.8	-
4.5	0	0.8242	0.1757	4.6	8.0
5.0	0	0.9037	9.634×10^{-2}	9.9	9.9
10.0	0	0.9825	1.746×10^{-2}	44	42
20.0	0	0.9934	6.619×10^{-2}	84	94
40.0	0	0.9971	2.953×10^{-2}	122	121
60.0	0	0.9981	1.900×10^{-3}	140	126
100.0	0	0.9989	1.109×10^{-3}	157	116

Table 9.4 - The distribution of cirazoline and observed and theoretical stability factors for the 2×10^{-3} M cirazoline hydrochloride-SDDS system at 50°C. $f_{(c)}$, $f_{(M)}$ and $f_{(aq)}$ = fractions of cirazoline distributed in the complex, micellar and aqueous (pseudo)phases respectively. Theoretical stability factors were calculated using equation 9.3 and $k_{(aq)} = 3.10 \times 10^{-5}$ s^{-1}, $k_{(M)} = 1.63 \times 10^{-7}$ s^{-1}, $K_A = 9.380 \times 10^3$ M^{-1}, CMC' = 4.00×10^{-7} M and $SOL_T = 4.40 \times 10^{-3}$ M.

[SDDS] ($Mx10^3$)	$(k_{(aq)}-k_{SDDS})^{-1}$ ($M^{-1}x10^5$)	$([S]^T-CMC')^{-1}$ ($M^{-1}x10^3$)	K_A ($M^{-1}x10^{-4}$)	$k_{(M)}$ ($s^{-1}x10^8$)
(a) 2×10^{-4} M, 30°C				
5.0	5.362	1666		
7.0	5.143	385	2.6	1.8
8.0	5.077	278		
(b) 2×10^{-3} M, 30°C				
10.0	5.050	216		
20.0	5.028	68.3	3.3	0.68
30.0	5.023	40.6		
(c) 2×10^{-3} M, 50°C				
5.0	0.3588	1000		
10.0	0.3304	167	0.94	16
20.0	0.3261	62.5		
40.0	0.3253	27.8		

Table 9.5 - Calculated K_A and $k_{(M)}$ values for (a) 2×10^{-4} M cirazoline hydrochloride-SDDS systems at 30°C, (b) 2×10^{-3} M cirazoline hydrochloride-SDDS systems at 30°C and (c) 2×10^{-3} M cirazoline hydrochloride-SDDS systems at 50°C.

together with the stability factors calculated using equation 9.3.

The fraction of cirazoline present as complex, micellar and aqueous species over the solubilization range for the 2 x 10^{-3} M cirazoline hydrochloride-SDDS system (30°C) was calculated assuming:

(i) $[CIRH^{+}_{(aq)}]$ = constant;

(ii) $[CIRH\text{-}DDS_{(M)}] \propto [DDS^{-}_{(M)}]$;

(iii) $[CIRH\text{-}DDS_{(C)}]$ at CMC' = $[CIRH\text{-}DDS_{(M)}]$ at SOL_T.

Observed and theoretical stability profiles for each system generally show good agreement (figures 9.7 to 9.9) and indicate equations 9.2 and 9.3 are satisfactory in describing the hydrolysis of cirazoline in the presence of SDDS. The predicted stabilizing effect due to complexation in the systems at 30°C is slightly less than that observed experimentally indicating that the K_s' value of 1.17 x 10^{-7} moles^2 litre^2 may be slightly too high or that 'pre-micellar' aggregation occurs below the CMC' of the system. For the 2 x 10^{-3} M cirazoline hydrochloride system at 30°C the decrease in stability due to initial aggregation is slightly more than predicted using equation 9.3. This may be due to experimental error or, alternatively, it may indicate a reduced stabilizing effect of aggregates saturated with cirazoline compared to unsaturated aggregates formed at higher SDDS concentrations.

The predicted stabilizing effect due to liquid complex formation at 50°C is greater than that observed experimentally and the expected decrease in stability in the initial solubilization region is not apparent. These discrepancies may be explained by adsorption/partitioning of dodecylsulphate into the complex phase (see section 9.2.3). The maximum in the observed stability profile is not

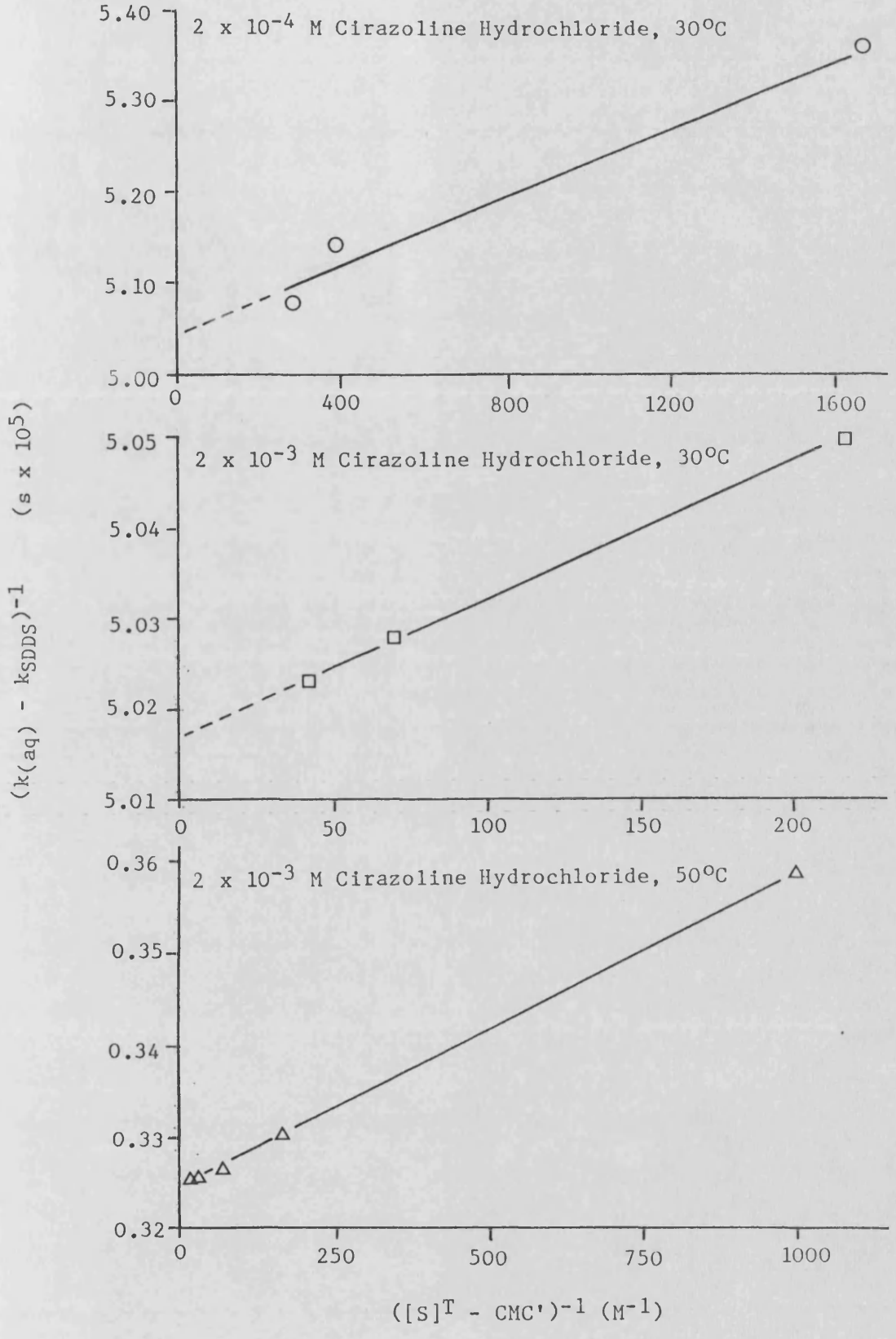

Figure 9.6 - The effect of micellar SDDS on the hydrolysis of cirazoline at each initial cirazoline hydrochloride concentration and temperature shown. Data plotted according to equation 1.91.

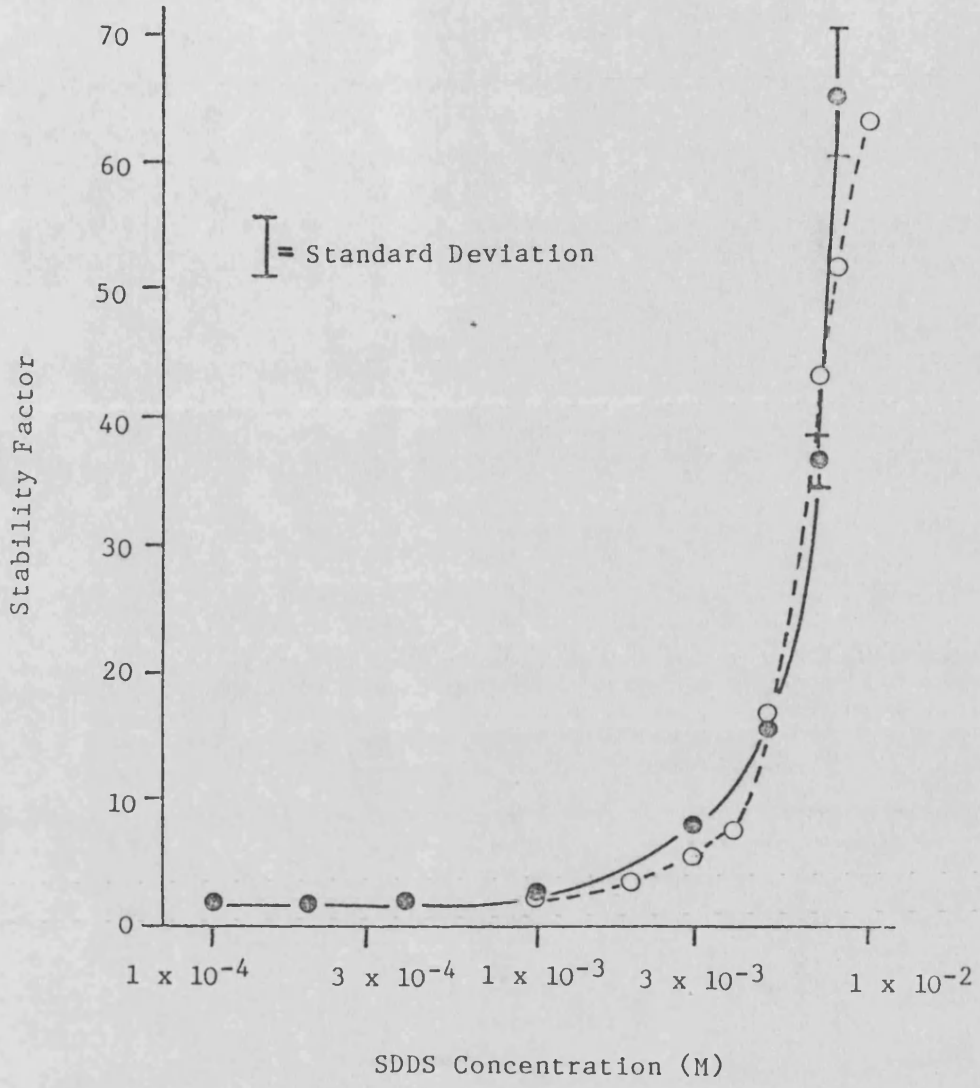

Figure 9.7 - Observed (—●—) and theoretical (--O--) 2 x 10^{-4} M cirazoline hydrochloride stability-SDDS concentration profiles. Plot of stability factor ($k_{(aq)}/k_{SDDS}$) against SDDS concentration for the hydrolysis at pH 7.0, 30°C. Theoretical profiles calculated using equation 9.3.

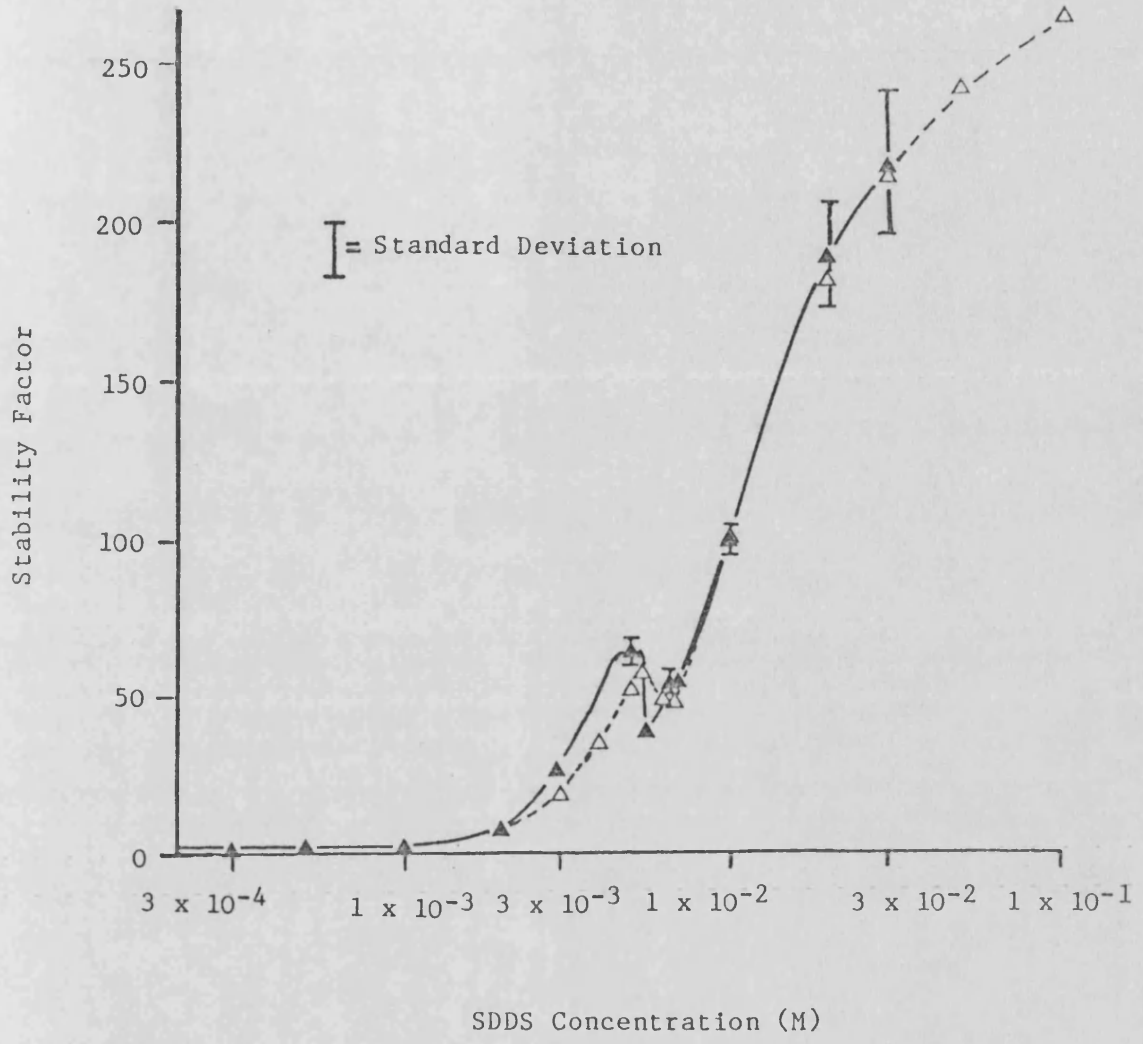

Figure 9.8 - Observed (—▲—) and theoretical (--△--) 2 x 10^{-3} M cirazoline hydrochloride stability-SDDS concentration profiles. Plot of stability factor ($k_{(aq)}/k_{SDDS}$) against SDDS concentration for the hydrolysis at pH 7.0, 30°C. Theoretical profiles calculated using equation 9.3.

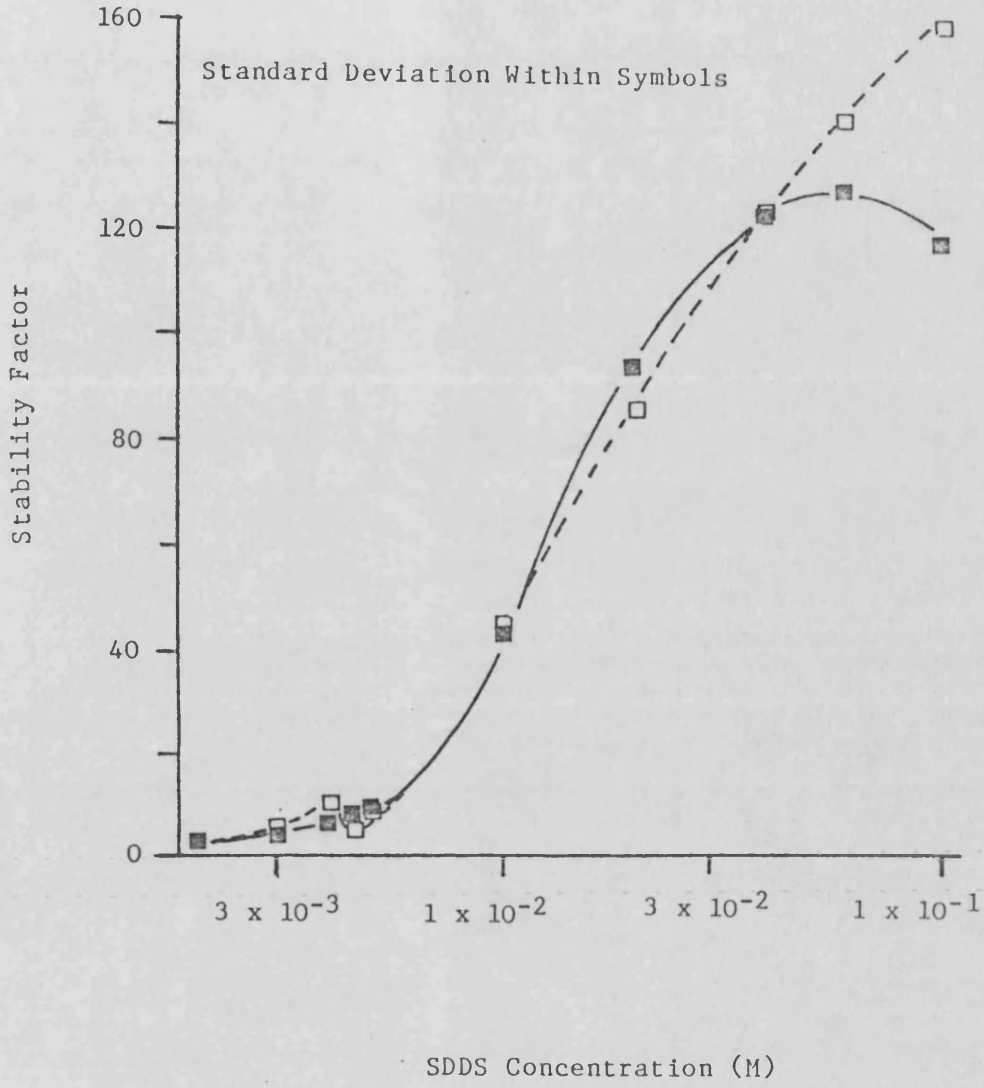

Figure 9.9 - Observed (—■—) and theoretical (--□--) 2 x 10^{-3} M cirazoline hydrochloride stability-SDDS concentration profiles. Plot of stability factor ($k_{(aq)}/k_{SDDS}$) against SDDS concentration for the hydrolysis at pH 7.0, 50°C. Theoretical profiles calculated using equation 9.3.

predicted by the Menger and Portnoy treatment and may be due to the high ionic strength of concentrated SDDS solutions (0.1 M).

K_A values for the system at 30°C determined using the 0.2 and 2×10^{-3} M cirazoline hydrochloride-SDDS kinetic data (2.6 and 3.3 x 10^4 M^{-1}, table 9.5) are in good agreement with K_A values determined by conductimetric titration (mean 2.9 (S.D. 0.2) x 10^4 M^{-1}, table 7.5) and solubility studies (mean 3.2 x 10^4 M^{-1}, table 7.10 and 7.11). The K_A value for the system at 50°C (0.94 x 10^4 M^{-1}) is lower than the value determined by conductimetric titration (2.2 x 10^4 M^{-1}, table 7.6) which is further evidence for the inaccuracy of K_A values determined by conductimetric titration for liquid complex systems.

Micellar stabilization of cirazoline may be associated with several mechanisms e.g.:

(a) proximity effects, i.e. a reduction in the pH at the surface of micelles due to repulsion of hydroxyl ions and attraction of hydronium ions, (sections 1.1.2, 1.5.1.2 and 8.3.2);

(b) medium effects, (sections 1.1.2 and 1.5.1.1) e.g.:

  (i) changes in the dielectric constant and/or ionic strength at the surface of micelles (section 8.3.4);

  (ii) formation of stable neutral cirazoline species (sections 4 and 8.3.2);

  (iii) a change in hydrolysis mechanism, e.g. enhanced exocyclic methylene exchange (sections 5 and 9.1).

Mechanisms (b)(i) and (b)(ii) are thought unlikely to provide the degree of stability observed experimentally. The imidazoline and aromatic moieties in cirazoline are fairly polar and are unlikely to be

buried deeply in the micelle (sections 1.3.2.3 and 1.4.3.2). The presence of anionic micelles usually increases the pK_a' of solubilized weak bases (section 1.5.1.1.) and no decrease in bulk pH was apparant which would accompany a transition from protonated to neutral cirazoline species (equation 4.1). Although no information is available as to the factors affecting the rate of exocyclic methylene exchange, (mechanism (b)(ii)), proximity effects are thought to be the prime mechanism for cirazoline stability in SDDS micelles (mechanism (a)). Support for this is provided by the effect of electrolyte on the reactivity of solubilized cirazoline and the calculated $k_{(M)}$ values at 30°C and 50°C (table 9.1). Although the values for $k_{(M)}$ at 30°C calculated from the 0.2 and 2 x 10^{-3} M cirazoline hydrochloride-SDDS data are not in very good agreement, (1.82 and 0.68 x 10^{-8} s^{-1} respectively), the mean value of 1.3 x 10^{-8} s^{-1} is identical to the calculated value for the uncatalysed (neutral water) reaction at 30°C (k_0, table 8.8 and equation 1.23). The $k_{(M)}$ value at 50°C is also similar to the predicted k_0 value (1.9 x 10^{-7} s^{-1} and 1.3 x 10^{-7} s^{-1} respectively) and indicates that the neutral water reaction is dominant at the micelle surface (i.e. $k_{(M)} = k_0$) which requires a reduction of >3 pH units at the micelle surface (figure 9.1).

Added electrolyte is known to reduce the degree of micellar effects on bimolecular reactions involving ionic reagents due to competition for micelle binding sites between the reactive ions and the added unreactive ions (section 1.5.2.2). The results in table 8.14 show a marked decline in the ability of 0.007 M SDDS to stabilize 2 x 10^{-3} M cirazoline hydrochloride upon addition of sodium chloride. A stability factor of 7.5 was estimated when calculations were compensated for the increase in aqueous stability and micelle concentration in 0.1 M NaCl.

The decreased stability in electrolyte solution is probably due to an increase in $k_{(M)}$ resulting from an increase in the local pH at the surface of the aggregates.

Using the assumptions that $k_{(M)} = k_O$ it is possible to predict the effect of SDDS on cirazoline hydrolysis at other initial cirazoline hydrochloride concentrations, pHs and temperatures using the values for K_A, $k_{(aq)}$, k_O and K_S' in tables 7.6, 8.6-8.8 and 6.7 to calculate cirazoline species fractions and thus solve equation 9.3. Figures 9.10-9.12 show predicted stability profiles for 2×10^{-3} M cirazoline hydrochloride-SDDS systems at 10-30°C, pH 7.0; pH 5-7 at 30°C; and for $0.2 - 5.0 \times 10^{-3}$ M cirazoline hydrochloride-SDDS systems at pH 7.0, 30°C.

Temperature is thus predicted to have a profound effect on the degree of stabilization afforded by both complexation and solubilization mechanisms, (figure 9.10). The stabilizing potency associated with complexation decreases with increasing temperature due to an increase in K_S' (figure 6.17). Micellar stabilizing potency increases with increasing temperature, however, due to an increase in the difference between the uncatalysed (k_O or $k_{(M)}$) and base catalysed (k_2) rate constants (table 8.8). A decrease in the CMC' of the system with increase in temperature also shifts solubilization effects to lower SDDS concentrations.

pH will not significantly affect the degree of stabilization due to complex formation as K_S' is predicted to be independent of pH except at very low or high pHs when associated ionic strength effects will become significant. The stabilizing effect due to solubilization is heavily dependent upon pH, however, (figure 9.11). The CMC' of the

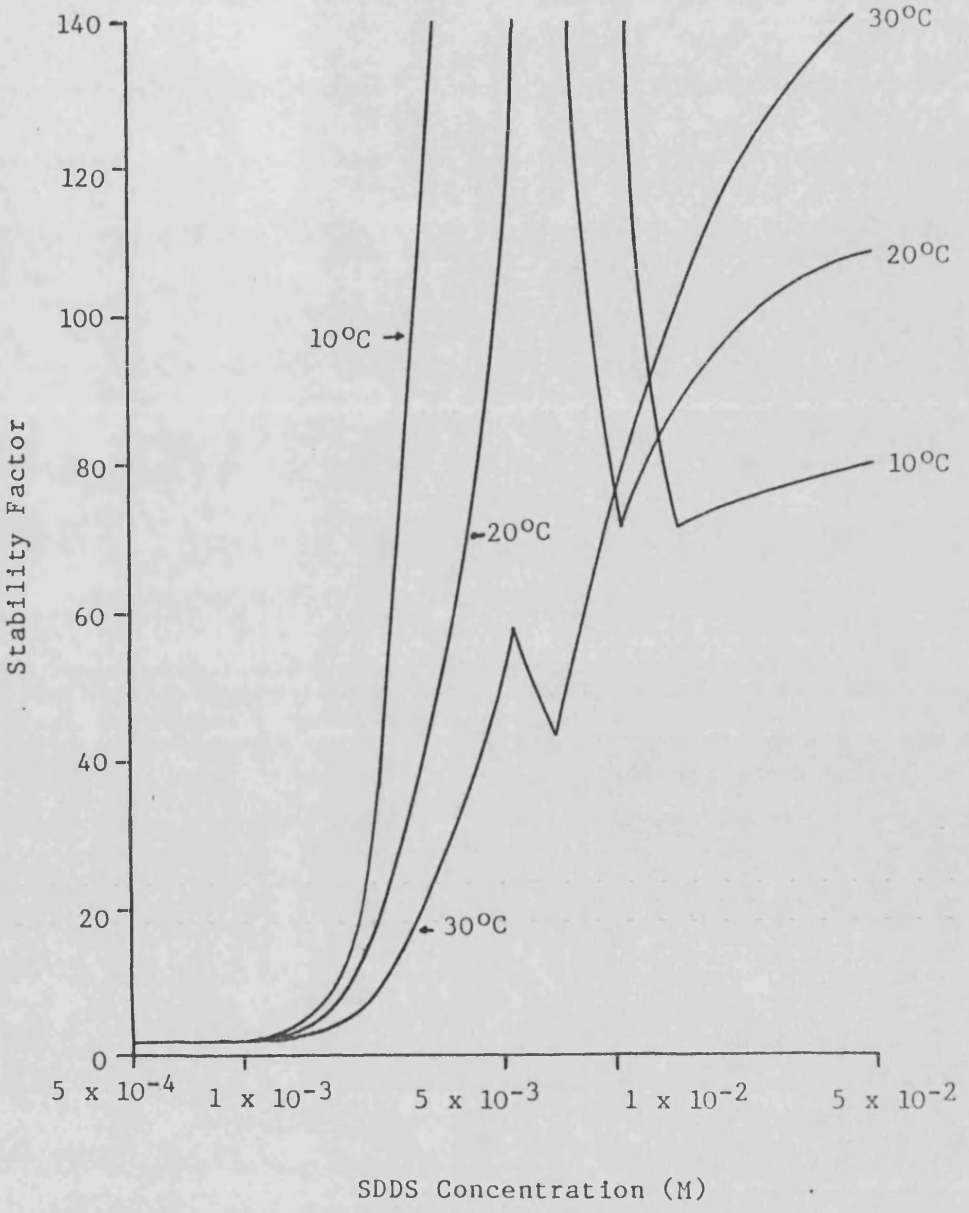

Figure 9.10 - Predicted effect of temperature on the cirazoline hydrochloride stability - SDDS concentration profile. Plot of stability factor ($k_{(aq)}/k_{SDDS}$) against SDDS concentration for the hydrolysis of 2×10^{-3} M cirazoline hydrochloride at pH 7.0 and each temperature shown. Profiles calculated using equation 9.3

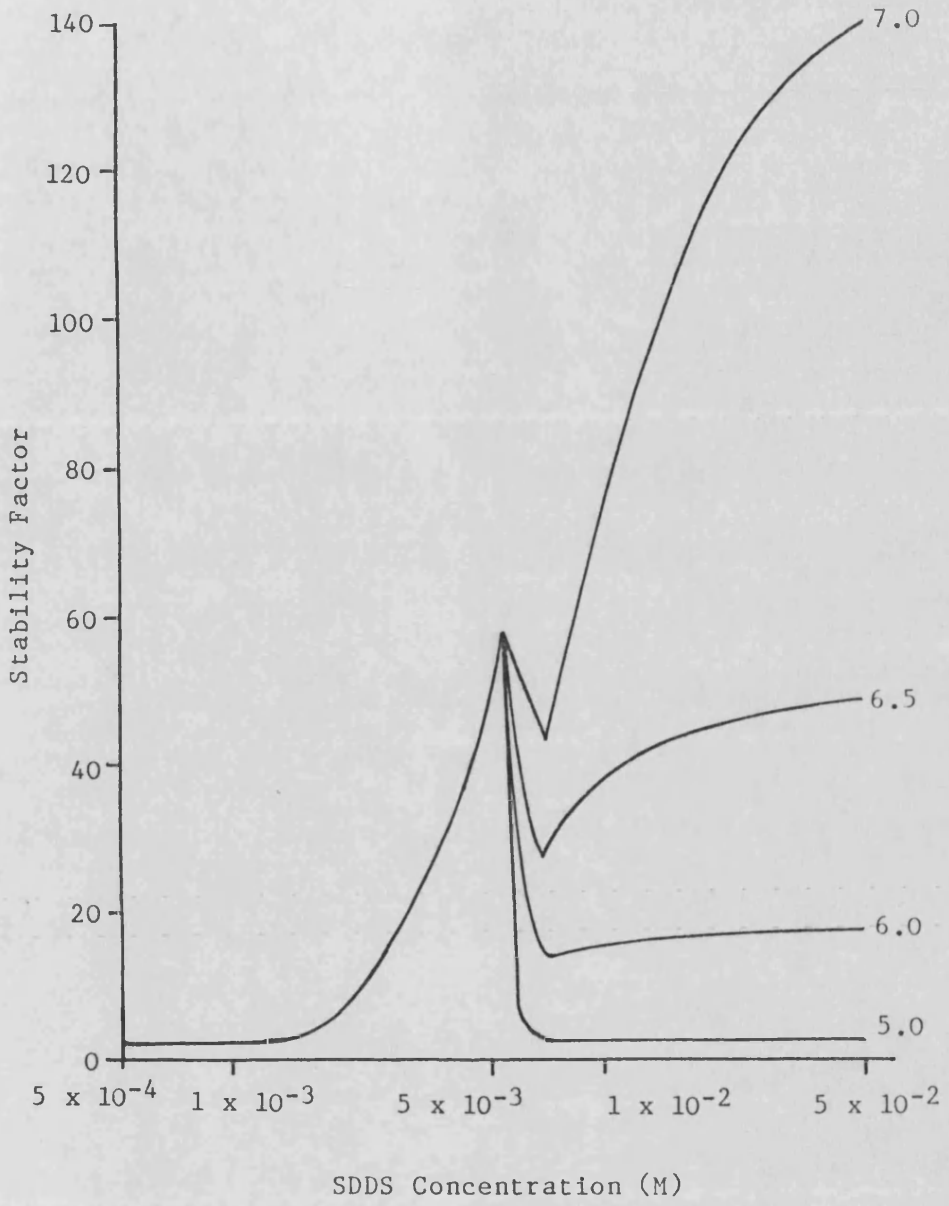

Figure 9.11 - Predicted effect of pH on the cirazoline hydrochloride stability - SDDS concentration profile. Plot of stability factor ($k_{(aq)}/k_{SDDS}$) against SDDS concentration for the hydrolysis of 2 x 10^{-3} M cirazoline hydrochloride at 30°C and each pH shown. Profiles calculated using equation 9.3

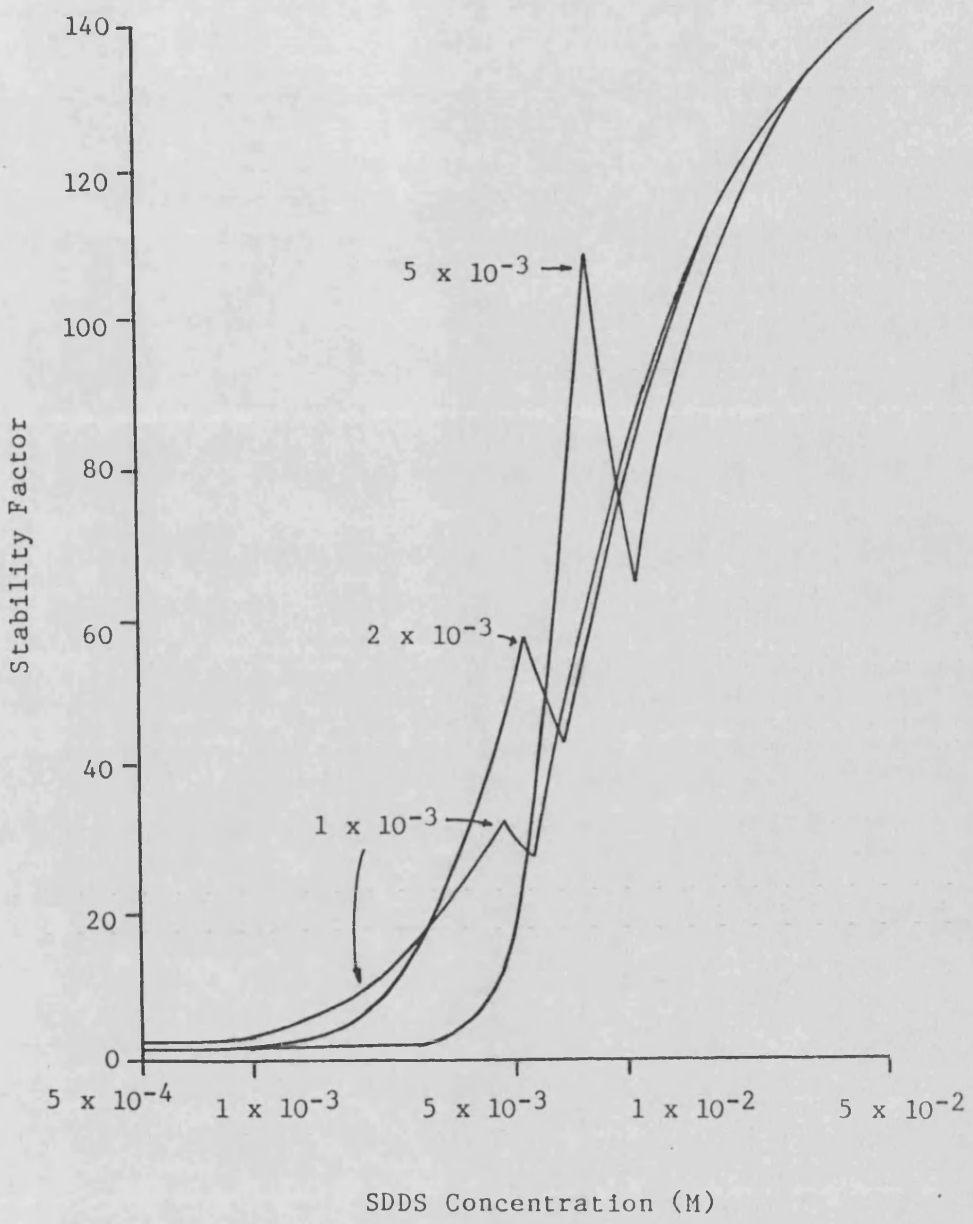

Figure 9.12 - Predicted effect of cirazoline concentration on the stability - SDDS concentration profile. Plot of stability factor ($k_{(aq)}/k_{SDDS}$) against SDDS concentration for the hydrolysis at pH 7.0, 30°C and each initial cirazoline hydrochloride concentration shown. Profiles calculated using equation 9.3

system will be approximately independent of pH but as pH decreases from 7.0 to 5.0, k_2 $[OH^-]$ -> k_0 (= $k_{(M)}$) and the stabilizing effect due to incorporation within micelles is lost.

Initial cirazoline hydrochloride concentration is predicted to have little effect on stability at high SDDS concentrations as under these conditions the vast majority of cirazoline is incorporated into SDDS micelles (figure 9.12). Stabilization in the complexation and initial solubilization regions is dependent upon initial cirazoline hydrochloride concentration, however, due to changes in the equimolar concentration and CMC' of the system.

It must be noted that a decrease in temperature and/or pH increases the overall stabiliy of cirazoline (i.e. k_{SDDS} decreases) and the degree of stabilization required is, therefore, not as great. However, the predictions shown in figures 9.10-9.12 indicate that care must be taken in extrapolating stability effects measured for one system to systems at different pH, temperature and/or initial cirazoline hydrochloride concentrations.

9.4 CONCLUSIONS

This study has shown that:

1. Cirazoline degrades in aqueous solution by uncatalysed and specific base catalysed hydrolysis of the protonated species. No significant acid catalysed hydrolysis or hydrolysis of the cirazoline free base species occurs. Equation 8.4 is satisfactory in characterising the stability pH profile. These results support the findings of Martin and Parcell[28], Savignac et al[29] and Ross et al[18] with respect to the mechanism of imidazoline hydrolysis.

2. Steric effects, inductive effects and exocyclic methylene acidity have been identified as factors contributing towards the stability of medicinal 2-substituted imidazolines. The poor stability of cirazoline (and fenoxazoline) is due to the presence of an ether linkage in the 2-substituent.

3. The interaction between cirazoline and dodecylsulphate ions in aqueous solution may be described in terms of ion-pair formation, complexation and micellization and solubilization. Aqueous, crystalline complex, liquid complex (coacervate) and micellar (pseudo)phases may all exist, the relative amounts of each being dependent upon the concentration of cirazoline hydrochloride and SDDS, temperature and presence of electrolyte. Metastable liquid complex and/or viscous solutions of aggregates may be formed upon rapid addition or bulk mixing of cirazoline hydrochloride and SDDS. Similar physicochemical phenomena are observed in cirazoline alkylsulphate (C_8 - C_{14}) systems and in a range of imidazoline dodecylsulphate systems.

4. Cirazoline dodecylsulphate ion-pair association constant, crystalline and liquid complex (coacervate) solubility products, CMC values, and the amount of SDDS required to solubilize cirazoline may be rapidly and reproducibly determined using an automated conductimetric titration technique. Cirazoline-micelle association constants and cirazoline:dodecylsulphate moiety ratios in aggregates may also be determined for systems in the presence of crystalline complex.

5. A temperature of transition from crystalline complex to stable liquid complex (coacervate) occurs for a range of cirazoline alkylsulphate systems. The transition temperature is a function

of alkylchain length and increases with increased hydrophobicity of the surfactant. The solubility of both complex forms increases with temperature and decreases with surfactant alkylchain length. Solubility and transition temperature are also a function of the imidazoline structure.

6. Cirazoline interacts strongly with micellar SDDS to form aggregates rich in cirazoline under saturated conditions. Added electrolyte decreases the CMC of the system, increases aggregate size and the viscosity of the system but has little effect on the interaction stoichiometry of cirazoline with micellar SDDS. Increased temperature decreases the CMC of the system and increases the capacity of SDDS micelles to incorporate cirazoline.

7. Cirazoline dodecylsulphate ion-pair formation has little or no effect on cirazoline stability but complexation and incorporation into SDDS micelles are potent mechanisms for stabilization at pH 7, 30°C in the absence of added electrolyte or buffer salts. Equation 9.2 allows prediction of the effect of SDDS on the rate of hydrolysis of cirazoline. Addition of electrolyte, reduction in pH (<7) and temperature are predicted to reduce micellar stabilizing effects. However, the latter two parameters are potent mechanisms for reducing the overall rate of hydrolysis.

8. Micellar stabilization is considered to be due to repulsion of hydroxide ion from the surface of micelles (proximity effects) and, at pH <7, the rate of hydrolysis within the micelles is governed by the rate of the uncatalysed hydrolysis reaction.

9.5 SUGGESTIONS FOR FUTURE WORK

The use of NMR as a tool in the elucidation of imidazoline hydrolysis and proton exchange mechanisms has been demonstrated. Further work in this area aimed at refining the technique, further testing of the proposed mechanism and expanding the research into a wider range of 2-imidazoline structures would be useful. Experiments at, e.g. pH 7.0, 50°C might enable simultaneous monitoring of exchange and ring cleavage reactions.

Work reported in this thesis and by a variety of other workers indicate that crystalline complex formation is not restricted to cirazoline dodecylsulphate systems. Factors affecting crystalline complex formation, solubility, temperature of transition to liquid complex (coacervate) and formation of metastable systems for a range of organic ion-ionic surfactant systems should be investigated further using such techniques as automated conductimetric titration, viscosity, DSC and hot stage microscopy techniques. Further probing for liquid crystal phases should also be considered.

A better characterisation of the solubilization region in liquid complex systems would be a useful area of future research, e.g. use of solubility and turbidity techniques to confirm CMC and SOL_T points. Inflexions in conductivity curves might be better defined in systems containing higher initial cirazoline hydrochloride concentrations. Replacement of glass wool as a means of entraping formed solid complex during conductimetric titrations would be advantageous and might allow more detailed analysis of conductivity curves.

The concept of organic ion cooperativity at the surface of aggregates should be tested e.g. by determining K_A values under unsaturated

conditions and extending the study to a variety of organic ion structures with varying degrees of aromaticity and hydrophobicity.

Production of 'metastable' and 'equilibrium' cirazoline hydrochloride-SDDS phase diagrams at a range of temperature and electrolyte concentrations and further investigation into the high viscosity of aggregated systems would be useful.

Kinetic studies into the effect of SDDS on the hydrolysis kinetics and mechanism of micellar stabilization of cirazoline should be repeated in more detail and extended to higher SDDS concentrations. This may be possible for solid complex systems by using slightly higher pH and temperature conditions e.g. pH 7.5, 35°C. The validity of equation 9.2 in predicting stability-SDDS concentration profiles should be further tested, e.g. at a variety of pH, temperature and initial cirazoline hydrochloride concentrations.

Finally, the effect of pharmaceutical excipients such as buffer salts, electrolyte and non-ionic additives (e.g. alcohols, glycerol) on the interaction and stabilizing effect of SDDS would be a useful area of further work.

APPENDIX 1

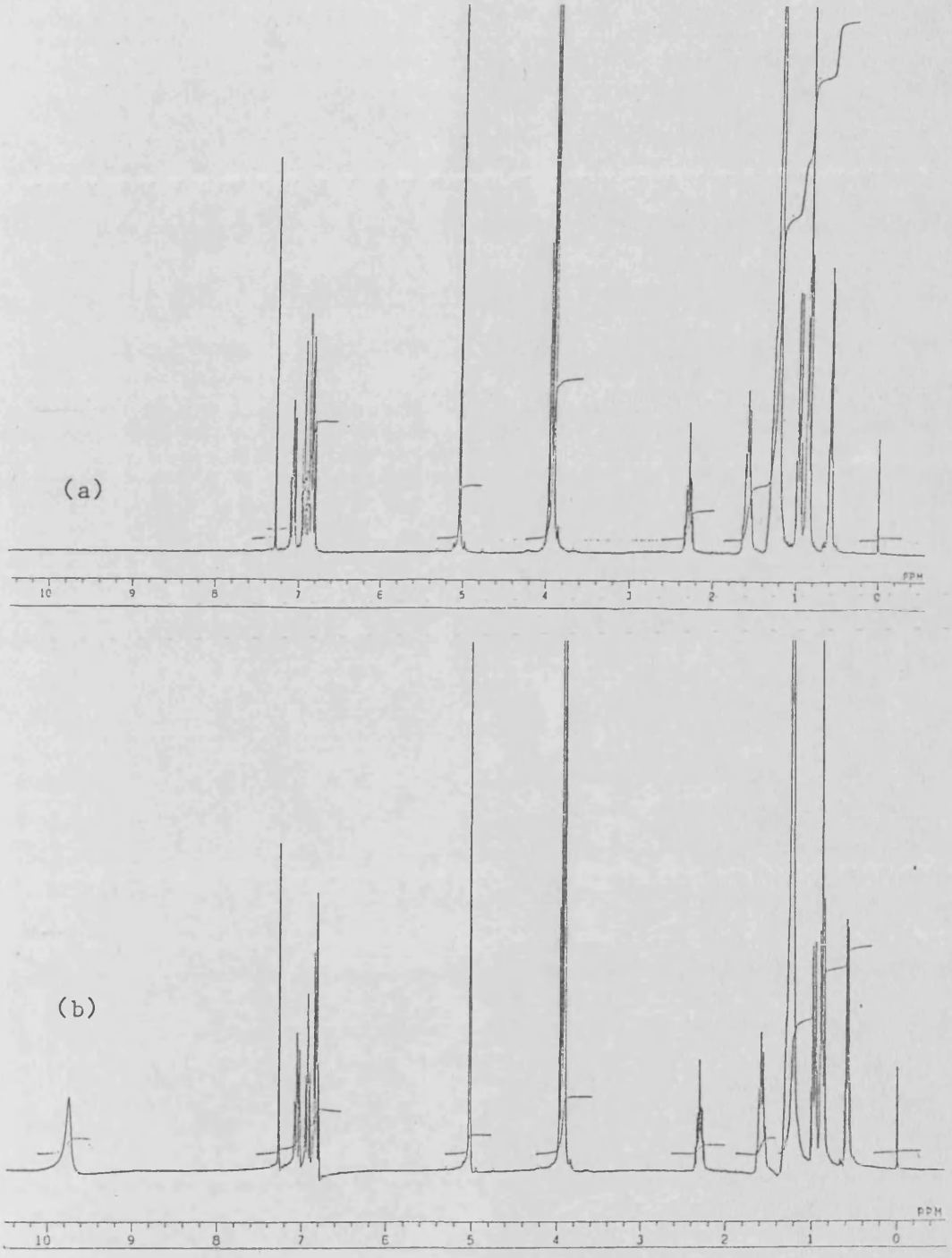

Chemical Shift (ppm)

Figure I.1 - Proton NMR spectrum for (a) cirazoline-octylsulphate, (CIRH-OS) and (b) cirazoline-decylsulphate, (CIRH-DS), in $CDCl_3$.

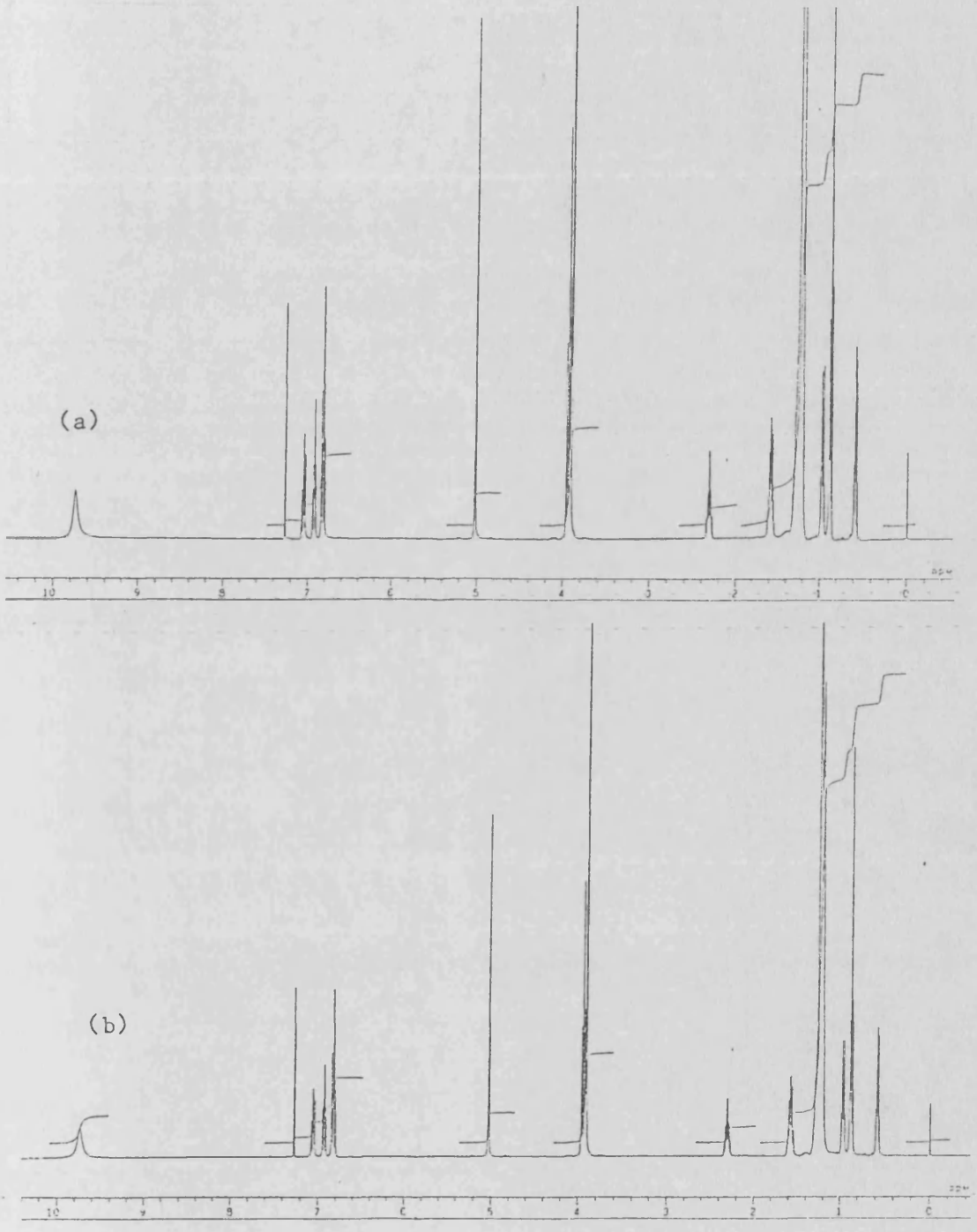

Chemical Shift (ppm)

Figure I.2 - Proton NMR spectrum for (a) cirazoline-dodecylsulphate, (CIRH-DDS) and (b) cirazoline-tetradecylsulphate, (CIRH-TDS) in $CDCl_3$.

APPENDIX 2

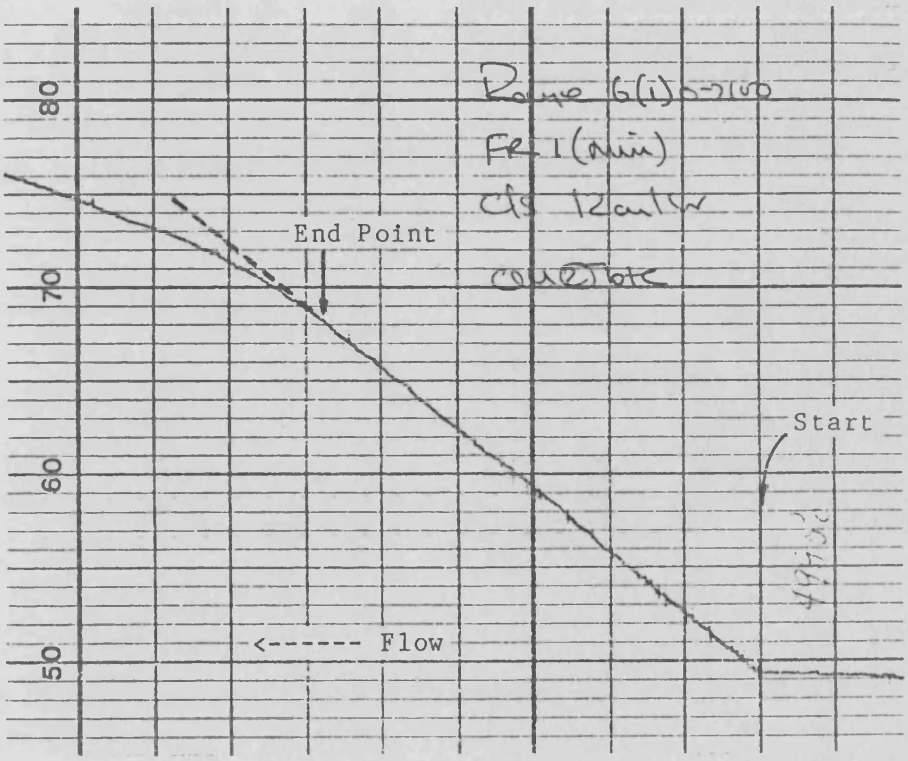

Figure II.1 - Conductimetric titration trace for SDDS (0.01 M) against cirazoline hydrochloride (1.5×10^{-3} M) at 50°C. Flow rate = 50.48 µl min^{-1}, chart speed = 12 cm hr^{-1}, chart conductivity range = 100 - 200 x 10^{-6} S.

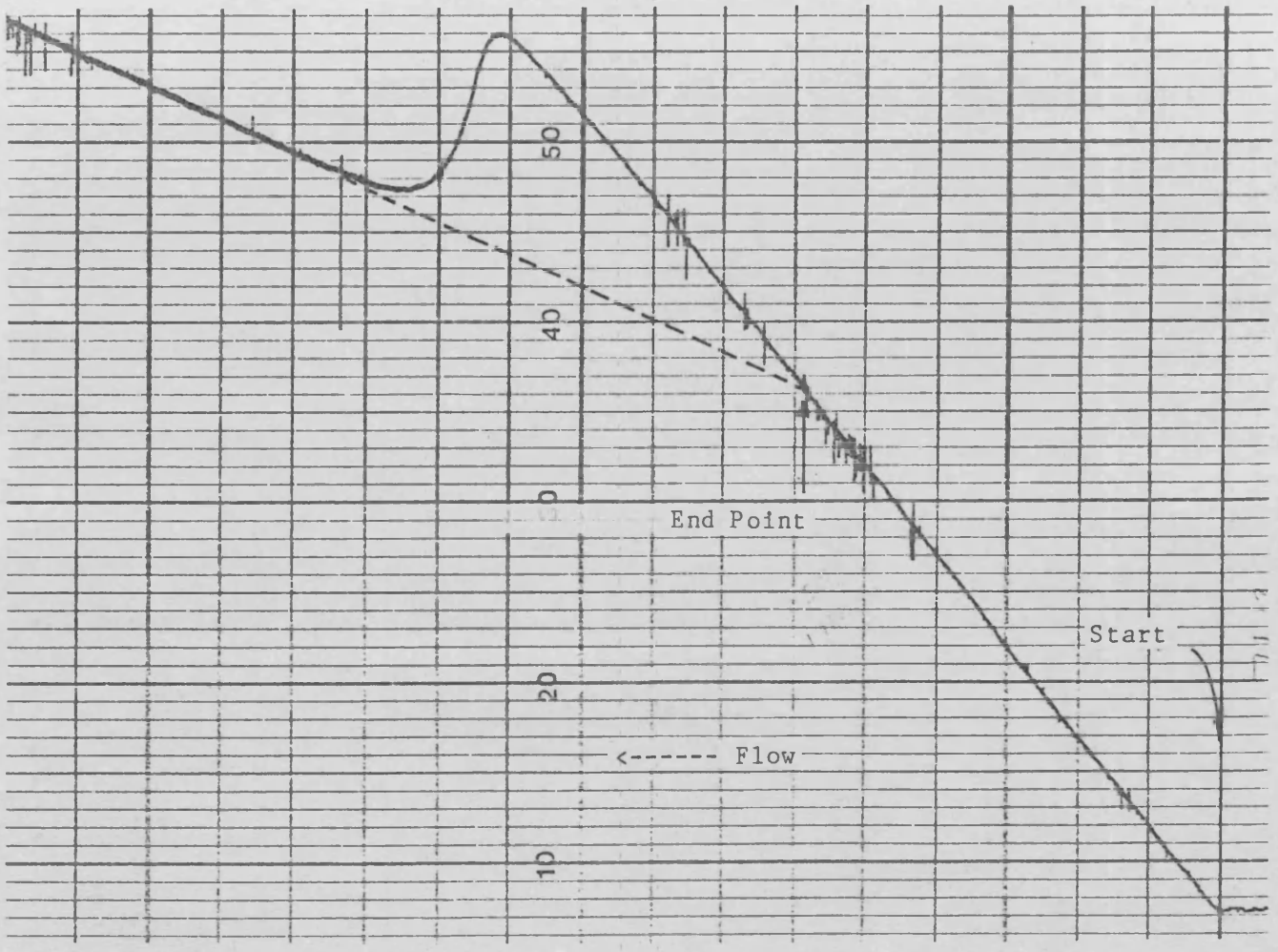

Figure II.2 - Conductimetric titration trace for SDDS (0.01 M) against cirazoline hydrochloride (1×10^{-3} M) at 30°C. Flow rate = 20.38 µl min^{-1}, chart speed = 12 cm hr^{-1}, chart conductivity range = 70 - 90 x 10^{-6} S.

APPENDIX 3

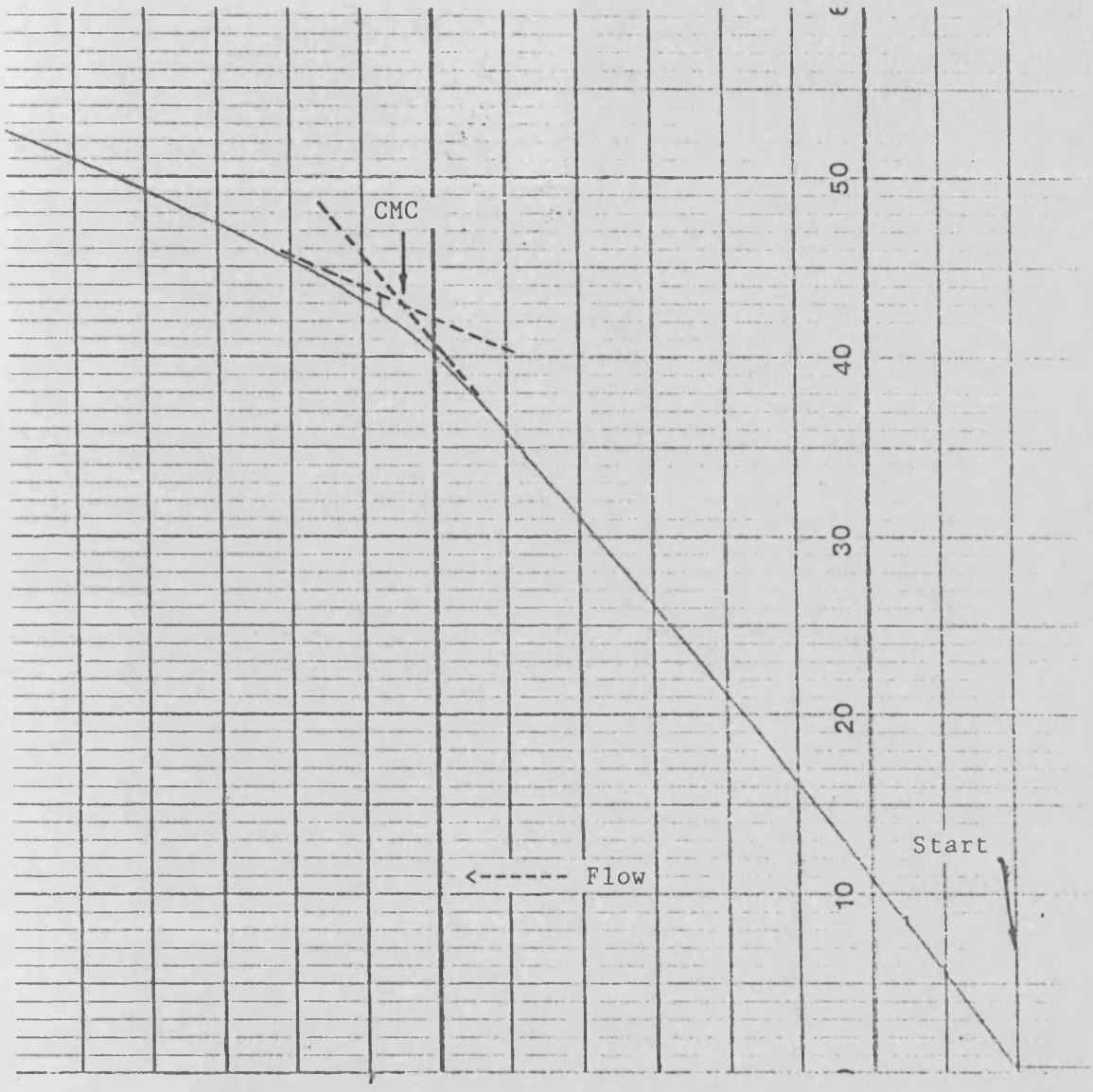

Figure III.1 - Conductimetric titration trace for SDDS (0.2 M) against double distilled water at 30°C. Flow rate = 50.48 µl min^{-1}, chart speed = 12 cm hr^{-1}, chart conductivity range = 0 - 1000 x 10^{-6} S.

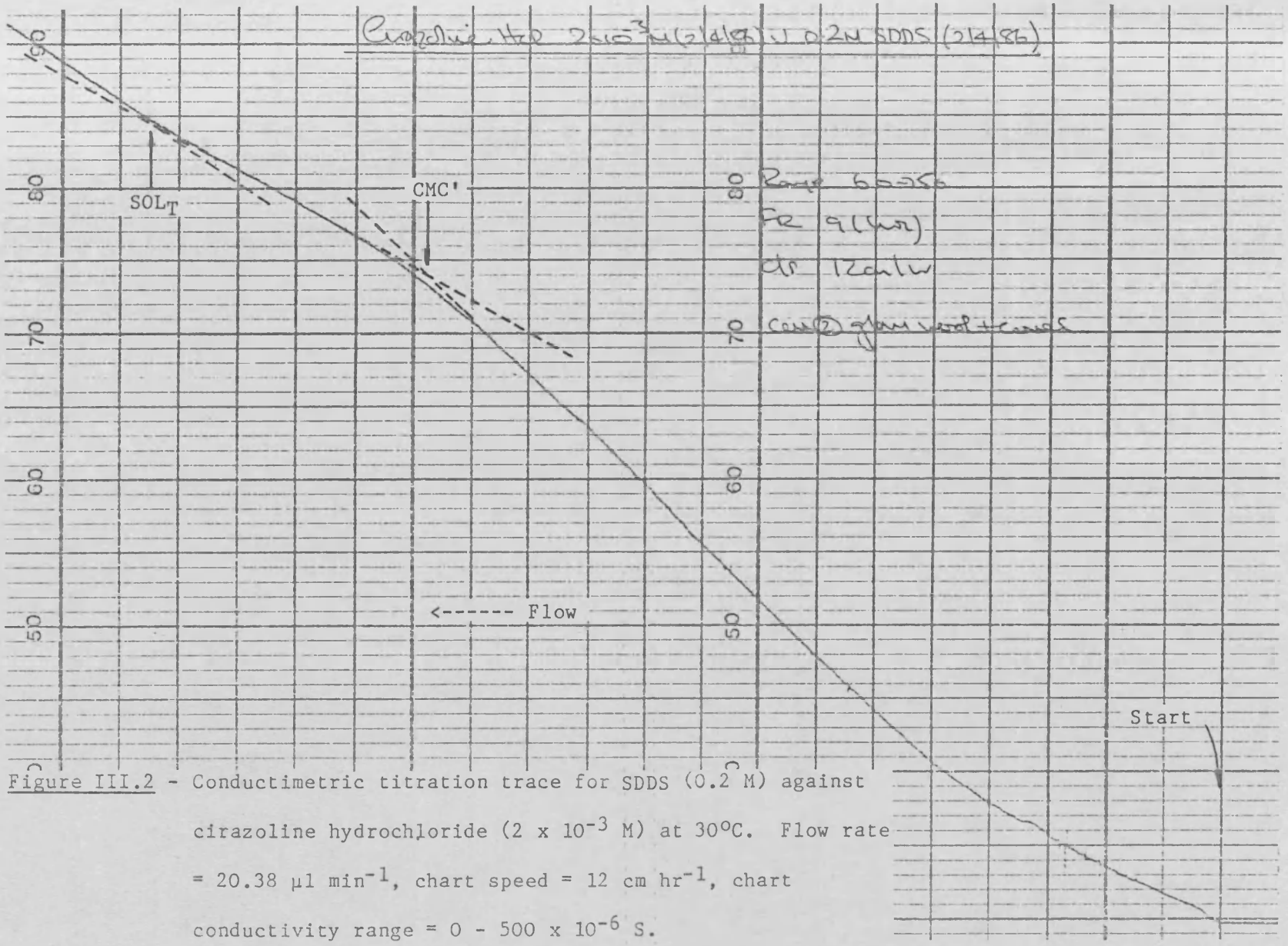

Figure III.2 - Conductimetric titration trace for SDDS (0.2 M) against cirazoline hydrochloride (2×10^{-3} M) at 30°C. Flow rate = 20.38 µl min^{-1}, chart speed = 12 cm hr^{-1}, chart conductivity range = 0 - 500 x 10^{-6} S.

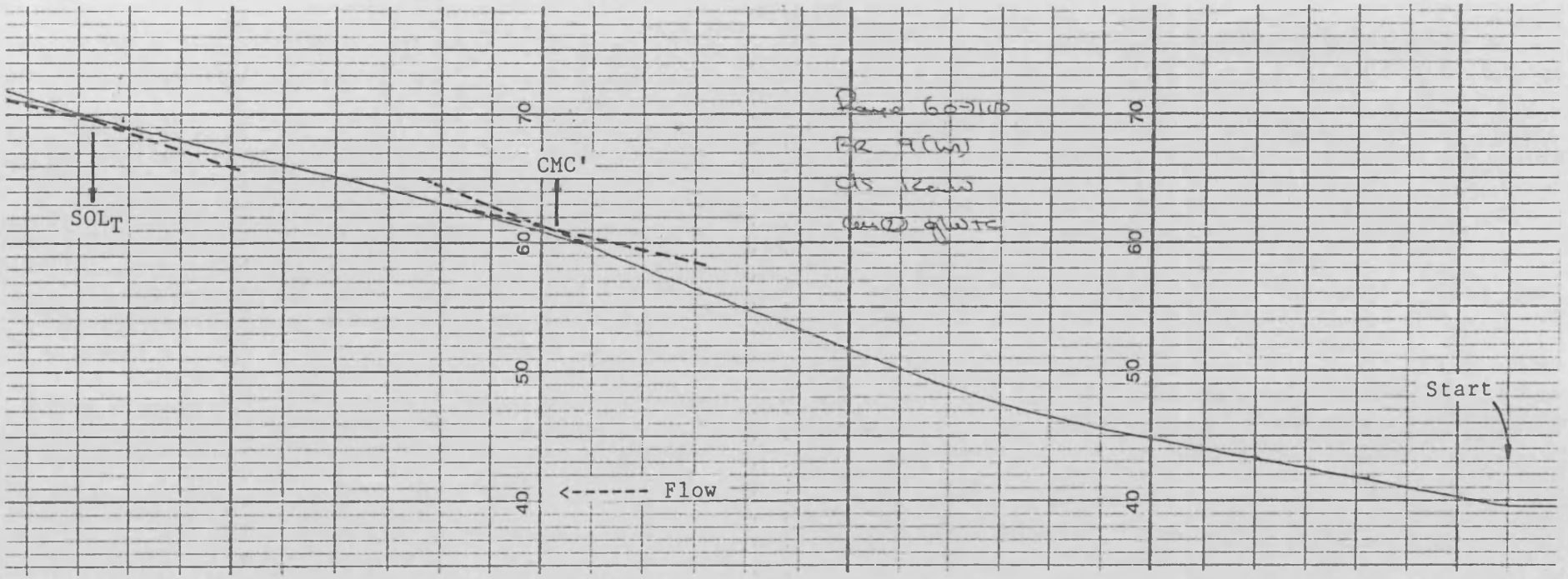

Figure III.3 - Conductimetric titration trace for SDDS (0.2 M) against cirazoline hydrochloride (5×10^{-3} M) at 30°C. Flow rate = 20.38 µl min^{-1}, chart speed = 12 cm hr^{-1}, chart conductivity range = 0 - 1000 x 10^{-6} S.

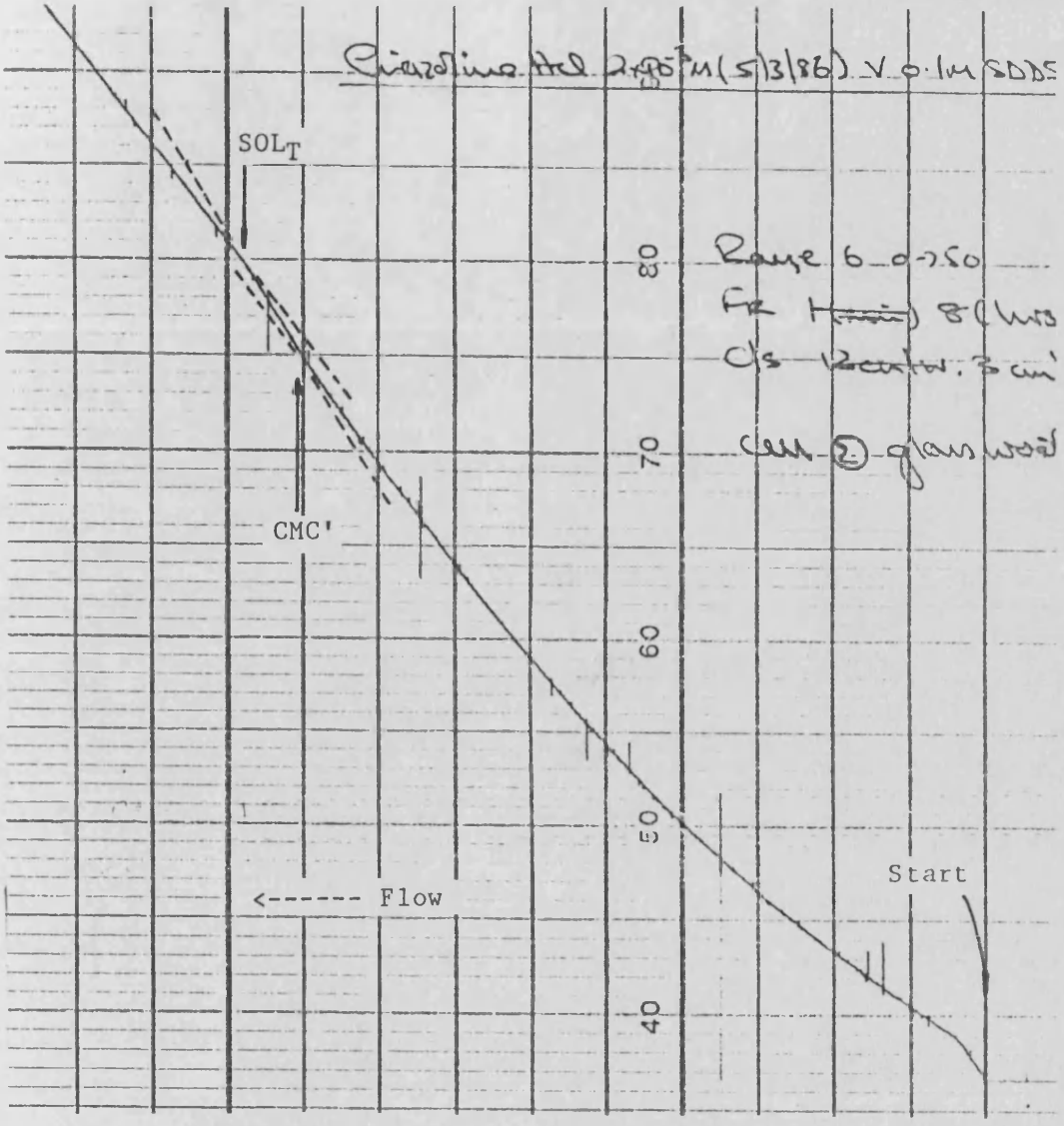

Figure III.4 - Conductimetric titration trace for SDDS (0.1 M) against cirazoline hydrochloride (2 x 10^{-3} M) at 40°C. Flow rate = 12.39 µl min^{-1}, chart speed = 3 cm hr^{-1}, chart conductivity range = 0 - 500 x 10^{-6} S.

REFERENCES

1. Connors, K.A., Amidon, G.L., Stella, V.J., 'Chemical Stability of Pharmaceuticals', 2nd ed., J. Wiley and sons, New York, (1986).

2. Mollica, J.A., Ahuja, S., Cohen, J., J. Pharm. Sci., 67, 443, (1978).

3. Garrett, E.R., 'Kinetics and Mechanism in Stability of Drugs', in Adv. Pharm. Sci., Bean, H.S., Beckett, A.H., Carless, J.E., eds., Vol 2, 1, Academic Press Inc., London, (1967).

4. Osol, A., ed., 'Remington's Pharmaceutical Sciences', Mack Publishing Co., Eastern Pennsylvania, (1980).

5. Martin, A., Swarbrick, J., Cammarata, A., 'Physical Pharmacy', 3rd ed., Lea and Febiger, Philadelphia, (1983).

6. Wilkinson, F., 'Chemical Kinetics and Reaction Mechanisms', Van Nostrand Reinhold Co., New York, (1980).

7. Frost, A.A., Pearson, R.G., 'Kinetics and Mechanism. A study of homogeneous chemical reactions', Chapman and Hall Ltd., London, (1953).

8. Laidler, K.J., 'Chemical Kinetics', 2nd ed., McGraw Hill Book Co., London, (1965).

9. Swinbourne, E.S., 'Analysis of Kinetic Data', Thomas Nelson and Sons Ltd., London, (1971).

10. Benson, S.W., 'Thermochemical Kinetics, methods for the estimation of thermochemical data and rate parameters', 2nd ed., John Wiley and Sons, London, (1976).

11. Robinson, R.A. and Stokes, R.H., 'Electrolyte Solutions', 2nd ed., Butterworths, London, (1965).

12. Reynolds, J.E.F., ed., 'Martindale - The Extra Pharmacopoeia', 28th ed., The Pharmaceutical Press, London, (1982).

13. 'The Pharmaceutical Codex', 11th ed., The Pharmaceutical Press, London, (1979).

14. Van Meel, J.C.A., DeJonge, A., Timmermans, P.B.M.W.M., Van Zwieten, P.A., J. Pharmacol. Exp. Ther., 219, 760, (1981).

15. Davies, D.J.G., Meakin, B.J., Stroud, N., Stevens, H.N.E., Proc. 2nd Int. Conf. Pharm. Tech., (Paris), II, 217, (1980).

16. Stroud, N., Davies, D.J.G., Stevens, H.N.E., Meakin, B.J., Proc. 4th Int. Conf. Surface and Colloid Sci., (Jerusalem), 374, (1981).

17. Fedynec, R.C., Lewis, G.A., Stevens, H.N.E., J. Pharm. Pharmacol., 33, 103P, (1981).

18. Ross, A.J., GO, M-V.C., Casey, D.L., Palling, D.J., J. Pharm. Sci., 76, 306, (1987).

19. Windholz, M., ed., 'The Merck Index', 10th ed., Merck and Co. Ltd., Rahway, USA, (1983).

20. Kountourellis, J.E., PhD Thesis, Unversity of Bath, (1981).

21. Kountourellis, J.E., Papadopoulos, N., Raptouli, A., Talanta, 31, 730, (1984).

22. Moffat, A.C., ed., 'Clarke's Isolation and Identification of Drugs' 2nd ed., The Pharmaceutical Press, London, (1986).

23. Hoffmann, K., 'Imidazole and its Derivitives', Part I, Interscience Publishers inc., London, (1953).

24. Katritzky, A.R., Rees, C.W., 'Comprehensive Heterocyclic Chemistry. The structure, reactions, synthesis and uses of heterocyclic compounds', Vol. 5, Pergammon Press, Oxford, (1984).

25. Harnsberger, B.G., Riebsomer, J.L., J. Heterocyclic Chem., 1, 188, (1964).

26. Harnsberger, B.G., Riebsomer, J.L., J. Heterocyclic Chem., 1, 229, (1964).

27. Fernandez, B.M., Lamden, S., J. Heterocyclic Chem., 18, 933, (1981).

28. Martin, R.B., Parcell, A., J.Am. Chem. Soc., 88, 4830, (1961).

29. de Savignac, A., Kabbage, T., Dupin, P., Calmon, M., J. Heterocyclic Chem., 15, 897, (1978).

30. Stern, M.J., King, L.D., Marcus, A.D., J. Amer. Pharm. Ass. Sci. Ed., 48, 641, (1959).

31. Yamana, T., Mizukami, Y., Nishida, M., Izaki, M., Shirai, K., Kitade, N., Yakuzaigaku, 27, 203, (1967).

32. Grabowska, I., Kraczkowska, A., Acta. Pol. Pharm., 40, 577, (1983).

33. Grabowska, I., Rajzer, D., Acta. Pol. Pharm., 41, 359, (1984).

34. Grabowska, I., Rajzer, D., Acta. Pol. Pharm., 41, 665, (1984).

35. Couper, A., in 'Surfactants', Tadros, Th.F., ed., 19, Academic Press, London, (1984).

36. Mukerjee, P., Ber. Bunsenges Phys. Chem., 82, 931, (1978).

37. Mukerjee, P., 'Micellization, Solubilization and Microemulsions', Mittal, K.L., ed., Vol. 1, 171, Plenum Press, New York, (1977).

38. Lindman, B., Wennerstrom, H., 'Solution Behaviour of Surfactants', Mittal, K.L., Fendler, E.J., ed., Vol. 1, 3, Plenum Press, New York, (1982).

39. Almgren, R., Aniansson, E.A.G., Wall, S.N., Holmaker, K., 'Micellization, Solubilization and Microemulsions', Mittal, K.L., ed., Vol. 1,329, Plenum Press, New York, (1977).

40. Franks, F., 'Water - a Comprehensive Treatise', Vol. 4, Ch. 2, Plenum Press, New York, (1977).

41. Attwood, D., Florence, A.T., 'Surfactant Systems, Their Chemistry, Pharmacy and Biology', Chapman and Hall, London, (1983).

42. Woolley, E.M., Burchfield, T.W., J. Phys. Chem., 89, 714, (1985).

43. Ruckenstein, E., Nagarajan, R., 'Micellization, Solubilization and Microemulsions', Mittal, K.L., ed., Vol. 1, 133, Plenum Press, New York, (1977).

44. Tanford, C., 'Micellization, Solubilization and Microemulsions', Mittal, K.L., ed., Vol. 1, 119, Plenum Press, New York, (1977).

45. Jonsson, B., Wennerstrom, H., J. Colloid Interfac. Sci., 80, 482, (1981).

46. Jonsson, B., Gunnarsson, G., Wennerstrom, H., 'Solution Behaviour of Surfactants', Mittal, K.L., Fendler, E.J., ed., Vol. 1, 317 Plenum Press, New York, (1982).

47. Takeda, K., Yasunaga, T., Vehara, H., 'Micellization, Solubilization and Microemulsions', Mittal, K.L., ed., Vol. 1., 305, Plenum Press, New York, (1977).

48. Lindman, B., in 'Surfactants', Tadros, Th.F., ed., 83, Academic Press, London, (1984).

49. Muller, N., 'Solution Chemistry of Surfactants', Mittal, K.L., ed., Vol. 1, 267, Plenum Press, New York, (1979).

50. Aniansson, G.E.A., Progr. Colloid and Polymer Sci., 70, 2, (1985).

51. Mukerjee, P., Mysels, K.J., 'CMCs of Aqueous Surfactant Systems', NSRDS-NBS 36, U.S. Government Printing Office, Washington D.C., (1971). (1971).

52. Jean, Y-C., Djermouni, B., Ache, H.J., 'Solution Chemistry of Surfactants', Mittal, K.L., ed., Vol. 1, 129, Plenum Press, New York, (1979).

53. Schara, M., Lasic, D.D., 'Solution Behaviour of Surfactants', Mittal, K.L., ed., Vol. 1, 475, Plenum Press, New York, (1982).

54. Meguro, K., Shoji, N., 'Solution Chemistry of Surfactants', Mittal, K.L., ed., Vol. 1, 407, Plenum Press, New York, (1979).

55. Mittal, K.L., ed., 'Micellization, Solubilization and Microemulsions', Vol. 1 and 2, Plenum Press, New York, (1979).

56. Mittal, K.L., ed., 'Solution Chemistry of Surfactants', Vol. 1 and 2, Plenum Press, New York, (1979).

57. Mittal, K.L., Fendler, E.J., ed., 'Solution Behaviour of Surfactants', Vol 1 and 2, Plenum Press, New York, (1982).

58. Mittal, K.L., Lindman, B., ed., 'Surfactants in Solution', Vol 1-3, Plenum Press, New York, (1984).

59. Tadros, Th.F., 'Surfactants', Academic Press, London, (1984).

60. McBain, J.W., Salmon, C.S., J. Am. Chem. SOC., 43, 426, (1920).

61. Hartley, G.S., 'Aqueous Solutions of Paraffin Chain Salts', Hermann and Cie, Paris, (1936).

62. Menger, F.M., 'Surfactants in Solution', Mittal, K.L. Lindman, B., ed., Vol. 1, 347, Plenum Press, New York, (1984).

63. Fromherz, P., 'Surfactants in Solution', Mittal, K.L., Lindman, B., ed., Vol. 1, 321, Plenum Press, New York, (1984).

64. Dill, K.A., Koppel, D.E., Cantor, R.S., Dill, J.D., Bendedouch, D., Chen, S-H., Nature, 309, 42, (1984).

65. Dill, K.A., 'Surfactants in Solution', Mittal, K.L., Lindman, B., ed., Vol. 1, 307, Plenum Press, New York, (1984).

66. Gruen, D.W.R., Progr. Colloid and Polymer Sci., 70, 6, (1985).

67. Gruen, D.W.R., de Lacey, E.H.B., 'Surfactants in Solution', Mittal, K.L., Lindman, B., ed., Vol. 1, 279, Plenum Press, New York, (1984).

68. Anacker, E.W., 'Solution Chemistry of Surfactants', Mittal, K.L., ed., Vol. 1, 247 Plenum Press, New York, (1979).

69. Gunnarsson, G., Jonsson, B., Wennerstrom, H., J. Phys. Chem., 84, 3114, (1980).

70. Beunen, J.A., Ruckenstein, E., J. Colloid Interfac. Sci., 96, 469, (1983).

71. Frahm, J., Diekmann, S., 'Surfactants in Solution', Mittal, K.L., Lindman, B., ed., Vol. 2, 897, Plenum Press, New York, (1984).

72. Charbit, G., Gaboriaud, R., Dorion, F., J. Colloid Interfac. Sci., 106, 265, (1985).

73. Backlund, S., Rundt, K., Birdi, K.S., Dalsager, S., Colloid and Polymer Sci., 259, 1105, (1981).

74. Lindman, B., Lindblom, G., Wennerstrom, H., Gustavsson, H., 'Micellization, Solubilization and Microemulsions', Mittal, K.L., ed., Vol. 1, 195, Plenum Press, New York, (1977).

75. Schott, H., J. Pharm. Sci., 62, 162, (1973).

76. Aniansson, E.A.G., Wall, S.N., Almgren, M., Hoffmann, H., Kielmann, I., Ulbricht, W., Zana, R., Lang, J., Tondre, C., J. Phys. Chem., 80, 905, (1976).

77. Tokiwa, F., Adv. Colloid Interfac. Sci., 3, 389, (1972).

78. Ben-Naim, A., 'Surfactants in Solution', Mittal, K.L., Lindman, B., ed., Vol. 2, 731, Plenum Press, New York, (1984).

79. Leibner, J.E., Jacobus, J., J. Phys. Chem., 81, 130, (1977).

80. Nakagawa, T., Shinoda, K., 'Colloidal Surfactants', Tamamushi, B.I., Isemura, T., eds., Academic Press, New York, (1963).

81. Almgren, M., Swarup, S., J. Phys. Chem., 87, 876, (1983).

82. Birdi, K.S., 'Micellization, Solubilization and Microemulsions', Mittal, K.L., ed., Vol. 1, 151, Plenum Press, New York, (1977).

83. Mukerjee, P., Adv. Colloid Interfac. Sci., 1, 241, (1967).

84. Hoffmann, H., Nusslein, H., Ulbricht, W., 'Micellization, Solubilization and Microemulsions', Mittal, K.L., ed., Vol. 1, 263, Plenum Press, New York, (1977).

85. Berr, S.S., Coleman, M.J., Marriot-Jones, R.R., Johnson, J.S., J. Phys. Chem., 90, 6492, (1986).

86. Gravsholt, S., J. Colloid Interfac. Sci., 57, 575, (1976).

87. Ulmius, J., Wennerstrom, H., Johansson, L., Lindblom, G., Gravsholt, S., J. Phys. Chem., 83, 2232, (1979).

88. Hoffmann, H., Rehage, H., Schorr, W., Thurn, H., 'Surfactants in Solution', Mittal, K.L., Lindman, B., ed., Vol. 1, 425, Plenum Press, New York, (1984).

89. Gamboa, C., Sepulveda, L., J. Colloid Interfac. Sci., 113, 566, (1986).

90. Sepulveda, L., Perez-Cotapos, J., J. Colloid Interfac. Sci., 109, 21, (1986).

91. Corrin, M.L., Harkins, W.D., J. Amer. Chem. Soc., 69, 683, (1947).

92. Tartar, H.V., J. Colloid, Interfac. Sci., 17 243, (1962).

93. Anacker, E.W., J. Colloid Interfac. Sci., 8, 402, (1953).

94. Mazer, N.A., Carey, M.C., Benedek, G.B., 'Micellization, Solubilization and Microemulsions', Mittal, K.L., ed., Vol. 1, 359, Plenum Press, New York, (1977).

95. Mazer, N.A., Benedek, G.B., Carey, M.C., J. Phys. Chem., 80, 1075, (1976).

96. Missel, P.J., Mazer, N.A., Benedek, G.B., Young, C.Y., Carey, M.C., J. Phys. Chem. 84, 1044, (1980).

97. Kratohvil, J.P., J. Colloid Interfac. Sci., 75, 271, (1980).

98. Rohde, A., Sackmann, E., J. Colloid Interfac. Sci., 70, 494, (1979).

99. Doughty, D.A., J. Phys. Chem., 87, 5286, (1983).

100. Corti, M., Degiorgio, V., 'Solution Chemistry of Surfactants', Mittal, K.L., ed., Vol. 1, 377, Plenum Press, New York, (1979).

101. Hayashi, S., Ikeda, S., J. Phys. Chem., 84, 744, (1980).

102. Nicoli, D.F., Dorshow, R.B., Bunton, C.A., 'Surfactants in Solution', Mittal, K.L., Lindman, B., ed., Vol. 1, 455, Plenum Press, New York, (1984).

103. Chang, N.J., Kaler, E.W., J. Phys. Chem., 89, 2996, (1985).

104. Chen, J-M., SU, T-M., Mou, C.Y., J. Phys. Chem., 90, 2418, (1986).

105. Mukerjee, P., 'Solution Chemistry of Surfactants', Mittal, K.L., ed., Vol. 1, 153, Plenum Press, New York, (1979).

106. Mukerjee, P., Pure and Applied Chem., 52, 1317, (1980).

107. Wan, L.S.C., J. Pharm. Sci., 55, 1395, (1966).

108. Larsen, J.W., Magid, L.J., Payton, V., Tetrahedron letters, 29, 2663, (1973).

109. Swarbrick, J., Darawala, J., J. Phys. Chem., 73, 2627, (1969).

110. Flockhart, B.D., J. Colloid Sci., 16, 484, (1961).

111. Goddard, E.D., Benson, G.C., Canad. J. Chem., 35, 986, (1957).

112. Stilbs, P., J. Colloid Interfac. Sci., 94, 463, (1983).

113. Stilbs, P., 'Surfactants in Solution', Mittal, K.L., Lindman, B., ed., Vol. 2, 917, Plenum Press, New York, (1984).

114. Shih, L.B., Williams, R.W., J. Phys. Chem., 90, 1615, (1986).

115. Hoiland, H., Kuammen, O., Backlund, S., Rundt., K., 'Surfactants in Solution', Mittal, K.L., Lindman, B., ed., Vol. 2, 949, Plenum Press, New York, (1984).

116. Moroi, Y., Sato, K., 'Surfactants in Solution', Mittal, K.L., Lindman, B., ed., Vol. 2, 963, Plenum Press, New York, (1984).

117. Mukerjee, P., Ray, A., J. Phys. Chem., 70, 2144, (1966).

118. Cordes, E.H., Pure and Applied Chem., 50, 617, (1978).

119. Tomlinson, E., Davis, S.S., Mukhayer, G.I., 'Solution Chemistry of Surfactants', Mittal, K.L., ed., Vol. 1, 3, Plenum Press, New York, (1979).

120. Mukhayer, G.I., Davis, S.S., Tomlinson, E., J. Pharm. Sci., 64, 147, (1975).

121. Mukhayer, G.I., Davis, S.S., J. Colloid Interfac. Sci., 53, 224, (1975).

122. Mukhayer, G.I., PhD Thesis, University of Aston, (1974).

123. Hoyer, H.W., Doerr, I.L., J. Phys. Chem., 68, 3494, (1964).

124. Barry, B.W., Russell, G.F.J., J. Pharm. Sci., 61, 502, (1972).

125. Davis, S.S., Bruce, P.E., Daniels, P., Feely, L., 'Surfactants in Solution', Mittal, K.L., Lindman, B., ed., Vol. 2, 1391, Plenum Press, New York, (1984).

126. Barry, B.W., Gray, G.M.T., J. Colloid Interfac. Sci., 52, 327, (1975).

127. Mukhayer, G.I., Davis, S.S., J. Colloid Interfac. Sci., 66, 110, (1978).

128. Tomlinson, E., Davis, S.S., J. Colloid Interfac. Sci., 66, 335, (1978).

129. Tomlinson, E., Davis, S.S., J. Colloid Interfac. Sci., 76, 563, (1980).

130. Lemordant, D., Gaboriaud, R., Fluid Phase Equilibria, 20, ,269, (1985).

131. Moroi, Y., Ikeda, N., Matuura, R., J. Colloid Interfac. Sci., 101, 285, (1984).

132. Moroi, Y., Sugii, R., Akine, C., Matuura, R., J. Colloid Interfac. Sci., 108, 180, (1985).

133. Barry, B.W., Gray, G.M.T., J. Pharm. Sci., 63, 548, (1974).

134. Mukhayer, G.I., Davis, S.S., J. Colloid Interfac. Sci., 56, 350, (1976).

135. Tomlinson, E., Davis, S.S., Mukhayer, G.I., 'Solution Chemistry of Surfactants', Mittal, K.L., ed., Vol. 2, 889, Plenum Press, New York, (1979).

136. Mukhayer, G.I., Davis, S.S., J. Colloid Interfac. Sci., 59, 350, (1977).

137. Davis, S.S., Mukhayer, G.I., J. Pharm. Pharmacol., 24, 129P, (1972).

138. Mukhayer, G.I., Davis, S.S., J. Colloid Interfac. Sci., 61, 582, (1977).

139. Sepulveda, L., J. Colloid Interfac. Sci., 46, 372, (1974).

140. Bunton, C.A., Sepulveda, L., J. Phys. Chem., 83, 680, (1979).

141. Hirose, C., Sepulveda, L., J. Phys. Chem., 83, 3689, (1979).

142. Zoltewicz, J.A., Munoz, S., J. Phys. Chem., 90, 5820, (1986).

143. Abe, M., Ohsato, M., Ogino, K., Colloid and Polymer Science, 262, 657, (1984).

144. Sato, H., Kawasaki, M., Kasatani, K., Nakashima, N., Yoshihara, K., Bull. Chem. Soc. Japan, 56, 3588, (1983).

145. Park, J.W., Kim, S-J., Bull. Korean Chem. Soc., 5, 121, (1984).

146. Park, J.W., Nam, H-L., Bull. Korean Chem. Soc., 5, 182, (1984).

147. Robinson, B.H., White, N.C., Mateo, C., Adv. Molecular Relaxation Processes, 7, 321, (1975).

148. James, A.D., Robinson, B.H., White, N.C., J. Colloid Interfac. Sci., 59, 328, (1977).

149. Almgren, M., Swarup, S., 'Surfactants in Solution', Mittal, K.L., Lindman, B., ed., Vol. 1, 613, Plenum Press, New York, (1984).

150. Malliaris, A., Binana-Limbele, W., Zana, R., J. Colloid Interfac. Sci., 110, 114, (1986).

151. Hiromitsu, I., Kevan, L., J. Phys. Chem., 90, 3088, (1986).

152. Gamboa, C., Sepulveda, L., J. Colloid Interfac. Sci., 113, 566, (1986).

153. Bunton, C.A., Pure and Applied Chem., 49., 969, (1977).

154. Linda, P., Rubessa, F., Savelli, G., La Chimica e L'Industria, 63, 333, (1981).

155. Patel, K.L., Saruagya, S., Katiyar, S.S., Indian Journal of Chemistry, 20, 788, (1981).

156. Bunton, C.A., 'Solution Chemistry of Surfactants', Mittal, K.L., ed., Vol. 2, 519, Plenum Press, New York, (1979).

157. Bunton, C.A., Catal. Rev. - Sci. Eng., 20, 1, (1979).

158. Brown, J.M., Colloid Science Vol. 3 - Specialist Periodical Reports (1974-77), 253.

159. Brown, J.M., Elliot, R.L., Colloid Science Vol. 4 - Specialist Periodical Reports (1977-81), 180.

160. Fendler, J.H., Fendler, E.J., 'Catalysis in Micellar and Macromolecular Systems', Academic Press, New York, (1975).

161. Sudholter, E.J.R., van de Langkruis, G.B., Nengberts, J.B.F., Journal of the Royal Netherlands Chemical Society, 99, 73, (1980).

162. Chaimovich, H., Aleixo, R.M.V., Cuccovia, I.M., Zanette, D., Quina, F.H., 'Solution Behaviour of Surfactants', Mittal, K.L., Fendler, E.J., ed., Vol. 2, 949, Plenum Press, New York, (1982).

163. Bunton, C.A., 'The Chemistry of Enzyme Action', Page, M.I., ed., 461, Elsevier Science Publishers, (1984).

164. Romsted, L.S., 'Surfactants in Solution, Mittal, K.L., Lindman, B., ed., Vol. 2, 1015, Plenum Press, New York, (1984).

165. Martinek, K., Yatsimirski, A.K., Levashov, A.V., Berezin, I.V., 'Micellization, Solubilization and Microemulsions', Mittal, K.L., ed., Vol. 2, 489, Plenum Press, New York, (1977).

166. Broxton, T.J., Ryan, T., Morrison, S.R., Aust. J. Chem., 37, 1895, (1984).

167. Cipiciani, A., Ebert, C., Germani, R., Linda, P., Lovrecich, M., Rubessa, F., Savelli, G., J. Pharm. Sci., 74, 1184, (1985).

168. Tsuji, A., Miyamoto, E., Matsuda, M., Nishimura, Yamana, T., J. Pharm. Sci., 71, 1313, (1982).

169. Broxton, T.J., Aust. J. Chem., 35, 1357, (1982).

170. Hartley, G.S., Trans. Faraday Soc., 30, 444, (1934).

171. Reddy, I.A.K., Katiyar, S.S., 'Solution Behaviour of Surfactants', Mittal, K.L., Fendler, E.J., ed., Vol. 2, 1017, Plenum Press, New York, (1982).

172. Funasaki, N., J. Phys. Chem., 83, 237, (1979).

173. Broxton, T.J., Aust. J. Chem., 34, 1615, (1981).

174. Menger, F.M., Portnoy, C.E., J. Amer. Chem. Soc., 89, 4698, (1967).

175. Romsted, L.S., 'Micellization, Solubilization and Microemulsions', Mittal, K.L., ed., Vol. 2, 509, Plenum Press, New York, (1977).

176. Quina, F.H., Politi, M.J., Cuccovia, I.M., Martins-Franchetti, S.M., Chaimovich, H., 'Solution Behaviour of Surfactants', Mittal, K.L., Fendler, E.J., ed., Vol. 2, 1125, Plenum Press, New York, (1982).

177. Quina, F.H., Chaimovich, H., J. Phys. Chem., 83, 1844, (1979).

178. Chaimovich, H., Bonilha, J.B.S., Politi, M.J., Quina, F.H., J. Phys. Chem., 83, 1851, (1979).

179. Quina, F.H., Politi, M.J., Cuccovia, I.M., Baumgarten, E., Martins-Franchetti, S.M., Chaimovich, H., J. Phys. Chem., 84, 361, (1980).

180. Tomlinson, E., Davis, S.S., Brown, J.E., 'Solution Chemistry of Surfactants', Mittal, K.L., ed., Vol. 2, 867, Plenum Press, New York, (1979).

181. Nogami, H., Hasegawa, J., Iwatsuru, M., Chem. Pharm. Bull., 18, 2297, (1970).

182. Nogami, H., Awazu, S., Iwatsuru, M., Chem. Pharm. Bull., 11, 1251, (1963).

183. Ionescu, L.G., Nome, F., 'Surfactants in Solution', Mittal, K.L., Lindman, B., ed., Vol. 2, 1107, Plenum Press, New York, (1984).

184. Katiyar, S.S., Patel, K.L., Indian Journal of Chemistry, 20, 1065, (1981).

185. Davis, S.S., Kinkel, J.F.M., Olejnik, O., Tomlinson, E., J. Pharm. Pharmacol., 33, 104P, (1981).

186. Schurgers, N., de Blaey, C.J., Tomlinson, E., J. Pharm. Pharmacol., 36, 45, (1984).

187. Olejnik, O., Davis, S.S., Int. J. Pharm., 30, 101, (1986).

188. Touitou, E., Fisher, P., J. Pharm. Sci., 75, 384, (1986).

189. Jonkman, J.H.G., Hunt, C.A., Pharm. Weekbl. Sci. ed., 5, 41, (1983).

190. Tomlinson, E., van Dooremalen, J.A.M., van Rooij, H.H., Wynne, H.J.A., Int. J. Pharm., 12, 87, (1982).

191. Suzuki, E., Tsukigi, M., Muranishi, S., Sezaki, H., Kakemi, K., J. Pharm. Pharmacol., 24, 138, (1972).

192. Shetewi, B.B., PhD Thesis, University of Bath, (1975).

193. Weast, R.C., ed. in Chief, 'CRC Handbook of Chemistry and Physics', 67th ed., CRC Press Inc., Florida, USA, (1986).

194. Parkins, D.A., PhD Thesis, University of Bath, (1986).

195. Bates, R.G., 'Determination of pH-Theory and Practice', 2nd ed., J. Wiley and Sons, London, (1973).

196. Pryde, A., Gilbert, M.T., 'Applications of High Performance Liquid Chromotagraphy', Chapman and Hall, London, (1979).

197. Colin, H., Krstulovic, A.M., Excoffier, J.L., Guiochon, G., 'A guide to the HPLC Literature', Vol. 1-3, John Wiley and Sons, New York, (1985).

198. Schram, S.B., 'The LDC basic book of Liquid Chromatography', Milton Roy, St. Petersburg, (1980).

199. Bristow, P.A., Knox, J.H., Chromatographia, 10, 279, (1977).

200. Perrin, D.D., Dempsey, B., ' Buffers for pH and Metal Ion Control', Chapman and Hall Ltd., London, (1974).

201. Albert, A., Serjeant, E.P., 'The Determination of Ionization Constants', Chapman and Hall Ltd., London, (1971).

202. Cresswell, C.J., Runquist, O.A., Campbell, M.M., 'Spectral Analysis of Organic Compounds', 2nd ed., Longman, UK, (1972).

203. Derome, A.E., 'Modern NMR Techniques for Chemistry Research' in 'Organic Chemistry Series', Vol. 6., Pergamon Press, Oxford, (1987).

204. Kasler, F., 'Quantitative Analysis by NMR Spectroscopy', Academic Press, London, (1973).

205. Berne, B.J., Pecora, R., 'Dynamic Light Scattering with Applications to Chemistry Biology and Physics', John Wiley and Sons Inc., New York, (1976).

206. Kasatani, K., Kawasaki, M., Sato, H., Nakashima, N., J. Phys. Chem., 89, 542, (1985).

207. Wilson, C.G., Tomlinson, E., Davis, S.S., Olejnik, O., J. Pharm. Pharmacol., 31, 749, (1981).

208. Lee, S.J., Kurihara-Bergstrom, T., Kim, S.W., Int. J. Pharm., 47, 59, (1987).

209. Green, P.G., Hadgraft, J., Int. J. Pharm., 37, 251, (1987).

210. Linfield, W.M., ed., 'Anionic Surfactants', 'Surfactants Science Series', Vol. 7, Marcel Dekker, New York, (1976).

211. Lucassen-Reynders, E.H., ed., 'Anionic Surfactants - Physical Chemistry of Surfactant Action', 'Surfactant Science Series', Vol. 11, Marcel Dekker, New York, (1981).